Lipodepsipeptide Antibiotics: Total Synthesis and Mechanism of Action Studies Using ^{19}F-NMR

by

Braden John Kralt

A thesis
presented to the University of Waterloo
in fulfillment of the
thesis requirement for the degree of
Doctor of Philosophy
in
Chemistry

Waterloo, Ontario, Canada, 2020

Examining Committee Membership

The following served on the Examining Committee for this thesis. The decision of the Examining Committee is by majority vote.

External Examiner	Dr. Robert Batey, PhD Professor, University of Toronto Biological and Organic Chemistry
Supervisor	Dr. Scott Taylor, PhD Professor, University of Waterloo Chemistry
Internal-external member	Dr. David Rose, PhD Professor, University of Waterloo Bioinformatics, Systematics, and Evolution
Other Members	Dr. Michael Chong, PhD Professor, University of Waterloo Synthetic Organic Chemistry
	Dr. Richard Manderville, PhD Professor, University of Guelph Chemistry and Toxicology
	Dr. Michael Palmer, MD Associate Professor, University of Waterloo Biochemistry

Author's Declaration

I hereby declare that I am the sole author of this thesis. This is a true copy of the thesis, including any required final revisions, as accepted by my examiners.

I understand that my thesis may be made electronically available to the public.

Abstract

Daptomycin is a calcium-dependent cyclic lipodepsipeptide that is used clinically in the treatment of infections caused by pathogenic Gram-positive organisms, such as methicillin-resistant *Staphylococcus aureus*. Another calcium-dependent cyclic lipodepsipeptide antibiotic, A54145D, also has biological activity against Gram-positive pathogenic organisms, but is not used clinically because it is approximately 4-fold less active than daptomycin. Unlike daptomycin, however, A54145D is not inhibited by lung surfactant *in vitro*, which makes A54145D a suitable lead compound for the development of other antibiotics that may find use in medical practice as an alternative treatment for community-acquired pneumonia caused by *Streptococcus pneumoniae*.

While the total synthesis of daptomycin has been reported, thus allowing for an efficient method for the generation of analogs of daptomycin, no similar synthesis for A54145D was reported at the start of these studies. To facilitate the development of future antibiotics, a total synthesis of A54145D was developed employing Fmoc-based solid-phase-peptide synthesis. This synthesis enabled us to confirm that the 3-hydroxyasparagine residue has the (2*S*,3*S*)-configuration (*threo*), and the 3-methoxyaspartate residue has the (2*S*,3*R*)-configuration (*erythro*) instead of the (2*S*,3*S*)-configuration (*threo*). Additional analogs of A54145D and A54145A$_1$ were synthesized to study the structure-activity relationships of these antibiotics, and it was determined that the threonine residue is not amenable for substitution, in that replacement of threonine caused a dramatic loss in biological activity. Furthermore, it was confirmed that the replacement of the uncommon amino acid 3-methoxyaspartate with

aspartate, and 3-hydroxyasparagine with asparagine resulted in a 16-fold reduction of biological activity.

To further elucidate the mechanism of action of cyclic lipodepsipeptide antibiotics, which is a matter of some controversy in the scientific literature, ten fluorinated analogs of daptomycin were constructed by semi-synthesis or total synthesis to study their interaction with model membranes using ^{19}F-NMR. These analogs exhibited activity against *Bacillus subtilis* equal to or approaching that of daptomycin. ^{19}F-NMR studies with a peptide that contained a trifluoromethyl moiety at the end of the lipid tail indicate that at concentrations of daptomycin and calcium that are representative of *in vivo* conditions, daptomycin does not aggregate in solution. Preliminary ^{19}F-NMR studies with a daptomycin analog containing the CF_3 group appended to the ornithine residue at position 6 in the presence of model membranes and varying amounts of calcium suggest that the ornithine residue of daptomycin interacts with biological membranes before the lipid tail does.

Acknowledgements

I would like to express my sincere gratitude and appreciation to Professor Scott Taylor, my research supervisor, for his patience, support, and guidance throughout the course of my graduate work at the University of Waterloo. I thank the other members of my advisory committee, Dr. Chong, Dr. Manderville, and Dr. Palmer for the roles they played in the completion of this thesis. I thank the University of Waterloo, the Department of Chemistry and NSERC for their financial support.

I would like to thank other staff members that supported me throughout my graduate work: Dr. Smith of the UW Mass-Spec facility, Jan Venne who assisted with many NMR experiments, and Julie Goll, Dr. Laura Ingram and Dr. Steven Forsey, for whom I served several TA roles.

I would like to thank the members of the Taylor research group, both past and present, for their assistance and friendships: Dr. Yaser Abdel-Karem, Matthew Diamandas, Yuhan Huang, Magda Karski, Duncan Li, Dr. Chuda Lohani, Dr. Samy Mohamady, Ryan Moreira, Michael Noden, Bradley Scott, Jacob Soley, Dr. Robert Taylor, Wayne Vuong, Joshua Williams, and Bo Zheng. In addition to these individuals, there were many other friends in the chemistry department at the University of Waterloo, past and present, who made the past several years more enjoyable.

This thesis would not have been possible without the love and support of my beautiful wife, Brigitte. I thank her for her enduring patience throughout the entirety of this journey.

Dedicated to Brigitte

Table of Contents

List of Figures

List of Tables

List of Schemes

Abbreviations

2-ClTrt-Cl-PS	2-chlorotrityl-chloride polystyrene resin
2-MP	2-methylpiperidine
4-MP	4-methylpiperidine
A54145A_1	A54145 Factor A_1
A54145D	A54145 Factor D
A54145E	A54145 Factor E
AA	amino acid
AABA	(2*S*,3*R*)-2-amino-3-azidobutanoic acid
AcOH	acetic acid
Ala	alanine
Alloc	allyloxycarbonyl
Asn	asparagine
Asp	aspartate
Boc	butyloxycarbonyl
BODIPY	boron-dipyrromethene
BOP	(benzotriazol-1-yloxy)tris(dimethylamino)phosphonium hexafluorophosphate
CAP	community-acquired pneumonia
CCCP	carbonyl cyanide *m*-chlorophenyl hydrazine
CD	circular dichroism
CDA	Calcium-dependent antibiotic
CFU	colony forming unit
CHO	formyl
CL	cardiolipin
cLPA	cyclic lipodepsipeptide antibiotic
DABA	(2*S*,3*R*)-2,3-diaminobutyric acid
DABCO	1,4-diazabicyclo[2.2.2]octane
Dap	daptomycin
DAPA	(2*S*)-2,3-diaminopropionic acid
DCA	dichloroacetic acid
DCM	dichloromethane
Dec	decanoyl
^{DH}Ala	dehydroalanine
^{DH}Asp	dehydroaspartic acid
DIAD	diisopropyl azodicarboxylate
DIC	*N,N'*-diisopropylcarbodiimide
DIPEA	*N*,*N*-diisopropylethylamine
DKP	diketopiperazine
DMAP	*N*,*N*-dimethyl-4-aminopyridine
DMB	dimethoxybenzyl
DMBA	*N,N'*-dimethylbarbituric acid
DMF	*N*,*N*-dimethylformamide
DMPC	dimyristoylphosphatidylcholine
DMPG	dimyristoylphosphatidylglycerol

DOPC	dioleoylphosphatidylcholine
DOPG	dioleoylphosphatidylglycerol
DTT	dithiothreitol
EDC	1-ethyl-3-(3-dimethylaminopropyl)carbodiimide
ee	enantiomeric excess
*e*MeOAsp	*L-erythro*-methoxyaspartate
equiv	equivalents
Fmoc	fluorenylmethoxycarbonyl
FRET	fluorescence resonance energy transfer
GFP	green fluorescent protein
GlcNAc	*N*-acetylglucosamine
Glu	glutamate
Gly	glycine
GUV	giant unilamellar vesicles
HCTU	2-(6-Chloro-1-H-benzotriazole-1-yl)-1,1,3,3-tetramethylaminium hexafluorophosphate
hCys	homocysteine
hCys(CF_3)	(trifluoromethyl)-homocysteine
HFIP	hexafluoroisopropanol
HOAsn	hydroxyasparagine
HOAsp	hydroxyaspartate
HOAt	1-hydroxy-7-azabenzotriazole
HOBt	hydroxybenzotriazole
HPLC	high performance liquid chromatography
Ile	isoleucine
ITC	isothermal titration calorimetry
Kyn	kynurenine
LB	Luria-Bertani
LD_{50}	lethal dose killing 50% of the test sample
LRMS	low-resolution mass spectrometry
LTA	lipoteichoic acid
LUV	large unilamellar vesicles
Lys	lysine
MeGlu	(2*S*,3*R*)-3-methylglutamate
MeOAsp	methoxyaspartate
mprF	multipeptide resistance factor
mRNA	messenger ribonucleic acid
MRSA	methicillin-resistant *Staphylococcus aureus*
MSSA	methicillin-susceptible *Staphylococcus aureus*
N-MePhe	*N*-methylphenylalanine
NBD	7-nitrobenzo-2-oxa-1,3-diazole
NBD-PE	NBD-labelled phosphatidylethanolamine
NHS	*N*-hydroxysuccinimide
NMP	*N*-methylpyrrolidinone
NMR	nuclear magnetic resonance
NRPS	non-ribosomal peptide synthetase

Orn	ornithine
PBu_3	tributylphosphine
PEG	polyethylene glycol
PG	phosphatidylglycerol
$PhSiH_3$	phenylsilane
PMe_3	trimethylphosphine
PNB	*p*-nitrobenzoate
PNBCOOH	*p*-nitrobenzoic acid
POPC	palmitoyloleoylphosphatidylcholine
POPG	palmitoyloleoylphosphatidylglycerol
PPh_3	triphenylphosphine
PS	polystyrene
PyBOP	benzotriazol-1-yl-oxytripyrrolidinophosphonium hexafluorophosphate
R_2	transverse relaxation rate
RP	reverse-phase
SAR	structure-activity relationship
Sar	sarcosine
Ser	serine
SIIS	solvent-induced isotopic shift
SNP	single-nucleotide polymorphism
SPPS	solid-phase peptide synthesis
STAB-H	sodium triacetoxyborohydride
SUV	small unilamellar vesicles
T_2	transverse relaxation time
TBAF	tetrabutylammonium fluoride
TBDMS	*tert*-butyldimethylsilyl
tBu	*tert*-butyl
TEMPO	(2,2,6,6-tetramethylpiperidin-1-yl)oxidanyl
^{TF}acetyl	trifluoroacetyl
^{TF}Dec	10,10,10-trifluorodecanoyl
TFE	trifluoroethanol
^{TF}ethyl	trifluoroethyl
^{TFM}benzoyl	*p*-trifluoromethylbenzoyl
^{TFM}benzyl	*p*-trifluoromethylbenzyl
^{TFM}Phe	*p*-trifluoromethylphenylalanine
THF	tetrahydrofuran
*t*HOAsn	*L-threo*-hydroxyasparagine
Thr	threonine
TIPS	triisopropylsilane
TMCL	tetramyristoylcardiolipin
*t*MeOAsp	*L-threo*-methoxyaspartate
tRNA	transfer ribonucleic acid
Trp	tryptophan
Trt	trityl
Val	valine

Chapter 1 – Introduction

1.0 – Antibiotics and Antibiotic Resistance

Sulfonamides were deployed as antibacterial agents in the 1930s, and ever since then, antibiotics have been used clinically to aid in the treatment of bacterial infections.[1,2] Antibiotics are compounds that kill bacteria (bactericidal) or prevent their proliferation (bacteriostatic). They can act on various cellular targets, including the cell wall, cell membrane, proteins, and even nucleic acids. Penicillin, for example, inhibits the final step in cell wall biosynthesis in Gram-positive bacteria.[3]

Many infections that were once fatal have become easily treatable through antibiotics. The introduction of antibiotics for the rapid treatment of pathogenic bacteria is easily one of the most important advances ever made in the field of medicine. Many antibiotics were discovered or developed between 1940 and 1960, and this time interval has been called the "Golden Age" of antibiotic development.[4] Between 1962 and 2000, no new major classes of antibiotics were introduced to clinic, until linezolid (2000), daptomycin (2003), and retapamulin (2007) were approved for clinical use (Figure 1.1).[4] More recently, fixadomycin and bedaquiline (Figure 1.1) were approved for clinical use (2012).[5,6] Regrettably, the search

for new antibiotics is not very economically profitable, and despite the urgent and on-going need for new antibiotics, limited research is underway.[7]

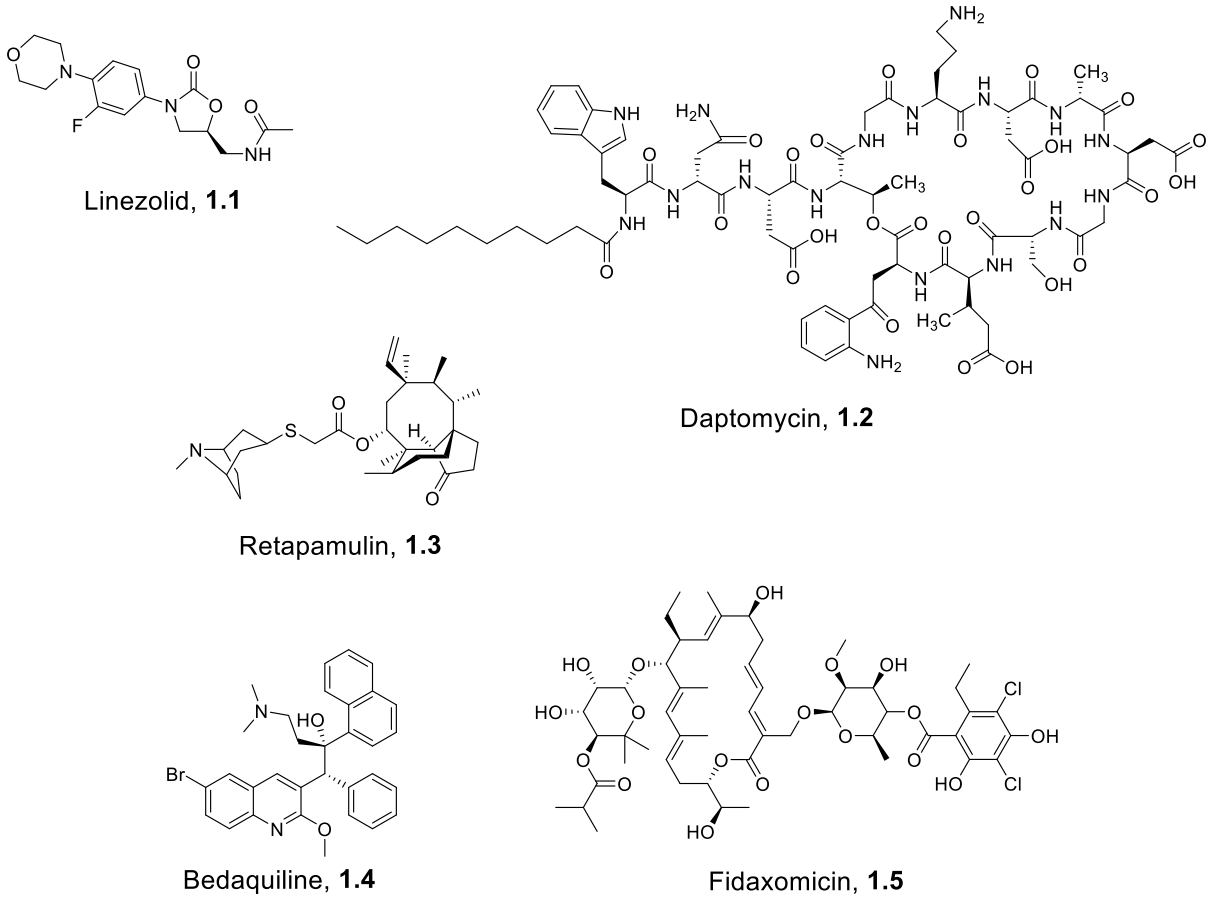

Figure 1.1: Novel antibiotics released in the 21st century. Each structure represents a different class. Linezolid, retapamulin, and fidaxomicin inhibit ribosomal protein synthesis.[8–10] Bedaquiline inhibits ATP synthase.[11]

The lack of research toward new antibiotics is concerning, as bacterial antibiotic resistance has been observed within several years of the deployment of any novel antibiotic (Figure 1.2).[1] Indeed, Clatworthy et al. discussed this trend in 2007, noting the dates of deployment and the dates of resistance observed. As an antibiotic is deployed to target a cellular component or function, bacteria adapt to their environment under selective pressure, and evolve resistance to the antibiotic.

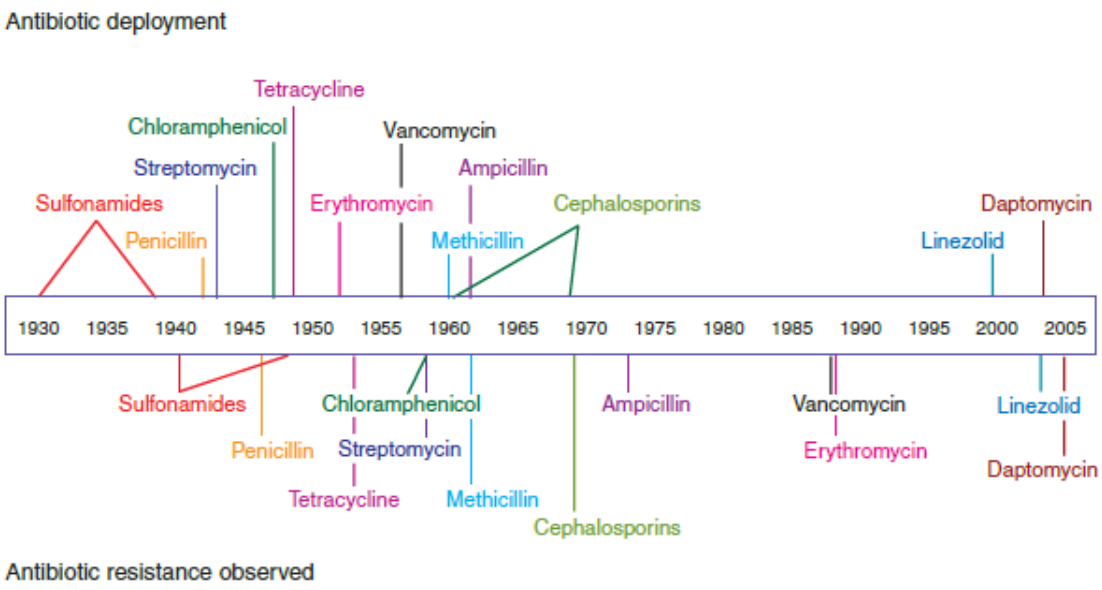

Figure 1.2: Timeline of antibiotic deployment and observed resistance. The year the antibiotic was deployed is depicted above the timeline, and the year resistance was observed is below. Figure taken from Clatworthy et al. and used with permission.[1]

The widespread resistance to antibiotics has led some to claim that we are living in a "post-antibiotic era".[12] The extensive use of antibiotics has led to the emergence of multi-drug resistant strains of bacteria including *Staphylococcus aureus*, *Mycobacterium tuberculosis*, and *Streptococcus pneumoniae*. Accordingly, humanity and bacteria are currently in an evolutionary arms race: as bacteria evolve resistance against our current arsenal of antibiotics, we must be continually developing new antibiotics, and this cycle will inevitably continue *ad infinitum*. Thus, overcoming antibiotic-resistant bacteria is not merely an end-goal, but a perpetual journey, and the issue of antibiotic resistance is an issue that is expected to become much more serious in the not-too-distant future.

Fortunately, physicians have at their disposal a handful of antibiotics for which widespread resistance has not yet developed. These are used as a last resort when all other antibiotics fail. One of these so-called last resort antibiotics is daptomycin.[13]

1.1 – Introduction to Cyclic Lipodepsipeptide Antibiotics

Daptomycin (Figures 1.1 and 1.3) is a cyclic lipodepsipeptide antibiotic (cLPA) that is used to treat serious skin infections caused by Gram-positive bacteria. It is a member of the A21978C family of antibiotics and is clinically approved for the treatment of infections caused by methicillin-resistant and methicillin-susceptible *S. aureus* (MRSA and MSSA, respectively), *Streptococcus pyogenes*, *Streptococcus agalactiae*, *Streptococcus dysgalactiae*, and vancomycin-resistant *Enterococci faecalis*.[13,14] Notably, daptomycin is not used clinically against *Streptococcus pneumoniae*, the source of community-acquired pneumonia. Although daptomycin is biologically active *in vitro* against *S. pneumonia*, daptomycin is suspected to be inhibited by lung surfactant *in vivo*.

Daptomycin consists of a macrocyclic peptide core containing ten amino acids, with an ester bond between the side-chain of Thr4 and the α-carboxylic acid of Kyn13. Attached to Thr4 is an exocyclic portion which contains an additional three amino acids and a lipid tail. The peptide contains three non-proteinogenic *L*-amino acids: ornithine at position 6 (Orn6), (2*S*,3*R*)-3-methylglutamate at position 12 (MeGlu12), and kynurenine at position 13 (Kyn13). Additionally, there are three non-proteinogenic *D*-amino acids (*D*-Asn2, *D*-Ala8, and *D*-Ser11). It is produced using non-ribosomal peptide synthetases (NRPSs) by *Streptomyces roseosporus* (See section 1.4 for a brief discussion on non-ribosomal peptide synthesis) and remains the only member of its class approved for clinical use.

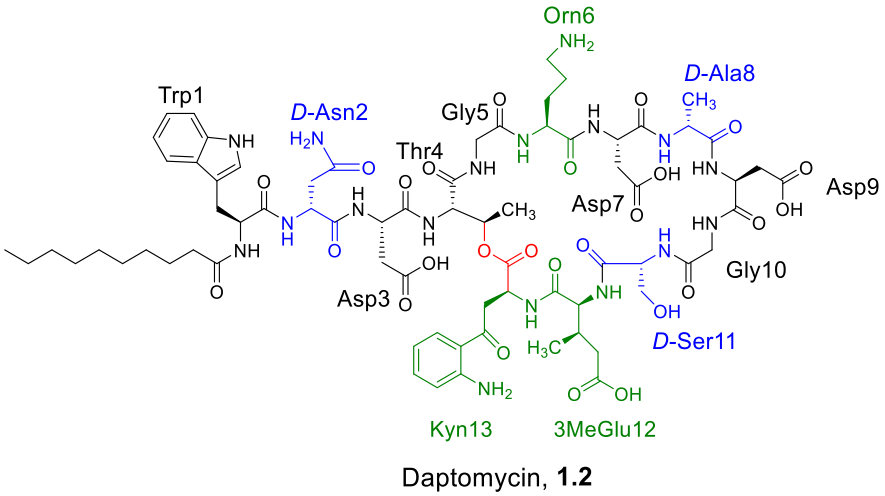

Figure 1.3: The structure of daptomycin (**1.2**). *D*-amino acids are shown in blue, and non-proteinogenic amino acids are shown in green. The depsi-bond between the side-chain of Thr4 and the α-carboxylic acid of Kyn13 is shown in red.

Members of the Calcium-Dependent Antibiotic (CDA) and A54145 families of antibiotics (Figure 1.4) are structurally related to daptomycin. The A54145 family also contains a macrocyclic peptide core containing ten amino acids, an exocyclic tripeptide and a lipid tail. In A54145, the depsi-bond is formed between the side-chain of Thr4 and the α-carboxylic acid of Ile13 or Val13. Three non-proteinogenic *D*-amino acids are found at the same locations as for daptomycin (*D*-Glu2, *D*-Lys8, and *D*-Asn11). The A54145 family of antibiotics consists of 8 different factors, whose structures vary at three different locations. Common to all A54145 factors are the non-proteinogenic amino acids hydroxyasparagine at position 3 (HOAsn3), sarcosine at position 4 (Sar4), and methoxyaspartate at position 9 (MeOAsp9). The factors vary at the lipid tail, which may be *n*-decanoyl, *iso*-decanoyl, or *anteiso*-undecanoyl; at position 12, which may be Glu or 3MeGlu; and at position 13, which may be Ile or Val. The A54145 family of antibiotics is synthesized non-ribosomally by *Streptomyces fradiae* (see section 1.4).

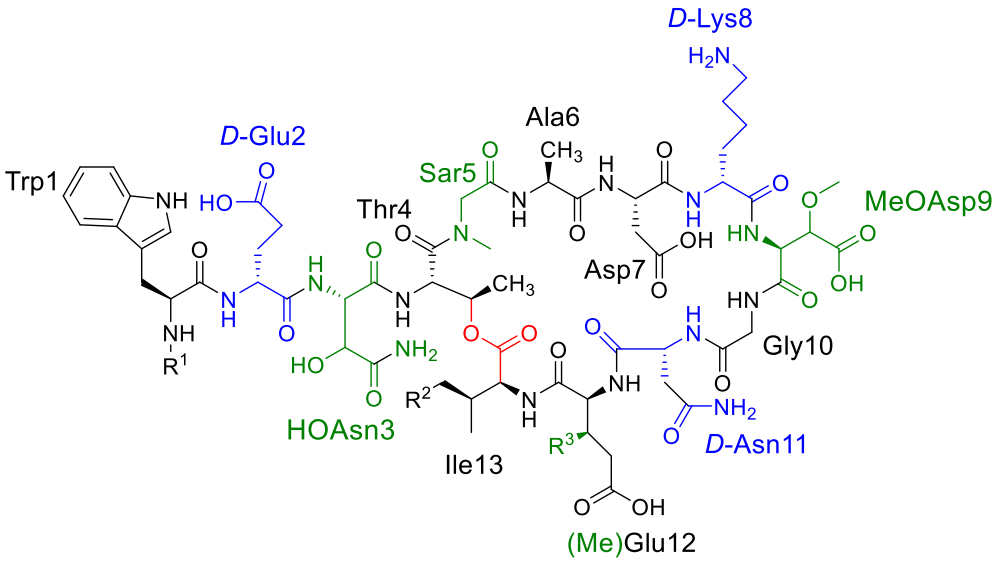

Compound	A54145 Factor	R^1	R^2	R^3
1.6	A	*iso*-decanoyl	$-CH_3$	-H
1.7	A_1	*n*-decanoyl	$-CH_3$	-H
1.8	B	*n*-decanoyl	$-CH_3$	$-CH_3$
1.9	B_1	*iso*-decanoyl	$-CH_3$	$-CH_3$
1.10	C	*anteiso*-undecanoyl	-H	$-CH_3$
1.11	D	*anteiso*-undecanoyl	$-CH_3$	-H
1.12	E	*anteiso*-undecanoyl	$-CH_3$	$-CH_3$
1.13	F	*iso*-decanoyl	-H	-H

Figure 1.4: The structure of the A54145 family of antibiotics. *D*-amino acids are shown in blue, and non-proteinogenic amino acids are shown in green. The depsi-bond between the side-chain of Thr4 and the α-carboxylic acid of Ile13/Val13 is shown in red.

No members of the A54145 family have been approved for clinical use. Factors that contain MeGlu12 are about 2-fold less active than daptomycin but are too toxic to mice.[15] Factors that contain Glu12 are about 2-fold less active than those containing MeGlu12 but are substantially less toxic. A54145 Factor D (A54145D), which contains Glu12, Ile13, and an *anteiso*-undecanoyl tail, has lower biological activity than daptomycin, but, somewhat surprisingly, *in vitro* studies demonstrate that A54145D retains most of its biological activity in the presence of lung surfactant.[16,17] Since inhibition by lung surfactant is the suspected

reason why daptomycin failed to meet non-inferiority criteria as a treatment for community-acquired pneumonia during clinical trials, A54145D's *in vitro* efficacy in the presence of lung surfactant makes it a promising starting point in the development of antibiotics that can be used to treat community-acquired pneumonia (CAP), a leading cause of death worldwide.[18,19]

1.2 – Proposed Mechanisms of Action of Cyclic Lipodepsipeptide Antibiotics

Most of the research to date pertaining to the mechanism of action of cLPAs has been done on daptomycin. It is assumed that A54145 behaves in a similar fashion. Despite over 30 years of studies to elucidate its mode of action, the exact mechanism by which daptomycin elicits its bactericidal effect is a matter of some controversy. The main proposed mechanisms are pore formation within the cell membrane, disruption of cell wall synthesis, and disruption of proper cell membrane function.

In 1985, the first reported study of the bacterial activity of the A21978C family of antibiotics was published. Eliopoulos et al. discovered that A21978C_1, which is daptomycin with an 8-methyldecanoyl tail instead of a decanoyl tail, only exhibited anti-bacterial activity if the growth medium was supplemented with calcium (Ca^{2+}).[20] Lakey et al. reported in 1986 that subjecting lipid membranes to A21978C (daptomycin) increased their conductivity and rendered them permeable to potassium, and that conductivity was proportional to the amount of Ca^{2+} added.[21] Finally, in 2004, researchers in the Hancock group used daptomycin's intrinsic fluorescence to show that daptomycin binds to membranes only in the presence of Ca^{2+}, and only when the membranes contain phosphatidylglycerol (PG) lipids.[22] Further, based upon circular dichroism studies (CD) studies, the Hancock group established that daptomycin undergoes a significant structural change upon membrane-binding.[22] While the exact mechanism by which daptomycin elicits its bactericidal activity is still controversial, it has

been well established that daptomycin requires calcium and phosphatidyl glycerol for biological activity, and that depolarization of the cell membrane occurs after being subjected to daptomycin.

1.2.1 – Disruption of Cell Wall Synthesis

There are several differences between Gram-positive and Gram-negative bacteria. Firstly, Gram-negative bacteria have two separate cell membranes: an inner membrane and an outer membrane (Figure 1.5). Secondly, Gram-positive bacteria have a much thicker peptidoglycan (also termed murein) layer, which acts as a cell wall. It is the synthesis of this peptidoglycan layer that is thought by some to be the site of action of daptomycin.

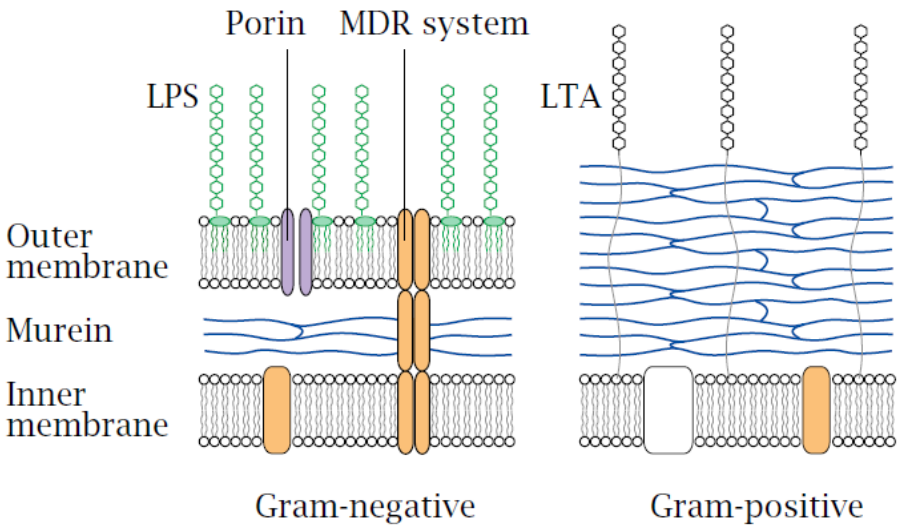

Figure 1.5: Structure of Gram-negative and Gram-positive membranes**.** Murein is referred to as peptidoglycan in this thesis. Figure taken and modified from Dr. Palmer's Biochemical Pharmacology course notes with permission.[23]

In 1985, Eliopoulos et al. studied A21978C_1 and observed that upon subjecting *Staphylococcus aureus* and *Streptococcus faecalis* to this compound for 180 minutes, incorporation of radio-labelled [^{14}C]-alanine was reduced by up to 50% of the control.[20] Since alanine is a precursor to *D*-alanine, which is incorporated into peptidoglycan during its

biosynthesis, the researchers concluded that daptomycin inhibits the peptidoglycan synthesis.[20] The same effect was also observed with authentic daptomycin (at the time named LY146032) by Allen et al.[24] Similarly, Mengin-Lecreulx et al. also reported in 1990 that daptomycin likely interferes in peptidoglycan synthesis, as treatment with daptomycin reduced the incorporation of another precursor, [^{14}C]-GlcNAc (*N*-acetylglucosamine), into peptidoglycan.[25]

In 1990 and 1993, researchers in the Satta group further refined this proposed mechanism of action.[26] In this work, the researchers determined that daptomycin was still active against *Enterococcus faecium* protoplasts (living cells which notably lack a cell wall, and are grown in osmotically protective media).[26,27] By comparing the number of colony forming units (CFUs) observed after treatment with daptomycin with the number of CFUs observed after treatment with vancomycin (a known peptidoglycan synthesis inhibitor), it was clearly demonstrated that inhibition of peptidoglycan synthesis alone cannot account for daptomycin's biological activity, as vancomycin was rendered ineffective, yet daptomycin still retained biological activity. The researchers determined that treating both *S. aureus* and *E. faecium* protoplasts with daptomycin reduced the incorporation of [^{14}C]-glycerol into lipoteichoic acid (LTA), the synthesis of which is known to occur in the cell membrane.[26,27] This led to the alternative hypothesis that daptomycin also inhibits the biosynthesis of LTA.

Further research by Boaretti and Canepari towards daptomycin's inhibition of LTA synthesis allowed for the isolation of so-called daptomycin-binding proteins in 1995, and the further purification of these proteins in 2000.[28,29] These isolated proteins, however, are only speculated to be related to LTA biosynthesis, and no direct evidence of daptomycin's binding and their subsequent inhibition was obtained. Further, these proteins were never characterized

or identified, and no research on the topic of daptomycin-binding proteins has been published since.[28]

Many of the studies which conclude that daptomycin inhibits peptidoglycan synthesis or LTA synthesis relied on the observation that radiolabeled precursors to peptidoglycan and LTA are not incorporated by cells subjected to daptomycin. However, protoplasts lacking a peptidoglycan-containing cell wall were killed by daptomycin, which would not be expected if daptomycin acted exclusively on peptidoglycan synthesis. Furthermore, Laganas et al. demonstrated in 2003 that rifampin-treated *S. aureus* were susceptible to daptomycin treatment.[30] Rifampin is a bacteriostatic antibiotic that causes the cessation of macromolecular synthesis including synthesis of LTA through RNA polymerase inhibition.[31] However, treatment with rifampin does not significantly affect cellular viability. If daptomycin's mechanism of action involved the inhibition of LTA biosynthesis, one might then expect that treating rifampin-arrested cells with daptomycin would not cause cell death. However, Laganas et al. found that daptomycin does indeed cause cell death of rifampin-arrested cells.[30] Thus, current evidence pointing to the hypothesis that daptomycin's mechanism of action involves inhibition of cell-wall biosynthesis does not completely explain daptomycin's mode of action.

1.2.2 – Disruption of Proper Cell Membrane Function

In 1986, Lakey and Lea observed that treatment of membranes with daptomycin increased their conductivity, proportional to the amount of calcium ions present, and from this proposed that daptomycin's activity involved incorporation into the bilayer membrane.[21] Several studies have offered some support to the idea that daptomycin acts directly on membranes of its target bacteria, causing adverse effects. For example, scanning electron

microscopy of daptomycin-treated *S. aureus* by Wale et al. resulted in gross morphological changes to the surface of the bacteria.[32]

Researchers at Cubist Pharmaceuticals in 2008 were able to isolate cells after daptomycin treatment and examine them intact using electron microscopy, and demonstrated that daptomycin, regardless of its interaction with lipid bilayers, does not result in bacterial cell lysis (up to concentrations of 4 µg/mL, 8 x the MIC), however does result in aberrant cell division septa.[33] In the same year, research in the Straus and Hancock groups demonstrated that the addition of daptomycin and Ca^{2+} to liposomes (model membranes) containing dioleoylphosphatidylglycerol (DOPG) and dioleoylphosphatidylcholine (DOPC) resulted in the fusion of large unilamellar vesicles (LUVs).[34] Despite the evidence of membrane fusion in model membranes, this is unlikely to be the mechanism of action *in vivo*, since the presence of the cell well would prevent membrane fusion of live cells.

In 2012, Pogliano et al. in collaboration with Cubist Pharmaceuticals studied the interaction of BODIPY-daptomycin with *B. subtilis*.[35] BODIPY-daptomycin is a synthetic variant of daptomycin which contains the BODIPY fluorophore, and can therefore be observed in live cells. The researchers noticed that BODIPY-daptomycin localizes in the cell membrane at nascent septa but is absent from pre-existing septa. Further, patches of daptomycin were found to co-localize with DivIVA-GFP, or the DivIVA protein with a green fluorescent protein (GFP) covalently attached. The authors proposed that daptomycin forms patches that attract the cell division protein DivIVA and incorrectly induce cell division. Further, sub-lethal concentrations of daptomycin resulted in abnormal membrane morphology, in that typically cylindrical *B. subtilis* appeared bent or curved following treatment with daptomycin. Finally, BODIPY-daptomycin co-localized with GFP-vancomycin, which is known to localize at

locations of peptidoglycan synthesis, further suggesting daptomycin's possible role in abnormal cell wall morphology. In accordance with these observations, a new mechanism of action was proposed that involved the abnormal functioning of the cell membrane (Figure 1.6). In this proposed mechanism of action, daptomycin at sub-lethal concentrations causes changes in cell-membrane curvature as a result of the large head-group volume of daptomycin and the small-volume tail. It was postulated that this negative membrane curvature is compensated on the inner leaflet by cardiolipin, which has a small-volume head group and a large-volume lipid volume. Patches of daptomycin recruit the DivIVA protein, incorrectly signaling the daptomycin-patch as a site of cell division. At above-lethal concentrations of daptomycin, discontinuities in the membrane result in the slow leakage of ions and the loss of membrane potential.

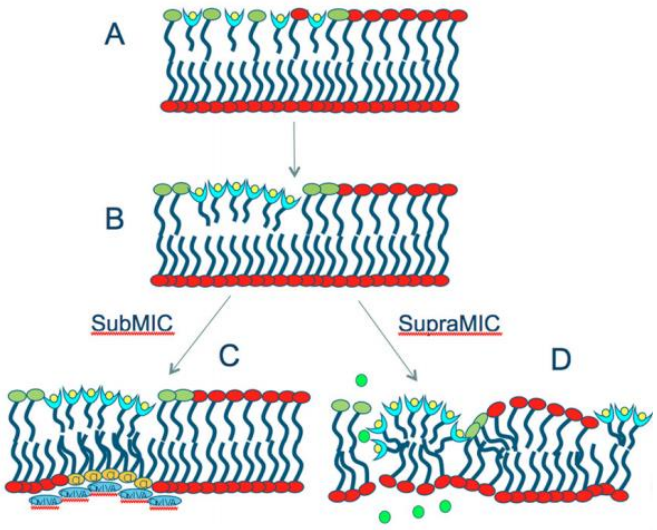

Figure 1.6: Proposed mechanism of action involving discontinuities in the membrane. Shown in the image is daptomycin (light blue cups with yellow circles), PG lipids (green lipids), cardiolipin (yellow lipids), potassium ions (green circles), and DivIVA (blue ovals). Taken from Pogliano et al. and used with permission.[35]

A novel hypothesis to the mechanism of action was also proposed by Chen et al. in 2014, which involved daptomycin-mediated lipid-extraction.[36] In this proposed mechanism of

action, the insertion of daptomycin into the model membrane displaces a pair of lipid molecules from the membrane, resulting in a major rearrangement of neighbouring lipids, called water pore defects, and these water pore defects allow for the permeation of ions through the membrane.[36] To support this hypothesis, the researchers analyzed giant unilamellar vesicles (GUVs) partially aspirated into a micropipette at constant vacuum, effectively producing a spherical part and cylindrical part of the vesicle (Figure 1.7). Treatment with daptomycin at concentrations above the minimum inhibitory concentration resulted in an initial increase in the volume of the cylindrical part of the vesicle, indicating association of daptomycin with the membrane, followed by a decrease in the cylindrical volume, indicating an increase in surface tension that could be caused by the loss of lipids from the membrane. This study fails to address, however, the results from Pogliano et al., who observed membrane curvature as the result of daptomycin treatment.[35] It is possible that daptomycin's ability to adjust membrane curvature might also increase the surface tension observed in this lipid-extraction study.

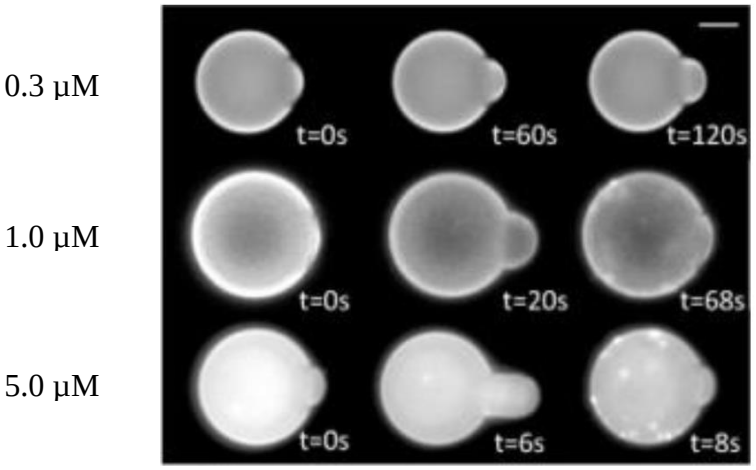

Figure 1.7: Membrane surface area changes of GUVs with treatment of daptomycin. Daptomycin concentrations are indicated. The top row represents sub-MIC concentrations, and the middle and bottom rows represent supra-MIC concentrations. Taken from Chen et al. and used with permission.[36]

Very recently, Müller et al. observed that daptomycin completely dislodges MurG and PlsX from the bacterial membrane, and based upon this, suggested an alternative mechanism of action.[37] It was proposed that daptomycin binds to fluid micro-domains (regions of increased fluidity), distorting the membrane resulting in even more fluid lipids at the site of membrane insertion (A,B Figure 1.8). The recruitment of other fluid lipids in the inner leaflet allows for daptomycin flipping from the outer to the inner leaflet, displacing the MurG protein, responsible for catalyzing the last synthesis step of peptidoglycan precursor lipid II, and PlsX, which is involved in phospholipid synthesis (C, Figure 1.8). Daptomycin present at the inner leaflet prevents the reassociation of MurG (D, Figure 1.8). Interestingly, this proposed mechanism of action relates the disruption of proper membrane function to the disruption of cell wall synthesis. Membrane depolarization is explained as a secondary effect of daptomycin's activity, instead of its primary effect: the boundaries between regions of increased fluidity and more rigid micro-domains are assumed to be weak spots that allow for leaking of protons through the membrane. Interestingly, this work observed the lysis of cell membranes at 4 μg/mL, contrary to the results of Cubist researchers in 2008.[33]

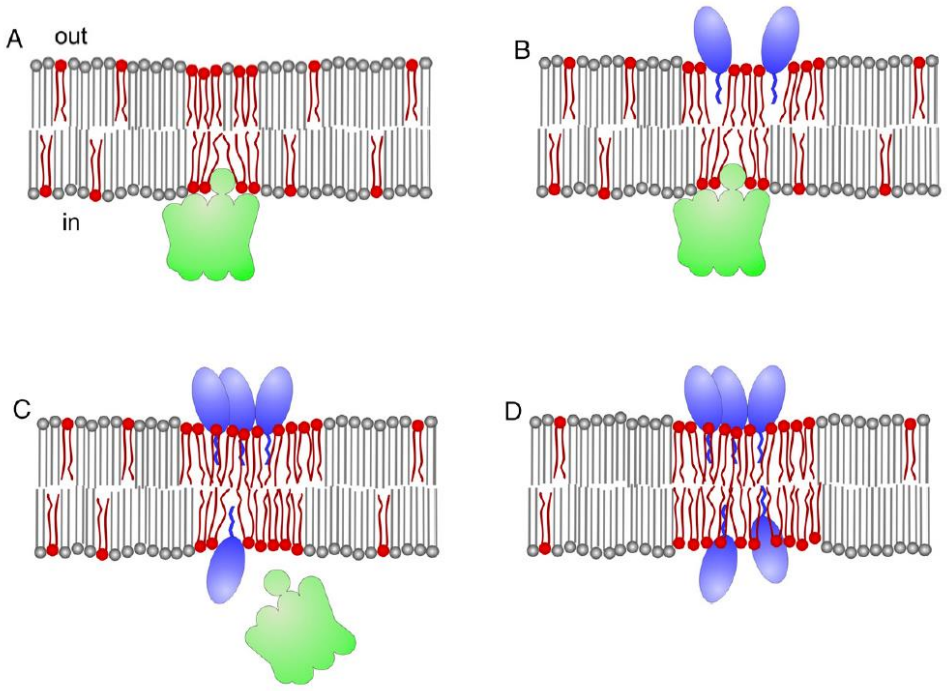

Figure 1.8: Proposed mechanism of action involving MurG and PlsX dislocation. Daptomycin inserts into fluidic domains of the membrane (A, B), dislodging peripheral proteins such as MurG and PlsX (C,D). MurG and PlsX (green) are involved in peptidoglycan synthesis and phospholipid synthesis. Figure taken from Müller et al. and used with permission.[37]

Additionally, it was demonstrated by Lee et al. in 2018 that daptomycin bound to membranes that contained cholesterol less effectively.[38] Since cholesterol increases the rigidity of biological membranes, this offers further support to the notion that daptomycin binds to regions of the membrane with increased fluidity.

A third mechanism of action widely accepted and supported by available evidence is the idea that daptomycin oligomerizes on bacterial membranes and forms a pore. This pore allows the leakage of cations from the cytosol, causing membrane depolarization and ultimately cell death.

1.2.3 – Oligomerization and Pore Formation

Initial studies by Lakey and Lea in 1986 demonstrated that treatment of biological membranes in the presence of calcium ions resulted in increased conductivity of model membranes.[21] Generally, increasing the calcium ion concentrations resulted in increased conductivity, suggesting that charged molecules or atoms were able to pass through the membrane. Lakey and Ptak in 1988 reconfirmed that daptomycin requires calcium for activity by observing the fluorescence changes of the intrinsically fluorescent kynurenine amino acid in lipids at increasing calcium concentrations.[39]

In 1991, researchers at Eli Lilly demonstrated on live cells that daptomycin disrupts membrane potential in *S. aureus* in a calcium-dependent fashion.[40] In this report, it was also observed that the greatest biological activity of daptomycin was observed when the membrane potential of growing cells was at its largest, suggesting that the energized membrane potential is a target of the antibiotic's action mechanism. Later that year, researchers at Eli Lilly reported that treatment by daptomycin reduced the potential-dependent uptake of glutamic acid and alanine, further suggesting that the energized membrane was the target for biological activity.[41] Expanding upon these results, in 2003 Jared Silverman et al. of Cubist Pharmaceuticals correlated the cell viability of daptomycin-treated *S. aureus* with a loss in membrane potential, and additionally, through the loss of potassium ions using a PBFI indicator (PBFI is a fluorescence ion indicator specific for potassium (K^+) ions).[42] Notably, the release of exclusively potassium from the cells would result in membrane hyperpolarization, so it is likely that daptomycin allows for the leakage of other ions from the cell in addition to potassium.[13] Additionally, recent research published by the Fišer group demonstrated that membranes with

higher potential were dissipated faster than membranes with lower potential when subjected to daptomycin, further suggesting that daptomycin's target is an energized membrane.[43]

The above observations support the mechanism of action which involves membrane depolarization, but they do not provide insights into how it exactly this biological activity is effected. In the 2003 work by Silverman et al., it was proposed that daptomycin oligomerizes on biological membranes, which ultimately leads to membrane depolarization, although no evidence was presented to support daptomycin oligomerization.

It wasn't until 2011 when researchers in the Palmer group reported that daptomycin oligomerizes on biological membranes.[44,45] Based on observed self-quenching of the NBD-fluorophore on NBD-daptomycin (NBD is 7-nitrobenzo-2-oxa-1,3-diazole, covalently attached to the Orn6 residue), and reduced self-quenching in the presence of native daptomycin, the presence of oligomers were deduced. Formation of oligomers were calcium ion dependent, and further, dependent upon the presence of DOPG lipids in the model membranes. Additionally, a daptomycin with a perylene moiety on its lipid tail formed excimers in the presence of PG membranes and calcium, further suggesting aggregation.

Researchers in the Palmer group in 2012 further estimated the subunit stoichiometry of membrane-associated daptomycin oligomers to be between 6 and 7 by quantifying fluorescence and fluorescence-resonance energy transfer (FRET) of the kynurenine of native daptomycin and the NBD-group of NBD-daptomycin.[46] Then, in 2014, members of the Palmer group utilized a pore-forming assay to further elucidate the mechanism of action of daptomycin. In this assay, daptomycin and CCCP (carbonyl cyanide *m*-chlorophenyl hydrazine, a known protonophore) are exposed to pyranine-containing liposomes with both pH and salt gradient, and these pore-formers mutually allow dissipation of both gradients. The

fluorescence of pyranine is pH-sensitive and increases at higher pH (Figure 1.9). Accordingly, antibiotics that allow for the dissipation of the membrane through ion leakage will incite a fluorescence increase.

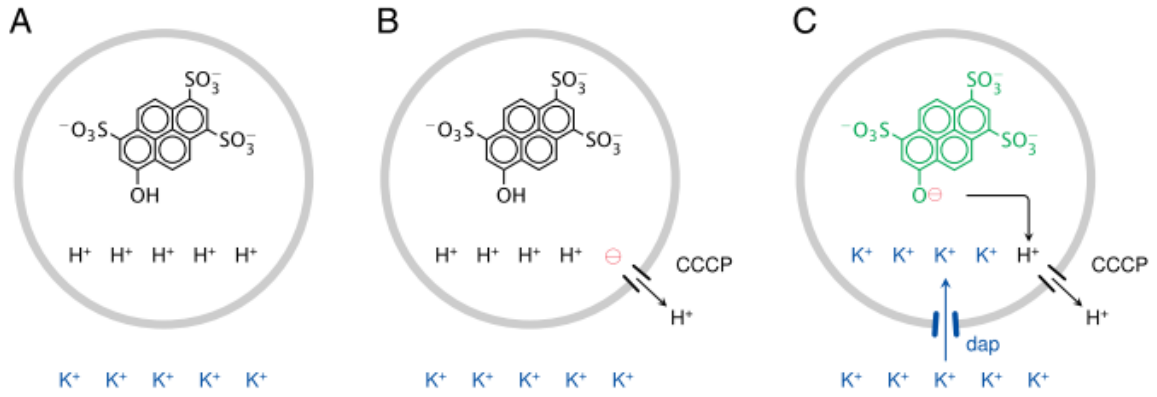

Figure 1.9: Schematic representation of the pyranine-based liposome permeabilization assay. Addition of CCCP alone (Panel B) allows for slow diffusion of protons, but addition of CCCP and daptomycin (Panel C) allows for rapid dissipation of both gradients. Taken from Zhang et al. and used with permission.[47]

A control for this assay employed valinomycin instead of daptomycin, an antibiotic which is selective for translocating potassium through the membrane. With daptomycin, it was observed that other cations, including sodium, magnesium, and cesium in addition to potassium could pass through the membrane, but larger cations such as choline or hexamethonium were translocated at a much slower rate, and anions such as chloride and cysteine were not translocated at all, suggesting that daptomycin forms pores selective for cations, with a preference for smaller, monoatomic ions over larger, molecular ions.

Also in 2014, the Palmer group proposed that the fully functioning pore formed by daptomycin involves the oligomerization of daptomycin on each leaflet of the biological membrane.[48] The study involved the use of the NBD fluorophore, which can be quenched in the presence of dithionite. When model membranes containing NBD-labelled phosphatidyl-

ethanolamine (NBD-PE) were subjected to dithionite, approximately half of the fluorescence was quenched, as would be expected since only the outer leaflet of the membrane contained the NBD label (Figure 1.10). Upon addition of detergent, which dissolves the model membranes, the remaining NBD signal was quenched. When NBD-daptomycin in model membranes was exposed to dithionite in the absence of cardiolipin, initially 50% of the NBD signal was quenched, and over the time-frame of six additional minutes, the remaining sample was slowly quenched. The presence of 10% or more cardiolipin (CL), a phospholipid derived from phosphatidyl glycerol which contains a single polar head group and four lipid tails, resulted in greater than 75% initial quenching the NBD signal upon addition of dithionite. Taken together, it suggests that cardiolipin prevents the translocation of daptomycin from the outer to the inner leaflet, and thus prevents the formation of a fully functioning pore (See resistance mechanisms, section 1.3.2).

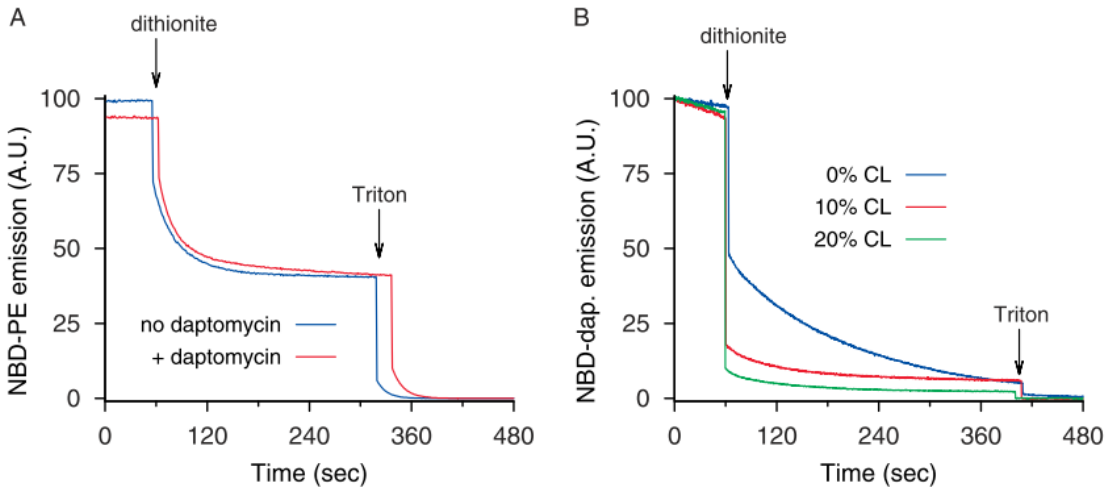

Figure 1.10: Evidence of daptomycin found on the inner- and outer- leaflets of model membranes through NBD fluorescence quenching by dithionite. Taken from Zhang et al. and used with permission.[48]

These data, combined with additional quantitative FRET studies as performed by the Palmer group in 2012,[46] allowed for a new model for daptomycin's mechanism of action to be

proposed (Figure 1.11). In this model, daptomycin binds to membranes in a Ca^{2+}- and PG-dependent fashion, and the acyl tail void volume caused by daptomycin having a single lipid tail and phospholipids having usually two causes deep insertion of the tetrameric leaflet to the membrane (Figure 1.11C). Spontaneous membrane translocation and then combination with a tetramer in the opposite leaflet forms the fully functional octameric pore (Figure 1.11D). In this proposed model, cardiolipin would indeed produce the observed effect – the extra acyl tail groups present because of cardiolipin would act to alleviate the void volume produced by daptomycin binding to membranes, which would reduce the deeper membrane insertion and therefore membrane translocation.

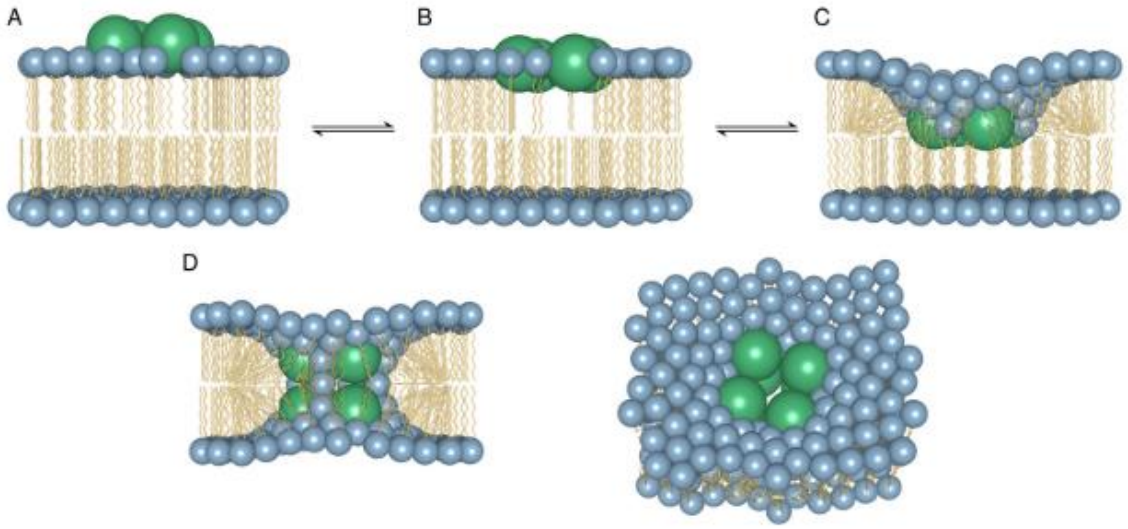

Figure 1.11: Updated model of daptomycin's action mechanism. Taken from Zhang et al. and used with permission.[48]

This model was further refined when Taylor et al. deduced that daptomycin and A54145D membrane binding involve the successive binding of two calcium ions.[49] Both isothermal titration calorimetry (ITC) and fluorescence techniques were used to establish that daptomycin binds to two equivalents of calcium in a stepwise fashion: after binding one

equivalent of calcium (at ~0.1 mM Ca^{2+}), acrylodan fluorophores appended to Orn6 of daptomycin and *D*-Lys8 of A54145D demonstrated localization in a membrane. With increased calcium present (~0.5 to 1.0 mM Ca^{2+}), an additional fluorescence change is observed, this time with the intrinsically fluorescent Trp1 residue of A54145D, or Kyn13 residue of daptomycin. Related to this is the research of Zhang et al., who studied an A54145D analog with a pyrene-butanoyl lipid tail.[50] The results of these studies suggest that the pyrene moiety forms an excimer (requiring close proximity, implying mutual presence and therefore oligomerization in the membrane) at calcium concentrations similar to the second transition proposed by Taylor et al.[49] These data suggest that the first interaction between daptomycin and biological membranes occurs at the Orn6 residue, and following this, the hydrophobic lipid tail and additional hydrophobic Trp1 and Kyn13 residues insert into the membrane. Similarly, these results suggest that the first interaction between A54145D and biological membranes occurs at the *D*-Lys8 residue, followed by the Trp1 and hydrophobic lipid tail.

In 2017, Taylor et al. further discovered that membrane permeabilization by daptomycin depends not only on the head groups of the membrane lipids, but also the acyl chain component of the lipids.[51] Functional octameric oligomers were formed only with DMPC/DMPG (dimyristoylphosphatidylcholine / dimyristoylphosphatidylglycerol) lipids. In the presence of DOPC/DOPG lipids, or POPC/POPG lipids (palmitoyloleoylphosphatidylcholine / palmitoyloleoylphosphatidylglycerol), membrane binding occurs, but instead of forming the octameric oligomer and properly functioning pore, tetrameric oligomerization on each leaflet is observed by FRET quantification, and no membrane permeabilization was observed. Additionally, a greater degree of NBD-daptomycin quenching by dithionite is observed in DOPC/DOPG membranes relative to DMPC/DMPG

membranes, suggesting an uneven distribution of daptomycin across the leaflets with a greater preference for the outer leaflet, indicating less membrane translocation. Further, in 2018, it was shown that as little as 10% DOPC in membranes containing DMPG and DMPC could inhibit proper pore formation.[52] Taken together, these studies may refute some of the recent action mechanism studies performed on DOPC/DOPG or POPC/POPG lipids signifying that daptomycin does not form a pore. Lee et al. studied the effect of daptomycin on DOPG/DOPC membranes and observed only a transient ion leakage upon binding of daptomycin.[38] Because of the temporary nature of ion leakage, they concluded that daptomycin does not form pores. Additionally, Kreutzberger et al. observed that giant unilamellar vesicles (GUVs) made of POPG and POPC that encapsulated smaller vesicles did not allow for daptomycin to translocate from the outer membrane to the inner membrane, on the basis that daptomycin was only observed on the outer vesicle membranes and not on the membranes of the interior vesicles.[53]

Direct evidence for the formation of an ion channel was observed by Seydlová et al. in 2018.[43] The researchers performed conductance measurements on planar lipid membranes, which allow for the analysis of pore-forming activities on membranes. In this assay, a single lipid bilayer separates two aqueous reservoirs. An external voltage is applied to the membrane, and the opening of a pore in the membrane is indicated by a jump in current through the membrane; conversely, the closing of a pore is indicated by a reduction in membrane current. Indeed, planar lipid membranes demonstrated clear evidence of pore formation, only after being subjected to daptomycin. Interestingly, the membrane pores formed by daptomycin had varying degrees of current fluctuation and were dependent upon the applied voltage across the membrane. The varying currents indicated that pores of varying diameters were formed, suggesting that pores can have varying subunit stoichiometry.

1.3 – Proposed Mechanisms of Resistance of cLPAs

Some studies attempt to directly elucidate the mechanism of action of antibiotics, but a more indirect approach is also sometimes used: studying the mechanisms of resistance that bacteria employ. By studying the mechanisms of resistance, some insights may be gained on how antibiotics function.

While resistance to daptomycin is not yet widespread, there have been numerous reports of reduced susceptibility of pathogenic bacteria to daptomycin. A growing body of literature is dedicated to the resistance mechanisms employed against daptomycin due to its current use as a last-resort antibiotic. It is possible that these studies can provide information on daptomycin's mode of action.

1.3.1 – Resistance by Changes to the Membrane Lipid Composition

Various genomic analyses have been performed on clinical isolates with reduced susceptibility to daptomycin. In a genomic analysis of *S. aureus* isolates with decreased susceptibility to daptomycin, Friedman et al. discovered several single-nucleotide polymorphisms (SNPs) in the *mprF* gene, which is associated with the multipeptide resistance factor (mprF) protein responsible for converting PG into lysyl-PG.[54] Peleg et al. also correlated daptomycin resistance with mutations in the *pgsA* and *cls2* genes, which are involved in the first step of PG synthesis and the synthesis of cardiolipin, respectively.[55] Notably, all of these genes involve to some extent the composition of the lipid bilayer, which is well-accepted to be the target of daptomycin's activity.

The *mprF* gene encodes for the multipeptide resistance factor protein, which appends a lysine into PG, forming lysyl-PG (Figure 1.12). Additionally, the mprF protein flips lysyl-

PG from the inner membrane leaflet to the outer membrane leaflet.[56,57] This protein has been correlated with reduced daptomycin susceptibility in several reports.[58,59] Mutations in this gene may result in increased lysyl-PG formation, or lysyl-PG translocation to the outer leaflet, which in turn may have effects on daptomycin's activity.

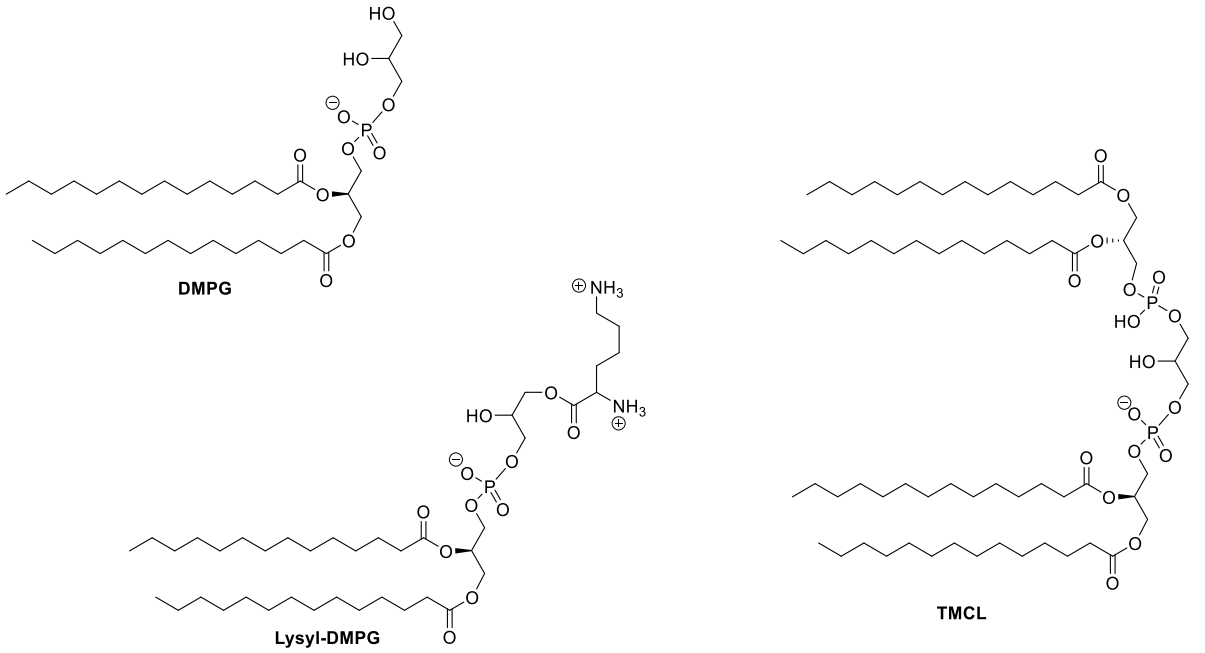

Figure 1.12: Dimyristoyl phosphatidyl glycerol (DMPG), lysyl-DMPG, and tetramyristoylcardiolipin (TMCL). Anionic DMPG is required for daptomycin's activity. TMCL and overall cationic lysyl-DMPG may reduce daptomycin's activity.

It is known that daptomycin requires PG for biological activity, and this may be due to the charge of the lipid. At physiological pH levels, daptomycin is trianionic, and upon binding to two equivalents of calcium, the Dap-2Ca^{2+} complex becomes cationic, and charge attraction between the daptomycin-calcium complex and negatively charged PG can be expected. However, when lysine is appended to PG, there may be charge repulsion between cationic lysyl-PG and cationic Dap-2Ca^{2+}. Hence, the presence of lysyl-PG in the membrane may be a resistance mechanism employed by bacteria. Indeed, Mishra et al. in 2013 noticed a significant

increase in lysyl-PG of isolates of *S. aureus* with reduced daptomycin susceptibility.[60] Admittedly, most of this lysyl-PG was located in the inner membrane leaflet, which may have an effect in reducing the translocation of daptomycin from the outer membrane leaflet to the inner membrane leaflet and therefore the formation of a properly functioning pore. In any case, the amount of PG present in the species analyzed invariably decreased, which may suggest that resistance is caused by increased presence of lysyl-PG in the membrane, or simply decreased PG-content.

Although the *mprF* gene is widely implicated in cases of increased resistance to daptomycin, Pillai et al. discovered that reduced susceptibility to daptomycin does not necessarily involve mutations to the *mprF* gene.[61] Another possible mechanism of increased resistance to daptomycin involves cardiolipin. It was demonstrated by the Palmer group that cardiolipin inhibits the translocation of daptomycin tetramers from the outer leaflet of the membrane to the inner leaflet.[48] Accordingly, it is to be expected that mutations in the *cls2* gene, which encodes cardiolipin synthase, an enzyme that forms cardiolipin from PG, are correlated with reduced susceptibility to daptomycin.[55] Indeed, Davlieva et al. in 2013 observed in isolates of daptomycin-resistant *Enterococci* that select mutations to *cls2* resulted in cardiolipin synthase with increased enzymatic activity, suggesting that the increased presence of cardiolipin is a mechanism of resistance employed by bacteria.[62]

1.3.2 – Resistance via Cell Wall Thickening

In 2017, Taylor et al. in the Palmer group studied the biological activity of a covalently linked daptomycin dimer (**1.14**, Figure 1.13).[63] The peptide, which consisted of two daptomycin nuclei (daptomycin less the lipid tail) tethered together by a linear C18 alkane with two carboxylic acid functional groups on either end. Peptide **1.14** was able to form pores on

model membranes similar to authentic daptomycin but had MIC's against *B. subtilis* 1046 that were at least 100-fold less active than authentic daptomycin. Interestingly, when the daptomycin dimer was assayed against *B. subtilis* PDC134 L-forms (variants of the bacteria that lack a cell wall), biological activity returned to levels approaching those of authentic daptomycin (0.2 µg/mL for daptomycin-dimer compared to 0.075 µg/mL for daptomycin). Taken all together, this suggests that the cell wall may have some effect on resistance to daptomycin, as the covalent daptomycin dimer may have had difficulty diffusing through the peptidoglycan layer.

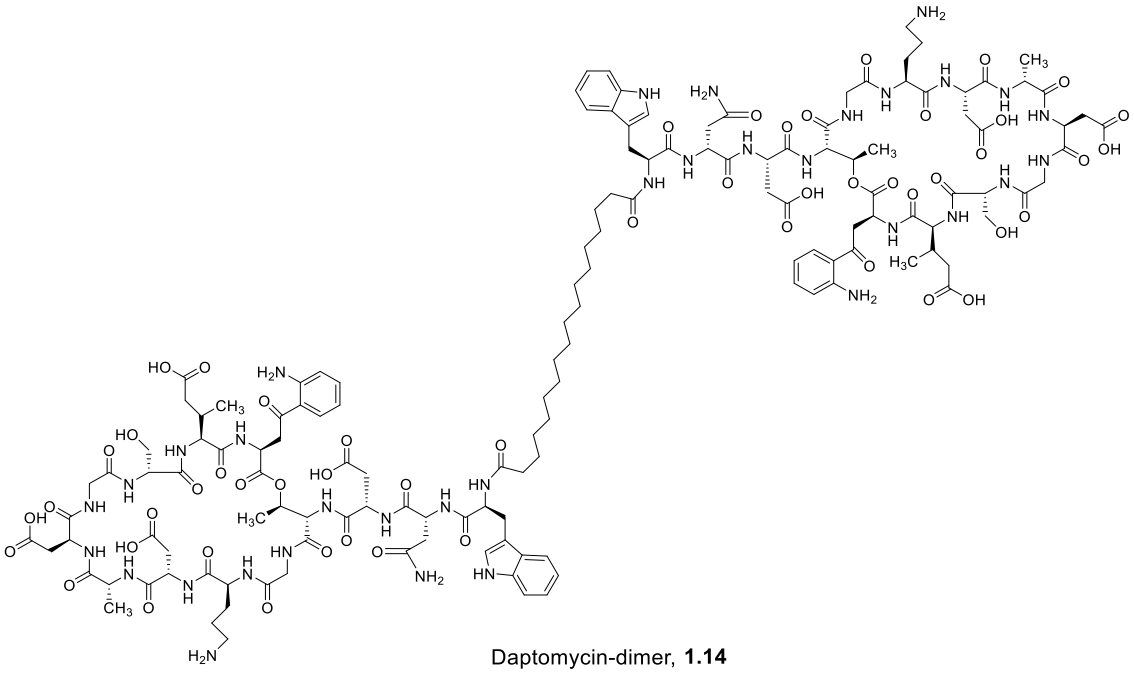

Figure 1.13: Covalently-linked daptomycin-dimer **1.14**.

It was also observed by Peleg et al. in 2012 with transmission electron microscopy that isolates of daptomycin-non-susceptible *S. aureus* demonstrated increased cell wall thickness relative to their daptomycin-susceptible counterparts.[55] In agreement with Taylor et al.'s results, it would seem that a thicker peptidoglycan layer may result in less effective diffusion

of daptomycin to the cell membrane, and since the cell membrane is the active target of daptomycin, this would subsequently reduce its biological activity. Again, it should also be noted that increased cell wall thickness is not a requirement of daptomycin resistance. Yang et al. in 2010 observed a daptomycin-resistant strain of MRSA which did not display a thicker cell wall, once again suggesting that there may be multiple mechanisms by which bacteria evolve resistance to daptomycin.[64]

1.3.3 – Resistance by Direct Inactivation of Daptomycin

In 2012, D'Costa et al. observed that antibiotic-producing soil bacteria are remarkably resistant to antibiotics and performed mechanistic studies on these resistances.[65] A library of soil bacteria demonstrated that daptomycin was almost universally ineffective against soil bacteria, and antibiotic inactivation was exceptionally high. It is worth noting that these mechanisms of resistance have not been observed in clinical isolates of daptomycin-resistant pathogenic bacteria but represent possible resistance mechanisms to daptomycin in general.

One resistance mechanism displayed by approximately 29% of species in the soil-bacterium library was removal of the acyl tail of daptomycin. As increased length of the lipid tail is associated with increased biological activity, it can be expected that complete removal of the tail would abolish it.[66] Additionally, 44% of soil-bacterium species demonstrated hydrolysis of the ester-bond in daptomycin, which was further shown to abolish biological activity.

In summary, the mechanisms of action associated with daptomycin, and the mechanisms of resistance to daptomycin displayed by bacteria, are complex, and the precise nature of daptomycin's biological activity is still a topic of some controversy.

1.4 – Natural synthesis of Daptomycin and A54145

In biological systems, proteins and peptides are typically translated from a primary mRNA transcript which was transcribed from DNA. Translation is mediated by organelles called ribosomes and amino acids are bought in close-proximity of the growing peptide through tRNAs. On the other hand, cLPAs are produced using non-ribosomal peptide synthetases (NRPSs), which are enzymes that synthesize peptides without the use of ribosomes.[66,67] Daptomycin's NRPSs are encoded by three different genes (*dptA*, *dptBC*, and *dptD*), and A54145's NRPSs are encoded by four genes (*lptA*, *lptB*, *lptC*, and *lptD*), each of which is responsible for the incorporation of several amino acids (Figure 1.14).[66–68]

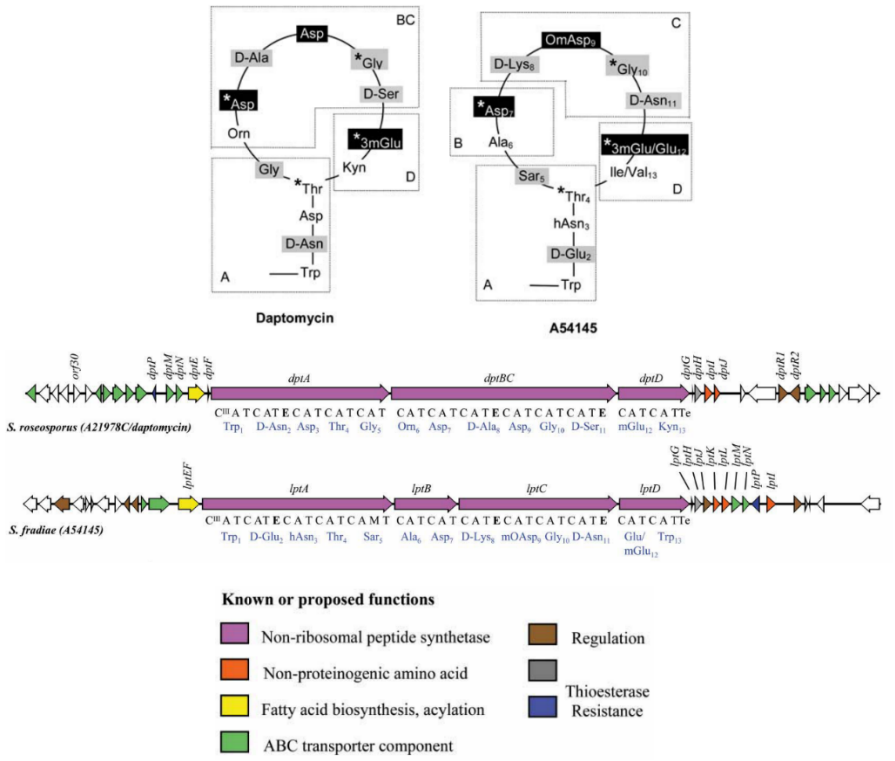

Figure 1.14: Core peptide structure and gene map of daptomycin and A54145 biosynthesis. (Top) Core peptide structures of daptomycin and A54145. The NRPS of each boxed region is encoded by a different gene. (Bottom) Gene maps for daptomycin and A54145. A – adenylation domain; T – thiolation domain; E – epimerase domain; M – methylation domain; TE – thioesterase domain. Images taken and modified with permission from Baltz et al.[66] and Miao et al.[67]

The gene maps in Figure 1.14 are labelled with appropriate domains that catalyze specific reactions in the synthesis of cLPAs, further described for daptomycin in Figure 1.15. Amino acids are activated by the adenylation domain (A), followed by tethering to the thiolation domain (T), forming a thioester (Figure 1.15A). The condensation domain (C) of the subsequent amino acid then catalyzes the formation of the peptide bond between this thioester and the following amino acid (Figure 1.15B). This cycle continues until the final amino acid (Kyn13 for daptomycin, Ile13 for A54145D) is adenylated and tethered by the T-domain, after which the peptide is cyclized between the Thr4 side-chain and the terminal amino acid by a thioesterase domain (Te). Within this synthesis, epimerase domains (E) are responsible for inverting the stereochemistry of standard *L*-amino acids to form *D*-amino acids, and in the case of A54145, a methylation domain (M) is responsible for the methylation of the α-amino group of Sar5. It is worth noting that these domains promote some degree of flexibility: the daptomycin NRPS can accommodate several lipid tails: *n*-decanoyl, *anteiso*-undecanoyl, *iso*-dodecanoyl, and *anteiso*-tridecanoyl tails.[68] A54145 has even more flexibility. Lipid tail incorporation can tolerate *n*-decanoyl, *iso*-decanoyl, and *anteiso*-decanoyl; position 12 can tolerate glutamic acid and 3-methylglutamic acid; and position 13 can tolerate valine or isoleucine, giving rise to the eight different factors of A54145 (Figure 1.4).

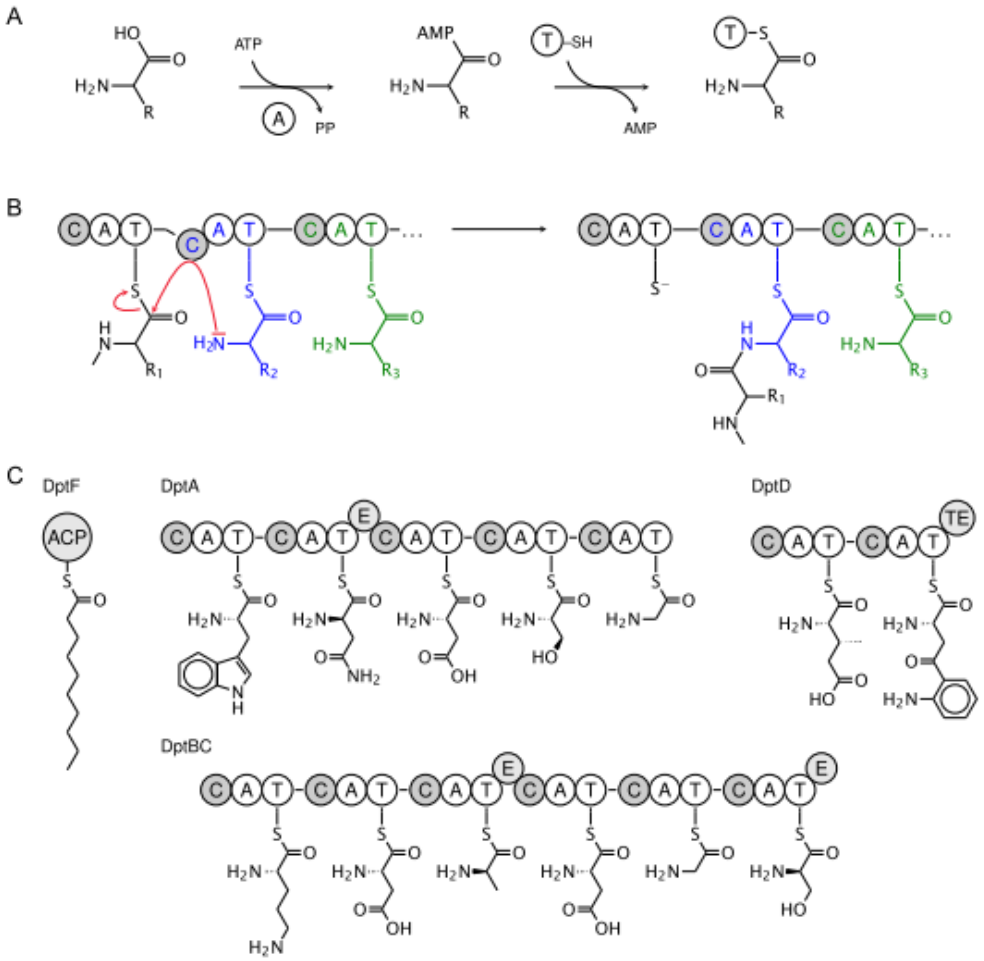

Figure 1.15: Schematic of the modular daptomycin synthase. (A) Each amino acid is activated by the adenylation domain, and converted to a thioester by a T domain. (B) The condensation domain acquires the growing peptide sequence from the previous module, forming a new peptide bond. (C) Synthesis of daptomycin is performed by three large enzymes, each responsible for the addition of multiple amino acids. Figure taken from Taylor and Palmer with permission.[13]

1.5 – Daptomycin and A54145 analogs

1.5.1 – Synthesis of Daptomycin analogs via Semi-Synthesis

Since the discovery of the A21978C family of antibiotics, researchers have attempted to introduce modifications to its structure to ascertain how biological activity is affected (structure-activity relationships, SARs) and to produce yet more effective antibiotics. Researchers at Lilly Research Laboratories obtained the A21978C complex, containing a

common peptide nucleus, and were able to modify its acyl tail.[69] First, a Boc-protecting group was added to the ornithine residue, followed by bacteria-assisted acyl tail removal, which was found to be most effective using *Actinoplanes utahensis* NRRL 12052 (Scheme 1.1). The product, Orn(Boc)DeacylDap (**1.15**), was then reacylated by treatment with activated esters in *N*,*N*-dimethylformamide (DMF), and the Boc-group removed with a short treatment with trifluoroacetic acid (TFA). Tails ranging from six carbons (hexanoyl) to sixteen carbons (hexadecanoyl) were added, and it was observed that increasing the tail length caused a marked increase in biological activity with a concurrent increase in toxicity against mice (Table 1.1).[69] The compound with the most favourable activity/toxicity profile possessed a decanoyl (Dec) tail, and was ultimately named daptomycin. Analogous studies on A54145A$_1$ published by the same company in 1990 also demonstrated increased biological activity as acyl tail length increased.[15,70]

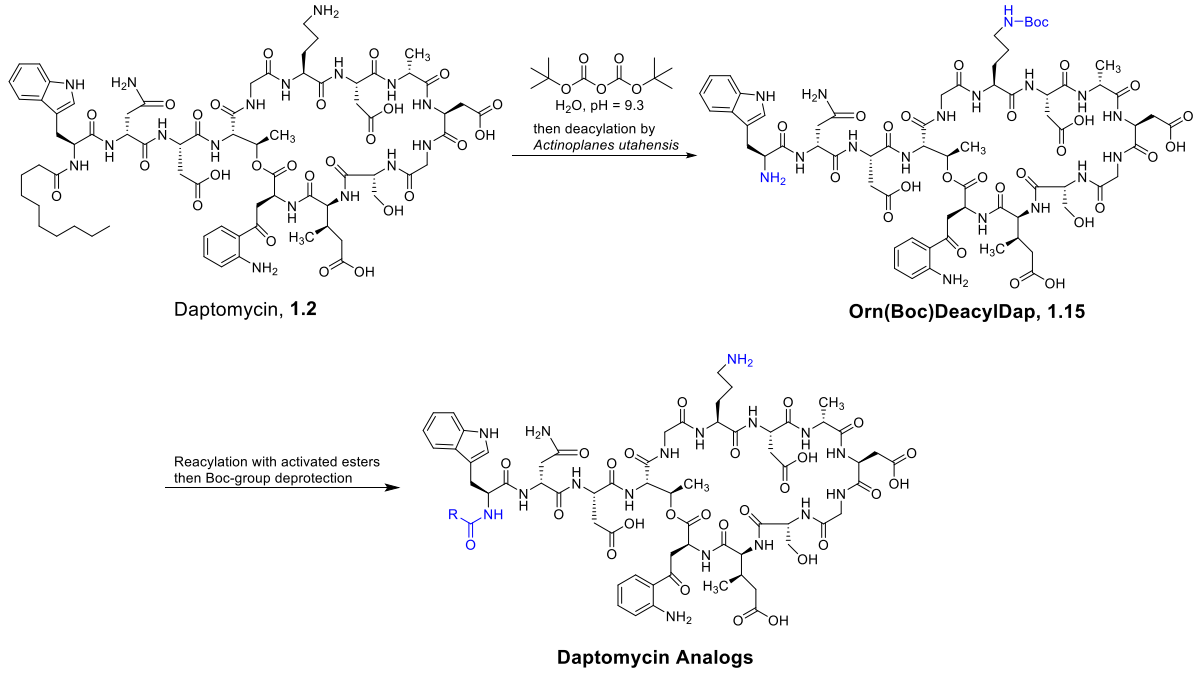

Scheme 1.1: Synthesis of daptomycin analogs with alternative lipid tails.

Table 1.1: Minimum inhibitory concentrations (MICs) of daptomycin and A54145A analogs with alternative lipid tails.[15,69,71]

Original antibiotic	New lipid tail	MIC (ug/mL)[a]	LD_{50} against mice (mg/kg, iv)
$A21978C_1$	*n*-heptanoyl	8	> 600
	n-octanoyl	4	> 600
	n-nonanoyl	8	> 600
	***n*-decanoyl**	**0.5**	**600**
	n-undecanoyl	0.25	450
	n-dodecanoyl	0.5	144
	n-tridecanoyl	0.125	112.5
	n-tetradecanoyl	0.5	62.5
	n-pentadecanoyl	1	56.3
	n-hexadecanoyl	1	50
$A54145A_1$	*n*-hexanoyl	>128	N.D.
	n-nonanoyl	32	>500
	iso-decanoyl	16	>500
	n-decanoyl	8	>500
	n-undecanoyl	2	>500
	n-dodecanoyl	1	321

[a] MICs performed against *S. aureus*.

In an effort to create even more potent and effective cLPAs, in 2003, researchers at Cubist Pharmaceuticals Inc. created 46 different analogs of daptomycin by appending various acyl groups to the side-chain of ornithine through nucleophilic acyl substitution with pentafluorophenyl esters (Scheme 1.2).[72,73] It was discovered that the ornithine residue is particularly amenable to substitution, resulting in minimal loss of bactericidal activity. Most interesting in this study is perhaps that these modifications to daptomycin's structure also modify the charge of daptomycin: by converting the basic amine to a non-basic amide functional group, the overall charge of these daptomycin analogs at physiological pH becomes -4 instead of -3. Nevertheless, biological activity remained: synthesized analogs were 1.6 to 32-fold less active than daptomycin.

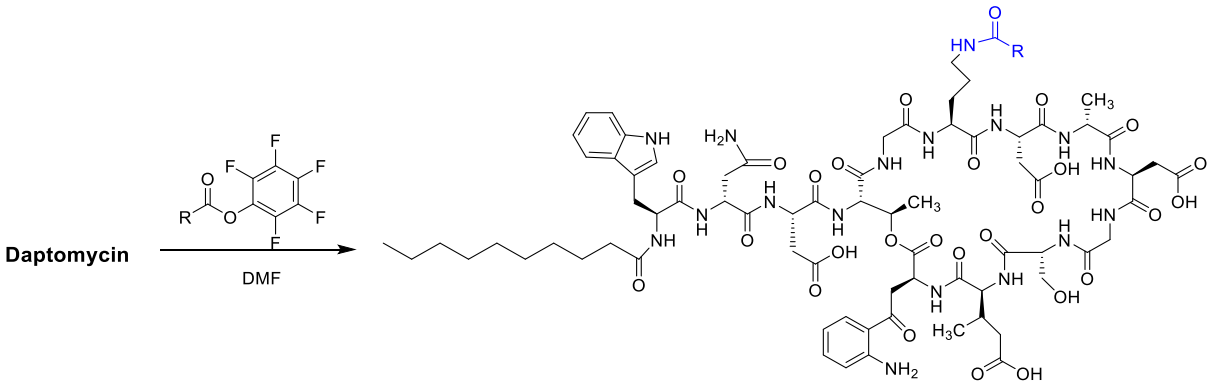

Scheme 1.2: General synthesis of Orn6-substituted daptomycin analogs by Hill et al.[72]

Researchers at Cubist Pharmaceuticals in 2012 developed an additional approach for modifying native daptomycin.[74] In this approach, the ornithine residue was protected with a carboxybenzyl (CBz) group and the lipid tail removed enzymatically using the previously patented deacylase protocol, yielding CBz-protected peptide **1.16** (Scheme 1.3).[75] Then, Trp1 was removed using Edman degradation with phenyl isothiocyanate. Boc-protected non-proteinogenic amino acids were then coupled to the resulting free amine as pentafluorophenyl esters, followed by Boc-deprotection and additional coupling to add the lipid tail. Finally, the CBz group was removed by hydrogenolysis, and the resulting peptide assessed for biological activity. Using this approach, 22 additional daptomycin analogs were obtained, which retained considerable biological activity as long as Trp1 was replaced with an amino acid with a highly lipophilic side-chain. Further, some modifications produced daptomycin analogs that retained biological activity in the presence of lung surfactant. These results suggest that the tryptophan residue of daptomycin may be interacting with a hydrophobic target and may also interact with a component of lung surfactant, although direct evidence of this is not available.

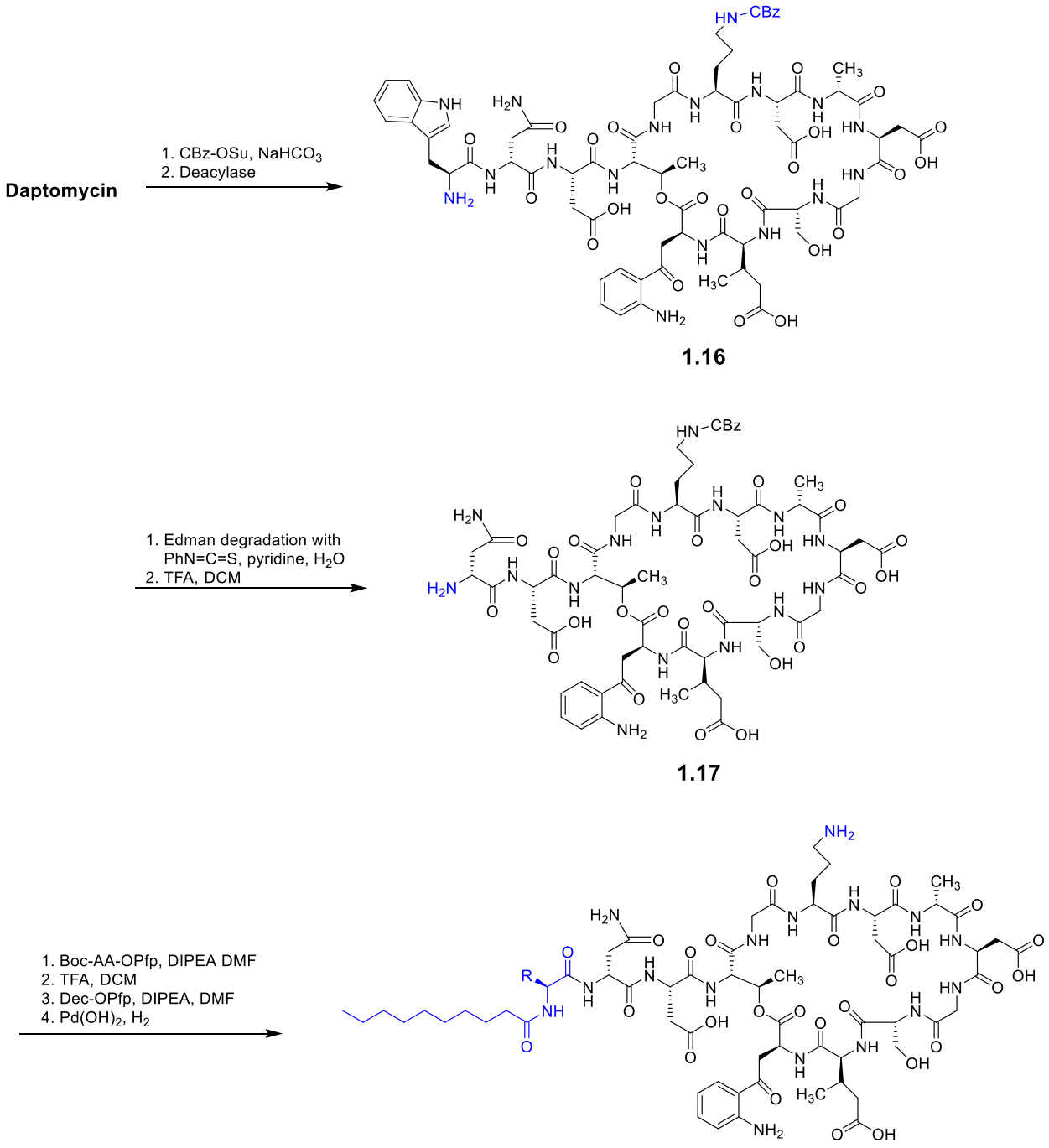

Scheme 1.3: Synthesis of Trp1→Xaa1 daptomycin analogs performed by He et al.[74]

Although direct modification of daptomycin via appending groups on to the Orn6 residue, modifying the lipid tail, and changing the Trp1 residue can provide valuable information on the structure-activity relationship of daptomycin and its analogs, its scope in

the synthesis of daptomycin analogs is limited to three different positions. For further probing the mechanism of action, it would be beneficial if there was an alternative synthesis that would allow for additional amino acid substitutions of daptomycin.

1.5.2 – Chemoenzymatic Synthesis of Daptomycin and A54145 Analogs

In 2004, researchers in the Marahiel group developed a chemoenzymatic route to the synthesis of daptomycin analogs.[76] In this approach, linear peptides bearing a C-terminal thioester, synthesized using solid-phase peptide synthesis, were subjected to CDA cyclase, which is the cyclization domain of the non-ribosomal peptide synthetase from *Streptomyces coelicolor* used to synthesize CDA *in vivo* (similar to Figure 1.14). The CDA cyclase domain effectively formed the macrocyclic core of daptomycin, and additional coupling of the Dec-Trp-Asn building block allowed for the generation of nine analogs of daptomycin. In all of these analogs, MeGlu12 was replaced with Glu12 and *D*-Asn2 was replaced with *L*-Asn2, as the correct *D* configuration of Asn2 was unknown at the time. All synthesized analogs were noticeably less biologically active than authentic daptomycin (probably in part due to the replacement of *D*-Asn2 with *L*-Asn2), but nevertheless this new approach allowed for increased flexibility when designing daptomycin analogs beyond lipid-tail substitution and appending groups to the Orn6 sidechain.

In 2006, the Marahiel group refined their chemo-enzymatic approach through biochemical isolation and characterization of the peptide cyclase domains from the daptomycin and A54145 non-ribosomal peptide synthetases, and with the added knowledge of the proper stereochemistry of *D*-Asn2,[77] the researchers synthesized a total of nine additional daptomycin-A54145 hybrids and assessed them for biological activity.[78] The researchers reported the chemoenzymatic synthesis of the single-mutant of daptomycin in which MeGlu12

is replaced with Glu12 (Dap-Glu12), and this analog was 5.5-fold less active than authentic daptomycin against *Bacillus subtilis* PY79. Further, this work also reported the synthesis of an A54145A_1 analog in which the uncommon amino acids HOAsn3 and MeOAsp9 were replaced with their proteinogenic counterparts, Asn3 and Asp9, and a second analog in which, in addition to these modifications, the Thr residue at position 4 was replaced with diaminopropionic acid (DAPA). These two analogs were adequately cyclized by the excised peptide cyclase domains and their MICs were both reported to be 25 μg/mL, a 12.5-fold decrease from that of authentic daptomycin.

Key limitations in the chemoenzymatic approach used in these studies is that synthesized linear peptides must be purified both before and after cyclization – from the point of view of developing a large number of analogs of daptomycin or A54145, it would be more advantageous if each analog required only one purification. Further, as the cyclase domain used is an enzyme, presumably with some sort of substrate specificity, it is unknown whether it would be completely effective in cyclizing any peptide sequence, which further limits is application to the synthesis of analogs of these antibiotics.

1.5.3 – Biosynthetic Approach to Daptomycin and A54145 Analogs

Between 2010 and 2014, the Baltz group synthesized analogs of daptomycin and A54145 using an enzymatic approach, in which the NRPSs of daptomycin and A54145 were modified to produce different antimicrobial products.[16,17,79] The biological activity of these analogs were assessed in the absence and presence of 1% bovine lung surfactant. Relative to native daptomycin, all daptomycin analogs had reduced activity in the absence of lung surfactant, although some analogs demonstrated increased activity in the presence of lung surfactant, again, relative to daptomycin's activity in the presence of lung surfactant.

A total of 25 analogs of A54145D and A54145E were synthesized with alternative amino acids at several positions throughout the peptide resulting in peptides with varying biological activities (Table 1.2), depending on the substitutions used. It seems that A54145E is significantly inhibited by lung surfactant, and many modifications to A54145E resulted in peptides with a more favourable biological activity profile (Table 1.2, entries 3 to 13). Most notably, the activity in the presence of lung surfactant increased by a factor of 16 when *D*-Glu2 and HOAsn3 were replaced with *D*-Asn2 and Asp3, respectively (Table 1.2, entry 4). Most modifications to A54145D resulted in a loss of biological activity both in the presence and absence of lung surfactant (Table 1.2, entries 14 to 27), however, replacement of Ile13 in A54145D with Kyn13 produced an analog that was 2-fold more biologically active than A54145D both in the presence and absence of lung surfactant, although it was still 2-fold less active than daptomycin in the absence of lung surfactant (Table 1.2, entry 28). A single substitution of MeOAsp with Asp in A54145D resulted in a drastic loss in biological activity (Table 1.2, entry 25), although some activity was restored slightly if HOAsn was also replaced with Asn (Table 1.2, entry 19).

While unable to produce analogs with improved biological activity relative to daptomycin, the Baltz group did synthesize two analogs with improved biological activity relative to A54145D. While these two derivatives would appear to have some potential for clinical application, they were not sufficiently active in mouse models, and thus were not pursued clinically.[80]

Table 1.2: MICs of A54145D and A54145E analogs synthesized by the Baltz group.[16,17,79]

Entry	Peptide	Amino acid at position								*S. aureus* MIC [a]	
		2	3	5	8	9	11	12	13	without surfactant	with surfactant
1	**Daptomycin**	*D*-Asn	Asp	Gly	*D*-Ala	Asp	*D*-Ser	MeGlu	Kyn	0.5	64
2	**A54145E**	*D*-Glu	HOAsn	Sar	*D*-Lys	MeOAsp	*D*-Asn	MeGlu	Ile	1	32
3	CB-182,575	*D*-Asn	HOAsn	Sar	*D*-Lys	MeOAsp	*D*-Asn	MeGlu	Ile	2	4
4	CB-182,561	*D*-Asn	Asp	Sar	*D*-Lys	MeOAsp	*D*-Asn	MeGlu	Ile	1	2
5	CB-182,363	*D*-Glu	Asn	Sar	*D*-Lys	MeOAsp	*D*-Asn	MeGlu	Ile	2	16
6	CB-182,597	*D*-Glu	Asn	Sar	*D*-Lys	HOAsp	*D*-Asn	MeGlu	Ile	1	16
7	CB-182,390	*D*-Glu	Asn	Sar	*D*-Lys	Asp	*D*-Asn	MeGlu	Ile	2	2
8	CB-182,571	*D*-Glu	HOAsn	Sar	*D*-Ala	MeOAsp	*D*-Asn	MeGlu	Ile	1	32
9	CB-182,549	*D*-Glu	HOAsn	Sar	*D*-Ser	MeOAsp	*D*-Asn	MeGlu	Ile	1	16
10	CB-182,510	*D*-Glu	HOAsn	Sar	*D*-Asn	MeOAsp	*D*-Asn	MeGlu	Ile	8	64
11	CB-182,443	*D*-Glu	HOAsn	Sar	*D*-Lys	Asp	*D*-Asn	MeGlu	Ile	2	4
12	CB-182,548	*D*-Glu	HOAsn	Sar	*D*-Lys	MeOAsp	*D*-Ala	MeGlu	Ile	1	16
13	CB-182,332	*D*-Glu	HOAsn	Sar	*D*-Lys	MeOAsp	*D*-Ser	MeGlu	Ile	2	16
14	**A54145D**	*D*-Glu	HOAsn	Sar	*D*-Lys	MeOAsp	*D*-Asn	Glu	Ile	2	4
15	CB-182,444	*D*-Asn	HOAsn	Sar	*D*-Lys	MeOAsp	*D*-Asn	Glu	Ile	8	8
16	CB-182,560	*D*-Asn	Asp	Sar	*D*-Lys	MeOAsp	*D*-Asn	Glu	Ile	8	16
17	CB-182,325	*D*-Glu	Asn	Sar	*D*-Lys	MeOAsp	*D*-Asn	Glu	Ile	32	32
18	CB-182,349	*D*-Glu	Asn	Sar	*D*-Lys	HOAsp	*D*-Asn	Glu	Ile	32	64
19	CB-182,348	*D*-Glu	Asn	Sar	*D*-Lys	Asp	*D*-Asn	Glu	Ile	16	32
20	CB-182,391	*D*-Glu	HOAsn	Gly	*D*-Lys	MeOAsp	*D*-Asn	Glu	Ile	16	32
21	CB-182,567	*D*-Glu	HOAsn	Sar	*D*-Ala	MeOAsp	*D*-Asn	Glu	Ile	4	8
22	CB-182,532	*D*-Glu	HOAsn	Sar	*D*-Ser	MeOAsp	*D*-Asn	Glu	Ile	8	8
23	CB-182,531	*D*-Glu	HOAsn	Sar	*D*-Asn	MeOAsp	*D*-Asn	Glu	Ile	16	16
24	CB-182,350	*D*-Glu	HOAsn	Sar	*D*-Lys	HOAsp	*D*-Asn	Glu	Ile	8	16
25	CB-182,333	*D*-Glu	HOAsn	Sar	*D*-Lys	Asp	*D*-Asn	Glu	Ile	32	64
26	CB-182,509	*D*-Glu	HOAsn	Sar	*D*-Lys	MeOAsp	*D*-Ala	Glu	Ile	8	16
27	CB-182,336	*D*-Glu	HOAsn	Sar	*D*-Lys	MeOAsp	*D*-Ser	Glu	Ile	64	128
28	CB-183,296	*D*-Glu	HOAsn	Sar	*D*-Lys	MeOAsp	*D*-Asn	Glu	Kyn	1	2

Modifications from A54145E and A54145D are indicated in red.
[a] Against *S. aureus* 42

This approach has proven effective in generating new daptomycin and A54145 analogs, but is ultimately limited by the repertoire of synthetase modules and their substrate specificities, similar to the chemoenzymatic approach previously discussed (section 1.5.2).

Changes to the growing peptide sequence may result in peptides that are not processed by the other domains in the NRPSs due to incompatibility of recombinantly adjoined modules. Additionally, to obtain a single analog in significant yields, bacterial genomes must be edited, and the resulting strains must be isolated and cultured. With the ultimate goal of developing new antibiotics that may find use in clinic, it would be advantageous in the screening stage to develop a more high-throughput method for synthesis, which allows for rapid synthesis and isolation, and avoids the use of genetic modifications and culturing of individual strains of bacteria. To that end, the total synthesis of antimicrobial peptides would be advantageous, as it would allow for a higher throughput method by which analogs can be synthesized and assayed for biological activity.

1.6 – The Total Synthesis of Daptomycin

1.6.1 – Fmoc-based Solid-Phase Peptide Synthesis

As a considerable part of this thesis deals with the synthesis of peptides using Fmoc-based solid-phase peptide synthesis (Fmoc-SPPS), a brief discussion of Fmoc-SPPS is warranted. Fmoc-SPPS is a technique used to synthesize peptides in which the growing peptide is covalently attached to an insoluble polystyrene (PS) resin. Attachment of the first amino acid is accomplished variously using carboxylic acids or amines, and the peptide is grown stepwise (Scheme 1.4). Each amino acid coupled to the resin is suitably protected by various blocking groups that temporarily mask reactivity allowing for a single reaction to occur.

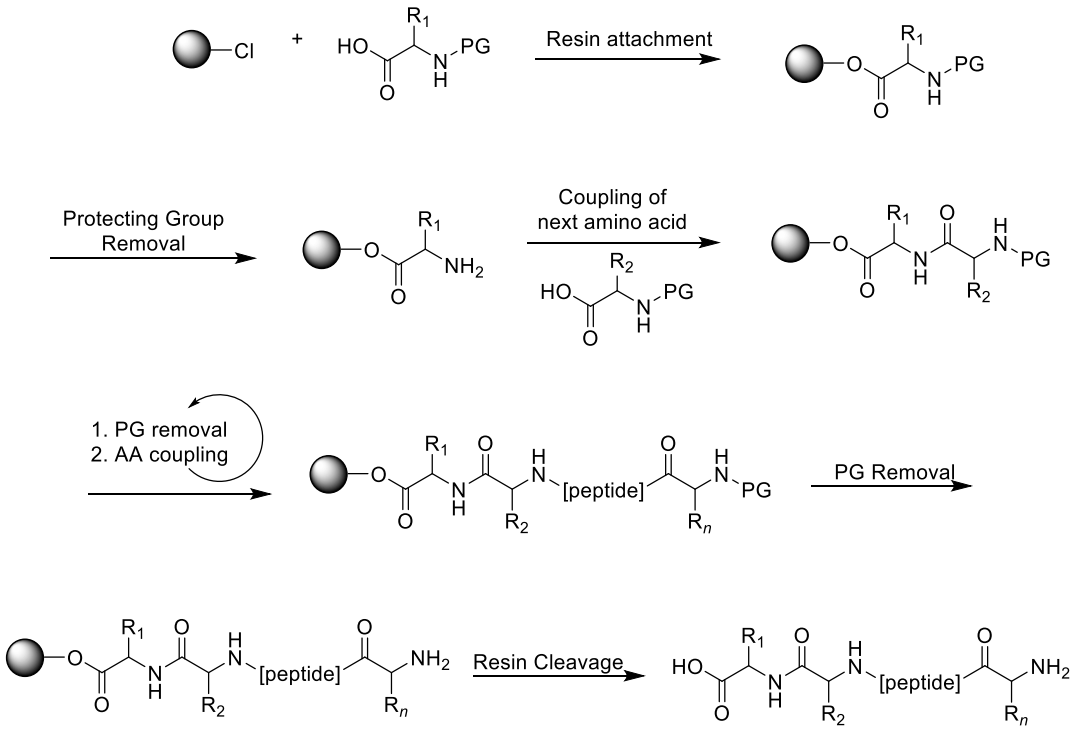

Scheme 1.4: General strategy for solid-phase peptide synthesis. In this scheme, PG = protecting group, AA = amino acid.

In Fmoc-SPPS, the α-amino groups of amino acids are protected with a fluorenylmethoxycarbonyl (Fmoc) group, which is base-labile and easily removed in the presence of 20% piperidine in DMF. Since piperidine is costly, 2-methylpiperidine (2-MP) or 4-methylpiperidine (4-MP) are often used as replacements. Commercially available amino acids with an Fmoc-protecting group on the α-amine group may also require a side-chain protecting group. There are many different protecting groups available to the organic chemist, but common protecting groups include butyloxycarbonyl (Boc) groups for amines, *tert*-butyl (tBu) groups for carboxylic acids, and *tert*-butyldimethylsilyl (TBDMS) groups or trityl (Trt) groups for alcohols (Figure 1.16). Boc-, tBu-, and Trt-protecting groups are easily removed by treatment with a strong acid such as TFA, and TBDMS groups can be removed by treatment with TFA or a fluoride ion, possibly in the form of tetrabutylammonium fluoride (TBAF).

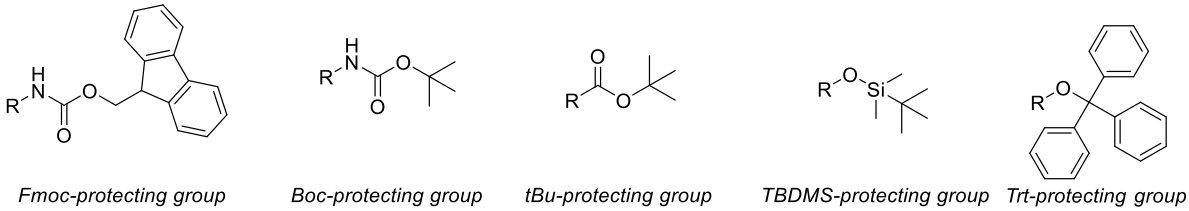

Figure 1.16: Common protecting groups in SPPS.

Several different linkers attaching the peptide to the PS resin can be used in SPPS, and chosen linkages chosen must be stable to the conditions used in forming the desired peptide. The Taylor lab most often uses the 2-chlorotrityl-chloride (2-ClTrt-Cl-PS) resin, which is a 2-ClTrt-Cl group attached to a polystyrene solid support (Figure 1.17). This 2-ClTrt-Cl group is stable to treatments of base but labile to weak acids. Other resins include the Wang resin, which possesses a benzyl alcohol linker that is resistant to weak acids but labile to strong acids such as TFA, and also the Merrifield resin, which is resistant to acids and bases, but labile to hydrogen fluoride and hydrogenolysis. In the case of 2-ClTrt-Cl-PS resin and Merrifield resin, attachment to the resin occurs by nucleophilic displacement of the chloride leaving group, but for the Wang resin, the alcohol acts as a nucleophile toward an activated ester of a carboxylic acid.

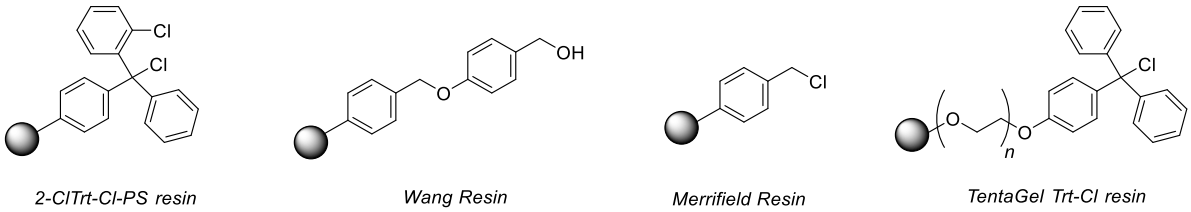

Figure 1.17: Commonly used linkers used in SPPS**.** The shaded circle represents the polystyrene solid support.

A variant of the 2-ClTrt-Cl-PS resin used occasionally in the Taylor lab is the TentaGel Trt-Cl resin, which contains a polystyrene matrix with a polyethylene glycol (PEG) linker

attached to the trityl chloride group (Figure 1.17). The PEG linker allows for more space between the polystyrene support and the peptide, which reduces peptide aggregation during SPPS and improves coupling yields. Both daptomycin and A54145D possess an ester bond between the side-chain of Thr4 and the α-carboxylic acid of Kyn13 (daptomycin) or Ile13 (A54145D), and in past syntheses of daptomycin and analogs, it was observed that the challenging depsi-bond formation could be made more efficient through the use of TentaGel Trt-Cl resin.[81,82]

Solid-phase peptide synthesis allows for the synthesis of complex peptides, and its main advantage is the ease of purification after each successive coupling step. Treating the solid support with excess coupling reagents or deprotection reagents facilitates the desired reaction, and the excess, unreacted reagents are simply rinsed away through a filter, leaving only the peptide-bound solid resin remaining. Accordingly, solid-phase peptide synthesis generally avoids the use of other purification methods such as column chromatography until the completion of last step of the synthesis.

1.6.2 – First Total Synthesis of Daptomycin by the Li Group

In 2013, the first total synthesis of daptomycin was reported by the Li group.[83] They started their synthesis by attaching the peptide to the support via the α-carboxylic acid of Gly10 (**1.18**, Scheme 1.5). The group employed Fmoc-SPPS to yield linear peptide **1.19**, containing the lipid tail and residues 1 to 10, after which the crucial ester-bond was to be formed yielding peptide **1.20**. However, the formation of the depsi-bond proved problematic and could not be achieved despite significant efforts.

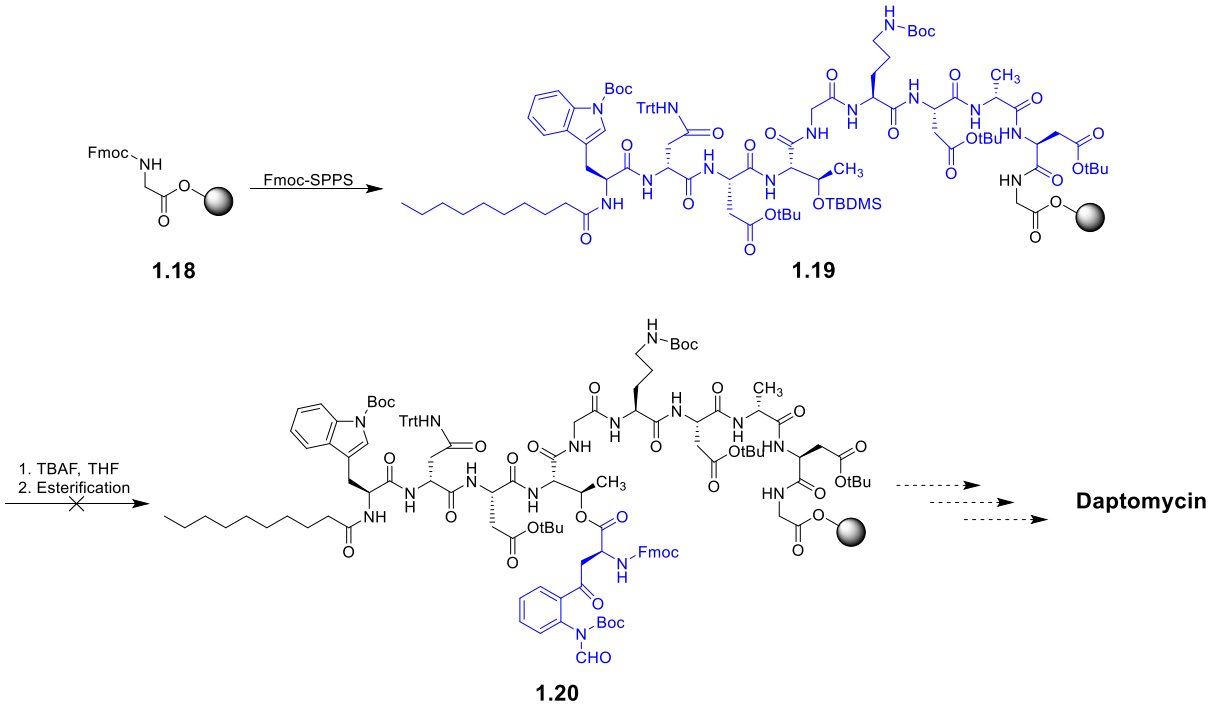

Scheme 1.5: First proposed route to daptomycin by the Li group.[83]

The researchers ultimately overcame the issue and achieved the synthesis of daptomycin by coupling on a tetra-amino acid building block **1.22** (with residues 13, 3, 4, and 5) to linear peptide **1.21** with the ester-bond pre-formed (Scheme 1.6), which was synthesized in solution. Fmoc-based SPPS from peptide **1.23** allowed for the incorporation of residues 12 and 11, yielding peptide **1.24**, and the azido protecting group on Asp3 was reduced with dithiothreitol (DTT) and *N*,*N*-diisopropylethylamine (DIPEA) in DMF. The azido group is sometimes used in addition to Fmoc-SPPS as it is completely orthogonal to the Fmoc-protecting group. Further Fmoc-based SPPS allows for the lipid tail and residues 1 and 2 to be installed, affording uncyclized daptomycin precursor, peptide **1.25**.

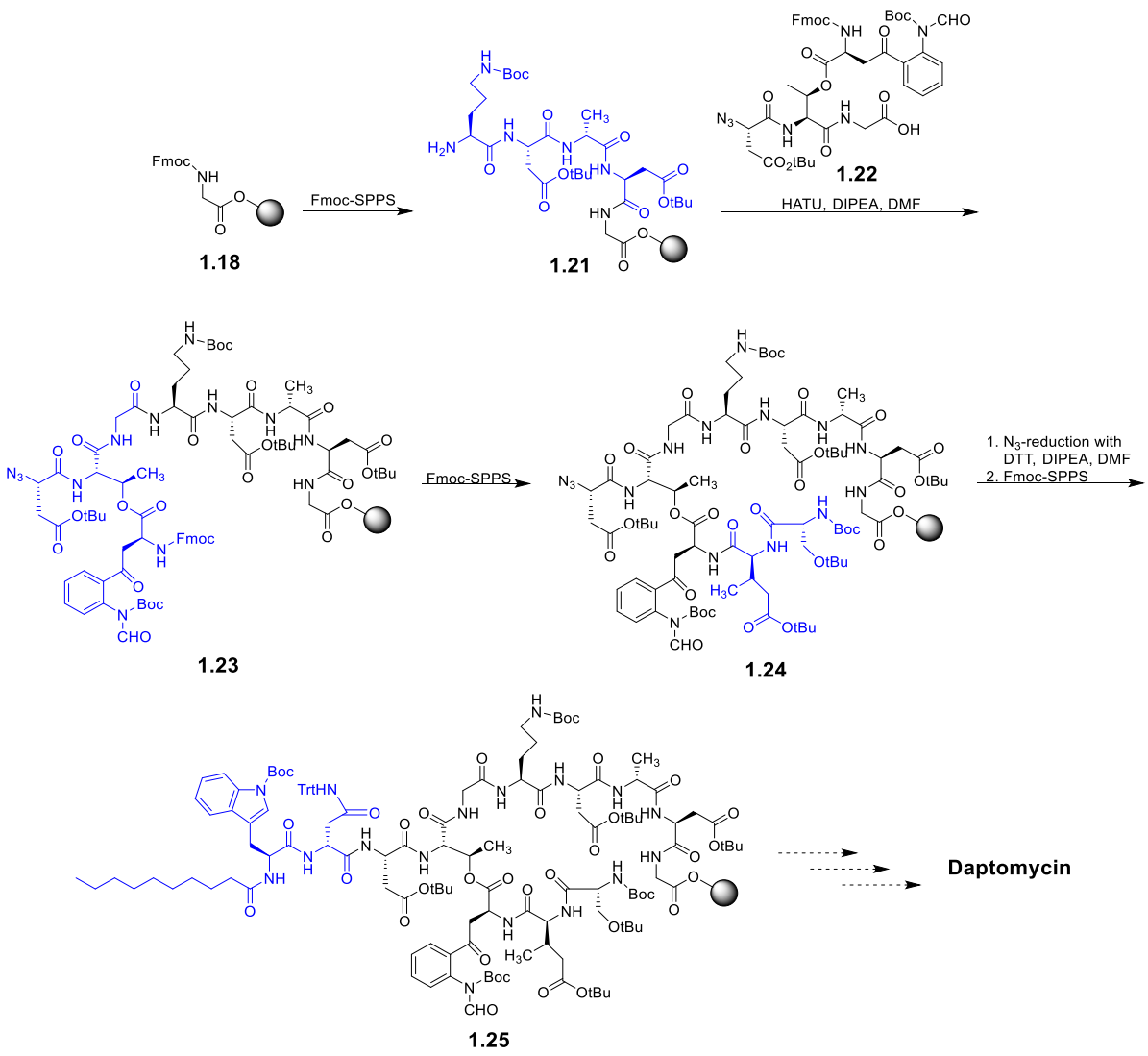

Scheme 1.6: Second route to daptomycin by the Li group, part 1.[83]

Linear precursor **1.25** was cleaved from the peptide with weakly acidic acetic acid (AcOH), trifluoroethanol (TFE) and dichloromethane (DCM) to keep side-chain protecting groups intact, yielding peptide **1.26** (Scheme 1.7). Coupling of the dimethyl acetal of salicylaldehyde mediated by benzotriazol-1-yl-oxy-tripyrrolidinophosphonium hexafluorophosphate (PyBOP) and DIPEA followed by global deprotection yielded branched peptide **1.27** in 17% yield, based on initial resin loading. Aldehyde **1.27** was converted to hemiaminal ether **1.28** with pyridine acetate buffer via chemoselective serine ligation and

macrocyclization, and further cleavage of the hemiaminal ether **1.28** with TFA and H_2O yielded daptomycin in 67% yield from aldehyde **1.27**.

The synthetic approach by the Li group was the first total synthesis of daptomycin reported. The main advantage of synthesizing analogs by total synthesis is that it enables the synthesis of many analogs in a relatively quick time-frame. The Li group's strategy, however, is not very conducive to the synthesis of analogs of daptomycin for multiple reasons. Firstly, without being able to form the depsi-bond on-resin, the researchers are required to synthesize a tetrapeptide building block in solution with the ester-bond pre-formed, and a new tetrapeptide building block must by synthesized whenever one of these four amino acid residues is to be substituted with an alternative amino acid. Secondly, the synthesis required two purifications by reverse-phase-(RP) high performance liquid chromatography (HPLC): one purification of intermediate **1.27** prior to serine ligation, and an additional purification at the end of the synthesis, making the strategy much more labour-intensive. Finally, the synthesis involves four separate in-solution steps to convert resin-bound peptide **1.25** to daptomycin, which would be extremely labour-intensive if large numbers of analogs were to be synthesized in this way. It would be far more advantageous if the ester bond of daptomycin could be formed on-resin, in addition to on-resin cyclization.

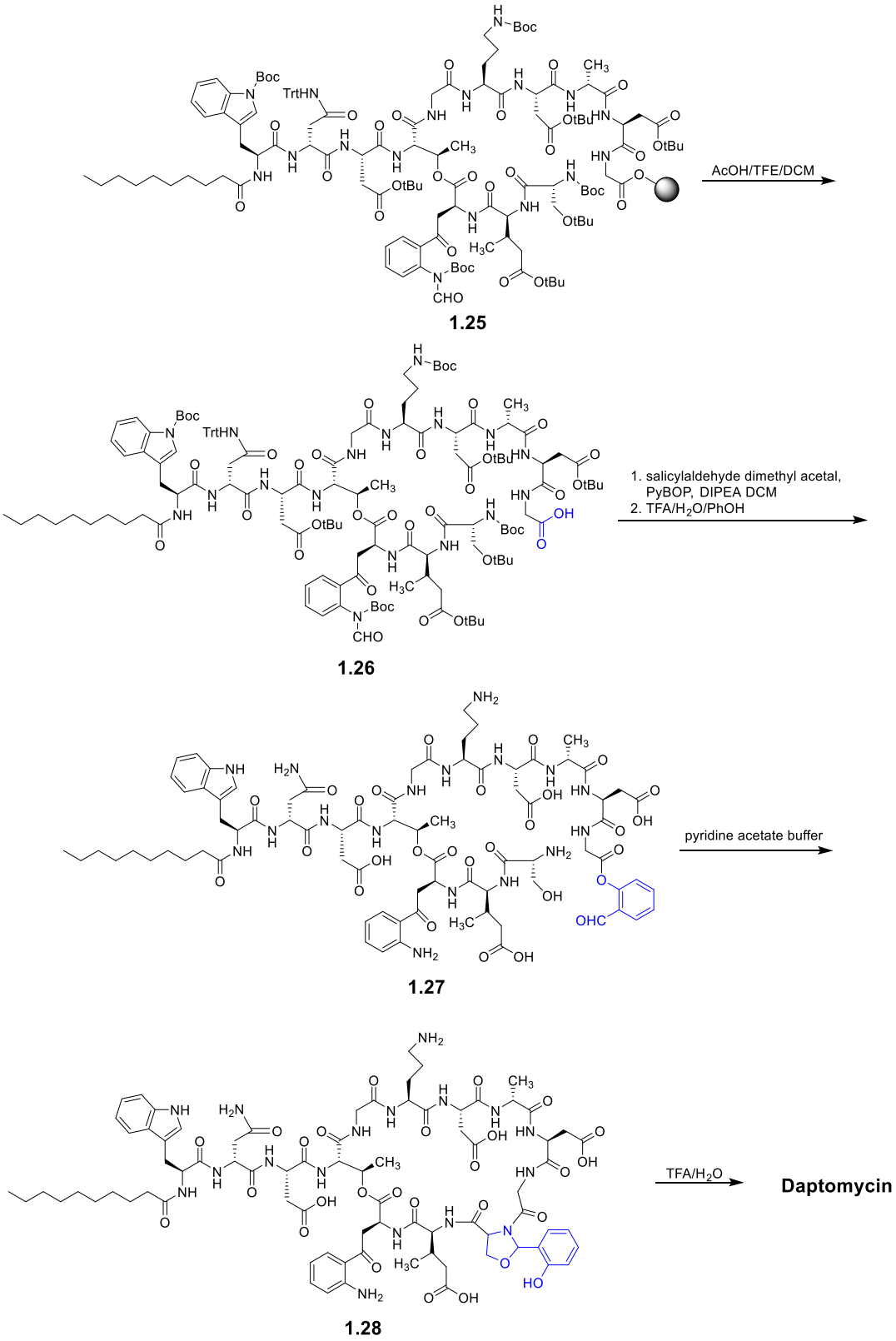

Scheme 1.7: Second route to daptomycin by the Li group, part 2.[83]

1.6.3 – Synthesis of Daptomycin Analogs by the Martin Group

In 2014, the Martin group reported a synthesis of daptomycin analogs which also involved an off-resin cyclization.[84] In one analog, MeGlu12 was replaced with Glu12, and Thr4 was replaced with DAPA4 (diaminopropionic acid), resulting in the conversion of the depsi-bond to a synthetically less challenging amide bond. A second analog contained both of these modifications, and moreover a Trp instead of Kyn13. Their strategy involved attaching the peptide to the solid-support by the α-carboxylic acid of Gly5 and employing Fmoc-SPPS to incorporate residues 1 through 4 plus the lipid tail (Scheme 1.8). DAPA4 was incorporated in the form of FmocDAPA(Alloc). Selective deprotection of the Alloc (allyloxycarbonyl) protecting group of peptide **1.29** with $Pd(PPh_3)_4$ and phenylsilane ($PhSiH_3$) provided a new branch point for further peptide elaboration of free amine **1.30**. Incorporation of residues 13 to 6 using Fmoc-SPPS yielded uncyclized Dap-DAPA4-Glu12 precursor **1.31**, which was cleaved from the resin with weakly acidic 20% hexafluoroisopropanol (HFIP) in DCM. The peptide, with protecting groups still intact, was subjected to off-resin cyclization followed by global deprotection of Boc-protecting groups with TFA, yielding Fmoc-DAPA4-Glu12 (**1.32**). In this strategy, the formation of the depsi-bond was not an inherent challenge as it was replaced with the less synthetically challenging amide bond. Further, it was observed that these two analogs were considerably less active than daptomycin (Dap-DAPA4-Glu12 was 80-fold less active, and Dap-DAPA4-Glu12-Trp13 was 160-fold less active when assayed against *S. aureus* ATCC 29213). Several amino acid substitutions were made in these analogs, so it is difficult to pin-point the exact cause of such a drastic reduction in biological activity. However, it is likely that the conversion of the depsi-bond to an amide bond resulted in a significant loss of activity, as Dap-Glu12, which contains an ester bond but otherwise resembles Dap-DAPA4-

Glu12, has been reported to be only 5.5-fold less active than native daptomycin when assayed against *B. subtilis* PY79.[78]

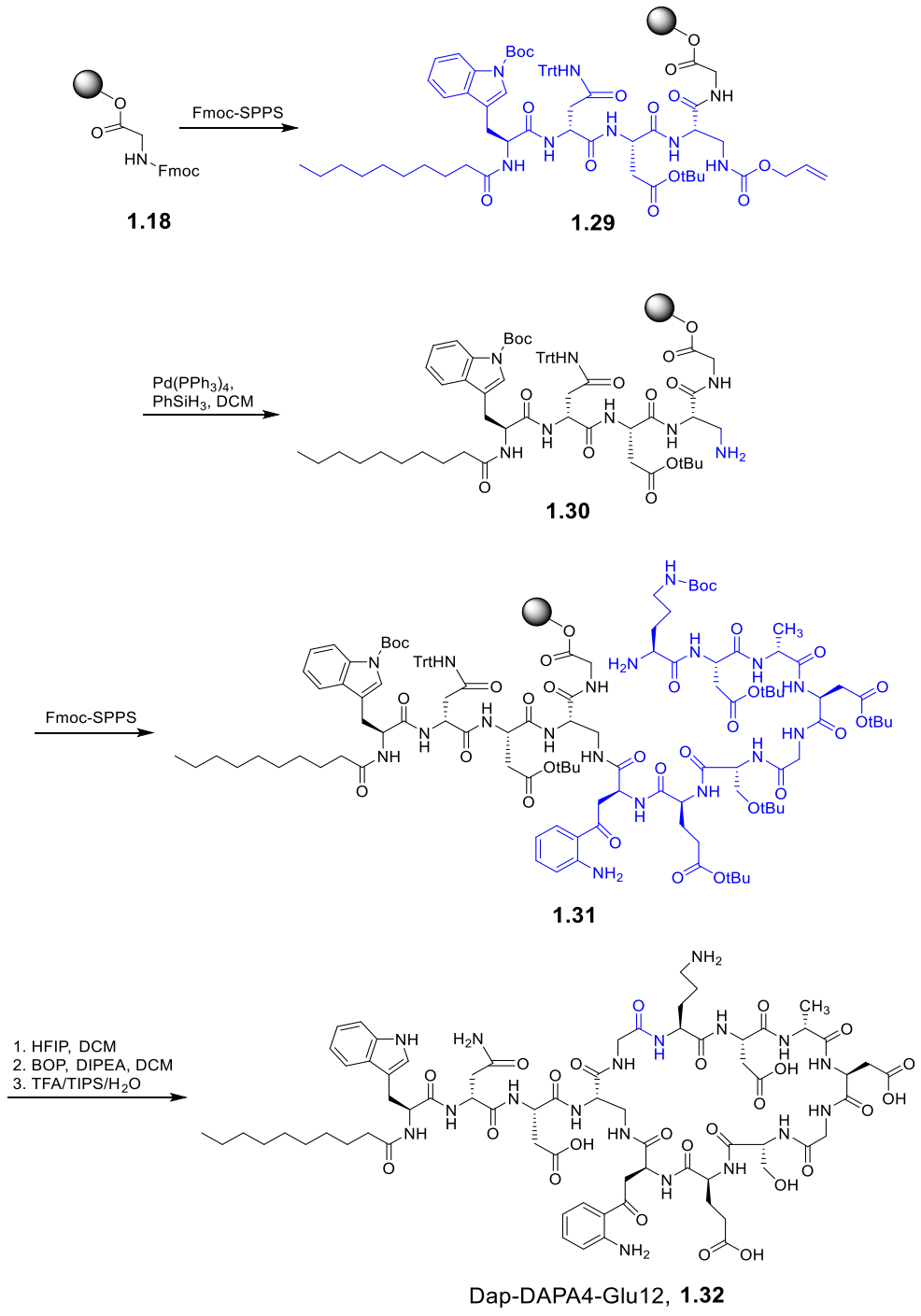

Scheme 1.8: Synthesis of Dap-DAPA4-Glu12 (**1.32**) by the Martin group.[84] Dap-DAPA4-Gu12-Trp13 was synthesized in the same manner except FmocTrp(Boc)OH was used instead of FmocKynOH.

1.6.4 – Total Synthesis of Daptomycin by the Taylor Group

Despite the advances of the Li group and the Martin group, a total synthesis of daptomycin suitable for the rapid generation of many analogs had not yet been achieved. In the Li group's synthesis, the use of solution-phase chemistry to synthesize their amino acid building blocks makes the rapid development of analogs more challenging and more time-consuming. In the Martin group's synthesis, the ester-bond crucial for daptomycin activity was completely omitted and replaced with an amide bond. These challenges were tackled by the Taylor group in 2015, who published the first entirely on-resin synthesis of daptomycin and analogs.[85]

The approach pioneered by Lohani et al. employed Fmoc- and N_3-SPPS, and the peptide was attached to the resin by the sidechain of Asp9 using DIPEA and FmocAsp(OH)Oallyl forming resin-bound FmocAspOallyl **1.33** (Scheme 1.9). Removal of the allyl group with $Pd(PPh_3)_4$ and *N,N'*-dimethylbarbituric acid (DMBA) and incorporation of Gly10 via the tosylate salt of allyl glycine produced resin-bound dipeptide **1.34**. In the first attempted synthesis, Fmoc-SPPS was used to introduce the lipid tail along with residues 1 to 8, but formation of the depsi-bond on complete linear peptide **1.35** with FmocKyn(CHO, Boc)OH yielding **1.36** was unsuccessful.

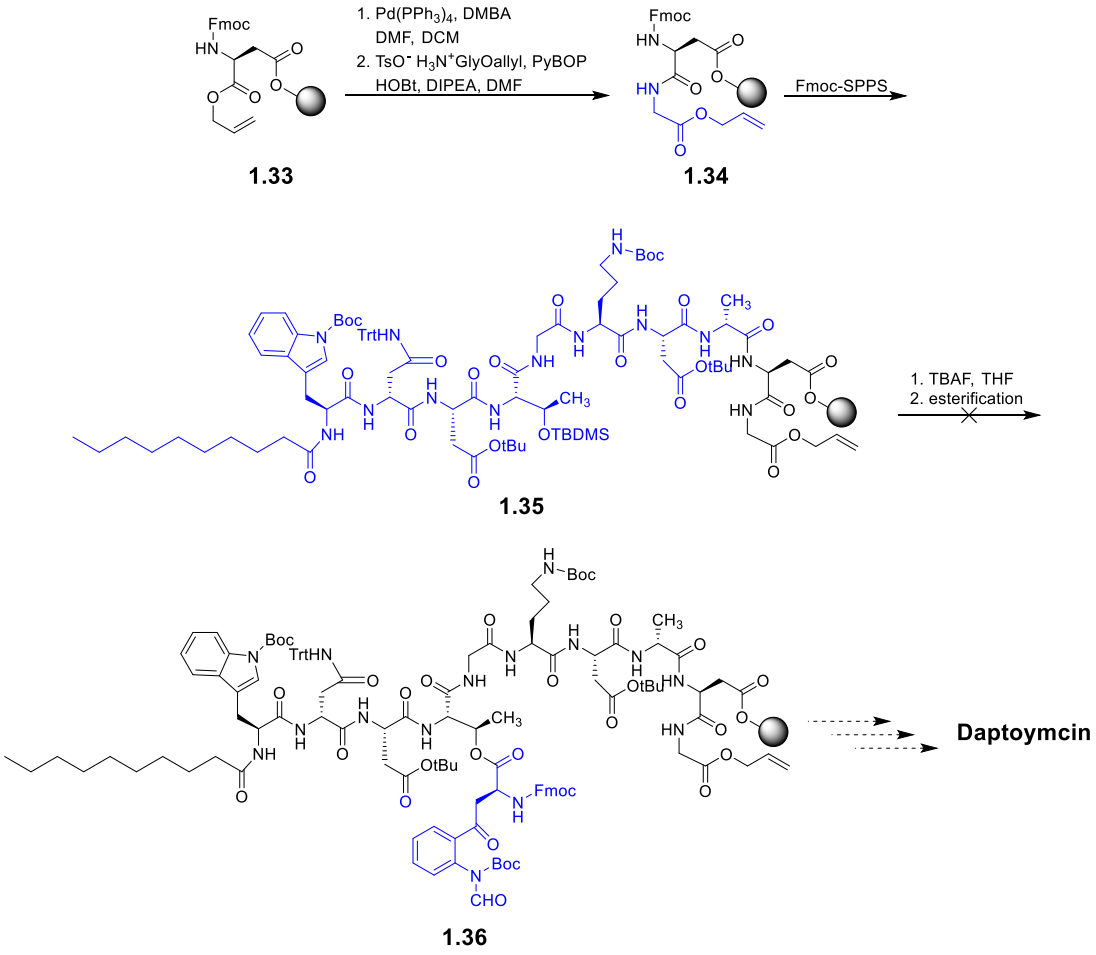

Scheme 1.9: First attempted route to daptomycin by the Taylor group.[85]

To resolve the challenging issue of depsi-bond formation, it was attempted on truncated peptide **1.37** containing azido-protected Asp3, which allowed for facile depsi-bond formation with Fmoc-Kyn(CHO, Boc)-OH when *N*,*N'*-diisopropylcarbodiimide (DIC) and *N*,*N*-dimethyl-4-aminopyridine (DMAP) were used as coupling reagents (Scheme 1.10), yielding peptide **1.38**. Residues 1 and 2 were introduced via azido acids N_3-D-Asn(Trt)OH and N_3Trp(Boc)OH, and their azido groups were converted to amino groups with trimethylphosphine (PMe_3) in dioxane and H_2O, followed by the incorporation of the lipid tail to yield branched peptide **1.36**. Further Fmoc-based SPPS yielded the uncyclized peptide **1.39**,

and removal of the allyl group with $Pd(PPh_3)_4$ and DMBA followed by on-resin cyclization with PyBOP, 1-hydroxy-7-azabenzotriazole (HOAt), and DIPEA, and finally global deprotection and resin cleavage with TFA resulted in daptomycin in a 9% overall yield.

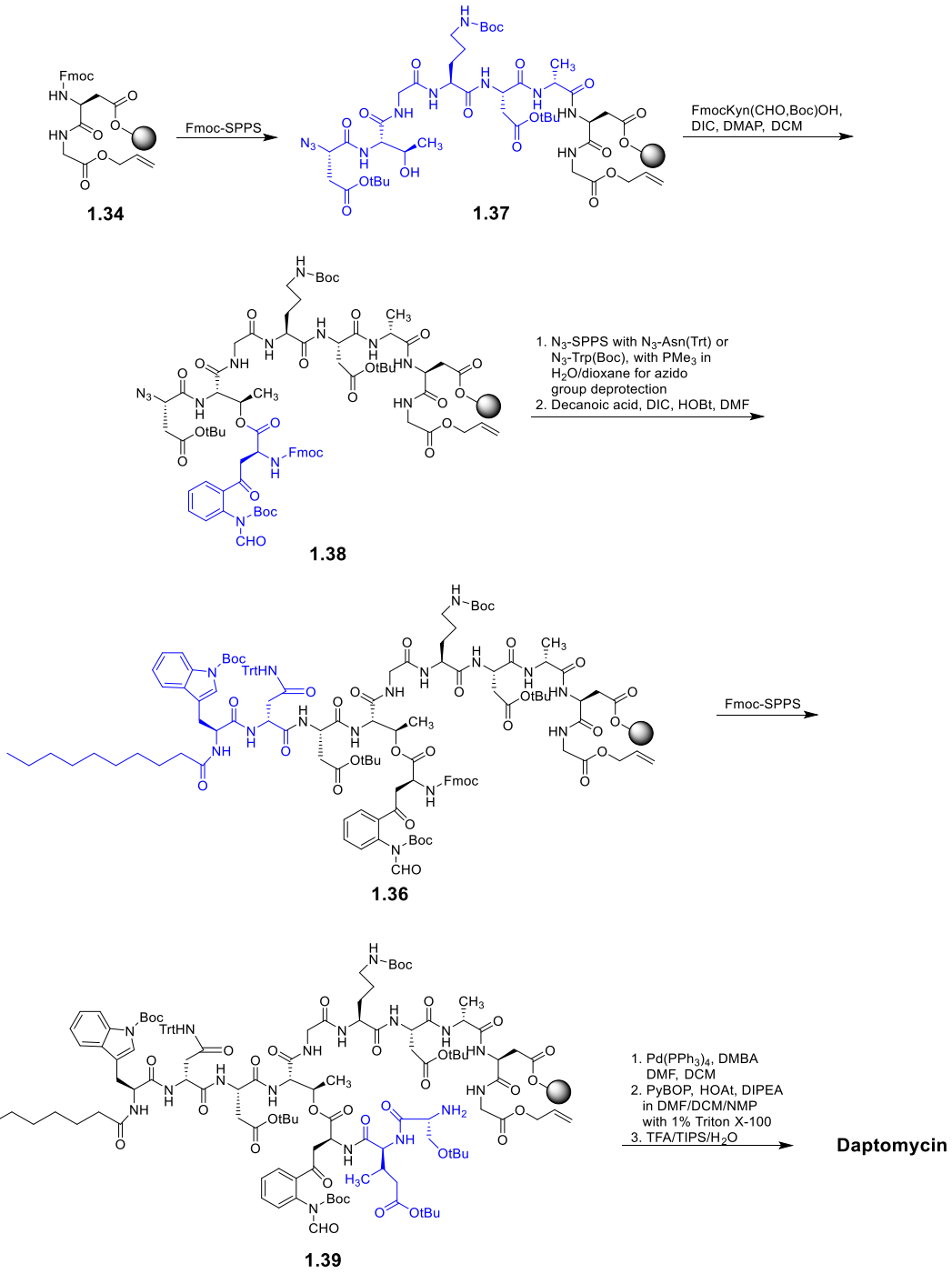

Scheme 1.10: First total synthesis of daptomycin and analogs achieved by the Taylor group.[85]

This synthesis was applied to three additional daptomycin analogs, and these analogs demonstrated that the non-proteinogenic amino acids MeGlu12 and Kyn13 could be replaced with Glu12 and Trp13 (Dap-Glu12-Trp13) with activity approaching that of native daptomycin (only 5-fold less active at 1.8 mM Ca^{2+}). Further, an analog was synthesized in which the stereochemistry of the β-methyl group of MeGlu12 was changed from 3*R* to 3*S*, and this was found to reduce biological activity by about 50-fold when assayed against *B. subtilis* ATCC 1046 at 5 mM Ca^{2+}, demonstrating that inversion of a single stereocenter in daptomycin can be detrimental to biological activity. In a subsequent publication, a similar approach was used to obtain Dap-Ser4-Glu12-Trp13, an analog in which the Thr4 residue was replaced with a Ser4 residue.[86] This modified approach involved the use of FmocSer(Trt)OH, whose trityl group was removed under weakly acidic 20% dichloroacetic acid (DCA) in DCM (v/v). Accordingly, a more acid-resistant Wang resin was used in its synthesis. Dap-Ser4-Glu12-Trp13 was at least 100-fold less active than daptomycin, and at least 20-fold less active than Dap-Glu12-Trp13. This approach, however effective in the development of daptomycin analogs, suffered in its use of three azido acids, N_3Trp(Boc)OH, N_3-*D*-Asn(Trt)OH, and N_3Asp(tBu)OH, which are not commercially available and therefore require in-lab synthesis. This makes the approach less amenable for a large-scale daptomycin library generation.

The Taylor group improved their synthesis of Dap-Glu12-Trp13 in 2016.[87] In the new approach, ester bond formation on truncated Fmoc-protected peptide **1.40** with N_3Trp(Boc)OH, DIC, and DMAP was achieved, thereby only requiring one azido acid in the synthesis of daptomycin analogs (Scheme 1.11). Branched peptide **1.41** was further elaborated with Fmoc-SPPS yielding peptide **1.42**. Reduction of azido-peptide **1.42** was achieved with DTT and DIPEA in DMF. Following this, Fmoc-SPPS yielded resin-bound, uncyclized peptide

1.43. Dap-Glu-12-Trp13 (**1.44**) was obtained analogously to the approach used in Scheme 1.10.

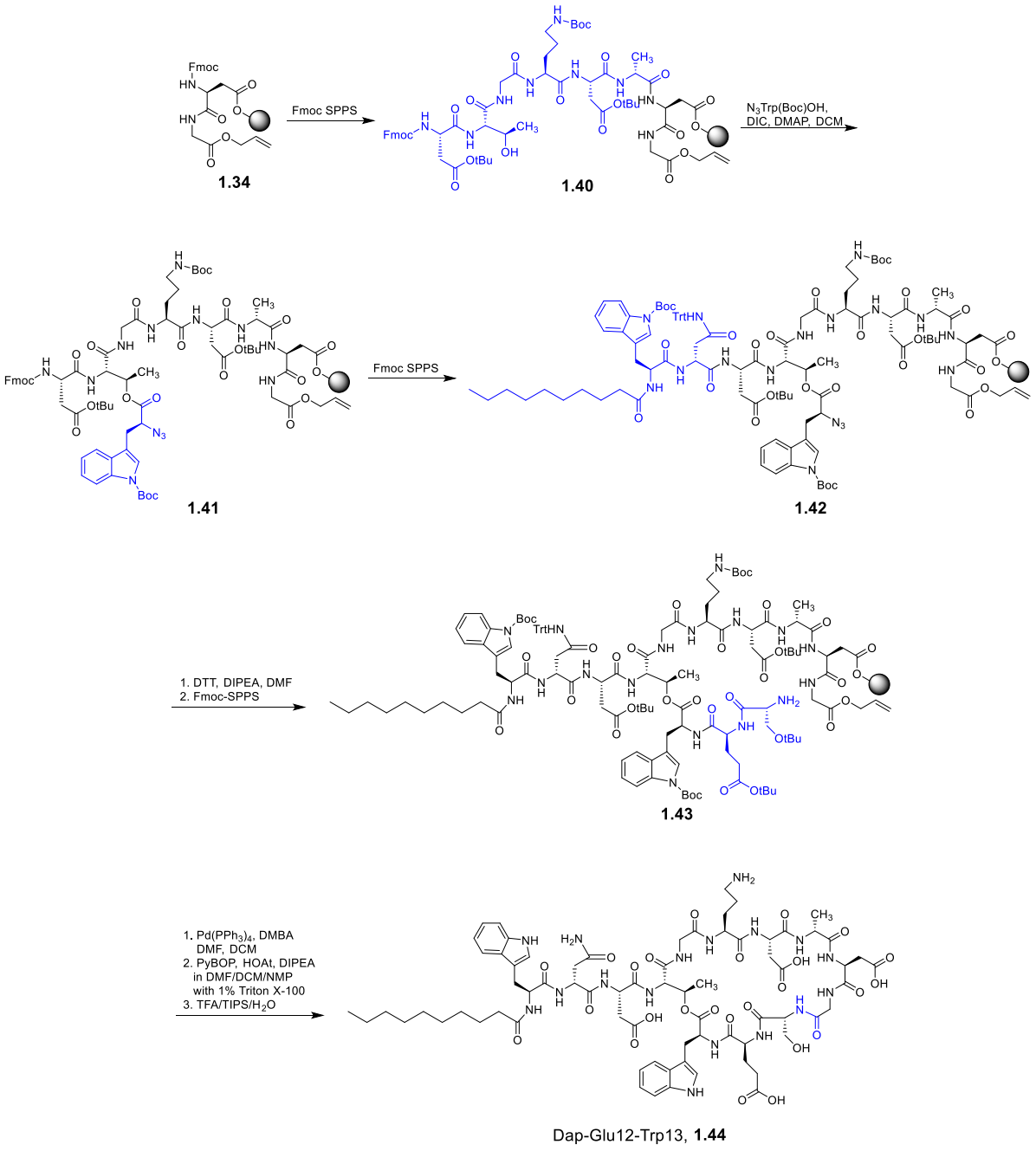

Scheme 1.11: Second strategy toward daptomycin analogs reported by the Taylor group.[87]

In 2018, the Taylor group improved their synthetic approach even further, obviating the need for azido acids altogether.[82] This new approach used Fmoc-SPPS on TentaGel Trt-Cl

resin, which contains a polystyrene matrix with a polyethylene glycol linker attached to the trityl chloride group (Section 1.6.1). It was observed that this resin choice facilitates the formation of the depsi-bond, which allowed for an entirely Fmoc-based synthesis of daptomycin and analogs (Scheme 1.12). Dipeptide **1.34** underwent Fmoc-SPPS to form linear peptide **1.45**, and depsi-bond formation proceeded via treatment with 10 equiv of FmocTrp(Boc)OH, 10 equiv of DIC, and 0.1 equiv of DMAP in DCM containing Triton X-100 (1%, v/v) yielding peptide **1.46**. Further elaboration of peptide **1.46** using the same conditions presented in Schemes 1.10 and 1.11 afforded Dap-Glu12-Trp13 (**1.44**). This synthetic approach also allowed for the synthesis of Dap-Lys6-Glu12-Trp13 (**1.47**, Figure 1.18), an analog in which the uncommon amino acids Orn6, MeGlu12 and Kyn13 are replaced with Lys6, Glu12, and Trp13. The biological activity of this compound was examined and determined to be only 2-fold less active than daptomycin against *B. subtilis*, and thus serves as a valuable starting point in the synthesis of a library of antibiotics.

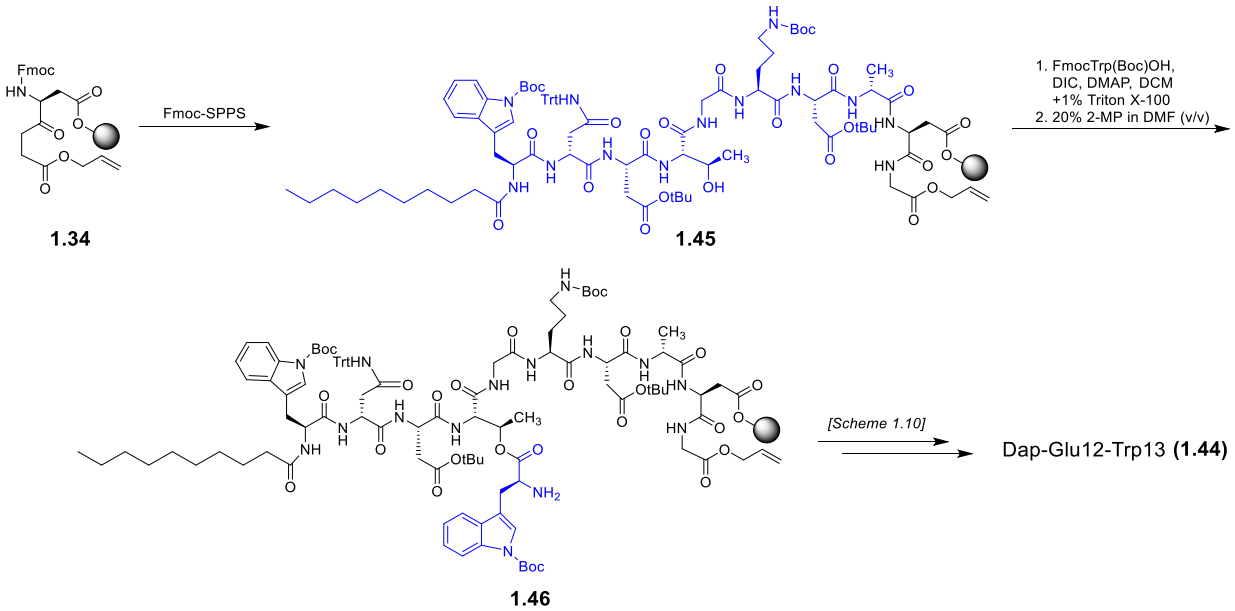

Scheme 1.12: Third successful route to daptomycin analogs by the Taylor group.[82]

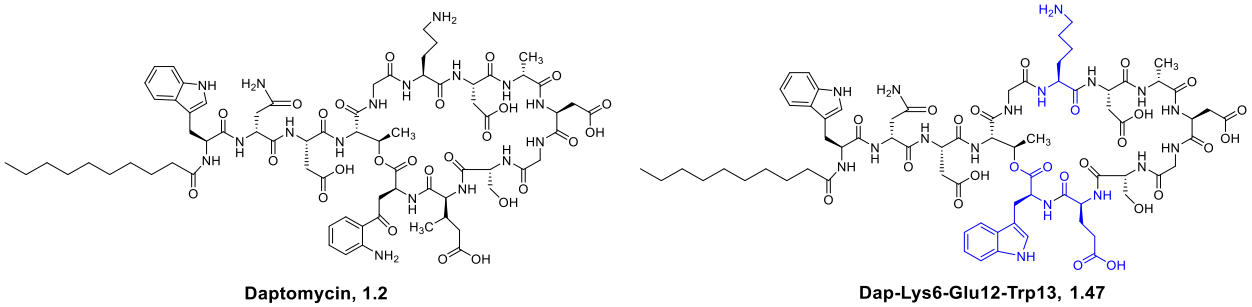

Figure 1.18: Daptomycin (**1.2**) compared with Dap-Lys6-Glu12-Trp13 (**1.47**)

With the optimized total synthesis of daptomycin, researchers in the Taylor group were able to conduct an alanine scan (replacement of individual amino acids of daptomycin with alanine) to probe attempt to determine which amino acid residues are tolerant to substitution.[81,82] It was determined that residues 6 and 11 are amenable to substitution with alanine or *D*-alanine, respectively, with a 2-fold loss of activity, and also that position 2 is somewhat amenable to substitution with *D*-alanine, with a 4-fold loss in activity, relative to Dap-Lys6-Glu12-Trp13. On the basis of these results, positions 2, 6, and 11 may be amenable to substitutions with other amino acids, yielding daptomycin analogs with improved biological activity. This is part of the long-term goals in the Taylor group: to develop of libraries of antibiotics using a split-and-pool solid-phase peptide approach (see section 3.1 for a description of the split-and-pool approach).

1.7 – Project Goals

1.7.1 – Total Synthesis of A54145D and analogs

From Section 1.5 and 1.6, it is clear that the development of a total synthesis of daptomycin enables the development of analogs which can provide information on biological activity and may have activity profiles similar to or better than that of authentic daptomycin. This may ultimately allow for the possible generation of new antibiotics which may find

clinical use. No analogous total chemical synthesis of A54145 had been reported prior to the studies presented in this thesis.

In Chapter 2, the objective is to achieve an efficient synthesis of A54145D using Fmoc-based peptide synthesis on solid-support. The synthesis of A54145D was achieved, and the results of these studies demonstrate a stereochemical revision in the side-chain of MeOAsp9 from *L-threo*-MeOAsp to *L-erythro*-MeOAsp. Additionally, it was determined that the stereochemistry of the methyl group on the 8-methyldecanoyl tail does not affect biological activity.

In Chapter 3, the objective is to conduct further structure-activity relationship studies of A54145 analogs. Two new syntheses for A54145 analogs were developed, and these studies indicate that Thr4 of A54145 is not amenable to substitution. Further, structure-activity relationship studies confirm previously reported results that substitution of HOAsn3 or MeOAsp9 results in a 16-fold loss of biological activity, but that the 8-methyldecanoyl tail of A54145D can be replaced with a decanoyl tail (yielding A54145A_1) with only slightly reduced biological activity against *B. subtilis*. Additionally, replacing the *anteiso*-undecanoyl tail, HOAsn, and MeOAsp with a decanoyl tail, Asn, and Asp, respectively, produces an analog with also a 16-fold loss in biological activity relative to A54145D, and a mere 4-fold loss in biological activity relative to A54145A_1.

1.7.2 – Probing the mechanism of action of Daptomycin using ^{19}F-NMR

From Section 1.3, it is evident that the exact mechanism by which daptomycin elicits its bactericidal mode of action it not completely elucidated, but that it involves association with the biological membrane in a PG- and Ca^{2+}-dependent fashion. One technique often used to probe interactions of biomolecules with lipid membranes involves ^{19}F-NMR. The fluorine

nucleus is sensitive to its chemical environment and known to adopt different chemical shifts and peak shapes in hydrophilic and hydrophobic environments. In Chapter 4, the synthesis of a total of ten fluorinated analogs of daptomycin is discussed, as are preliminary NMR studies that probe the nature of daptomycin's interaction with biological membranes. These preliminary findings indicate that the ornithine residue interacts with model membranes prior to the lipid tail, and that aggregation of daptomycin analogs does not occur in solution at physiological concentrations of daptomycin and calcium.

Chapter 2 – The Total Synthesis of A54145D

2.1 – Introduction

No members of the A54145 family have been developed into clinically useful drugs. The most potent natural factors (Factors B, B1, and E) contain MeGlu12, and while they are only 2-fold less active than daptomycin (**1.2**, Figure 2.1), they are found to be toxic to mice.[15,17] For example, the LD_{50} for A54145B is low, at only 28 mg/kg.[15,80] Factors containing Glu12, such as A54145D (**1.11**, Figure 2.1), are about 2-fold less potent than those containing MeGlu, but are substantially less toxic in mouse models (>500 mg/kg).[15,17]

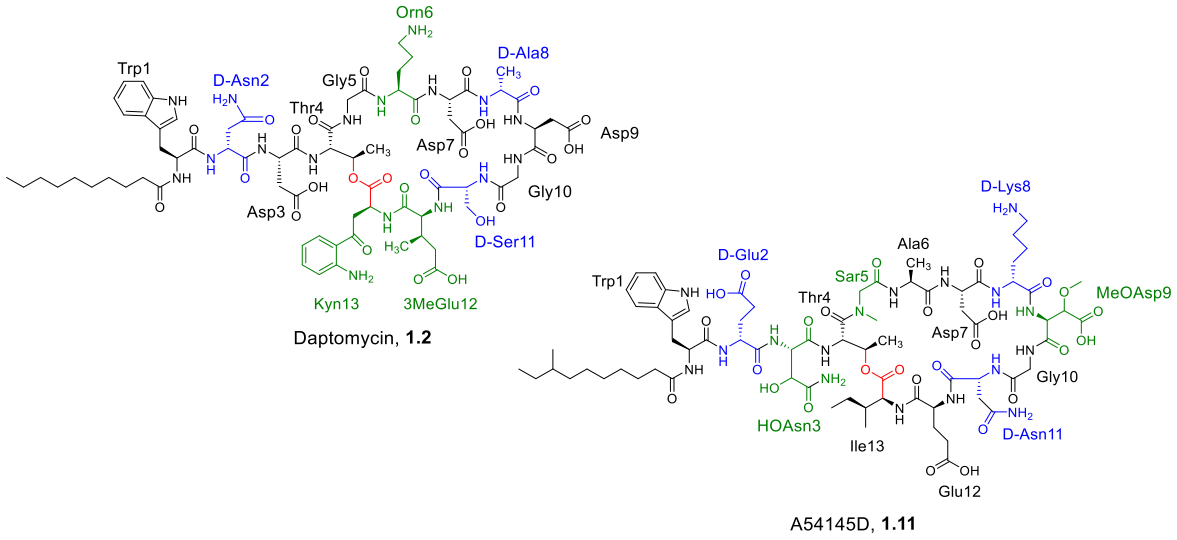

Figure 2.1: Structures of daptomycin (**1.2**) and A54145D (**1.11**).

Daptomycin did not meet non-inferiority standards in clinical trials for treating community-acquired pneumonia (CAP). A possible cause for this failure is its inhibition by lung surfactant.[19] Unlike daptomycin, A54145D is not severely inhibited by lung surfactant. This characteristic of A54145D prompted the development of combinatorial biosynthesis methodologies for preparing cLPAs based on the A54145D peptide core.[16,17] Although several A54145D analogs were obtained that exhibited good activity, low toxicity, and low inhibition by surfactant, none were sufficiently active in mouse models for *S. pneumoniae* to pursue clinically.[80] Nevertheless, these results are promising when one considers that the key *in vitro* criteria (good activity, low toxicity, and low inhibition by surfactant) were met even though the number of analogs prepared represented only a very small fraction of the potential chemical space. It is possible that the development of an efficient chemical approach to the synthesis of A54145D and its analogs will enable researchers to access a larger portion of the available chemical space, which could ultimately lead to the development of a cLPA suitable for the treatment of CAP that is resistant to conventional therapy.

2.1.1 – Research Objectives

The main objectives of the work described in this chapter are to synthesize A54145D and elucidate the stereochemistry of the side chains of HOAsn and MeOAsp. An additional objective is to establish the importance of the stereochemistry of the 8-methyldecanoyl lipid tail to biological activity. It would also be desirable if the synthesis of A54145D was amenable to the synthesis of large numbers of analogs.

2.1.2 – Stereochemical Considerations for A54145D

A54145 Factor D contains four amino acids with two stereogenic centers. Both isoleucine at position 13 and threonine at position 4 have known stereochemistry. However, at

positions 3 and 9 are HOAsn and MeOAsp, respectively, and although they are often depicted in the literature as having the *2S*,3*S*-configuration, the absolute configuration of the position 3 stereocenter was not unambiguously established at the start of these studies. It was suggested by Strieker et al. that the HOAsn of CDA was likely (2*R*,3*S*) based upon bioinformatic studies of the CDA NRPSs.[88] Notably, the NRPSs for CDA include an epimerase domain (Section 1.4) which converts *L*-HOAsn (2*S*,3*S*) to *D*-HOAsn (2*R*,3*S*). The analogous A54145 NRPSs lack this epimerase domain for HOAsn3, and since the two antibiotics are both produced by two *Streptomyces* species (*S. fradiae* for A54145, and *S. coelicolor* for CDA), we proceeded with the assumption that A54145 contains HOAsn with a (2*S*,3*S*) configuration, or *L-threo*-HOAsn. Unfortunately, no bioinformatic studies have been performed for MeOAsp. Nevertheless, we further assumed that the amino acids were synthesized *in vivo* through a common intermediate and that both amino acids were of the *L-threo* configuration.

2.2 – Results and Discussion

2.2.1 – First Proposed Synthesis of A54145D

In our first approach for the synthesis of A54145D, we envisioned attaching the resin to the side-chain of MeOAsp9 via Fmoc-*L-threo*-MeOAspOallyl (Fmoc-*t*MeOAspOallyl) (Scheme 2.1), which resembles the approach used by Lohani et al. and Barnawi et al. (Scheme 1.9, Section 1.6.4).[82,85] Removal of the allyl group of resin-bound Fmoc-*t*MeOAspOallyl (**2.1**) with $Pd(PPh_3)_4$ and DMBA followed by the coupling of the tosylate salt of allyl glycine ($TsO^-H_3N^+$GlyOallyl) would produce dipeptide **2.2**. The reason for choosing this particular dipeptide is two-fold. Firstly, final cyclization steps of cyclic peptides can cause racemization of the C-terminal amino acid during activation of the carboxylic acid. By employing Gly10 as the C-terminal amino acid in this cyclization step, we can avoid the formation of two epimers

entirely, as glycine is inherently achiral. Secondly, this dipeptide would permit on-resin cyclization, which, from the perspective of ultimately generating a multitude of peptides via a split-and-pool SPPS approach on macro-beads, is advantageous for library genesis. While off-resin cyclization is possible, it would require a separate reaction flask for each macro-bead (each individual peptide in the library), whereas on-resin cyclization can be done with limitless macro-beads in the same reaction cartridge. For a description of Fmoc-SPPS on macro-beads, refer to section 3.1.

Elaboration of peptide **2.2** via Fmoc-SPPS employing DIC/hydroxybenzotriazole (HOBt) would yield linear peptide **2.3**, which contains the unprotected hydroxyl group of Thr4 as the branch point for depsi-bond formation. Forming the depsi-bond with N_3IleOH and DIC/DMAP would produce peptide **2.4**, which would further undergo elaboration via Fmoc SPPS yielding peptide **2.5**. We expected that reduction of the azido group with tributylphosphine (PBu_3) in the presence of the symmetric anhydride of FmocGlu(tBu)OH in tetrahydrofuran (THF)/H_2O, followed by further Fmoc-SPPS, would yield the uncyclized peptide **2.6**, which, after removal of the allyl protecting group with $Pd(PPh_3)_4$ and DMBA, would allow for an on-resin cyclization. Global deprotection and resin cleavage using TFA/TIPS/H_2O would yield A54145D.

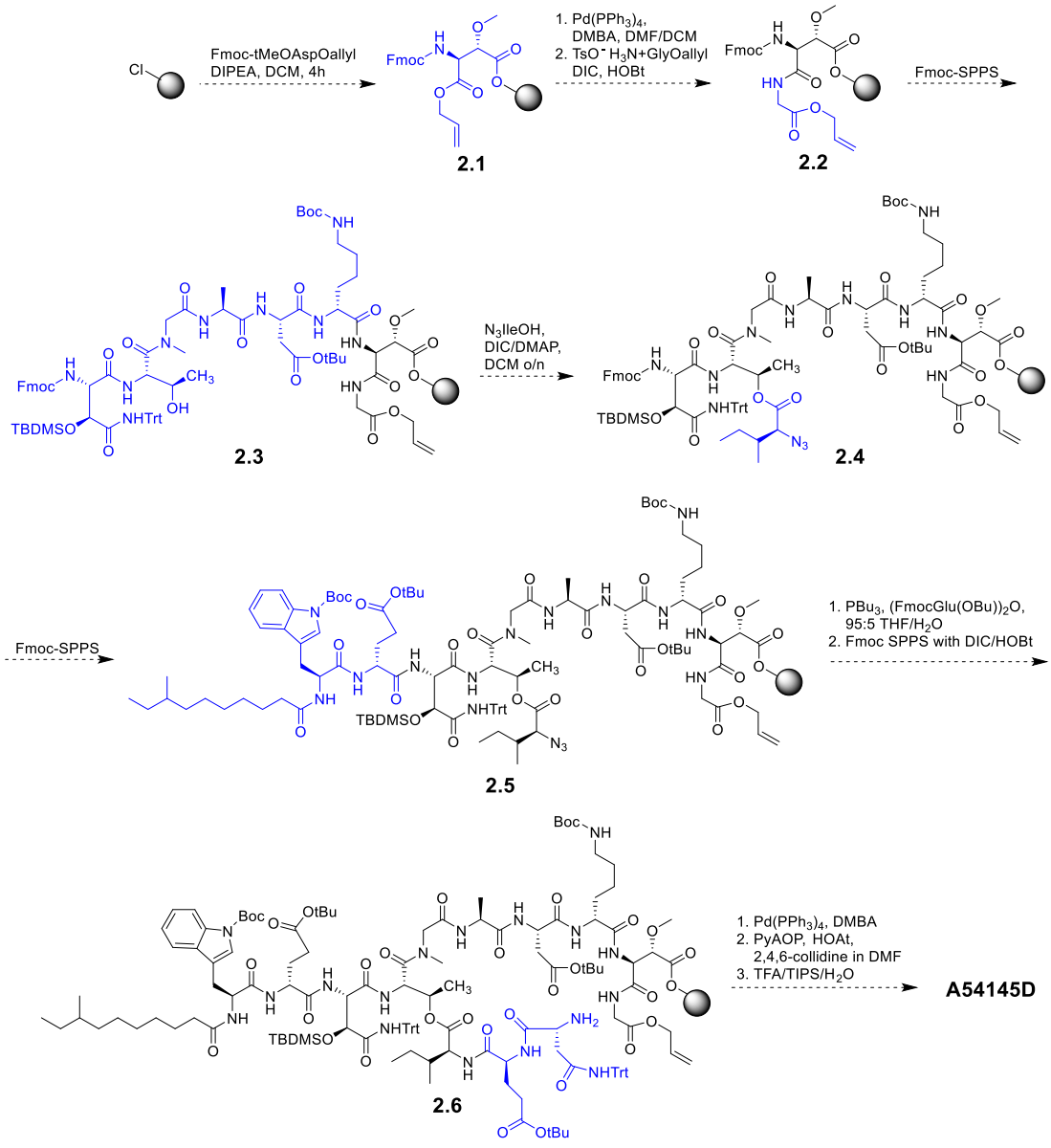

Scheme 2.1: First proposed synthesis of A54145D (i.e., A54145-*t*HOAsn3-*t*MeOAsp9).

For this synthesis, suitably protected amino acids were required. Attachment of the peptide by the side-chain of MeOAsp9 would require Fmoc-*t*MeOAspOallyl, and subsequent synthesis would require Fmoc-*L*-*threo*-HOAsn(Trt, TBDMS)-OH and (±)-8-methyldecanoic acid.

2.2.1.1 – Synthesis of Non-Commercially Available Amino Acids and the Lipid Tail

For the synthesis of Fmoc-*t*MeOAspOallyl, an asymmetric aminohydroxylation reaction, performed by Professor Scott Taylor, using the conditions of von Eckardstein et al.[89] was performed on ester **2.7**[90] to give compound **2.8** in excellent yield (Scheme 2.2). Methylation of the free hydroxyl group using MeI/Ag_2O gave compound **2.9** in good yield. Oxidation of the phenyl ring followed by esterification of the resulting acid using allyl bromide gave compound **2.10** in 52% yield (2 steps). Finally, removal of the *tert*-butyl and Boc-protecting groups using acid followed by Fmoc protection of the free amino group gave compound **2.11** in 87% yield.

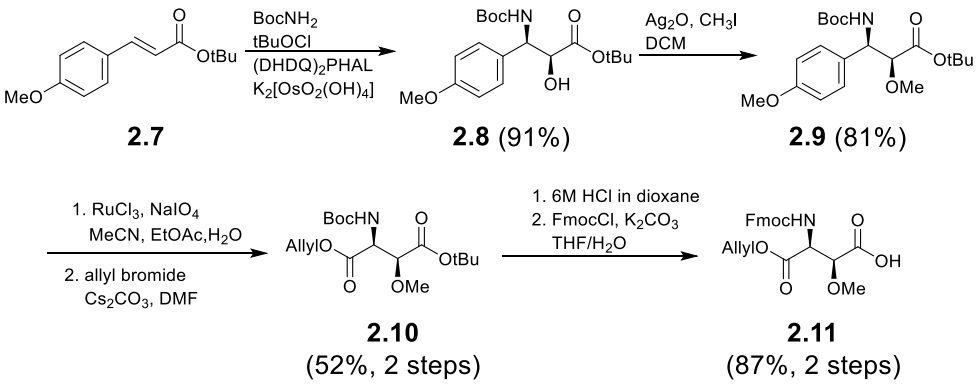

Scheme 2.2: Synthesis of Fmoc-*t*MeOAspOallyl **(2.11)**.

Fmoc-*t*HOAsn(Trt, TBDMS)OH was synthesized by Ryan Moreira, a graduate student in the Taylor group, by tritylation of Fmoc-*t*HOAsn(TBDMS)OH.[91] The 8-methyldecanoyl lipid tail of A54145D is not commercially available and therefore also required synthesis. We elected to use a racemic tail, and so (±)-8-methyldecanoic (**2.14**) was prepared (Scheme 2.3). This involved a Wittig reaction between phosphonium bromide salt **2.12**, produced using the procedure by Motoshima et al.[92], and (±)-2-methylbutanal which gave alkene **2.13** in 66%

yield. Lipid **2.14** was obtained in good yield by subjecting **2.13** to hydrogenation and then NaOH (aq).

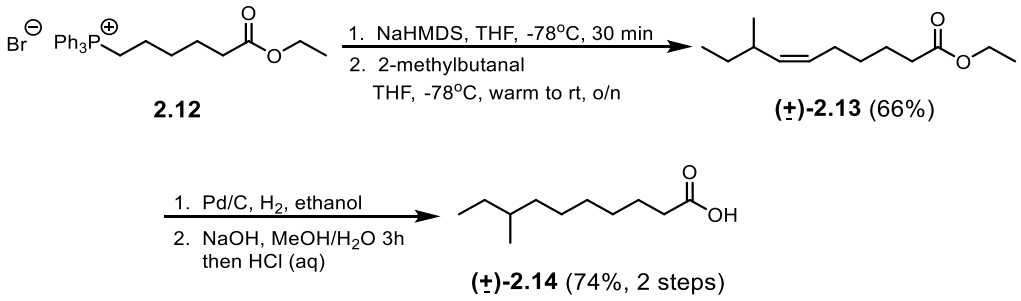

Scheme 2.3: Synthesis of (±)-8-methyldecanoic acid (**2.14**).

2.2.2 – First Approach to A54145D

Fmoc-*t*MeOAspOallyl (**2.11**) was attached to TentaGel-TrtCl resin via its side chain COOH group (Scheme 2.4). Removal of the allyl group of amino acid **2.1** followed by installation of $TsO^{-}H_3N^{+}$GlyOallyl gave dipeptide **2.2**. However, when the peptide was elongated using standard Fmoc-SPPS, it was found that the amount of peptide remaining attached to the resin decreased with each successive amino acid coupling. Specifically, following resin cleavage with TFA, tripeptide **2.17** was observed by HPLC (Figure 2.2) and by low-resolution mass spectrometry (LRMS), but further elaboration using Fmoc-SPPS to produce peptide **2.18** yielded an HPLC chromatogram almost devoid of any peaks after cleavage of the peptide from the resin. We suspected that aspartimide formation had occurred during Fmoc-SPPS, in the presence of 4-MP as a base. This would cause the peptide to be cleaved slowly from the resin throughout the synthesis. This result was unexpected, because similar side-reactions were not observed in the total synthesis of daptomycin and its analogs by other researchers.[82,85] It is likely that the presence of the electron-withdrawing methoxy group of MeOAsp9 promotes aspartimide formation.

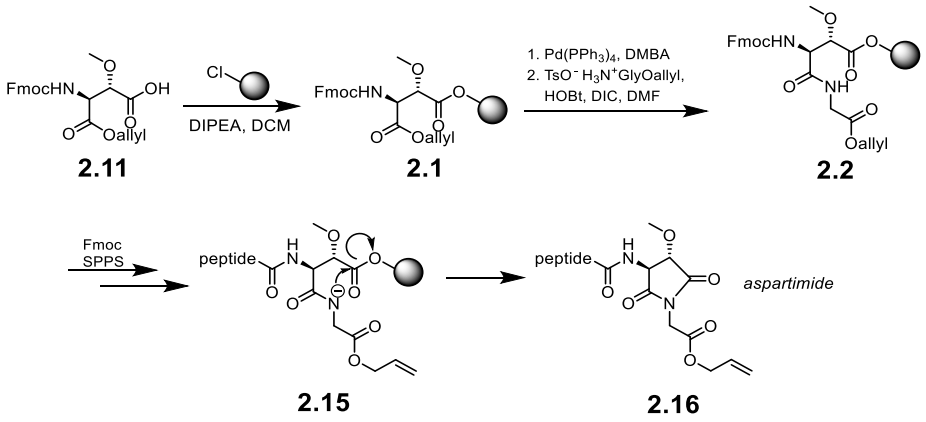

Scheme 2.4: Putative aspartimide formation during Fmoc-SPPS of A54145D.

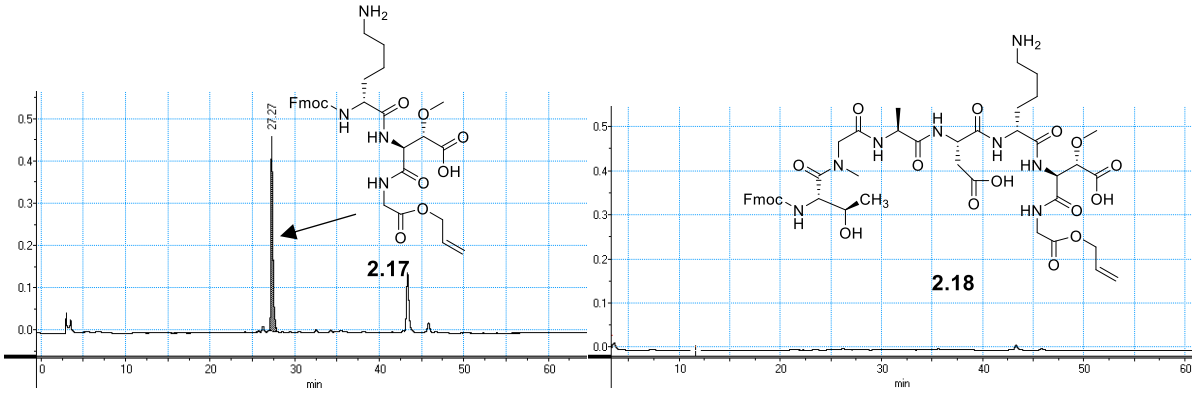

Figure 2.2: HPLC Chromatograms demonstrating loss of peptide from the resin. It was suspected that aspartimide formation between Gly10 and *t*MeOAsp9 cleaved the peptide from the resin.

To overcome the issue of aspartimide formation, we prepared dipeptide **2.19**, in which the amide nitrogen of Gly10 was protected with a dimethoxybenzyl (DMB) group (Scheme 2.5).[84] Unfortunately, we found that upon removal of the Fmoc group, the resulting dipeptide **2.20** underwent extremely rapid diketopiperazine (DKP) formation (**2.21**), as indicated by HPLC analysis and LRMS, in which the free amine produced upon Fmoc-deprotection engages in nucleophilic acyl substitution of the nearby allyl ester, forming a highly stable, six-membered ring product. DKP-formation is a common side reaction when *N*-alkylated amino acids are used in SPPS.[93,94]

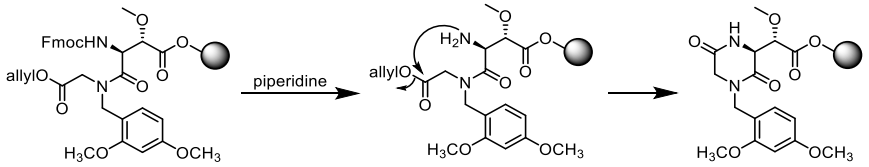

Scheme 2.5: DKP formation upon Fmoc-deprotection of peptide **2.19**.

In 2018, researchers in the Brimble group synthesized jahanyne, **2.22**, which is a highly *N*-methylated natural product (Figure 2.3).[93] In their synthesis, the peptide was attached to the resin by the α-carboxylic acid of proline, which is extremely susceptible to DKP formation. The researchers were able to avoid DKP formation between *N*-methylphenylalanine and proline with shortened treatments of 2-MP in DMF (20%, v/v). Encouraged by this observation, we assessed whether this strategy would be feasible in our synthesis of tripeptide **2.23**.

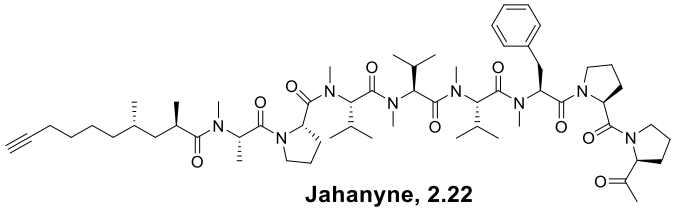

Figure 2.3: Structure of jahanyne, a highly *N*-methylated natural product.

Dipeptide **2.19** was subjected to a single 1-minute treatment of 20% 2-MP in DMF (v/v) before the coupling of Fmoc-*D*-Lys(Boc)OH with DIC/HOBt. The resulting HPLC trace demonstrated unpromising results, in that the major peak corresponded to starting material (**2.26**), and two peaks corresponding to DKP product (**2.24**) and desired product (**2.17**) were observed, with the DKP product being more significant (Figure 2.4). Thus, it was concluded that other strategies would need to be employed.

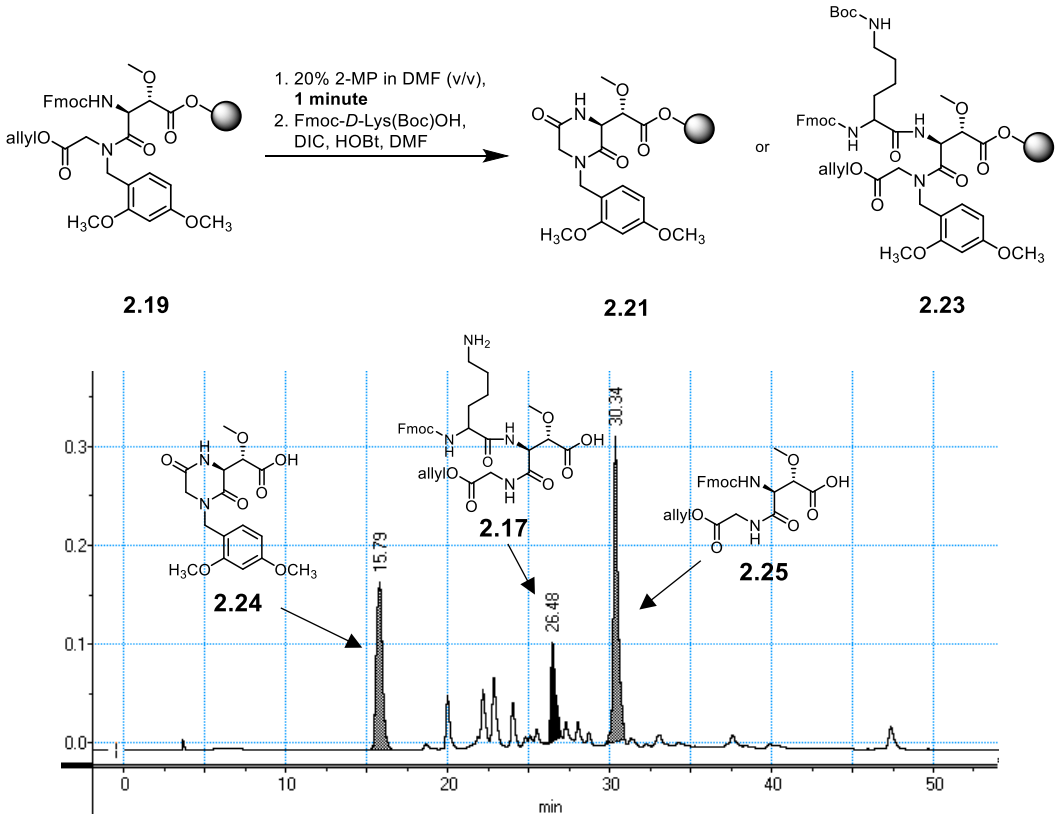

Figure 2.4: HPLC chromatogram after one minute of Fmoc-deprotection of peptide **2.19** and subsequent resin cleavage. Reduced deprotection times were not effective in eliminating the formation of DKP side-product **2.21**/**2.24**.

Due to the difficulties encountered using the on-resin cyclization route, we decided to pursue an off-resin cyclization strategy, in which the peptide would be attached to the resin by the α-carboxylic acid of Gly10 (Scheme 2.6). One significant difference between this strategy and the strategy presented in Scheme 2.1 is that following the incorporation of all amino acids, the peptide would be cleaved from the resin with a weakly acidic solution of TFA in DCM (1%, v/v), keeping the side-chain protecting groups intact. Off-resin cyclization would then occur before global deprotection with TFA/triisopropylsilane (TIPS)/H_2O (95:2.5:2.5 v/v), yielding A54145D-*t*HOAsn3-*t*MeOAsp9.

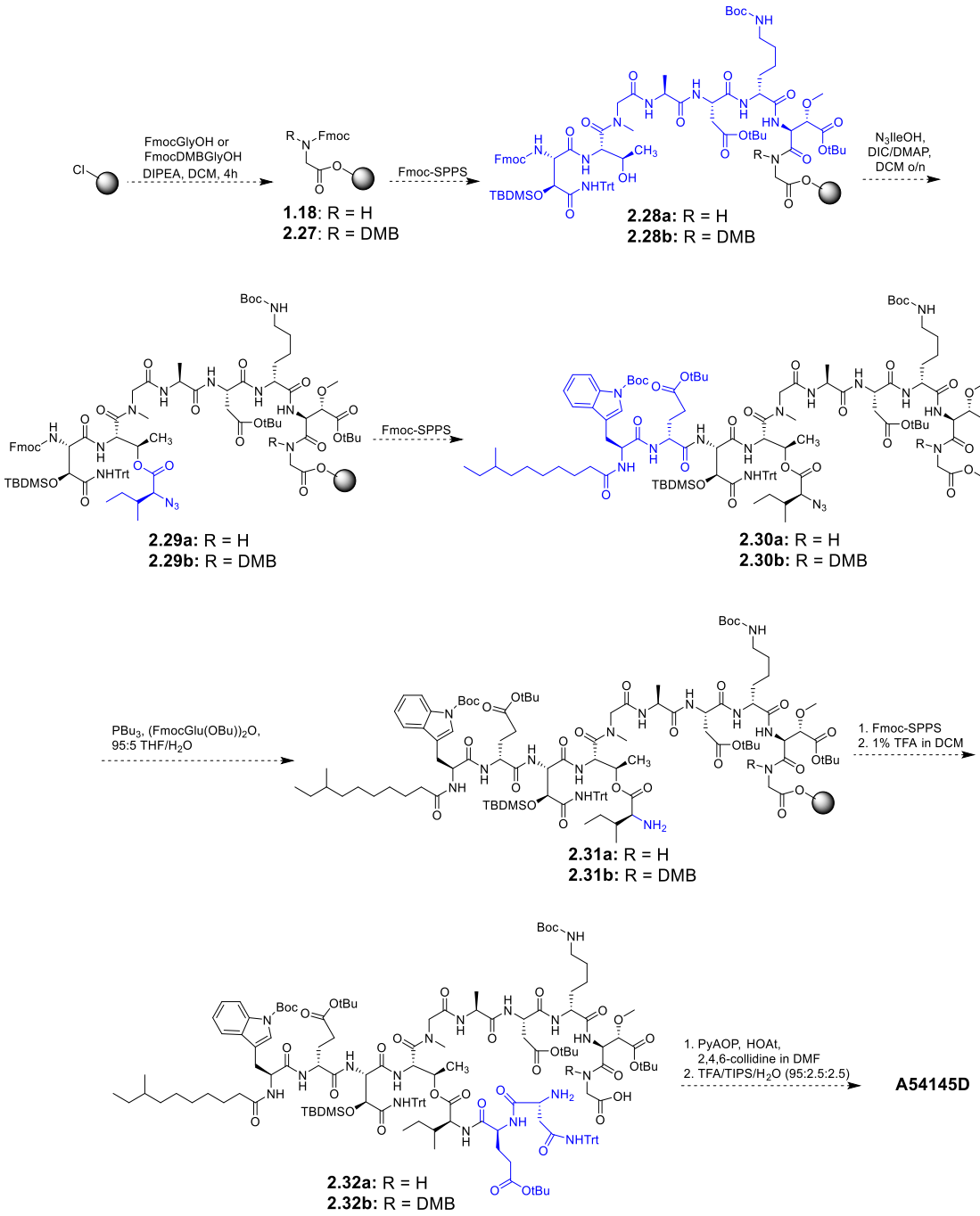

Scheme 2.6: Alternative proposed synthesis of A54145-*t*HOAsn3-*t*MeOAsp9.

Resin-bound glycine (**1.18**) was subjected to 20% 4-MP in DMF, and Fmoc-*L-threo*-MeOAsp(tBu)OH (**2.33**, prepared by Ryan Moreira of the Taylor group)[91] was introduced with DIC/HOBt, yielding dipeptide **2.34** (Scheme 2.7). After coupling of the third amino acid (*D*-

Lys8), we considered it prudent to check if the desired tripeptide **2.35** was obtained, since we had already observed that aspartimide formation could occur upon Fmoc-deprotection of the resin-bound dipeptide. RP-HPLC analysis of the cleaved tripeptide revealed two peaks (Figure 2.5), both with a mass corresponding to the desired product as indicated by LRMS. In the mechanism of aspartimide formation shown in Scheme 2.8, two isomeric products are formed: an α-MeOAsp product and a β-MeOAsp product. The presence of these closely eluting peaks with the same target mass further supports the supposition that the methoxy group of MeOAsp9 promotes aspartimide formation.

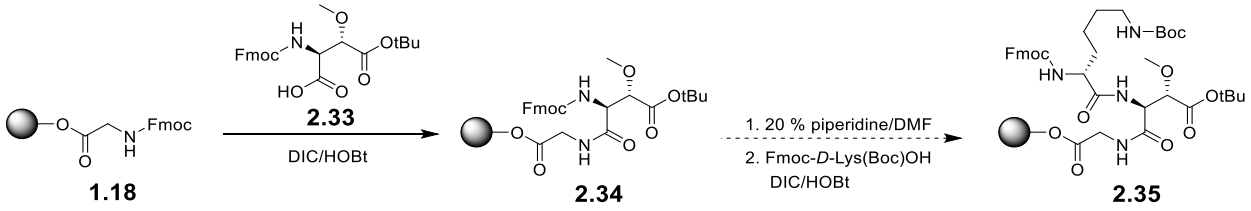

Scheme 2.7: Attempted synthesis of tripeptide **2.35** from **1.18**.

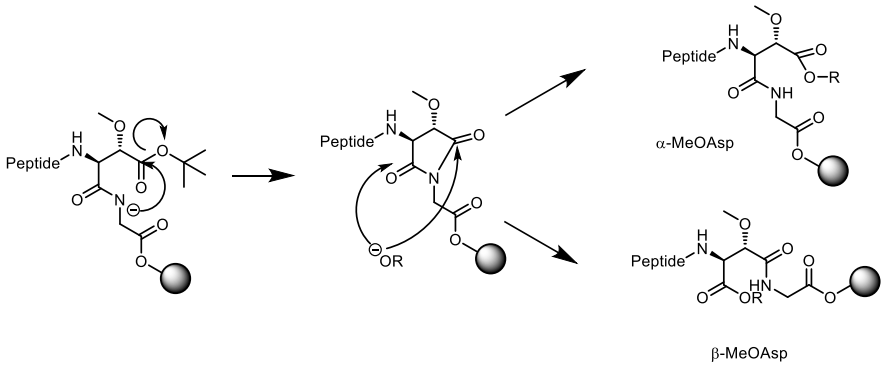

Scheme 2.8: Mechanism of aspartimide formation, leading to two isomeric products.

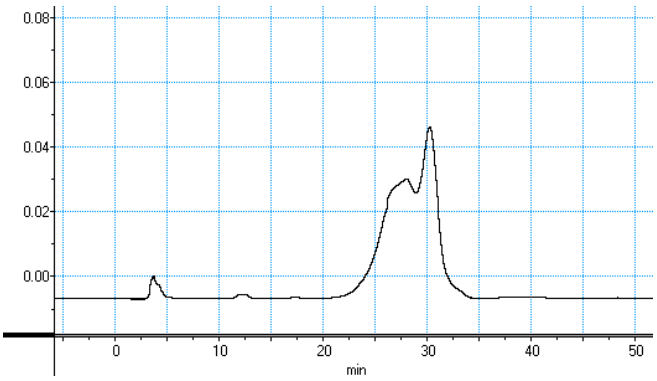

Figure 2.5: Aspartimide formation indicated by RP-HPLC. Peptide **2.35** was cleaved from the resin and analyzed by RP-HPLC. Both closely eluting peaks above had a mass corresponding to the desired peptide, suggestive of aspartimide formation (See Scheme 2.8).

In another attempt, DMB-protected Gly was attached to the resin followed by the addition of Fmoc-*t*MeOAsp(tBu)OH, yielding dipeptide **2.36** (Scheme 2.9). Unsurprisingly, attempts to incorporate Fmoc-*D*-Lys(Boc)OH also resulted in DKP formation, which is evident from almost complete absence of peaks in the HPLC chromatogram of the cleaved product (Figure 2.6). DKP formation had resulted in cleavage of the peptide from the resin.

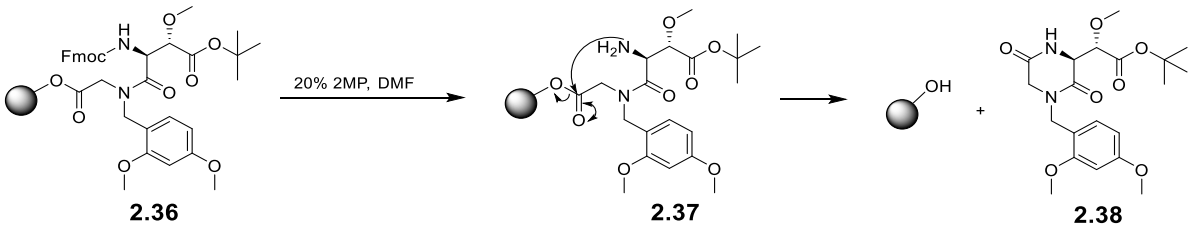

Scheme 2.9: DKP formation upon Fmoc-deprotection of dipeptide **2.36**.

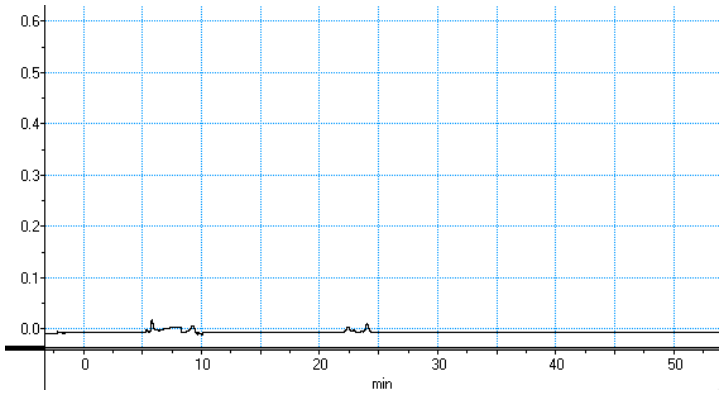

Figure 2.6: HPLC chromatogram showing very little peptide product after attempted coupling of Fmoc-*D*-Lys(Boc)OH to dipeptide **2.37**. Following resin cleavage, very little of any product was detected, indicating DKP formation upon deprotection of dipeptide **2.36**.

The strategy employed thus far involved final cyclization of the peptide between *D*-Asn11 and Gly10, chosen because glycine is achiral and thus immune to epimerization during the cyclization step. Attachment of the peptide to the resin by the sidechain of MeOAsp9 or by the α-carboxylic acid of Gly10 had proven unsuccessful due to aspartimide formation in the absence of a DMB protecting group, and DKP formation in the presence of one. We reasoned that DKP formation might be avoided if tripeptide **2.23** was obtained by the coupling of DMBGlyOallyl to dipeptide **2.39** (Scheme 2.10). In this approach, there would never be a free amino group capable of DKP formation with the allyl ester of Gly10. It should be noted, however, that the activated ester of the C-terminal end of a peptide chain is more susceptible to racemization than a single carbamate-protected amino acid, and epimerized products may be expected.

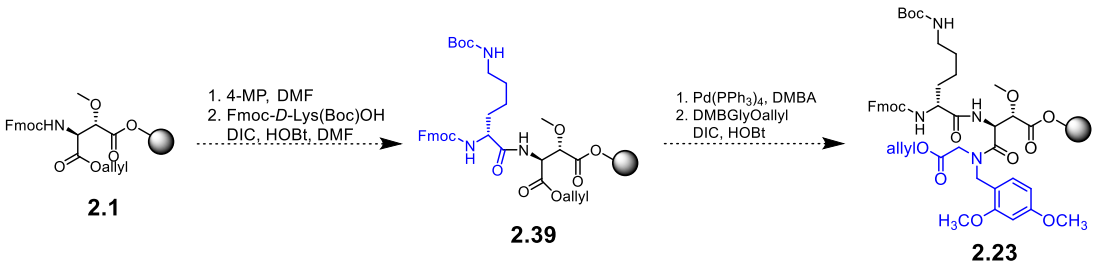

Scheme 2.10: Alternative approach to the synthesis of tripeptide **2.23**.

Dipeptide **2.39** was obtained in excellent purity employing Fmoc-SPPS, with an HPLC chromatogram consisting of a single peak following resin cleavage. After attempting to introduce DMBGlyOallyl to dipeptide **2.39**, the HPLC chromatogram revealed several different peaks (Figure 2.7), and one minor peak (t_r = 27.5 min) corresponded to the desired tripeptide **2.23** as indicated by LRMS. Another expected peak (t_r = 18.6 min) corresponded to the DMB-alcohol cleavage by-product, **2.40**. No evidence of the starting material Fmoc-*D*-Lys-*t*MeOAspOallyl or its allyl-deprotected Fmoc-*D*-Lys-*t*MeOAspOH counterpart was observed, indicating that the first step of the reaction sequence involving allyl deprotection goes to completion, as is expected using these conditions,[82,85] and further, that the allyl deprotected product Fmoc-*D*-Lys-*t*MeOAspOH necessarily underwent a subsequent reaction. The question remained, which reaction corresponded to the major product observed by HPLC?

While Fmoc-*D*-Lys-*t*MeOAspOH was not observed, we were surprised to find that the major peak (t_r = 22.5 min) on the HPLC chromatogram corresponded to Fmoc-*D*-Lys-^{DH}Asp-OH, **2.41** (Figure 2.7), where ^{DH}Asp is dehydroaspartic acid, formed by the elimination of the methoxy group. Further, an additional peak (t_r = 32.0) was found to correspond to tripeptide Fmoc-*D*-Lys-^{DH}Asp-(DMB)Gly-OH, **2.42**. Taken together, the presence of these peaks led us to conclude that the methoxy group had been eliminated in a side reaction during activation of the allyl deprotected peptide. We propose that O-acyl urea intermediate **2.43** underwent an intramolecular acid-base reaction and removed the proton from the α-position of *t*MeOAsp (Scheme 2.11). Elimination of the methoxy group, likely by an $E1_{CB}$ mechanism, yielded Fmoc-D-Lys-^{DH}Asp-OH after cleavage from the resin (**2.41**). Dipeptide **2.43** could also undergo the expected amino acid coupling, yielding tripeptide **2.23** (Scheme 2.11). By HPLC

and LRMS, it was also demonstrated that the DMB-protecting group of tripeptide **2.42** was not removed during resin-cleavage involving a 1-hour treatment of 95:2.5:2.5 TFA/TIPS/H_2O.

While it may have been possible to avoid this side reaction by using different coupling reagents, the high probability that this route would lead to, at the very least, epimerization of the MeOAsp residue via oxazalone formation or via direct α-deprotonation prompted us to explore an alternative route.

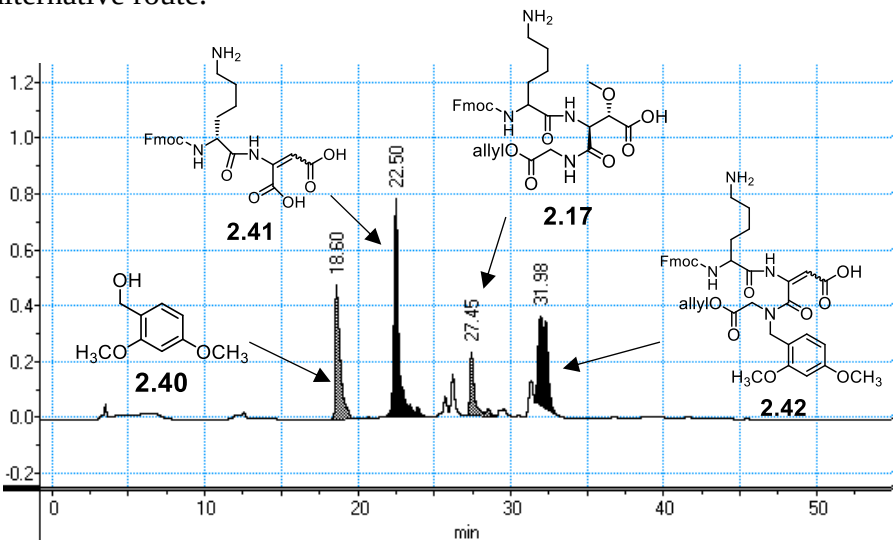

Figure 2.7: HPLC chromatogram of cleaved products after attempted synthesis of **2.23**.

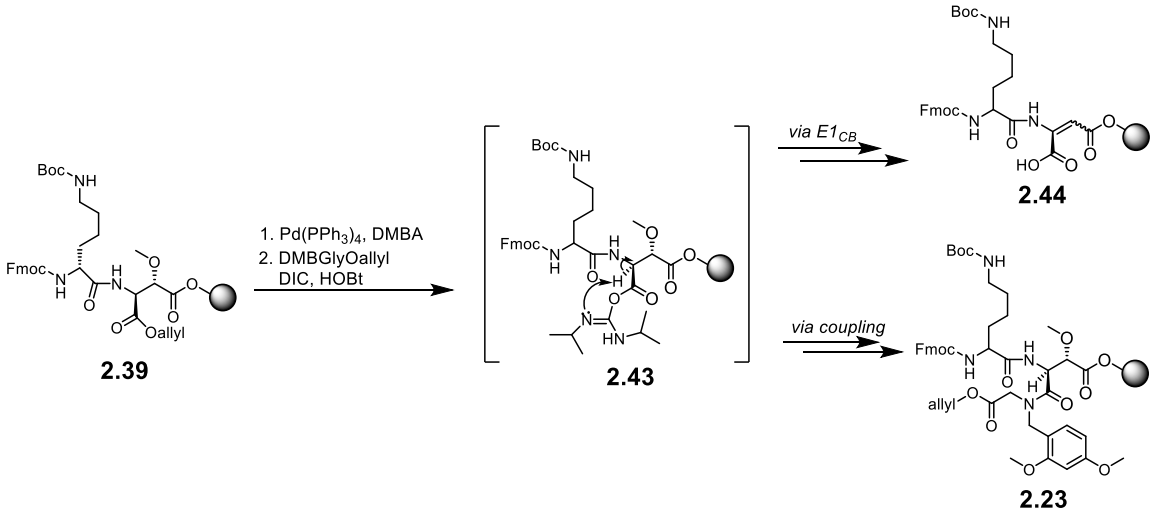

Scheme 2.11: Proposed mechanism leading to Fmoc-*D*-Lys-^{DH}AspOH (**2.44**)

2.2.3 – Second Approach to A54145D

The key advantage of our previously attempted routes to A54145D was that the final cyclization was to take place between *D*-Asn11 and Gly10, thus avoiding issues of epimerization, as Gly10 is achiral. This strategy was successfully employed by Lohani et al. in their total synthesis of daptomycin.[85] A54145D has an additional achiral amino acid: Sar5. With this in mind, we envisioned a total synthesis of A54145D which would begin with attachment of Sar5 to the resin through its α-carboxyl group, yielding **2.45** (Scheme 2.12). Incorporation of residue 4 would yield dipeptide **2.46**, and residue 3 would yield tripeptide **2.47**. Formation of the depsi-bond with N_3IleOH would yield branched peptide **2.48**, and subsequent Fmoc-SPPS would yield **2.49**. Reduction of the azido group followed by further Fmoc-SPPS would yield uncyclized peptide **2.50**, and resin cleavage, off-resin cyclization, and finally global deprotection would yield A54145D (A54145D-*t*HOAsn3-*t*MeOAsp9).

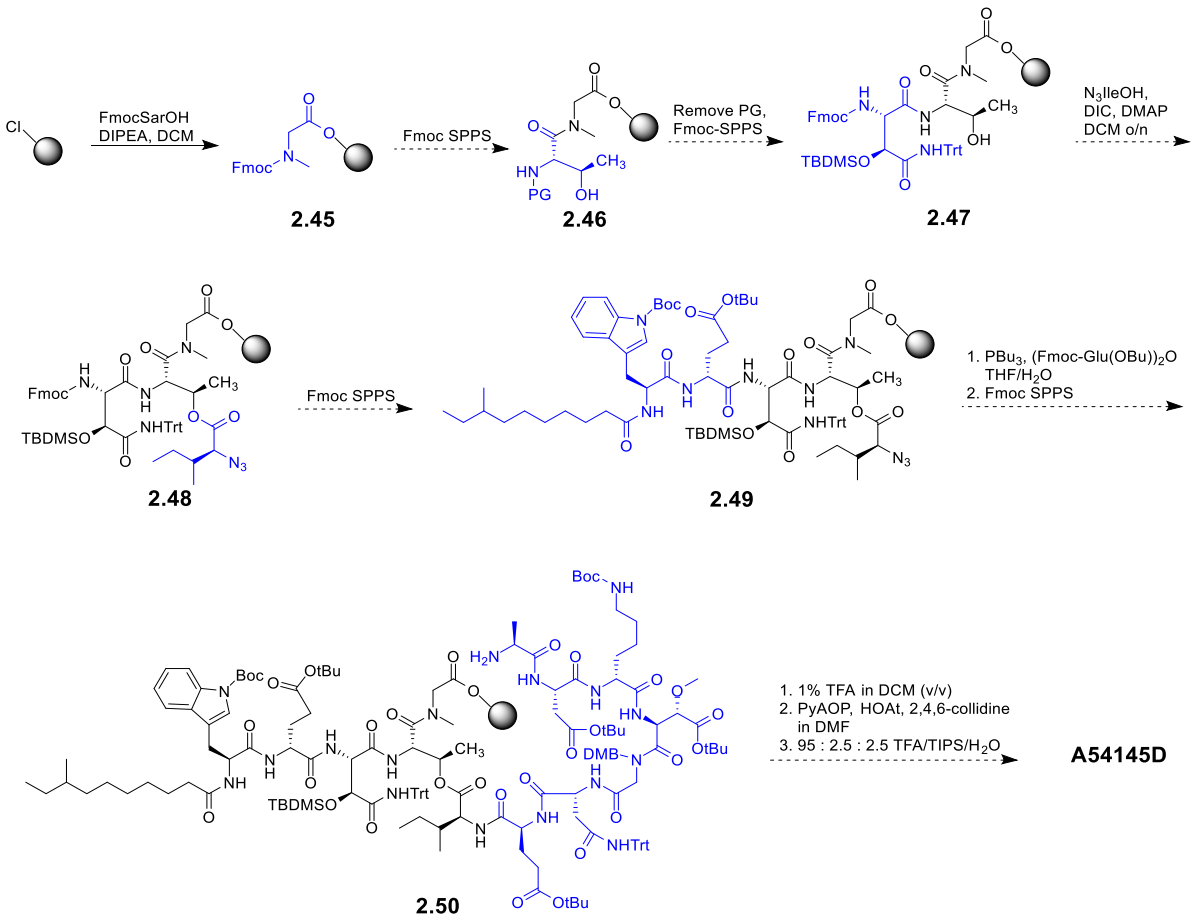

Scheme 2.12: Proposed synthesis of A54145D via Sar5 resin-attachment.

This approach was expected to be advantageous for several reasons. Firstly, the Taylor lab had shown that formation of the ester bond in daptomycin became more difficult with increasing length of the peptide containing the Thr residue, and it was very difficult when the lipid tail was present.[85] We therefore expected that forming the ester-bond in **2.48** would be less synthetically challenging than the initial approaches discussed above, which involved forming a depsi bond on octapeptide **2.3** (Scheme 2.1). Additionally, aspartimide formation between Gly10 and *t*MeOAsp9 could be avoided with the use of a DMB-protecting group, while simultaneously avoiding DKP formation between *t*MeOAsp9 and Gly10. However, a disadvantage of attaching the peptide to the resin by Sar5 is that FmocAA-Sar esters (where

AA is any amino acid) can also undergo DKP formation of the terminal amino group upon deprotection of the Fmoc group.[95] Nevertheless, we expected that DKP formation during the deprotection of peptide **2.46** could be reduced using carefully selected deprotection conditions.

2.2.3.1 – Attempts to Avoid DKP Formation between Thr4 and Sar5

Knowing that DKP formation might be an issue in our synthesis, we spent some time optimizing a method for the determination of exactly how much DKP was being formed, through Fmoc loading checks at each stage of the synthesis. In all our studies, resin-loading was estimated using a procedure modified from Gude et al.[96]

In 2002, Gude et al. reported a method for the quantification of Fmoc-derivatized solid phase supports.[96] In their approach, an aliquot of the resin is treated with 20 mL 2% DBU in DMF to remove the Fmoc group. The reaction mixture is subsequently diluted in acetonitrile and the dibenzofulvene product quantified by absorbance based on a molar coefficient of 7624 mol^{-1} L cm^{-1} at 304 nm. Employing Beer-Lambert's law, A = εbc, where A is the absorbance, ε is the molar extinction coefficient, b is the path-length of the cuvette, and c is the concentration of dibenzofulvene deprotection product, and accounting for the dilution factor and the initial volume, the researchers were able to quantify resin-loading according to the following equation:

$$Loading_{(mmole/g)} = Absorbance_{304\,nm} \times \frac{163.96}{mg\ resin}$$

This equation is used to estimate the loading of a peptide on resin when the substitution of the resin is low, as is the case for TentaGel TrtCl resin (theoretical loading = 0.23 mmol/g). However, when the theoretical loading is high, with 2-ClTrt-Cl resin (theoretical loading = 1.5 mmol/g), the equation above fails to accurately assess the loading.

Consider the situation where 2-ClTrt-Cl-PS with a theoretical loading of 1.5 mmol/g is used in peptide synthesis. Choosing an initial scale of 0.1 mmol would require 66 mg of resin, and if the loading of the first amino acid (FmocSarOH) was 95% efficient, then the amount of FmocSarOH present on the resin after the initial coupling would be approximately 30 mg (311 g/mol * 0.1 mmol * 0.95 = 30 mg). Therefore, an aliquot of resin chosen for loading is approximately 31% amino acid by mass, and 69% of the mass corresponds to the original resin (30 mg / (30 + 66) mg *100% = 31%), meaning that a large portion of the aliquot chosen for Fmoc quantification should not be considered in the resin-loading calculation. On the other hand, if low-loading TentaGel Trt-Cl resin with a theoretical loading of 0.23 mmol/g was used, an initial scale of 0.1 mmol would require 435 mg of resin. If the loading of the first amino acid was 95% efficient, the mass of FmocSarOH present after the initial coupling would still be 30 mg, which accounts for approximately 6% of the resin's new total mass (30 mg / (30 + 435) mg *100% = 6%). In practice, the mass of the resin does increase significantly when 2-ClTrt-Cl-PS resin is used (as is expected, given that all amino acids have a higher mass than chlorine), further demonstrating that the mass of the peptide must be accounted for when determining the amount of resin-loading.

The equation presented by Gude et al.[96] makes no consideration of the mass of the peptide in its calculation. In our approach to quantifying resin loading, we used 2 mL of 2% DBU in DMF, and accounting for the mass of the peptide, a new equation was developed:

$$Loading_{(mmole/g)} = \frac{Abs_{304} * 16.396}{(mg\ resin) - Abs_{304} * \left(\frac{MW - 35.45}{1000}\right) * 16.396}$$

In this new equation, where MW = molecular weight of the amino acid, the actual mass of the resin is corrected with the additional term in the denominator, which removes the portion

of mass that is the direct result of coupling an amino acid to the resin. The other advantage of this modified equation is that it can be used to determine the loading of the resin at multiple stages of the synthesis, since the increased mass of the peptide is accounted for. The loading of a tripeptide can be determined just as easily as the loading of a single amino acid. This is advantageous, as it allows for the determination of DKP formation, simply by quantifying the amount of Fmoc signal present both before and after amino acid coupling attempts.

Efforts to circumvent DKP formation were reported by Thieriet et al. in 1997.[97] In this approach, the *N*-terminus of dipeptides bearing an *N*-terminal Alloc protecting group were deprotected under neutral conditions using $Pd(PPh_3)_4$ and $PhSiH_3$ as the allyl scavenger, in the presence of an activated amino acid. This tandem deprotection-coupling procedure was reported to reduce DKP formation to as little as 2%. In 2001, Zorn et al. reported that $Pd(PPh_3)_4$ and DABCO (1,4-diazabicyclo[2.2.2]octane) could also be used, and successfully applied these conditions to the deprotection and subsequent coupling of an activated amino acid to an *N*-terminal Alloc-protected proline-proline dipeptide on a Wang resin, which is highly prone to DKP formation when deprotected.[98] Inspired by these observations, we attempted to synthesize model tripeptide **2.51** (FmocAsn(Trt)ThrSarOH) by coupling FmocAsn(Trt)OH to resin-bound AllocThrSar (**2.46a**, Table 2.1, entries 1-4). Following the attempted amino acid coupling, a portion of the peptide was cleaved from the resin with 95:2.5:2.5 TFA/TIPS/H_2O and analyzed by RP-HPLC to detect the desired peptide. If desired peptide was present, the quantity was then determined by performing a resin-loading analysis.

Initial attempts to form tripeptide **2.51** using the approaches of Thieriet et al. and Zorn et al. were unsuccessful (Table 2.1, entry 1). On both TentaGel Trt-Cl resin and 2-ClTrt-Cl-PS resin, deprotection of the Alloc group using these tandem conditions failed to yield the desired

peptide. It is unknown whether DKP formation had caused cleavage of the peptide from the resin, or if the deprotected peptide simply failed to react with the activated ester under these conditions, because DCM was used as the solvent. Deallylations using DMBA as the allyl scavenger and DCM as a solvent for both the deallylation and the coupling reactions, performed either in tandem or sequentially, produced only trace amounts of desired tripeptide (entries 2 and 3). However, when allyl deprotection was performed using $Pd(PPh_3)_4$/DMBA in DCM, followed by coupling of activated FmocAsn(Trt)OH in DMF, the desired tripeptide was obtained in a 44% yield on TentaGel Trt-Cl resin, and 49% on 2-ClTrt-Cl resin (Table 2.1, entry 4). This supports the notion that DCM is ineffective as a solvent for peptide coupling reactions. No further attempts for tandem deprotection-coupling were made, although it may be of interest to attempt tandem Alloc-deprotections and Fmoc-amino acid couplings with DMF as the solvent in an attempt to ameliorate this issue.

Siow et al. in their synthesis of jahanyne reported that DKP formation could be minimized using 2-MP and short Fmoc deprotection times. Accordingly, we attempted to reduce DKP formation using 2-MP and carefully controlled reaction times. When three 10-minute iterations of 2-MP in DMF were used for Fmoc deprotection of Fmoc-protected dipeptide **2.47b**, none of the desired peptide was obtained when the peptide was attached to TentaGel Trt-Cl resin (Table 2.1, entry 5). Surprisingly, when 2-ClTrt-Cl-PS resin was used, with three 10-minute iterations of 20% 2-MP treatment, the desired peptide was obtained in a 26% yield. Reducing the deprotection to two 5-minute iterations (entry 6) formed the desired peptide in 34% yield with TentaGel, and 73% yield with 2-ClTrt-Cl. When the deprotection time was reduced to only two 1-minute iterations of 20% 2-MP in DMF, the desired tripeptide **2.51** was obtained in almost quantitative yield (Entry 7).

Table 2.1: Conditions examined for coupling FmocAsn(Trt)OH to peptides **2.46a** or **2.46b**.

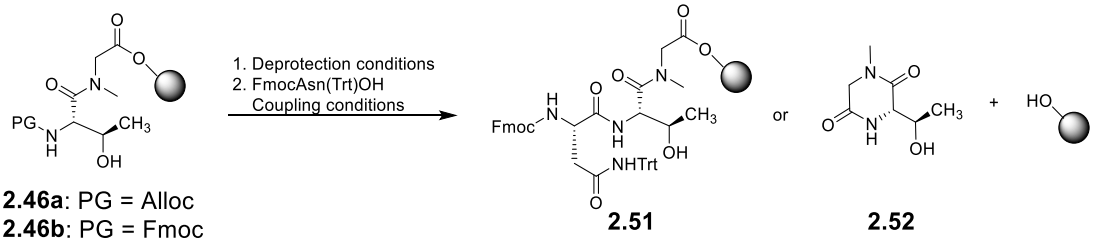

2.46a: PG = Alloc
2.46b: PG = Fmoc

2.51 **2.52**

Entry	PG	Deprotection Conditions	Coupling Reagents	sequential or tandem	Yield of **2.51** (%)
1	Alloc	12 equiv of DABCO or $PhSiH_3$, 0.2 equiv of $Pd(PPh_3)_4$, DCM	3 equiv of AA/HOBt/EDC or DIC	tandem[a]	0[c]
2	Alloc	10 equiv of DMBA, 0.2 equiv of $Pd(PPh_3)_4$, DCM	4 equiv of AA/HOBt/DIC	tandem[b]	0[d]
3	Alloc	10 equiv of DMBA, 0.2 equiv of $Pd(PPh_3)_4$, DCM, 1 h	4 equiv of AA/HOBt/DIC in DCM	sequential	trace[d]
4	Alloc	10 equiv of DMBA, 0.2 equiv of $Pd(PPh_3)_4$, DCM, 1 h	4 equiv of AA/HOBt/DIC in DMF	sequential	44[d], 49[e]
5	Fmoc	20% 2-MP in DMF, 3 x 10 min	4 equiv of AA/HOBt/DIC in DMF	sequential	0[d], 26[e]
6	Fmoc	20% 2-MP in DMF, 2 x 5 min	4 equiv of AA/HOBt/DIC in DMF	sequential	34[d], 73[e]
7	Fmoc	20% 2-MP in DMF, 2 x 1 min	4 equiv of AA/HOBt/DIC in DMF	sequential	99[e]

[a] Tandem reaction conducted for 2 h. [b]Tandem reaction conducted for 4 h. [c] TentaGel or 2-ClTrt-Cl resin. [d]TentaGel resin. [e]2-ClTrt-Cl resin.

It is possible that the ester bond between sarcosine and the resin is more susceptible to attack by the amino group of the unprotected threonine residue with TentaGel resin than 2-ClTrt-Cl-PS resin. Because of the PEG linker found in TentaGel, the peptide attached to TentaGel is expected to have more mobility in solution, and this could increase the rate of DKP formation.

We initially used Fmoc-*t*HOAsn(Trt, TBDMS)OH for the synthesis of A54145D. Thus, peptide **2.46b** was deprotected using the conditions outlined in entry 7 in Table 2.1 and Fmoc-*t*HOAsn(Trt, TBDMS)OH was coupled to the resulting deprotected dipeptide using DIC/HOBt. However, the coupling was sluggish and, based upon the lower than expected signal intensities by analytical RP-HPLC of subsequent amino acid couplings, we suspected

that increased DKP formation was again an issue. Therefore, we decided to try the less sterically encumbered Fmoc-*t*HOAsn(TBDMS)OH building block.[91] In this case, the coupling proceeded smoothly and tripeptide **2.53** was formed in almost quantitative yield (Scheme 2.13).

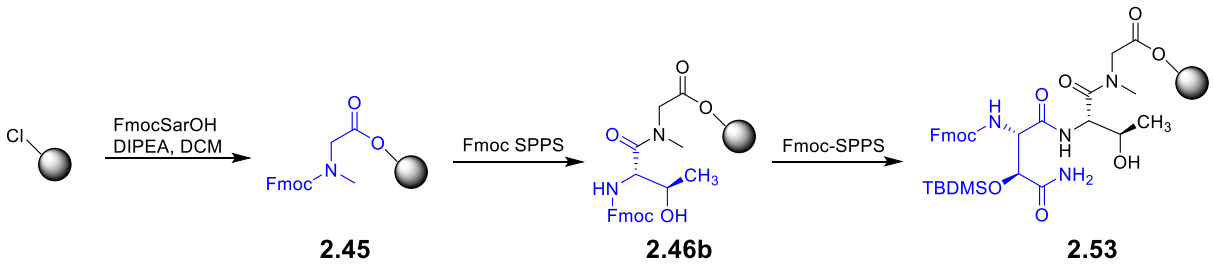

Scheme 2.13: Synthesis of tripeptide **2.53** after shortened deprotection times.

2.2.3.2 – Difficulties in Deprotection of Resin-bound FmocSar

While DKP formation could be avoided using reduced deprotection times on 2-ClTrt-Cl-PS resin, it is worth mentioning the difficulty experienced in attempting to remove the Fmoc group of resin-bound FmocSar (**2.45**, Scheme 2.13). Typically, the Fmoc-group can be removed without issue from resin-bound amino acids using two 10-minute treatments with 20% piperidine in DMF, and this was indeed the case for FmocSarOH bound to TentaGel Trt-Cl resin. Unfortunately, attempts to remove the Fmoc group from **2.45** proved problematic, which has received little mention in the literature.

In the first attempted synthesis of dipeptide **2.46a**, **2.45** was subjected to 20% 4-MP in DMF (1 x 5 min, 1 x 20 min) and the resulting unprotected sarcosine allowed to react with AllocThrOH with DIC/HOBt. After Alloc-removal and coupling of FmocAsn(Trt)OH in DCM (Table 2.1, entry 3), a portion of the resin was cleaved for HPLC analysis, revealing a single peak as shown in Figure 2.8. While the presence of a single peak in an analytical RP-HPLC

chromatogram is generally desired during HPLC analysis, we were dismayed when LRMS revealed this peak to correspond to FmocSarOH. The presence of this protected amino acid indicated that when FmocSarOH is the only amino acid attached to 2-ClTrt-Cl resin, it is more resistant to Fmoc-deprotection than other amino acids, and this observation was only slightly ameliorated when the resin was allowed to swell for longer periods of time. We were initially surprised by this result, but came upon the work of Malakoutikhah et al., who reported in 2008 alternative Fmoc-deprotection conditions to remove the Fmoc group from resin-bound Fmoc-*N*-methylphenylalanine (Fmoc-*N*-MePheOH).[99] In their work, most Fmoc-groups were removed by simple treatment of 20% piperidine in DMF (2 x 1 min, 1 x 10 min), but this was not the case for resin-bound Fmoc-*N*-MePheOH. Removal of the Fmoc-group in resin-bound Fmoc-*N*-MePheOH required an additional 5-minute treatment with 1,8-diazabicyclo[5.4.0]undec-7-ene (DBU), toluene, and piperidine in DMF (5%, 5%, 20%, v/v).

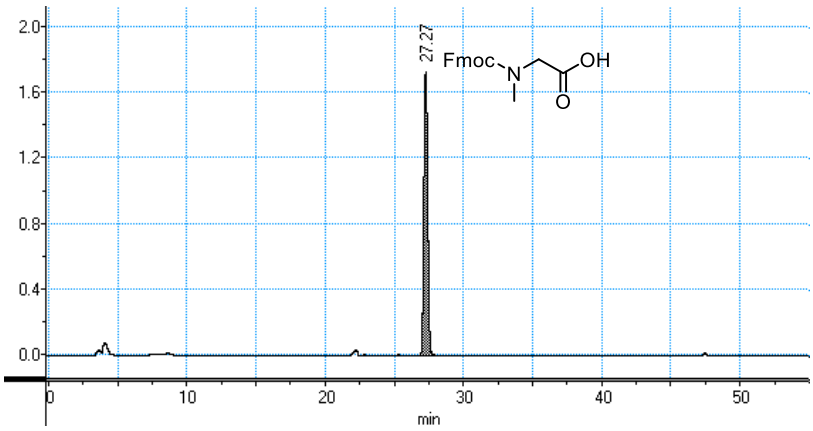

Figure 2.8: Presence of FmocSarOH observed after attempted formation of tripeptide **2.51**.

To resolve this issue, **2.45** was subjected to conditions similar to those reported by Malakoutikhah et al., except 4-MP was used in place of piperidine. Nevertheless, protected FmocSarOH was still observed by HPLC and LRMS (Figure 2.9A). However, treatment of the peptide with an extended 75-minute treatment of DBU, toluene and 4-MP in DMF (5%, 5%,

20%, v/v) effectively removed the Fmoc-group quantitatively (Figure 2.9B). Furthermore, extended deprotection times (3 x 30 min) with 20% 4-MP in DMF (Figure 2.9C) or with 5% DBU (3 x 30 min) in DMF (Figure 2.9D) were also effective in removing the Fmoc-group. It is worth noting that the HPLC chromatograms in Figures 2.8 and 2.9 can detect FmocSarOH because of the presence of the chromophoric fluorenyl group. However, the product of Fmoc-deprotection, unprotected sarcosine, possesses no chromophore, and therefore is not detectable by HPLC analysis using a UV detector. Accordingly, these HPLC chromatograms will only show the lack of starting material, and not the presence of product. Having finally established conditions suitable for completely removing the Fmoc-group of FmocSarOH while avoiding DKP formation of FmocThrSarOH, we were poised to continue our synthesis of A54145D.

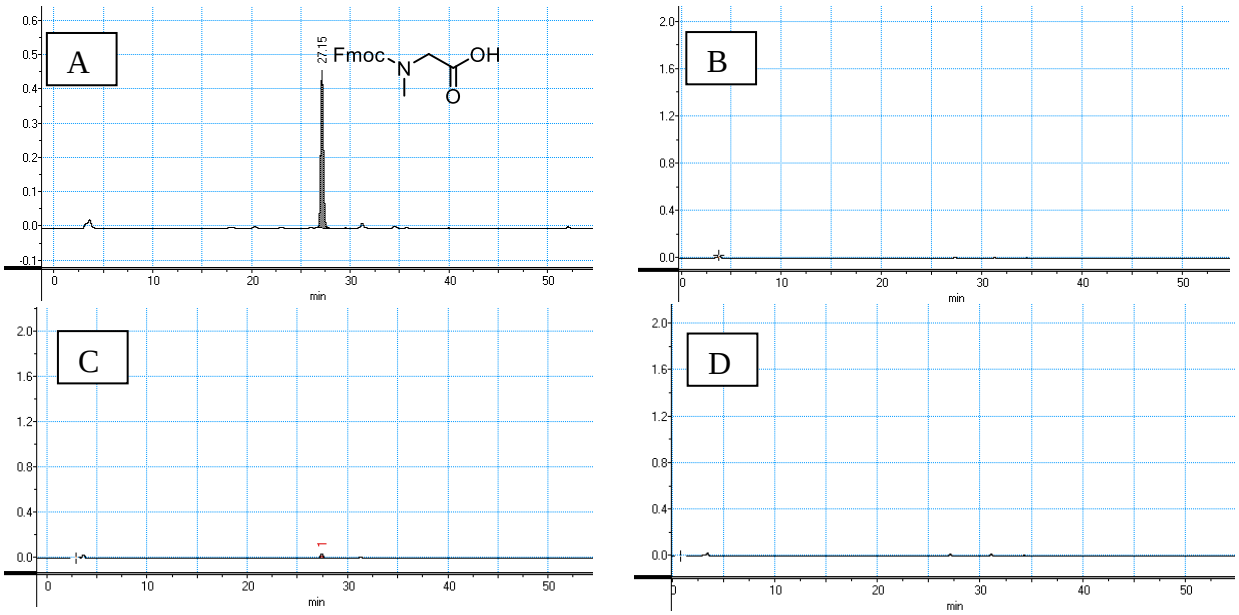

Figure 2.9: Attempted Fmoc-deprotections of FmocSar on 2-ClTrt-Cl resin. (A) partial deprotection observed when employing the conditions used by Malakoutikhah et al.[99] (B) Complete deprotection observed after extended treatment with 5:5:20:70 DBU/Toluene/ 4-MP/DMF. (C) Complete deprotection observed after extended treatment with 20% 4-MP in DMF. (D) Complete deprotection observed after extended treatment with 5% DBU in DMF.

2.2.3.3 – Total Synthesis of A54145D-*t*HOAsn-*t*MeOAsp

Tripeptide **2.53** was obtained in almost quantitative yield from **2.46b** employing two 1-minute iterations of 20% 2-MP in DMF, followed by coupling of Fmoc-*t*HOAsn(OTBDMS)OH with DIC and DMAP (Scheme 2.14). Ester bond formation between tripeptide **2.53** and N_3IleOH (synthesized according to the procedure of Kim et al.,[100] except that imidazole-1-sulfonyl azide hydrochloride[101,102] was used in place of triflic azide) with DIC/DMAP was performed without issue after one 12 h coupling, and no subsequent epimerization of Ile13 was observed. Fmoc-SPPS was used to incorporate *D*-Glu2, Trp1, and racemic lipid **2.14** into peptide **2.54** to give peptide **2.55**. At this point, we noticed that the cleavage cocktail 95:2.5:2.5 TFA/TIPS/H_2O was no longer effective in removing the TBDMS protecting group from *t*HOAsn(OTBDMS), indicating that at a later point in the synthesis, it would need to be removed by treatment with TBAF.

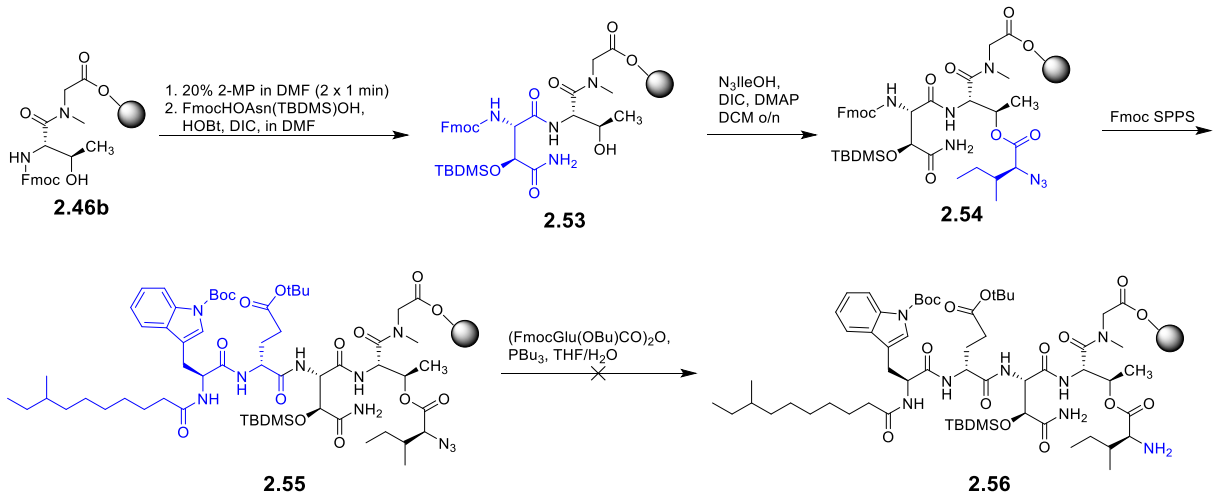

Scheme 2.14: Unsuccessful synthesis of peptide **2.56**.

Reduction of the N_3 group of peptide **2.55** was attempted with PBu_3 in 95:5 THF/H_2O in the presence of the symmetric anhydride of FmocGlu(tBu)OH,[103] but HPLC analysis of the

reduced product indicated a complex mixture of products (Figure 2.10). The major product (t_r = 30 min) could not be identified, and the desired product (t_r = 40 min, **2.57**) was only present in minute amounts. Reduction of the azido group using alternative conditions of DTT and DIPEA was sluggish. In fact, two overnight attempts of azido reduction using DTT and DIPEA resulted in less than 50% reduction as indicated by HPLC.

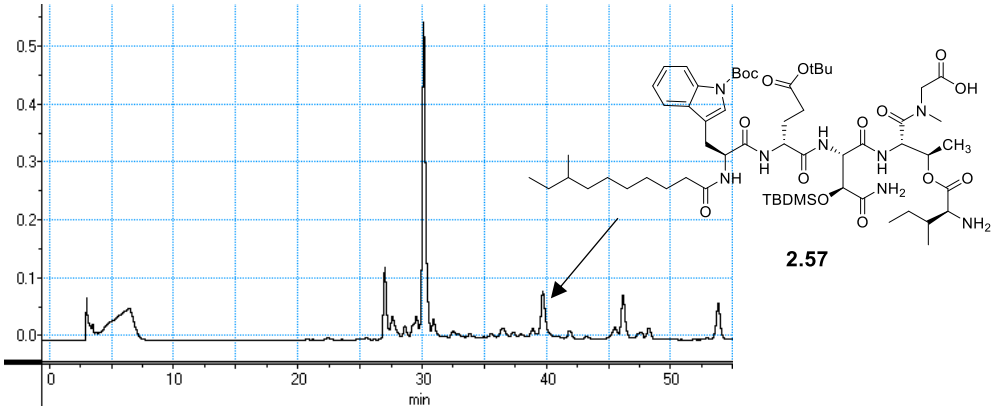

Figure 2.10: HPLC chromatogram of crude peptide after azido-reduction of **2.55** with PBu_3 and resin cleavage.

Fortunately, we found that if the TBDMS group was removed with TBAF and AcOH in THF prior to N_3 reduction, the desired peptide **2.58** could be obtained almost quantitatively, suggesting that the TBDMS group participates in unknown side reactions under our reduction conditions (Scheme 2.15). Furthermore, it was suspected that the TBDMS protecting group participated in side-reactions during TFA cleavage conditions. When the progress of the reaction was analyzed by HPLC, it was found that the presence of the TBDMS protecting group resulted in somewhat complex HPLC chromatograms. However, once the TBMDS group was removed with TBAF, the apparent purities of the compounds as judged by HPLC significantly improved. Presumably, the silyl ether underwent some side reactions during the resin-cleavage step with 95:2.5:2.5 TFA/TIPS/H_2O, although the nature of these side reactions is unknown.

It is worth noting that, despite the presence of the symmetric anhydride of FmocGlu(tBu)OH during N_3 group reduction, the major product was indeed peptide **2.58** and not the FmocGlu(tBu)-coupled counterpart, consistent with previous studies in the Taylor lab.[103] The presence of the symmetric anhydride of FmocGlu(tBu)OH during azido group reduction prevents cleavage of the ester bond during this step. Accordingly, subsequent Fmoc-SPPS still required standard coupling of FmocGlu(tBu)OH using DIC/HOBt.

Standard Fmoc-SPPS from **2.58** was used to introduce residues 12 to 6 to give peptide **2.59** (Scheme 2.15). A DMB-protecting group on Gly10 was used to prevent aspartimide formation between *t*MeOAsp9 and Gly10. Peptide **2.59** was cleaved from the resin using 1% TFA in DCM (v/v) to give peptide **2.60**, which was cyclized using PyAOP/HOAt/2,4,6-collidine, followed by global deprotection with TFA/TIPS/H_2O to yield crude A54145-*t*HOAsn3-*t*MeOAsp9. Purification by semi-preparative RP-HPLC gave the target peptide in an 8% yield based on initial resin loading.

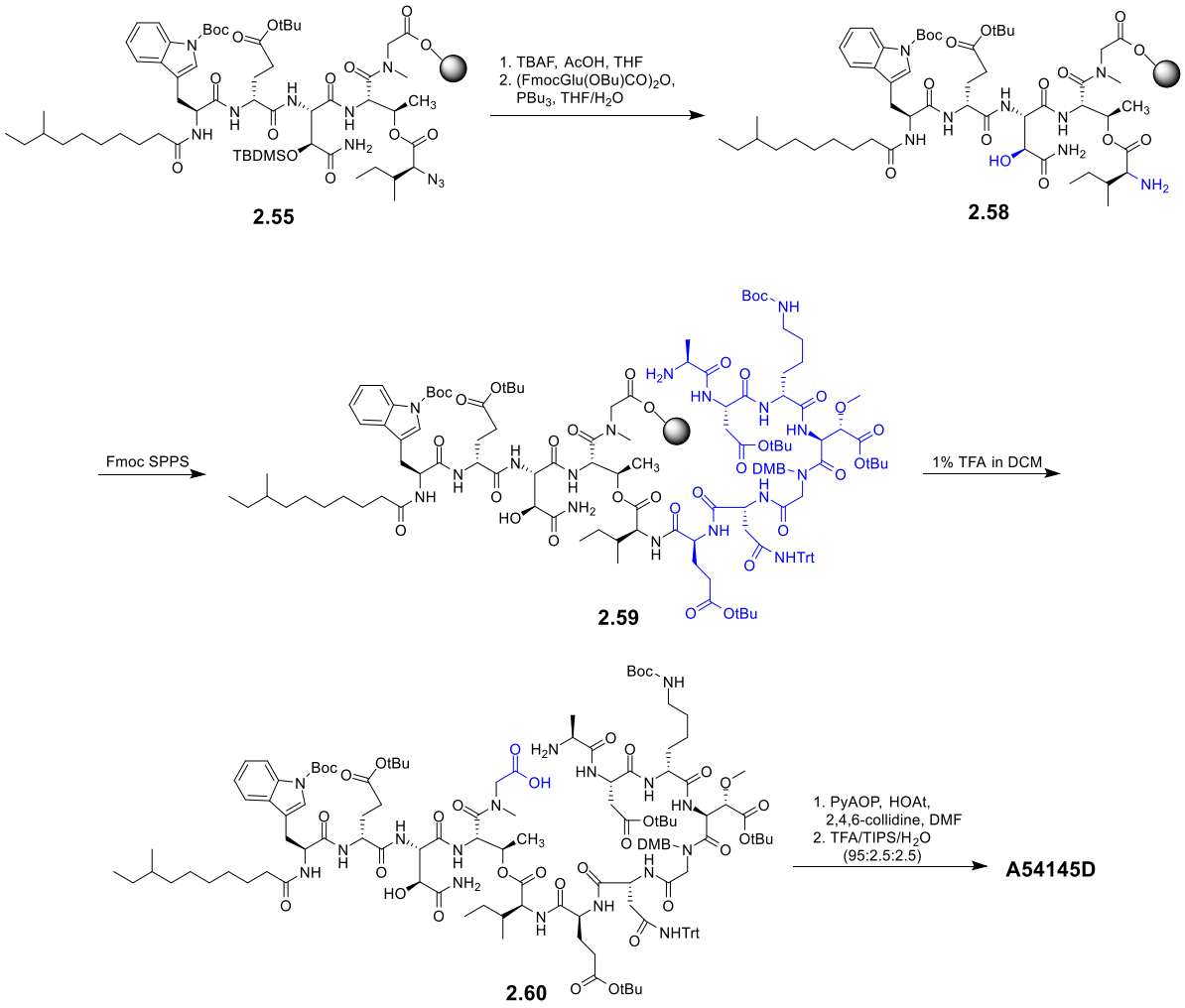

Scheme 2.15: Successful synthesis of A54145-*t*HOAsn3-*t*MeOAsp9.

The antimicrobial activity of authentic A54145D, generously provided by Jared Silverman previously of Cubist Pharmaceuticals, now owned by Merck and Co., and the activity of our synthesized A54145D-*t*HOAsn3-*t*MeOAsp9 were determined against *B. subtilis* ATCC 1046 (Table 2.2). The synthesized A54145D-*t*HOAsn3-*t*MeOAsp9 exhibited an MIC that was at least 64 times greater than that of authentic A54145D, signifying poorer biological activity, which suggested to us that the configuration of the side chain of the HOAsn3 residue and/or the MeOAsp9 residue in the synthetic peptide was incorrect. Since bioinformatics

studies strongly suggested that the HOAsn residue is the *L-threo* isomer,[88] we assumed that the problem was most likely with the MeOAsp residue.

Table 2.2: MICs of A54145D peptides.

entry	peptide	MIC (μg/mL)[a]
1	Authentic A54145D	0.5
2	A54145D-tHOAsn3-*t*MeOAsp9[b]	>32
3	A54145D-tHOAsn3-*e*MeOAsp9[c]	0.5
4	A54145D-(8*R*)-*anteiso*	0.5
5	A54145D-(8*S*)-*anteiso*	0.5

[a]Against *B. subtilis* ATCC 1046. 1.25 mM Ca^{2+} present.
[b]Putative structure of A54145D
[c]Actual structure of A54145D (see below)

2.2.3.4 – Total Synthesis of A54145D-*t*HOAsn3-*e*MeOAsp9

To test whether the low biological activity was indeed due to incorrect stereochemistry at the MeOAsp residue, Fmoc-*L-erythro*-MeOAsp(tBu)OH (Fmoc-*e*MeOAsp(tBu)OH, **2.65** in Scheme 2.16) was prepared by Ryan Moreira. The configuration of the alcohol in **2.61**[91] was inverted by first treating **2.61** with diisopropyl azodicarboxylate (DIAD), triphenylphosphine (PPh_3) and *p*-nitrobenzoic acid (PNBCOOH), and the resulting PNB ester **2.62** was then subjected to NaN_3.[104] This gave the corresponding *erythro* isomer **2.63** in excellent yield. Methylation of the alcohol in **2.63** with MeI/Ag_2O in diethyl ether at reflux gave ether **2.64** in almost quantitative yield. Removal of the benzyl group in **2.64** using Bobbit's salt[91] and oxidation of the *in situ* generated alcohol using NaO_2Cl/NaOCl gave acid Fmoc-*e*MeOAsp(tBu)OH (**2.65**) in 80% yield.

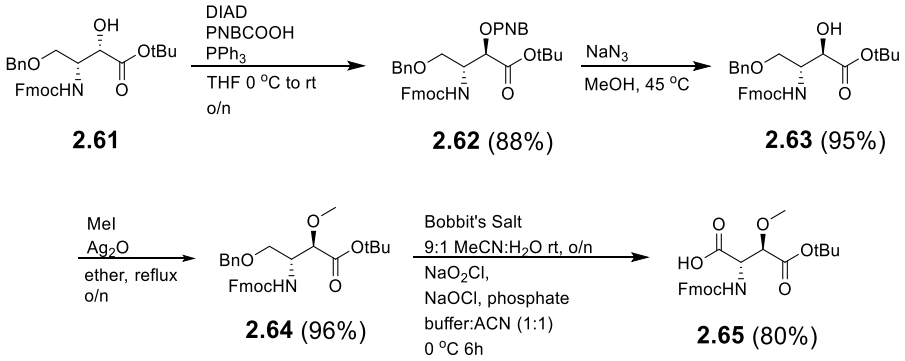

Scheme 2.16: Synthesis of Fmoc-*L*-*erythro*-MeOAsp(tBu)OH, **2.65**.

A54145D-*t*HOAsn3-*e*MeOAsp9 was prepared using the same route that was used for the *threo* isomer (Schemes 2.13, 2.14, and 2.15). After purification, the synthesized peptide was co-injected with authentic A54145D for HPLC analysis, and the two compounds co-eluted (Figure 2.11). The biological activity of A54145D-*t*HOAsn3-*e*MeOAsp9 was identical to the biological activity of authentic A54145D (Table 2.2, entry 3), indicating that this newly synthesized compound was indeed A54145D.

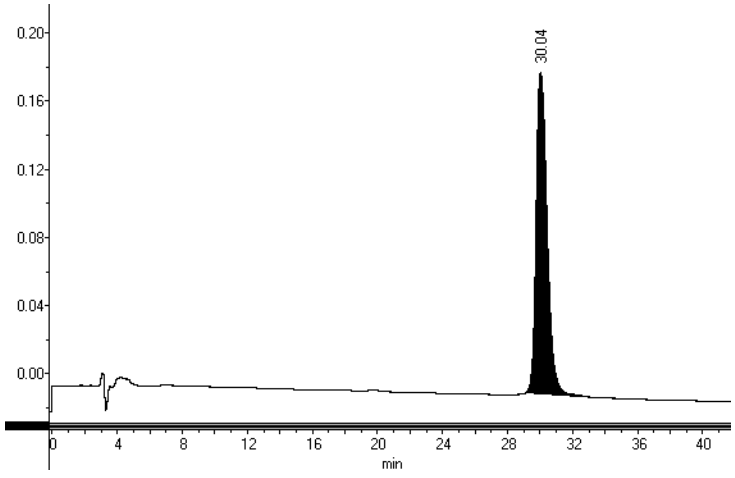

Figure 2.11: Co-injection of A54145D-*t*HOAsn3-*e*MeOAsp9 and authentic A54145D.

2.2.3.5 – Characterization of A54145D-*t*HOAsn3-*e*MeOAsp9

The ^{1}H-NMR spectrum of A54145D had been reported previously by Cubist Pharmaceuticals in the patent literature.[105] As an additional confirmation that our synthesized compound was indeed the same as authentic A54145D, we obtained a ^{1}H-NMR spectrum in D_2O. However, a direct comparison was challenging because of line-broadening issues that occur due to aggregation of the peptide (Figure 2.12).

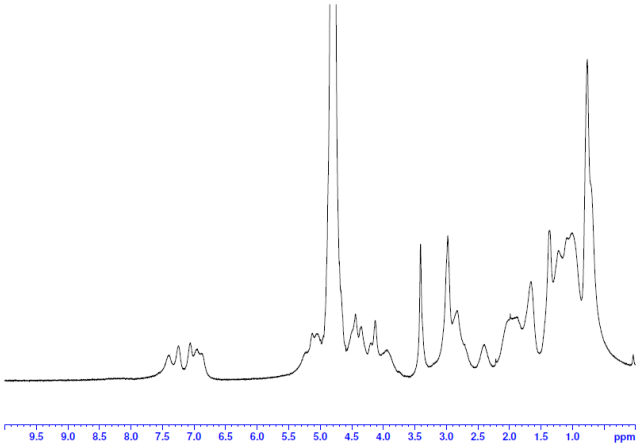

Figure 2.12: ^{1}H-NMR of A54145D-*t*HOAsn3-*e*MeOAsp9 (300 MHz, D_2O). As is the case with the literature ^{1}H-NMR spectrum of A54145D,[105] severe line broadening is observed.

To address the line-broadening problem, the nucleus of A54145D (A54145D without the lipid tail) was synthesized in the same manner as A54145D (Schemes 2.13, 2.14, and 2.15), except that Trp1 was incorporated into the resin as BocTrp(Boc)OH, no lipid tail was attached, and Fmoc-*e*MeOAsp(tBu)OH was used instead of Fmoc-*t*MeOAsp(tBu)OH. The ^{1}H-NMR of the synthetic nucleus was a good match to its literature spectrum (Figure 2.13),[106] which further indicated that we had indeed produced authentic A54145D, and that MeOAsp9 is of the *L-erythro*-configuration and not the *L-threo*-configuration as is often depicted in the literature. Additionally, this also confirmed that HOAsn in A54145D is of the *L-threo*-configuration.

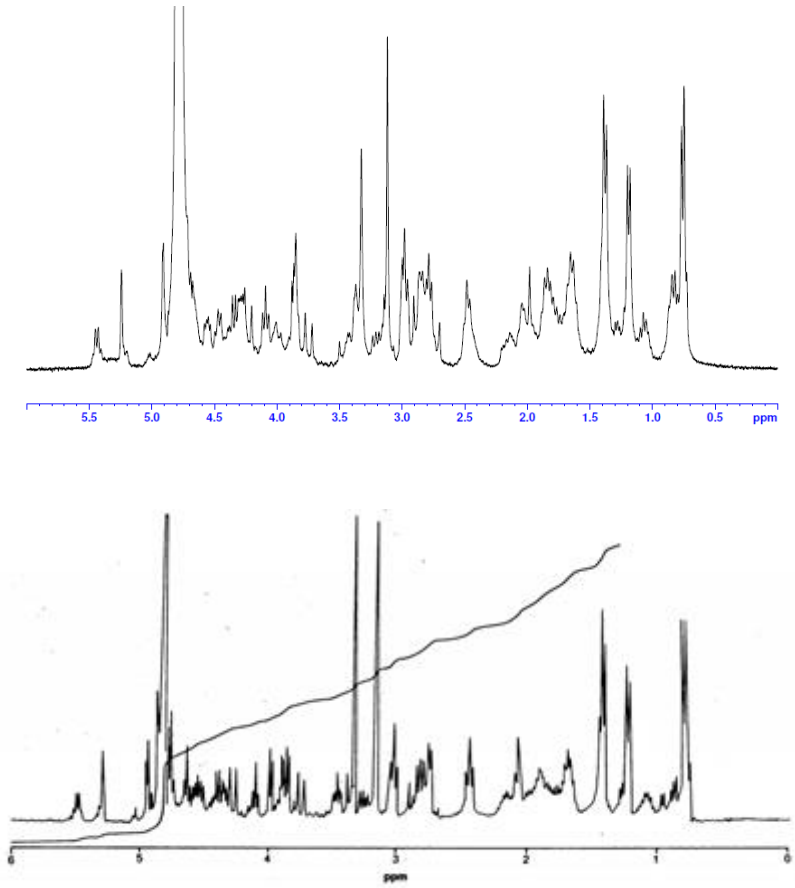

Figure 2.13: ^{1}H-NMR of synthetic A54145D-nucleus (300 MHz, D_2O, *top*) and literature spectrum (270 MHz, D_2O, *bottom*).[106]

After the comparison of the ^{1}H-NMR of our synthesized nucleus to the ^{1}H-NMR data found in the patent literature,[106] we then proceeded to completely characterize it by 1D and 2D NMR spectroscopy. An aliquot of 5 mg of the peptide was dissolved in 0.5 mL of D_2O and analyzed with 1D NMR experiments including ^{1}H-NMR, and 2D NMR experiments including ^{1}H-^{13}C HSQC, ^{1}H-^{13}C HMBC, ^{1}H-COSY, ^{1}H-TOCSY and ^{1}H-ROESY (See Figures A.1 to A.6, and Table A.1 in Appendix A).

In assigning the chemical shifts of each amino acid residue, the ^{1}H-^{13}C HSQC, ^{1}H-^{13}C HMBC, ^{1}H-COSY spectra were used to assign the chemical shifts of Trp1, Thr4, and Ile13. The ^{1}H-COSY was used to assign the chemical shifts of Sar5 and Ala6, and subsequently, ^{1}H-

^{13}C HMBC was used to assign the chemical shifts of the methyl groups of Sar5 and *e*MeOAsp9. Both the ^{1}H-COSY and the ^{1}H-TOCSY spectra were used to assign the chemical shifts of the remaining amino acids, and the ^{1}H-ROESY spectra was used to distinguish between *D*-Glu2 and Glu12, Asp7 and *D*-Asn11, and *t*HOAsn3 and *e*MeOAsp9. Following the assignments of each proton signal, the assignments of each carbon signal were made using the ^{1}H-^{13}C HSQC spectrum. Additionally, with DMSO-d_6 as the solvent, line broadening issues observed for synthesized A54145D-*t*HOAsn3-*t*MeOAsp9 and A54145D-*t*HOAsn3-*e*MeOAsp9 were avoided, and therefore, we also completely characterized these two compounds with ^{1}H-NMR, and 2D experiments ^{1}H-^{13}C HSQC, ^{1}H-^{13}C HMBC, ^{1}H-COSY, ^{1}H-TOCSY and ^{1}H-ROESY (Figures A.7 to A.12 for A54145D-*t*HOAsn3-*e*MeOAsp9, Figures A.13 to A.18 for A54145D-*t*HOAsn3-*t*MeOAsp9; and Table A.2 in Appendix A). Additionally, synthetic A54145D was characterized by MS/MS peptide sequencing (See Figure D.1 and Figure D.2 in Appendix D).

2.2.4 – Assessing the Role of Lipid Tail Stereochemistry in Biological Activity of A54145D

Although the configuration of the *anteiso*-lipid in A54145D has never been determined, Kaneda has reported that *anteiso*-lipids in Gram-positive bacteria have the *S*-configuration.[107] Furthermore, it was also established by Boeck and Wetzel that supplementing *S. fradiae* with isoleucine in the growth medium significantly increased the output of A54145 factors C, D and E (those with the *anteiso*-undecanoyl tail) from 17% of the total antibiotic to 66% of the total antibiotic.[108] From these data, it may be inferred that the side chain of isoleucine ultimately ends up in the *anteiso*-decanoyl lipid tail, and since the side-chain of isoleucine possesses *S*-stereochemistry, the notion that the lipid tail may be of the *S*-configuration is further substantiated. The fact that our synthetic A54145D, which contained a racemic lipid, exhibited the same activity as authentic A54145D suggests that the stereochemistry of the lipid does not

affect activity or that the lipid in A54145D is actually racemic. To determine if this is indeed the case, we prepared A54145D (containing the correct *L-erythro*-MeOAsp isomer) bearing either (*R*)-8-methyldecanoic or (*S*)-8-methyldecanoic acid (A54145D-(8*R*)-*anteiso* and A54145D-(8*S*)-*anteiso*, respectively). (8*R*)- and (8*S*)-methyldecanoic acid were prepared using the same route used to prepare (±)-8-methyldecanoic (Scheme 2.3, Section 2.2.1.1) except (*R*)- or (*S*)-2-methylbutanal was used instead of (±)-2-methylbutanal. (*S*)-2-Methylbutanal was readily prepared by (2,2,6,6-tetramethylpiperidin-1-yl)oxidanyl (TEMPO) oxidation of commercially available (*S*)-2-methylbutanol.[109] However, (*R*)-2-methylbutanol and (*R*)-2-methylbutanal are either not commercially available or prohibitively expensive. Ryan Moreira prepared (*R*)-2-methylbutanal using a route similar to that developed by Yang et al. for the synthesis of (*R*)-2-methylpentanal (Scheme 2.17).[110] (1*S*)-2,10-camphorsultam, **2.66**, was treated with butyryl chloride in the presence of triethylamine (TEA) and DMAP which gave sulfonamide **2.67** in 69% yield. Methylation at the 2-position of the butyryl portion of **2.67** with sodium hexamethyldisilazide (NaHMDS)/methyl iodide (MeI) gave compound **2.68** in 79 % yield. Treatment of **2.68** with diisobutylaluminum hydride (DIBAL) gave (*R*)-2-methylbutanal (**2.69**) in 33 % yield. The yield obtained for compound **2.69** was quite low, due to the volatility of this compound. We found it best to not remove all the solvent after chromatography, but instead to use it as a 40% solution in DCM in the subsequent Wittig reaction (Scheme 2.3).

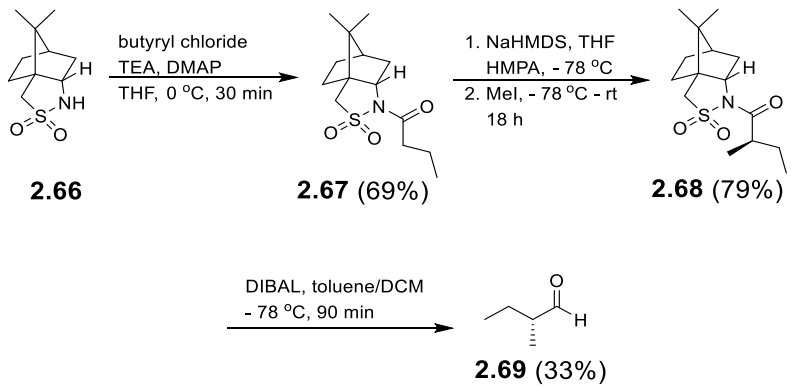

Scheme 2.17: Synthesis of (*R*)-2-methylbutanal (**2.69**).

With the enantiomerically pure lipid tails in hand, two more A54145D peptides were synthesized using the same route outlined in Schemes 2.13, 2.14 and 2.15, except that Fmoc-*e*MeOAsp(tBu)OH, and (8*R*)- or (8*S*)-methyldecanoic acid were used. The biological activities of A54145D-(8*R*)-*anteiso* and A54145D-(8*S*)-*anteiso* were determined against *B. subtilis* ATCC 1046 (Table 2.2, entries 4 and 5), and it was found that the biological activities of these two compounds were identical to those of authentic A54145D and A54145D-*t*HOAsn3-*e*MeOAsp9. While these results fail to ascertain the true stereochemistry of the lipid tail in A54145D, they nevertheless demonstrate that the biological activity of A54145D is unaffected by the stereochemistry of the lipid tail.

2.3 – Conclusions

Very recently, and while the work described here was nearing completion, Chen et al. reported the total synthesis of A54145 factors A, A1, B, B1 and F, the stereochemical revision of the MeOAsp, and also confirmed that the HOAsn3 residue is the L-*threo* isomer.[111] Their approach was to attach the peptide to the resin via Gly10 (**1.18** in Scheme 2.6, Section 2.2.2); however, the yields obtained were low (3 %). Our studies suggest that the low yields may have

been due to aspartimide formation. Having to make the ester bond on a 10-mer containing the lipid tail may also have contributed to the low yields. In contrast, we have devised a more efficient synthesis of A54145D. Consistent with the studies of Chen et al.,[111] we found that the MeOAsp9 residue has the 2*S*,3*R* configuration. In addition, we demonstrated that the stereochemistry of the *anteiso*-undecanoyl lipid tail does not affect biological activity.

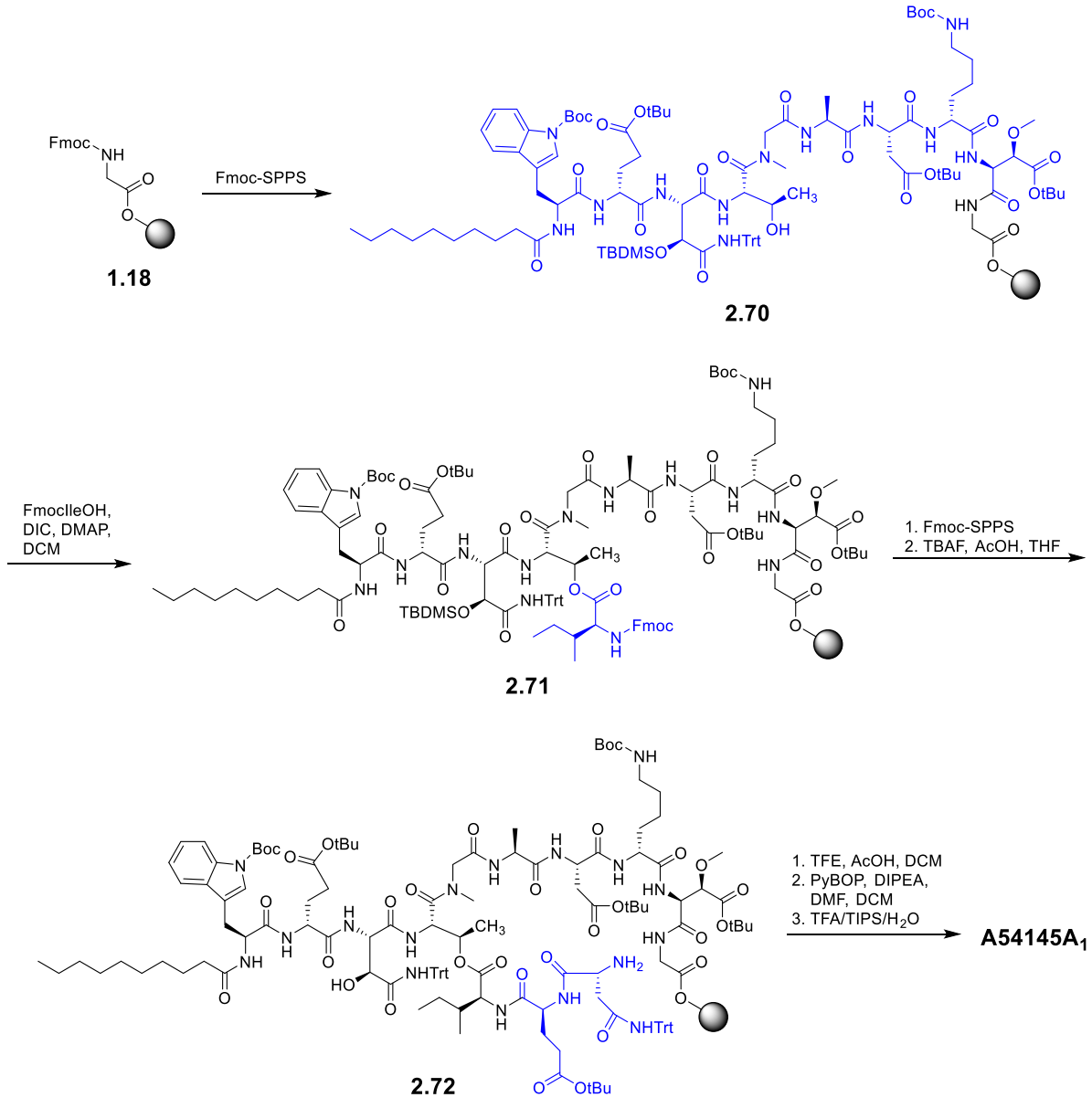

Scheme 2.18: Synthesis of A54145A$_1$ reported by Chen et al.[111]

The total synthesis of A54145D reported here is more efficient than that of Chen et al.,[111] and key challenges in the synthesis have been overcome. This total synthesis opens the door for the synthesis of A54145D analogs to establish SARs, which could lead to the development of novel antibiotics for treating CAP. For example, can the non-proteinogenic amino acids be replaced with more commercially available ones? Are other amino acids in the structure of A54145D amenable to substitution without loss of activity? With a successful approach for the synthesis of A54145D analogs in hand, we turned our attention to the synthesis of A54145D analogs. This research is presented in Chapter 3.

2.4 – Experimental

2.4.1 – General Experimental

All reagents used for peptide synthesis were obtained from commercial sources including coupling reagents, resins, and Fmoc amino acids. ACS grade *N,N'*-dimethylformamide (DMF), 4-methylpiperidine (4-MP), 2-methylpiperidine (2-MP), TFA, dimethylbarbituric acid (DMBA), and triisopropylsilane (TIPS) were purchased from commercial suppliers and used without further purification. CH_2Cl_2 (DCM) was distilled from calcium hydride under nitrogen. THF was distilled from sodium metal and benzophenone under nitrogen. Peptide synthesis was performed manually using a rotary mixer for agitation.

Peptide syntheses were monitored by treating small aliquots of resin with 95:2.5:2.5 TFA/TIPS/H_2O for 1.5 h, removing the solvent by N_2 stream, re-dissolving the peptide in 1:1 MeCN/H_2O and analyzing by RP-HPLC and LRMS.

Analytical HPLC was accomplished with a reversed-phase C18 column (10 µm, 250 mm × 4.6 mm, 1 mL/min flow rate). Peptides were purified by reversed phase semi-preparative

HPLC using a C18 column (10 µm, 150 mm × 20 mm, 10 mL/min flow rate). High resolution positive ion electrospray (ESI+) mass spectra were obtained using an orbitrap mass spectrometer, dissolving samples in 1:1 MeOH/H_2O + 0.1% formic acid.

Resin loading was estimated using a procedure modified from Gude et al.[96] Resin containing the first amino acid, di- or tripeptide were subjected to 2 mL of 2% DBU in DMF (v/v) for 30 minutes. The suspension was diluted to 10 mL with acetonitrile, of which 1 mL was further diluted to 12.5 mL with acetonitrile. Absorbance of this solution was observed in triplicate at 304 nm with a reference solution as a blank. Resin loading was estimated by substitution of appropriate values into the equation in section 2.2.3.1.

2.4.2 – Procedure for Assessing Minimum Inhibitory Concentrations (MICs)

The antibacterial activity of the synthetic peptides and authentic A54145D was determined using a broth microdilution assay.[112] Overnight bacterial cultures were grown in Luria-Bertani (LB) broth and then diluted to approximately 1×10^6 CFU/mL according to the measured optical density at 600 nm (OD600). Twofold serial dilutions were used to prepare a series of peptide solutions in LB broth, which were then inoculated with an equal volume of diluted bacterial culture in 96-well microplates. Plates were incubated for 24 h at 37 °C, and then the MIC was determined by the lowest concentration at which there was no visible growth of bacteria.

2.4.3 – General Procedures for Fmoc-SPPS

Procedure for resin activation and resin attachment*:* 2-ClTrt-Cl-PS resin or TentaGel Trt-Cl resin was treated with 3.6 equiv of thionyl chloride and 7.2 equiv of pyridine in dry DCM at reflux for 2 h. Following the reflux, the resin was transferred to a disposable polyethylene cartridge equipped with a filter and rinsed extensively (6 x 30 s) with dry DCM. To this was

added the first amino acid (4 equiv) and DIPEA (8 equiv) in dry DCM, and the peptide was agitated for 4 h. Following the reaction time, the cartridge was rinsed with DCM (3 x 3 min) and capped with DCM/methanol (MeOH)/DIPEA (17:2:1, v/v, 3 x 10 min). The resin was then rinsed with DCM (3 x 5 min).

General procedure for Fmoc-Removal*:* The resin was swelled in DMF for 5 min before the addition of 20% 4-MP in DMF (v/v, 1 x 5 min, 1 x 20 min). For the removal of Fmoc groups after the formation of the depsi bond, the resin was treated with 20% 2-MP in DMF (v/v, 3 x 10 min). Following Fmoc-deprotection, the resin was rinsed with DMF (3 x 5 min) and DCM (3 x 5 min).

General procedure for Amino Acid Coupling*:* The resin was swelled in DMF for 5 min before the addition of FmocAAOH (4 equiv), HOBt (4 equiv), and DIC (4 equiv) in DMF. The cartridge was agitated for 4 h at room temperature before the reagents were filtered and the resin subsequently rinsed with DMF (3 x 5 min) and DCM (3 x 5 min).

General procedure for Allyl Group Removal: The resin was swelled in dry DCM. The solvent was removed by filtration, and to the cartridge was added DMBA (10 equiv) and $Pd(PPh_3)_4$ (0.2 equiv) in 3:1 DCM/DMF (v/v). The mixture was mixed by N_2 stream for 1 h, and following the reaction time, the unreacted $Pd(PPh_3)_4$ was quenched by further rinses with 1% sodium diethyldithiocarbamate trihydrate in DMF (m/v, 5 x 5 min). The resin was further rinsed with DMF (3 x 5 min) and DCM (3 x 5 min).

General procedure for Amino Acid Coupling in the N → C direction*:* The resin was swelled in DMF for 5 min, and HOBt (4 equiv) and DIC (4 equiv) added as a solution in DMF. The free carboxylic acid was allowed to activate for 5 min before the addition of H_2NAAOAllyl (4

equiv), and the cartridge was agitated for 4 h. Following the reaction, the resin was rinsed with DMF (3 x 5 min) and DCM (3 x 5 min).

General procedure for Depsi-Bond Formation: FmocIleOH or N_3IleOH (10 equiv) were dissolved in dry DCM followed by the addition of DIC (10 equiv). The suspension was mixed for 1 h before filtration and transfer to the peptide containing an unprotected alcohol of Thr4. Following the addition of the amino acid and DIC, DMAP (0.1 equiv) was added to the cartridge, and the cartridge was agitated overnight (12 h). The following day, the resin was rinsed with DCM (3 x 5 min), DMF (3 x 5 min), and finally with DCM (3 x 5 min).

2.4.4 – Experimental Procedures for Synthesized Compounds

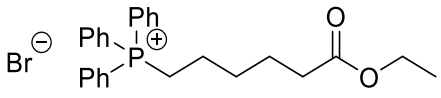

2.12

(6-Ethoxy-6-oxohexyl)triphenylphosphonium bromide (**2.12**). Compound **2.12** was synthesized according using a procedure by Motoshima and coworkers.[92] To a 50 mL round-bottom flask was added ethyl 6-bromohexanoate (2.01 mL, 11.3 mmol, 1.07 eq.), triphenylphosphine (2.77 g, 10.5 mmol, 1 eq.), and dry acetonitrile (15 mL). The mixture was refluxed for 7 h, concentrated, and purified by column chromatography employing a slow gradient of chloroform to 19:1 chloroform-methanol. The desired product was obtained as a beige, amorphous solid (3.43 g, 67%). ^{1}H-NMR (300 MHz, $CDCl_3$) δ: 7.79-7.65 (m, 15H), 3.99 (q, 2H, J = 7.1 Hz), 3.73-3.69 (m, 2H), 2.19 (t, 2H, J = 7.1 Hz), 1.61-1.56 (m, 6H), 1.14 (t, 2H, J = 7.1 Hz). ^{13}C-NMR (75 MHz, $CDCl_3$) δ: 173.5, 135.1, 133.6, 130.5, 118.2, 60.2,

33.7, 29.7, 24.3, 22.9, 22.3, 14.2. ^{31}P-NMR (121 MHz, $CDCl_3$) δ: 25.3. HRMS (ESI+): *m/z* $[M]^+$ calcd for $C_{26}H_{30}O_2P$: 405.19779; found: 405.19741.

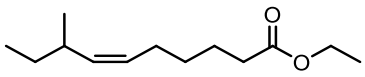

(±)-2.13

(±)-Ethyl (*Z*)-8-methyldec-6-enoate ((±)-2.13). The following procedure was used to prepare **(±)-2.13**, **(*S*)-2.13** and **(*R*)-2.13** using either (±)- or (*S*)-2-methylbutanal, or (*R*)-2-methylbutanal (**2.69**). To a 100 mL round-bottom flask was added **2.12** (1.02 g, 2.10 mmol, 1 equiv) and the flask was purged with argon gas. Dry THF (50 mL) was added and the mixture was cooled to -78 ^{o}C in a slurry of dry ice in acetone. A 1.0 M solution of NaHMDS in THF (2.1 mL, 2.1 mmol, 1 equiv) was slowly added over 5 min and the resulting orange solution was stirred for 30 min at -78 ^{o}C. A solution of (±)-2-methylbutanal (231 µL, 2.00 mmol, 0.95 equiv) in THF (5 mL) was transferred to the reaction mixture. The solution was allowed to warm to room temperature and stirred overnight. The reaction was quenched with saturated sodium bicarbonate and the product was extracted with ethyl acetate (2 x 50 mL). The organic layers were combined, dried with sodium sulfate, and concentrated *in vacuo*. The residue was subjected to flash chromatography (95% hexane/5% ethyl acetate, R_f = 0.3) which provided pure **(±)-2.13** as a colorless oil (0.305 g, 66% yield). The yields of **(*S*)-2.13** and **(*R*)-2.13** were 71% and 69% respectively. ^{1}H-NMR (300 MHz, $CDCl_3$) δ: 5.22 (1H, td, *J* = 7.2, 10.8 Hz), 5.04 (1H, app. t, *J* = 9.9 Hz), 4.04 (2H, q, *J* = 7.2 Hz), 2.22 (2H, t, *J* = 7.5 Hz), 1.97 (2H, q, *J* = 7.3 Hz), 1.57 (2H, app. quint, *J* = 7.6 Hz), 1.36-1.04 (7H, m), 0.85 (3H, d, *J* = 6.7 Hz), 0.76 (3H, t, *J* = 7.4 Hz). ^{13}C-NMR (75 MHz, $CDCl_3$) δ: 173.5, 136.4, 127.8, 60.0, 34.1, 33.3, 30.2, 29.3, 27.0, 24.5, 20.9, 14.1, 11.8. HRMS-ESI$^+$: *m/z* $[M + H]^+$ calcd for $C_{13}H_{25}O_2$: 213.1849;

found 213.1849. The ^{1}H-NMR spectra of **(*S*)-2.13** and **(*R*)-2.13** were identical to that of **(±)-2.13**.

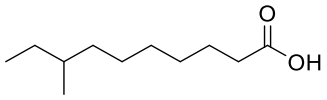

(±)-2.14

(±)-8-Methyldecanoic acid (**(±)-2.14**). The following procedure was used to prepare **(±)-2.14**, **(*S*)-2.14**, and **(*R*)-2.14** using either **(±)-2.13**, **(*S*)-2.13**, or **(*R*)-2.13**. Compound **(±)-2.13** (201 mg, 0.95 mmol) was added to a 50 mL round-bottom flask equipped with a stir bar. To this was added ethanol (25 mL) and 10% Pd/C (40 mg, 0.04mmole, 0.04 equiv) and the flask was purged with argon gas. The flask was then flushed with H_2 and allowed to stir overnight at room temperature. The mixture was filtered over celite and the filtrate was concentrated yielding a colorless oil {^{1}H-NMR (300 MHz, $CDCl_3$) δ: 4.06 (2H, q, J = 7.0 Hz), 2.22 (2H, t, J = 7.4 Hz), 1.56 (2H, m), 1.35-0.95 (15H, m), 0.88-0.72 (6H, m). ^{13}C-NMR (75 MHz, $CDCl_3$) δ: 173.7, 60.0, 36.5, 34.3, 29.5, 29.4, 29.1, 26.8, 24.9, 19.1, 14.1, 11.3. HRMS-ESI^{+}: *m/z* $[M + H]^{+}$ calcd for $C_{13}H_{27}O_2$: 215.20056; found 215.20134}. The oil (176 mg, 0.82 mmol) was dissolved in a solution of 1:1 MeOH and 0.6 M NaOH (aq) (25 mL). After 3 h, the reaction was acidified to pH 1 with 1 M HCl and the product extracted into ethyl acetate (2 x 50 mL). The organic layers were dried with Na_2SO_4 and the solvent removed by rotary evaporation yielding pure **(±)-2.14** as a colorless oil (153 mg, 77%). The yields of **(*S*)-2.14** and **(*R*)-2.14** were 78% and 79% respectively. ^{1}H-NMR (300 MHz, $CDCl_3$) δ: 11.74 (1H, br. s), 2.33 (2H, t, J = 7.5 Hz), 1.59 (2H, app. quint, J = 7.3 Hz), 1.39-1.00 (11H, m), 0.88-0.76 (6H, m); ^{13}C-NMR (75 MHz, $CDCl_3$) δ: 183.6, 39.4, 37.2, 37.0, 32.5, 32.3, 32.0, 29.7, 27.5, 22.0, 14.2; HRMS-ESI^{-}: *m/z* $[M-H]^{-}$ calcd for $C_{11}H_{21}O_2$: 185.1547; found 185.1552. The ^{1}H-NMR spectra

of **(*S*)-2.14** and **(*R*)-2.14** were identical to that of **(±)-2.14**. **(*S*)-2.14**: $[\alpha]^{22}_{D}$ +4.7° (c 0.20, $CHCl_3$) (lit.,[113] $[\alpha]^{25}_{D}$ +6.1° (1.14, $CHCl_3$)). **(*R*)-2.14**: $[\alpha]^{22}_{D}$ -4.4° (c 0.20, $CHCl_3$).

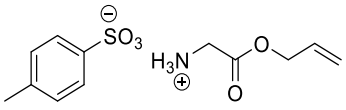

2.73

$TsO^{-}H_3N^{+}$GlyOAllyl (**2.73**). Glycine (21 g, 0.280 mol, 1 equiv) was added to a solution of toluene (75 mL) and allyl alcohol (66.6 mL, 0.979 mol, 3.5 equiv). To this solution was added *p*-toluenesulfonic acid monohydrate (p-TsOH·H_2O, 55.9 g, 0.294 mol, 1.05 equiv). The solution was stirred under reflux equipped with a Dean-Stark trap overnight. Following the reaction, the mixture was concentrated to obtain a dark oil. This was triturated with ethyl acetate overnight and the resulting solid was rinsed with chilled ethyl acetate yielding the desired product as beige crystals (80.4 g, 88%). ^{1}H-NMR (300 MHz, CD_3OD) δ: 7.69 (2H, d, J = 7.9 Hz), 7.22 (2H, d, J = 7.8 Hz), 5.95 (1H, m), 5.36 (1H, d, J = 17.2 Hz), 5.26 (1H, d, J = 10.4 Hz), 4.71 (2H, d, J = 5.5 Hz), 3.85 (2H, s), 2.36 (3H, s). ^{13}C-NMR (75 MHz, CD_3OD): δ: 166.8, 142.0, 140.3, 131.3, 128.4, 125.5, 118.1, 66.3, 39.6, 19.9. HRMS (ESI+): *m/z* $[M+H]^+$ calcd for $C_5H_{10}NO_2$: 116.07061, found 116.07093.

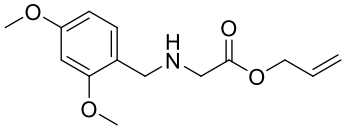

2.74

Allyl (2,4-dimethoxybenzyl)glycinate (**2.74**). Compound **2.74** was synthesized based upon a procedure by the Martin Group.[84] To 1,2-dichloroethane (100 mL) was added 2,4-dimethoxybenzaldehyde (3.0 g, 18 mmol, 1 equiv) and triethylamine (7.5 mL, 54 mmol, 3 equiv), and the solution was stirred vigorously. To the stirring solution was added compound

2.73 (7.24 g, 27 mmol, 1.5 equiv), followed by the portion-wise addition of STAB-H (7.69 g, 36.2 mmol, 2.1 equiv). The resulting mixture was stirred overnight. Following the reaction, the mixture was quenched with the addition of sat. $NaHCO_3$ (aq) (30 mL), and the desired product extracted with DCM (3 x 15 mL). The organic layers were dried and concentrated, and the residue was further purified by flash chromatography (1:1 EtOAc/DCM containing 0.5% NH_4OH). Fractions containing the desired product were pooled and concentrated yielding the desired product as a clear oil (4.79 g, quant.). ^{1}H-NMR (300 MHz, $CDCl_3$) δ: 7.06 (1H, d, J = 7.9 Hz), 6.39-6.33 (2H, m), 5.88 (1H, ddt, J = 16.3, 10.7, 5.8 Hz), 5.24 (1H, dd, J = 1.2 Hz, 17.2 Hz), 5.22 (1H, d, J = 10.4 Hz), 4.53 (2H, d, J = 5.8 Hz), 3.76 (3H, s), 3.73 (3H, s), 3.69 (2H, s), 2.03 (1H, s). ^{13}C-NMR (75 MHz, $CDCl_3$) δ: 175.0, 163.1, 161.6, 134.9, 133.4, 122.9, 121.3, 106.5, 101.3, 68.1, 58.15, 58.13, 52.8, 50.9. HRMS (ESI+): *m/z* $[M+H]^+$ calcd for $C_{14}H_{20}NO_4$: 266.1387; found: 266.1395.

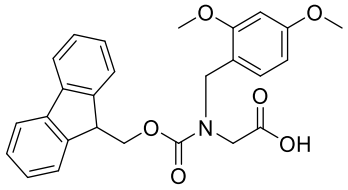

2.75

FmocDMBGlyOH (**2.75**). Compound **2.74** (4.79 g, 18 mmol, 1 equiv) was suspended in 1,4-dioxane (20 mL). To this was added 1M NaOH (aq) (20 mL) portionwise, 4 mL added every five min. After 1 h, hydrolysis of the allyl ester was confirmed by TLC. The reaction mixture was diluted with sat. $NaHCO_3$ (aq) (50 mL), and a suspension of 9-fluorenylmethyl *N*-succinimidyl carbonate (Fmoc-OSu, 6.39 g, 19 mmol, 1.05 equiv) in 1,4-dioxane (25 mL) was added to the stirring mixture dropwise. The mixture was allowed to stir overnight at room temperature. Following the reaction, the mixture was concentrated *in vacuo* to remove the

dioxane, and water was added to achieve a total volume of 100 mL. Solid citric acid was added to achieve neutral pH. The mixture was extracted with EtOAc (3 x 100 mL), and the organic layers were combined and dried over Na_2SO_4 before concentration by rotary evaporation. The product was then purified by column chromatography with a slow gradient of DCM to 10% MeOH in DCM. Fractions containing the desired product were pooled and concentrated to obtain compound **2.75** (6.66 g, 76%) as a beige solid. Characterization data agreed with literature.[84] ^{1}H NMR (300 MHz, $CDCl_3$) δ: 7.74 (2H, t, J = 7.4 Hz), 7.53 (2H, d, J = 7.4 Hz), 7.38-7.25 (4H, m), 6.78 (1H, d, J = 7.7), 6.42 (1H, s), 6.34 (1H, d, J = 7.9 Hz), 4.54-4.40 (4H, m), 4.27-4.21 (1H, m), 4.06 (1H, s), 3.91 (1H, s), 3.78 (3H, s), 3.75 (3H, s). ^{13}C NMR (75 MHz, $CDCl_3$) δ: 178.4, 163.4, 161.4, 159.8, 146.8, 144.2, 134.5, 133.5, 130.6, 130.0, 127.9, 127.8, 122.8, 120.2, 120.0, 107.1, 101.2, 70.7, 58.3, 58.1, 51.2, 50.1, 49.1. HRMS (ESI+): *m/z* $[M+H^+]^+$ calcd for $C_{26}H_{26}NO_6$: 448.17546; found 448.17594.

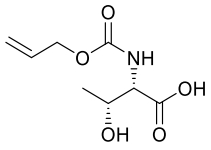

2.76

AllocThrOH (**2.76**). To saturated Na_2CO_3 (aq) (39 mL) was added unprotected threonine (3.0 g, 25 mmol, 1.0 equiv). To the ice-cooled stirring solution was added a solution of allyl chloroformate (2.94 mL, 28 mmol, 1.1 equiv) in 1,4-dioxane (60 mL) dropwise over 1 h. The ice-bath was removed and the mixture stirred at room temperature for an additional 2 h. Following the reaction, the mixture was diluted with 150 mL of water and washed with ether (3 x 150 mL). The aqueous layer was acidified to pH 2 with 1 M HCl, and the product extracted with EtOAc (3 x 100 mL). The organic phase was dried (Na_2SO_4), and concentrated. The residue was then dissolved in saturated $NaHCO_3$ (aq) (150 mL), washed with ether (3 x 100

mL), and reacidified to pH 2 with 1 M HCl (aq). A final extraction with EtOAc (3 x 100 mL), followed by the drying of the organic phase with Na_2SO_4 and subsequent solvent removal by rotary evaporation yielded compound **2.76** as a clear oil (3.74g, 73%). Characterization data matched the literature.[114] ^{1}H NMR (300 MHz, CD_3OD) δ: 5.98 (1H, m), 5.31 (1H, d, J = 17.2 Hz), 5.18 (1H, d, J = 10.5 Hz), 4.55 (2H, d, J = 5.1 Hz), 4.29-4.24 (1H, m), 4.13 (1H, d, J = 2.8 Hz), 1.20 (3H, d, J = 6.4 Hz). ^{13}C NMR (75 MHz, CD_3OD) δ: 177.0, 160.3, 135.6, 119.6, 70.1, 68.5, 62.3, 22.2. HRMS (ESI+): m/z $[M+H^+]^+$ calcd for $C_8H_{14}NO_5$: 204.08665; found: 204.08704.

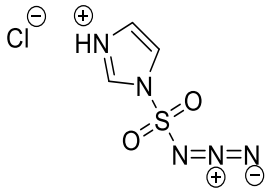

2.77

Imidazole-1-sulfonyl azide hydrochloride (**2.77**). According to a procedure by Goddard-Borger et al., and Ji and coworkers[101,102], sulfuryl chloride (16.1 mL, 200 mmol, 1 equiv) was added dropwise to an ice-chilled suspension of sodium azide (13 g, 200 mmol, 1 equiv) in acetonitrile (200 mL). The ice-bath was removed and the mixture was stirred overnight at room temperature. The mixture was chilled in a new ice-bath, after which imidazole (25.9 g, 380 mmol, 1.9 equiv) was added portion-wise over 10 min. The resulting slurry was stirred for 3 h at room temperature. The mixture was diluted with EtOAc (400 mL), washed with water (2 x 400 mL), and finally washed with saturated $NaHCO_3$ (aq) (2 x 200 mL). The organic phase was dried over Na_2SO_4 and filtered. To this organic phase was added a solution of HCl in EtOH [obtained by adding acetyl chloride (21.3 mL, 300 mmol) drop-wise to ice-cooled dry ethanol (75 mL)] dropwise while stirring. The precipitate was filtered and rinsed with ethyl acetate (3

x 50 mL) to give **2.77** as white needles (27.7 g, 66%). ^{1}H-NMR (D_2O) δ: 9.38 (1H, s), 7.94 (1H, s), 7.53 (1H, s). HRMS (ESI+): *m/z* $[M]^+$ calcd for $C_3H_4N_5O_2S$, 174.00802; found, 174.00815.

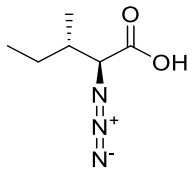

2.78

N_3IleOH (**2.78**). To a stirring solution of methanol (14 mL) and water (7 mL) was added isoleucine (1.0 g, 7.6 mmol, 1 equiv). To this was added compound **2.77** (1.93 g, 9.2 mmol, 1.2 equiv) and copper(II) sulfate pentahydrate (20 mg, 0.076 mmol, 0.01 equiv). To the stirring suspension was added potassium carbonate (2.83 g, 20.5 mmol, 2.7 equiv) and the reaction was stirred overnight at room temperature excluding light. After the reaction time, the mixture was concentrated to one-third its volume, diluted with water (25 mL) and acidified to pH 1 with 1 M HCl (aq). The aqueous solution was extracted with DCM (3 x 25 mL), and the combined organic layers were dried over Na_2SO_4 and subsequently the organic solvent removed *in vacuo*. The crude oil was then diluted in saturated $NaHCO_3$ (aq) (25 mL) and washed with diethyl ether (1 x 30 mL). The aqueous phase was again adjusted to pH 1 with 1 M HCl (aq) and further extracted with DCM (3 x 30 mL). The combined organic layers were dried over Na_2SO_4, and the solvent removed by rotary evaporation yielding compound **2.78** (890 mg, 74%) as a clear oil. Characterization data agreed with the literature.[100] ^{1}H-NMR (300 MHz, $CDCl_3$) δ: 11.1 (br. s), 3.76 (1H, d, J = 5.9 Hz), 1.98-1.89 (1H, m), 1.54-1.18 (2H, m), 0.96 (3H, d, J = 6.8 Hz), 0.86 (3H, t, J = 7.4 Hz). ^{13}C-NMR (75 MHz, $CDCl_3$) δ: 179.2, 69.9, 39.9, 27.6, 18.6, 13.9.

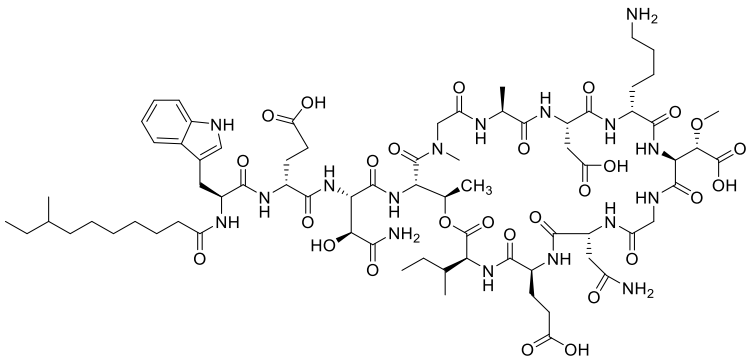

A54145D-*t*HOAsn3-*t*MeOAsp9

A54145D-*t*HOAsn3-*t*MeOAsp9. The following describes the optimized synthesis of A54145-*t*HOAsn3-*t*MeOAsp9. 2-Cl-TrtCl-PS (theoretical substitution = 1.5 mmol/g, 66.7 mg, 0.1 mmol, 1 equiv) was activated in dry DCM with thionyl chloride (26 µL, 3.6 equiv) and pyridine (58 µL, 7.2 equiv) under reflux for 2 h. The resin was transferred to a disposable peptide cartridge and rinsed 6 x with dry DCM, followed by loading with FmocSarOH (4 equiv) and DIPEA (8 equiv) in 1 mL dry DCM for 2 h, twice. The resin was capped with 17:2:1 DCM/MeOH/DIPEA (3 x 10 min) and the loading efficiency determined to be 1.40 mmol/g. Removal of the Fmoc group from resin-bound FmocSar was performed with four 30-min iterations of 20% 4-methylpiperidine in DMF (v/v). All Fmoc-amino acids (4 equiv) and the lipid tail (4 equiv) were activated for 5 min using HOBt (4 equiv) and DIC (4 equiv) in DMF (2 mL) and then coupled for 4 h, except for Fmoc-*t*MeOAsp(tBu)-OH, which was coupled for 12 h. Removal of the Fmoc-group from resin-bound FmocThrSar was performed with two 1-min iterations of 20% 2-methylpiperidine in DMF (v/v), and all other Fmoc-removals were performed with three 10-min iterations of 20% 2-methylpiperidine in DMF. Following installation of FmocHOAsn(TBDMS)OH, yielding peptide **2.53**, synthesis of peptide **2.54** was achieved by treating peptide **2.53** with N_3IleOH (10 equiv), pre-activated with DIC (10 equiv) by stirring in DCM (2 mL) for 1 h, followed by the addition of DMAP (0.1 equiv). Depsi-

bond completion was monitored by HPLC. The next amino acids, *D*-Glu2, Trp1, and 8-methyldecanoic acid ((±)-**2.14**), were introduced using the above general procedure, yielding peptide **2.55**. The removal of the TBDMS group of Asn(OTBDMS) was afforded by treating the resin with TBAF (3 equiv), and acetic acid (3 equiv) in THF (2 mL) for 1 h. After the removal of the TBDMS group, the azido group was reduced by treatment of the peptide with PBu_3 (3 equiv), and $(FmocGlu(tBu)CO)_2O$ (5 equiv, formed by the addition of 10 equiv FmocGlu(tBu)OH and 5 equiv DIC to 2 mL dry THF and stirring for 1 h) in THF for 5 minutes, followed by the addition of 0.1 mL H_2O and further stirring for 16 h, yielding peptide **2.58**. The remaining amino acids were introduced using the coupling and deprotection protocol mentioned above, affording peptide **2.59**. The peptide was cleaved from the resin by treatment with 1% TFA in DCM (5 x 10 mins) affording peptide **2.60** after solvent removal by rotary evaporation. Peptide **2.60** was subjected to PyAOP (5 equiv), HOAt (5 equiv), and 2,4,6-collidine (10 equiv) in DMF (100 mL, 1 mM) overnight for cyclization. The solvent was removed by high-vacuum rotary evaporation, and the crude solid was treated with 95:2.5:2.5 TFA/TIPS/H_2O (v/v, 15 mL) for global deprotection of side-chain protecting groups for 1.5 h. The TFA was removed under stream of N_2, and the peptide precipitated with diethyl ether. The suspension was centrifuged, and the pellet was redissolved in 9:1 H_2O/CH_3CN. The target compound was purified by preparative RP-HPLC employing an isocratic gradient of 40:60 CH_3CN / H_2O (+0.1% TFA). Fractions containing the target product were pooled and lyophilized giving A54145D-*t*HOAsn3-*t*MeOAsp9 as a white powder (12.3 mg, 8% yield based on resin loading), judged to be > 95% pure by analytical RP-HPLC (Figure B.1 in Appendix B). HRMS-ESI^+ (*m/z*): calcd for $C_{73}H_{113}N_{17}O_{27}$ $[M+2H]^{2+}$, 829.8990; found 829.8992 (Figure C.1 in Appendix C). The peptide was also characterized by NMR (^1H, as

well as 2D: HSQC, HMBC, COSY, TOCSY, ROESY. See Figures A.13-A.18 and Table A.2 in Appendix A).

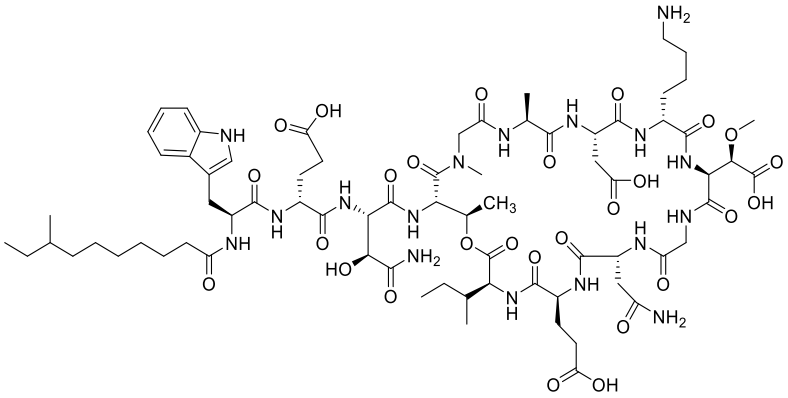

A54145D-*t*HOAsn3-*e*MeOAsp9

A54145D-*t*HOAsn3-*e*MeOAsp9: A54145D-*t*HOAsn3-*e*MeOAsp9 was synthesized according to the procedure used for A54145D-*t*HOAsn3-*t*MeOAsp9, except that Fmoc-*e*MeOAsp(tBu)OH was used in place of Fmoc-*t*MeOAsp(tBu)OH. The desired compound was isolated as a white powder (12.4 mg, 8% yield), judged to be >95% pure by analytical RP-HPLC (Figure B.2 in Appendix B). HRMS-ESI$^+$ (*m/z*): calcd for $C_{73}H_{113}N_{17}O_{27}$ $[M+2H]^{2+}$, 829.8990; found 829.9010 (Figure C.2 in Appendix C). The peptide was also characterized by NMR (^{1}H, as well as 2D: HSQC, HMBC, COSY, TOCSY, ROESY. See Figures A.7-A.12 and Table A.2 in Appendix A), and its sequence characterized by MS/MS (See Figures D.1 and D.2 in Appendix D).

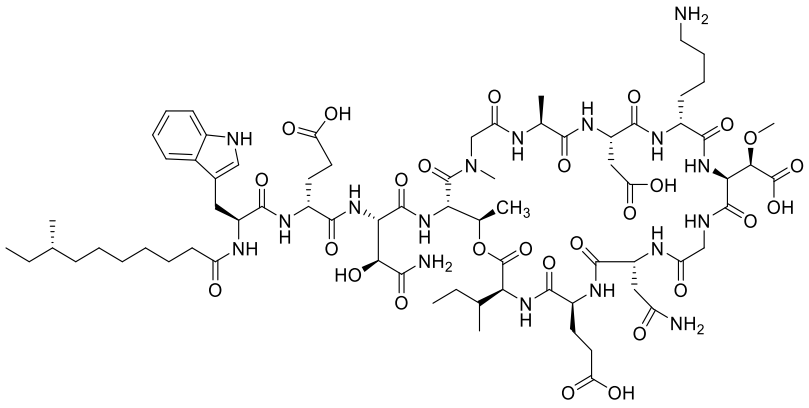

A54145D-(8*S*)-*anteiso*

A54145D-(8*S*)-*anteiso*: A54145D-(8*S*)-*anteiso* was synthesized according to the procedure used for A54145D-*t*HOAsn3-*t*MeOAsp9, except that Fmoc-*e*MeOAsp(tBu)OH was used in place of Fmoc-*t*MeOAsp(tBu)OH, and (*S*)-8-methyldecanoic acid were used in place of (±)-8-methyldecanoic acid. A54145D-(8*S*)-*anteiso* was isolated as a white powder (16.6 mg, 11% yield based on resin loading), judged to be >95% pure by analytical RP-HPLC (Figure B.3 in Appendix B). HRMS-ESI$^+$ (*m/z*): calcd for $C_{73}H_{113}N_{17}O_{27}$ $[M+2H]^{2+}$, 829.8990; found 829.8986 (Figure C.3 in Appendix C).

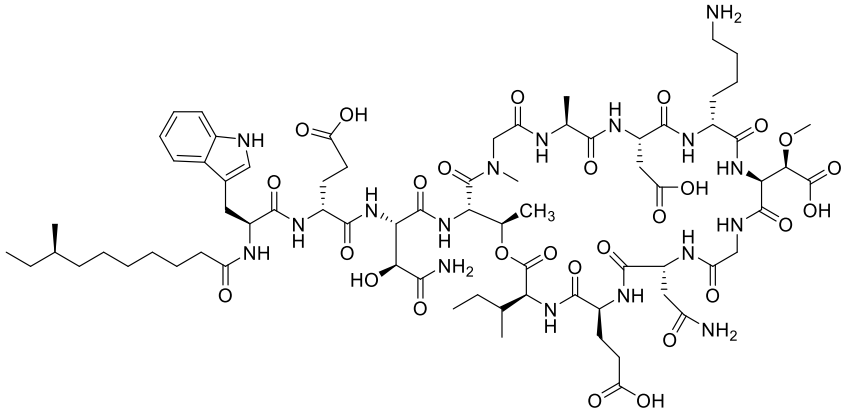

A54145D-(8*R*)-*anteiso*

A54145D-(8*R*)-*anteiso*: A54145D-(8*R*)-*anteiso* was synthesized according to the procedure used for A54145D-*t*HOAsn3-*t*MeOAsp9, except that Fmoc-*e*MeOAsp(tBu)OH was used in

place of Fmoc-*t*MeOAsp(tBu)OH, and (*R*)-8-methyldecanoic acid were used in place of (±)-8-methyldecanoic acid. A54145D-(8*R*)-*anteiso* was isolated as a white powder (16.7 mg, 11% yield based on resin loading), judged to be >95% pure by analytical RP-HPLC (Figure B.4 in Appendix B). HRMS-ESI$^+$ (*m/z*): calcd for $C_{73}H_{113}N_{17}O_{27}$ $[M+2H]^{2+}$, 829.8990; found 829.8991 (Figure C.4 in Appendix C).

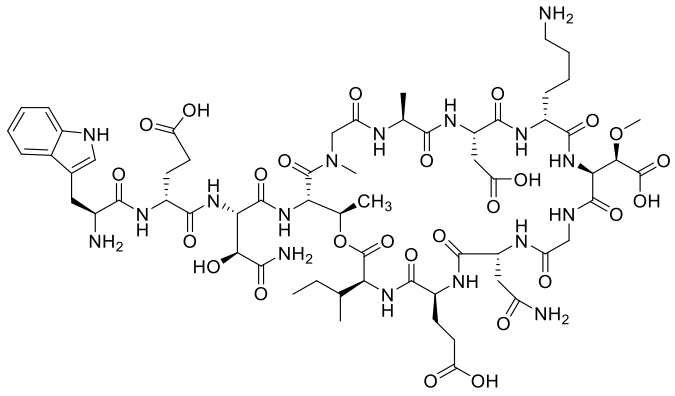

A54145D-nucleus

A54145D-nucleus: The nucleus of A54145D, used for characterization purposes, was synthesized according to the procedure used for A54145D-*t*HOAsn3-*t*MeOAsp9, except that Fmoc-*e*MeOAsp(tBu)OH was used in place of Fmoc-*t*MeOAsp(tBu)OH, and BocTrp(Boc)OH was used instead of FmocTrp(Boc)OH. No lipid tail was coupled to the peptide. The peptide was purified using preparative RP-HPLC employing an isocratic solution of 16:84 CH_3CN / H_2O (+ 0.1% TFA), yielding A54145D-nucleus as a white powder (12.0 mg, 9% based on resin-loading). The compound was judged to be >95% pure based on analytical HPLC (Figure B.5 in Appendix B). HRMS-ESI$^+$ (*m/z*): calcd for $C_{62}H_{93}N_{17}O_{26}$ $[M+2H]^{2+}$, 745.8233; found 745.8244 (Figure C.5 in Appendix C). The peptide was also characterized by NMR (^{1}H, as well as 2D: HSQC, HMBC, COSY, TOCSY, ROESY. See Figures A.1-A.6 and Table A.1 in Appendix A).

Chapter 3 – Structure Activity Relationships of A54145

3.1 – Introduction

The development of new drugs often involves performing structure-activity relationship (SAR) studies on known drugs or known biologically active compounds to learn more about the mechanism of action of the drug and identify moieties which are amenable to substitution or modification. Such studies sometimes result in the development of new, more active, or differently-acting drugs. Various SAR studies have been performed on daptomycin, which include modification to the lipid tail, appending groups onto the ornithine residue, and substituting different amino acids (see sections 1.5 and 1.6). Except for some work by the Baltz group in between 2010 and 2014 (Table 1.2, section 1.5.3), much less research is available for A54145D. In this chapter we report our initial studies on the synthesis of several analogs of A54145D and A54145A_1 and their *in vitro* biological activity.

3.1.1 – Split-and-Pool Method of Fmoc-SPPS Employing Macro-beads

A long-term goal in the Taylor lab is to synthesize large numbers of daptomycin and A54145 analogs and evaluate these analogs for their biological activity. Such studies might

provide non-toxic daptomycin or A54145 analogs that are highly active in both the absence and presence of lung surfactant and would also be useful for mechanism of action studies.

One method that enables rapid synthesis of large numbers of peptides is the split-and-pool approach. This approach to peptide synthesis is illustrated in Figure 3.1. In this example, the beads are split into three different reaction vials. The first amino acid is attached to the beads using a different amino acid (AA_1, AA_2, or AA_3) for each vial. The beads from all three vials are then pooled and then equally split back into three separate vials. Then, the second amino acid is coupled, again, using a different amino acid (AA_4, AA_5, AA_6) for each vial. When this process is repeated a third time (with AA_7, AA_8, AA_9), each vial contains nine different peptides attached to the beads, and each resin bead contains multiple copies of only one peptide. In Figure 3.1, three iterations of three amino acids yields a library of 27 variants ($3^3 = 27$). This process can be repeated as often as desired, and exponential growth results in a large library of analogs synthesized, in a relatively short time-frame, with each macro-bead possessing a single peptide. Just three iterations applied to all 20 proteinogenic amino acids would yield 8000 different variants ($20^3 = 8000$).

One of the challenges of applying the split-and-pool approach to synthesizing daptomycin or A54145 analogs is assessing the synthesized peptides for biological activity. Since A54145 and daptomycin function by first inserting into the bacterial cell membrane, the peptides will have to be cleaved off of the beads in order to assess their biological activity. This means that individual beads must be picked out of the mixture, and the peptide cleaved from the resin, and then assessed for activity. This also means that each individual bead must produce enough peptide for biological screening and spectral identification. Solid-phase combinatorial synthesis is typically performed on beads with diameters of 50-500 μm with a

loading of 0.1 to 0.5 mmol/g.[115] If such beads were used for daptomycin or A54145 library construction, then only pmol or low nmol amounts of peptide would be produced per bead, which is not enough for our purposes. Consequently, high loading macro-beads (500-560 μm or higher in diameter, 1.0-1.5 mmol/g loading) will have to be used to make the daptomycin and A54145 libraries. Unfortunately, reaction rates decrease with increasing resin bead diameter, since library preparation on macro-beads is hindered by slow reagent diffusion into the polymer matrix and sluggish reaction rates.[115] Consequently, we are aware of only one report describing the synthesis of a cyclic peptide library on macrobeads.[116]

The problem of slow reaction rates on macro-beads can be overcome by using longer reaction times and a large excess of reagents. However, as depsi-bond formation is already very challenging on "regular" resin beads, we expected that it will be particularly challenging on macro-beads. Therefore, it would be advantageous if the ester bond in A54145 could be replaced with an amide bond, as amide bonds are easier to form than ester bonds. It would also be advantageous for the cyclization of the peptides to be done on-resin. With an on-resin cyclization, each individual peptide at the end of the synthesis need only be cleaved from the resin and purified by HPLC. However, a synthesis employing an off-resin cyclization would involve extra steps: each peptide would have to be cleaved from the resin while keeping protecting groups intact, the peptide would then be cyclized, and then the side-chain protecting groups removed, followed by purification. Most problematically, these steps would require a different reaction vessel for each peptide (each different macro-bead), and this accordingly would make the synthesis significantly more laborious. In Chapter 2, the total synthesis of A54145D was reported, and while this opens the door to the generation of many more A54145D analogs, the strategy cannot be applied to synthesis on macro-beads using a split-

and-pool approach because of the off-resin cyclization and potential difficulties in making the depsi-bond.

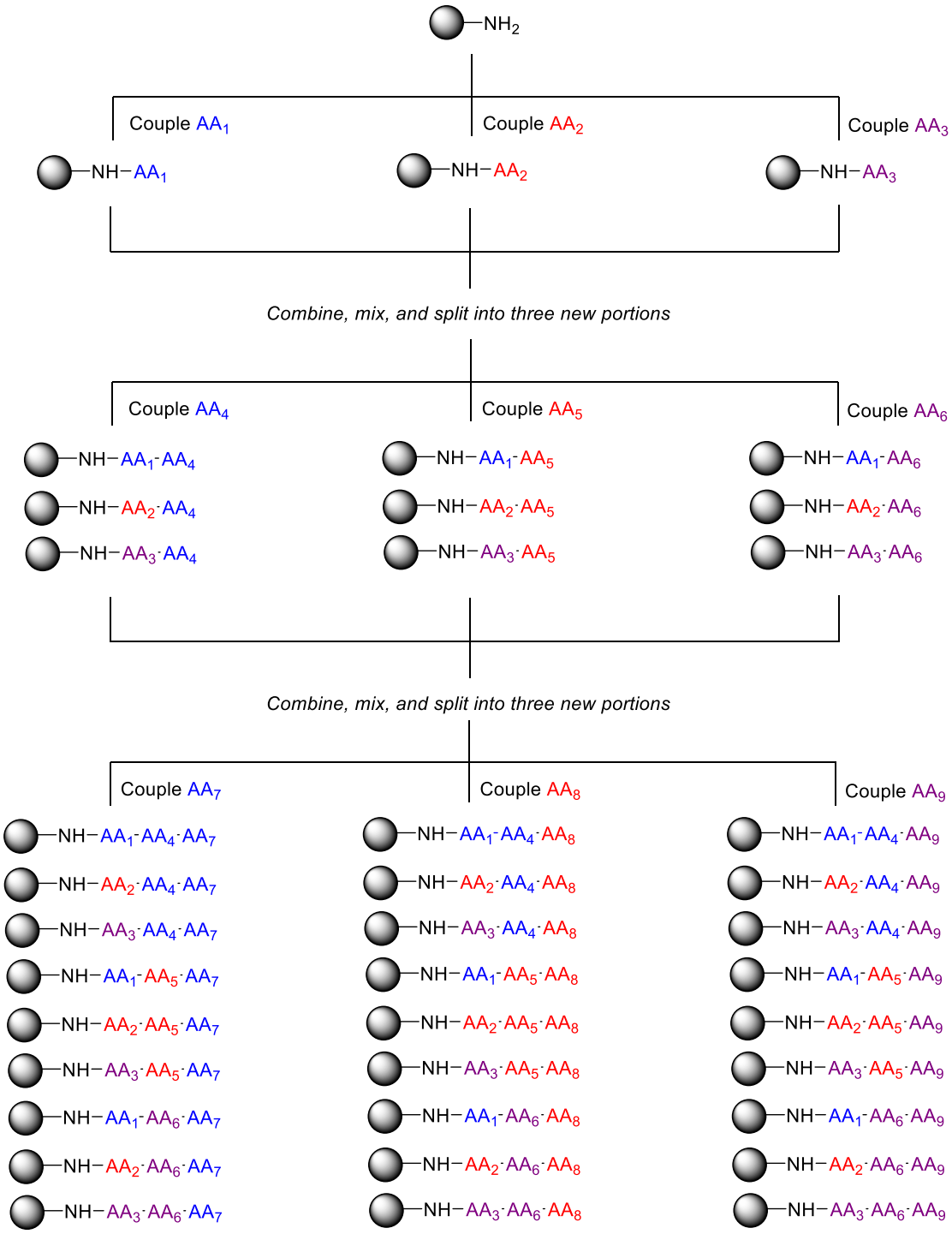

Figure 3.1: The split-and-pool approach to peptide library synthesis.

3.1.2 – Previous A54145 Analogs Synthesized as a Starting Point for Library Genesis

In 2006, Kopp et al. reported the chemoenzymatic synthesis of an A54145A_1 analog in which the non-proteinogenic amino acids HOAsn3 and MeOAsp9 were replaced with their proteinogenic counterparts, Asn3 and Asp9 (**3.1**), as well as a second analog in which, in addition to these modifications, the Thr residue at position 4 was replaced with (2*S*)-2,3-diaminopropionic acid (DAPA) (**3.2**, Figure 3.2).[78] The MICs of these two peptides were both reported to be 25 μg/mL against *B. subtilis* PY79. Although notably less active than both daptomycin and A54145D, this result suggests that replacing the ester bond in A54145D with an amide linkage has no effect on biological activity. The identical biological activities of these two analogs were surprising to us, since, as we and others have shown, when the ester bond in daptomycin analogs is replaced with an amide bond, the biological activity is significantly reduced.[84,117] If Kopp et al.'s result is correct, it is significant for two reasons. First, it would be expected that the chemical synthesis of A54145 analogs containing an amide bond would be less challenging than analogs containing an ester bond at this position. This would be advantageous for library construction on macro-beads. Second, a study by D'Costa et al. has shown that resistance to daptomycin can occur by enzymatic hydrolysis of the ester bond (section 1.3.3).[65] It is likely that such a resistance mechanism could also result in the deactivation of other cyclic lipodepsipeptide antibiotics such as A54145 and its analogs. It is possible that this mechanism of resistance could be circumvented by replacing the ester bond with an amide bond.

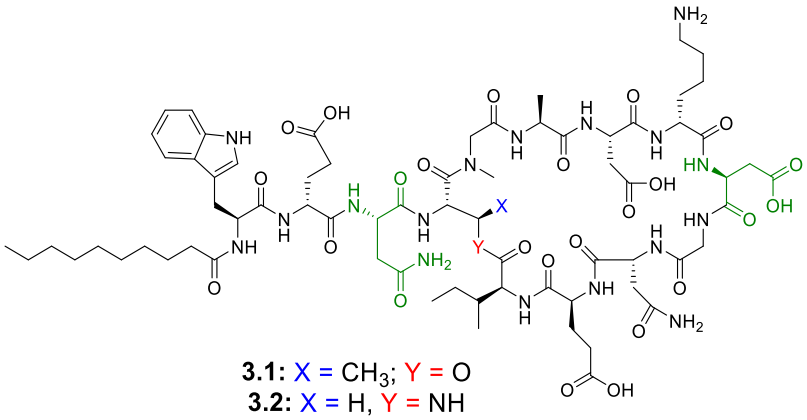

Figure 3.2: Structures of analogs **3.1** and **3.2.** Deviations from A54145A$_1$ are shown in green.

3.1.3 – Research Objectives

The main objectives of the work described in this chapter is to synthesize peptides **3.1** and **3.2**, as well as other analogs that contain Asn and/or Asp in place of HOAsn and MeOAsp, and to use these analogs to determine the roles of the ester bond in A54145's biological activity. Additionally, another objective of this work is to evaluate the importance of the ester bond and these two uncommon amino acids on the activity of A54145D or A54145A$_1$.

3.2 – Results and Discussion

3.2.1 – A54145A$_1$-Asn3-DAPA4-Asp9 (Peptide **3.2**)

In Chapter 2, the total synthesis of A54145D was discussed (Schemes 2.13, 2.14, and 2.15). The peptide was attached to the resin via Sar5 and the ester bond was formed between the side chain of the Thr residue in resin-bound tripeptide **2.53** and N_3IleOH to give peptide **2.54**. Fmoc SPPS was used to introduce residues 1 and 2 and the lipid tail into peptide **2.54** to give peptide **2.55**. Upon removal of the TBDMS group and reduction of the azido group in peptide **2.55**, the resulting peptide **2.58** was further elaborated via Fmoc-SPPS to give peptide **2.59**, which was cleaved from the resin, yielding **2.60**, cyclized in solution, and then globally

deprotected to give A54145D. An on-resin cyclization strategy, which involved attaching the peptide to the resin via the side chain COOH of a MeOAsp9-Gly10 dipeptide (Scheme 2.4) was attempted but was unsuccessful due to aspartimide formation between Gly10 and MeOAsp9. Attempts to circumvent this problem by protecting the amide nitrogen of Gly10 with a dimethoxybenzyl (DMB) group were unsuccessful due to very rapid diketopiperazine formation. This is in contrast to previous work in the Taylor lab, whose successful syntheses of daptomycin and its analogs were readily achieved using an on-resin cyclization strategy by attaching the peptide to the resin via the side chain of an Asp9-GlyOallyl10 dipeptide (**1.34**, Scheme 1.10, Section 1.6.4).[82,85,87,103] The finding that aspartimide formation occurs with MeOAsp but not Asp suggests that the presence of the electron withdrawing 3-methoxy group was promoting aspartimide formation. As A54145A$_1$-Asn3-Asp9 (**3.1**) and A54145A$_1$-Asn3-DAPA4-Asp9 (**3.2**) contain Asp and not MeOAsp at position 9, we reasoned that an on-resin cyclization strategy could be used for the synthesis of these two analogs.

3.2.1.1 – Proposed Synthesis of A54145A$_1$-Asn3-DAPA4-Asp9 (**3.2**)

In the first proposed synthesis of compound **3.2**, we envisioned attaching the peptide to 2-ClTrt-Cl-PS resin by the side-chain of Asp9, using FmocAsp(OH)GlyOallyl as the initial building block, yielding dipeptide **1.34** (Scheme 3.1), analogous to the synthesis of daptomycin by Lohani et al.[82,85] Fmoc-based SPPS with commercially available amino acids and Fmoc-β-azidoAlaOH[118,119] would yield peptide **3.3**. The azido group in Fmoc-β-azidoAlaOH would be used as a protecting group for the amino group in the DAPA residue, as the azido group is orthogonal to Fmoc-, Boc-, and allyl protecting groups. After the completion of linear peptide **3.3**, the azido group would be reduced, yielding amine **3.4**. Peptide **3.4** would undergo further

Fmoc-SPPS yielding branched peptide **3.5**. Removal of the allyl group followed by on-resin cyclization and then resin cleavage and global deprotection would afford target compound **3.2**.

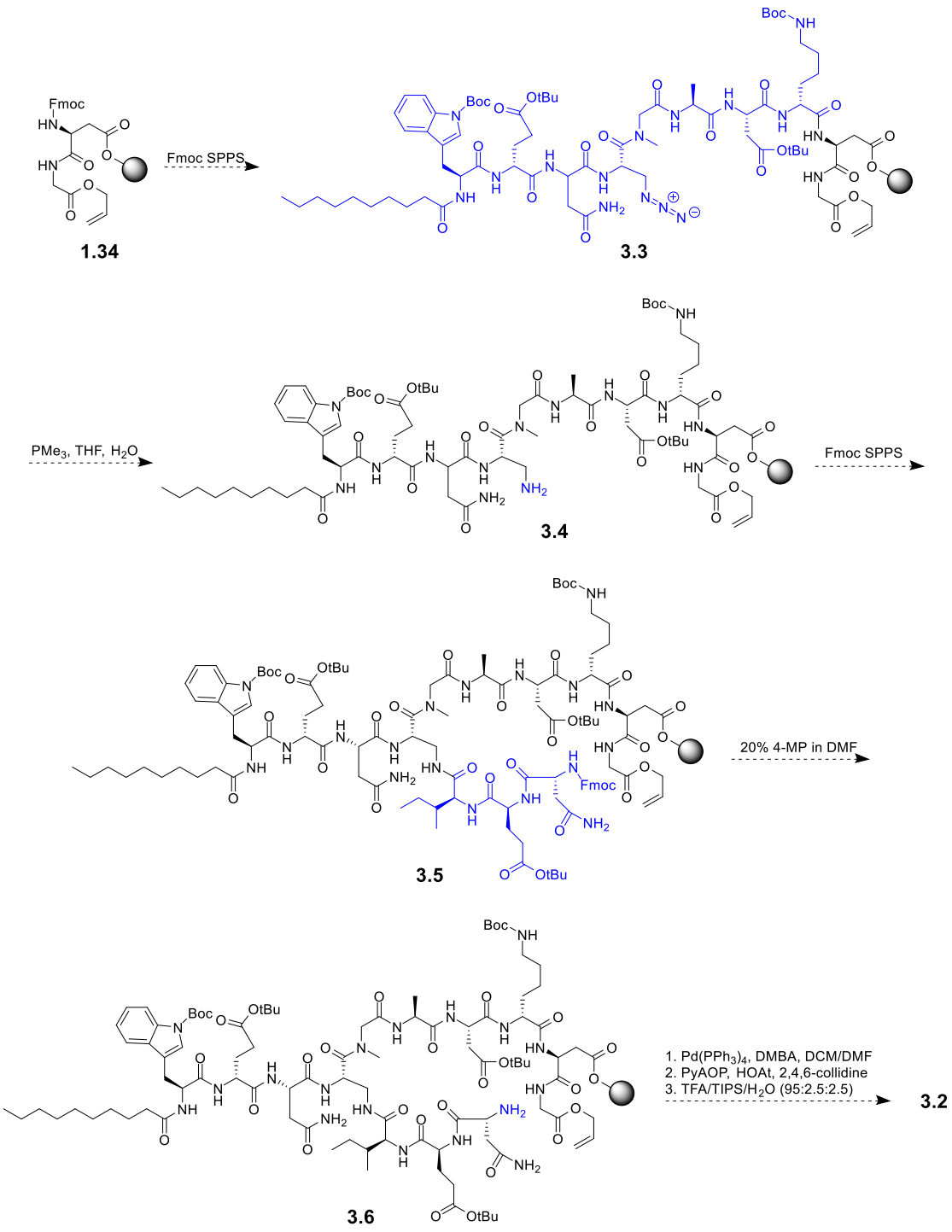

Scheme 3.1: First proposed route to peptide **3.2**.

3.2.1.2 – Total Synthesis of A54145A$_1$-Asn3-DAPA4-Asp9 (**3.2**)

Dipeptide **3.8** was synthesized using our previously reported procedure.[86] First, FmocAsp(tBu)OH was coupled to $TsO^-H_3N^+$GlyOallyl (**2.73**) yielding dipeptide **3.7** (Scheme 3.2). The *tert*-butyl group in dipeptide **3.7** was removed using TFA. FmocAspGlyOallyl (**3.8**) was coupled to 2-ClTrt-Cl resin with DIPEA without issue, yielding dipeptide **1.34**. The loading levels attained for this initial coupling typically were determined to be 60-70%. Standard Fmoc-based SPPS employing DIC and HOBt as coupling reagents transformed dipeptide **1.34** into linear peptide **3.3** without issue.

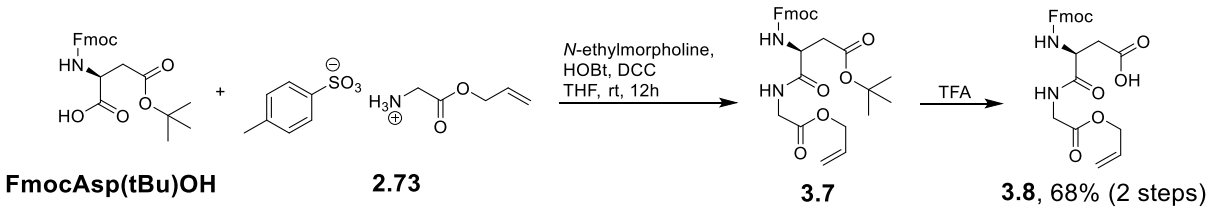

Scheme 3.2: Synthesis of dipeptide **3.8**.

DAPA was introduced into peptide **3.3** as Fmoc-β-azidoAla, which was synthesized by slightly modified literature procedures (Scheme 3.3).[118,119] Lau and Spring reported the synthesis of Fmoc-β-azidoAla, **3.10**, through a Hofmann rearrangement starting from FmocAsnOH yielding FmocDAPAOH (**3.9**). FmocDAPAOH was converted to Fmoc-β-azidoAla through the use of a diazo transfer reagent, imidazole-1-sulfonyl azide hydrochloride (**2.77**). In Lau and Spring's synthesis, bis(trifluoroacetoxy)iodobenzene was used to achieve the Hofmann rearrangement. We found that the reaction also worked when diacetoxyiodobenzene was used, but with a lower yield (57% versus 80%) (Scheme 3.3). Since diacetoxyiodobenzene is considerably less expensive, we elected to use this reagent in our synthesis.

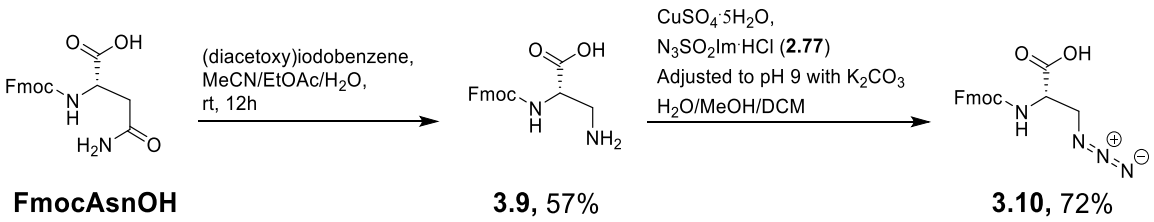

Scheme 3.3: Synthesis of Fmoc β-azidoAla (**3.10**).

At this point we should mention an observation that we made when cleaving Trp(Boc)-bearing peptides from resins using TFA/TIPS/H_2O. Upon cleavage of such peptides from the resin using TFA/TIPS/H_2O, two peaks were sometimes observed in the analytical HPLC chromatogram, one of which corresponded to the target peptide, and the second, which consistently eluted 1-2 minutes before the target peptide, and which had a mass that was 44 amu larger than the target peptide as determined by LRMS. This additional peak was also temporary; repeated injections on the same day showed different relative peak areas of these two signals (Figure 3.3), and subsequent injection the following day showed a complete absence of the additional peak. Consistent with this observation is the hypothesis of a temporary CO_2-adduct of the Trp-containing peptide, in which the Boc-protected tryptophan residue undergoes a stepwise deprotection (Scheme 3.4). The first step is fast, involving the loss of the *tert*-butyl group, and the second step is slow, involving decarboxylation.

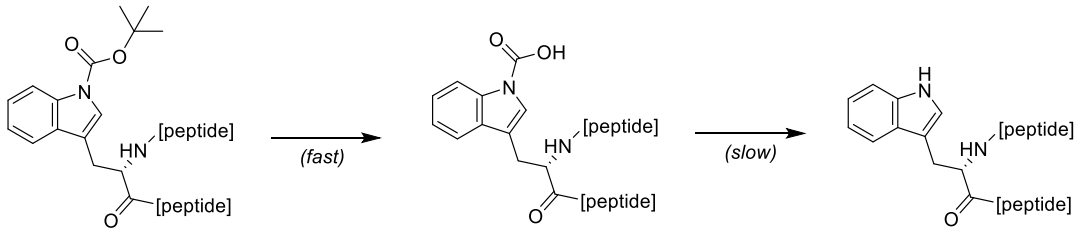

Scheme 3.4: Products formed upon the treatment of peptides containing Trp(Boc) residues with TFA/TIPS/H_2O.

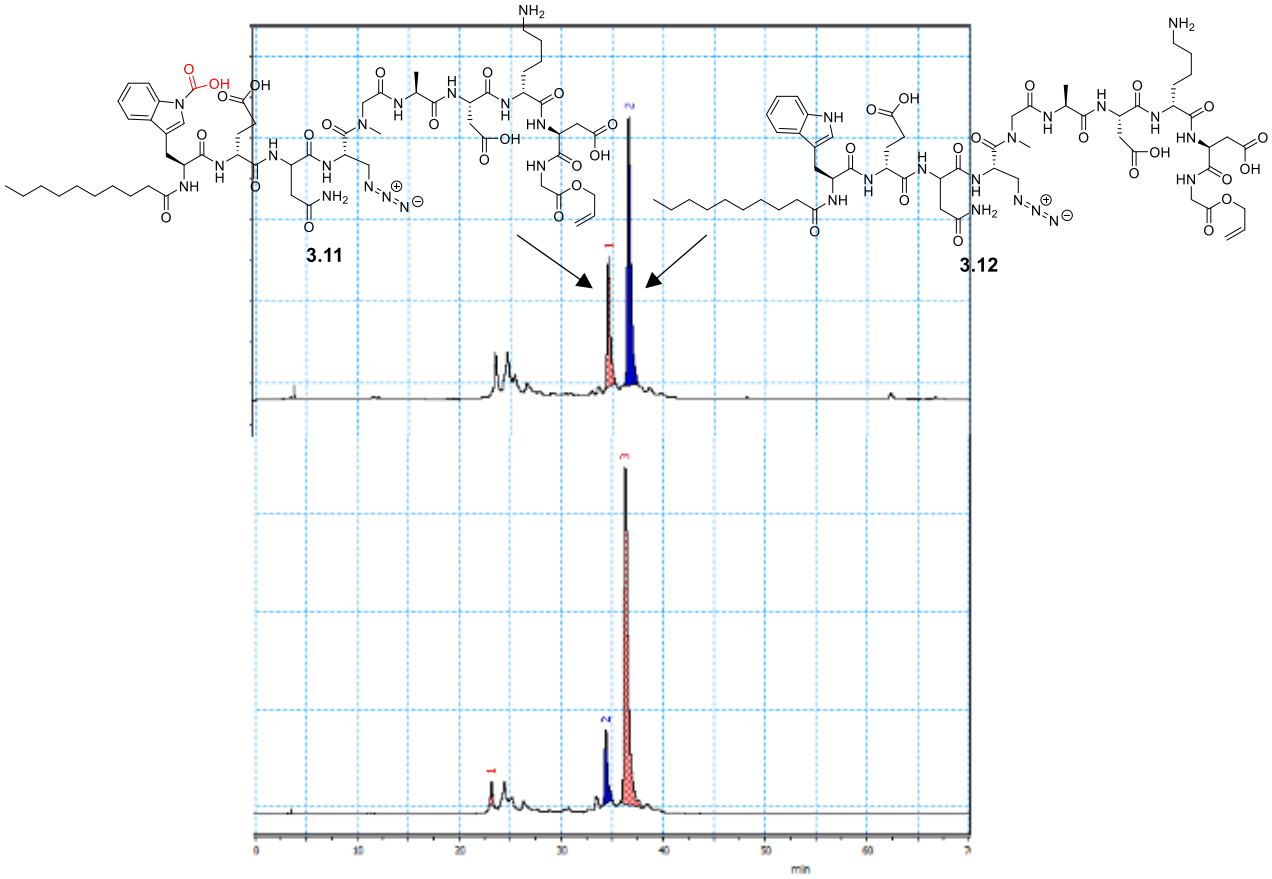

Figure 3.3: RP-HPLC chromatograms of the crude mixture obtained after treating peptide **3.3** with TFA/TIPS/H_2O. Both spectra correspond to the same sample, but the bottom spectrum was injected several hours after the first.

Following the successful synthesis of linear peptide **3.3**, the azido group in peptide **3.3** was reduced using PMe_3 in a 1:1 mixture of THF and H_2O, yielding peptide **3.4**. Surprisingly, subsequent coupling of FmocIleOH employing DIC and HOBt were inefficient, producing some of the desired compound, but a considerable amount of unreacted starting material remained. To remedy this, we attempted the conditions developed by Thakkar et al., which involved using HOBt/PyBOP/DIPEA as coupling reagents in DMF/DCM/NMP (*N*-methylpyrrolidinone) (3:2:2) containing 1% Triton X-100 (called "Magic Mixture").[120] It was suspected that the lipid in the peptide was promoting aggregation, or perhaps causing the peptide to adopt a tertiary structure that shielded the branch point from reacting efficiently, and

that the detergent, Triton X-100, might prevent or minimize this problem. Of note, Magic Mixture was originally developed to assist with challenging on-resin cyclizations. To our delight, Magic Mixture was effective in the incorporation of Ile13 and Glu12.

However, the use of Magic Mixture was not effective for the incorporation of *D*-Asn11. HPLC analysis of the crude uncyclized peptide **3.5** by RP-HPLC and LRMS indicated the presence of an undesired side-product that was 18 amu less than the target product, which was consistent with asparagine dehydration (Figure 3.4). To alleviate this problem, peptide **3.15** was constructed in which *D*-Asn11 was incorporated with a Trt protecting group (Scheme 3.5). It is interesting to note that asparagine dehydration was not observed when incorporating Asn3 to the peptide using DIC/HOBt, signifying that the dehydration of asparagine may be dependent upon the coupling reagents used.

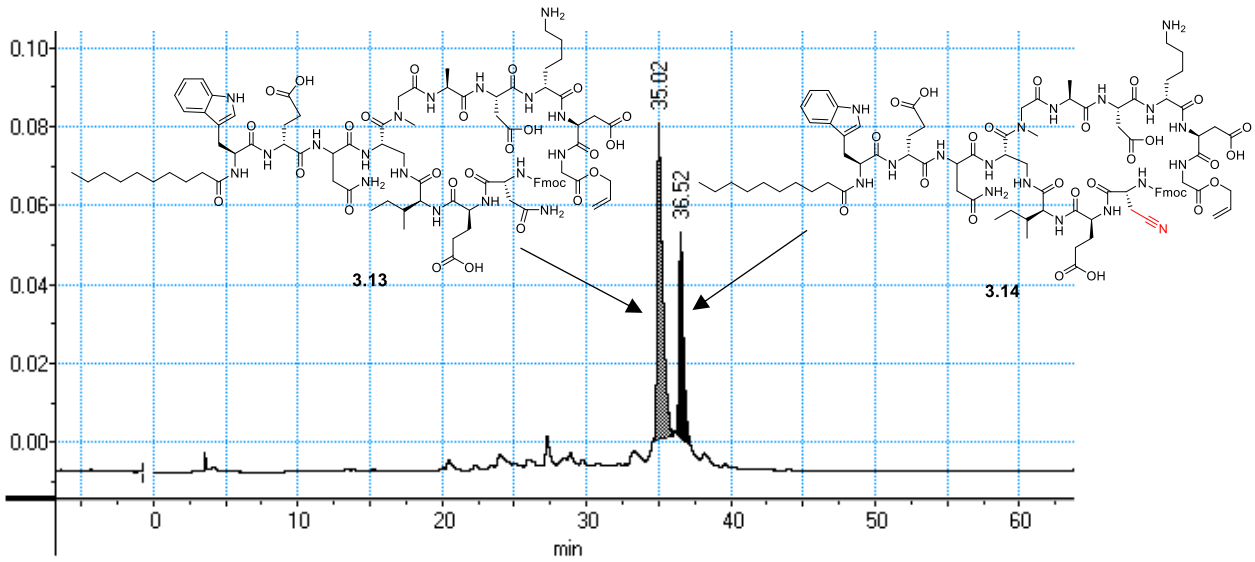

Figure 3.4: RP-HPLC chromatograms demonstrating *D*-Asn11 dehydration. The peptide was analyzed by HPLC one day after cleavage with TFA/TIPS/H_2O to avoid spectrum convolution as a result of the temporary CO_2-adduct from Trp(Boc)-deprotection.

Fmoc-deprotection of **3.15** yielded corresponding amine **3.16**. The next two steps in the synthesis of compound **3.2** involved removing the allyl protecting group and the on-resin cyclization. The allyl group was removed without issue with 0.2 equiv of $Pd(PPh_3)_4$ and DMBA (10 equiv) in 3:1 DCM/DMF (v/v). The mixture was treated with several rinses of 1% sodium diethyldithiocarbamate trihydrate in DMF (w/v) to remove the palladium catalyst. Cyclization using Magic Mixture was expected to be successful (as these conditions were initially developed for challenging cyclizations); however, it was observed that these conditions resulted in the incomplete formation of the final amide bond. After one cyclization attempt, cyclization efficiency was estimated to be 30% by HPLC, and after two cyclization attempts, cyclization efficiency was estimated to be 60%. Despite incomplete cyclization, the peptide was then cleaved from the resin with TFA/TIPS/H_2O and then purified by semi-preparative RP-HPLC, affording compound **3.2** in a 6% yield based on initial resin loading.

Although compound **3.2** was successfully synthesized, the strategy suffered from an inefficient cyclization. With the long-term goal to develop an approach amenable for library generation, it would be advantageous to develop cyclization conditions that can consistently and reliably result in quantitative cyclization. We decided to examine the cyclization conditions used by Knerr and van der Donk, who employed PyAOP/HOAt/2,4,6-collidine in DMF, to form several macrolactams of Epilancin 15X analogs.[121] It was found that we could quantitatively cyclize peptide **3.16** with these alternative conditions. Using these conditions, peptide **3.2** was obtained in a 13% yield based on initial resin loading (Scheme 3.5). Analysis by MS/MS was attempted on the cyclic peptide, and the spectrum obtained very closely matched a literature MS/MS spectrum (See Figures D.3 and D.4 in Appendix D).[78]

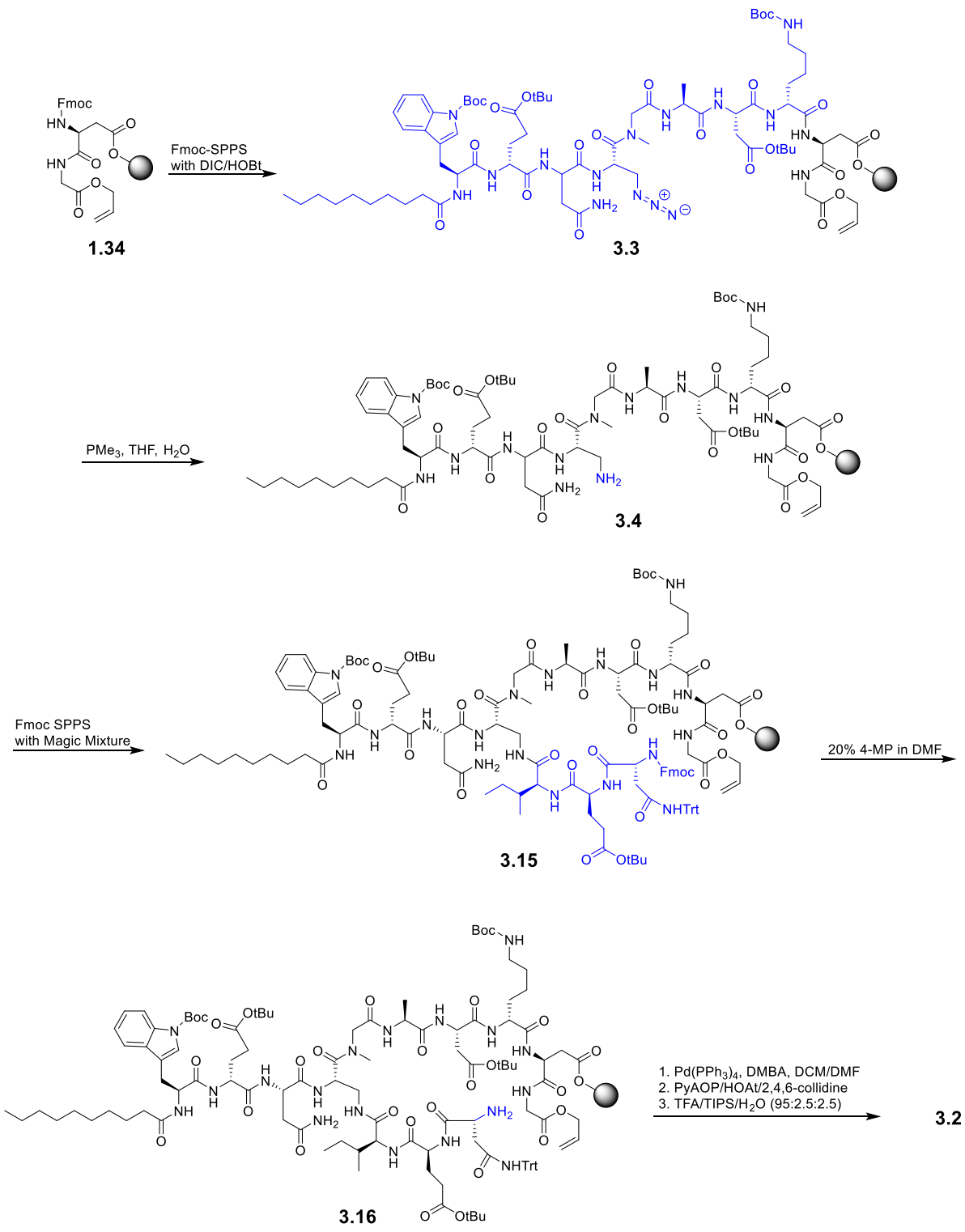

Scheme 3.5: Total synthesis of A54145A$_1$-Asn3-DAPA4-Asp9 (**3.2**).

3.2.1.3 – Assessing the Biological Activity of Peptide **3.2**

The biological activity of peptide **3.2** was assessed as reported by Kopp et al., against *B. subtilis* PY79 at 1.8 mM Ca^{2+}. Peptide **3.2** was not biologically active up to tested concentrations of 128 µg/mL; however, Kopp et al. reported an MIC of 25 µg/mL for this peptide.[78] The reason for the discrepancy between our work and the work of Kopp et al. is unknown. Our results are consistent with previous research reported by the Taylor group and the Martin group, who both found a significant reduction in biological activity when the ester bond of daptomycin is replaced with an amide bond.[84,117]

Some of the biological activity of peptide **3.2** could be restored if the minimum inhibitory concentrations are measured at elevated calcium concentrations. While the synthesized analog was not active at lower calcium concentrations (1.8 mM), at 100 mM calcium, the MIC was reduced to 10 µg/mL, which suggests that this compound may have a reduced affinity for calcium. Such observations have been observed with many moderately active daptomycin analogs synthesized in the Taylor group,[82] although the increased biological activity at higher levels of calcium is irrelevant to potential antibiotic leads *in vivo*, as the free concentration of calcium in blood plasma is 1.25 mM.

Peptide **3.2** was also subjected to a membrane binding assay routinely performed by members of the Taylor and Palmer groups.[49,50,117] The structures of daptomycin and A54145D possess intrinsic fluorophores in the form of Trp1 and Kyn13 in daptomycin, and Trp1 in A54145D. Upon insertion into a hydrophobic environment such as a model membrane, the fluorescence signals of these amino acids undergo a characteristic blue shift, or a hypsochromic shift. In this assay, solutions of analogs in the presence of model membranes are subjected to increasing amounts of calcium, and the fluorescence emission spectrum is observed. Plotting

the fluorescence spectra as a function of calcium concentration (Figure 3.5) demonstrates that membrane binding depends on calcium concentration.

For native A54145D, calcium concentrations between 0.1 and 0.5 mM result in an observable blue shift in the presence of 1:1 DMPC/DMPG lipids, signifying membrane insertion.[48,49] However, for peptide **3.2**, insertion into the model membranes is never observed, even at calcium concentrations up to 50 mM, consistent with the lack of biological activity of this compound.

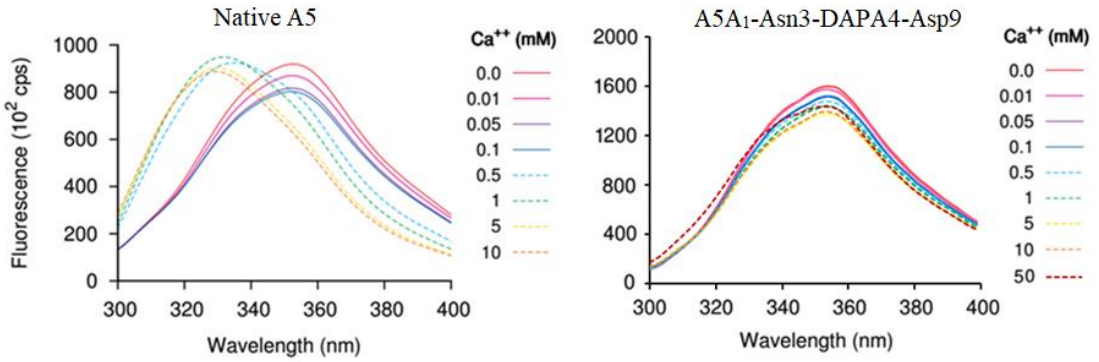

Figure 3.5: Membrane binding curves of native A54145D[49] and peptide **3.2**. Between 0.1 and 0.5 mM Ca^{2+}, the Trp1 of native A54145D undergoes a hypsochromic shift, indicating insertion into the hydrophobic membrane.

3.2.2 – A54145A$_1$-Asn3-Asp9 (Peptide **3.1**)

3.2.2.1 – Proposed Synthesis of A54145A$_1$-Asn3-Asp9 (**3.1**)

After establishing that compound **3.2** was not biologically active, in contradiction with the results of Kopp et al.[78], we turned our attention to compound **3.1**, which contains Thr4 instead of DAPA4. It was suspected that if this compound exhibited good activity, a library of analogs of A54145A$_1$ would still be feasible, if the challenging esterification reaction could be highly optimized.

We envisioned a synthesis of peptide **3.1** analogous to the published syntheses of daptomycin analogs by Barnawi et al., who used TentaGel Trt-Cl and exclusively Fmoc-protected amino acids in their synthesis.[82] Dipeptide **1.34** would be elaborated by standard Fmoc-SPPS yielding linear peptide **3.17** (Scheme 3.6). The depsi-bond would be attempted using DIC and DMAP in the presence or absence of Triton X-100, yielding **3.18**, and further Fmoc-SPPS would yield peptide **3.19**. Allyl deprotection followed by on-resin cyclization using the conditions used for uncyclized peptide **3.16** (PyAOP/HOAt/2,4,6-collidine), and then global deprotection and resin cleavage would yield peptide **3.1**.

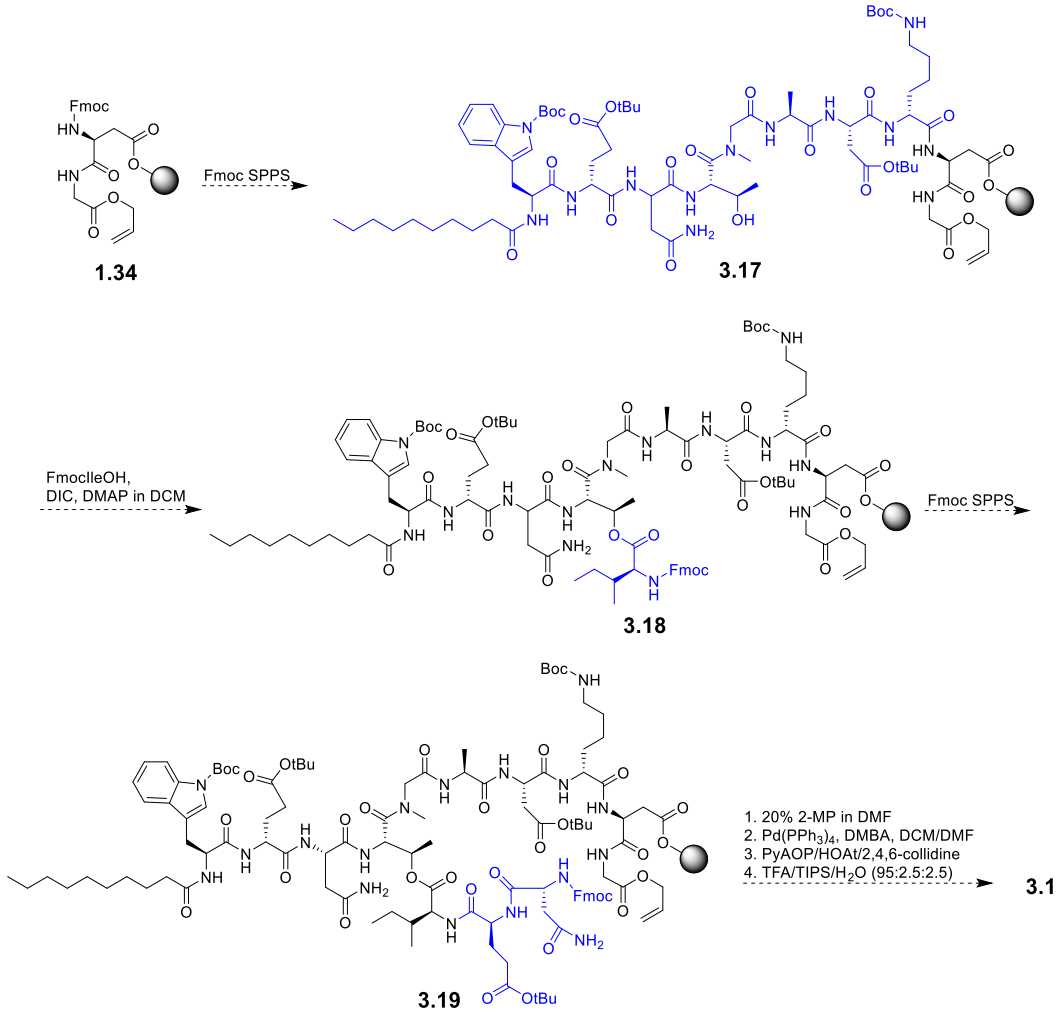

Scheme 3.6: First proposed synthesis of peptide **3.1**.

3.2.2.2 – First Attempted Synthesis of Compound **3.1**.

At this time in the Taylor lab, conditions were developed that significantly decreased the amino acid coupling times. In the synthesis of peptide **3.2**, amino acids were coupled using 4-hour reactions with DIC/HOBt, or 4-hour reactions with HOBt/PyBOP/DIPEA. It was found by Dr. Chuda Lohani, a former post-doctoral fellow in the Taylor group, that peptide coupling times could be reduced to 1 hour by using 2-(6-chloro-1-H-benzotriazole-1-yl)-1,1,3,3-tetramethylaminium hexafluorophosphate (HCTU)/*N*-methylmorpholine (NMM). Accordingly, the synthesis of linear peptide **3.17** from dipeptide **1.34** was attempted employing HCTU/NMM as coupling reagents, using 2-ClTrt-Cl-PS resin.

Linear peptide **3.17** was synthesized using HCTU/NMM as coupling agents, and the resulting crude peptide was analyzed by HPLC. To our dismay, numerous peaks were present in the HPLC chromatogram of the crude mixture (Figure 3.6A). The crude mixture was also analyzed by LRMS, and a complex mass spectrum was obtained (Figure 3.6B); however, several sets of peaks in the spectrum were separated by consistent mass differences. For example, the 44 amu difference between the peak at *m/z* = 1300.6 and *m/z* = 1344.6; *m/z* = 1199.5 and *m/z* = 1243.5; *m/z* = 1085.5 and *m/z* = 1129.5; and *m/z* = 956.5 and *m/z* = 1000.4 is indicative of a temporary CO_2-deprotection adduct on four different peptides, the result of the stepwise removal of Trp1's Boc-protecting group (Scheme 3.4). The difference between the peak at *m/z* = 1300.6 and *m/z* = 1199.5 is indicative of a peptide that lacks the threonine residue. The difference between the peak at *m/z* = 1300.6 and *m/z* = 1085.5 is indicative of a peptide lacking two amino acids: threonine and asparagine. Finally, the difference between the peak at *m/z* = 1300.6 and *m/z* 956.5 corresponds to lacking three amino acids: threonine, asparagine, and *D*-glutamic acid.

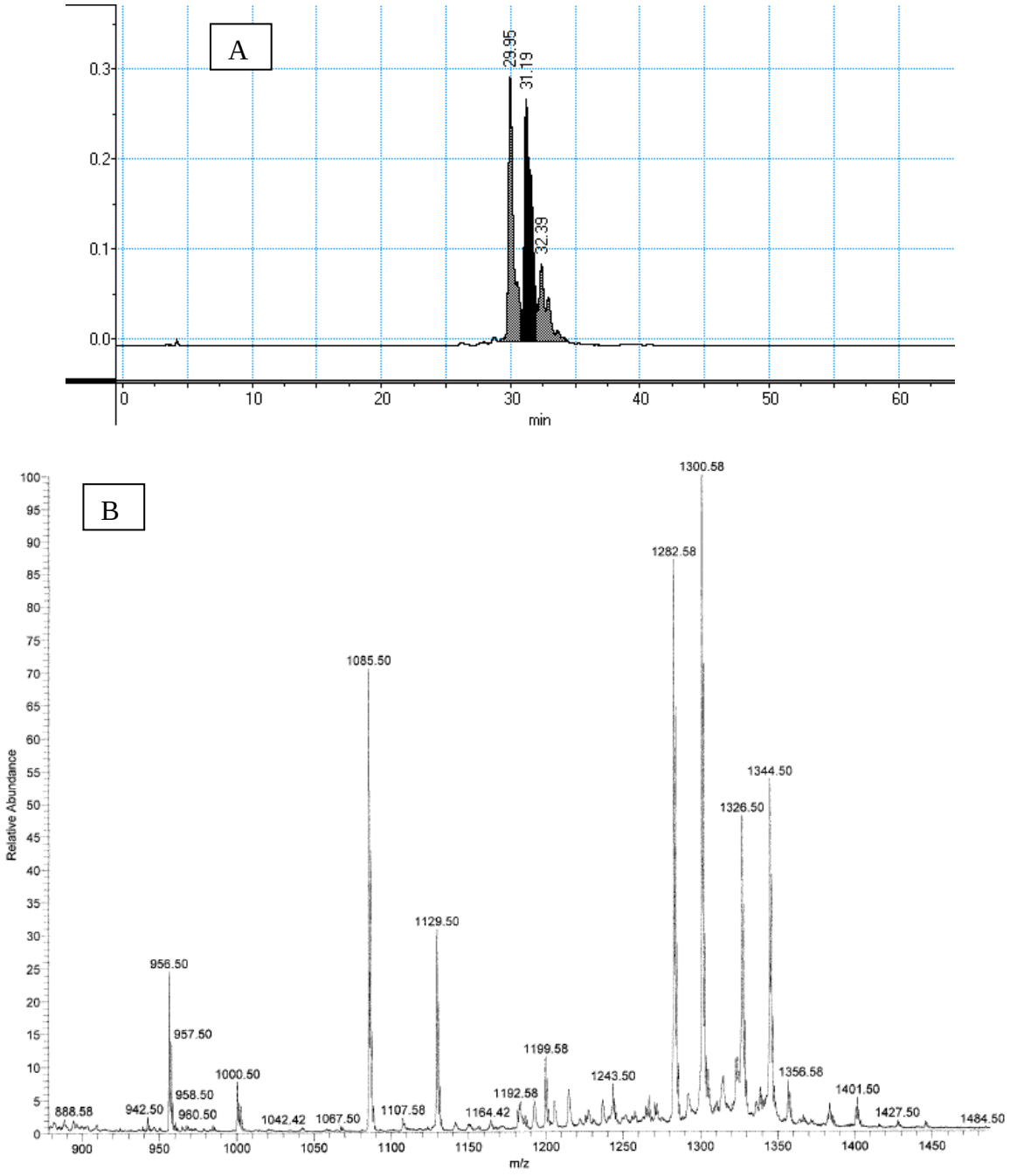

Figure 3.6: Problematic synthesis of linear peptide **3.17** using HCTU/NMM. (A) RP-HPLC chromatogram of crude peptide **3.17** indicates side-reactions occurred. (B) LRMS of crude peptide **3.17** indicating presence of side-products (target *m/z* = 1300.6).

From the analysis of the crude mass spectrum, it was apparent that Thr4, Asn3, and *D*-Glu2 were not being coupled efficiently during the synthesis. There are two conceivable

reasons why this might be the case. Firstly, it was possible that Fmoc-deprotection of sarcosine was not 100% effective and the treatments with 20% 4-MP in DMF (v/v) did not ensure quantitative Fmoc-deprotection. Supporting this hypothesis was the observation that resin-bound FmocSar required extended deprotection times to completely remove the Fmoc group in our synthesis of A54145D (Figure 2.9, Section 2.2.3.2). Admittedly, this issue was not observed in the synthesis of peptide **3.2**. Alternatively, it was possible that the new coupling conditions were not conducive to ensuring quantitative coupling onto sarcosine. As an *N*-methylated amino acid, the *N*-methyl group may sterically hinder the amine nucleophile, thus reducing its nucleophilicity. Perhaps complete coupling does not take place in the reduced reaction times. Either of these two possibilities could account for a crude mass-spectrum similar to what was observed (Figure 3.6B).

Since we had not encountered this issue in our synthesis of compound **3.2**, linear hexapeptide **3.20** was resynthesized using HCTU/NMM as coupling reagents until Sar5, and then Thr4 was incorporated using the previous coupling reagents DIC/HOBt, yielding heptapeptide **3.21** in a near quantitative yield (Scheme 3.7). This indicated that the issue observed in Figure 3.6 was due to inefficient amino acid coupling onto the secondary amine of sarcosine under HCTU/NMM conditions, and not due to inefficient Fmoc-deprotection of sarcosine.

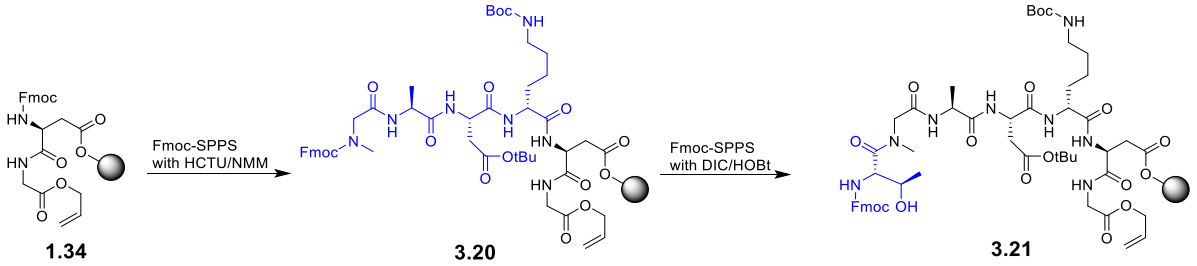

Scheme 3.7: Successful synthesis of heptapeptide **3.21** using HCTU/NMM and DIC/HOBt.

Also present in Figure 3.6B was a peak at *m/z* = 1282.6, which is 18 amu less than the target peak at 1300.6, signifying possible dehydration of Asn. Dehydration was observed previously when PyBOP/HOBt/DIPEA were used as coupling reagents for *D*-Asn11 in the synthesis of peptide **3.2**. This problem was addressed by employing Fmoc-*D*-Asn(Trt)OH instead of Fmoc-*D*-AsnOH. It was suspected that these new coupling reagents, in addition to failing to quantitatively couple amino acids onto sarcosine, were also mediating the dehydration of Asn3. However, we were concerned that protecting Asn3 with a Trt group would increase the difficulty of successfully forming the depsi bond, due to steric bulk of the peptide. Instead of using FmocAsn(Trt)OH, we returned to using DIC/HOBt as coupling reagents. To confirm that Asn-dehydration was occurring during this coupling using HCTU/NMM, the analytical HPLC chromatogram of the peptide was obtained before and after the incorporation of FmocAsnOH, employing DIC/HOBt as coupling reagents, and employing HCTU/NMM as coupling reagents. As we expected, HCTU/NMM facilitated dehydration (Figure 3.7). Fortunately, dehydration was avoided when DIC/HOBt were used as coupling reagents (Figure 3.7; Scheme 3.8), which meant that we would not need to resort to the potentially problematic Trt protecting group, which could interfere with depsi-bond formation. Continuing the synthesis, octapeptide **3.24** was elaborated to linear peptide **3.17** employing DIC/HOBt as coupling reagents without further issue (Scheme 3.8). Following the completed synthesis of linear peptide **3.17**, the next step of the synthesis involved the challenging formation of the ester bond.

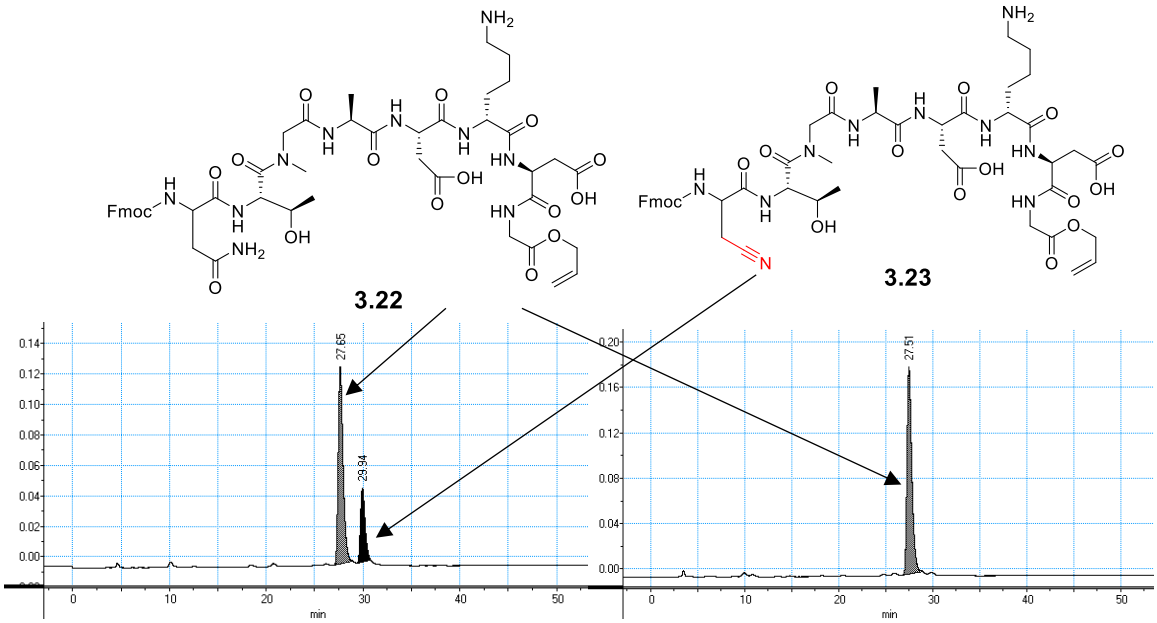

Figure 3.7: HPLC chromatograms of the crude octapeptide **3.24** after cleavage from the resin. (Left) Crude **3.24** obtained after coupling of FmocAsnOH using HCTU/NMM. (Right) Crude **3.24** obtained using after coupling of FmocAsnOH using DIC/HOBt.

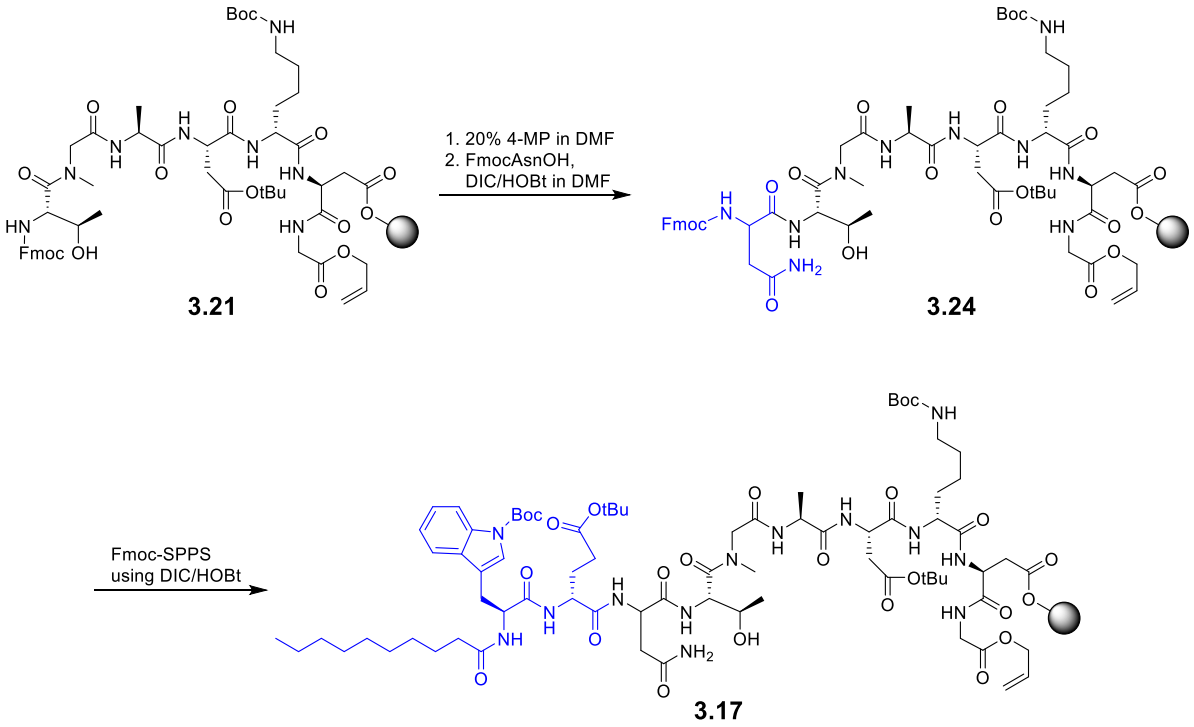

Scheme 3.8: Successful synthesis of linear peptide **3.17**.

Formation of the depsi-bond in peptide **3.18** was performed using the conditions of Barnawi et al.[82] FmocIleOH (10 equiv) and DIC (10 equiv) were mixed in dry DCM for 1 h before being filtered and added to the peptide cartridge. Then, DMAP (0.1 equiv) was added, followed by Triton X-100 to a final concentration of 1% (v/v). After one overnight coupling, the depsi-bond was observed to be ~55% complete, as indicated by RP-HPLC analysis. After a second attempt, the depsi-bond appeared to be ~70% complete. After a third attempt, the depsi-bond appeared to be ~75% complete, and finally, after a fourth attempt, the depsi-bond appeared to be ~80% complete (Figure 3.8). Clearly, formation of the depsi-bond is a synthetically challenging step. However, since the purpose of making peptide **3.1** at this stage in our studies was to compare its biological activity to that of peptide **3.2**, we proceeded with the synthesis, despite incomplete depsi-bond formation.

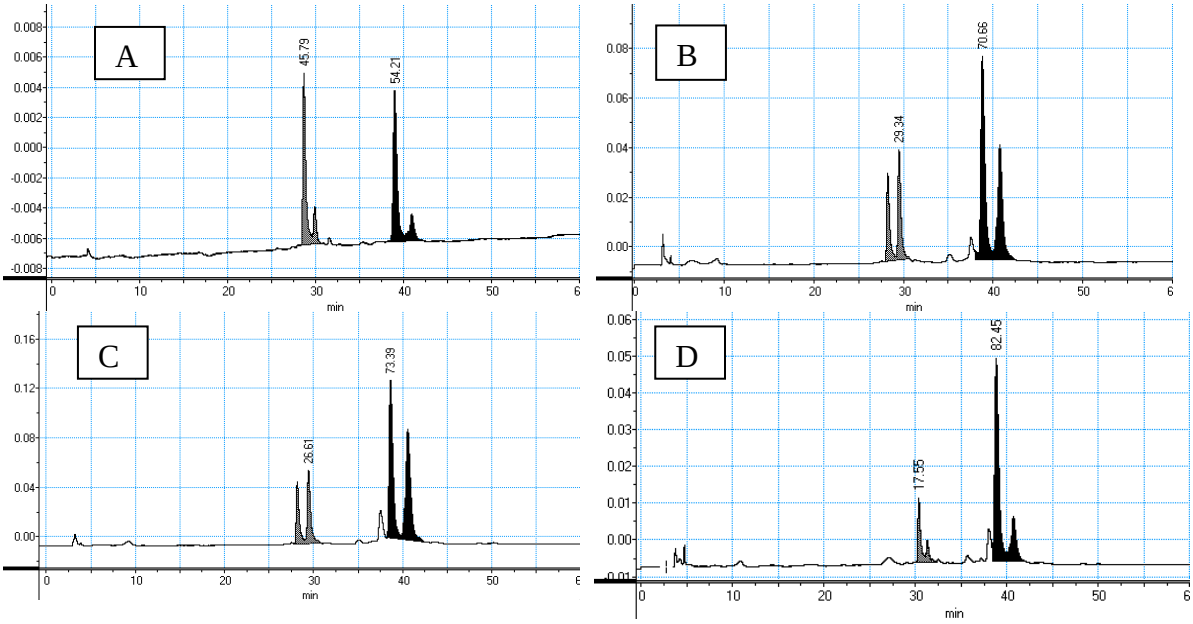

Figure 3.8: RP-HPLC chromatograms of the crude mixture obtained after coupling of FmocIleOH to peptide **3.17** after resin cleavage. Grey peaks correspond to starting material, and black peaks correspond to desired product. (A) First o/n coupling; (B) second o/n coupling; (C) third o/n coupling; (D) fourth o/n coupling.

Following the formation of the depsi-bond, Fmoc-deprotections were conducted using 20% 2-MP in DMF (v/v), to reduce possible aminolysis of the newly formed ester bond.[85] Incorporation of Glu12 with DIC/HOBt proceeded without issue, but upon coupling of Fmoc-*D*-AsnOH with DIC/HOBt, dehydration of *D*-asparagine was once again observed (t_r = 39.7 min vs t_r = 41.6 min, Figure 3.9A). This was unexpected, as this dehydration was not observed with Asn3 with these identical coupling conditions. The reason for this discrepancy is unknown, but nevertheless, the problem was once again solved by using Fmoc-*D*-Asn(Trt)OH (t_r = 36.0 min, Figure 3.9B).

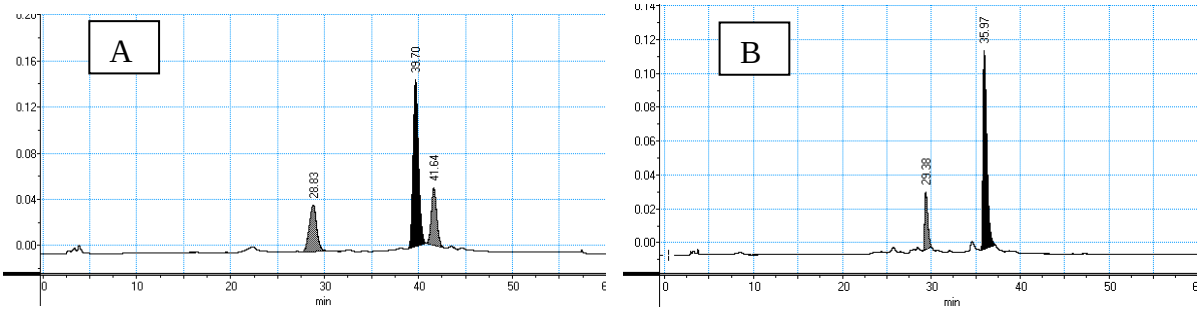

Figure 3.9: RP-HPLC chromatograms after resin cleavage of the crude mixture obtained after using Fmoc-*D*-AsnOH (A) or Fmoc-*D*-Asn(Trt)OH (B) to incorporate residue 11. Black peaks correspond to desired peptide **3.19**. The peak at 29 minutes in each chromatogram corresponds to linear peptide **3.17**, which lacks the depsi fragment. The peak at 41.6 min in chromatogram A corresponds to the peptide resulting from the dehydration of peptide **3.19**.

With peptide **3.19** completed, albeit with some incomplete depsi-bond formation, the only remaining steps in the synthesis of compound **3.1** involved removal of the last Fmoc-protecting group, removal of the allyl group, and the on-resin cyclization. These steps were attempted according to the synthesis of compound **3.2** (Scheme 3.5). The completed peptide was cleaved from the resin with TFA/TIPS/H_2O and HPLC analysis of the final crude peptide revealed three rather strong, closely eluting peaks amongst a variety of other less prominent peaks (Figure 3.10). MS analysis of one of the three more intense peaks (t_r = 33.5 min)

corresponded to peptide **3.25**. Presumably, a pyrrolidine contaminant originating from commercially available PyAOP, or originating from the breakdown of PyAOP *in situ*, reacted with the activated carboxylic acid of linear peptide **3.27** (Scheme 3.9).[122]

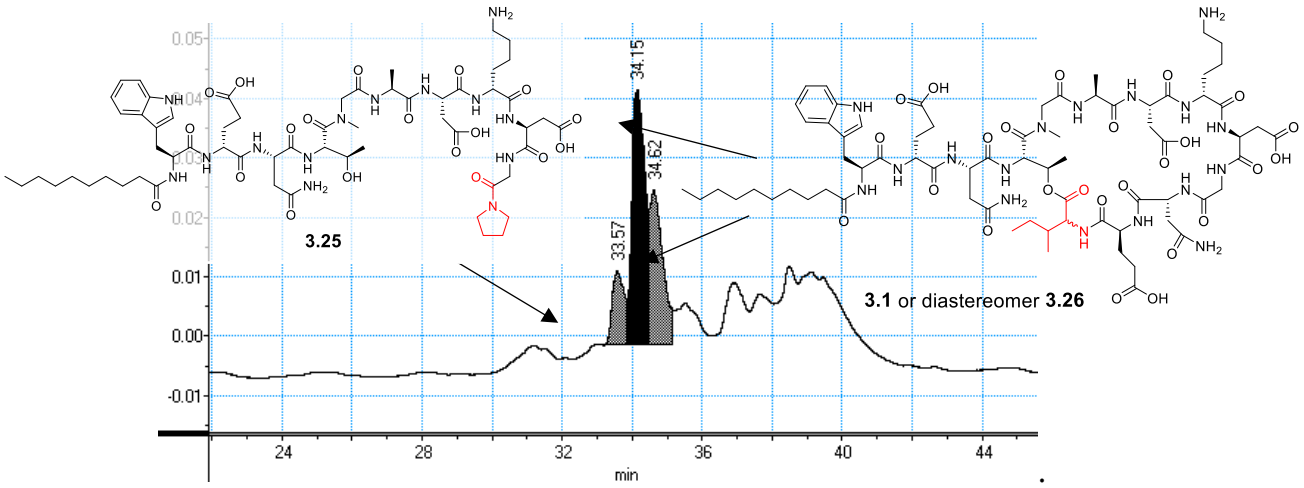

Figure 3.10: Analytical RP-HPLC chromatogram of crude peptide product **3.1**.

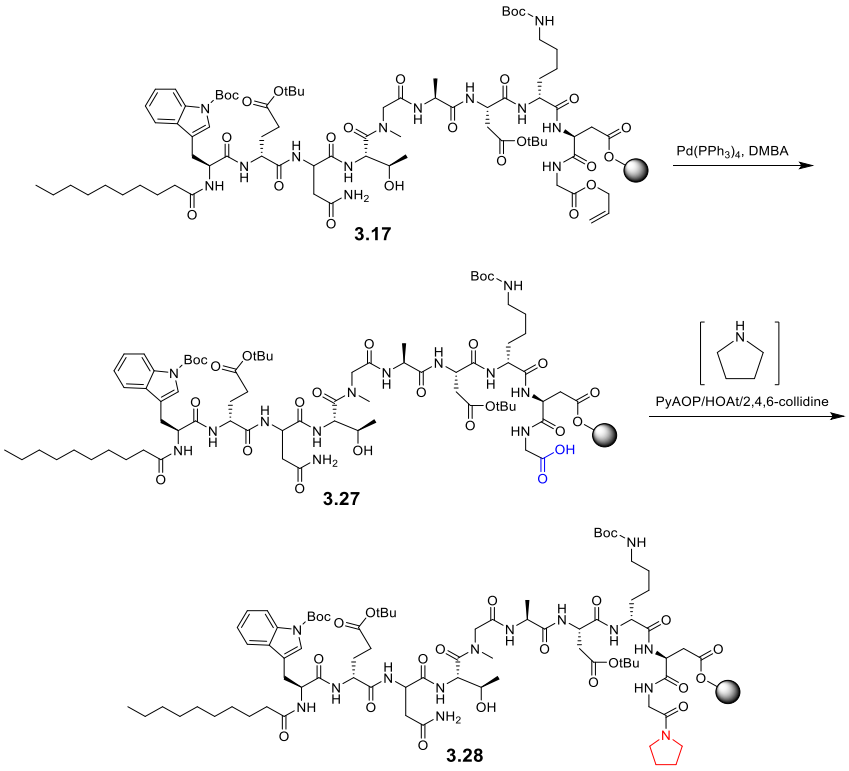

Scheme 3.9: Formation of **3.28** from linear peptide **3.17**.

The two other strong peaks (Figure 3.10, t_r = 34.1 min, t_r = 34.6 min) both had masses corresponding to the final peptide, suggesting that at some point in the synthesis, epimerization had occurred that was only observable upon the completion of the peptide. These compounds corresponding to these two peaks were separated by preparative RP-HPLC, and it was found that only one of these peptides (t_r = 34.6 min) was biologically active against *B. subtilis* PY79.

The presence of the epimeric products in this synthesis, combined with the lack of these epimeric products in the synthesis of compound **3.2**, suggested to us that epimerization occurred during the depsi-bond formation step. This problem was not avoided with the use of TentaGel resin, which has been shown by the Taylor lab to facilitate ester bond formation in comparison to standard PS resin. It was suspected that the epimerization was the result of the extended reaction times that were required for the formation of the depsi-bond. Accordingly, efforts were made to improve this step of the synthesis.

3.2.2.3 – Improving the Synthesis of A54145A$_1$-Asn3-Asp9 (**3.1**)

One of the mechanisms by which an amino acid can racemize during SPPS is via the oxazolone pathway of carbamate-protected amino acids (Scheme 3.10). It is by this mechanism that we suspected epimerization of Ile13 to have occurred during the formation of the depsi bond.

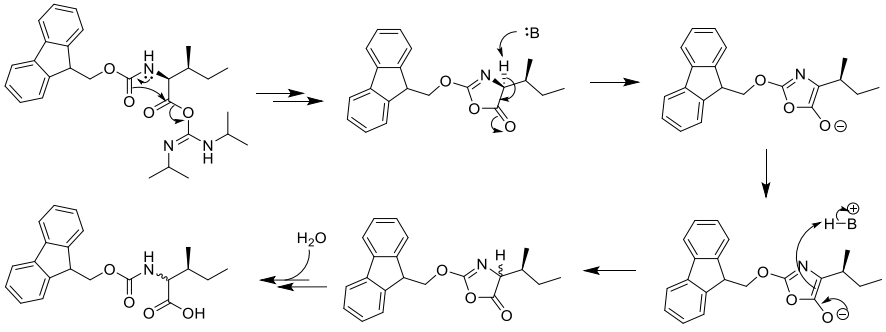

Scheme 3.10: Epimerization via oxazalone formation.

We therefore attempted to make the ester bond using N_3IleOH as a building block instead of FmocIleOH, anticipating that the less sterically demanding azido group would make formation of the ester bond easier. Surprisingly, the formation of the depsi-bond between peptide **3.17** and N_3IleOH was very sluggish, regardless of the resin used, and after three overnight couplings, less than 50% of peptide **3.17** was converted into peptide **3.29** as determined by resin-cleavage and analysis by RP-HPLC (Scheme 3.11). Evidently, the formation of the depsi-bond had proven itself to be very challenging on full-length peptide **3.17**.

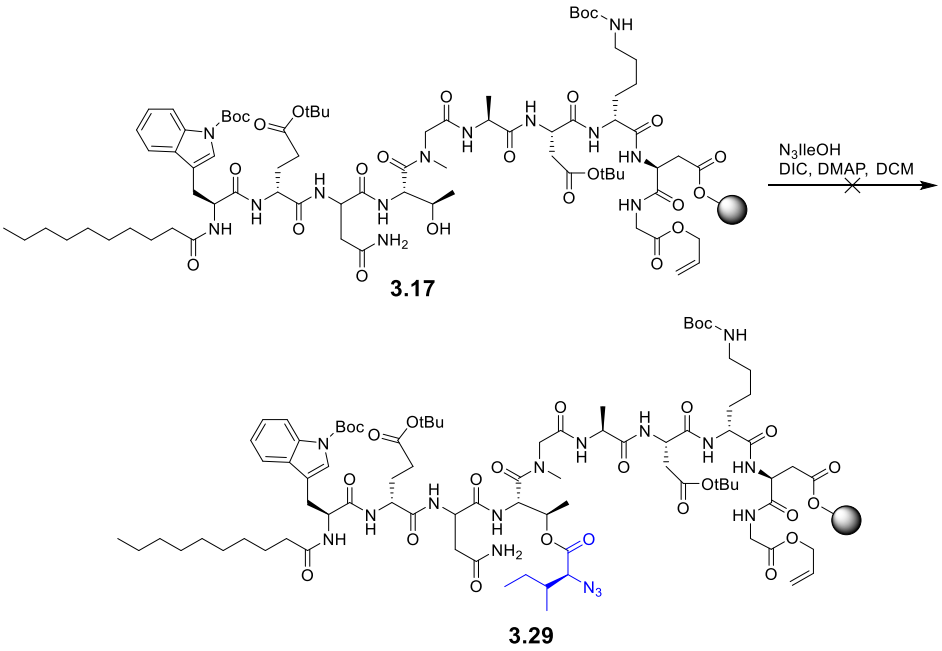

Scheme 3.11: Unsuccessful depsi-bond formation with N_3IleOH and peptide **3.17**.

During a previous synthesis of daptomycin, it was demonstrated that formation of the ester bond in daptomycin became more difficult as the length of the peptide containing the Thr residue increased,[85] and was very difficult when the lipid tail was present. Therefore, we attempted to form the depsi-bond on truncated peptide **3.24**, as demonstrated in Scheme 3.12.

Since this synthesis involved the use of a Fmoc-protected *N*-terminal amino acid, it also necessitated the use of orthogonally protected N_3IleOH at the branch point.

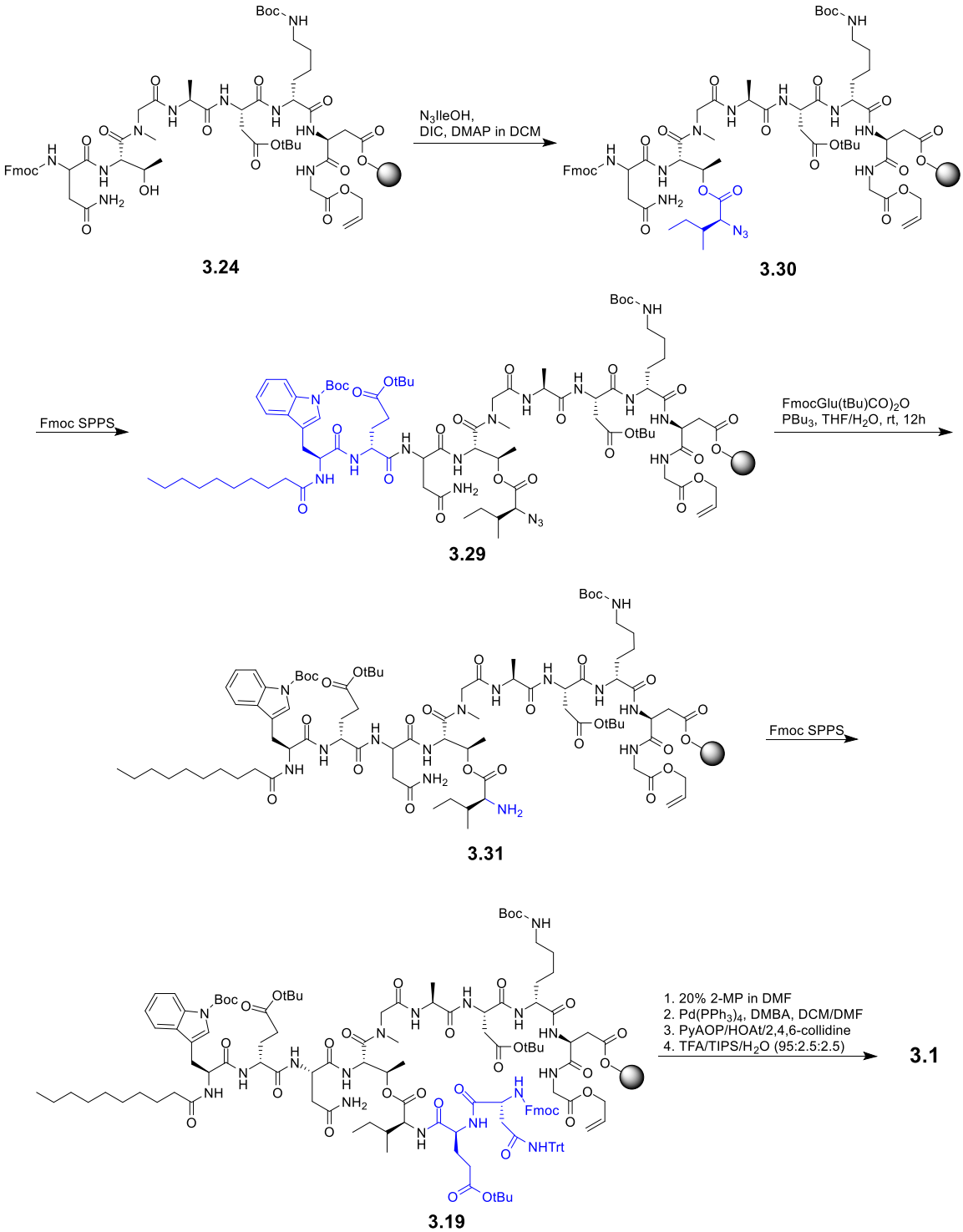

Scheme 3.12: Alternative route to A54145A$_1$-Asn3-Asp9 (**3.1**).

Formation of the depsi-bond between peptide **3.17** and N_3IleOH depended on the choice of resin. With TentaGel Trt-Cl resin, the depsi bond was formed in near quantitative yields after 2 overnight couplings. With 2-ClTrt-Cl-PS resin, the depsi-bind was achieved after three overnight couplings. Further elaboration of the branched peptide **3.30** using Fmoc-SPPS with DIC/HOBt, and 20% 2-MP in DMF to minimize aminolysis of the newly formed ester, yielded branched peptide **3.29**. The azido group in peptide **3.29** was reduced to the corresponding amine **3.31** using PBu_3 in 95:5 THF/H_2O in the presence of the symmetric anhydride of FmocGlu(tBu)OH following literature procedures.[103] Further peptide elaboration using Fmoc SPPS (DIC/HOBt) and 20% 2-MP in DMF gave peptide **3.19**. Fmoc-removal with 2-MP in DMF, followed by allyl group removal using the same conditions as for peptide for peptide **3.16**, followed by on-resin cyclization with PyAOP/HOAt/2,4,6-collidine in DMF, and then resin cleavage and global deprotection with TFA/H_2O/TIPS (95:2.5:2.5), afforded crude peptide **3.1**. After purification by RP-HPLC, peptide **3.1** was obtained, free from epimerization, in 7% yield when TentaGel Trt-Cl resin was used, and 9% yield when 2-ClTrt-Cl-PS resin was used. The sequence of the peptide was confirmed with MS/MS (See Figures D.5 and D.6 in Appendix D).

3.2.2.4 – Biological activity of Compound **3.1**

The biological activity of compound **3.1** was assessed against *B. subtilis* PY79 at 1.8 mM Ca^{2+}. Gratifyingly, A54145A_1-Asn3-Asp9 was found to exhibit an MIC against *B. subtilis* PY79 of 32 µg/mL, in close agreement with Kopp et al., which was 25 µg/mL.[78] These results, in conjunction with the MIC obtained for A54145A_1-Asn3-DAPA4-Asp9, are consistent with our previous studies on daptomycin, which demonstrate that when the ester bond of

daptomycin analogs is replaced with an amide bond, the biological activity is significantly reduced.[84,117]

3.2.3 – SARs of Position 4 Mutants of A54145A$_1$-Asn3-Asp9

There are two key structural differences between A54145A$_1$-Asn3-DAPA4-Asp9 (**3.2**) and A54145A$_1$-Asn3-Asp9 (**3.1**). The first difference is the inherent replacement of the amide-bond in **3.2** with an ester bond in **3.1**. The second difference is the lack of the γ-methyl group of threonine in **3.2**. To elucidate if one or both of these changes affect biological activity, we envisioned the synthesis of two additional A54145A$_1$ analogs (Figure 3.11). The first analog was one in which Thr4 in A54145A$_1$-Asn3-Asp9 was replaced with Ser (A54145A$_1$-Asn3-Ser4-Asp9, **3.32**), and the second analog was one in which DAPA4 in A54145A$_1$-Asn3-DAPA4-Asp9 was replaced with (2*S*,3*R*)-2,3-diaminobutyric acid (DABA4) (A54145A$_1$-Asn3-DABA4-Asp9, **3.33**). Assessing the biological activities of these two analogs would provide insight into which change most adversely affects the biological activity of A54145A$_1$.

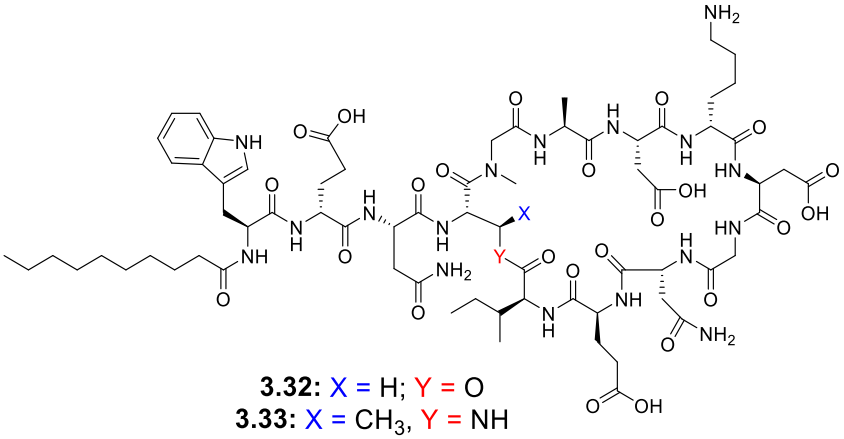

Figure 3.11: Structures of A54145A$_1$-Asn3-Asp9 analogs **3.32** and **3.33**.

3.2.3.1 – Synthesis of A54145A$_1$-Asn3-Ser4-Asp9 (**3.32**)

Serine contains a primary alcohol group and is therefore a better nucleophile than threonine, which contains a secondary alcohol group. Because of this, we hypothesized that our synthesis of peptide **3.1** would not be applicable toward the synthesis of peptide **3.32** as we expected O-acylation of unprotected Ser4 to be a significant issue. We therefore decided to use of side-chain protected FmocSer(Trt)OH in our synthesis, which has an acid-labile trityl protecting group that can be easily removed under mildly acidic conditions, such as 1% TFA in DCM, or 20% hexafluoroisopropanol (HFIP) in DCM. Accordingly, for SPPS synthesis of A54145A$_1$-Asn3-Ser4-Asp9, a more acid-resistant Wang linker would be needed, as the conditions to remove the trityl protecting group from Ser4 would also facilitate resin cleavage from trityl-based resins. We envisioned a modified synthesis in which the initial dipeptide **3.8** was attached to the resin with DIC and DMAP (Scheme 3.13). Unfortunately, when using dipeptide **3.8**, this approach suffered from very low resin-loading. We attempted to improve the loading by preparing resin-bound dipeptide **1.34** in a stepwise fashion (Scheme 3.14); however, the loading was only slightly better.

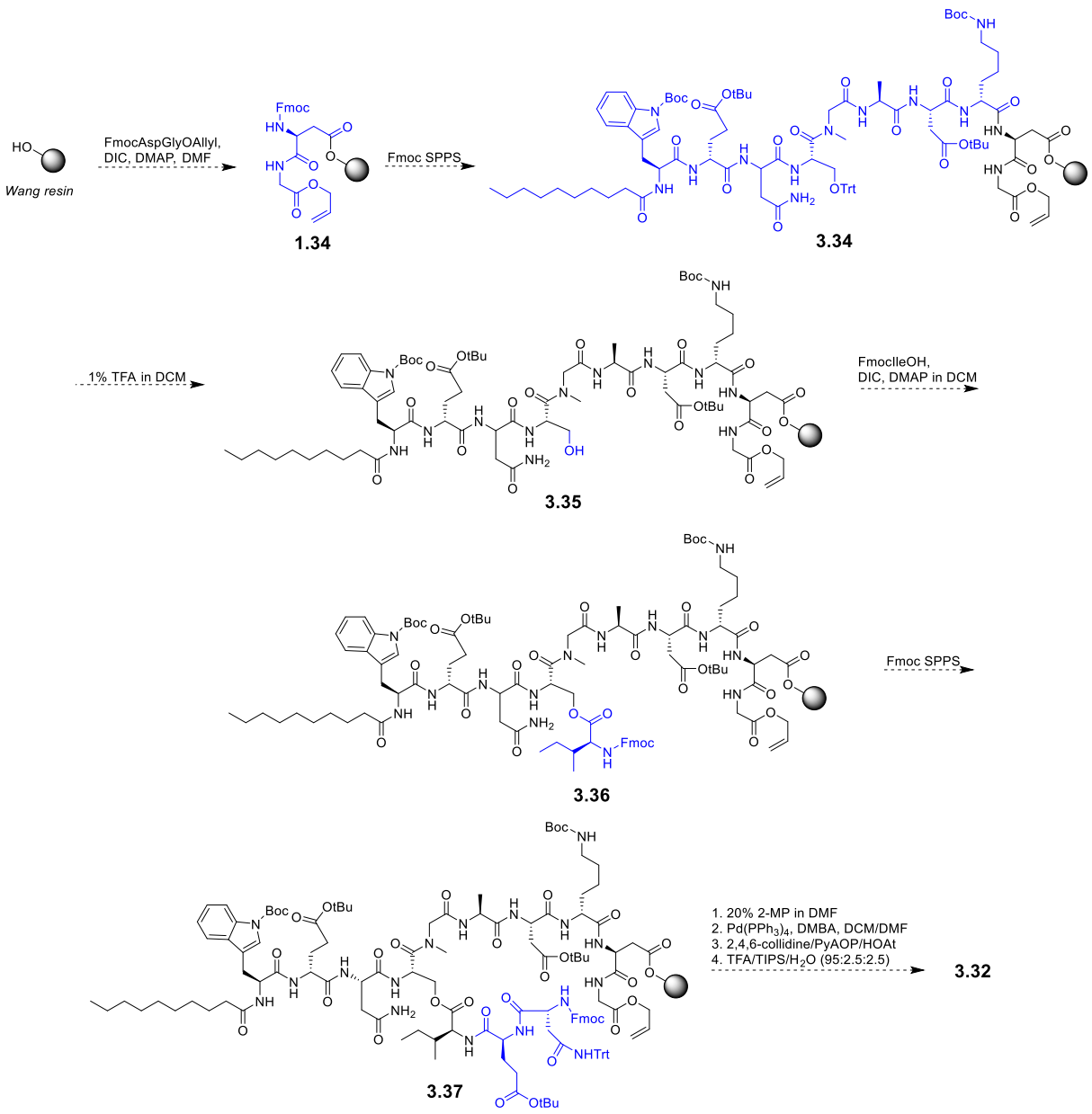

Scheme 3.13: First proposed route to peptide **3.32**.

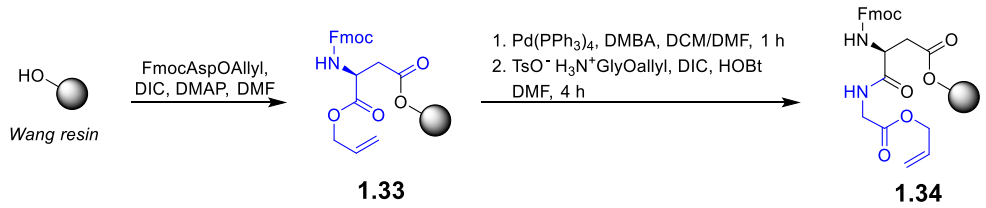

Scheme 3.14: Alternative route to dipeptide **1.34** on Wang resin.

To avoid the problem of low-resin loading using a Wang resin, we decided to use TBDMS-protected serine as a building block, since this allowed us to use TentaGel Trt-Cl resin, which is usually much easier to load than a standard PS Wang resin (Scheme 3.15). Synthesis of linear peptide **3.38** was successfully achieved using DIC/HOBt-mediated amino acid couplings as indicated by RP-HPLC and LRMS. However, after treatment of linear peptide **3.38** with 0.1 M TBAF in DMF to remove the TBDMS group (and form peptide **3.35**), subsequent analyses indicated that a majority of the peptide (>95%) based on relative HPLC signals had been cleaved from the resin.

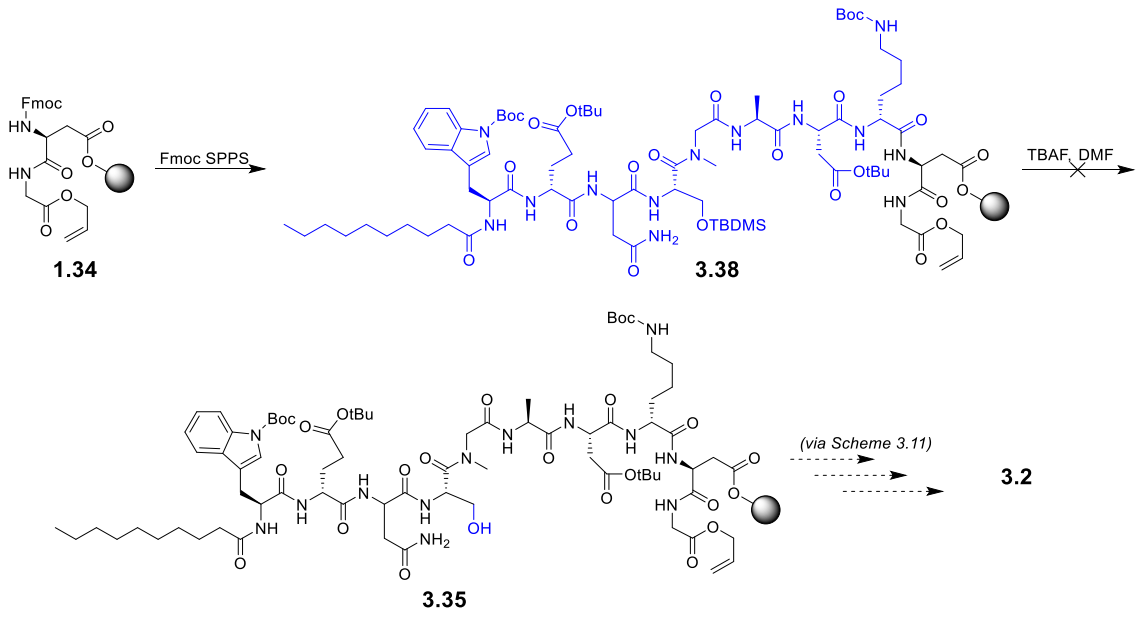

Scheme 3.15: Second proposed route to **3.32**.

We had assumed that the use of side-chain unprotected FmocSerOH in the synthesis of A54145A$_1$-Asn3-Ser4-Asp9 would be unsuccessful due to O-acylation. Nevertheless, we decided to attempt the synthesis using unprotected FmocSerOH as a building block in the hope that O-acylation would not be a major issue (Scheme 3.16). Surprisingly, the use of DIC/HOBt

coupling reagents to transform dipeptide **1.34** into linear peptide **3.35** was very successful, as the HPLC chromatogram of this sample was analyzed and found to contain a single major peak corresponding to peptide **3.35** by LRMS (Figure 3.12). Furthermore, the subsequent depsi-bond formation attempt with FmocIleOH and DIC/DMAP was observed to go to completion after a single overnight coupling. However, after further elaboration with DIC/HOBt couplings, followed by allyl deprotection and on-resin cyclization, we were surprised to find that, once again, two epimeric products were observed by RP-HPLC.

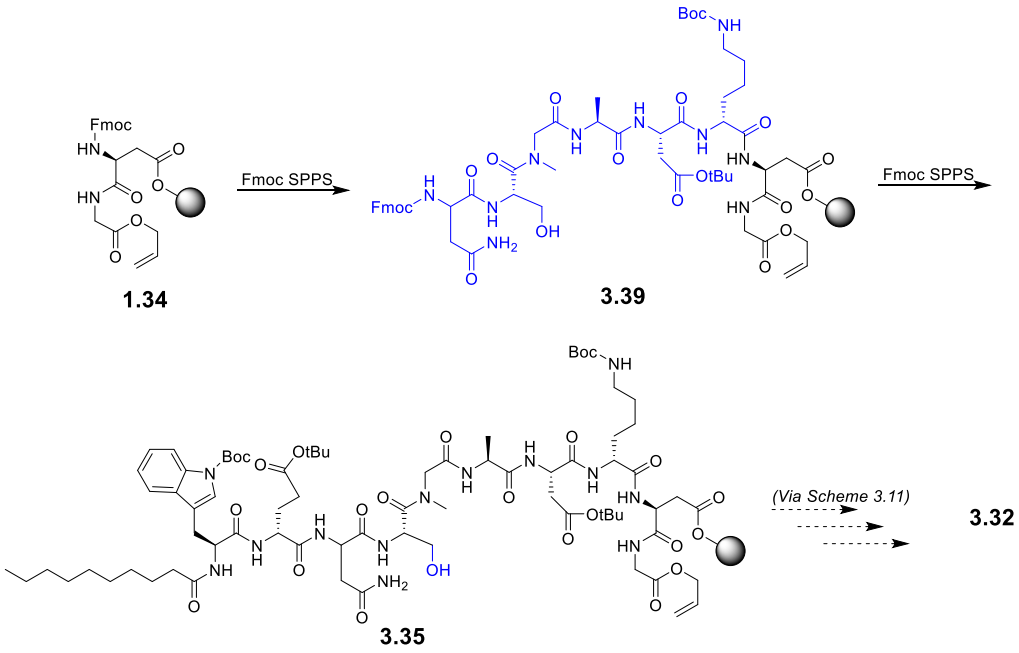

Scheme 3.16: Third proposed route to **3.32**.

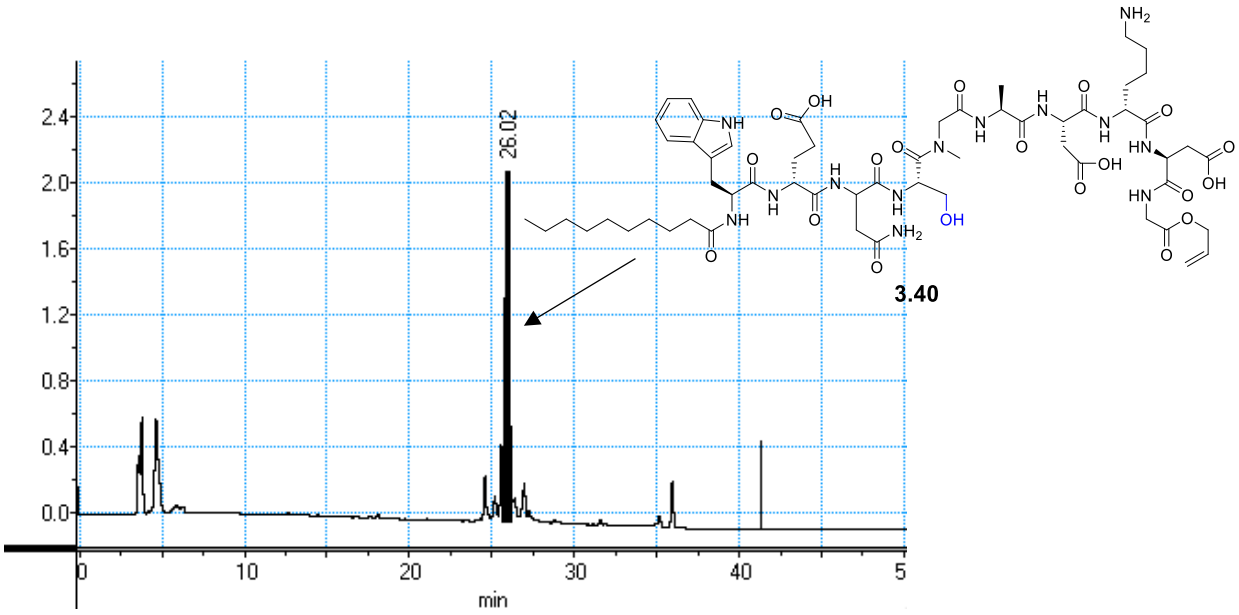

Figure 3.12: RP-HPLC chromatogram of crude peptide **3.35** after resin cleavage forming peptide **3.40**.

Ultimately, we found that the synthesis of **3.32** could be achieved using an approach analogous to that used for **3.1** (Scheme 3.17). Truncated peptide **3.39** containing unprotected Ser4 was synthesized from dipeptide **1.34**. Ester-bond formation with N_3IleOH was quantitatively achieved after two overnight coupling attempts yielding **3.41**, and subsequent peptide elaboration using Fmoc-SPPS with DIC/HOBt, and 2-MP in DMF for Fmoc-removal yielded **3.42**. Reduction of the azido group yielded the corresponding amine **3.43**, and further Fmoc-SPPS yielded **3.37**. Removal of the last Fmoc-group, allyl deprotection, on-resin cyclization, and resin-cleavage with TFA/TIPS/H_2O (95:2.5:2.5) yielded peptide **3.32** in 7% yield after purification by preparative RP-HPLC. No evidence of isoleucine epimerization was observed using this approach. As a novel compound, this peptide was characterized using 1D NMR experiments including ^{1}H-NMR, and 2D NMR experiments including ^{1}H-^{13}C HSQC, ^{1}H-COSY, ^{1}H-TOCSY and ^{1}H-ROESY (See Figures A.19 to A.23, and Table A.3 in Appendix A). Additionally, the amino acid sequence was confirmed with MS/MS (See Figures D.7 and D.8 in Appendix D).

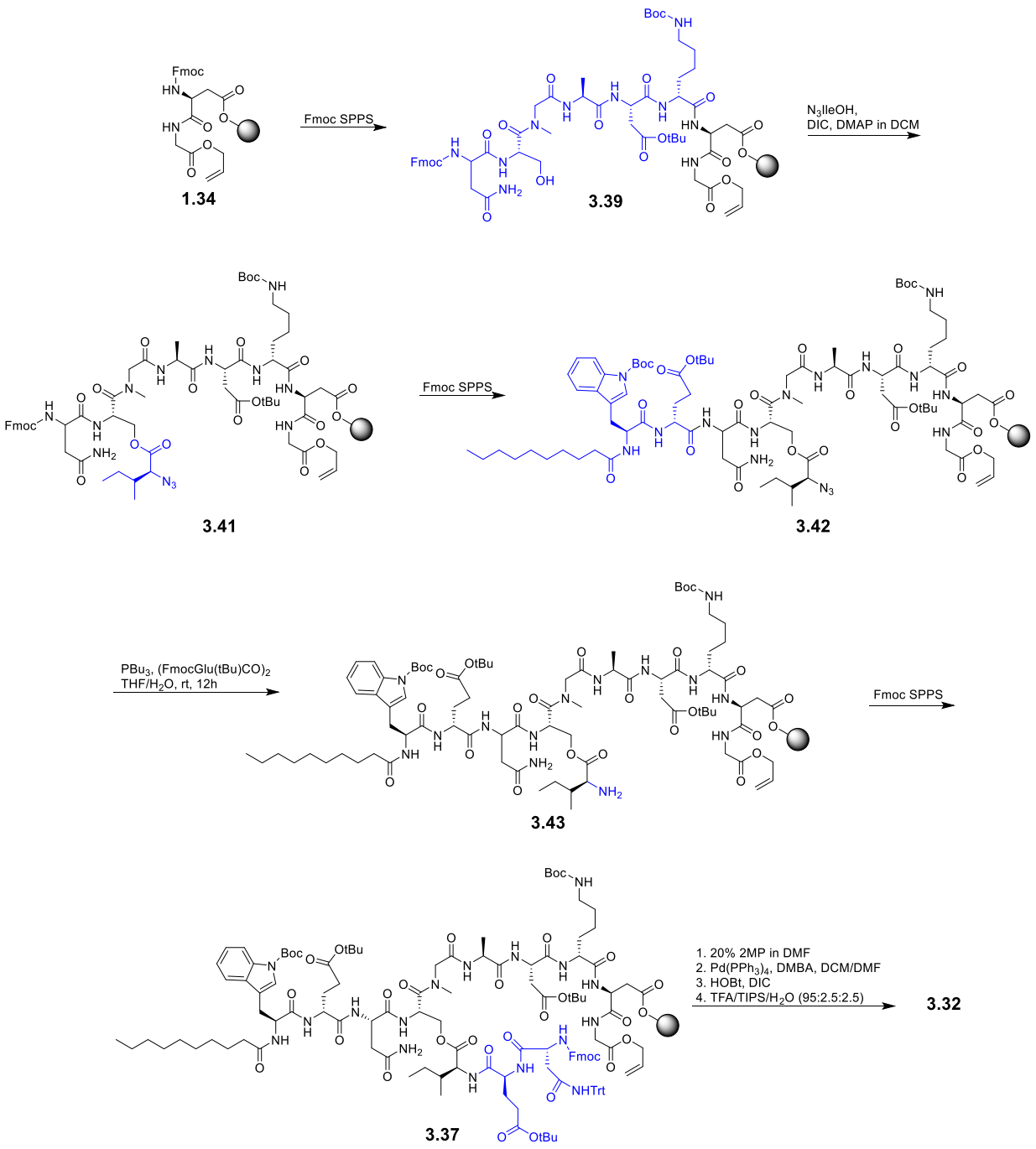

Scheme 3.17: Successful synthesis of A54145A$_1$-Asn3-Ser4-Asp9 (**3.32**).

3.2.3.2 – Synthesis of A54145A$_1$-Asn3-DABA4-Asp9 (**3.33**)

In addition to A54145A$_1$-Asn3-Ser4-Asp9 (**3.32**), we synthesized A54145A$_1$-Asn3-DABA4-Asp9 (**3.33**), in which DAPA4 was replaced with (2*S*,3*R*)-2,3-diaminobutyric acid (DABA). Synthesis of this peptide took place as depicted in Scheme 3.5, except Fmoc-(2*S*,3*R*)-2-amino-3-azidobutanoic acid[117] (FmocAABA, synthesized by Ryan Moreira of the Taylor Group) was used instead of Fmoc-β-azidoAla, and azido group reduction was performed with DTT and DIPEA in DMF. However, this required three 1 h iterations to completely reduce the azido group to the corresponding amine. Further peptide elaboration using DIC/HOBt was readily achieved, and subsequent allyl deprotection, on-resin cyclization, and resin cleavage afforded A54145A$_1$-Asn3-DABA4-Asp9 (**3.33**) after HPLC purification in 15% yield. This novel peptide was completely characterized using 1D NMR experiments including ^{1}H-NMR, and 2D NMR experiments including ^{1}H-^{13}C HSQC, ^{1}H-COSY, ^{1}H-TOCSY and ^{1}H-ROESY (See Figures A.24 to A.28, and Table A.3 in Appendix A) and the amino acid sequence was confirmed with MS/MS (See Figures D.9 and D.10 in Appendix D).

3.2.3.3 – SARs of Position 4 Mutants of A54145A$_1$-Asn3-Asp9

With the completion of these two additional A54145A$_1$ analogs, we were then poised to assess how position 4 affects biological activity. We had previously demonstrated that when Thr4 was replaced with DAPA4, biological activity was reduced by at least 4-fold. The synthesized peptides A54145A$_1$-Asn3-Ser4-Asp9 and A54145A$_1$-Asn3-DABA4-Asp9 were assessed for biological activity and both analogs were shown to have at least a 4-fold reduction in biological activity compared to A54145A$_1$-Asn3-Asp9 when assayed against *B. subtilis* PY79 at 1.8 mM Ca^{2+} (Table 3.1). While we were unable to assess whether the ester bond or the γ-methyl group in Thr4 of A54145A$_1$-Asn3-Asp9 was more important for biological

activity, we were nevertheless able to conclude that both of these functional groups are crucial for biological activity.

Table 3.1: MICs of Position 4 mutants of A54145A$_1$-Asn3-Asp9

entry	peptide	MIC (μg/mL)	
		This work	Kopp et al.[78]
1	A54145A$_1$-Asn3-DAPA4-Asp9 (**3.2**)	>128[a]	25[a]
2	A54145A$_1$-Asn3-Asp9 (**3.1**)	32[a], 8[b]	25[a]
3	A54145A$_1$-Asn3-Ser4-Asp9 (**3.32**)	>128[a]	---
4	A54145A$_1$-Asn3-DABA4-Asp9 (**3.33**)	>128[a]	---

[a]Against *B. subtilis* PY79, 1.8 mM Ca^{2+} present
[b]Against B. subtilis ATCC 1046, 1.25 mM Ca^{2+} present

Interestingly, when the biological activity of peptide **3.1** was assayed against *B. subtilis* ATCC 1046 at 1.25 mM Ca^{2+}, it was observed to be 4-fold more active compared to its activity against *B. subtilis* PY79. This corresponds to only a 16-fold loss in biological activity relative to unmodified A54145D (Table 2.2, Section 2.2.3.3, entries 1 and 3) instead of the 50-fold loss in activity we were expecting as per the results of Kopp et al.[78]

Although our initial idea of using A54145A$_1$-Asn3-DAPA4-Asp9 as a starting point for library genesis using a split-and-pool approach with macro-beads would ultimately not be viable due to the lack of biological activity of A54145A$_1$-Asn3-DAPA4-Asp9, we nevertheless developed a synthesis of using A54145A$_1$-Asn3-Asp9 which is amenable for library generation. Current preliminary studies in the Taylor lab are working towards making a library of daptomycin analogs using a split-and-pool macro-bead approach, and it is likely that this approach will be applicable toward the synthesis of A54145A$_1$-Asn3-Asp9. Challenging steps involve the formation of the ester bond with N_3IleOH, but this has been shown to go to near completion after three depsi-bond formation attempts.

3.2.4 – Assessing the Importance of HOAsn3 and MeOAsp9 to Biological Activity

A54145D was previously synthesized and found to be very biologically active against *B. subtilis* ATCC 1046 (MIC = 0.5 µg/mL, Table 2.2, Section 2.2.3.3). However, making three simultaneous changes to the structure of A54145D to obtain A54145A$_1$-Asn3-Asp9 (8-methyldecanoyl → decanoyl; HOAsn3 → Asn3; MeOAsp9 → Asp9) resulted in a 16-fold loss in biological activity. To determine which of these changes contributed the most to this loss of activity, as well as to determine if activity could be restored with only a single substitution to A54145D's structure, we proceeded to synthesize mutants of A54145D which replaced these non-proteinogenic amino acids in isolation with their proteinogenic counterparts. This is additionally advantageous in the context of synthesizing a library of A54145D analogs. Replacement of either of the two non-proteinogenic amino acids would greatly ease the synthetic challenges of building such a library.

Nguyen et al. prepared a variety of A54145D analogs using a biosynthetic approach (section 1.5.3), including one where HOAsn3 was replaced with Asn3, and another in which MeOAsp9 was replaced with Asp9.[16] Each of these analogs were reported to be 16-fold less active than A54145D against a strain of *S. aureus*, indicating that these two uncommon amino acids are important for its biological activity. They also reported an analog in which HOAsn3 and MeOAsp9 were replaced with *both* Asn3 and Asp9, which was only 8-fold less active than A54145D.[16]

To confirm that the HOAsn residue is indeed essential for good activity, A54145D-Asn3 (**3.44**, Figure 3.13) was prepared according to the method employed in synthesizing A54145D (Schemes 2.13, 2.14, and 2.15), except that FmocAsnOH was used instead of Fmoc-*t*HOAsn(OTBDMS)OH and Fmoc-*e*MeOAsp(tBu)OH was used instead of Fmoc-

*t*MeOAsp(tBu)OH. Accordingly, there was no need for TBDMS removal with TBAF. A54145D-Asn3 was obtained in a 10% yield, characterized by MS/MS sequencing (Figures D.11 and D.12 in Appendix D). Further, to confirm that the MeOAsp residue is indeed essential for good activity, A54145D-Asp9 (**3.45**, Figure 3.13) was also prepared according to Schemes 2.13, 2.14, and 2.15 except that FmocAsp(tBu)OH was used instead of Fmoc-*t*MeOAsp(tBu)OH. A54145D-Asp9 was obtained in an overall 14% yield, and characterized by MS/MS sequencing (Figures D.13 and D.14 in Appendix D).

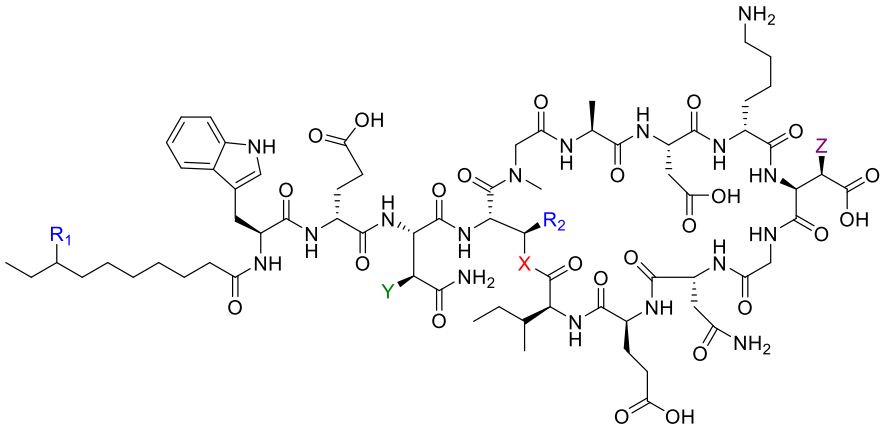

	R_1	R_2	X	Y	Z	Activity
1.11 (A54145D)	CH_3	CH_3	O	OH	OMe	+++
3.1	H	CH_3	O	H	H	+
3.2	H	H	NH	H	H	---
3.32	H	H	O	H	H	---
3.33	H	CH_3	NH	H	H	---
3.44	CH_3	CH_3	O	H	OMe	+
3.45	CH_3	CH_3	O	OH	H	+
1.7 ($A54145A_1$)	H	CH_3	O	OH	OMe	++

Figure 3.13: Summary of A54145D/A_1 analogs and their relative biological activities.

In agreement with Nguyen et al.,[16] substitution of either of these non-proteinogenic amino acids in A54145D resulted in a 16-fold loss of biological activity when tested against *B. subtilis* ATCC 1046 (Table 3.2) – the same degree of activity loss reported with *S. aureus* 42. Interestingly, these two compounds were about 4-fold more active against *B. subtilis* ATCC 1046 than *S. aureus* 42. Perhaps even more interestingly, peptides **3.44** and **3.45** were as active as the A54145D triple mutant A54145A$_1$-Asn3-Asp (**3.1**) which suggests a compensatory effect of multiple substitutions, and further, implies that peptide **3.1** is a valuable starting point for the development of many A54145 analogs.

Table 3.2: MICs of A54145D, A54145A$_1$, and A54145D analogs

entry	peptide	MIC (μg/mL)	
		This work	Literature
1	A54145D (**1.11**)	0.5[a]	2[16,b], 2-4[15,c]
2	A54145D-Asn3 (**3.44**)	8[a]	32[16,b]
3	A54145D-Asp9 (**3.45**)	8[a]	32[16,b]
4	A54145A$_1$ (**1.7**)	2[a]	4-8[15,c]

[a]Against *B. subtilis* ATCC 1046, 1.25 mM Ca^{2+} present; [b] Against *S. aureus* 42, 1.25 mM Ca^{2+} present; [c] Against several other strains of *S. aureus*.

3.2.5 – Effect of Acyl Tail Substitutions on A54145D and A54145A$_1$ and Daptomycin

From the point of view of preparing a large number of A54145D analogs for biological evaluation, it would be more convenient if the *anteiso*-undecanoyl lipid in A54145D could be replaced with a lipid that is commercially available and relatively inexpensive. For these reasons, *anteiso*-undecanoic acid must be synthesized (Scheme 2.3). A54145A$_1$ (**1.7**, Figure 3.13) is identical to A54145D except that it contains an *n*-decanoyl lipid instead of an *anteiso*-undecanoyl lipid. Counter et al. demonstrated that A54145D possesses biological activity that is 2- to 4-fold higher than A54145A$_1$ against various strains of *Staphylococcus*, but we were

interested in assessing how this subtle change affects biological activity against *Bacillus subtilis*.[15]

A54145A$_1$ was synthesized according to Schemes 2.13, 2.14, and 2.15, except that commercially available decanoic acid was used to install the lipid (and Fmoc-*e*MeOAsp(tBu)OH was used instead of Fmoc-*t*MeOAsp(tBu)OH). The target compound was obtained in overall 12% yield, whose sequence was confirmed with MS/MS sequencing (Figures D.15 and D.16 in Appendix D). We found that A54145A$_1$ was 4-fold less active than A54145D against *B. subtilis* ATCC 1046, which is approximately the same relative reduction in activity against *S. aureus* as reported by Counter et al. (Table 3.2).[15] This indicates that the methyl group at position 8 of the lipid in A54145D can be omitted with only a modest reduction in biological activity, and signifies that this lipid tail can be replaced with a decanoyl tail in the future development of A54145A$_1$ or A54145D analogs.

Eliopoulos et al. reported that the MICs of 8-methyldecanoyl daptomycin (8-MeDec-Dap), against various strains of *Staphylococcus, Streptococcus,* and *Listeria,* were 1 to 4-fold less than daptomycin.[20,123] We prepared 8-MeDec-Dap via a semi-synthesis approach (Scheme 3.18). The succinimidyl ester of 8-methyldecanoic acid was coupled to Orn(Boc)-deacyldaptomycin (Orn(Boc)deacylDap) in the presence of TEA. Orn(Boc)deacylDap was generously provided by Cubist Pharmaceuticals Inc, now part of Merck & Co. The Boc-group on the Orn residue was removed with TFA/thioanisole scavenger to produce 8-MeDec-Dap, which was purified by preparative RP-HPLC. MIC studies with 8-MeDec-Dap against *B. subtilis* revealed that the addition of the methyl group to the 8-position of increased biological activity 1.5-fold (Table 3.3), consistent with the studies of Eliopoulos et al.[12a,b] Hence, it appears that substituting the decanoyl lipid in daptomycin with 8-MeDec-Dap does not

significantly affect its activity against *B. subtilis*, but does modestly affect the activity of A54145D against *B. subtilis.*

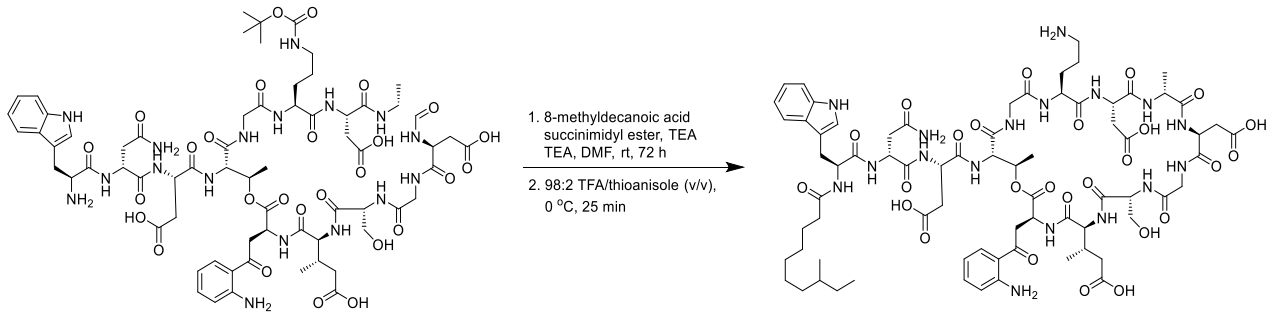

Scheme 3.18: Synthesis of 8-MeDec-Dap (**3.46**) from Orn(Boc)DeacylDap.

The strategy demonstrated in Scheme 3.18 was also used to synthesize two additional analogs of daptomycin in which the lipid tail was replaced with a pentadecanoyl tail, or 10-methyldodecanoyl lipid. Unsurprisingly, these analogs with a longer acyl tail were very biologically active, more-so than authentic daptomycin (Table 3.3). Previous literature has demonstrated that longer acyl tails on daptomycin provide increased biological activity but also increased the toxicity of the analogs *in vivo* (Table 1.1, section 1.5.1).

Table 3.3: MICs of daptomycin and daptomycin analogs with alternative lipid tails

entry	peptide	MIC (μg/mL)[a]
1	Daptomycin (**1.2**) (i.e., decanoyl lipid tail)	0.75
2	8-methyldecanoyl-daptomycin (**3.46**)	0.5
3	10-methyldodecanoyl-daptomycin (**3.47**)	0.25
4	pentadecanoyl-daptomycin (**3.48**)	0.25

[a] Against *B. subtilis* ATCC 1046, 1.25 mM Ca^{2+} present

3.3 – Conclusions

In this chapter, analogs of A54145D and A54145A_1 were prepared and evaluated for their *in vitro* biological activity. It was discovered that, contrary to the results obtained by Kopp

et al., the activity of A54145A$_1$ is significantly compromised when the ester bond is replaced with an amide bond. Both the ester bond and the γ-methyl group in Thr4 of A54145A$_1$-Asn3-Asp9 were found to be crucial for biological activity. This result is consistent with studies performed by the Taylor and Martin groups, who have reported that the activity of daptomycin is significantly compromised when the ester bond is replaced with an amide bond, and that both the ester bond and the γ-methyl group in Thr4 of daptomycin are crucial for biological activity.[84,117] Consequently, it will not be prudent to make libraries of the A54145 factors in which the ester bond is replaced with an amide bond. However, it might be possible to use the route outlined in Schemes 3.7, 3.8, and 3.12 to make libraries of the A54145 factors even though the synthetically challenging ester bond will be present.

We also performed studies to determine if either of the uncommon amino acids HOAsn and MeOAsp could be replaced with their common amino-acid counter-parts. A single substitution of HOAsn with Asn, or of MeOAsp with Asp resulted in a 16-fold decrease in biological activity. However, a double substitution of HOAsn with Asn and MeOAsp with Asp also resulted in a 16-fold loss in biological activity relative to A54145D, but a 4-fold loss in biological activity relative to A54145A$_1$. It is unlikely that it will be possible to replace MeOAsp with amino acids other than Asp or 3-hydroxyAsp[79] as position 9 is part of the Ca^{2+}-binding DXDG motif, and it has been shown that replacing Asp9 in daptomycin with Asn results in complete loss of activity.[76]

In both Chapter 2 and Chapter 3, many challenges in the total synthesis of these A54145 analogs were encountered, which are summarized in Figure 3.14. The challenges encountered, and the strategies employed to overcome them, will also be of value to future total syntheses of cyclic lipodepsipeptide antibiotics.

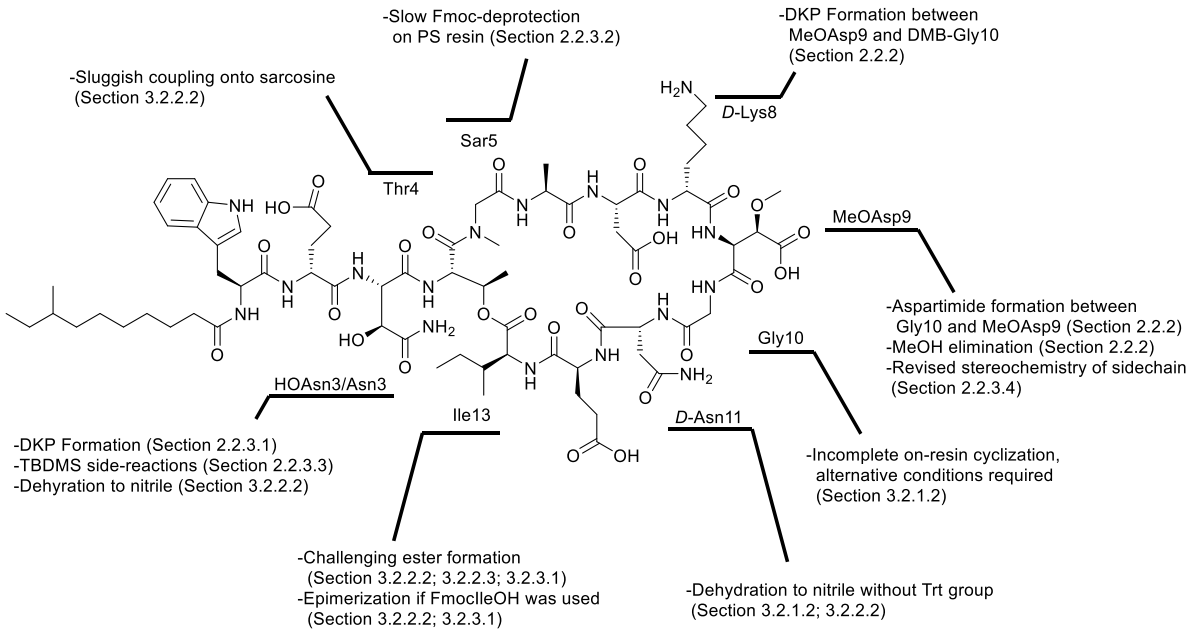

Figure 3.14: Summary of issues encountered in the synthesis of A54145D and analogs.

3.3.1 – Future Studies

In the development of antibiotics related to A54145, it is possible that small structural changes to the structure of A54145D may tune its biological activity in the presence and absence of lung surfactant. For this reason, having the total synthesis available for A54145 analogs containing both MeOAsp9 or Asp9 is advantageous.

Future work in the Taylor lab will be to synthesize new analogs of A54145D and A54145A$_1$. Substitutions to either MeOAsp9 or HOAsn3 result in a 16-fold loss in biological activity in isolation, but the Baltz group has shown that additional substitutions can compensate and restore some biological activity (Table 1.2, entries 16 and 17, entries 19 and 25). The results reported here comparing peptide **3.1** with A54145A$_1$ (**1.7**) are in complete agreement with the results of the Baltz group, in that both the non-proteinogenic HOAsn and MeOAsp can be replaced with Asn3 and Asp9 with only a 4-fold loss in biological activity, relative to A54145A$_1$. It may be worthwhile to conduct an alanine scan of peptide **3.1**, to determine if

there are any amino acids of A54145A$_1$-Asn3-Asp9 that are amenable to substitution, much like the alanine scan performed on daptomycin by Barnawi et al.[81,82] With a synthetic strategy for A54145D analogs containing MeOAsp9 available, in addition to a synthetic strategy for A54145D analogs containing Asp9, the synthesis of these analogs are quite feasible.

The A54145 family of antibiotics contains 8 different factors, illustrated in Figure 1.4 (Section 1.1). These factors arise from the inherent flexibility of suitable substrates in A54145's NRPSs. There are three options for the lipid tail (*anteiso*-undecanoyl, *n*-decanoyl, and *iso*-decanoyl), two options for position 13 (isoleucine and valine), and two options for position 12 (glutamate and 3-methylglutamate). All possible combinations of these variations produce, in theory, a total of twelve members in the A54145 family – it is therefore surprising that A54145 produces only 8 factors by *Streptomyces fradiae.* It may be of interest to synthesize these remaining A54145 family members (Table 3.4) and assess their biological activities.

Table 3.4: Structures and MICs of the "entire" A54145 family.[15]

A54145 Factor	Position 12	Position 13	Lipid Tail	MIC[a] (µg/mL)
B$_1$	MeGlu	Ile	*iso*-decanoyl	0.5 – 2.0
B	MeGlu	Ile	*n*-decanoyl	0.5 – 2.0
E	MeGlu	Ile	*anteiso*-undecanoyl	0.25 – 2.0
--	MeGlu	Val	*iso*-decanoyl	---
--	MeGlu	Val	*n*-decanoyl	---
C	MeGlu	Val	*anteiso*-undecanoyl	2.0 – 4.0
A	Glu	Ile	*iso*-decanoyl	0.5 – 2.0
A$_1$	Glu	Ile	*n*-decanoyl	1.0 – 8.0
D	Glu	Ile	*anteiso*-undecanoyl	0.5 – 4.0
F	Glu	Val	*iso*-decanoyl	2.0 – 32
--	Glu	Val	*n*-decanoyl	---
--	Glu	Val	*anteiso*-undecanoyl	---

[a] Against several *S. aureus* strains

Daptomycin and A54145D both contain DXDG calcium-binding motifs; however, two of the amino acids vary between them: Asp7-D-Lys8-MeOAsp9-Gly10 in A54145, and Asp7-

D-Ala8-Asp9-Gly10 in daptomycin. It may be of interest to generate hybrid daptomycin-A54145D analogs, in which the calcium-binding DXDG motif of A54145 (containing MeOAsp) is replaced with the DXDG motif of daptomycin (containing Asp). This series of substitutions would change the ionization state of the peptide at physiological pH from -3 to -4, since the basic *D*-Lys8 is replaced with a neutral *D*-Ala8, which may affect biological activity. To compensate, an additional analog could be synthesized in which position 6 of A54145D (Ala) is also replaced by position 6 of daptomycin (Orn), resulting in a peptide with the same net charge in solution. With the calcium-binding motif of daptomycin, the hybrid peptide may have a higher calcium affinity and therefore increased biological activity, while maintaining A54145D's activity in the presence of lung surfactant.

Ultimately, with the synthesis of A54145D in place, we are poised to synthesize many more analogs of A54145D or A54145A_1, some of which may have improved biological activity and may retain biological activity in the presence of lung surfactant. If sufficiently active in mouse models, they may find use as an alternative treatment for community-acquired pneumonia.

3.4 – Experimental

3.4.1 – General Experimental

The membrane binding assay used to study the interaction of A54145A_1-Asn3-DAPA4-Asp9 with model membranes was performed as described in Taylor et al.[49]

3.4.2 – Experimental Procedures for Synthesized Compounds

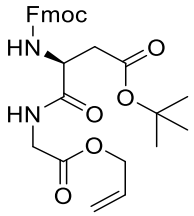

3.7

FmocAsp(tBu)GlyOAllyl (3.7). To dry THF (90 mL) was added the tosylate salt of allyl glycine (**2.73**) (7.0 g, 24.4 mmol, 1 equiv), *N*-ethylmorpholine (3.08 mL, 24.4 mmol, 1 equiv) and HOBt (3.29 g, 24.4 mmol, 1 equiv). The suspension was stirred and cooled to 0 ^{o}C. To this was added FmocAsp(tBu)OH (10.0 g, 24.4 mmol, 1 equiv) and the resulting mixture was stirred vigorously. A solution of DCC (5.54 g, 26.8 mmol, 1.1 equiv) in dry THF (35 mL) was added and the mixture allowed to stir at 0 ^{o}C for 30 min. The ice bath was removed and the mixture was further stirred at room temperature for 16 h. Following the reaction, the DCU by-product was removed by filtration, and the filtrate concentrated *in vacuo*. The product was purified by column chromatography using 30:70 EtOAc/hexane to yield Compound **3.7** (10.9 g, 86% yield) as a thick oil. ^{1}H-NMR (300 MHz, $CDCl_3$) δ: 7.74 (2H, t, J = 7.5 Hz), 7.57 (2H, d, J = 7.3 Hz), 7.38 (2H, t, J = 7.4 Hz) 7.29 (2H, t, J = 7.4 Hz), 5.95-5.82 (2H, m), 5.29 (1H, d, J = 20.2 Hz), 5.23 (1H, d, J = 10.4 Hz), 4.64-4.42 (5H, m), 4.22 (1H, t, J = 6.8 Hz), 4.12-3.95 (2H, m), 2.89 (1H, d, J = 20.2), 2.65 (1H, dd, J = 16.5, 6.2), 1.44 (9H, s). ^{13}C-NMR (75 MHz, $CDCl_3$): δ: 171.0, 170.9, 169.0, 156.1, 143.7, 141.3, 131.4, 127.8, 127.1, 125.1, 120.0, 119.0, 81.9, 67.3, 66.0, 51.1, 47.1, 41.4, 37.4, 28.0. HRMS (ESI+): *m/z* $[M+H]^+$ calcd for $C_{28}H_{33}N_2O_7$, 509.22823, found 509.22835.

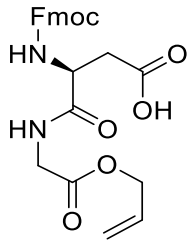

3.8

FmocAspGlyOAllyl (3.8). FmocAsp(tBu)GlyOAllyl (**3.7**) (10.9, 21.4 mmol) was added to a round-bottom flask and was cooled in an ice bath. Pre-chilled trifluoroacetic acid (50 mL) was added and the mixture was stirred at 0 ^{o}C for 6 h. The solvent was removed by vacuum, and trace TFA removed azeotropically with toluene three times. Toluene was removed azeotropically with methanol, and methanol was removed azeotropically with chloroform. The crude product was suspended in chloroform and filtered to yield the purified product as a white solid (7.7 g, 79%). Characterization data matched the literature.[86] ^{1}H- NMR (300 MHz, $CDCl_3$) δ: 7.78 (2H, d, J = 7.5 Hz), 7.65 (2H, d, J = 7.5 Hz), 7.38 (2H, t, J = 7.3 Hz), 7.29, (2H, t, J = 7.4 Hz), 5.91 (1H, m), 5.30 (1H, d, J = 17.1 Hz), 5.19 (1H, d, J = 10.4 Hz), 4.61-4.55 (3H, m), 4.38-4.22 (3H, m), 3.95 (2H, s), 2.83-2.67 (2H, m). ^{13}C-NMR (75 MHz, DMSO-d_6): 172.1, 172.0, 169.8, 156.3, 144.2, 141.1, 132.7, 128.1, 127.5, 125.8, 120.5, 118.3, 66.2, 65.2, 51.6, 47.0, 41.2, 36.7. HRMS (+ESI) *m/z*: calcd for $C_{24}H_{25}N_2O_7$: 453.16563, found 453.16568.

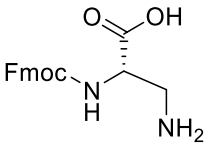

3.9

(*S*)-2-((((9H-Fluoren-9-yl)methoxy)carbonyl)amino)-3-aminopropanoic acid (3.9). Compound **3.9** was synthesized using procedures from Picha and coworkers and Lau and coworkers.[118,119] FmocAsnOH (11.1 g, 31.3 mmol, 1 equiv) was added to a stirring mixture of

acetonitrile (50 mL), ethyl acetate (50 mL), and water (25 mL) at room temperature. To the stirred suspension was added (diacetoxyiodo)benzene (12.1 g, 37.6 mmol, 1.2 equiv), and the reaction was stirred overnight. The solvent was removed *in vacuo* and the suspension was dissolved in water (150 mL). The solution was acidified to pH 1 with concentrated HCl, and the acidified solution was washed with ethyl acetate (3 x 100 mL). The aqueous phase as adjusted to pH 6 with 2M NaOH, and the precipitated was filtered and washed with water three times, chilled ethanol once, and diethyl ether five times. The solid was dried under vacuum to give compound **3.9** as a beige solid (5.83 g, 57%). ^{1}H NMR (300 MHz, DMSO) δ: 8.48 (br. s, 1H), 7.86 (2H, d, J = 7.4 Hz), 7.73 (2H, d, J = 7.2 Hz), 7.39 (2H, t, J = 7.3 Hz), 7.30 (2H, t, J = 7.3 Hz), 6.81 (br. s, 1H), 4.30-4.21 (3H, m), 3.71 (1H, m), 2.98 (1H, m), 2.78 (1H, m), 1.88 (1H, s).

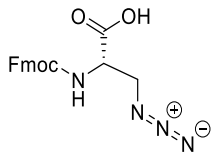

3.10

Fmoc-β-azidoalanine-OH (3.10). Compound **3.10** was synthesized according to a previous method by Lau et al.[118] Compound **3.9** (1.0 g, 3.1 mmol, 1 equiv) was dissolved in a biphasic mixture of water (15 mL), MeOH (30 mL) and DCM (25 mL), according to the procedure by Lau and Spring.[118] To this was added copper(II) sulfate pentahydrate (5 mg, 0.02 mmol, 0.006 equiv) and compound **2.77** (2.0 g, 9.5 mmol, 3.1 equiv). The mixture was stirred vigorously overnight. The mixture was further diluted with additional DCM (30 mL), and the aqueous phase was isolated. The organic phase was extracted with saturated $NaHCO_3$ (2 x 50 mL), and the combined aqueous phases were washed with diethyl ether (2 x 50 mL). The aqueous phase was adjusted to pH 2 with concentrated HCl and extracted with diethyl ether (3 x 60 mL). The

ether layers were dried over Na_2SO_4 and concentrated under reduced pressure to give Fmoc-β-Ala(N_3)OH as a beige, amorphous solid (0.75 g, 72%). ^{1}H-NMR (300 MHz, $CDCl_3$) δ: 11.0 (1H, br. s), 7.76 (2H, d, J = 7.5 Hz), 7.60 (2H, d, J = 7.4 Hz), 7.40 (2H, t, J = 7.4 Hz), 7.32 (2H, t, J = 7.5 Hz), 6.0 (1H, s), 4.62-4.41 (3H, m), 4.22 (1H, t, J = 6.9 Hz), 3.79-2.70 (3H, m). ^{13}C-NMR (75 MHz, $CDCl_3$) δ: 175.8, 159.2, 146.4, 144.2, 130.8, 130.1, 128.0, 123.0, 70.5, 56.7, 55.2, 49.9.

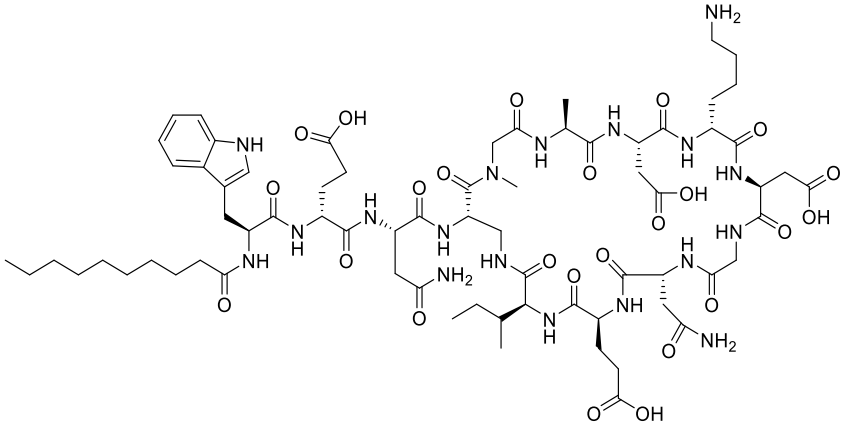

A54145A$_1$-Asn3-DAPA4-Asp9, 3.2

A54145A$_1$-Asn3-DAPA4-Asp9 (3.2). 2'-Cl-TrtCl polystyrene resin (theoretical substitution = 1.5 mmol/g, 66.7 mg, 0.1 mmol, 1 equiv) was activated in dry DCM with thionyl chloride (26 µL, 3.6 equiv) and pyridine (58 µL, 7.2 equiv) under reflux for 2 h. The resin was transferred to a disposable peptide cartridge and rinsed 6 x with dry DCM, followed by loading with Fmoc-Asp(OH)GlyOAllyl (4 equiv) and DIPEA (8 equiv) in dry DCM for 4 h. The cartridge was briefly rinsed with DCM (3 x 5 min), followed by capping with 17:2:1 DCM/MeOH/DIPEA (3 x 10 min). The resin was rinsed thoroughly with DMF (3 x 5 min) and DCM (3 x 5 min), and the loading efficiency estimated to be 1.04 mmol/g. All Fmoc groups were removed by treatment with 20% 4-methylpiperidine in DMF (v/v) for 5 minutes, followed by a second treatment for 20 minutes. The lipid tail and residues 1-8 were activated (4 equiv)

for 5 min using HOBt (4 equiv) and DIC (4 equiv) in DMF (2 mL) and then coupled for 4 h. Residues 13-11 were activated (5 equiv) for 5 min with HOBt (5 equiv), PyBOP (5 equiv), and DIPEA (10 equiv) in 3:2:2 DCM/DMF/NMP with 1% Triton X-100 (2 mL) and then coupled for 4 h. After each Fmoc deprotection and each amino acid coupling, the resin was rinsed with DMF (3 x 5 min) and DCM (3 x 5 min). Following the synthesis of linear peptide **3.3**, the azido group was reduced by treatment with PMe_3 (4 equiv) in 1:1 THF/H_2O overnight, which afforded peptide **3.4**. Further elaboration by Fmoc-SPPS resulted in branched peptide **3.16**, whose allyl group was removed by treatment with $Pd(PPh_3)_4$ (0.2 equiv) and DMBA (10 equiv) in 3:1 DCM/DMF (v/v) using a N_2 gas inlet for agitation. Unreacted palladium was quenched by rinsing the resin with 1% (m/v) sodium diethyldithiocarbamate trihydrate in DMF (5 x 3 min). The resulting peptide was cyclized by two 1.5 h treatments of PyAOP (5 equiv), HOAt (5 equiv), and 2,4,6-collidine (10 equiv) in DMF (2 mL). Resin cleavage and global deprotection was mediated through treatment with 95:2.5:2.5 TFA/H_2O/TIPS (v/v) for 1.5 h. The cleavage cocktail was concentrated by N_2 stream and the peptide precipitated by the addition of chilled diethyl ether. The suspensions were centrifuged, and the pellets resuspended in 9:1 H_2O/MeCN and purified by preparative RP-HPLC employing an isocratic solution gradient of 35:65 CH_3CN / H_2O (+0.1% TFA). Fractions containing the desired product were pooled and concentrated under vacuum. The residue was resuspended in water, frozen, and lyophilized affording A54145A_1-Asn3-DAPA4-Asp9 (**3.2**) as a white powder (36 mg, 13% based on resin loading), which was judged to be >95% pure by analytical RP-HPLC (Figure B.6 in Appendix B). HRMS (ESI+) m/z: $[M+2H]^{2+}$ Calcd for $C_{70}H_{110}N_{18}O_{24}$, 792.3886; Found 792.3911 (Figure C.6 in Appendix C). Limited sequence data using MS/MS was also obtained (Figures D.3 and D.4 in Appendix D).

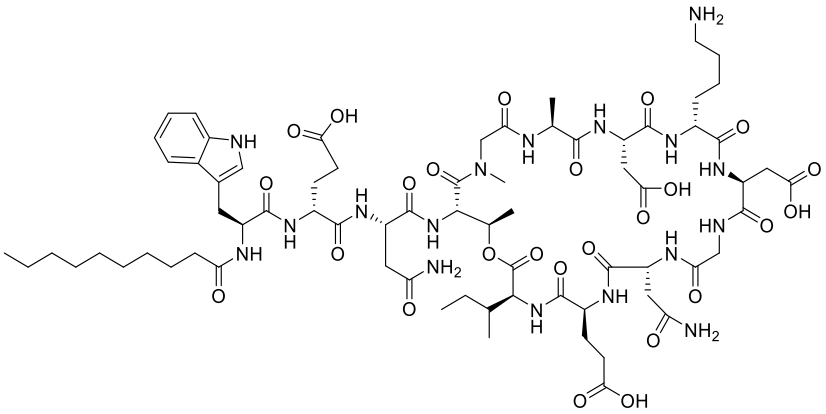

A54145A1-Asn3-Asp9, 3.1

A54145A$_1$-Asn3-Asp9 (3.1). TentaGel TrtCl resin (theoretical loading, 0.23 mmol/g, 435 mg, 0.1 mmol, 1 equiv) was activated in dry DCM with thionyl chloride (3.6 equiv) and pyridine (7.2 equiv) under reflux for 2 h. The resin was transferred to a disposable peptide cartridge and rinsed 6 x with dry DCM, followed by loading with FmocAspGlyOAllyl (4 equiv) and DIPEA (8 equiv) in dry DCM for 4 h. The cartridge was briefly rinsed with DCM (3 x 5 min), followed by capping with 17:2:1 DCM/MeOH/DIPEA (3 x 10 min). The resin was rinsed thoroughly with DMF (3 x 5 min) and DCM (3 x 5 min), and loading efficiency was estimated to be 0.17 mmol/g. Prior to the formation of the depsi bond, all Fmoc groups were removed by treatment with 20% 4-MP in DMF (v/v) for 5 minutes, followed by a second treatment for 20 min. All Fmoc-amino acids (4 equiv) and the lipid tail (4 equiv) were activated for 5 min using HOBt (4 equiv) and DIC (4 equiv) in DMF (2 mL) and then coupled for 4 h. Peptide **3.24** underwent on-resin esterification by treatment with N_3IleOH (10 equiv), pre-activated with DIC (10 equiv) by stirring in DCM (2 mL) for 1 h, followed by the addition of DMAP (0.1 equiv), for 12 h. The progress of the depsi-bond formation was monitored by analytical HPLC until peptide **3.30** was obtained in a satisfactory yield. Following the installation of the depsi bond, all Fmoc-deprotections were performed using three 10-min iterations of 20% 2-

methylpiperidine in DMF (v/v). Fmoc-SPPS with DIC/HOBt coupling starting from peptide **3.30** yielded branched peptide **3.29**. The azido group in the peptide **3.29** was reduced by treatment of the peptide with PBu_3 (3 equiv), and $(FmocGlu(tBu)CO)_2O$ (5 equiv) (formed by the addition of 10 equiv FmocGlu(tBu)OH and 5 equiv DIC to 2 mL dry THF and stirring for 1 h) for 5 min, followed by the addition of 0.1 mL H_2O and further stirring for 16 h, yielding peptide **3.31**. Further Fmoc-SPPS allowed the incorporation of the remaining two amino acids, yielding peptide **3.19**. Removal of the Fmoc group was performed with 20% 2-MP in DMF, followed by allyl deprotection with $Pd(PPh_3)_4$ (0.2 equiv) and DMBA (10 equiv) in 3:1 DCM/DMF (v/v) for 1 h using a N_2 gas inlet for agitation. Unreacted palladium was quenched by rinsing the resin with 1% (m/v) sodium diethyldithiocarbamate trihydrate in DMF (5 x 3 min). The resulting peptide was cyclized by two 1.5 h treatments of PyAOP (5 equiv), HOAt (5 equiv), and 2,4,6-collidine (10 equiv) in DMF (2 mL). Resin cleavage and global deprotection was mediated through treatment with 95:2.5:2.5 TFA/H_2O/TIPS (v/v) for 1.5 h. The cleavage cocktail was concentrated by N_2 stream and the peptide precipitated by the addition of chilled diethyl ether. The suspensions were centrifuged, and the pellets resuspended in 9:1 H_2O/MeCN. The target compound was purified by preparative RP-HPLC employing a linear gradient of 37% CH_3CN/63% H_2O (+0.1% TFA) to 38% CH_3CN/62% H_2O (+ 0.1% TFA) over 50 min. Fractions containing the desired product were pooled and lyophilized giving A54145A_1-Asn3-Asp9 (**3.1**) as a white powder (8 mg, 7% based on resin loading), which was judged to be >95% pure by analytical RP-HPLC (Figure B.7 in Appendix B). HRMS (ESI+) m/z: $[M+2H]^{2+}$ Calcd for $C_{71}H_{111}N_{17}O_{25}$, 799.8885; Found 799.8879 (Figure C.7 in Appendix C). Sequence data was also obtained with MS/MS (Figures D.5 and D.6 in Appendix D).

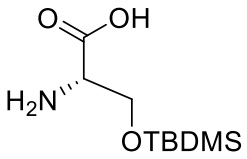

3.49

NH_2-Ser(OTBDMS)-OH (**3.49**). Compound **3.49** was obtained according to a procedure by Luo et al.[124] To a stirred suspension of L-serine (2 g, 19.0 mmol, 1 equiv) in DMF (20 mL) was added imidazole (2.59 g, 38.1 mmol, 2.0 equiv) and *tert*-butyldimethylsilyl chloride (3.15 g, 20.9 mmol, 1.1 equiv). The mixture was stirred over night at room temperature, after which the DMF was removed by high-vacuum rotary evaporation. The oily residue was then stirred in 1:1 H_2O/hexane vigorously for 4 h. The white solid was filtered off, rinsed with hexane, and air-dried to give compound **3.49** as a white solid (3.52 g, 84%). ^{1}H-NMR (300 MHz, $CDCl_3$) δ: 4.04 (1H, dd, J = 3.9 Hz, J = 11.1 Hz), 3.97 (1H, dd, J = 6.0 Hz, J = 11.0 Hz), 3.60 (1H, m), 0.92 (9H, s), 0.11 (6H, s).

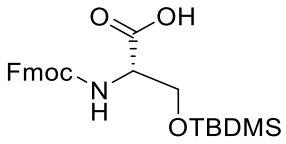

3.50

Fmoc-Ser(OTBDMS)-OH (**3.50**). Compound **3.50** was obtained according to a procedure by Aguda et al.[125] To a solution of NH_2-Ser(OTBDMS)-OH (**3.49**) (1 g, 4.6 mmol, 1.0 equiv) in a 1:1 mixture of 1,4-dioxane and water (50 mL) was added Na_2CO_3 (0.966 g, 0.91 mmol, 2.0 equiv) and Fmoc-OSu (1.69 g, 5.0, 1.1 equiv) at room temperature. The resulting mixture was stirred overnight, resulting in a clear solution. This solution was acidified with 2N HCl to pH 1 and extracted with ethyl acetate (3 x 75 mL). Evaporation of the organic layer afforded the crude product as a clear oil. The crude product was purified by column chromatography using

a slow gradient of 100% DCM to 97:3 DCM/MeOH, to afford the desired compound **3.50** as a yellow amorphous solid (1.59 g, 79%). ^{1}H NMR (300 MHz, $CDCl_3$) δ: 7.68 (2H, d, J = 7.4 Hz), 7.55 (2H, d, J = 6.5 Hz), 7.39 (2H, t, J = 7.3), 7.30 (2H, t, J = 7.4), 5.63 (1H, d, J = 8.1 Hz), 4.44-4.33 (3H, m), 4.24 (1H, t, J = 7.08), 4.14 (1H, d, J = 9.5), 3.87 (1H, d, J = 7.3), 0.89 (9H, s), 0.06 (6H, s).

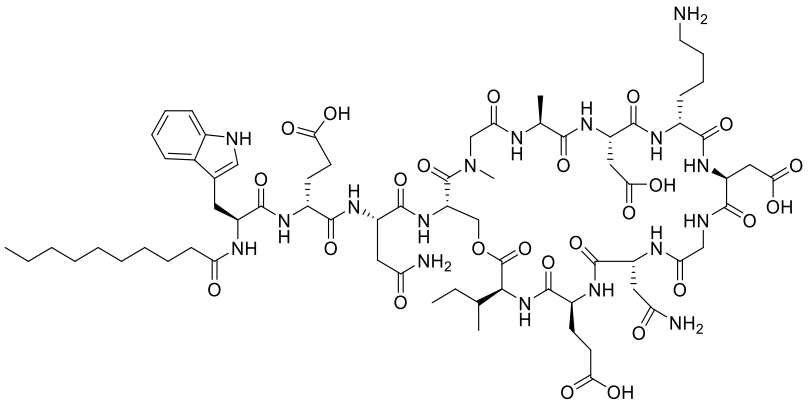

A54145A$_1$-Asn3-Ser4-Asp9, 3.32

A54145A$_1$-Asn3-Ser4-Asp9 (3.32). A54145A$_1$-Asn3-Ser4-Asp9 was synthesized according to the procedure for A54145A$_1$-Asn3-Asp9, except that FmocSerOH was used instead of FmocThrOH. The target compound was purified by preparative RP-HPLC employing a linear gradient of 36% CH_3CN/64% H_2O (+0.1% TFA) to 37% CH_3CN/63% H_2O (+ 0.1% TFA) over 50 min. Fractions containing the desired product were pooled and lyophilized giving A54145A$_1$-Asn3-Ser4-Asp9 (**3.32**) as a white powder (7 mg, 7% based on resin loading), which was judged to be >95% pure by analytical RP-HPLC (Figure B.8 in Appendix B). HRMS (ESI+) m/z: $[M+2H]^{2+}$ calcd for $C_{70}H_{109}N_{17}O_{25}$, 792.8807; Found 792.8777 (Figure C.8 in Appendix C). The peptide was characterized by NMR (Figures A.19 to A.23 and Table A.3 in Appendix A) and sequenced by MS/MS (Figures D.7 and D.8 in Appendix D).

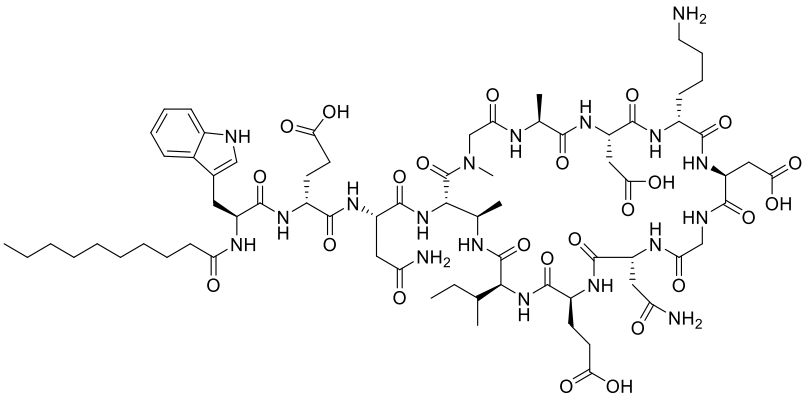

A54145A1-Asn3-DABA4-Asp9 (3.33)

A54145A$_1$-Asn3-DABA4-Asp9 (3.33). A54145A$_1$-Asn3-DABA4-Asp9 was synthesized according to the procedure for A54145A$_1$-Asn3-DAPA4-Asp9 except that Fmoc-(2*S*,3*R*)-2-amino-3-azidobutanoic acid[117] (FmocAABA) was used instead of Fmoc-β-azidoAlaOH. The reduction of the azido was also slower for this peptide and required three overnight treatments with 2 M DTT and 1 M DIPEA in DMF, with the complete azido reduction monitored by analytical RP-HPLC. All amino acids were introduced with DIC/HOBt couplings. The target compound was purified by preparative RP-HPLC employing a linear gradient of 37% CH_3CN/63% H_2O (+0.1% TFA) to 38% CH_3CN/62% H_2O (+ 0.1% TFA) over 50 min. Fractions containing the desired product were pooled and lyophilized giving A54145A$_1$-Asn3-DABA4-Asp9 (**3.33**) as a white powder (42 mg, 15% based on resin loading), which was judged to be >95% pure by analytical RP-HPLC (Figure B.9 in Appendix B). HRMS (ESI+) m/z: $[M+2H]^{2+}$ Calcd for $C_{71}H_{110}N_{18}O_{24}$, 799.3965; Found 799.3948 (Figure C.9 in Appendix C). The peptide was characterized by NMR (Figures A.24 to A.28 and Table A.3 in Appendix A) and limited sequence data obtained by MS/MS (Figures D.9 and D.10 in Appendix D).

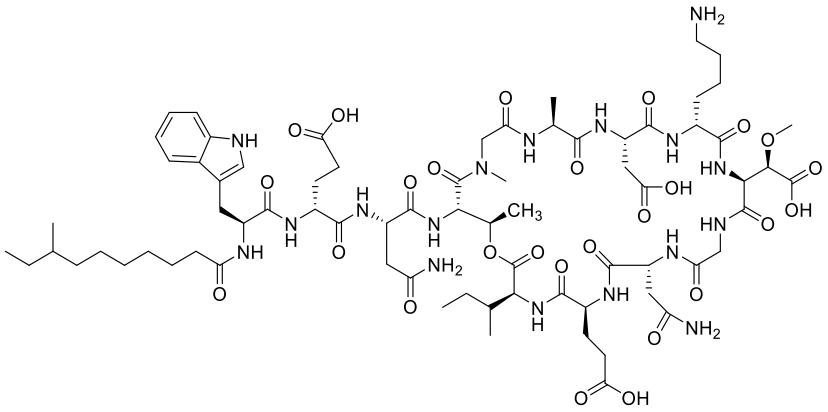

A54145-Asn3, 3.44

A54145D-Asn3 (**3.44**). A54145D-Asn3 was synthesized using the procedure we developed for the synthesis of A54145D (Chapter 2) except FmocAsnOH was used in place of Fmoc-*t*HOAsn(OTBDMS)OH at position 4. The target compound was purified by preparative RP-HPLC employing a linear gradient of 40% CH_3CN/60% H_2O (+0.1% TFA) to 41% CH_3CN/59% H_2O (+0.1% TFA) over 40 min. Fractions containing the desired compound were pooled and lyophilized giving A54145D-Asn3 (**3.44**) as a white powder (4 mg, 10% yield based on resin loading), judged to be >95% pure by analytical RP-HPLC (Figure B.10 in Appendix B). HRMS (ESI+) m/z: $[M+2H]^{2+}$ calcd for $C_{73}H_{113}N_{17}O_{26}$ 821.9016; Found 821.9017 (Figure C.10 in Appendix C). Sequence data was obtained by MS/MS (Figures D.11 and D.12 in Appendix D).

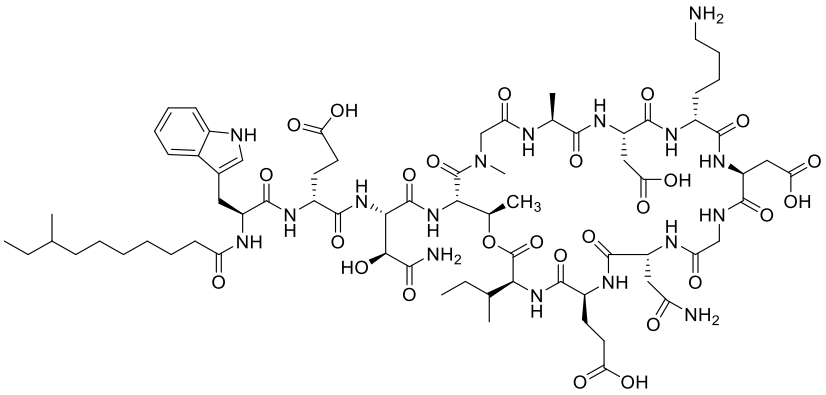

A54145D-Asp9, 3.45

A54145D-Asp9 (**3.45**). A54145D-Asp9 was synthesized using the procedure we developed for the synthesis of A54145D (Chapter 2) except FmocAsp(tBu)OH was used in place of Fmoc-*erythro*-MeOAsp(tBu)OH at position 9. The target compound was purified by preparative RP-HPLC employing a linear gradient of 39% CH_3CN/61% H_2O (+0.1% TFA) to 40% CH_3CN/60% H_2O (+0.1% TFA) over 40 min. Fractions containing the desired compound were pooled and lyophilized giving A54145D-Asp9 (**3.45**) as a white powder (6 mg, 14 % yield based on resin loading), judged to be > 95% pure by analytical RP-HPLC (Figure B.11 in Appendix B). HRMS (ESI+) m/z: $[M+2H]^{2+}$ Calcd for $C_{72}H_{111}N_{17}O_{26}$ 814.8938; Found 814.8965 (Figure C.11 in Appendix C). Sequence data was obtained by MS/MS (Figures D.13 and D.14 in Appendix D).

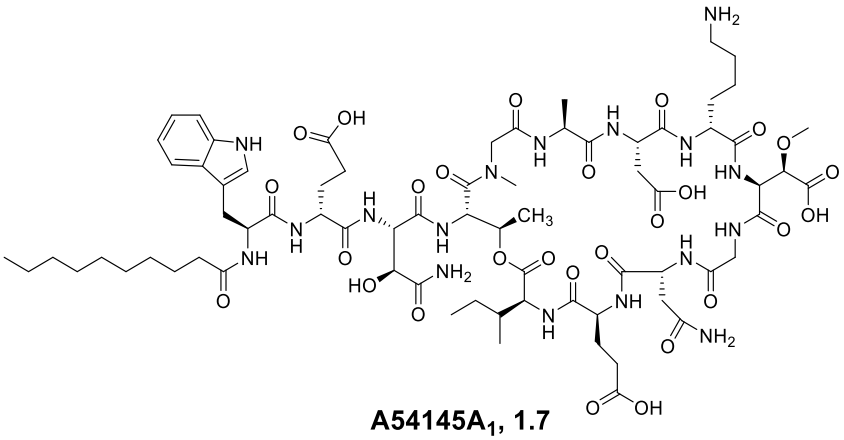

A54145A$_1$, 1.7

A54145A$_1$ (**1.7**). A54145A$_1$ was synthesized using the procedure we developed for the synthesis of A54145D (Chapter 2) except commercially available decanoic acid was used to install the lipid tail. The target compound was purified by preparative RP-HPLC employing a linear gradient of 39% CH_3CN/61% H_2O (+0.1% TFA) to 40% CH_3CN/60% H_2O (+0.1% TFA) over 40 minutes. Fractions containing the desired compound were pooled and lyophilized giving A54145A$_1$ (**1.**7) as a white powder (5 mg, 12 % yield based on resin loading), judged to be > 95% pure by analytical RP-HPLC (Figure B.12 in Appendix B). HRMS (ESI+) m/z: $[M+2H]^{2+}$ calcd for $C_{72}H_{111}N_{17}O_{27}$ 822.8912; Found 822.8910 (Figure C.12 in Appendix C). Sequence data was obtained by MS/MS (Figures D.15 and D.16 in Appendix D).

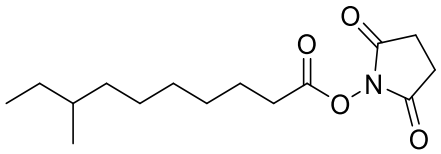

3.51

8-Methyldecanoic acid succinimidyl ester (**3.51**). (±)-8-Methyldecanoic acid (54 mg, 0.29 mmol, 1 equiv) was added to a 25 mL round-bottom flask. To this was added a solution of *N*-hydroxysuccinimide (50 mg, 4.4 mmol, 1.5 equiv) in dry DCM (10 mL) until dissolution. To

the stirring solution was added EDC (93 mg, 4.8 mmol, 1.67 equiv) and DMAP (3.5 mg, 0.029 mmol, 0.1 equiv). The solution was stirred at room temperature overnight, after which TLC indicated the reaction was complete. The mixture was diluted with EtOAc (15 mL), and the organic phase was washed with 0.1M HCl (aq) (1 x 15 mL), then washed with sat. $NaHCO_3$ (aq) (1 x 15 mL), and finally washed with brine (1 x 15 mL). The organic phase was dried with Na_2SO_4 and further purified by column chromatography (7:3 hexane/EtOAc). 8-Methyldecanoic acid succinimidyl ester (**3.51**) was obtained as a white solid (43 mg, 94%). ^{1}H NMR (300 MHz, $CDCl_3$, δ): 2.81 (2H, s), 2.56 (2H, t, J = 7.3 Hz), 1.73 (2H, t, J = 7.1 Hz), 1.60-1.08 (13H, m), 0.85-0.81 (6H, m). ^{13}C NMR (75 MHz, $CDCl_3$, δ): 172.1, 171.6, 39.4, 37.2, 33.8, 32.3, 31.7, 29.7, 28.5, 27.5, 22.1, 14.3. HRMS (ESI+) *m/z*: $[M+H]^+$ calcd for $C_{15}H_{26}NO_4$, 284.1856; found, 284.1849.

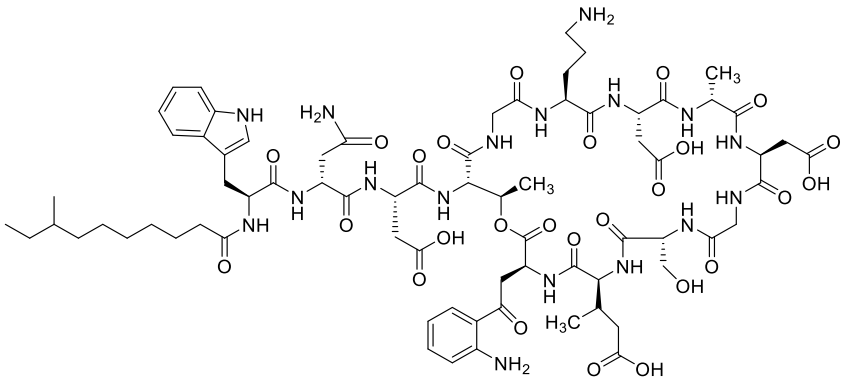

8-MeDec-Dap 3.46

8-MeDec-Dap (3.46). Orn(Boc)DeacylDap (20 mg, 0.013 mmol, 1 equiv) was added to dry DMF (400 µL) in a 7-mL scintered glass vial equipped with a stir bar. To this was added 8-methyldecanoic acid succinimidyl ester (**3.51**) (5.4 mg, 0.019 mmol, 1.5 equiv) and TEA (17.8 µL, 0.13 mmol, 10 equiv), and the reaction was allowed to stir for 72 h. The reaction was concentrated to dryness on a high-vacuum rotary evaporator, resuspended in TFA with 2% thioanisole (v/v) for 20 mins at 0 ^{o}C to remove the Boc-group. Once again, the solvents were

removed by rotary evaporation, and the residue resuspended in water, frozen, and lyophilized. Following lyophilization, the residue was resuspended in 9:1 H_2O/CH_3CN (10 mL). The mixture was then purified by preparative RP-HPLC employing a linear gradient of 40% CH_3CN/60% H_2O (+0.1% TFA) to 44% CH_3CN/56% H_2O (+ 0.1% TFA) over 40 min. Fractions containing the desired product were pooled and lyophilized, giving 8-MeDec-Dap as an off-white powder (8.7 mg, 42%). The compound was judged to be >95% pure by analytical HPLC (Figure B.13 in Appendix B). HRMS (ESI+) m/z: $[M+2H]^{2+}$ Calcd for $C_{73}H_{105}N_{17}O_{26}$, 817.8703; found, 817.8707 (Figure C.13 in Appendix C).

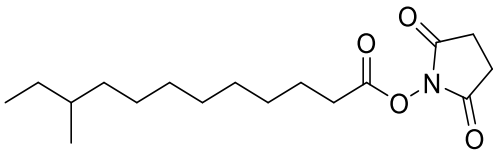

3.52

2,5-Dioxopyrrolidin-1-yl 10-methyldodecanoate (3.52). To a 25 mL round-bottom flask was added 10-methyldodecanoic acid (25 mg, 0.116 mmol, 1 equiv). To this was added a solution of NHS (19.8 mg, 0.172 mmol, 1.5 equiv) in dry DCM (5 mL) until dissolution. The reaction was cooled to 0 ^oC in an ice bath. To the chilled stirring solution was added EDC (37.0 mg, 0.193 mmol, 1.67 equiv) and DMAP (1.4 mg, 0.012 mmol, 0.1 equiv). The solution was stirred at 0 ^oC for 1 h, after which the ice-bath was removed and the mixture stirred for an additional 20 h as monitored by TLC. Following the reaction time, the mixture was diluted with EtOAc (15 mL). The organic phase was washed with 0.1 M HCl (aq) (1 x 15 mL), then washed with sat. $NaHCO_3$ (aq) (1 x 15 mL), and finally washed with brine (1 x 15 mL). The organic phase was dried of Na_2SO_4 and further purified by column chromatography with a mobile phase of 1:1 EtOAc-hexane, to yield the desired product **3.52** as a white solid (34 mg, 95%). ^{1}H-NMR (300 MHz, $CDCl_3$) δ: 2.81 (4H, s), 2.58 (2H, t, J = 7.4 Hz), 1.72 (2H, app. quint., J = 7.2 Hz),

1.38-1.04 (16H, m), 0.85-0.81 (6H, m). ^{13}C- NMR (75 MHz, $CDCl_3$) δ: 172.1, 171.6, 39.5, 37.3, 33.8, 32.8, 32.4, 32.3, 32.0, 31.7, 29.0, 28.5, 27.4, 22.1, 14.3. HRMS (ESI+): *m/z* $[M+H^+]^+$ calcd for $C_{17}H_{30}NO_4$: 312.21693, found 312.21668.

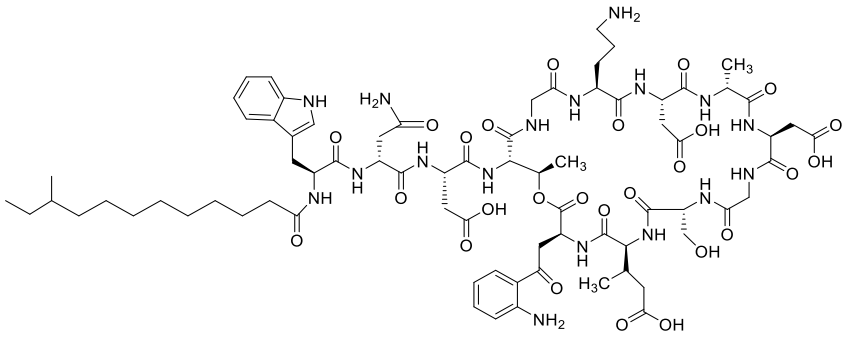

10-methyldodecanoyl-daptomycin, 3.47

10-Methyldodocanoyl-daptomycin (**3.47**). To a 7 mL glass vial was added Orn(Boc)DeacylDap (10 mg, 6.4 µmol, 1 equiv). The vial was equipped with a stir bar, and dry DMF (200 µL) was added. To this was added triethylamine (9 µL, 0.065 mmol, 10 equiv) and compound **3.52** (2.9 mg, 9.6 µmol, 1.5 equiv) and the suspension was stirred for 72 h. The reaction was concentrated on a high-vacuum rotary evaporator and redissolved in water followed by lyophilization. Then, the crude product was stirred in a solution of TFA (1 mL) containing thioanisole (2% v/v) for 25 min in an ice-bath. The solution was concentrated *in vacuo*, and the residue redissolved in dry DMF, with the solvent being removed once more. The oily residue was dissolved in water and lyophilized before purification by preparative HPLC using a Clipeus C18 10 µm column employing a linear gradient of 57:43 H_2O (+0.1 % TFA) / acetonitrile to 54:46 H_2O (+0.1 % TFA) / acetonitrile. Fractions containing the desired compound were pooled and concentrated, suspended in water and lyophilized to obtain the desired product as a white powder (2.5 mg, 24%), judged to be >95 pure by RP-HPLC (Figure

B.14 in Appendix B). HRMS (ESI+): *m/z* $[M+2H^+]^{2+}$ calcd for $C_{75}H_{109}N_{17}O_{26}$: 831.88593, found 831.88348 (Figure C.14 in Appendix C).

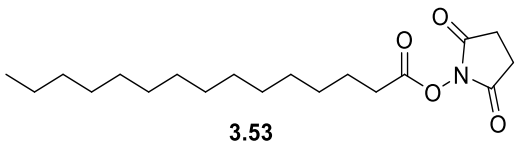

3.53

2,5-Dioxopyrrolidin-1-yl pentadecanoate (3.53). Pentadecanoic acid (28 mg, 0.116 mmol, 1 equiv) was added to a 25 mL round-bottom flask. To this was added a solution of NHS (19.8 mg, 0.172 mmol, 1.5 equiv) in dry DCM (5 mL) until dissolution. The reaction was cooled to 0 ^oC in an ice bath. To the chilled stirring solution was added EDC (37.0 mg, 0.193 mmol, 1.67 equiv) and DMAP (1.4 mg, 0.012 mmol, 0.1 equiv). The solution was stirred at 0 ^oC for 1 h, after which the ice-bath was removed and the mixture stirred for an additional 20 h as monitored by TLC. Following the reaction time, the mixture was diluted with EtOAc (15 mL). The organic phase was washed with 0.1 M HCl (aq) (1 x 15 mL), then washed with sat. $NaHCO_3$ (aq) (1 x 15 mL), and finally washed with brine (1 x 15 mL). The organic phase was dried with Na_2SO_4 and further purified by column chromatography with a mobile phase of 1:1 EtOAc-hexane, to yield the desired product **3.53** as a white solid (48 mg, 95%). ^{1}H-NMR (300 MHz, $CDCl_3$) δ: 2.81 (4H, s), 2.58 (2H, t, J = 7.5 Hz), 1.70 (2H, app. quint., J = 7.2 Hz), 1.38-1.21 (23H, m), 0.86 (3H, t, J = 6.8 Hz). ^{13}C- NMR (75 MHz, $CDCl_3$) δ: 169.2, 168.7, 31.9, 30.9, 29.6, 29.5, 29.3, 29.1, 28.8, 25.6, 24.6, 22.7. HRMS (ESI+): *m/z* $[M+H]^+$ calcd for $C_{19}H_{34}NO_4$: 340.24824, found 340.24849.

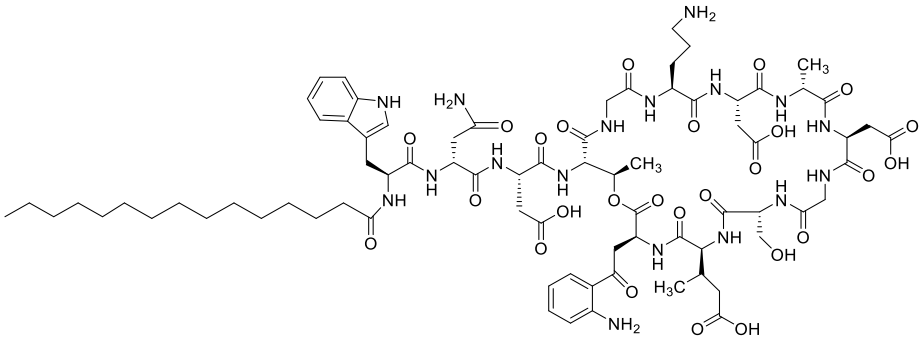

pentadecanoyl daptomycin, 3.48

Pentadecanoyl-daptomycin (**3.48**). To a 7 mL glass vial was added Boc-Deacyl-Dap (10 mg, 6.4 µmol, 1 equiv). The vial was equipped with a stir bar, and dry DMF (200 µL) was added. To this was added triethylamine (9 µL, 0.065 mmol, 10 equiv) and compound **3.52** (3.3 mg, 9.6 µmol, 1.5 equiv) and the suspension was stirred for 72 hours. The reaction was concentrated on a high-vacuum rotary evaporator and redissolved in water followed by lyophilization. Then, the crude product was stirred in a solution of TFA (1 mL) containing thioanisole (2% v/v) for 25 minutes in an ice-bath. The solution was concentrated *in vacuo*, and the residue redissolved in dry DMF, with the solvent being removed once more. The oily residue was dissolved in water and lyophilized before purification by preparative HPLC using a Clipeus C18 10 µm column employing a linear gradient of 51:49 H_2O (0.1 % TFA) / acetonitrile to 50:50 H_2O (0.1 % TFA) / acetonitrile. Fractions containing the desired compound were pooled and concentrated, suspended in water and lyophilized to obtain the desired product **3.48** as a white powder (2.4 mg, 22%), judged to be >95% pure by RP-HPLC (Figure B.15 in Appendix B). HRMS (ESI+): *m/z* $[M+2H^+]^{2+}$ calcd for $C_{77}H_{113}N_{17}O_{26}$: 845.90158, found 845.89821 (Figure C.15 in Appendix C).

Chapter 4 – Mechanism Studies of Fluorinated Analogs of Daptomycin

4.1 – Introduction

It is apparent from the discussion on daptomycin and related antibiotics in Chapter 1 that there are still many questions concerning their mechanism of action. Fluorescence spectroscopy, employing fluorescently labelled daptomycin or using the intrinsic fluorescence of daptomycin, has been used extensively, and very effectively, for studying daptomycin's interaction with model and bacterial membranes. However, due to FRET between Trp1 and Kyn13, only the Kyn residue can be employed for intrinsic fluorescent studies and, besides the lipid tail, the Orn residue is the only residue to which a fluorophore can be attached. It would be beneficial for mechanism of action studies if we could monitor the interaction of other residues of daptomycin with membranes.

4.1.1 – ^{19}F-NMR for Studying Biochemical and Biological Systems

Solid- and solution-state ^{19}F-NMR have been used to study the interaction of proteins and peptides, including antimicrobial peptides, with membranes.[126–129] The ^{19}F nucleus is a particularly useful probe for studying molecular interactions. It is present at 100% isotopic abundance and in ^{19}F-NMR, its nucleus has a very wide chemical shift range.[126] The fluorine

atom is often considered isosteric with hydrogen due to its similar size, and it can often replace hydrogen in small molecules with minimal effect on their binding to enzymes and proteins.[130] It is also absent from most biomolecules and biological systems, which allows the ^{19}F-NMR spectra of fluorinated compounds in biological systems to be free from extraneous signals.[126,128]

Solution state ^{19}F-NMR has been used to study the interaction of fluorinated peptides or proteins with biological membranes. Some examples are discussed below.

In 2003, Afonin et al. used ^{19}F-NMR to study the interactions of a fluorinated variant of PGLa, a cationic antimicrobial peptide, with liposomes.[131] It was observed that binding to liposomes only occurred when anionic DMPG lipids were present. The T_2 (transverse relaxation time, or spin-spin relaxation time) of the ^{19}F signal substantially decreased from 298 milliseconds to <25 milliseconds when DMPG liposomes were present, signifying that the PGLa antibiotic had moved from a highly fluid solvent to the less mobile membrane with slower tumbling. The authors monitored the ^{19}F-NMR signal of the fluorinated PGLa as a function of increasing concentration of DMPG liposomes: when the liposomes were added stepwise to the sample tube, the integral of the ^{19}F-NMR signal progressively decreased and finally disappeared. They concluded that the observed signal originated from the free form only, since any peptide bound to the vesicles would have given rise to a signal that is several orders of magnitude broader and could not be distinguished from the baseline.

Anderluh et al. observed the interaction of fluorinated equinatoxin II analogs with bicelles by solution state ^{19}F-NMR.[132] Equinatoxin II is a pore-former, known to require the presence of sphingomyelin in membranes for lytic activity. Researchers constructed a strain of *E. coli* that was auxotrophic for tryptophan, and thus could only survive if tryptophan was

present in the growth medium. The mutant strain was then grown in the presence of 5-fluorotryptophan, causing all five Trp residues in equinatoxin II to be replaced with the fluorinated amino acid. Incubating the fluorinated equinatoxin II analog with micelles or bicelles containing only DMPC resulted in a slight change in chemical shift for some of the fluorinated Trp residues, suggesting initial membrane interaction, even in the absence of sphingomyelin. Subsequent titration of sphingomyelin lipids caused additional chemical shift changes to the signals of specific fluorinated residues, suggesting a conformational change or deeper membrane insertion. While it had previously been established that equinatoxin II interacts reversibly with membranes containing PC only and irreversibly in membranes containing PC and sphingomyelin,[133] the changes in frequency of the specific ^{19}F resonances using ^{19}F-NMR allowed the researchers to propose several possible orientations of the peptide's insertion into membranes.

It has also been shown that the fluorine signal from a water-soluble molecule is deshielded by about 0.2 *ppm* when the solvent is changed from water to deuterium oxide (D_2O), in which the magnitude of the solvent-induced isotope shift (SIIS) is an indication of the extent to which a fluorine nucleus is exposed to solvent.[134] Fluorine nuclei exposed to solvent will be shifted by about 0.2 *ppm*, whereas fluorine nuclei buried in a protein, or a membrane, and subsequently unexposed to solvent, do not experience any SIIS. Therefore, using a combination of deuterated and non-deuterated solvents, in conjunction with chemical shift changes expected upon localization in slowly-tumbling chemical environments, the relative chemical shift of the ^{19}F signal can shed light on the nature of its chemical environment. The Marsh group has used this phenomenon to study membrane protein interactions.

In 2010 and 2011, the Marsh group introduced trifluoroethylglycine into a known membrane-binding protein called MSI-78 and observed shielding of the trifluoromethyl tag upon introduction of increasing concentrations of small unilamellar vesicles or bicelles containing DMPG and DMPC.[135,136] It was observed that upon addition of even low concentrations of small unilamellar vesicles (SUVs), peak broadening and chemical shift shielding of up to 1.0 *ppm* was observed, once again suggesting insertion into the membrane with slower tumbling. The researchers also observed SIIS effects of these protein analogs and, as would be expected, the fluorine signals of residues consistently experienced an upfield shift of 0.08 – 0.11 *ppm* in the absence of vesicles. However, for fluorine signals of mutant proteins in which hydrophobic residues were replaced with trifluoroethylglycine, there were very small or completely lacking upfield relative shifts when bicelles were present, signifying that these trifluoromethyl tags were not exposed to the deuterated solvent. Finally, while the fluorine signals of all fluorinated residues broadened in the presence of model membranes, T_2 values were smallest for the residues expected to be localized in the hydrophobic interior of the bicelle.

In 2013, the Marsh group synthesized (perfluoro-*tert*-butyl)homoserine and introduced it to varying locations in MSI-78. Fluorinated MSI-78 analogs were then analyzed in the presence of bicelles containing DMPG and DMPC, as discussed above. Once again, the researchers observed significant peak-broadening and shielding of the fluorinated *tert*-butyl group ranging from 0.02 *ppm* to 0.41 *ppm*, depending upon its location in the peptide.[137] The key advantage in this work over the previous study was that the fluorinated amino acid used contained 9 equivalent fluorine atoms instead of three or less, requiring smaller amounts of fluorinated MSI-78 analog for membrane-binding studies.

In 2010, the Pielak group observed a different phenomenon when studying the interaction of α-synuclein with small unilamellar vesicles containing varying head groups and lipid tails.[138] This peptide is associated with Parkinson's disease and other neurodegenerative disorders and is hypothesized to interact with membranes. However, previous studies provided contradictory descriptions of the interaction: some results indicated that the *N*-terminal amino acids lie on the surface of the membrane, and other results indicated that the *N*-terminal amino acids are anchored into the membrane. To elucidate the mechanism of membrane interaction, researchers replaced the four tyrosine residues of α-synuclein with 3-fluorotyrosine (1 in the *N*-terminal region, 3 in the C-terminal region). They observed that the highly cationic *N*-terminal region bound to SDS micelles and DOPC/DOPG membranes strongly, whereas the C-terminal region did not, based upon the complete disappearance of the fluorine signal of 3-fluorotyrosine of only one of the four fluorinated amino acids. The fluorine signal was broadened beyond detection due to the slow tumbling in the interior of the SUVs. Similarly, an α-synuclein variant was constructed where four tyrosine residues were replaced with *p*-trifluoromethylphenylalanine, whose interactions with SUVs mirrored the above results. These fluorinated analogs were used to assess the importance of lipid composition to membrane binding, and it was observed (once again based upon broadening beyond detection) that the *N*-terminal region is strongly anchored in the SUVs. Additionally, SUV-binding was both head-group and lipid-specific. The strongest binding was to anionic DOPC/DOPG SUVs, consistent with the cationic-nature of the *N*-terminal region. Interestingly, weakest SUV-binding was observed between α-synuclein and DMPG/DMPC lipids, which was attributed to the increase in curvature of these liposomes.

4.1.2 – Research Objectives

Several groups have attempted to study the mechanism of action of daptomycin via ^{1}H- or ^{13}C-spectroscopy. All of these groups have reported significant pH-dependent and concentration-dependent (both daptomycin and calcium concentration) line-broadening in the ^{1}H- and ^{13}C spectra of daptomycin, both in the presence and absence of Ca^{2+}.[139] Based on these results, it has been proposed that daptomycin forms micelles *in vivo* which deliver daptomycin to bacterial membranes.[22,139–141] These studies will be discussed in more detail in Section 4.2.5.1.

Besides the finding that daptomycin can form aggregates under certain conditions, little else pertaining to daptomycin's mechanism of action can be inferred from ^{1}H-or ^{13}C-NMR studies. Most other mechanism of action studies have involved appending different fluorophores to daptomycin, such as to the lipid tail or to the Orn6 residue (See Section 1.2.3)[44,46,49], or using the intrinsically fluorescent Trp1 and Kyn13 residues While effective, these strategies are limited to only a few locations on the entire daptomycin structure, and accordingly can only provide limited mechanistic insights.

The objective of this chapter is to determine if ^{19}F-NMR can be used to probe the interaction of fluorinated daptomycin analogs with model membranes, and whether or not it can provide new information on the mechanism of action of daptomycin. We anticipate that ^{19}F-NMR may be used to answer questions such as: (1) Which amino acid residues are embedded within the membrane, and which (if any) reside in the aqueous environment surrounding the membrane? (2) Which regions of the antibiotic associate with the biological membrane first, or initiate interactions between daptomycin and the membrane? We propose that these questions can be answered through synthesizing analogs of daptomycin with

trifluoromethyl tags at various locations, and subsequently analyzing these compounds in the presence of model membranes using ^{19}F-NMR. Answering these questions will provide insights regarding the mechanism of daptomycin's membrane binding, which will hopefully lead to the rational development of more potent and clinically valuable antibiotics.

4.2 – Results and Discussion

4.2.1 –Fluorinated Daptomycin Analogs by Semi-Synthesis

4.2.1.1 – 10,10,10-Trifluorodecanoyl-daptomycin (**4.5**)

The first fluorinated analog we chose to synthesize placed the trifluoromethyl tag at the end of the lipid tail of daptomycin (Dap-^{TF}Dec0 (**4.5**), Scheme 4.1). Phosphonium bromide salt **2.12**, prepared using a literature procedure,[92] reacted with NaHMDS and 4,4,4-trifluorobutanal yielding alkene **4.1** in 59% yield. Alkene **4.1** was subjected to hydrogenation to yield alkane **4.2** in 96% yield, and then the ester moiety in **4.2** was hydrolyzed using 1:1 MeOH/0.6 M NaOH (aq) to afford carboxylic acid **4.3** in a 79% yield. Carboxylic acid **4.3** was activated by treatment with *N*-hydroxysuccinimide (NHS), DMAP, and EDC (1-ethyl-3-(3-dimethylaminopropyl)carbodiimide) affording activated ester **4.4** in 82% yield. Compound **4.4** was coupled to the *N*-terminus of Orn(Boc)DeacylDap (**1.15**), and the crude peptide was subjected to TFA containing 2% thioanisole as a scavenger which gave target peptide **4.5** in 25% yield after purification by semi-preparative RP-HPLC (two steps).

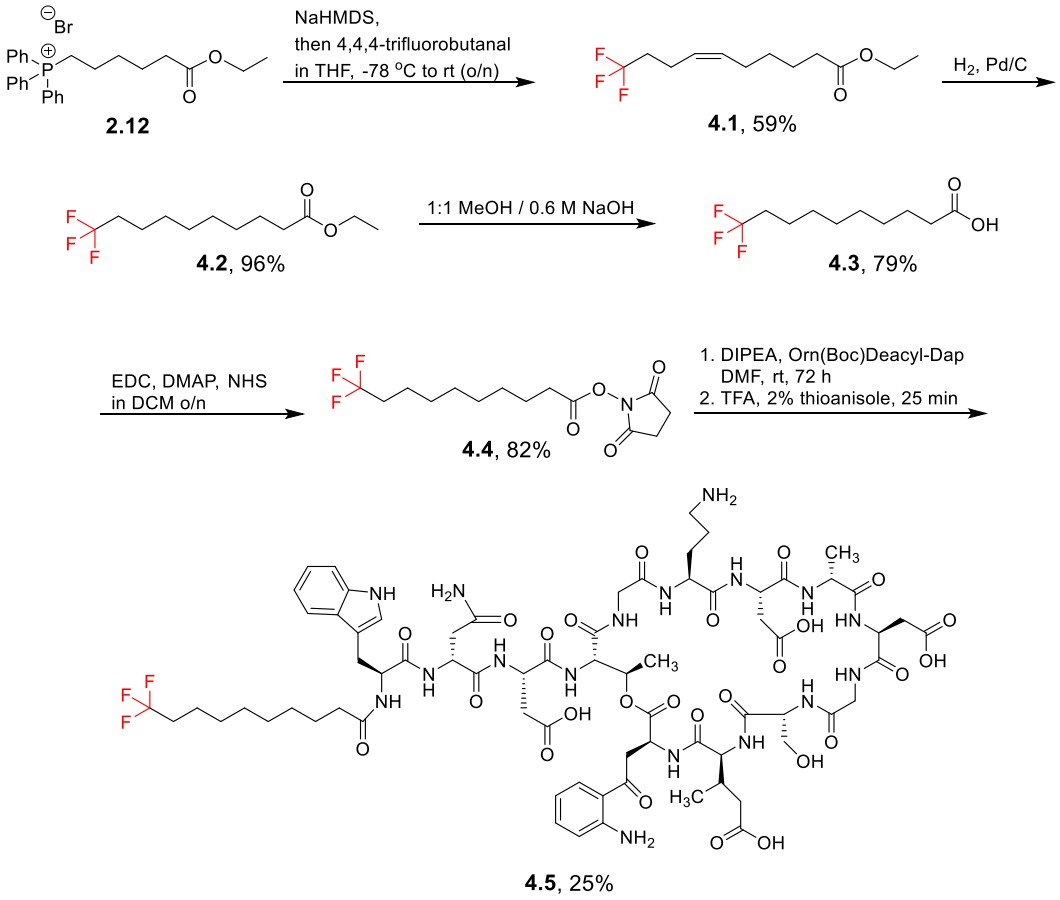

Scheme 4.1: Semi-synthesis of peptide **4.5**.

4.2.1.2 – Appending fluorinated moieties to Orn6

The amino group on the Orn residue of daptomycin appears to be necessary for optimal biological activity. Hill and co-workers examined the activity of various daptomycin analogs in which the Orn residue was acylated (usually with substituted benzoyl groups or amino acids).[72] In general, analogs containing acyl groups that did not contain a free amino group were less active (1.6 to 32-fold) than daptomycin against MSSA, MRSA, and *Enterococcus faecium*, and *E. faecalis*. When the acyl group contained a free amino group (primary or secondary amine), very little or no loss of activity was evident against MSSA or MRSA; however, in general, such analogs were less active (sometimes much less active) than

daptomycin against *E. faecium* or *E. faecalis*. The authors concluded that a free amino group was important, but not essential for activity. Additionally, Ghufran Barnawi in the Taylor group has shown that replacing the Orn6 residue with alanine results in a 7-fold loss of activity against *B. subtilis*.[82]

It is not unreasonable to expect that the positive charge associated with the basic Orn6 residue in daptomycin is involved in membrane-binding of the antibiotic to the lipid membrane, especially since daptomycin requires the anionic PG to function. Fluorescence studies employing daptomycin and daptomycin labelled at the Orn reside with the fluorophore acrylodan (acrylodan-Dap) and model membranes suggest that daptomycin's interactions with membranes are *initiated* by the ornithine residue (section 1.2.3).[49,50] However, the acrylodan tag had an adverse effect on daptomycin's activity with acrylodan-dap being approximately 10-fold less active than daptomycin.[13,49] It is possible that interaction of acrylodan-Dap with the membranes may have been driven by hydrophobic interactions between the acrylodan moiety and the membranes which are not present in unlabeled daptomycin. ^{19}F-NMR studies using daptomycin tagged with fluorinated groups on the Orn residue may shed some light as to if or at what stage in membrane binding the Orn residue interacts with membranes, and the environment surrounding the Orn residue.

We envisioned preparing several daptomycin analogs tagged with a trifluoromethyl group on the Orn residue (Figure 4.1). By performing ^{19}F-NMR studies on analogs that contain a phenyl-based tag (**4.6** and **4.8**), and those that don't bear a phenyl group (**4.7** and **4.9**), we would be able to determine if the physical properties of the tags (size and hydrophobicity) affect our results. Moreover, in analogs **4.8** and **4.9**, the amino group is converted to a non-basic amide. In analogs **4.6** and **4.7**, the primary amino group in Orn6 becomes a secondary

amine. The amino group in **4.6** should still be basic enough to be protonated under neutral conditions. The amino group in **4.7** may, however, be un-ionized at neutral pH. Considering that the pKa of ammonium is 9.25, and the pKa of 2,2,2-trifluoroethylammonium is 5.61, it appears that the addition of a trifluoroethyl group reduces the acidity of ammonium species by approximately 3.5-4.0 pK_A units due to the inductive effect of three fluorine atoms.[142,143] If appending a trifluoroethyl group to the protonated Orn residue has an effect of similar magnitude, then the pK_A of the protonated ornithine residue may decrease from 10.7, as reported by Qiu et al.[144], to between 6.7 and 7.2. At physiological pH values of 7.4 to 7.5, therefore, less than half of the daptomycin molecules in aqueous solution will bear a positive charge.

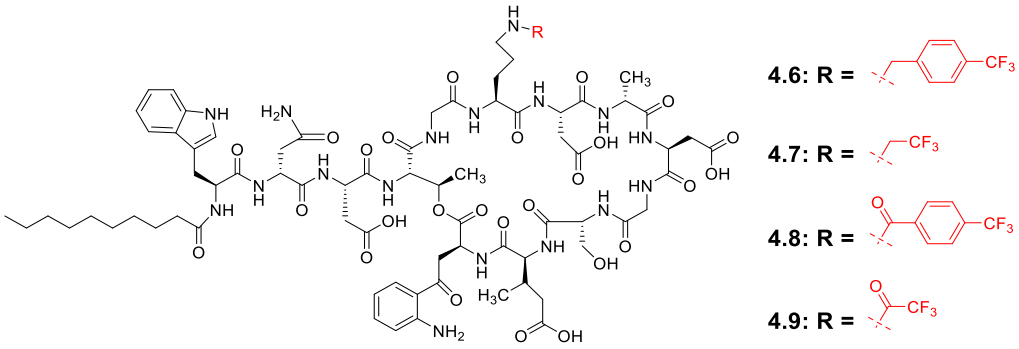

Figure 4.1: Structures of peptides **4.6** to **4.9**.

Analog **4.6** was prepared in moderate yield by reductive amination of *p*-trifluoromethylbenzaldehyde (**4.10**) with daptomycin using sodium triacetoxyborohydride (STAB-H) (Scheme 4.2). The synthesis of compound **4.7** was more challenging. Our first attempt involved direct alkylation of daptomycin with trifluoroethyl trifluoromethanesulfonate. Although some of **4.7** was formed (as determined by MS), the major product had a *m/z* = 1602 (18 Da less than daptomycin), suggesting that daptomycin had undergone a dehydration reaction. It is possible that under these conditions, the unprotected

alcohol of D-Ser11 reacted with the trifluoroethyl trifluoromethanesulfonate and the resulting trifluoroethyl ether was subsequently eliminated by either E2 or $E1_{CB}$ mechanism. We were unable to separate this side-product from **4.7** by RP-HPLC.

On the basis of several patent procedures,[145–148] we attempted to prepare **4.7** by reductive amination of the hydrate of trifluoroacetaldehyde or the ethyl hemiacetal of trifluoroacetaldehyde with daptomycin in TFA. Unfortunately, the desired product was obtained in only trace amounts. Ultimately, the reductive amination conditions that were used for preparing **4.6** were applied to the synthesis of **4.7** using the hemiacetal of trifluoroacetaldehyde (**4.11**) (Scheme 4.2). The reductive amination seemed to stop after about 50% completion, and efforts to drive the reaction to completion by supplementing with additional hemiacetal and STAB-H were unsuccessful. Regardless, even though the reaction did not go to completion, peptide **4.7** was obtained in 35% yield after purification by preparative RP-HPLC.

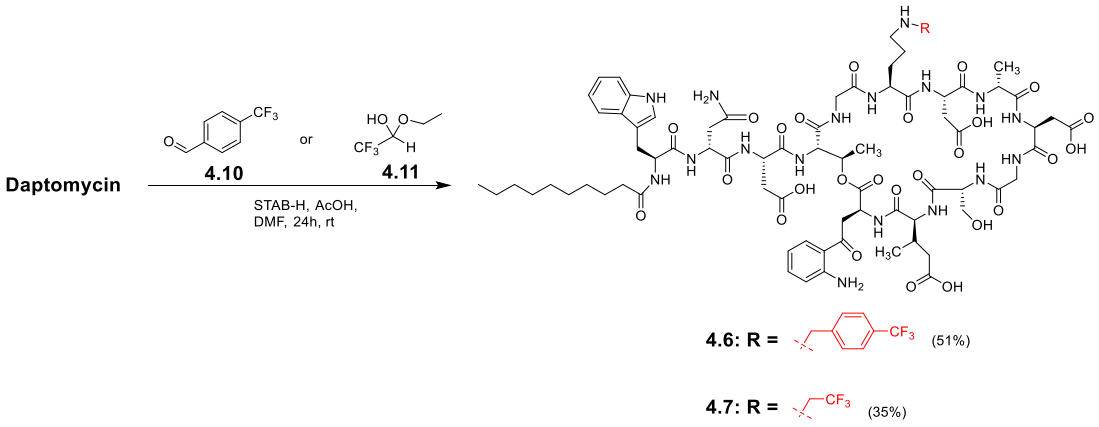

Scheme 4.2: Synthesis of peptides **4.6** and **4.7**.

Peptides **4.8** and **4.9** were synthesized in moderate yields by reacting daptomycin with the succinimidyl ester of trifluoromethylbenzoic acid (**4.13**) or ethyl trifluoroacetate (**4.14**) in the presence of DIPEA in DMF for 72 h (Scheme 4.3).

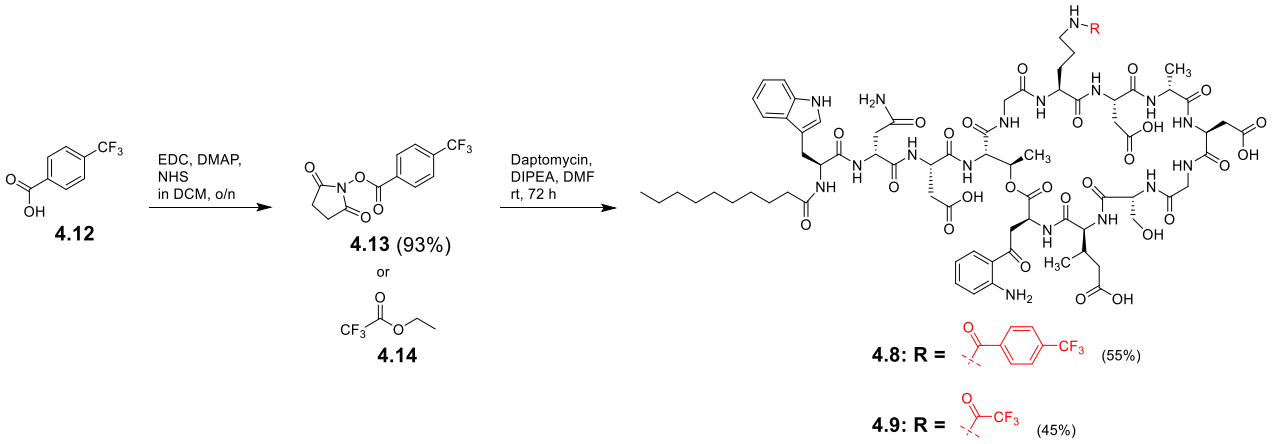

Scheme 4.3: Synthesis of peptides **4.8** and **4.9**.

4.2.2 –Fluorinated Daptomycin Analogs by Total Synthesis

The added value of employing ^{19}F-NMR to study the mechanism by which daptomycin interacts with membranes is that fluorine can be introduced in other amino-acid positions, instead of just the lipid tail, position 1, and position 6. Based upon the results of previous syntheses of daptomycin analogs, we expected that positions would tolerate amino acid substitutions with fluorinated amino acids, with a minimal loss in biological activity. For example, Ghufran Barnawi, a former graduate student in the Taylor group, performed an alanine scan of Dap-Lys6-Glu12-Trp13 (an analog of daptomycin that has activity approaching that of daptomycin but does not contain the synthetically challenging MeGlu12 residue, or the other two uncommon amino acids, Kyn and Orn). These studies revealed that *D*-Ser11 can be replaced with *D*-Ala with only a minor loss in biological activity, which suggests that this position may be amenable to substitutions with other amino acids, possibly including fluorinated ones.[81,82] Nguyen produced an analog of daptomycin in which the decanoyl lipid tail and *D*-Ala8 were replaced with 8-methyldecanoyl lipid tail and with *D*-Ser8, respectively, observing only a two-fold loss of activity.[16] This also suggests that *D*-Ala8 may be amenable to substitution. More recently, the Taylor group prepared analogs of Dap-Lys6-Glu12-Trp13

in which the *D*-Ala8 was substituted with almost all of the other 19 common amino acids.[149] It was found that *D*-Ala8 could be substituted with Ser, Met, or Arg with only a 2.5 to 5-fold loss of activity. He et al. revealed that substitution of Trp1 of daptomycin with *p*-trifluoromethylphenylalanine produced an analog that was only 2-fold less active than daptomycin.[74] Since the Taylor lab had already established an efficient synthesis of Dap-Lys6-Glu12-Trp13, we envisioned introducing fluorinated residues into Dap-Lys6-Glu12-Trp13 at positions 1, 8, and 11 by total synthesis.

4.2.2.1 – Synthesis of Dap-^{TFM}Phe1-Lys6-Glu12-Trp13 (**4.15**)

He et al. synthesized daptomycin bearing a *p*-trifluoromethylphenylalanine residue at position 1 (Dap-^{TFM}Phe1) by removing the acyl tail of CBz-protected (Orn-protected) daptomycin with a deacylase, yielding **1.16** (Scheme 1.3, Section 1.5.1).[74] Following the removal of Trp1 by Edman degradation, the *N*-terminus of the resulting peptide was then reacted with an active ester of *N*-Boc-protected *p*-trifluoromethylphenylalanine. Removal of the Boc-protecting group followed by introduction of the decanoyl tail and subsequent CBz-group removal gave Dap-^{TFM}Phe1 in an overall yields ranging from 10% to 25% starting from daptomycin. Due to limited quantities of daptomycin available, we decided it would be more prudent to synthesize the analogous Dap-^{TMF}Phe1-Lys6-Glu12-Trp13 (**4.15**, Figure 4.2) by total synthesis employing Fmoc-SPPS as per Scheme 1.12 (Section 1.6.4). For this, Fmoc-^{TFM}PheOH (**4.16**, Figure 4.2) was needed.

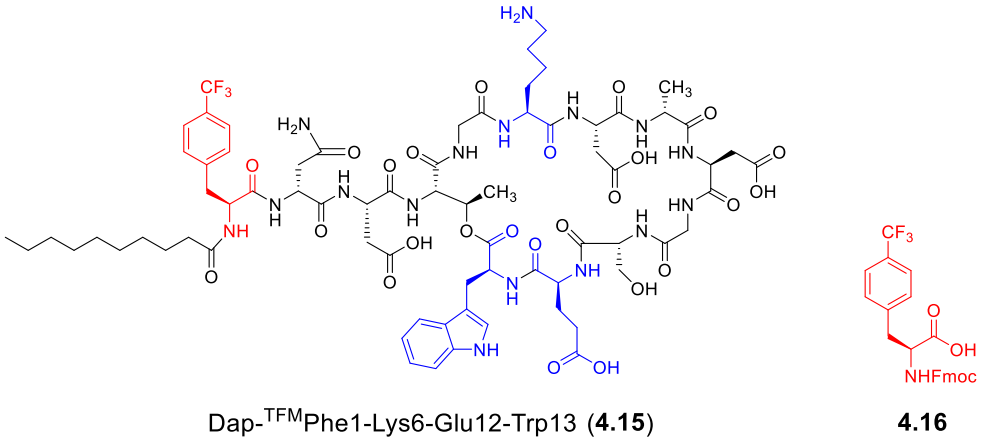

Figure 4.2. Structures of Dap-^{TMF}Phe1-Lys6-Glu12-Trp13 (**4.15**) and Fmoc-^{TFM}PheOH (**4.16**).

While amino acid **4.16** is commercially available, it is prohibitively expensive. In 2000, Chris Kotoris, a former graduate student in the Taylor group, developed a synthesis of Fmoc-^{TFM}PheOH (Scheme 4.4).[150] Although the overall yield was only 8.1%, the starting material and reagents were relatively inexpensive, so we decided to prepare **4.16** using this procedure (Scheme 4.5). For reasons unknown, we were able to obtain a much higher yield than Kotoris on the first step of the synthesis. We were also able to significantly increase the yield of racemic *N*-acetyl^{TFM}PheOH (**4.19**) by reversing the order of hydrogenation and hydrolysis steps and using an acetone-water mixture for the hydrolysis step. However, we were unable to reproduce Kotoris' yield (50% - essentially quantitative) with regards to the acylase step to get **4.20**. The deacetylation of **4.19** using acylase 1 from *Aspergillus niger* at 42 ^{o}C was slow as determined by analytical RP-HPLC, requiring a two-week reaction time, continually monitoring the pH of the reaction and supplying fresh enzyme. Purification of the zwitterionic product was also problematic, and ultimately required purification by preparative RP-HPLC. The desired amino acid was obtained in a very poor yield of 7% (14% of the desired enantiomer). We are unable to explain why this was occurring.

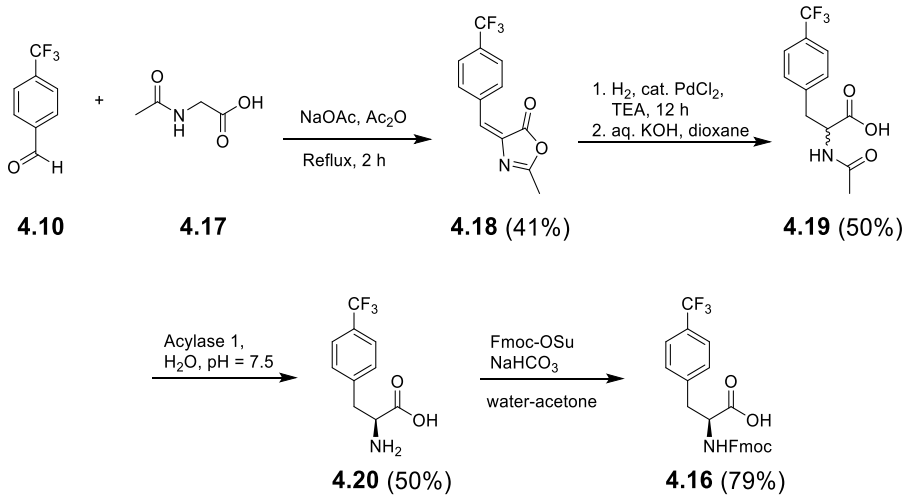

Scheme 4.4: Synthesis of **4.16** via the route developed by Kotoris and Taylor.[150]

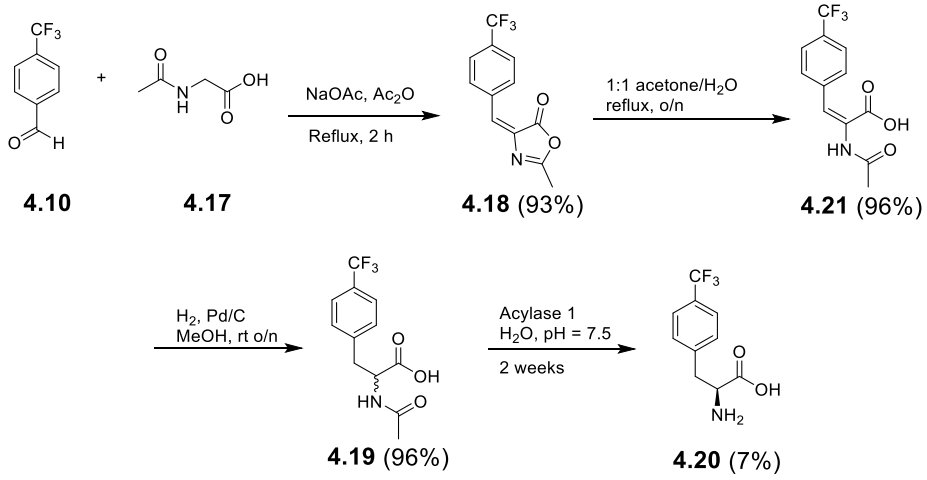

Scheme 4.5: Synthesis of **4.20** via the route developed by Kotoris and Taylor[150] with modifications.

One particularly effective way to prepare chiral phenylalanine derivatives is by using Williams' lactone as a chiral auxiliary (**4.24** in Scheme 4.6). This auxiliary has been used before in the Taylor group to prepare highly enantioenriched (>97% enantiomeric excess, *ee*) phenylalanine derivatives.[151] Although there are several other literature syntheses of ^{TFM}PheOH,[152–155] and Williams' lactone had never been used to prepare **4.16**, we chose to prepare **4.16** using Williams' lactone as the route is short, straightforward, and provides amino

acids in very high *ee*.[151,156–158] Williams' lactone (**4.24**) is commercially available but very expensive. We synthesized this lactone according to a modified procedure from Dastlik and co-workers (Scheme 4.6).[159] Subjecting the auxiliary to NaHMDS and then *p*-trifluoromethylbenzyl bromide gave **4.26** in 54% yield. Hydrogenolysis of **4.26** gave **4.20**. Crude compound **4.20** was subjected to Fmoc-OSu in biphasic 1,4-dioxane and saturated $NaHCO_3$ (aq) to afford compound **4.16** in 67% yield (two steps). The overall yield was 27%. To determine the *ee* of this compound, an aliquot of crude **4.20** was subjected to the pentafluorophenyl ester of *R*-Mosher's acid under Schotten-Baumann conditions overnight, and another aliquot subjected to the pentafluorophenyl ester of racemic Mosher's acid. The crude mixture was analyzed by ^{19}F-NMR and based upon the integrations of the Mosher's acid CF_3 groups of the corresponding amides, the *ee* of compound **4.20**, and correspondingly **4.16**, was determined to be 97% (Figure 4.3).

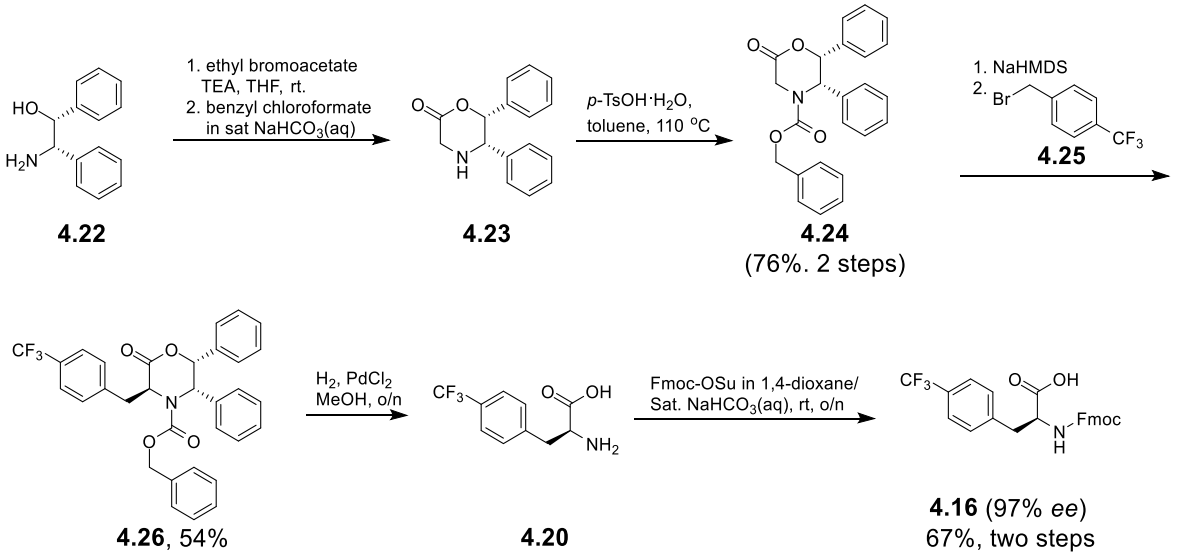

Scheme 4.6: Successful synthesis of compound **4.16** using Williams' lactone.

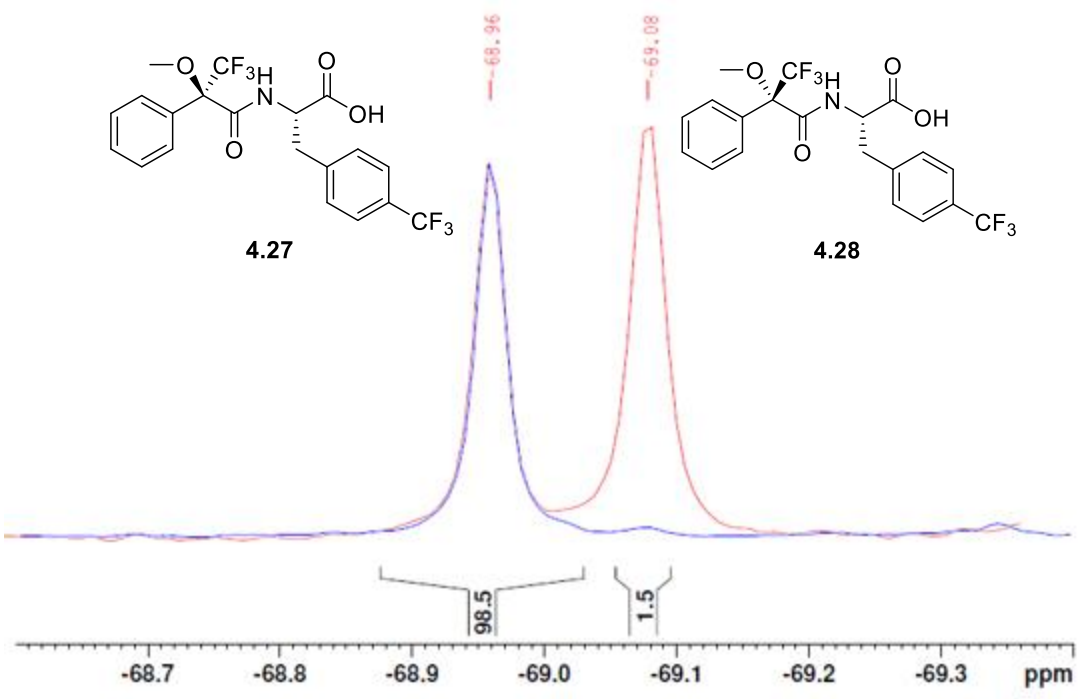

Figure 4.3: Establishing the *ee* of ^{TFM}PheOH. Coupling of **4.20** to the pentafluorophenyl ester of racemic Mosher's acid (red trace) revealed two diastereomeric ^{19}F-NMR signals, and coupling of **4.20** to the pentafluorophenyl ester of *R*-Mosher's acid demonstrates that the *ee* of **4.20**, and subsequently **4.16**, is 97%.

With the enantomerically enriched amino acid in hand, we were poised to introduce this amino acid into daptomycin via Fmoc-SPPS. The route employed by Barnawi et al. in their synthesis of daptomycin analogs was used (see Scheme 1.12, section 1.6.4). Peptide **4.15** was obtained in a 10% yield after purification by semi-preparative RP-HPLC.

4.2.2.2 – Synthesis of Dap-Lys6-D-Ser(CF_3)11-Glu12-Trp13 (**4.38**)

Barnawi and co-workers reported in 2018 that *D*-Ser11 of Dap-Lys6-Glu12-Trp13 could be replaced with *D*-Ala with only a minor decrease (~4-fold) in biological activity against *B. subtilis* ATCC 1046.[82] We anticipated that replacement of *D*-Ser with *D*-Ser(CF_3) would not significantly affect biological activity. In 2015, Liu et al. reported the synthesis of BocSer(CF_3)OMe (**4.30**) in 56% yield via silver-mediated trifluoromethylation of BocSerOMe

(Scheme 4.7). We anticipated that we could use this approach to prepare Fmoc-*D*-Ser(CF_3)OH (**4.36**, Scheme 4.8). This was advantageous, as it allowed for us to buy our enantiomerically pure starting material in the form of Boc-*D*-SerOMe.

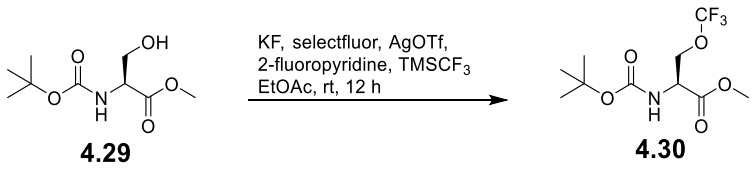

Scheme 4.7: Liu et al.'s synthesis of **4.30**.[160]

Boc-*D*-SerOMe was converted to Boc-*D*-Ser(CF_3)OMe in 35% yield using Liu et al.'s procedure (Scheme 4.8).[160] The Boc-protecting group was removed with TFA; however, hydrolysis of methyl ester **4.33** with LiOH was unsuccessful, producing a complex mixture of products. We suspected that the treatment with LiOH to hydrolyze the methyl ester might be causing some unknown side-reactions (possibly elimination of CF_3O- and formation of a dehydroalanine derivative, which may have decomposed to form other species). We were also concerned that treatment with LiOH might result in racemization. Therefore, we instead elected to use Boc-*D*-SerOtBu (**4.32**) as a starting material. Fortuitously, this was converted into Boc-*D*-Ser(CF_3)OtBu (**4.34**) in 51% yield using the conditions reported by Liu et al. (Scheme 4.8). The Boc-group and *tert*-butyl group were cleanly removed by TFA, and the resulting crude product converted to Fmoc-*D*-Ser(CF_3)OH (**4.36**) with Fmoc-OSu under basic conditions in 63% yield (two steps).

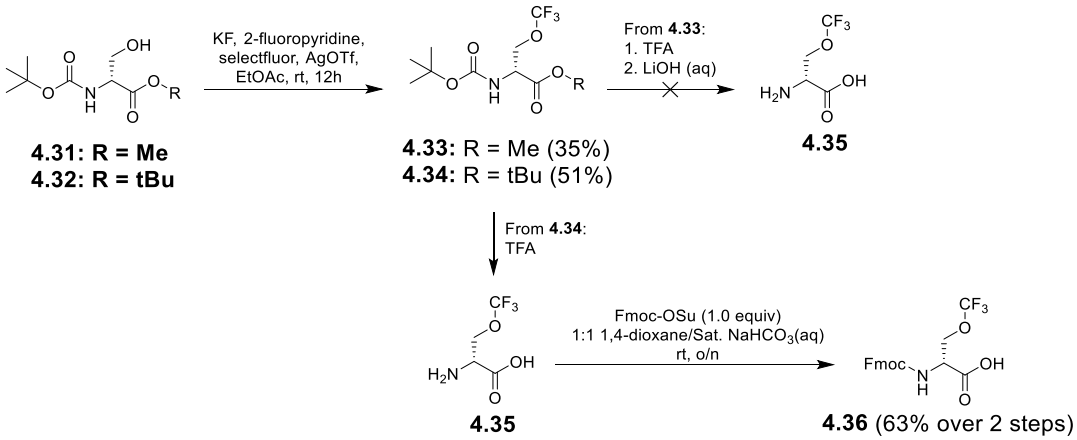

Scheme 4.8: Successful synthesis of Fmoc-*D*-Ser(CF_3)OH (**4.36**).

With the desired amino acid in hand, we attempted to synthesize Dap-Lys6-*D*-Ser(CF_3)11-Glu12-Trp13 (**4.38**), using the same route that was used for making Dap-^{TFM}Phe1-Lys6-Glu12-Trp13 (Scheme 1.12, Section 1.6.4). The HPLC chromatogram of the crude material showed many peaks (Figure 4.4). One of the major products had a mass corresponding to the desired product **4.38** (*m/z* = 1684) while the other had a mass corresponding to **4.37**, specifically with a loss of 84 Da (*m/z* = 1600). We suspected that CF_3O^- was eliminated from peptide **4.39** during removal of the Fmoc group during 20% 2-MP in DMF, yielding resin-bound dehydroalanine peptide **4.41** (Scheme 4.9). Upon cleavage from the resin and global deprotection using TFA, H_2O, and the reducing agent TIPS, the dehydroalanine was reduced to *D*/*L* alanine to give peptide **4.37** as a mixture of epimers at Ala11. The extent of elimination, as determined by peak areas of the two products, was about 55%. The desired product was obtained in 4% yield after purification by semi-preparative RP-HPLC.

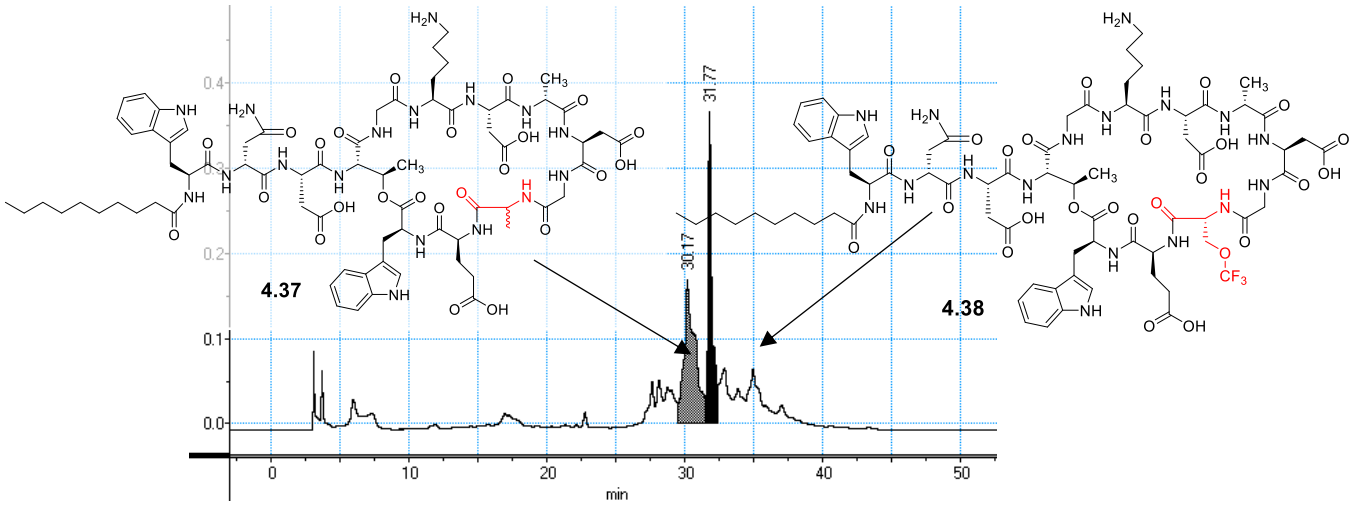

Figure 4.4: HPLC chromatogram of crude Dap-Lys6-*D*-Ser(CF_3)11-Glu12-Trp13 (**4.38**).

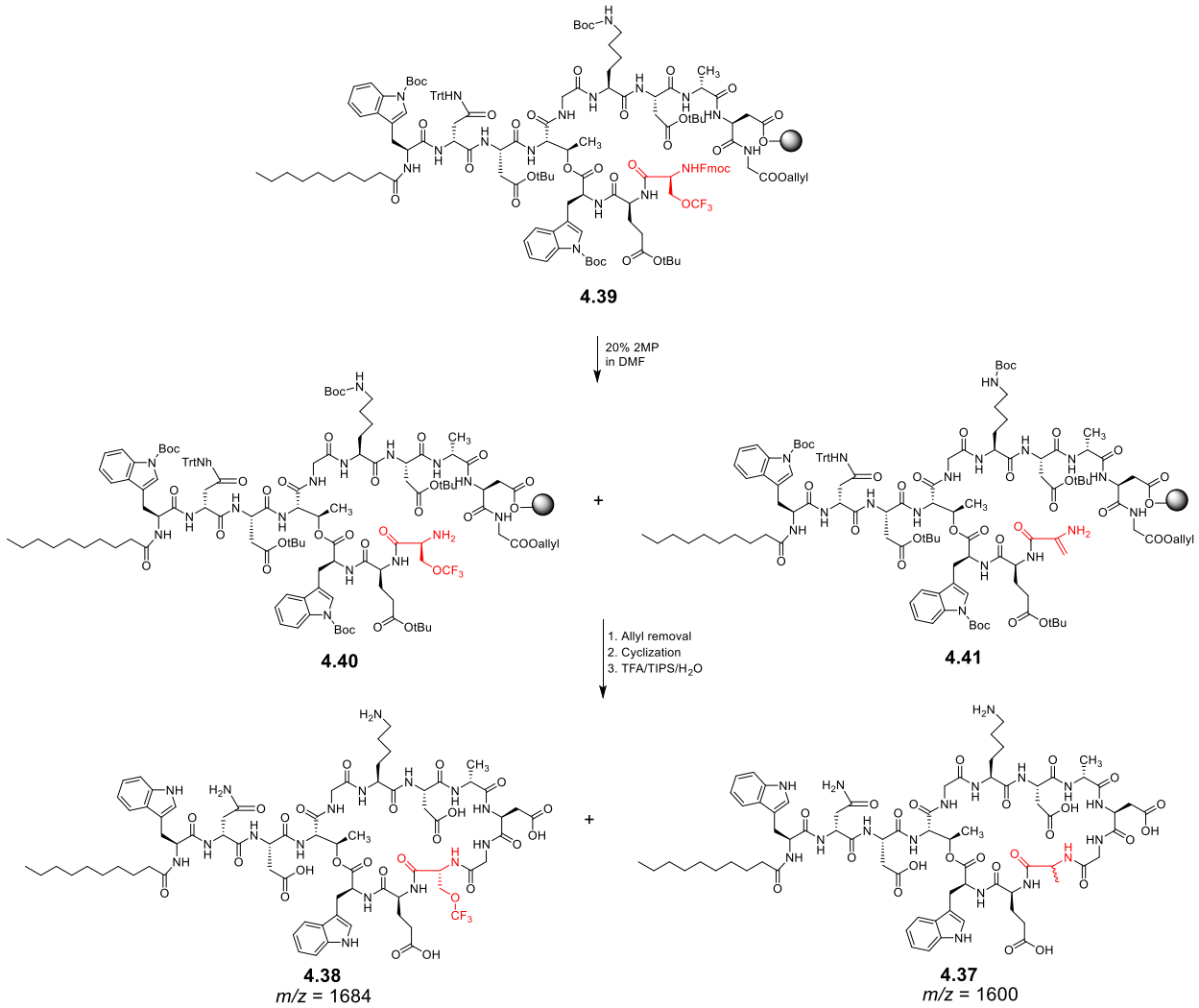

Scheme 4.9: Proposed sequence of side reactions resulting in peptide **4.37**.

Barnawi et al. reported that substitution of *D*-Ala8 with *L*-Ala8 was detrimental to biological activity, which suggested to us that the stereochemistry of amino acids in the 8-position of daptomycin must be of the *D*-configuration. We initially hoped that Fmoc-*D*-Ser(CF_3)OH could be introduced to position 8, allowing for the synthesis of Dap-Lys6-*D*-Ser(CF_3)8-Glu12-Trp13, but due to the issues faced in the synthesis of peptide **4.38**, this was not attempted. In Barnawi's route to Dap-Lys6-Glu12-Trp13, the *D*-Ser resiude at position 11 is subjected to a single treatment of 2-MP in DMF. The position 8 amino acid, *D*-Ala, is subjected to 11 treatments of 2-MP or 4-MP during the course of the synthesis, and so little or no Dap-Lys6-*D*-Ser(CF_3)8-Glu12-Trp13 would have been present at the end of the synthesis, especially since a single treatment resulted in about 55% elimination. Accordingly, we turned our attention to an amino acid that would avoid elimination of the trifluoromethyl tag.

4.2.2.3 – Synthesis of Dap-Lys6-*D*-hCys(CF_3)8-Glu12-Trp13 (**4.55**)

Michael Noden and Julian Marlyn, a graduate student and a former undergraduate student in the Taylor group, respectively, have shown that when *D*-Ala8 in Dap-Lys6-Glu12-Trp13 is replaced with *D*-Met, only a 2.5-fold decrease in activity results.[149] Therefore, we decided to replace *D*-Ala8 with *D*-trifluoromethylhomocysteine (*D*-hCys(CF_3)OH, also known as trifluoromethionine). This required the synthesis of Fmoc-*D*-hCys(CF_3)OH (**4.52**).

In 2014, Brown et al. reported the synthesis of Fmoc-*L*-hCys(CF_3)OH by electrophilic trifluoromethylation of Fmoc-*L*-hCys(Trt)OH, **4.42**, using Togni's reagent.[161] Briefly, **4.42** was subjected to TFA and TIPS to remove the Trt group (Scheme 4.10). The residue was dissolved in a mixture of DCM and methanol and subjected to Togni's reagent (**4.44**), and stirred overnight, yielding Fmoc-*L*-hCys(CF_3)OH (**4.45**). While this strategy could have been applied to the synthesis of Fmoc-*D*-hCys(CF_3)OH, the starting materials Fmoc-*D*-

hCys(Trt)OH and Togni's reagent were prohibitively expensive and instead we decided to pursue a different route.

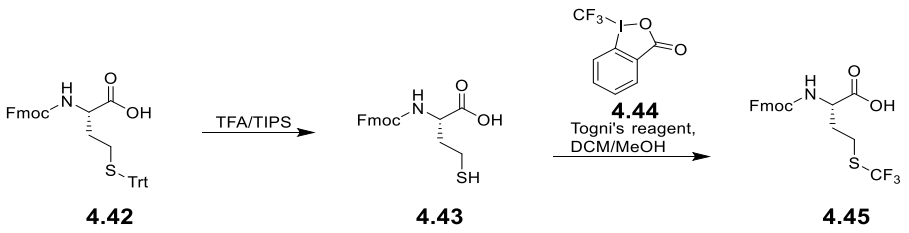

Scheme 4.10: Synthesis of Fmoc-hCys(CF_3)OH by Brown et al.[161]

In 1997, the Honek group reported the synthesis of *L*-hCys(CF_3)OH (**4.49**) from racemic homocysteine thiolactone (**4.46**), employing acylase 1 at the end of their synthesis, which catalyzes the hydrolysis of *N*-acetyl groups for *L*-amino acids only (Scheme 4.11).[162] This route was appealing to us as the reagents were relatively inexpensive and the route was short and straightforward. However, in our case, we required the *D*-amino acid, so acylase 1 could not be used. Fortunately, Amano Enzyme Inc. has a *D*-amino acid acylase available, which catalyzes the hydrolysis of *N*-acetyl groups and is highly selective for *D*-amino acids. Further, its optimal substrate (both in terms of activity and stereoselectivity) is *DL*-*N*-acetylmethionine. Since *N*-acetylmethionine and *N*-acetyl-hCys(CF_3) are very similar, we anticipated that *D*-aminoacylase would be very effective in the chiral resolution of our desired *D*-amino acid.

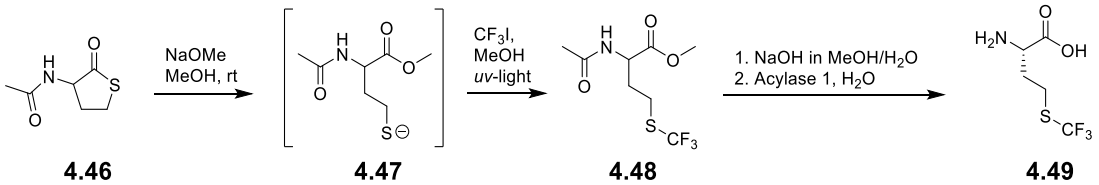

Scheme 4.11: Synthesis of *L*-hCys(CF_3) by the Honek group.[162]

Accordingly, amino acid **4.52** was synthesized beginning from the hydrochloride salt of homocysteine thiolactone and acetic anhydride at reflux (Scheme 4.12), yielding **4.46** in a 73% yield. Compound **4.46** was subjected to NaOMe in MeOH and subsequently treated with CF_3I under UV radiation yielding **4.48** in a 72% yield. The methyl ester was hydrolyzed with NaOH (aq), and the resulting mixture was adjusted to pH 7.5 with 0.1 M HCl (aq). The solution was brought to 30 ºC and then subjected to *D*-aminoacylase for 3 days. The crude product, **4.51**, used without further purification, was treated with Fmoc-OSu under alkaline conditions, which yielded the desired compound **4.52**, in 30% yield over two steps. To determine the *ee* of this compound, an aliquot of crude **4.51** was subjected to the pentafluorophenyl ester of *R*-Mosher's acid under Schotten-Baumann conditions overnight, and another aliquot subjected to the pentafluorophenyl ester of racemic Mosher's acid. The crude mixture was analyzed by ^{19}F-NMR and based upon the integrations of the Mosher's acid CF_3 groups of the corresponding amides, the *ee* of compound **4.51**, and subsequently **4.52**, was determined to be 94.2% (Figure 4.5).

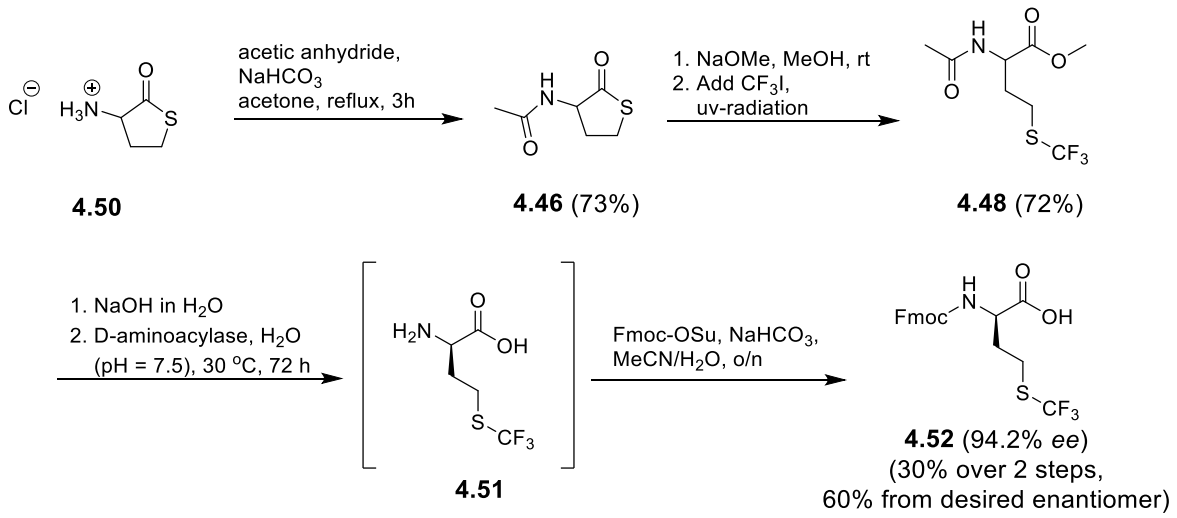

Scheme 4.12: Successful synthesis of Fmoc-*D*-hCys(CF_3)OH (**4.52**).

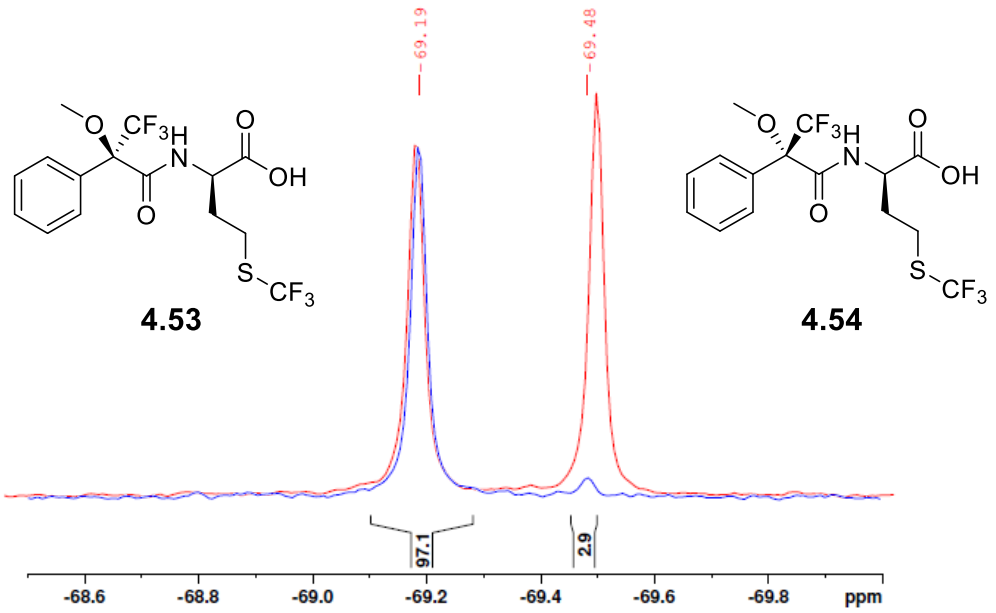

Figure 4.5: Establishing the *ee* of *D*-hCys(CF_3). Coupling of **4.51** to the pentafluorophenyl ester of racemic Mosher's acid (red trace) revealed two diastereomeric ^{19}F-NMR signals, and coupling of **4.51** to the pentafluorophenyl ester of *R*-Mosher's acid demonsrates that the *ee* of **4.51**, and subsequently **4.52**, is 94.2%.

With **4.52** in hand, we then synthesized Dap-Lys6-*D*-hCys(CF_3)8-Glu12-Trp13 (**4.55**, Figure 4.6) using the route outlined in Scheme 1.12 (Section 1.6.4). Unlike the incorporation of *D*-Ser(CF_3), no products resulting from elimination were observed, and after purification by RP-HPLC, peptide **4.55** was obtained in 11% yield based on resin loading.

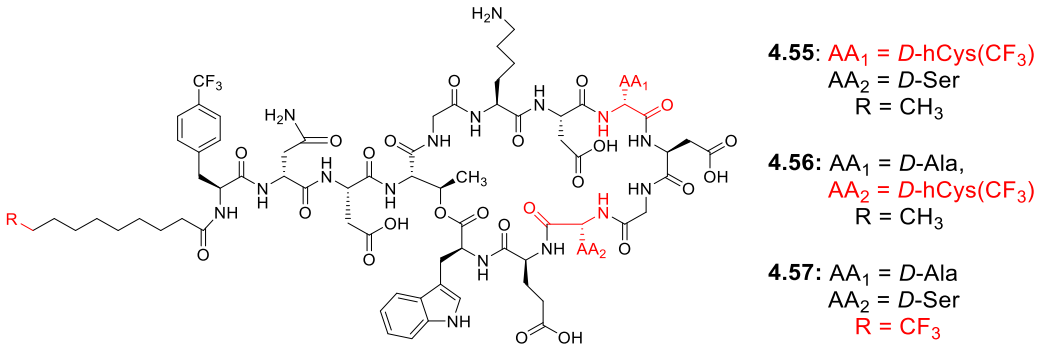

Figure 4.6: Structures of **4.55**, **4.56**, and **4.57**.

Additionally, we synthesized Dap-Lys6-*D*-hCys(CF_3)11-Glu12-Trp13 (**4.56**, Figure 4.6) using the route outlined in Scheme 1.12 (Section 1.6.4). Once again, elimination was not an issue, and the desired product was obtained after purification by RP-HPLC in 2% yield based on resin loading.

4.2.2.4 – Synthesis of Dap-^{TF}Dec0-Lys6-Glu12-Trp13 (**4.57**)

We also prepared Dap-Lys6-Glu12-Trp13 bearing a 10,10,10-trifluorodecanoyl residue (Dap-^{TF}Dec0-Lys6-Glu12-Trp13, **4.57**, Figure 4.6) by total synthesis (11% yield) according to procedures for the other Dap-Lys6-Glu12-Trp13 analogs described above (i.e., Scheme 1.12), except that 10,10,10-trifluorodecanoic acid (**4.3**) was used in place of decanoic acid.

4.2.3 – Biological Studies

The MICs of the fluorinated daptomycin analogs were determined against *B. subtilis* ATCC 1046 using a standard broth dilution assay. The results are presented in Table 4.1.

Peptides bearing a 10,10,10-trifluorodecanoyl lipid (**4.5** (entry 2) and **4.57** (entry 8)) exhibited the same activity as their decanoyl counter parts (entries 1 and 7). The daptomycin analog containing the *p*-^{TFM}benzyl group (**4.6**, entry 3) on Orn6 was only 2.7-fold less active than daptomycin, whereas the analog containing the *p*-^{TFM}benzoyl group on Orn6 (**4.8**, entry 4) was 5.3-fold les active than daptomycin. In this case, the presence of an amino group is slightly beneficial for activity, or, the carbonyl moiety in the benzoyl group is slightly detrimental to activity. The ^{TF}ethyl (**4.7**, entry 5) and ^{TF}acetyl (**4.9**, entry 6) daptomycin derivatives were both 5.3-fold less active than daptomycin. Peptide **4.7** was 2-fold less active than its benzyl-counterpart, but peptide **4.9** had the same activity as its benzoyl-counterpart,

indicating that, in this case, the type of linkage to the Orn residue (amine versus amide) does not affect activity. In any case, all of these daptomycin analogs (**4.5** to **4.9**) exhibited similar biological activity as daptomycin. In addition, all of the Dap-Lys6-Glu12-Trp13 analogs containing fluorinated amino acids (**4.38**, **4.55**, and **4.56**) exhibited similar biological activity, being only 2- to 5-fold less active than their parent compound, Dap-Lys6-Glu12-Trp13 (**1.47**).

Table 4.1: MICs of fluorinated daptomycin analogs against *B. subtilis* ATCC 1046.

Entry	Compound	Lipid Tail	Position 1	Position 6 [b]	Position 6 appendage	Position 8	Position 11	Position 12 [b]	Position 13 [b]	MIC [a] (μg/mL)
1	**1.2**	decanoyl	Trp	Orn	---	*D*-Ala	*D*-Ser	MeGlu	Kyn	0.75
2	**4.5**	trifluoro-decanoyl	Trp	Orn	---	*D*-Ala	*D*-Ser	MeGlu	Kyn	0.75
3	**4.6**	decanoyl	Trp	Orn	*p*-^{TFM}benzyl	*D*-Ala	*D*-Ser	MeGlu	Kyn	2
4	**4.8**	decanoyl	Trp	Orn	*p*-^{TFM}benzoyl	*D*-Ala	*D*-Ser	MeGlu	Kyn	4
5	**4.7**	decanoyl	Trp	Orn	^{TF}ethyl	*D*-Ala	*D*-Ser	MeGlu	Kyn	4
6	**4.9**	decanoyl	Trp	Orn	^{TF}acetyl	*D*-Ala	*D*-Ser	MeGlu	Kyn	4
7	**1.47**	decanoyl	Trp	Lys	---	*D*-Ala	*D*-Ser	Glu	Trp	1.5
8	**4.57**	trifluoro-decanoyl	Trp	Lys	---	*D*-Ala	*D*-Ser	Glu	Trp	1.5
9	**4.15**	decanoyl	^{TFM}Phe	Lys	---	*D*-Ala	*D*-Ser	Glu	Trp	8
10	**4.55**	decanoyl	Trp	Lys	---	*D*-hCys(CF_3)	*D*-Ser	Glu	Trp	4
11	**4.56**	decanoyl	Trp	Lys	---	*D*-Ala	*D*-hCys(CF_3)	Glu	Trp	2
12	**4.38**	decanoyl	Trp	Lys	---	*D*-Ala	*D*-Ser(CF_3)	Glu	Trp	8

[a] 1.25 mM Ca^{2+} added.

[b] Blue shaded cells represent deviations from daptomycin corresponding to peptide **1.47**, Dap-Lys6-Glu12-Trp13.

4.2.4 – Trifluoroacetate counter-ion (TFA^-) after RP-HPLC Purification

In all of the ^{19}F-NMR studies described in this thesis, the solvent is H_2O, with D_2O in a glass insert used for a lock signal. All ^{19}F-NMR spectra showed two fluorine signals, one of which was determined to be the trifluoroacetate (TFA^-) counter-ion (δ = -76 *ppm*) as a result of purification by RP-HPLC (water containing 0.1% TFA was employed as part of the mobile phase). For example, Figure 4.7 shows the ^{19}F-NMR spectra of compound **4.5** after HPLC purification, of daptomycin after being subjected to HPLC, and of daptomycin that was not

subjected to HPLC. The ^{19}F-NMR spectrum of compound **4.5** shows the peak due to the CF_3 group on the lipid tail at approximately -66 *ppm* and a peak at about -76 *ppm* due to TFA^-. The ^{19}F-NMR spectrum of daptomycin, after being subjected to HPLC, only shows a single peak at -76 *ppm*, corresponding to TFA^-. The ^{19}F-NMR spectrum of daptomycin that was not subjected to HPLC shows no peaks.

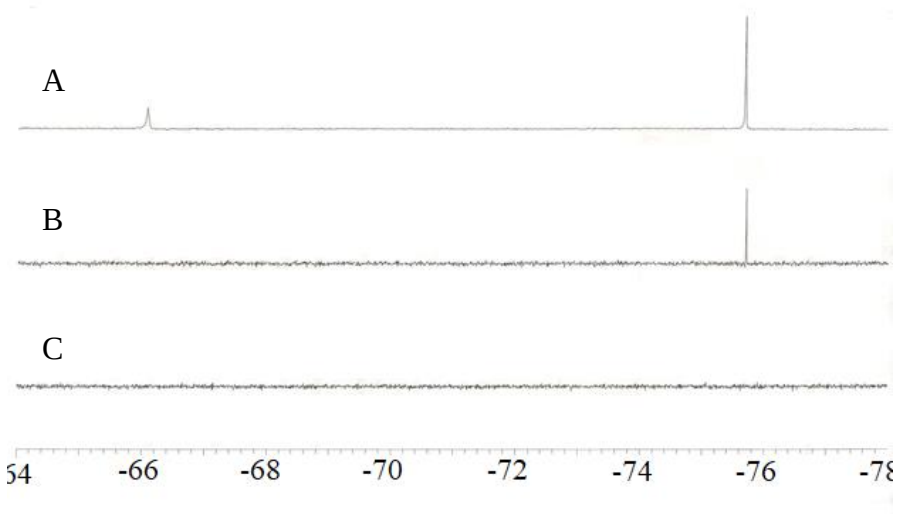

Figure 4.7: ^{19}F-NMR spectrum of (A) compound **4.5** after HPLC purification; (B) daptomycin after being subjected to HPLC, and of (C) daptomycin that was not subjected to HPLC. The TFA counterion appears at -76 *ppm*.

4.2.5 – ^{19}F-NMR Studies of Fluorinated Analogs

4.2.5.1 – ^{19}F-NMR Studies on Daptomycin Aggregation

It has been shown that, under certain conditions, daptomycin can form aggregates. NMR spectroscopy has been used to study the aggregation of apo-Dap (Ca^{2+}-free daptomycin) by examining line-broadening in the ^{1}H- and ^{13}C-NMR spectra of apo-Dap as a function of apo-Dap concentration and pH. The effect of pH on apo-Dap aggregation has been studied by Ball et al. using NMR spectroscopy.[139] They reported that the ^{1}H-NMR spectrum of a solution

of 0.8 mM apo-Dap at pH 7.8 exhibited little or no line broadening. Decreasing the pH to 5.2 and 2.4 resulted in increasing line broadening, characteristic of aggregation, such that the spectrum at pH 2.4 was difficult to analyze. This was particularly true at elevated apo-Dap concentrations of 3-5 mM.

Qiu and Kirsch reported that at pH 6.5, even when the concentration of apo-Dap was very high (21.2 mM), no significant line broadening in the ^{1}H-NMR spectrum was evident.[163] Qiu and Kirsch also studied the effect of pH on apo-Dap oligomerization using fluorescence spectroscopy and dynamic light scattering (DLS). Since daptomycin possesses intrinsically fluorescent Kyn13, whose fluorescence intensity increases in non-polar environments compared with polar, aqueous ones, an increase in fluorescence intensity signifies localization in a hydrophobic environment. The critical aggregation concentration (CAC) values of apo-Dap were identified by an upward inflection of the fluorescence emission intensity for Kyn13 and were also found to be pH-dependent. At pH 3-5, the CAC was determined to be 0.12-0.2 mM of apo-Dap. At pH values of 5.5-6.5, no upward inflections were detected up to 0.3 mM apo-Dap. Using DLS, they also determined that the hydrodynamic radius of apo-Dap at pH 4.0 above 0.2 mM increased, indicating aggregation. At pH 6.5, the hydrodynamic radius remained constant up to 7.32 mM, suggesting a lack of aggregation.

The tendency for apo-Dap to oligomerize under acidic conditions can be explained by the ionization state of apo-Dap. Between pH 2.5-4, apo-Dap exists primarily as a neutral or monoanionic species. As the pH increases to 7, the dianionic and trianionic forms dominate. Based on pK_A values assigned to the acidic residues, deprotonation of the Asp3 and MeGlu12 residues occurs as pH increased from 4 to 7 and these residues are located near the hydrophobic portions of daptomycin's amphipathic structure.[144] Since the structure of the monoanionic

species has been compared to a surfactant, ionization of the acid residues close to the lipid tail and hydrophobic portions of daptomycin would destabilize aggregates formed by hydrophobic interactions, and thus reduce aggregation.[163]

In summary, apo-Dap aggregates under acidic conditions at concentrations above 0.12 – 0.20 mM but does not appear to aggregate at neutral or near neutral pH, even at very high concentrations.

Since daptomycin is known to require calcium for biological activity, NMR studies have also been performed on daptomycin with calcium present. It has been shown that significant line broadening in the ^{1}H-NMR spectrum occurs upon the addition of just 0.3 equivalents of Ca^{2+} to 0.8 mM daptomycin at pH 5.0.[139] The Hancock and Straus groups reported that an aqueous solution of 2 mM daptomycin at pH 6.6 exhibited well-resolved resonances in the ^{1}H- and ^{13}C-NMR spectra; however, the addition of 5 mM Ca^{2+} resulted in significant line broadening.[22] Using ultracentrifugation, the Hancock and Straus groups reported that a 2.5 mM solution of daptomycin containing 1 molar equivalent of Ca^{2+} at pH 7.0 forms micelles consisting of 14 daptomycin monomers.[164] On the basis of these results, the Hancock and Straus groups suggested that daptomycin forms micelles *in vivo*, and the micelles act as vehicles to deliver daptomycin to the bacterial membrane, where the daptomycin micelle dissociates into monomers which allows daptomycin insertion into the bilayer.

Qiu and Kirsch also studied the effect of Ca^{2+} on daptomycin oligomerization using fluorescence spectroscopy (using the intrinsic fluorescence of the Trp and Kyn residues).[163] At pH 6.5, in the presence of 10 mM Ca^{2+}, the CAC of daptomycin was determined to be 0.50 mM. Limited studies were also performed using 1.0 mM Ca^{2+} in phosphate-buffered saline at pH 7.4 at daptomycin concentrations ranging from 0.011 to 0.0157 mM. As daptomycin

concentrations increased from 0.011 to 0.026 mM, the fluorescence spectral patterns or Trp and Kyn were not changed, except for an increase in emission intensity from these residues with increasing daptomycin concentration. When the daptomycin concentrations increased from 0.065 to 0.157 mM, there was an increase of the emission intensity from Kyn13 and a decrease in emission intensity from Trp1, suggesting that increased FRET between Trp1 and Kyn13 was occurring. The increased FRET occurring may suggest aggregation, although it should be noted that the slight increase in Kyn fluorescence seemed to parallel the slight increase observed when the Ca^{2+} concentration was increased from 0.011 to 0.026 mM – that is to say, Kyn13 emission intensity might not have been increasing between 0.065 and 0.157 mM Ca^{2+} *because* of FRET from Trp. Nevertheless, the researchers interpreted these fluorescence changes as being due to daptomycin aggregation and concluded that daptomycin forms aggregates at physiological plasma concentrations of 0.06 mM[165,166] (or 100 μg/mL) and physiological Ca^{2+} concentration (1.25 mM), and that daptomycin aggregation is critical for achieving its therapeutic effect. However, it has been pointed out by Taylor and Palmer that such daptomycin concentrations still substantially exceed daptomycin's MIC (0.75 μg/mL), and would only occur in human plasma immediately after application of the drug, as 90% of the total amount of daptomycin is protein-bound, most likely in its monomeric form.[167,168]

Although the above studies indicate that daptomycin undergoes oligomerization in the presence of calcium, these studies were conducted using daptomycin concentrations that were far greater than MIC values of daptomycin. More recently, Muraih et al. have examined daptomycin oligomerization at concentrations close to those required for antibacterial activity using fluorescence spectroscopy.[44] Because kynurenine has a very low fluorescence intensity in aqueous solution, both in the presence and absence of Ca^{2+}, Muraih et al. elected to use a

highly sensitive FRET assay to study daptomycin oligomerization and used daptomycin labelled at Orn6 with NBD (NBD-Dap, **4.58**, Figure 4.8) or Alexa Fluor 350 (Alexa-Dap, **4.59**, Figure 4.8). These fluorophores allow for FRET from Alexa-Dap to NBD-Dap if the two moieties are found in close proximity, and due to their high fluorescence intensity, could be studied at very low concentrations (0.175 µM Alexa-Dap, 0.88 µM NBD-Dap; corresponding to 0.3 µg/mL and 1.4 µg/mL of daptomycin, respectively). They found that no FRET between Alexa-Dap and NBD-Dap occurred in solution in both the absence and presence of Ca^{2+}. In contrast, strong FRET was observed only in the presence of both Ca^{2+} and DMPC/DMPG liposomes, suggesting that daptomycin only oligomerizes on membranes in the presence of Ca^{2+} These studies suggest that daptomycin does not form aggregates in solution at its MIC concentration, which indicates that pre-aggregation of daptomycin in solution is not necessary for daptomycin to interact with membranes and exert its biological effects.

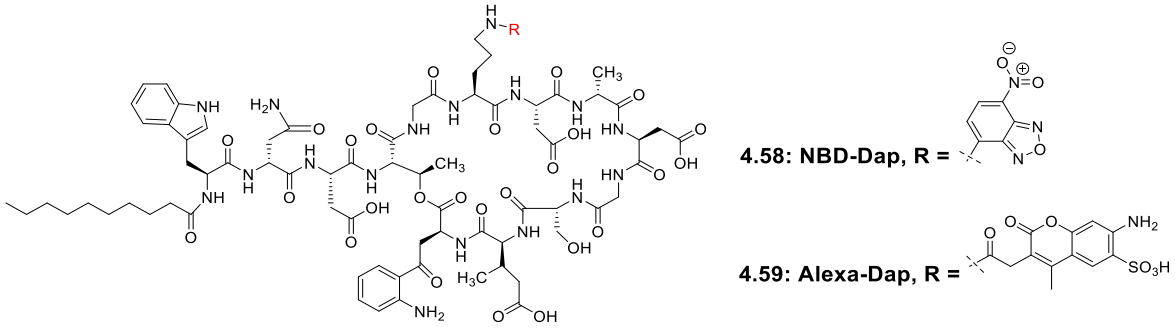

Figure 4.8: Structures of NBD-Dap (**4.58**) and Alexa-Dap (**4.59**).

We wished to determine if ^{19}F-NMR can be used to study daptomycin aggregation. We began these studies using an unbuffered solution of peptide **4.5**, at concentrations ranging from 10-500 µM, in Milli-Q water (pH = 4.8). Solutions were examined by ^{19}F-NMR at 37 ^{o}C (Figure 4.9).

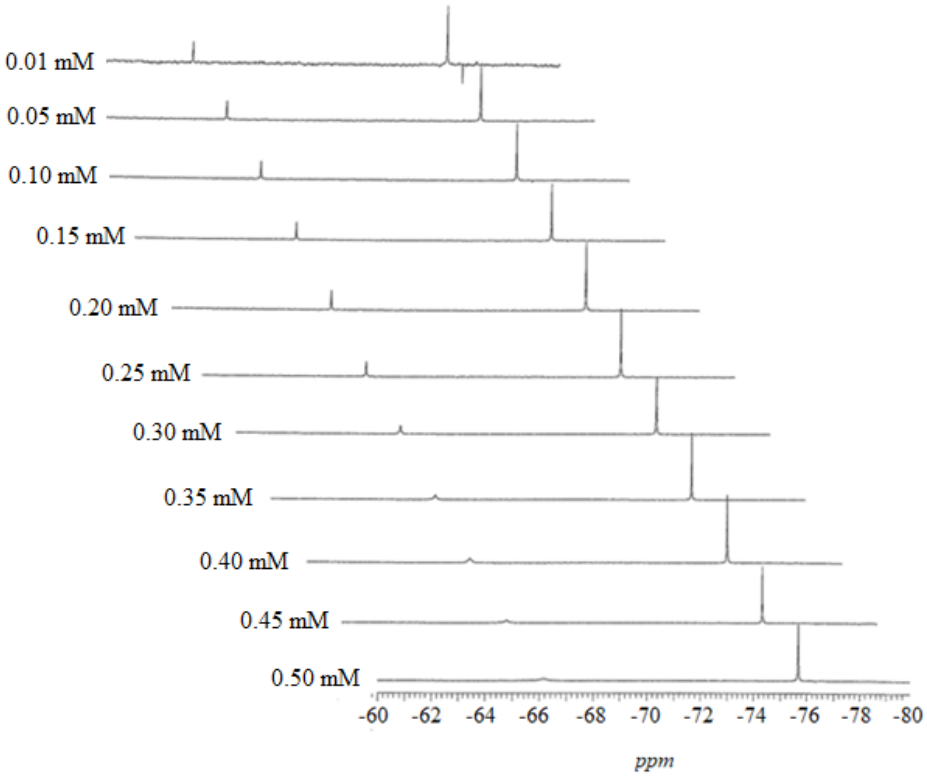

Figure 4.9: ^{19}F-NMR spectra of peptide **4.5** (0.01-0.500 mM) in Milli-Q water.

The chemical shift remained the same at all daptomycin concentrations. Qualitatively, broadening of the peaks was observed at approximately 0.25 mM of the peptide. Figure 4.10A shows the relationship between peak area (relative to the TFA counter-ion) and peptide concentration, Figure 4.10B shows the relationship between peak height (relative to the TFA counter-ion) and peptide concentration, and Figure 4.10C shows the relationship between peptide concentration and the width of the peak at half of the height of the peak, signifying broadening. Peak area (panel A) does not change with peptide concentration. Peak height does not begin to diminish significantly until the peptide concentration is greater than 0.20 mM. The peak width at half-height is constant up to 0.20 mM but then begins to increase in a linear fashion up to 0.45 mM. From the plot of the peak width at half-height versus peptide concentration, we are able to determine the critical aggregation concentration of daptomycin

under these conditions. These results are consistent with those of Qiu and Kirsch (discussed above) who, using fluorescence spectroscopy, determined the CAC of daptomycin to be 0.20 mM at pH 5.0.

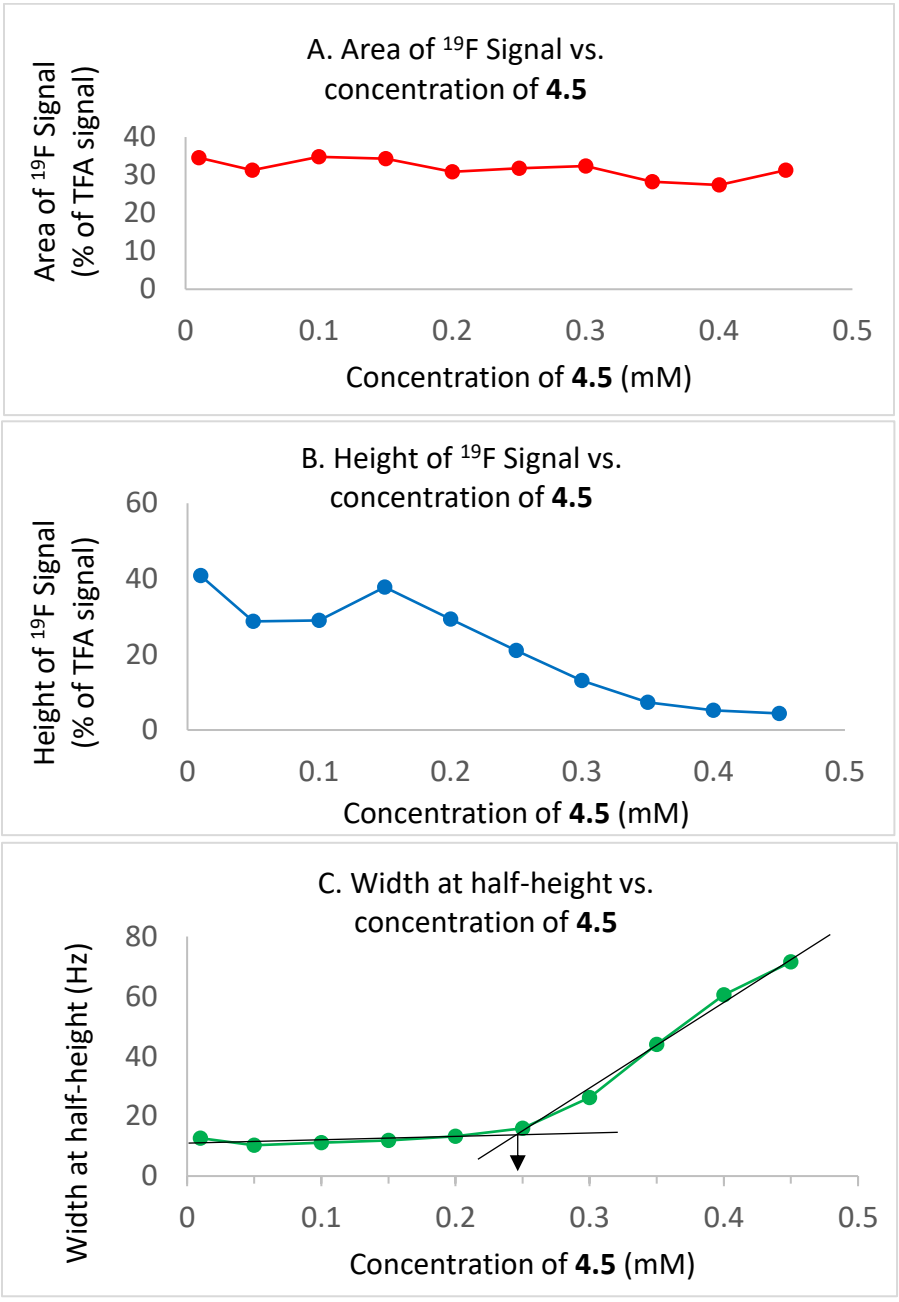

Figure 4.10: The effect of concentration of peptide in Milli-Q water on peptide **4.5** ^{19}F-NMR signal characteristics. (A) Total peak area, (B) peak height, and (C) peak width at half height. In panel C, where the two lines intersect represents the critical aggregation concentration of daptomycin (0.25 mM). We were unable to obtain accurate data at 0.5 mM due to excessive line broadening.

For obvious reasons, a solution of daptomycin in Milli-Q water (approximate pH = 4.8) does not represent biologically relevant conditions. Human plasma contains ions like sodium and calcium and is buffered at approximately pH = 7.4. Accordingly, we sought to determine the critical aggregation concentrations of compound **4.5** in buffered solutions in the presence and absence of calcium.

A solution of peptide **4.5** in 20 mM HEPES (pH 7.4) containing 150 mM NaCl was analyzed ^{19}F-NMR at 37 ^{o}C, both with and without the physiological concentration of daptomycin (1.25 mM $CaCl_2$). The chemical shift remained the same at all daptomycin concentrations. Unlike in unbuffered Milli-Q water, the peaks did not broaden at the higher concentrations, but remained relatively constant (Figure 4.11). Although the Hancock and Straus groups reported that the ^{1}H-NMR spectrum of an aqueous solution of daptomycin at pH 6.6 containing Ca^{2+} exhibited significant line broadening, the concentration of daptomycin used in their experiment (2 mM) was much greater than daptomycin's MIC (approximately 1.5 μM) and the concentration of Ca^{2+} (2.5 to 5 mM) was well above physiological concentrations (1.25 mM), making these results meaningless in terms of their relevance to daptomycin's mechanism of action.[167,168] Our results support the findings of Muraih et al.[44] that indicate that, at MIC concentrations of daptomycin and in the presence of physiological concentrations of Ca^{2+}, daptomycin does not form aggregates in solution under physiological conditions, and that pre-aggregation of daptomycin in solution is probably not necessary for daptomycin to interact with membranes and exert its biological effects.

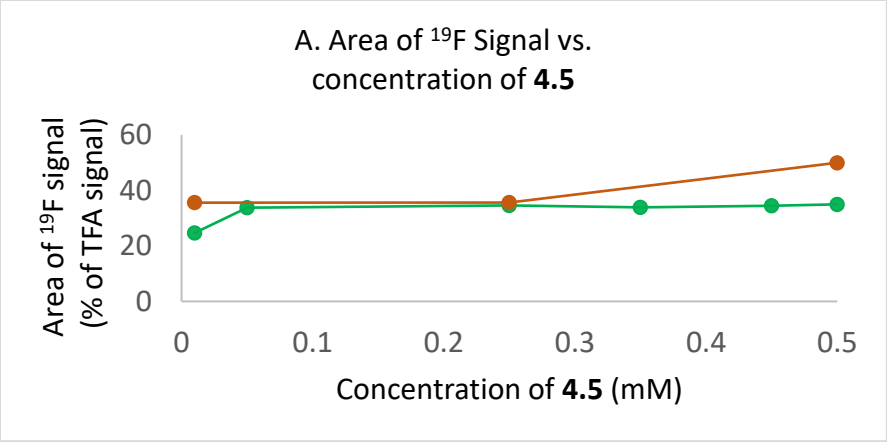

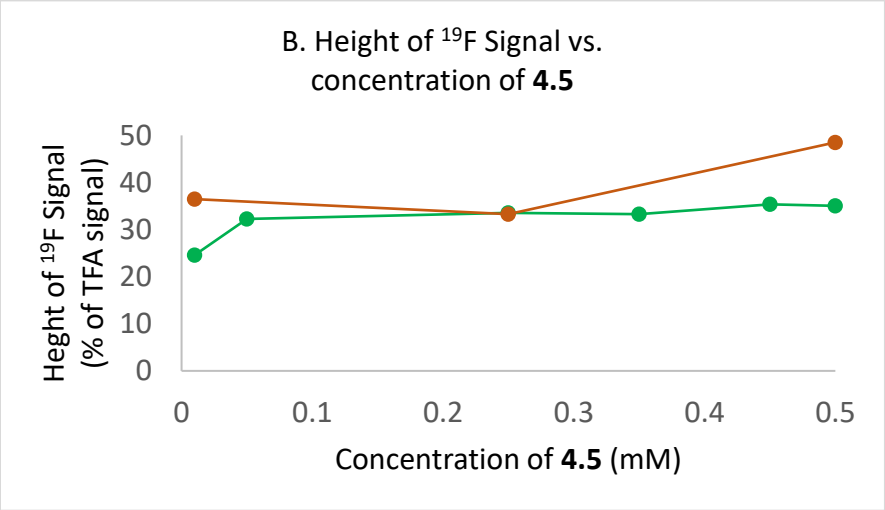

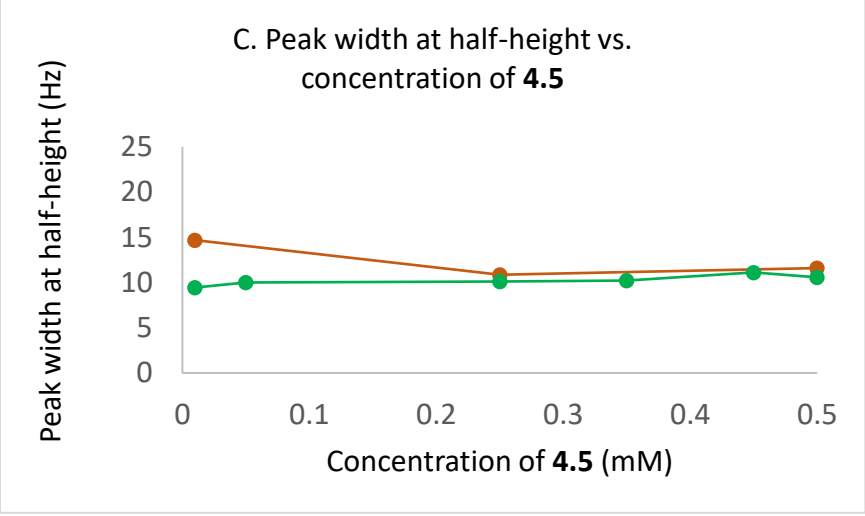

Figure 4.11: The effect of the concentrations of peptide **4.5** in buffered aqueous solution on ^{19}F-NMR peak characteristics in the presence (1.25 mM, orange line) and absence (green line) of Ca^{2+}. (A) Total peak area, (B) peak height, and (C) peak width at half-height. No aggregation of peptide **4.5** is observed, up to concentrations of 0.5 mM, ten times higher than concentrations of daptomycin found *in vivo* after daptomycin injections.

4.2.5.2 – ^{19}F-NMR Studies of Peptide **4.5** in the Presence of Liposomes

Our next step was to obtain ^{19}F-NMR spectra of peptide **4.5** in the presence of model membranes. To this end, ^{19}F-NMR spectra of 0.025 mM solutions of peptide **4.5** in HEPES buffer (20 mM, pH 7.4, 150 mM NaCl) containing liposomes (0.250 mM total lipid) and varying amounts of Ca^{2+} were recorded. One liposome sample consisted of a 1:1 mixture of DOPG and DOPC, while another liposome consisted of only DOPC lipids. Since daptomycin is known to require PG in its mechanism of action, interactions with liposomes containing DOPC were not expected.

The ^{19}F-NMR spectra of peptide **4.5** in solutions containing the DOPG/DOPC (1:1) liposomes and varying amounts of Ca^{2+} are shown in Figure 4.12. The ^{19}F-NMR spectra of peptide **4.5** in solutions containing the DOPC liposomes and varying amounts of Ca^{2+} are shown in Figure 4.13. Neither the chemical shift, nor the peak width at half-height (Figure 4.14B) changes as a function of Ca^{2+} concentration with either the DOPG/DOPC or DOPC liposomes. The peak area does not change as a function of Ca^{2+} concentration with the DOPC; however, the peak area does change as a function of Ca^{2+} concentration with the DOPG/DOPC liposomes (Figure 4.14A). Clearly, the peptide is not interacting with the DOPC liposomes, which is consistent with the mechanism of action of daptomycin in liposomes. It is interesting that with the DOPG/DOPC liposomes, that the peak width-at half-height (used to represent peak broadening) does not change while peak area decreases. This suggests that we are observing only the free, unbound form of the peptide. Any peptide bound to the liposomes should give rise to a signal that is broader (and possibly not observable) and probably has a chemical shift that is different from the free, unbound form. A similar phenomenon has been

reported by Afonin et al. during their ^{19}F-NMR studies on the interaction of PGLa, and by Pielak and co-workers during their ^{19}F-NMR studies on α-synuclein, mentioned above.[131,138]

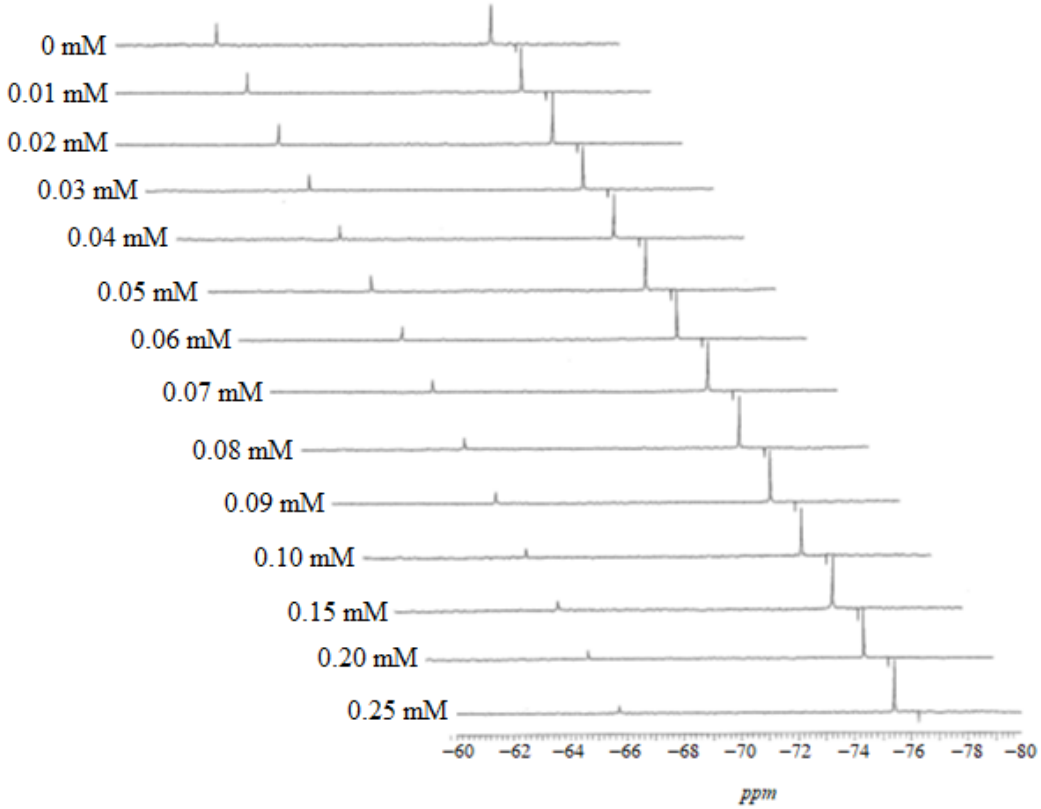

Figure 4.12: ^{19}F-NMR spectra of peptide **4.5** (0.025 mM) in HEPES buffer (pH 7.4, 150 mM NaCl, containing DOPG/DOPC (1:1) liposomes (0.250 mM) and varying amounts of Ca^{2+}.

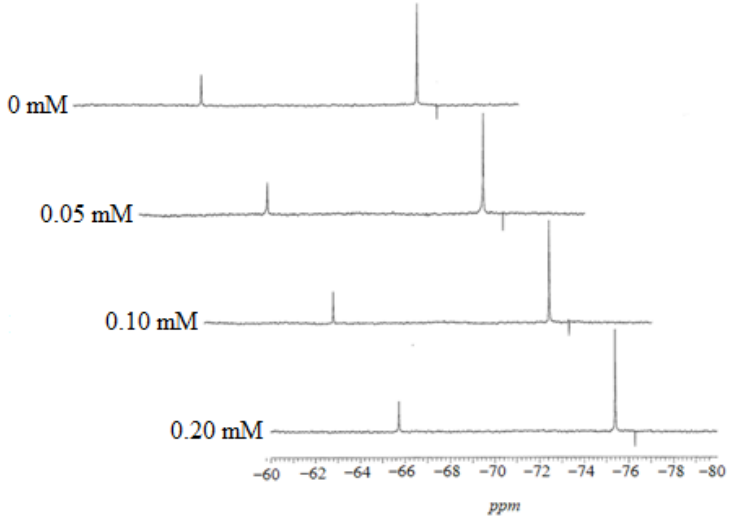

Figure 4.13: ^{19}F-NMR spectra of peptide **4.5** (0.025 mM) in HEPES buffer (pH 7.4, 150 mM NaCl) containing DOPC liposomes (0.250 mM) and varying amounts of Ca^{2+}.

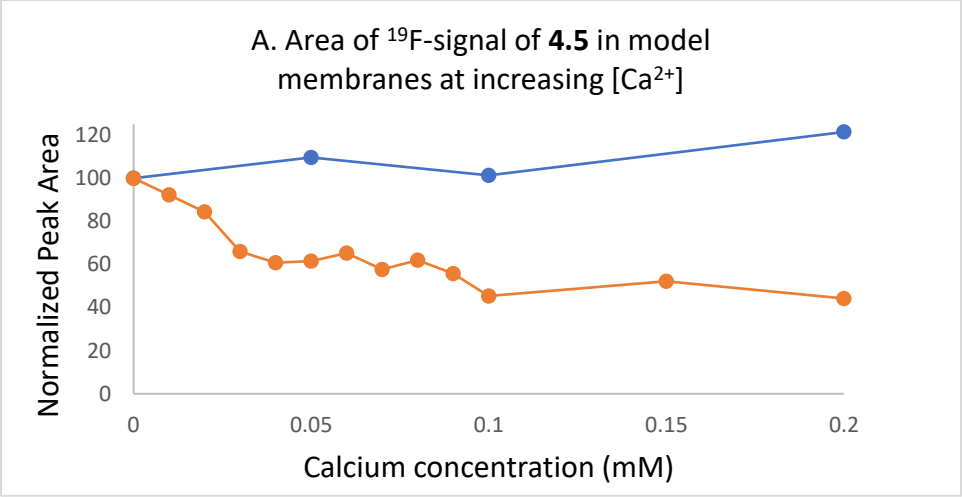

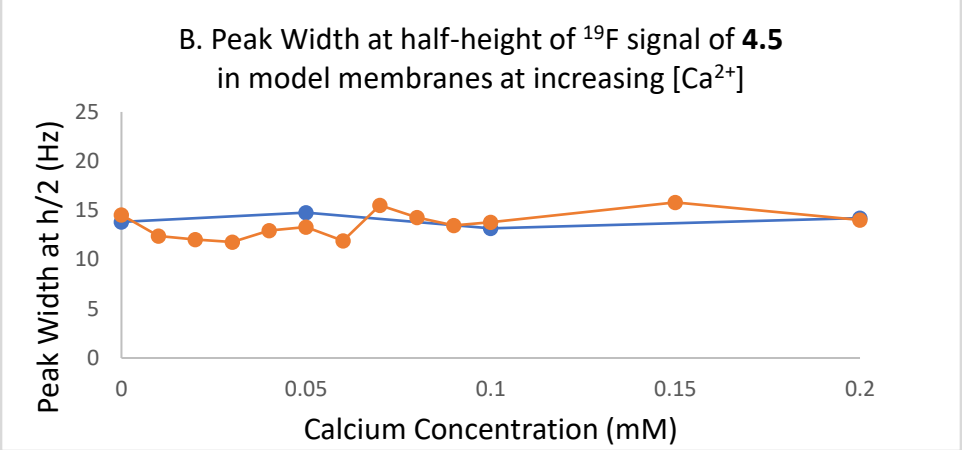

Figure 4.14: ^{19}F-NMR spectra characteristics of peptide **4.5** in buffered (pH 7.4) solutions containing lipids as a function of calcium concentration. Orange lines represent DOPG/DOPC (1:1) liposomes, blue lines represent DOPC liposomes. (A) Total peak area, (B) peak width at half-height.

4.2.5.3 – ^{19}F-NMR Studies of Peptide **4.6** in the Presence of Liposomes

Next, we examined the interaction of ornithine analog **4.6** with membranes using ^{19}F-NMR. ^{19}F-NMR spectra of 0.025 mM solutions of peptide **4.6** in HEPES buffer (20 mM, pH 7.4, 150 mM NaCl) containing liposomes (0.250 mM) and varying amounts of Ca^{2+} were recorded. One liposome consisted of a 1:1 mixture of DOPG and DOPC, while another liposome consisted of only DOPC lipids.

The ^{19}F-NMR spectra of peptide **4.6** in the presence of DOPC liposomes did not change significantly with Ca^{2+} concentration, indicating that this peptide was not interacting strongly with these liposomes (Figure 4.15). In contrast, the ^{19}F-NMR spectra of peptide **4.6** in the presence of the DOPG/DOPC liposomes changed dramatically with Ca^{2+} concentration (Figure 4.16). First, we noticed that even in the absence of Ca^{2+} that the height of the peak corresponding to peptide **4.6** in the presence of DOPG/DOPC liposomes was significantly less than the height of the peak corresponding to peptide **4.6** in the presence of DOPC liposomes (28% relative to the TFA peak versus 43% relative to the TFA peak). This suggests that, even in the absence of Ca^{2+}, the Orn residue is interacting with PG. This may be due to the electrostatic interactions between peptide **4.6**, which still bears a protonated amino group on the Orn residue, and the negative charge on PG. Due to the small size of the peaks in the DOPG/DOPC spectra (Figure 4.16), it was challenging to accurately determine the peak width at half-height; nevertheless, it appears that in the presence of the DOPG/DOPC liposomes that this characteristic does not change with increasing Ca^{2+} concentration. In contrast, in DOPG/DOPC liposomes, peak area decreases dramatically with Ca^{2+} concentrations, and the peak is undetectable at just 0.100 mM Ca^{2+} (Figure 4.17). These results again suggest that we are observing only the free, unbound form of the peptide. It can be concluded that the trifuoromethyl tag on **4.6** is strongly associated with the hydrophobic membrane at these levels of calcium.

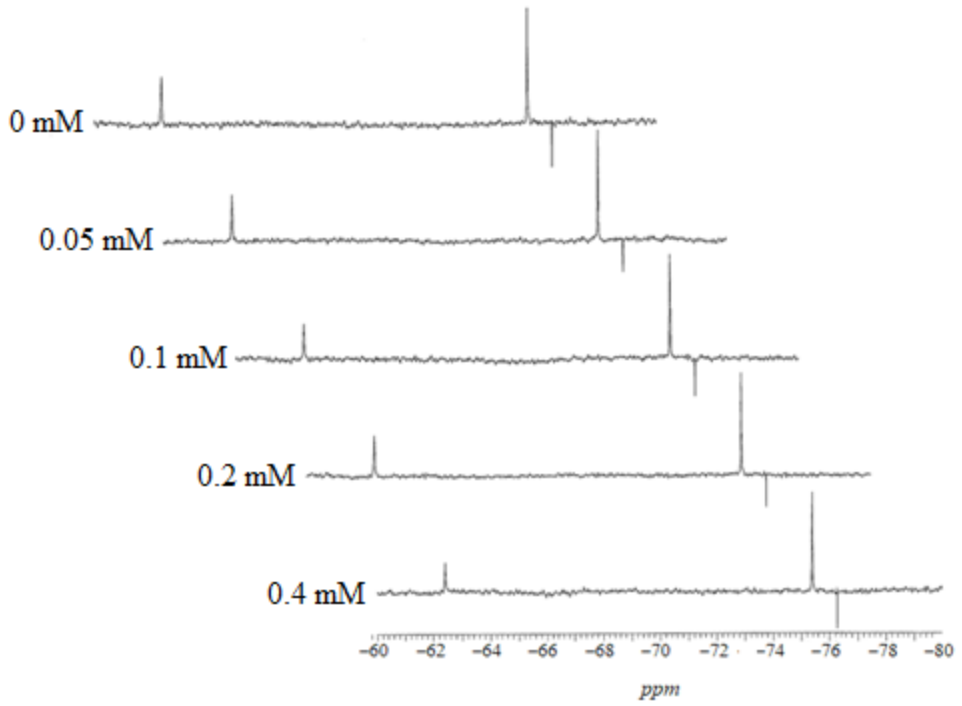

Figure 4.15: ^{19}F-NMR spectra of peptide **4.6** (0.025 mM) in HEPES buffer (pH 7.4, 150 mM NaCl), containing DOPC liposomes (0.250 mM) and varying amounts of Ca^{2+}.

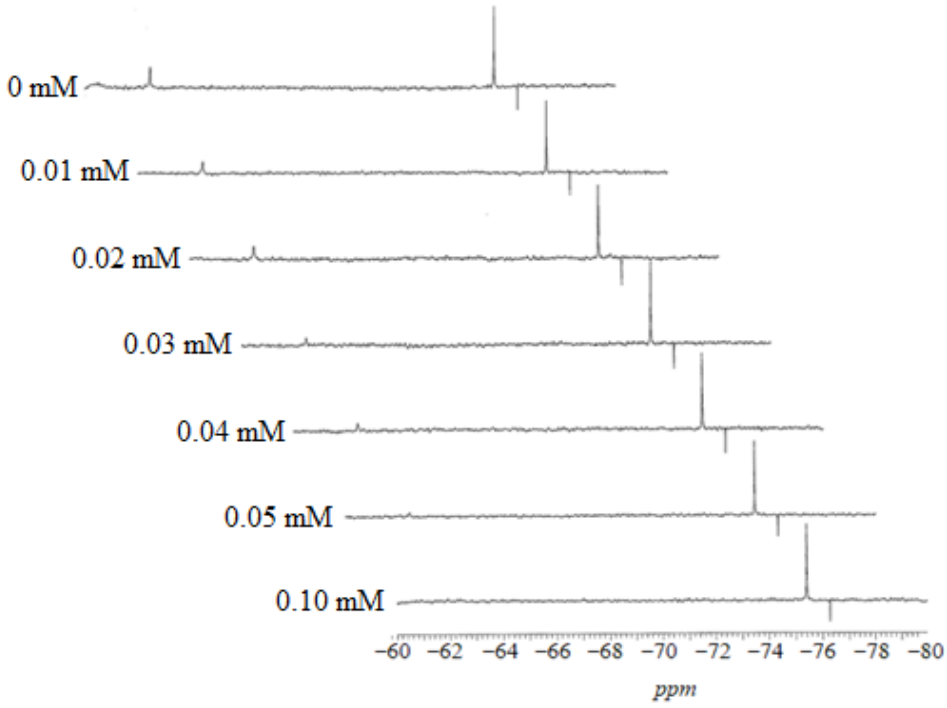

Figure 4.16: ^{19}F-NMR spectra of peptide **4.6** (0.025 mM) in HEPES buffer (pH 7.4, 150 mM NaCl), containing DOPG/DOPC (1:1) liposomes (0.250 mM) and varying amounts of Ca^{2+}.

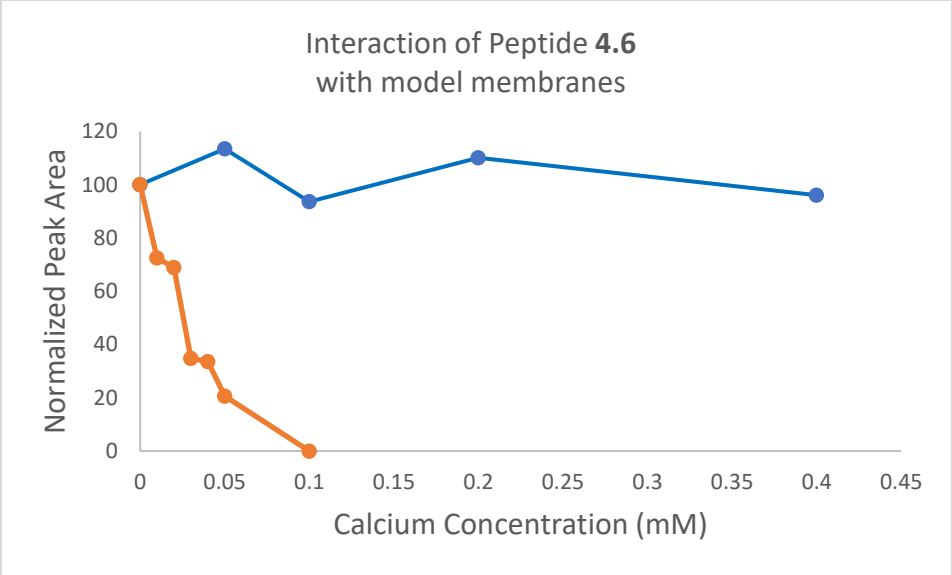

Figure 4.17: Areas of the peaks of peptide **4.6** in buffered (pH 7.4) solutions containing lipids as a function of calcium concentration. Orange lines represent DOPG/DOPC (1:1) liposomes, blue lines represent DOPC liposomes.

The interaction of peptide **4.6** with DOPG/DOPC liposomes was observed at calcium concentrations much lower than those observed with compound **4.5**. A graph illustrating the dependency of the peak area on Ca^{2+} concentration for both peptides **4.5** and **4.6** is shown in Figure 4.18. The area of the ^{19}F-signal of compound **4.6** decreased rapidly at concentrations between 0 and 0.05 mM Ca^{2+} and was completely undetectable at just 0.100 mM Ca^{2+}. In contrast, with peptide **4.5**, it takes considerably higher calcium concentrations for the area of the ^{19}F signal in peptide **4.5** to decrease, and even at the highest Ca^{2+} concentration examined, 0.250 mM, the peak did not completely disappear. Indeed, between 0.100 and 0.250 mM of Ca^{2+}, the peak area does not change appreciably. It is possible that the peak does not completely disappear because we did not use sufficiently high concentrations of Ca^{2+} to promote complete association of the lipid portion of peptide **4.5** with the liposome. Daptomycin exhibits maximal antibacterial activity at 1.25 mM Ca^{2+}. It will be interesting to see whether the peak area of peptide **4.5** would decrease (and eventually disappear) at Ca^{2+} concentrations between 0.25

mM and 1.25 mM. If so, then this would suggest that daptomycin interacts with membranes via two successive Ca^{2+} binding events as has been suggested by Palmer and Taylor groups (section 1.2.3).[49,51]

Previous results published by the Palmer and Taylor groups in the changes in fluorescence of daptomycin and of fluorescently labelled daptomycin suggested that the Orn residue initiates daptomycin interactions (section 1.2.3).[49] Our results are entirely consistent with these findings in that the trifluoromethylbenzyl moiety on the Orn residue in peptide **4.6** interacts with liposomes prior to the trifluoromethyl tag of compound **4.5** (Figure 4.18). Extending this to unlabeled daptomycin, one can conclude that the Orn residue interacts with membranes before the lipid tail.

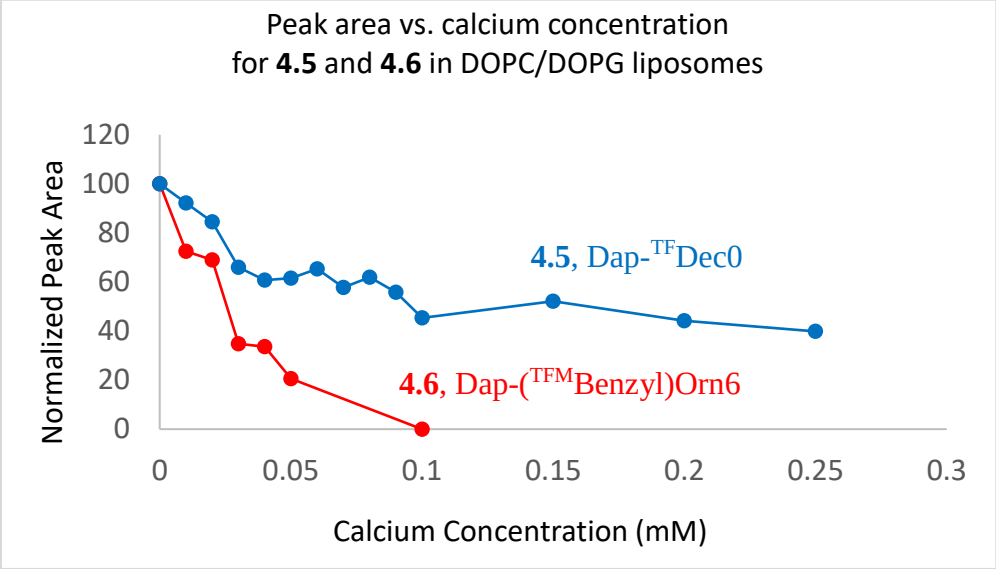

Figure 4.18: Peak area of the ^{19}F-signal of peptides **4.5** and **4.6** as a function of calcium in DOPG/DOPC membranes. Peak areas are normalized to the area of the signal at 0 mM Ca^{2+}.

4.3 – Summary and Conclusions

A total of ten fluorinated analogs of daptomycin were prepared. Analogs containing the trifluoromethyl group at either the lipid tail or Orn6 were prepared via semi-synthesis. Analogs containing the trifluoromethyl group at positions 1, 8, or 11 were prepared via total synthesis, as well as a Dap-Lys6-Glu12-Trp13 analog which contained the trifluoromethyl group on the lipid tail. All of the analogs were found to retain good biological activity against *B. subtilis* ATCC 1046 in comparison to their parent compounds (daptomycin or Dap-Lys6-Glu12-Trp13).

Using ^{19}F-NMR and peptide **4.5**, which bears a CF_3 group at the end of the lipid tail, we demonstrated that under physiological pH and physiological Ca^{2+} concentration, that daptomycin does not form aggregates at daptomycin concentrations up to at least 0.5 mM. These results support the findings of Muraih et al.[44], that at MIC concentrations of daptomycin, and in the presence of physiological concentrations of Ca^{2+}, daptomycin does not form aggregates in solution, and that preaggregation of daptomycin in solution is probably not necessary for daptomycin to interact with membranes and exert its biological effects.

^{19}F-NMR studies with peptides **4.5** and **4.6** suggest that the Orn6 residue of daptomycin interacts with biological membranes before the lipid tail does, as made evident by the observation that the trifluoromethyl signal for peptide **4.6** broadens beyond detection at Ca^{2+} concentrations lower than that observed for peptide **4.5**.

Due to time constraints, it was not possible to probe the interaction of peptides **4.7** to **4.9**, **4.15**, **4.38**, or **4.55** to **4.57** with model membranes using ^{19}F-NMR. Nevertheless, one of our objectives, which was to determine if ^{19}F-NMR can be used to probe the interaction of daptomycin with model membranes, has been achieved. It is clear from the above studies that

^{19}F-NMR can indeed be used to study daptomycin's interaction with model membranes. Whether or not it can provide *new* information on the mechanisms of action of daptomycin remains to be seen. We anticipate that future ^{19}F-NMR studies on all of the peptides synthesized in this chapter will indeed provide new information. A summary of these future studies is presented below.

4.3.1 – Future Studies

The studies involving the interaction of fluorinated analogs **4.5** and **4.6** with model membranes were performed on a Bruker 500 MHz NMR Spectrometer, and to obtain the spectra shown above with an acceptable signal-to-noise ratio, fluorinated daptomycin analogs were analyzed at concentrations of 0.025 mM, which is higher than the concentration of free daptomycin seen *in vivo*. Additionally, these NMR experiments involved 8000 scans requiring 12-hour NMR experiments. To support future ^{19}F-NMR studies on these compounds, the University of Waterloo received a grant for the purchase an installation of a ^{19}F-probe for a Bruker 600 MHz Spectrometer, which will assist future ^{19}F-NMR studies in terms of reduced time required for each NMR experiment, and additionally, reduced concentration of daptomycin analogs needed. The Taylor group is anxiously waiting for this new probe to be installed before ^{19}F-NMR studies will continue.

In the performed experiments, fluorinated analogs in the presence of lipids and increasing calcium concentration were analyzed by ^{19}F-NMR, and higher calcium resulted in a smaller magnitude of ^{19}F signal present in DOPG/DOPC membranes only, with no observable change in DOPC membranes. These studies were performed up to calcium concentrations of at most 0.4 mM, which is less than the physiological concentration of Ca^{2+} (1.25 mM). Accordingly, with DOPC membranes, it will be necessary to increase the

concentration of Ca^{2+} to at least 1.25 mM, to be absolutely certain that this method can be used to corroborate the overwhelming scientific consensus that daptomycin does not interact with DOPC liposomes under physiological concentrations of free calcium.

All synthesized peptides will be analyzed by ^{19}F-NMR in the presence of liposomes containing DOPG/DOPC as presented in Section 4.2.5.2 and 4.2.5.3. So far, the trifluoromethyl tags studied reside on a hydrophobic lipid tail, and on a hydrophobic benzyl group, and indicate localization within the hydrophobic bilayer of model membranes. It is possible that the trifluoromethyl tag of other fluorinated daptomycin analogs will demonstrate localization in the aqueous surroundings to the membranes. The placement of trifluoromethyl tags at varying locations of daptomycin's structure will hopefully shed light on the chemical environments associated with the different amino acid residues of daptomycin.

Instead of increasing calcium concentrations, an alternative version of this experiment can involve studying the fluorinated analogs in the presence of calcium and increasing the lipid concentration present. In doing so, we would expect to see a slow disappearance of the ^{19}F signal as liposomes are added, signifying membrane insertion, analogous to the observations of Afonin et al., who saw a decrease in the ^{19}F-signal of fluorinated α-synuclein upon addition of negatively charged liposomes.[131] In the studies performed in this thesis, the total peptide to lipid ratio is 1:10 (thus a 1:5 ratio of peptide to DOPG). Starting the experiments with no liposomes present and slowly increasing the amount of liposomes present would provide valuable information of the stoichiometry of daptomycin-DOPG binding. Additionally, the ratio of DOPG to DOPC can be varied to observe how this affects membrane binding using ^{19}F-NMR, in addition to including cardiolipin, or lipids with myristoyl acyl groups instead of oleoyl acyl groups.

Typically T_2 relaxation times are determined from measuring the peak-width at half height (λ, $\lambda = 2R_2$, and $R_2 = 1/T_2 \rightarrow T_2 = 2\lambda$).[169] In our studies, this is not possible due to the observed disappearance of the peaks of interest. To solve this problem, we can determine the T_2 values using CPMG T_2 experiments, as performed by the Marsh group for fluorinated analogs of MSI-78, an antimicrobial peptide.[135–137]

Additionally, these studies can be repeated with D_2O as the solvent instead of H_2O to observe the solvent induced isotopic shift (SIIS) effect. Trifluoromethyl tags on residues that are found in an aqueous environment will display a change in chemical shift of about 0.2 *ppm* in D_2O relative to water, but trifluoromethyl tags residing in a hydrophobic environment will not experience any SIIS effect.[170]

In this chapter, fluorinated analogs of daptomycin were synthesized. With the synthesis available for analogs of A54145A$_1$ and A54145D (Chapter 2 and 3), we are also poised to synthesize fluorinated analogs of A54145D and conduct the same studies to shed greater insights on the mechanism of action of A54145D as well. It is assumed to behave in a similar fashion to daptomycin, but due to some differences in the locations of its charged residues (e.g., *D*-Asn2 and Asp3 in daptomycin, vs. *D*-Glu2 and HOAsn3 in A54145; as well as Orn6 and *D*-Ala8 in daptomycin, vs. Ala6 and *D*-Lys8 in A54145), subtle differences in their membrane binding patterns may be expected.

4.4 – Experimental

4.4.1 – Procedure for ^{19}F-NMR studies

All NMR of fluorinated daptomycin analogs presented in this thesis were obtained on a Bruker 500 MHz NMR spectrometer with temperature set to 37 ^{o}C. For self-aggregation

studies in water, a 400-µL sample was prepared at the desired concentration of analog, added to an NMR tube, and a glass insert with D_2O was inserted. Samples with analog concentrations of 0.025 mM or less were subjected to 8000 scans with a delay time of 5 seconds, and samples with a higher concentration were subjected to 1000 scans.

All ^{19}F-NMR studies involving model membranes were performed at a final analog concentration of 0.025 mM, and accordingly subjected to 8000 scans with a relaxation time of 5 seconds. For these studies, liposomes were prepared by Dr. Robert Taylor, previously of the Taylor and Palmer lab, following previously reported procedures.[49,51,63] Each individual NMR experiment was performed on a freshly prepared solution of liposomes, buffer, calcium, and fluorinated analog.

4.4.2 – Procedure for *ee* Determination of Synthesized Fluorinated Amino Acids

For Trifluoromethylphenylalanine:

Following hydrogenation of **4.26** yielding **4.20**, an aliquot of the crude product (1 mg) was suspended in 1:1 H_2O/MeCN (200 µL). To this was added the pentafluorophenyl ester of *R*-Mosher's acid, or the pentafluorophenyl ester of *R/S*-Mosher's acid in excess (4 mg, >2 eq) and triethylamine (2 µL, >3 eq) (accounting for the mass of the bi-benzyl by-product after hydrogenation, the actual mass of unprotected trifluoromethylphenylalanine was necessarily less than 1 mg). The reaction was stirred at room temperature overnight. Following the reaction, the entire crude mixture was suspended in $CDCl_3$ and analyzed by ^{19}F-NMR. Peaks were observed that corresponded to unreacted starting Mosher's pentafluorophenyl ester, and hydrolyzed Mosher's acid and pentafluorophenol. The presence of unreacted Mosher's acid pentafluorophenyl ester indicated that all of the amino acid had been converted to its corresponding Mosher's amide. To elucidate the *ee* of compound **4.20**, and subsequently **4.16**,

the relative integrations of the diastereomeric Mosher's acid CF_3 signals were compared (See Figure 4.3).

For Trifluoromethylhomocysteine:

Following the enzymatic resolution to obtain crude **4.51**, an aliquot of the crude product (1 mg) was suspended in 1:1 H_2O/MeCN (200 µL). To this was added the pentafluorophenyl ester of *R*-Mosher's acid, or the pentafluorophenyl ester of *R/S*-Mosher's acid in excess (4 mg, >2 eq) and triethylamine (2 µL, >3 eq) (accounting for the mass of unreacted *N*-acetyl-*L*-trifluoromethylhomocysteine, the actual mass of unprotected *D*-trifluoromethylhomocysteine was necessarily less than 1 mg). The reaction was stirred at room temperature overnight. Following the reaction, the entire crude mixture was suspected in $CDCl_3$ and analyzed by ^{19}F-NMR. Peaks were observed that corresponded to unreacted starting Mosher's pentafluorophenyl ester, and hydrolyzed Mosher's acid and pentafluorophenol. To elucidate the *ee* of compound **4.51**, and subsequently **4.52**, the relative integrations of the diastereomeric Mosher's acid -CF_3 signals were compared (See Figure 4.5).

4.4.3 – Experimental Procedures for Synthesized Compounds

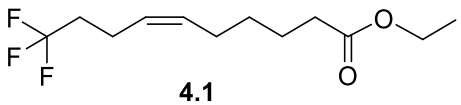

4.1

Ethyl 10,10,10-trifluorodec-6-enoate (4.1). To a 100 mL round-bottom flask was added phosphonium salt **2.12** (1.02 g, 2.1 mmol, 1.0 eq.) and purged with argon gas. Dry THF (50 mL) was added and the mixture was cooled to -78 ^oC in a slurry of dry ice in acetone. Sodium hexamethyldisilazide (1 mol/L in THF, 2.1 mL, 2.1 mmol, 1.0 eq.) was slowly added and the resulting brown solution was stirred for 30 minutes at -78 ^oC. A solution of 4,4,4-

trifluorobutyraldehyde (0.265 g, 2.0 mmol, 1.0 equiv) was dissolved in THF (5 mL) and transferred to the reaction mixture. The solution was allowed to warm to room temperature and was stirred overnight. The reaction was quenched with saturated sodium bicarbonate and the product was extracted with ethyl acetate (2 x 50 mL). The organic layers were combined, dried with sodium sulfate, and concentrated *in vacuo*. The residue was purified by flash chromatography with 95:5 hexane/ethyl acetate, yielding compound **4.1** as a clear oil (0.312 g, 59%). ^{1}H-NMR (300 MHz, $CDCl_3$) δ: 5.43 (1H, dt, J = 10.4, 7.5 Hz), 5.32 (1H, dt, J = 10.9, 6.8 Hz), 4.11 (2H, d, J = 7.1 Hz), 2.31-2.24 (4H, m), 2.14-2.01 (4H, m), 1.59 (2H, app. quint., J = 7.6 Hz), 1.37 (2H, app. quint., J = 7.7 Hz), 1.24 (3H, t, J = 7.1 Hz). ^{13}C-NMR (75 MHz, $CDCl_3$) δ: 173.6, 131.4, 128.7, 126.4, 60.1, 34.2, 33.8, 28.9, 26.7, 24.5, 19.9, 14.2. ^{19}F-NMR (282 MHz, $CDCl_3$) δ: -66.8 (t, J = 10.0 Hz). HRMS (ESI+): *m/z* $[M+H]^+$ calcd for $C_{12}H_{20}F_3O_2$: 253.14099; found 253.14094.

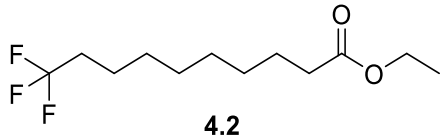

4.2

Ethyl 10,10,10-trifluorodecanoate (4.2). Compound **4.1** (245.5 mg, 0.97 mmol, 1 equiv) was added to a 50 mL round-bottom flask purged with argon. To this was added 10% Pd/C (37 mg) and the flask was re-purged with argon gas. The flask was then flushed with hydrogen gas and allowed to stir overnight at room temperature. The mixture was filtered over celite and the filtrate was concentrated. The hydrogenated product was obtained as a clear oil (239 mg, 96%). ^{1}H-NMR (300 MHz, $CDCl_3$) δ: 4.11 (2H, q, J = 7.1 Hz), 2.28 (2H, t, J = 7.5 Hz), 2.12-1.96 (2H, m), 1.62-1.48 (4H, m), 1.30-1.22 (11H, m). ^{13}C-NMR (75 MHz, $CDCl_3$): δ: 173.6, 127.2, 60.0, 34.1 (2C), 33.5, 28.9 (2C), 28.5, 24.8, 21.7, 14.0. ^{19}F-NMR (282 MHz, $CDCl_3$) δ: -66.7

(t, J = 10.9 Hz). HRMS (ESI+): *m/z* $[M+H]^+$ calcd for $C_{12}H_{22}F_3O_2$: 255.15664, found 255.15646.

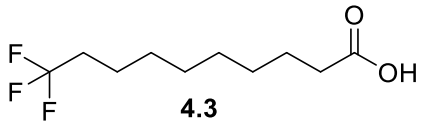

4.3

10,10,10-Trifluorodecanoic acid (4.3). Compound **4.2** (168 mg, 0.66 mmol) was dissolved in a 1:1 solution of methanol and 0.6 M NaOH (8 mL), and reaction completion was monitored by TLC. After 3 h, the reaction was acidified with 1 M HCl and the product was extracted with ethyl acetate twice. The organic layers were dried and evaporated yielding compound **4.3** as a beige solid (118 mg, 79%). ^{1}H-NMR (300 MHz, $CDCl_3$) δ: 11.26 (1H, br. s), 2.34 (2H, t, J = 7.1 Hz), 2.12-1.96 (2H, m), 1.65-1.48 (4H, m), 1.31-1.24 (8H, m). ^{13}C-NMR (75 MHz, $CDCl_3$) δ: 180.6, 127.2, 34.0, 33.6, 28.90, 28.86, 28.6, 24.5, 21.8. ^{19}F-NMR (282 MHz, $CDCl_3$) δ: -66.7 (t, J = 10.6 Hz). HRMS (ESI+): *m/z* $[M+H]^+$ calcd for $C_{10}H_{18}F_3O_2$: 225.10969, found 225.10992.

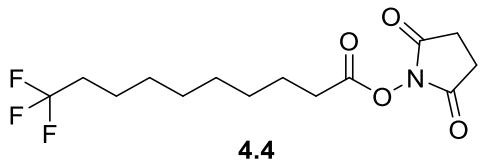

4.4

2,5-Dioxopyrrolidin-1-yl 10,10,10-trifluorodecanoate (4.4). Compound **4.3** (112.9 mg, 0.499 mmol, 1 equiv) was added to a 50 mL round-bottom flask. To this was added a solution of *N*-hydroxysuccinimide (NHS; 96 mg, 0.834 mmol, 1.67 equiv) in dry DCM (8 mL) until dissolution. The reaction as cooled to 0 ^{o}C in an ice bath. To the chilled stirring solution was added 1-ethyl-3-(3-dimethylaminopropyl)carbodiimide (EDC; 114 mg, 0.734 mmol, 1.47 equiv) and DMAP (6 mg, 0.050 mmol, 0.1 equiv). The solution was stirred at 0 ^{o}C for 1 h,

after which the ice-bath was removed and the mixture stirred for an additional 20 h as monitored by TLC. Following the reaction time, the mixture was diluted with EtOAc (15 mL). The organic phase was washed with 0.1 M HCl (aq) (1 x 15 mL), then washed with sat. $NaHCO_3$ (1 x 15 mL), and finally washed with brine (1 x 15 mL). The organic phase was dried of Na_2SO_4 and further purified by column chromatography with a mobile phase of 1:1 EtOAc-hexane, to yield the desired product as a white solid (132.6 mg, 82%). ^{1}H-NMR (300 MHz, $CDCl_3$) δ: 2.82 (4H, s), 2.59 (2H, d, J = 7.3 Hz), 2.12-1.95 (2H, m), 1.73 (2H, app. quint, J = 7.2 Hz), 1.52-1.23 (10 H, m). ^{13}C- NMR (75 MHz, $CDCl_3$) δ: 169.2, 168.6, 127.2, 33.4, 30.8, 28.74, 28.65, 28.46, 28.41, 25.5, 24.4, 21.7. ^{19}F-NMR (282 MHz, $CDCl_3$) δ: -66.7 (t, J = 10.6 Hz). HRMS (ESI+): *m/z* $[M+H]^+$ calcd for $C_{14}H_{21}F_3NO_4$: 324.14172, found 324.14168.

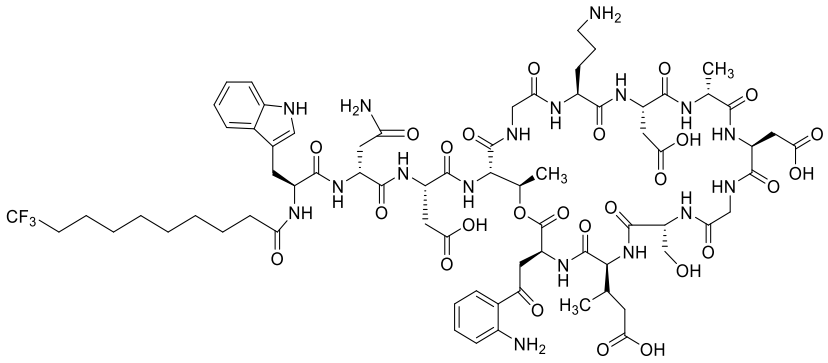

4.5

10,10,10-Trifluorodecanoyl-daptomycin (4.5). To a 7 mL glass vial was added Boc-Deacyl-Dap (10 mg, 6.4 µmol, 1 equiv). The vial was equipped with a stir bar, and dry DMF (200 µL) was added. To this was added triethylamine (9 µL, 0.065 mmol, 10 equiv) and compound **4.4** (3.1 mg, 9.6 µmol, 1.5 equiv) and the suspension was stirred for 72 h. The reaction was concentrated on a high-vacuum rotary evaporator and redissolved in water followed by lyophilization. Then, the crude product was stirred in a solution of TFA (1 mL) containing thioanisole (2% v/v) for 25 minutes in an ice-bath. The solution was concentrated *in vacuo*,

and the residue redissolved in dry DMF, with the solvent being removed once more. The oily residue was dissolved in water and lyophilized before purification by preparative HPLC using a Clipeus C18 10 µm column employing an isocratic gradient of 63% H_2O (0.1 % TFA) to 37% acetonitrile. Fractions containing the desired compound were pooled and concentrated, suspended in water and lyophilized to obtain the desired product as a white powder (2.7 mg, 25%), judged to be >95% pure by RP-HPLC (Figure B.16 in Appendix B). HRMS (ESI+): *m/z* $[M+H]^+$ calcd for $C_{72}H_{98}F_3N_{17}O_{26}$: 1674.68938, found 1674.69360; *m/z* $[M+2H]^{2+}$ calcd for $C_{72}H_{100}FN_{17}O_{26}$: 837.84833, found 837.84793 (Figure C.16 in Appendix C).

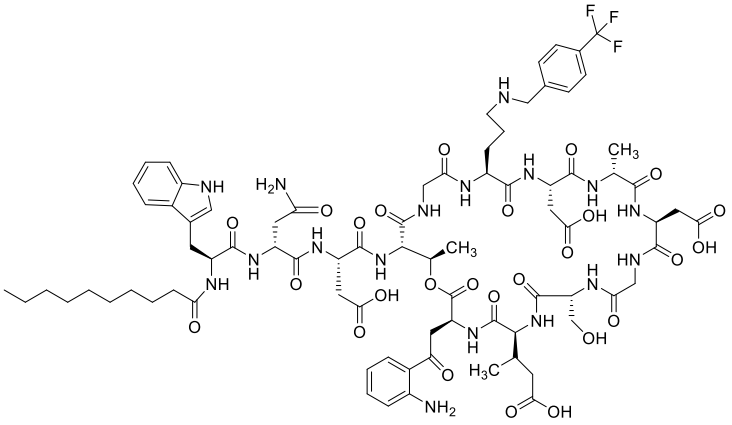

4.6

Dap-Orn(^{TFM}Benzyl)6 (**4.6**): Daptomycin (50 mg, 0.031 mmole, 1.0 equiv) was added to DMF (1 mL) in a scintered-glass vial equipped with a stirbar. To the stirring suspension was added *p*-trifluoromethylbenzaldehyde (**4.10**, 10.7 mg, 0.062 mmole, 2.0 equiv) and sodium-triacetoxyborohydride (STAB-H, 13.1 mg, 0.062 mmole, 2.0 equiv). Glacial acetic acid (1.7 µL, 0.031 mmole, 1.0 equiv) was added. The reaction was stirred at room temperature for 72 h, after which the solution was removed *in vacuo*. The residue was dissolved in water and lyophilized before purification by preparative HPLC using a Clipeus C18 10 µm column employing an isocratic gradient of 59% H_2O (0.1 % TFA) / 41% acetonitrile to 51% H_2O (0.1

% TFA) / 49% acetonitrile over 40 min. Fractions containing the desired compound were pooled and concentrated, suspended in water and lyophilized to obtain the desired product as a slightly yellow powder (28.2 mg, 51%), judged to be >95% pure by RP-HPLC (Figure B.17 in Appendix B). HRMS (ESI+): *m/z* $[M+2H]^+$ calcd for $C_{80}H_{108}F_3N_{17}O_{26}$: 889.87963, found 889.87801 (Figure C.17 in Appendix C).

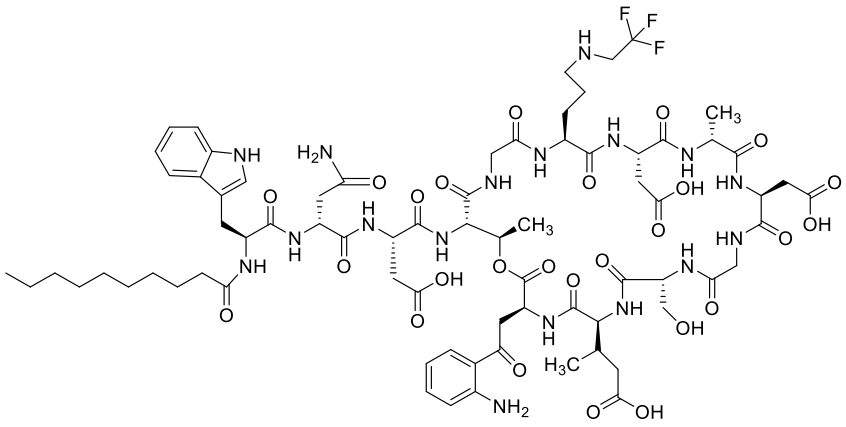

4.7

Dap-Orn(^{TF}ethyl)6 (4.7). Daptomycin (50 mg, 0.031 mmol, 1 equiv) was suspended in DMF (1 mL) in a scintered glass vial equipped with a stir bar. To this was added ethyl trifluoroacetalydehyde hemiacetal (9.9 µL, 0.062 mmol, 2 equiv) and STAB-H (13.1 mg, 0.062 mmole, 2 equiv). Glacial acetic acid (1.7 µL, 0.031 mmol, 1 equiv) was added, the reaction allowed to stir at room temperature for 72 h. To increase the completion of the reaction, further aliqouts of STAB-H (1 equiv) and ethyl-trifluoroacetaldehyde hemiacetal (1 equiv) were added but as determined by analytical HPLC, the reaction ceased after 50% completion. The solvent was removed by rotary evaporation, and the peptide was resuspended in H_2O and concentrated to dryness once more. The crude product was redissolved in H_2O, frozen, and lyophilized. The crude product was purified by preparative HPLC using a Clipeus C18 10 µm column employing a linear gradient of 59 % H_2O (0.1 % TFA) / 41% acetonitrile to 52 % H_2O (0.1 %

TFA) / 48 % acetonitrile over 40 min. Fractions containing the desired compound were pooled and concentrated, suspended in water and lyophilized to obtain the desired product as a white powder (18.4 mg, 35%), judged to be >95% pure by RP-HPLC (Figure B.18 in Appendix B). HRMS (ESI+): *m/z* $[M+2H]^{2+}$ calcd for $C_{74}H_{104}F_3N_{17}O_{26}$: 851.86398, found 851.86551 (Figure C.18 in Appendix C).

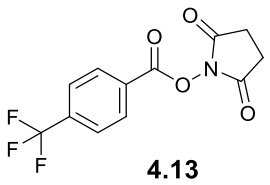

4.13

2,5-Dioxopyrrolidin-1-yl 4-(trifluoromethyl)benzoate (**4.13**). Compound **4.13** was synthesized modified from a procedure developed by Rubin et al.[171] To a 25-mL round-bottom flask was added 4-(trifluoromethyl)benzoic acid (**4.12**, 200 mg, 1.05 mmol, 1.0 equiv), *N*-hydroxysuccinimide (202 mg, 1.76 mmol, 1.67 equiv), and DCM (6 mL). To the vigorously stirred solution was added EDC (296 mg, 1.55 mmol, 1.5 equiv) and DMAP (12.8 mg, 0.11 mmole, 0.1 equiv). The suspension was stirred at room temperature overnight. Following the reaction time, the mixture was diluted with EtOAc (15 mL). The organic phase was washed with 0.1 M HCl (aq) (1 x 15 mL), then washed with Sat. $NaHCO_3$ (1 x 15 mL), and finally washed with brine (1 x 15 mL). The organic phase was dried of Na_2SO_4 and further purified by column chromatography with a mobile phase of 1:1 EtOAc-hexane, to yield the desired product as a white solid (280 mg, 93%). ^{1}H-NMR (300 MHz, $CDCl_3$) δ: 8.26 (2H, d, J = 7.8 Hz), 7.79 (2H, d, J = 8.0 Hz), 2.92 (4H, s). ^{19}F-NMR (282 MHz, $CDCl_3$) δ: -63.7 (s). ^{13}C-NMR (75 MHz, $CDCl_3$) δ: 171.8, 163.8, 139.0, 133.9, 131.4, 128.8, 126.1, 28.5. HRMS (ESI+): *m/z* $[M+H^+]^+$ calcd for $C_{12}H_9F_3NO_4$: 288.04782; found: 288.04906.

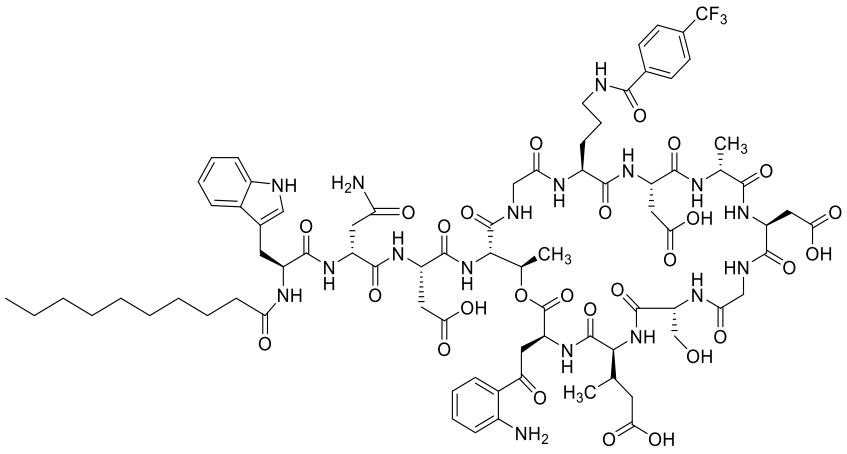

4.8

Dap-Orn(^{TFM}Benzoyl)^{6} (4.8). Native daptomycin (50 mg, 0.031 mmol, 1 equiv) was added to a 7-mL scintillation vial containing dry DMF (1 mL). To this was added compound **4.13** (13.3 mg, 0.046 mmol, 1.5 equiv), and triethylamine (43 µL, 0.31 mmol, 10 equiv) and the reaction mixture was allowed to stir for 48 h at room temperature, after which the reaction progress was confirmed complete by HPLC. Following the reaction, the mixture was dissolved in 50 mL of Milli-Q water and concentrated. This process was repeated leaving an oily residue, which was suspended in water, and subsequently frozen and lyophilized to yield crude **4.8** as a yellow powder. The crude product was purified by preparative HPLC using a Clipeus C18 10 µm column employing a linear gradient of 60 % H_2O (0.1 % TFA) / 40% acetonitrile to 50 % H_2O (0.1 % TFA) / 50% acetonitrile over 40 min. Fractions containing the desired compound were pooled and concentrated, suspended in water and lyophilized to obtain the desired product as a white powder (30.5 mg, 55%), judged to be >95% pure by RP-HPLC (Figure B.19 in Appendix B). HRMS (ESI+): *m/z* $[M+2H]^{2+}$ calcd for $C_{80}H_{106}F_3N_{17}O_{27}$: 896.86296, found 896.87057 (Figure C.19 in Appendix C).

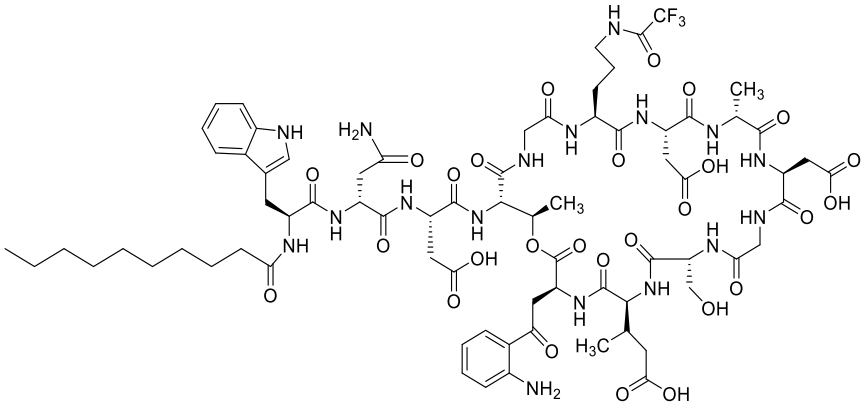

4.9

Dap-Orn(^{TF}**acetyl)6** (**4.9**). Native daptomycin (25 mg, 0.015 mmol, 1 equiv) was added to a 7-mL scintillation vial equipped with a stir bar, followed by the addition of DMF (1 mL). To this was added DIPEA (3.9 µL, 0.039 mmol, 2.5 equiv), and ethyl trifluoroacetate (2.6 µL, 0.02 mmol, 1.4 equiv). The mixture was stirred for 16 h at room temperature and the reaction completion monitored by HPLC. The solvent was removed by rotary evaporation, and the peptide was resuspended in H_2O and concentrated to dryness once more. The crude product was redissolved in H_2O, frozen, and lyophilized. The crude product was purified by preparative HPLC using a Clipeus C18 10 µm column employing a linear gradient of 60 % H_2O (0.1 % TFA) / 40% acetonitrile to 52 % H_2O (0.1 % TFA) / 48 % acetonitrile over 40 min. Fractions containing the desired compound were pooled and concentrated, suspended in water and lyophilized to obtain the desired product as a white powder (11.9 mg, 45%), judged to be >95% pure by RP-HPLC (Figure B.20 in Appendix B). HRMS (ESI+): *m/z* $[M+2H]^{2+}$ calcd for $C_{74}H_{102}F_3N_{17}O_{27}$: 858.85361, found 858.85537 (Figure C.20 in Appendix C)

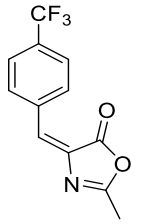

4.18

(*E*)-2-Methyl-4-(4-(trifluoromethyl)benzylidene)oxazol-5(4H)-one (**4.18**). To a round-bottom flask was added *p*-trifluoromethylbenzaldehyde (1.5 mL, 3.66 mmol, 1 equiv), acetic anhydride (1.72 mL, 18.3 mmol, 5.0 equiv), *N*-acetylglycine (557 mg, 4.76 mmol, 1.3 equiv), and sodium acetate (395 mg, 4.76 mmol, 1.3 equiv). The solution was stirred at reflux under argon for 1 h. Following the reaction time, the reaction was quenched with the addition of ice (10 g), and the reaction further stirred for 1h. The precipitous product was filtered and the obtained as a yellow solid (818 mg, 93%). Characterization data matched literature data.[172] ^{1}H-NMR (300 MHz, $CDCl_3$) δ: 8.18 (2H, d, J = 8.2 Hz), 7.68 (2H, d, J = 8.3 Hz), 7.13 (1H, s), 2.43 (3H, s). ^{19}F-NMR (282 MHz, $CDCl_3$) δ: -63.3 (s).

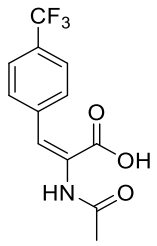

4.21

(*E*)-2-Acetamido-3-(4-(trifluoromethyl)phenyl)acrylic acid (**4.21**). Compound **4.18** (800 mg, 3.13 mmole) was added to reagent grade acetone (20 mL) and water (20 mL) in a round-bottom flask and heated to reflux for 12 h. Following the reaction, the reaction mixture was acidified with 1M HCl, and the product extracted with ethyl acetate (3 x mL). The organic phases were dried over sodium sulfate and concentrated, leaving the product as a yellow

residue without future purification (821 mg, 96%). Characterization data matched the literature.[173] ^{1}H-NMR (300 MHz, DMSO-d_6) δ: 9.53 (1H, s), 7.71 (4H, app. s), 7.17 (1H, s) 1.95 (3H, s). ^{19}F-NMR (282 MHz, DMSO-d_6) δ: -61.4 (s).

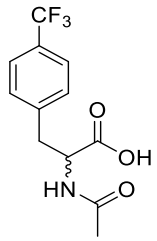

4.19

2-Acetamido-3-(4-(trifluoromethyl)phenyl)propanoic acid (**4.19**). Compound **4.21** (750 mg, 2.75 mmole, 1 equiv) was dissolved in methanol, and 10% Pd/C (90 mg, 0.08 mmole, 0.03 equiv) was added. The reaction vessel was purged with hydrogen gas and equipped with a hydrogen balloon, and the reaction stirred overnight. The reaction was filtered over celite and solvents removed *in vacuo* to yield target product **4.19** as a yellow solid (726 mg, 96%). Characterization data matched the literature.[153] ^{1}H-NMR (300 MHz, DMSO-d_6) δ: 8.19 (1H, d, J = 8.2 Hz), 7.62 (2H, d, J = 8.2 Hz), 7.42 (2H, d, J = 8.1 Hz), 4.42 (1H, m), 3.11 (1H, dd, J = 13.6 Hz, J = 4.7 Hz), 2.91 (2H, dd, J = 13.2 Hz, J = 9.5 Hz), 1.75 (3H, s). ^{19}F-NMR (282 MHz, DMSO-d_6) δ: -61.0 (s).

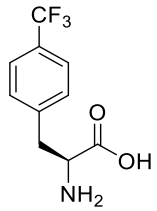

4.20

(*S*)-2-Amino-3-(4-(trifluoromethyl)phenyl)propanoic acid (**4.20**). To Compound **4.19** (700 mg, 2.54 mmole, 1 equiv) in water (20 mL) was added Acylase 1 from *Aspergillus niger* (1

mg). The reaction mixture was brought to 42 °C and adjusted to pH 7.5 with $NaHCO_3$ (aq). Over the course of two weeks, the pH was manually readjusted to 7.5 with $NaHCO_3$ (aq), and fresh enzyme continually added. After 2 weeks, the reaction appeared 50% complete by analytical RP-HPLC. The mixture was made acidic through the addition of 1 M HCl, and the solution washed with ethyl acetate to remove the unreacted *D*-enantiomer starting material. The aqueous phase was neutralized with $NaHCO_3$, and the aqueous phase concentrated by high-vacuum rotary evaporation. The residue was resuspended in 9:1 H_2O/MeCN and purified by RP-HPLC employing a linear gradient of 90 % H_2O (0.1 % TFA) / 10% acetonitrile to 10 % H_2O (0.1 % TFA) / 90 % acetonitrile over 50 min. The desired amino acid was obtained as a white powder (41.4 mg, 7%). Characterization data matched the literature.[155] ^{1}H-NMR (300 MHz, D_2O) δ: 7.62 (2H, d, J = 8.1 Hz), 7.38 (2H, d, J = 8.0 Hz), 4.23 (1H, app. t, J = 6.7 Hz), 3.31 (1H, dd, J = 14.6 Hz, J = 5.9 Hz), 3.19 (1H, dd, J = 14.6 Hz, J = 7.5 Hz).

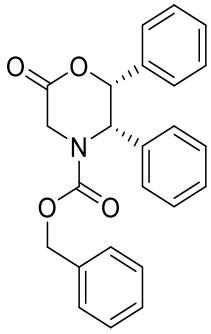

4.24

Benzyl (2*R*,3*S*)-6-oxo-2,3-diphenylmorpholine-4-carboxylate (**4.24**). Williams' lactone was synthesized according to a modified procedure from Dastlik et al.[159] Dry THF (22 mL) was added to (1*R*,2*S*)-2-amino-1,2-diphenylethanol (2.12 g, 10 mmol, 1 equiv) and stirred to form a suspension under argon. To this was added NEt_3 (2.2 mL, 15.5 mmol, 1.55 equiv), followed by the dropwise addition of ethyl bromooacetate (1.65 mL, 15.5 mmol, 1.55 equiv) over 1 h.

After the addition of ethyl chloroacetate, the mixture was stirred for an additional hour at room temperature, before being cooled to 0 ºC and filtered. The precipitate was rinsed with chilled THF and the filtrates were evaporated to dryness to yield a white solid. This was diluted with DCM (25 mL) and saturated $NaHCO_3$ (25 mL) and cooled on ice. Benzyl chloroformate (1.66 mL, 11 mmol, 1.1 equiv) was added to the vigorously stirred solution over 1 h, after which the mixture stirred for an additional 1 h. The two layers were separated by liquid-liquid extraction, and the aqueous layer was extracted with DCM. Combined organic layers were dried with sodium sulfate and evaporated to dryness. The residue was dissolved in toluene (22 mL) and *p*-TsOH·H_2O (190 mg, 1.0 mmol, 0.1 equiv) was added. The solution was concentrated to approximately half the initial volume and then cooled to room temperature. The crystals were collected by suction filtration and rinsed with toluene and hexane. Then, the product was further purified by flash chromatography with 20% EtOAc in hexane, affording Compound **4.24** as a white solid (2.97 g, 76%). ^{1}H-NMR (500 MHz, DMSO-d_6, 120 ºC) δ: 7.35-7.10 (13H, m), 6.74 (1H, s), 6.72 (1H, s), 6.23 (1H, s), 5.33 (1H, s), 5.12 (1H, d, J = 7.6 Hz), 5.07 (1H, d, J = 7.6 Hz), 4.66 (1H, d, J = 10.7 Hz), 4.60 (1H, d, J = 10.6 Hz). ^{13}C-NMR (123.3 MHz, DMSO-d_6, 120 ºC) δ: 166.4, 153.1, 135.7, 135.5, 134.1, 127.52, 127.46, 127.3, 127.0, 126.8, 126.6, 125.6, 78.9, 66.3, 59.0, 53.9, 44.8.

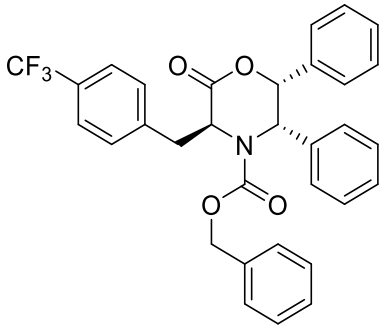

4.26

Benzyl (3*S*,5*S*,6*R*)-2-oxo-5,6-diphenyl-3-(4-(trifluoromethyl)benzyl)morpholine-4-carboxylate (**4.26**). Compound **4.24** (1.03 g, 2.66 mmole, 1 equiv) was dissolved in anhydrous THF (50 mL) and cooled to -78 ^{o}C in an acetone-dry ice bath under argon. To the stirring solution was added dropwise a solution of NaHMDS in THF (1 M, 2.66 mL, 2.66 mmole 1 equiv) dropwise and the reaction allowed to stir at -78 ^{o}C for 30 minutes. Then, *p*-trifluoromethylbenzyl bromide (**4.25**, 700 mg, 2.93 mmole, 1.1 equiv) as a solution in anhydrous THF (20 mL) was added dropwise, and the stirring suspension allowed to warm slowly to room temperature, followed by additional overnight stirring. Ethyl acetate (20 mL) was added followed by sat. $NaHCO_3$ (aq) (30 mL) to quench the reaction. The mixture was transferred to a separatory funnel and the layers separated. The aqueous phase was washed with ethyl acetate (3 x 50 mL), and the organic phase was dried over sodium sulfate and concentrated. The residue was then purified by column chromatography with 9:1 hexane/EtOAc. Purified fractions were pooled and concentrated yielding compound **4.26** as a white solid (785 mg, 54%). ^{1}H-NMR (500 MHz, DMSO-d_6, 120 ^{o}C) δ: 7.67 (2H, d, J = 7.6 Hz), 7.53 (2H, d), 7.30-7.15 (7H, m), 7.10 (2H, t, J = 7.6 Hz), 6.98 (2H, d, J = 7.1 Hz), 6.61 (2H, d, J = 7.5 Hz), 5.88 (1H, s), 5.29 (1H, d, J = 3.1 Hz), 5.16 (1H, dd, J = 8.6, 4.6 Hz), 5.03 (2H, s), 3.61 (1H, dd, J = 13.8, 8.7 Hz), 3.53 (1H, dd, J = 13.9, 4.5 Hz). ^{13}C-NMR (125.8 MHz, DMSO-d_6, 120 ^{o}C) δ: 166.7, 140.7, 135.4, 133.9, 129.6, 127.5, 127.1, 126.9, 126.8, 126.7, 125.7, 124.5, 77.6, 66.5, 59.5, 57.9. ^{19}F-NMR (470.6 MHz, DMSO-d_6, 120 ^{o}C) δ: -61.4. HRMS (ESI+): *m/z* $[M+H]^+$ calcd for $C_{32}H_{27}F_3NO_4$: 546.1887, found 546.1862.

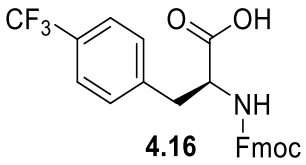

4.16

(*S*)-2-((((9H-Fluoren-9-yl)methoxy)carbonyl)amino)-3-(4-(trifluoromethyl)phenyl)propanoic acid (**4.16**). Compound **4.26** (751 mg, 1.37 mmole, 1 equiv) was dissolved in ethanol and $PdCl_2$ (7.3 mg, 0.041 mmole, 0.03 equiv) was added. The reaction vessel was purged with hydrogen gas, and equipped with a hydrogen balloon, followed by overnight stirring. The following day, the mixture was filtered over celite and the solvents removed to obtain a residue which was immediately resuspended in 1,4-dioxane (30 mL) and sat. $NaHCO_3$ (aq) (30 mL). To this mixture was added Fmoc-OSu (462 mg, 1.37 mmole, 1 equiv) and the mixture allowed to stir at room temperature overnight. The mixture was acidified with 1 M HCl (aq) to pH 1 and the desired product extracted to ethyl acetate (3 x 25 mL). The organic phase was dried over Na_2SO_4 and the solvent removed by rotary evaporation. The residue was then subjected to column chromatography with 9:1 hexane/EtOAc + 0.5% acetic acid. The purified compound was then dissolved in toluene to azeotropically remove trace acetic acid, yielding the desired compound as a white solid (420 mg, 67%). The *ee* of **4.16** was determined to be 97%, as described in section 4.4.2. Characterization data agreed with the literature.[152] ^{1}H-NMR (300 MHz, MeOD-d_3) δ: 7.75 (2H, d, J = 7.4 Hz), 7.58-7.49 (4H, m), 7.41-7.32 (4H, m), 7.25 (2H, t, J = 6.33 Hz), 4.45-4.10 (4H, m), 3.29 (1H, m), 3.05-2.95 (1H, m). ^{13}C-NMR (75 MHz, MeOD-d_3) δ: 159.8, 146.6, 145.0, 44.0, 132.5, 131.4, 130.2, 129.6, 127.7, 122.4, 69.4, 49.7, 39.7. ^{19}F-NMR (282 MHz, MeOD-d_3) δ: -64.1. HRMS (ESI+): *m/z* $[M+H]^+$ calcd for $C_{25}H_{21}F_3NO_4$: 456.14172, found 456.14237.

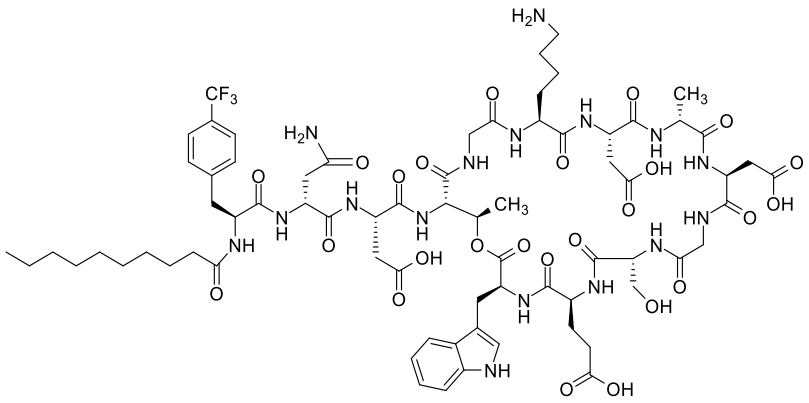

4.15

Dap-^{TFM}Phe1-Lys6-Glu12-Trp13 (**4.15**). 2-ClTrt-Cl-PG resin (theoretical substitution = 1.5 mmol/g, 66.7 mg, 0.1 mmol, 1 equiv) was activated in dry DCM with thionyl chloride (26 µL, 3.6 equiv) and pyridine (58 µL, 7.2 equiv) under reflux for 2 h. The resin was transferred to a disposable peptide cartridge and rinsed 6 x with dry DCM, followed by loading with FmocAsp(OH)GlyOallyl (**3.8**, 4 equiv) and DIPEA (8 equiv) in dry DCM. The resin was capped with 17:2:1 DCM/MeOH/DIPEA (3 x 10 min) and the loading efficiency determined to be 1.21 mmol/g. Removal of the Fmoc groups were performed with 20% 4-MP in DMF (v/v, 1 x 5 min, 1 x 20 min) before the formation of the depsi bond, and 20% 2-MP in DMF (v/v, 3 x 10 min) after the formation of the depsi bond). All Fmoc-amino acids including **4.16** (4 equiv) and the lipid tail (4 equiv) were activated for 5 min using HOBt (4 equiv) and DIC (4 equiv) in DMF (2 mL) and then coupled for 4 h. Following installation of the decanoyl tail, the depsi-bond formation was achieved FmocTrp(Boc)OH (10 equiv) with DIC (10 equiv) and DMAP (0.1 equiv). Residues 12 and 11 were introduced using standard coupling procedures. Deprotection of the allyl group was achieved with $Pd(PPh_3)_4$ (0.2 equiv) and DMBA (10 equiv) in 3:1 DCM/DMF for 1 h. On-resin cyclization was afforded by treating the peptide to PyAOP (5 equiv), HOAt (5 equiv) and 2,4,6-collidine (10 equiv), and the peptide was cleaved with 95:2.5:2.5 TFA/TIPS/H_2O. The deprotection cocktail was removed under an N_2 stream, and

the peptide resuspended in 4:1 H_2O/MeCN (v/v). The crude product was purified by preparative HPLC using a Clipeus C18 10 µm column employing a linear gradient of 58 % H_2O (0.1 % TFA) / 42% acetonitrile to 51 % H_2O (0.1 % TFA) / 49 % acetonitrile over 40 minutes. Fractions containing the desired compound were pooled and concentrated, suspended in water and lyophilized to obtain the desired product as a white powder (15 mg, 10% based on resin loading), judged to be >95% pure by RP-HPLC (Figure B.21 in Appendix B). HRMS (ESI+): *m/z* $[M+2H]^{2+}$ calcd for $C_{72}H_{99}F_3N_{16}O_{25}$: 823.35324, found 823.35421 (Figure C.21 in Appendix C).

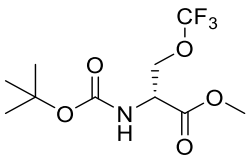

4.33

Methyl *N*-(*tert*-butoxycarbonyl)-*O*-(trifluoromethyl)-*D*-serinate (**4.33**). Compound **4.33** was obtained according to the procedure by Liu et al., performed in a N_2 box at room temperature.[160] To a round-bottomed flask containing anhydrous ethyl acetate (10 mL) equipped with a stirbar was added Boc-*D*-SerOMe (0.439 g, 2.0 mmole, 1 equiv), AgOTf (1.54 g, 6.0 mole, 3 equiv), Selectfluor™ (1.06 g, 3.0 mmole, 1.5 equiv), KF (0.465 g, 8.0 mmole, 4 equiv), 2-fluoropyridine (0.516 mL, 6.0 mmole, 3.0 equiv), and trifluoromethyl trimethylsilane (0.886 mL, 6.0 mmole, 3.0 equiv). The reaction was stirred overnight at room temperature, after which the vessel was removed from the N_2 box. The reaction was filtered through a plug of silica, eluted with ethyl acetate, and concentrated, and the product purified by column chromatography with (9:1 hexane/EtOAc, yielding the desired product as a clear oil (201 mg, 35% yield). ^{1}H-NMR (300 MHz, $CDCl_3$) δ: 5.34 (1H, d, J = 7.2 Hz), 4.55 (1H, app. d, J = 7.8 Hz), 4.36 (1H, dd, J = 10.0, 2.4 Hz), 4.23 (1H, dd, J = 9.9, 2.9 Hz), 3.80 (3H, s), 1.45 (9H, s).

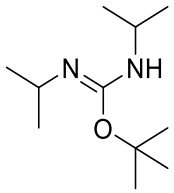

4.58

***tert*-Butyl *N,N'*-diisopropylcarbamimidate (4.58)**. To a flame-dried purged flask equipped with a stir-bar was added *tert*-butanol (4.9 mL, 51.6 mmol, 1.3 equiv) and *N,N'*-diisopropylcarbodiimide (6.13 mL, 39.6 mmol, 1.0 equiv). To this was added copper (I) chloride (75 mg, 0.76 mmol, 0.02 equiv) and the reaction vessel was sealed. The reaction was stirred at room temperature for 20 h, after which the reaction progress was monitored by ^{1}H-NMR to reveal no remaining diisopropylcarbodiimide. The vessel was concentrated *in vacuo* to remove any remaining *tert*-butanol and subsequently distilled over reduced pressure to obtain the purified product as a clear oil (5.28 g, 66.5%, mixture of *E/Z* isomers). Compound **4.58** was stored in a freezer until use. ^{1}H-NMR (300 MHz, $CDCl_3$) δ: 3.73-3.59 (1H, m), 3.24-3.08 (1H, m), 1.48-1.34 (9H, m), 1.10-1.01 (12H, m).

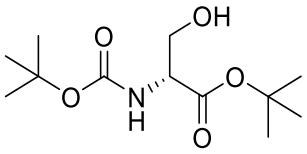

4.32

***tert*-Butyl (*tert*-butoxycarbonyl)-*D*-serinate (4.32).** To a solution of Boc-*D*-serine (1.25 g, 6.1 mmole, 1 equiv) in THF (20 mL) was added compound **4.58** (1.83 g, 9.1 mmole, 1.5 equiv). The mixture was refluxed for 2.5 h after which a second addition of compound **4.58** occurred (1.83 g, 9.1 mmole, 1.5 equiv). The reaction was stirred at reflux overnight. The mixture was cooled to room temperature, filtered to remove the diisopropylurea by-product, and

concentrated *in vacuo*. The crude product was then purified by flash chromatography employing a gradient of 1:1 hexane/ethyl acetate, yielding the desired compound **4.32** as a clear oil (1.02 g, 51%). Characterization data matched with the literature.[174] ^{1}H-NMR (300 MHz, $CDCl_3$) δ: 5.40 (1H, br. s), 4.23 (1H, br. s), 3.88 (2H, br. s), 2.35 (1H, br. s), 1.47 (9H, s), 1.44 (9H, s). ^{13}C-NMR (75 MHz, $CDCl_3$): δ: 169.9, 155., 82.3, 79.9,77.5, 77.1, 76.6, 63.7, 56.3, 28.3, 27.9. HRMS (ESI+): *m/z* $[M+H]^+$ calcd for $C_{12}H_{24}NO_5$: 262.16490, found 262.16492.

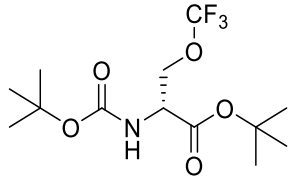

4.34

***tert*-Butyl *N*-(*tert*-butoxycarbonyl)-*O*-(trifluoromethyl)-*D*-serinate** (**4.34**). Compound **4.34** was obtained according to the procedure by Liu et al., performed in a N_2 box at room temperature.[160] To a round-bottomed flask containing anhydrous ethyl acetate (30 mL) equipped with a stirbar was added **4.32** (2.26 g, 8.7 mmole, 1 equiv), AgOTf (6.67 g, 26.0 mole, 3 equiv), Selectfluor^{TM} (4.60 g, 13.0 mmole, 1.5 equiv), KF (2.01 g, 34.6 mmole, 4 equiv), 2-fluoropyridine (2.24 mL, 26.0 mmole, 3.0 equiv), and trifluoromethyl trimethylsilane (3.84 mL, 26.0 mmole, 3.0 equiv). The reaction was stirred overnight at room temperature, after which the vessel was removed from the N_2 box. The reaction was filtered through a plug of silica, eluted with ethyl acetate, and concentrated, and the product purified by column chromatography with (9:1 hexane/EtOAc, yielding the desired product as a clear oil (1.45 g, 51% yield). ^{1}H-NMR (300 MHz, $CDCl_3$) δ: 5.33 (1H, br. s), 4.39 (1H, m), 4.32 (1H, d, J = 9.5 Hz), 4.19 (1H, d, J = 9.2 Hz), 1.45 (9H, s), 1.43 (9H, s). ^{13}C-NMR (75 MHz, $CDCl_3$): δ: 167.5,

155.1, 121.4, 83.3, 80.3, 67.5, 53.2, 28.2, 27.8. ^{19}F-NMR (282 MHz, $CDCl_3$) δ: -61.5 (s). HRMS (ESI+): *m/z* $[M+H]^+$ calcd for $C_{13}H_{23}F_3NO_5$; 330.15228, found 330.15231.

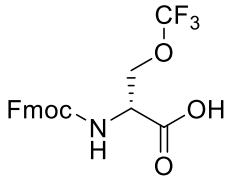

4.36

***N*-(((9H-Fluoren-9-yl)methoxy)carbonyl)-*O*-(trifluoromethyl)-*D*-serine** (**4.36**). Compound **4.34** (600 mg, 1.8 mmole, 1 equiv) was suspended in TFA (30 mL) and stirred for 4 h at room temperature. The reaction completion was monitored by ^{1}H-NMR spectroscopy, and following the reaction, the solvent was removed by rotary evaporation. The residue was resuspended in 1,4-dioxane (20 mL) and sat. $NaHCO_3$ (aq) (20 mL), followed by the addition of Fmoc-OSu (614 mg, 1.8 mmole, 1 equiv). The reaction was stirred at room temperature overnight after which the reaction mixture was acidified to pH = 1 with 1 M HCl. The reaction mixture was extracted with ethyl acetate (3 x 30 mL), and the organic layer was dried over Na_2SO_4 and concentrated. The residue was then purified by column chromatography employing a slow gradient of DCM to 5% MeOH in DCM, yielding the desired product as a white solid (453 mg, 63% over two steps). ^{1}H-NMR (300 MHz, MeOD-d_3) δ: 7.70 (2H, d, J = 7.4 Hz), 7.60 (2H, d, J = 7.1 Hz), 7.32 (2H, t, J = 7.3 Hz), 7.24 (2H, t, J = 7.4 Hz), 4.57 (1H, t, J = 4.1 Hz), 4.45-4.25 (4H, m), 4.14 (1H, t, J = 7.0 Hz). ^{13}C-NMR (75 MHz, MeOD-d_3): δ:170.2, 157.0, 143.8, 141.1, 127.4, 126.8, 124.9, 121.6, 119.5, 66.9, 53.1, 48.5, 46.9. ^{19}F-NMR (282 MHz, MeOD-d_3) δ: -62.5 (s). HRMS (ESI+): *m/z* $[M+H]^+$ calcd for $C_{19}H_{17}F_3NO_5$; 396.10533, found 396.10530.

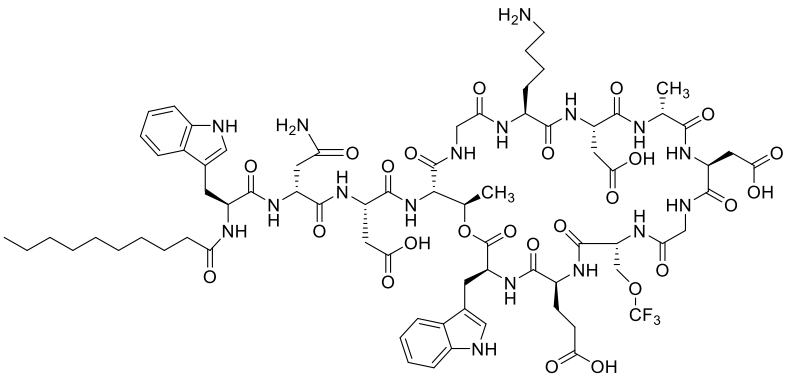

4.38

Dap-Lys6-*D*-Ser(CF$_3$)11-Glu12-Trp13 (**4.38**). Peptide **4.38** was synthesized in the same manner as **4.15**, except that FmocTrp(Boc)OH was used instead of amino acid **4.16**, and Fmoc-*D*-Ser(CF$_3$)OH was used instead of Fmoc-*D*-SerOH. The crude product was purified by preparative HPLC using a Clipeus C18 10 µm column employing a linear gradient of 60 % H_2O (0.1 % TFA) / 40% acetonitrile to 56 % H_2O (0.1 % TFA) / 44 % acetonitrile over 40 min. Fractions containing the desired compound were pooled and concentrated, suspended in water and lyophilized to obtain the desired product as a white powder (5.7 mg, 4% based on resin loading), judged to be >95% pure by RP-HPLC (Figure B.22 in Appendix B). HRMS (ESI+): *m/z* $[M+2H]^{2+}$ calcd for $C_{74}H_{102}F_3N_{17}O_{25}$: 842.85869, found 842.86197 (Figure C.22 in Appendix C).

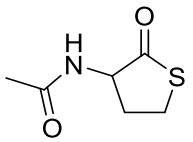

4.46

(±)-*N*-(2-Oxotetrahydrothiophen-3-yl)acetamide (4.46). To reagent-grade acetone (50 mL) was added *DL*-homocysteine thiolactone hydrochloride (1.0 g, 6.51 mmol, 1.0 equiv), $NaHCO_3$ (1.15 g, 13.7 mmol, 2.1 equiv), and acetic anhydride (1.23 mL, 13.0 mmol, 2.0 equiv). The suspension was brought to reflux for 3 h, after which the reaction was filtered, and the filtrate concentrated by rotary evaporation. Trace acetic acid by-product was removed azeotropically with toluene. Trace toluene was removed azeotropically with methanol, and trace methanol was removed azeotropically with chloroform, yielding the desired product **4.46** as a white solid (1.34 g, 73%). Characterization data matched the literature.[175] ^{1}H-NMR (300 MHz, $CDCl_3$) δ: 6.77 (1H, br. s), 4.53 (1H, m), 3.29-3.14 (2H, m), 2.73-2.66 (1H, m), 2.00-1.85 (4H, m). ^{13}C- NMR (75 MHz, $CDCl_3$) δ: 208.8, 174.2, 62.1, 34.2, 30.3, 25.7, 25.0, 24.0.

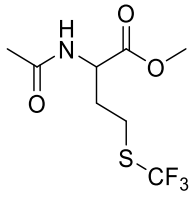

4.48

(±)-*N*-Acetyltrifluoromethionine methyl ester (4.48). Sodium metal (1.80 g, 78.3 mmol, 2.5 equiv) was added portion-wise to dried methanol (155 mL) in a 250 mL round bottom flask over ice and stirred until dissolution occurred. To this was added compound **4.46** (5.0 g, 31.4 mmol, 1 equiv) and the reaction was stirred at 0 ^{o}C for 40 minutes. The mixture was equipped with a dry-ice condenser and CF_3I (g) (18.5 g, 94.4 mmol, 3 equiv) was added. The mixture was then irradiated by UV light (350 nm) for 1 h. Following this reaction time, another installment of CF_3I (g) (6.2 g, 31.5 mmol, 1 equiv) was added, and the reaction further subjected to UV light for an additional 1 h. The solvent was removed *in vacuo* and redissolved in DCM (200 mL) and subsequently washed with sat. $NaHCO_3$ (1 x 100 mL) and brine (1 x

100 mL). The organic layer was dried over Na_2SO_4 and concentrated. The residue was further purified by chromatography in silica gel using 3:1 EtOAC/hexane as the mobile phase. Purification using this method afforded the desired compound **4.48** (5.86 g, 72%) as a clear oil. Characterization data matched with the literature.[176] ^{1}H-NMR (300 MHz, $CDCl_3$) δ: 6.12 (1H, br. s), 4.72 (1H, dt, J = 7.7, 5.0 Hz), 3.77 (3H, s), 2.92-2.86 (2H, m), 2.32-2.23 (1H, m), 2.08-1.99 (4H, m). ^{13}C- NMR (75 MHz, $CDCl_3$) δ: 172.0, 170.6, 130.8, 52.6, 51.1, 32.7, 26.0, 22.8. ^{19}F-NMR (282 MHz, $CDCl_3$) δ: -41.6.

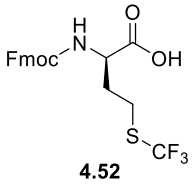

4.52

***N*-(((9H-Fluoren-9-yl)methoxy)carbonyl)-*S*-(trifluoromethyl)-*D*-homocysteine** (**4.52**). Compound **4.48** (1.99 g, 7.68 mmole, 1 equiv) was suspended in water (20 mL) in a 50 mL round-bottom flask equipped with a stir bar. To this was added NaOH(s) (338 mg, 8.44 mmole, 1.1 equiv), and the reaction was stirred for 1 h at room temperature to hydrolyze the methyl ester and the reaction monitored by TLC. At the completion of hydrolysis, the solution was then adjusted to pH 7.5 with HCl (aq) and heated to 30 ^{o}C followed by the addition of *D*-aminoacylase (50 mg). The reaction was gently stirred at 30 ^{o}C for 24 h. After the reaction time, the solution was made basic by the addition of $NaHCO_3$(s) (1.5 g), and an equal volume of MeCN was added. To the stirring suspension was added Fmoc-OSu (1.29 g, 3.84 mmole, 0.5 equiv), and the reaction stirred vigorously overnight. The mixture was made acidic (pH = 1) through the addition of 1 M HCl (aq), and the product extracted to ethyl acetate (3 x 50 mL). The organic layer was dried over Na_2SO_4 and concentrated. The residue was then purified by column chromatography, with a mobile phase of 9:1 hexane/EtOAc + 0.5% acetic acid,

yielding compound **4.52** as a slightly yellow solid (986 mg, 30% yield, 60% yield of desired enantiomer). The *ee* of **4.52** was determined to be 94.2%, described in Section 4.4.2. Characterization data closely matched that for the enantiomeric compound.[161] ^{1}H-NMR (300 MHz, MeOD-d_3) δ: 7.68(2H, d, J = 7.4 Hz), 7.58 (2H, app. t, J = 6.2 Hz), 7.30 (2H, t, J = 7.3 Hz), 7.23 (2H, t, J = 7.3 Hz), 4.31 (2H, d, J = 7.0 Hz), 4.10 (1H, t, J = 6.8 Hz), 3.05-2.85 (2H, m), 2.30-1.95 (2H, m). ^{13}C-NMR (75 MHz, MeOD-d_3): δ: 176.2, 160.1, 146.8/146.5, 144.1, 134.2, 130.3, 129.6, 127.7, 122.4, 69.4, 55.4, 49.9, 34.6. ^{19}F-NMR (282 MHz, MeOD-d_3) δ: -43.0 (s). HRMS (ESI+): *m/z* $[M+H]^+$ calcd for $C_{20}H_{19}F_3NO_4S$; 426.09814, found 426.09879.

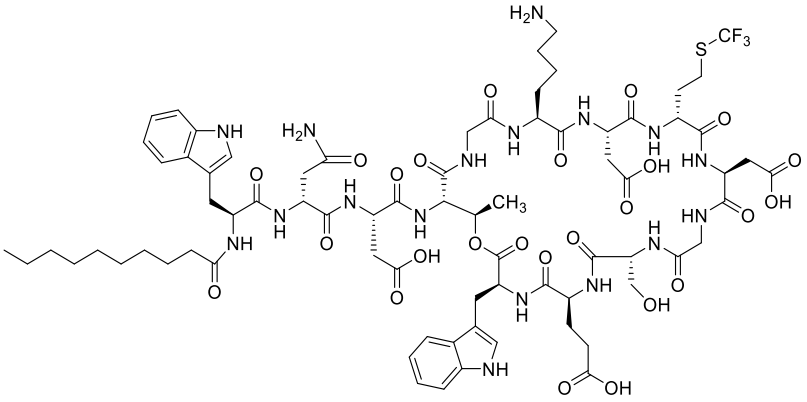

4.55

Dap-Lys6-*D*-hCys(CF$_3$)8-Glu12-Trp13 (**4.55**). Peptide **4.55** was synthesized in the same manner as (**4.16**), except that FmocTrp(Boc)OH was used instead of amino acid **4.16**, and Fmoc-*D*-hCys(CF$_3$)OH was used instead of Fmoc-*D*-AlaOH. The crude product was purified by preparative HPLC using a Clipeus C18 10 µm column employing an isocratic gradient of 57 % H_2O (0.1 % TFA) / 43% acetonitrile over 40 min. Fractions containing the desired compound were pooled and concentrated, suspended in water and lyophilized to obtain the desired product as a white powder (2.9 mg, 2% based on resin loading), judged to be >95%

pure by RP-HPLC (Figure B.23 in Appendix B). HRMS (ESI+): *m/z* $[M+2H]^{2+}$ calcd for $C_{75}H_{104}F_3N_{17}O_{25}S$: 865.85355, found 865.85547 (Figure C.23 in Appendix C).

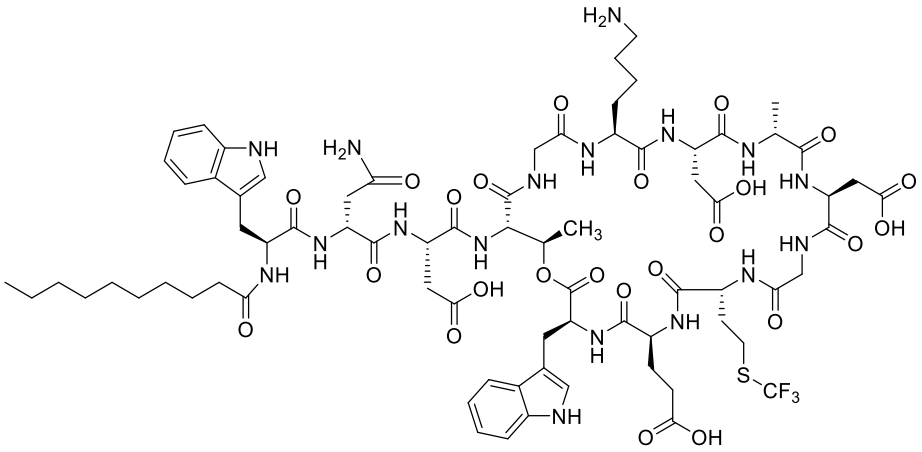

4.56

Dap-Lys6-*D*-hCys(CF$_3$)11-Glu12-Trp13 (**4.56**). Peptide **4.56** was synthesized in the same manner as (**4.16**), except that FmocTrp(Boc)OH was used instead of amino acid **4.16**, and Fmoc-*D*-hCys(CF_3)OH was used instead of Fmoc-*D*-SerOH. The crude product was purified by preparative HPLC using a Clipeus C18 10 µm column employing an isocratic gradient of 56 % H_2O (0.1 % TFA) / 44% acetonitrile over 40 min. Fractions containing the desired compound were pooled and concentrated, suspended in water and lyophilized to obtain the desired product as a white powder (16 mg, 11% based on resin loading), judged to be >95% pure by RP-HPLC (Figure B.24 in Appendix B). HRMS (ESI+): *m/z* $[M+2H]^{2+}$ calcd for $C_{75}H_{104}F_3N_{17}O_{24}S$: 857.85510, found 857.85792 (Figure C.24 in Appendix C).

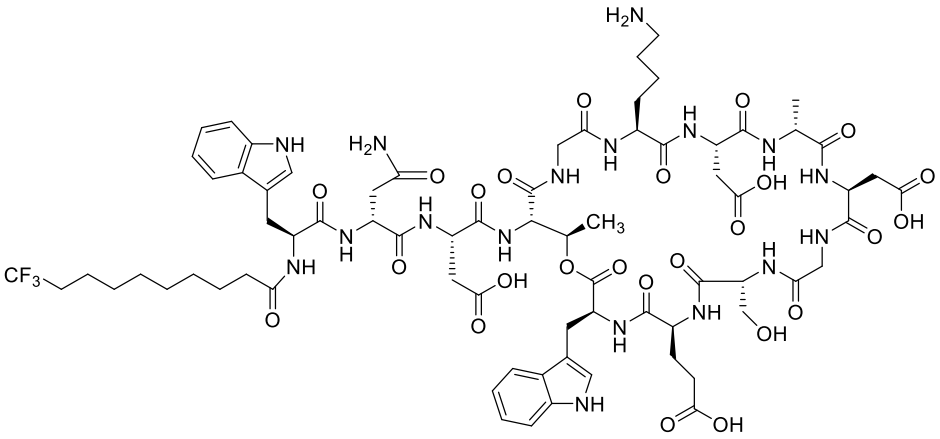

4.57

Dap-^{TF}Dec0-Lys6-Glu12-Trp13 (**4.57**). Peptide **4.57** was synthesized in the same manner as **4.15**, except that FmocTrp(Boc)OH was used instead of amino acid **4.16**, and 10,10,10-decanoic acid (**4.3**) was used instead of decanoic acid. The crude product was purified by preparative HPLC using a Clipeus C18 10 µm column employing an isocratic gradient of 61 % H_2O (0.1 % TFA) / 39% acetonitrile over 40 min. Fractions containing the desired compound were pooled and concentrated, suspended in water and lyophilized to obtain the desired product as a white powder (16 mg, 11% based on resin loading), judged to be >95% pure by RP-HPLC (Figure B.25 in Appendix B). HRMS (ESI+): *m/z* $[M+2H]^{2+}$ calcd for $C_{73}H_{100}F_3N_{17}O_{25}$: 835.85087, found 835.85226 (Figure C.25 in Appendix C).

Publications

Kralt, B.; Moreira, R.; Palmer, M.; Taylor, S.D. Total synthesis of analogs of A54145D and A54145A$_1$ for structure-activity relationship studies. *J. Org. Chem.* **2020**, *ahead of print at the time of submission*: DOI: 10.1021/acs.joc.9b02922

Kralt, B.; Moreira, R.; Palmer, M.; Taylor, S.D. Total synthesis of A54145 Factor D. *J. Org. Chem.* **2019**, *84* (18), 12021-12030.

Beriashvili, D.; Taylor, R.M.; **Kralt, B.**; Abu Mazen, N.; Taylor, S.D.; Palmer, M. Mechanistic studies on the effect of membrane lipid acyl chain composition on daptomycin pore formation. *Chem. Phys. Lipids* **2018**, *216*, 73-79.

Mohamady, S.; **Kralt, B**.; Samwel, S.K.; Taylor, S.D. Efficient one-pot, two-component modular synthesis of 3,5-disubstituted pyrazoles. *ACS Omega* **2018**, *3* (11), 15566-15574.

Lohani, C.R.; Soley, J.; **Kralt, B.**; Palmer, M.; Taylor, S.D. α-Azido esters in depsipeptide synthesis: C-O bond cleavage during azido group reduction. *J. Org. Chem.* **2016**, *81* (23), 11831-11840.

Mostafa, Y.A.; **Kralt, B.**; Rao, P.P.N.; Taylor, S.D. A-ring substituted 17β-arylsulfonamides of 17β-aminoestra-1,3,5(10)-trien-3-ol as highly potent reversible inhibitors of steroid sulfatase. *Bioorg. Med. Chem.* **2015**, *23* (17), 5681-5692

Appendix A: NMR Characterization Data for A54145D

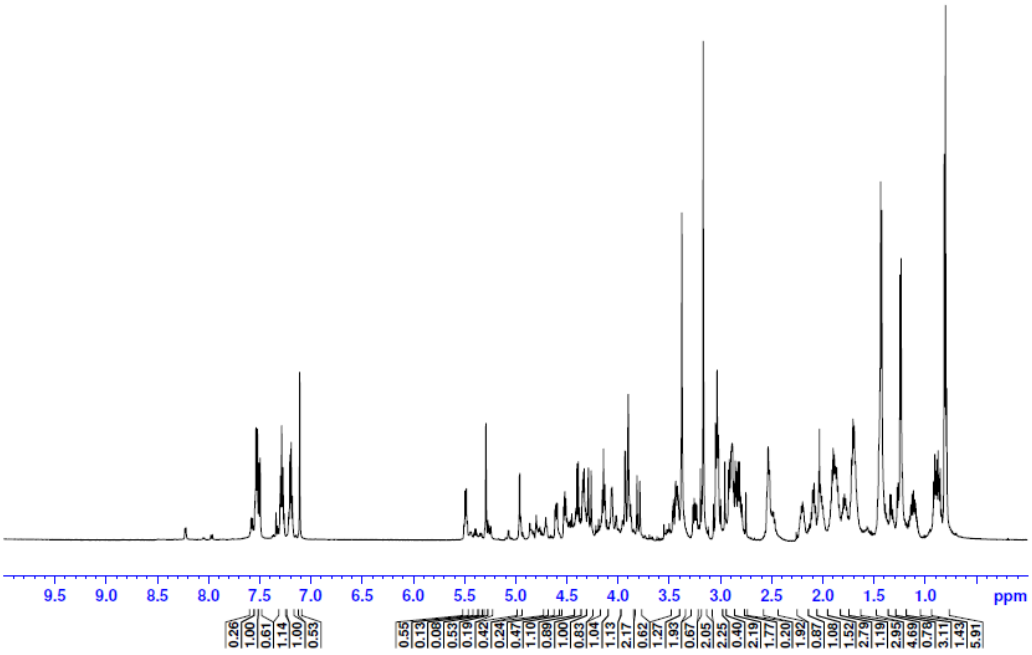

Figure A.1: ^{1}H-NMR spectrum of A54145D-nucleus (600 MHz, D_2O).

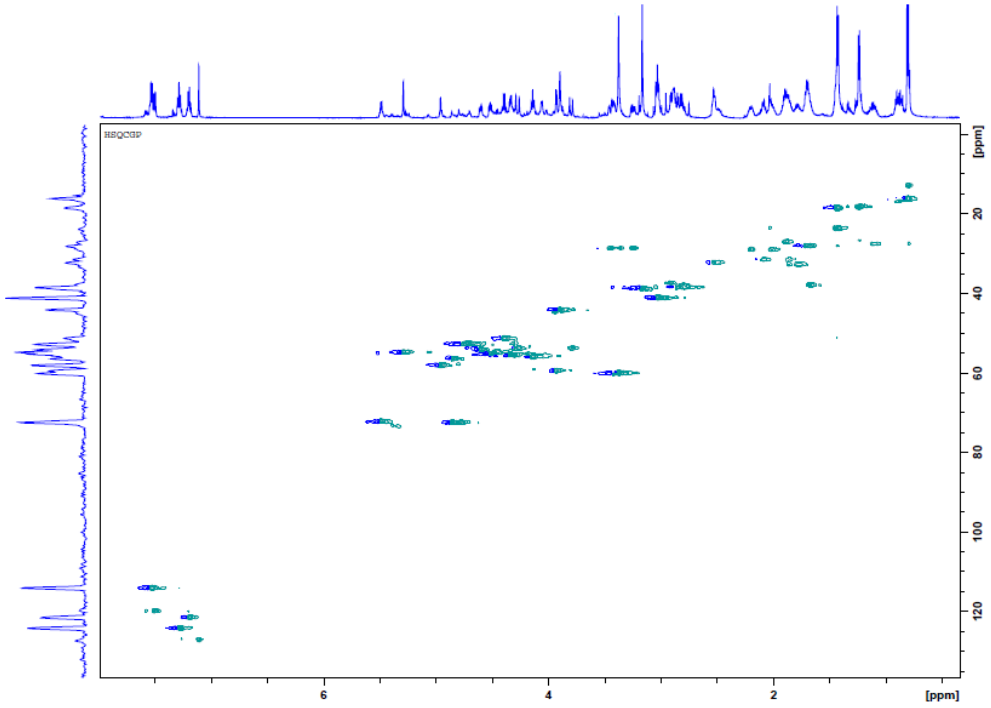

Figure A.2: ^{1}H-^{13}C HSQC spectrum of A54145D-nucleus (600 MHz, D_2O).

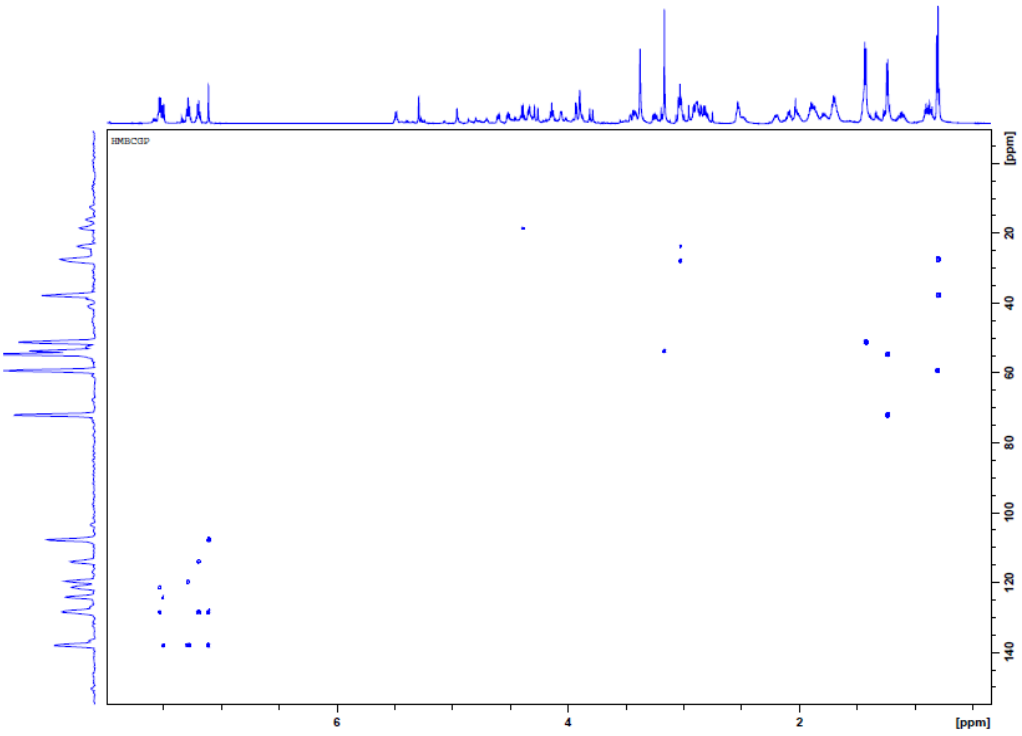

Figure A.3: ^{1}H-^{13}C HMBC spectrum of A54145D-nucleus (600 MHz, D_2O).

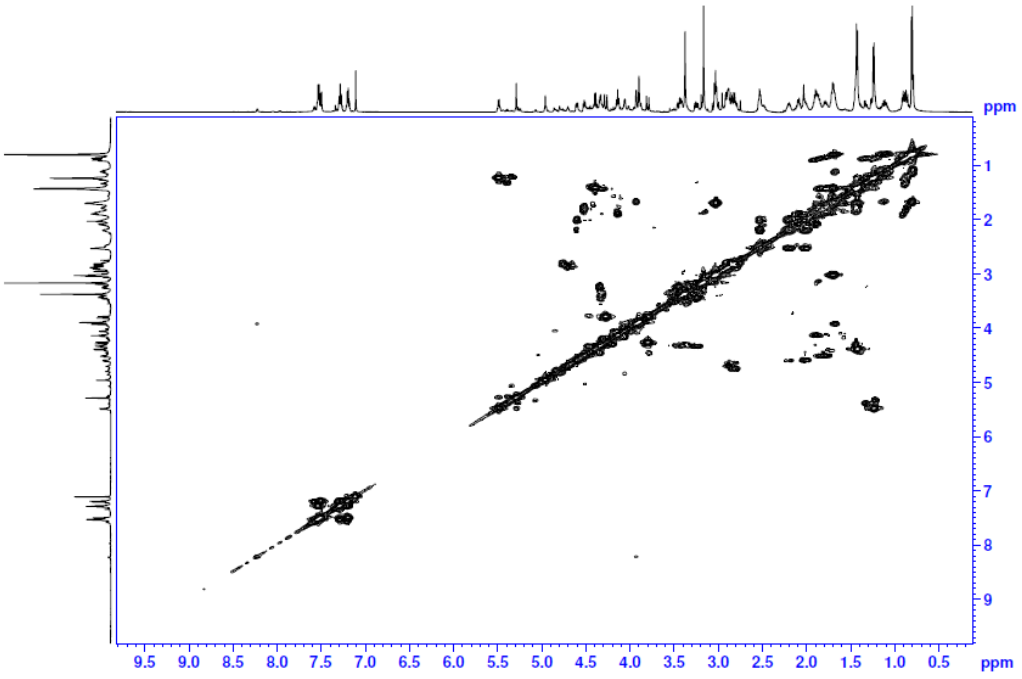

Figure A.4: ^{1}H-COSY spectrum of A54145D-nucleus (600 MHz, D_2O).

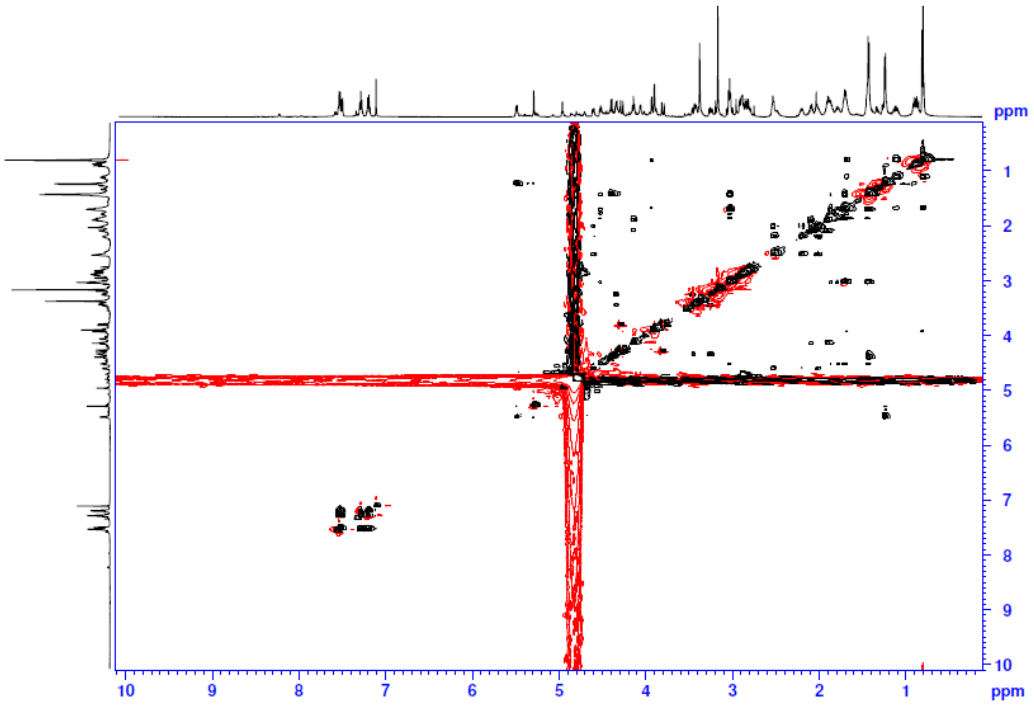

Figure A.5: ^{1}H-TOCSY spectrum of A54145D-nucleus (500 MHz, D_2O).

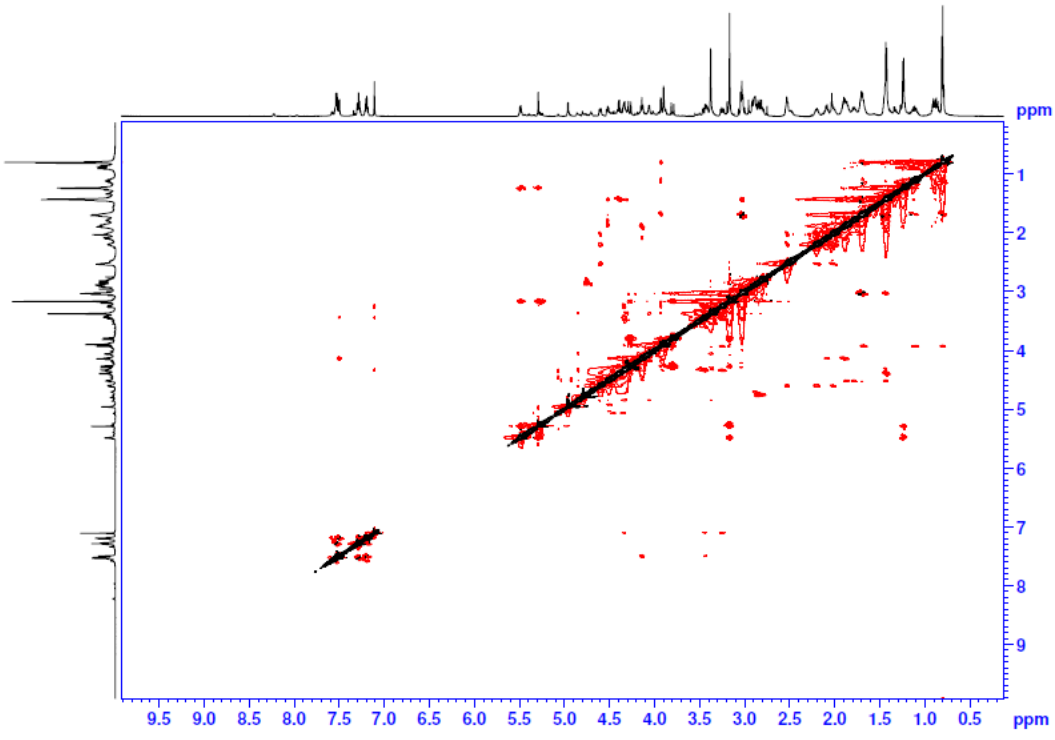

Figure A.6: ^{1}H-ROESY spectrum of A54145D-nucleus (600 MHz, D_2O).

Table A.1: HSQC/HMBC peak correlations for A54145D-nucleus

	A5D-nucleus (600 MHz, D_2O)				A5D-nucleus (600 MHz, D_2O)		
		^1H major conformer [minor conformer]	^{13}C major conformer [minor conformer]			^1H major conformer [minor conformer]	^{13}C major conformer [minor conformer]
Trp[1]	$C^{\alpha}H$	4.35	55.4	*e*MeOAsp[9]	$C^{\alpha}H$	4.05	55.7
	$C^{\beta}H_2$	3.25, 3.43	28.6		$C^{\beta}H$	4.86	72.6
	C^2H	7.10	127.2		O-CH_3	3.38	59.9
	C^3	---	107.9	Gly[10]	$C^{\alpha}H_2$	3.90	44.1
	C^{3a}	---	128.5	D-Asn[11]	$C^{\alpha}H$	4.76	52.8
	C^4H	7.50 [7.58][a]	119.9		$C^{\beta}H_2$	2.80, 2.86	41.1
	C^5H	7.18	121.5	Glu[12]	$C^{\alpha}H$	4.61	54.1
	C^6H	7.28	124.2		$C^{\beta}H_2$	2.01, 2.20	28.9
	C^7H	7.53	114.1		$C^{\gamma}H_2$	2.53 [2.48][a]	32.1 [32.3][a]
	C^{7a}	---	138.0	Ile[13]	$C^{\alpha}H$	3.95	59.4
D-Glu[2]	$C^{\alpha}H$	4.13	56.0		$C^{\beta}H$	1.67 [1.86][a]	37.8
	$C^{\beta}H_2$	1.89	27.1		$C^{\gamma}H_2$	1.10 [1.23][a]	27.5 [26.7][a]
	$C^{\gamma}H_2$	2.09	31.5		$C^{\delta}H_3$	0.80 [0.86] [a]	12.9 [12.23][a]
*t*HOAsn[3]	$C^{\alpha}H$	4.95	58.0		$C^{\gamma}H_3$	0.80 [0.86] [a]	16.2 [15.32][a]
	$C^{\beta}H$	4.79	72.5				
Thr[4]	$C^{\alpha}H$	5.30 [5.26][a]	54.8				
	$C^{\beta}H$	5.50 [5.40][a]	72.1 [73.4][a]				
	$C^{\gamma}H_3$	1.24 [1.33][a]	18.30				
Sar[5]	N^{α}-CH_3	3.17	38.6				
	$C^{\alpha}H_2$	3.80, 4.28	53.8				
Ala[6]	$C^{\alpha}H$	4.40	51.3				
	$C^{\beta}H_3$	1.43	18.5				
Asp[7]	$C^{\alpha}H$	4.70	52.8				
	$C^{\beta}H_2$	2.90 [2.95][a]	37.4				
D-Lys[8]	$C^{\alpha}H$	4.53 [4.48][a]	55.3 [54.8][a]				
	$C^{\beta}H_2$	1.78, 1.86	32.6				
	$C^{\gamma}H_2$	1.43	23.7				
	$C^{\delta}H_2$	1.70	28.0				
	$C^{\epsilon}H_2$	3.03	41.1				

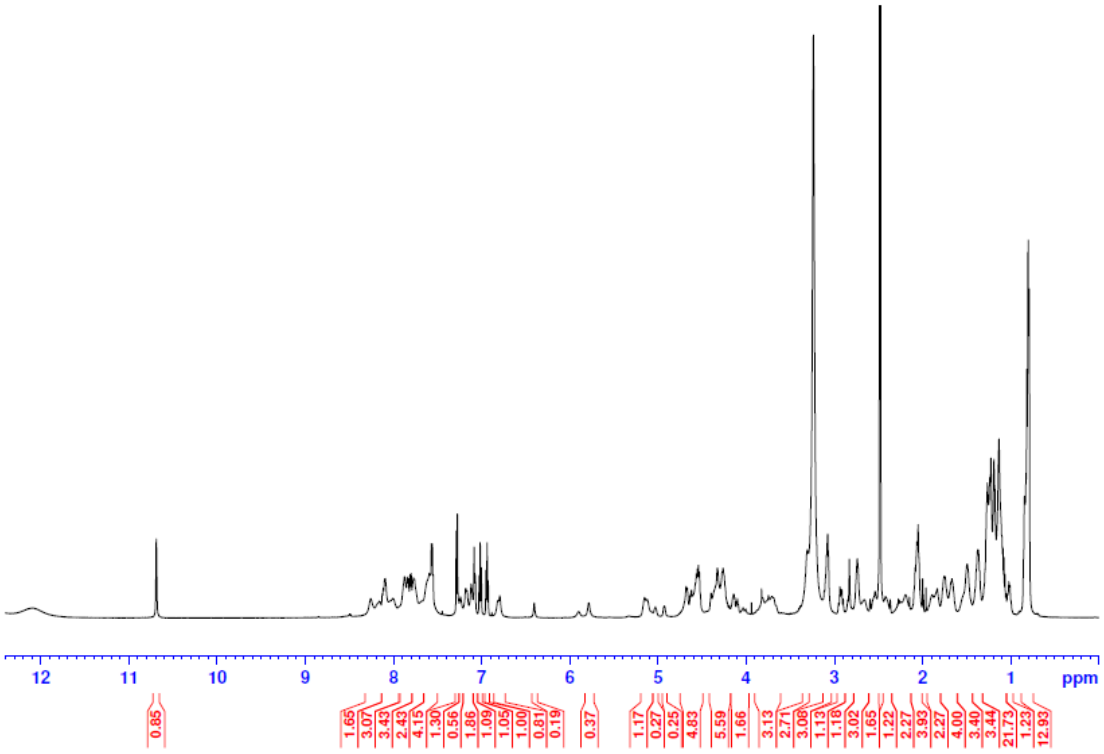

Figure A.7: ^{1}H-NMR spectrum of A54145D-*t*HOAsn3-*e*MeOAsp9 (600 MHz, d_6-DMSO).

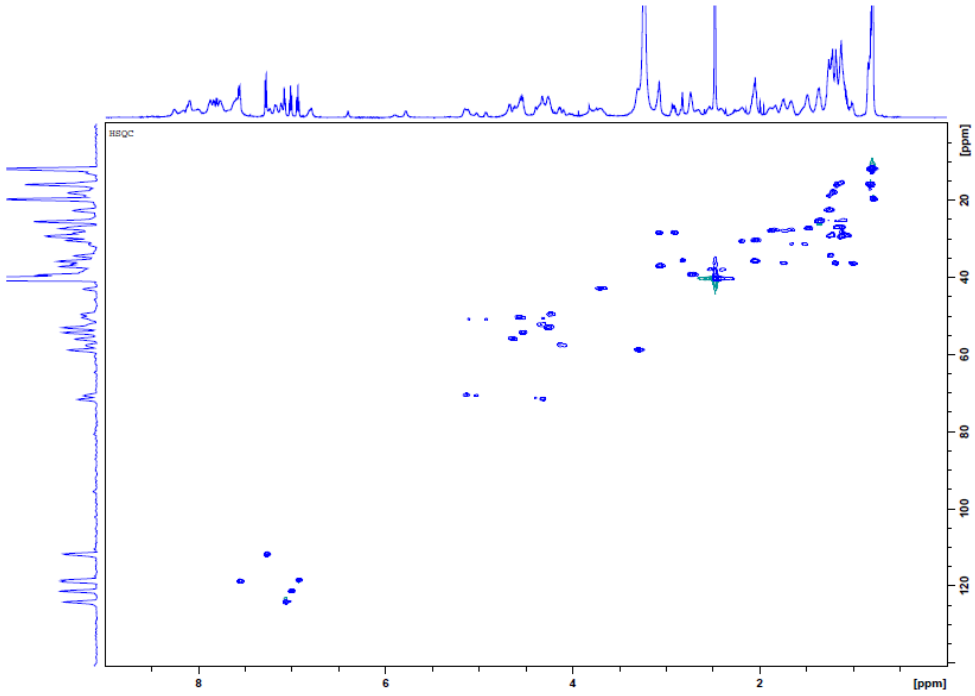

Figure A.8: ^{1}H-^{13}C HSQC spectrum of A54145D-*t*HOAsn3-*e*MeOAsp9 (600 MHz, d_6-DMSO).

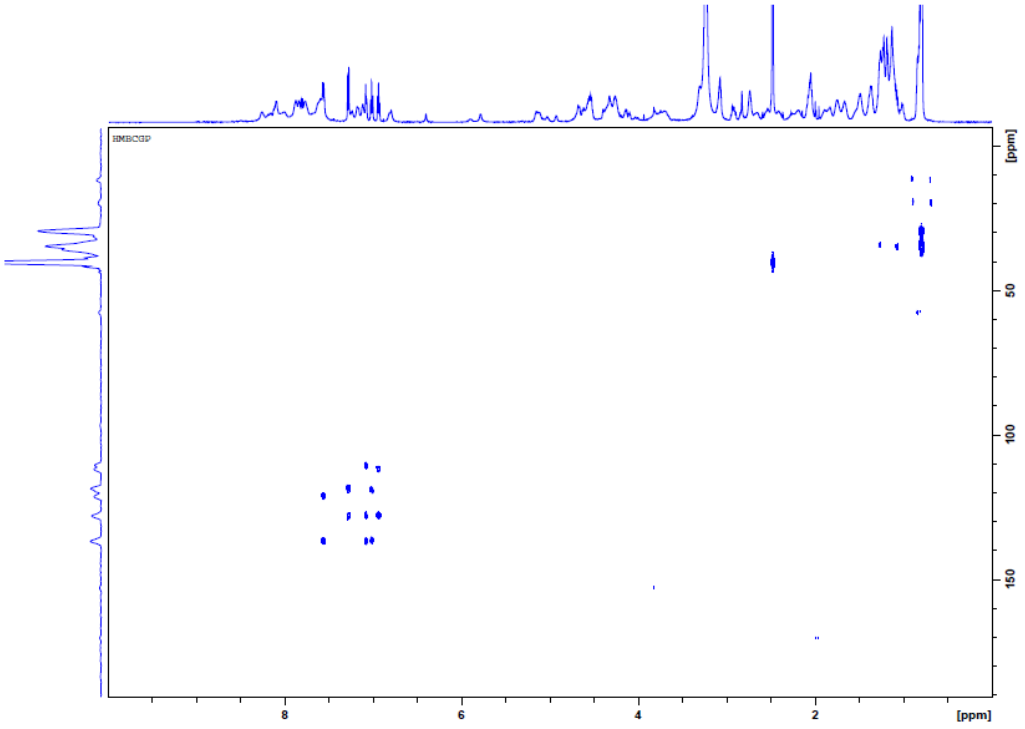

Figure A.9: ^{1}H-^{13}C HMBC spectrum of A54145D-*t*HOAsn3-*e*MeOAsp9 (600 MHz, d_6-DMSO).

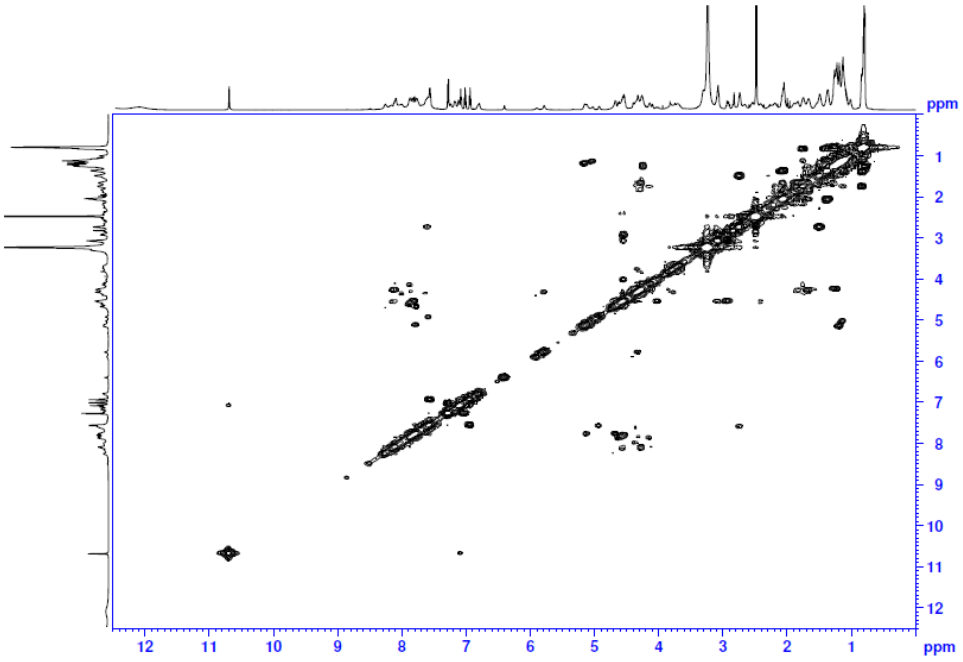

Figure A.10: ^{1}H-COSY spectrum of A54145D-*t*HOAsn3-*e*MeOAsp9 (600 MHz, d_6-DMSO).

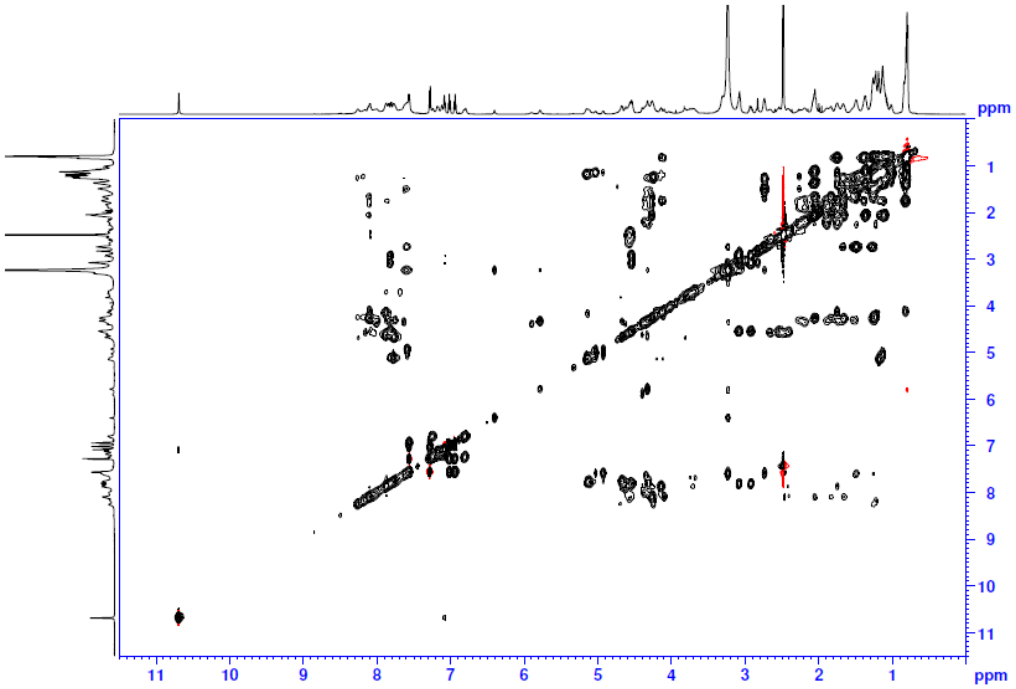

Figure A.11: ^{1}H-TOCSY spectrum of A54145D-*t*HOAsn3-*e*MeOAsp9 (600 MHz, d_6-DMSO).

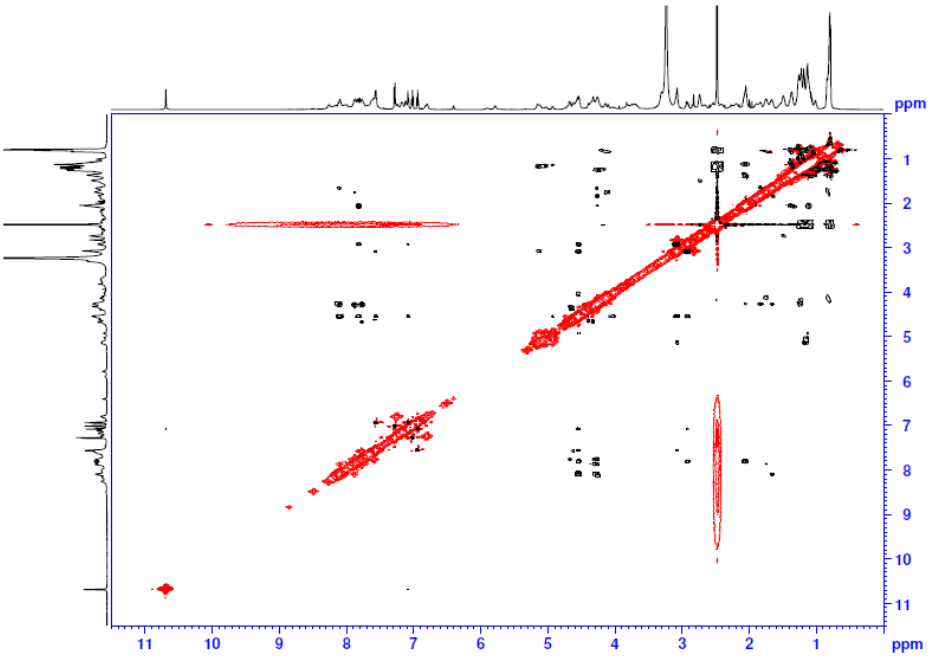

Figure A.12: ^{1}H-ROESY spectrum of A54145D-*t*HOAsn3-*e*MeOAsp9 (600 MHz, d_6-DMSO).

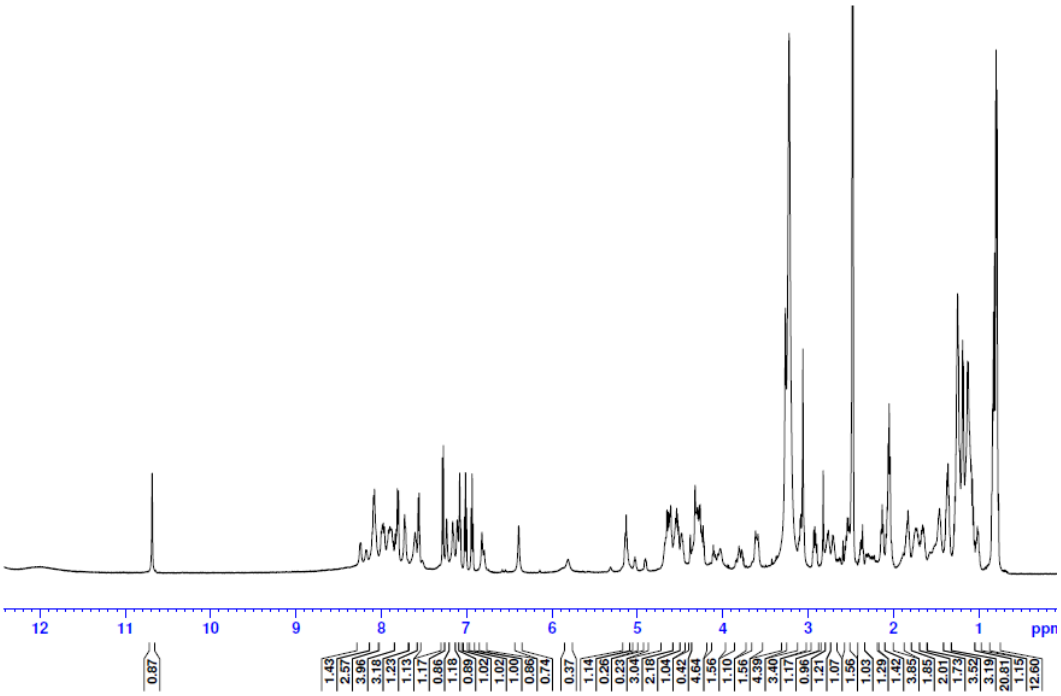

Figure A.13: ^{1}H-NMR spectrum of A54145D-*t*HOAsn3-*t*MeOAsp9 (600 MHz, d_6-DMSO).

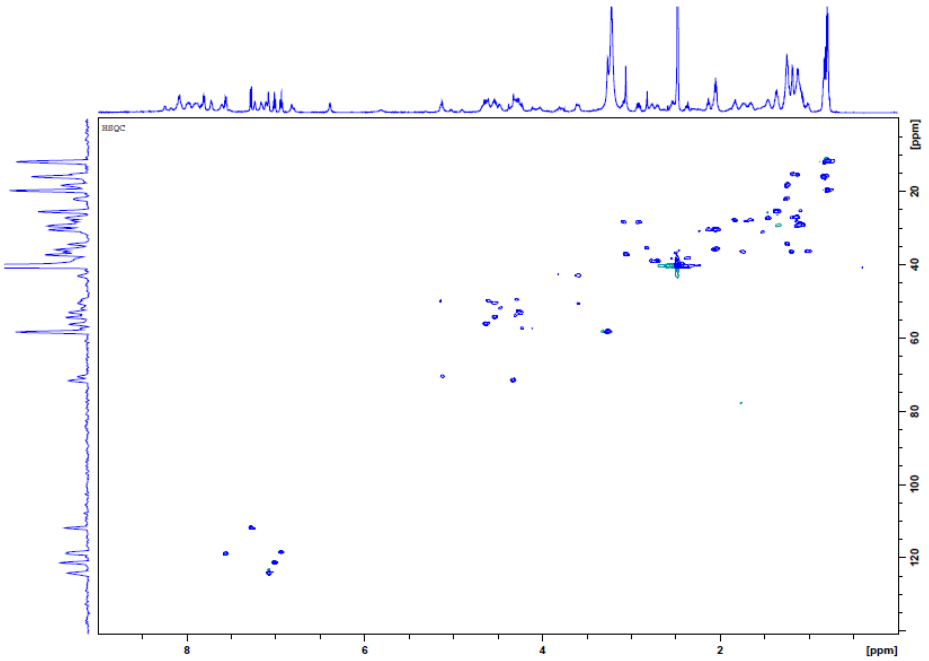

Figure A.14: ^{1}H-^{13}C HSQC spectrum of A54145D-*t*HOAsn3-*t*MeOAsp9 (600 MHz, d_6-DMSO).

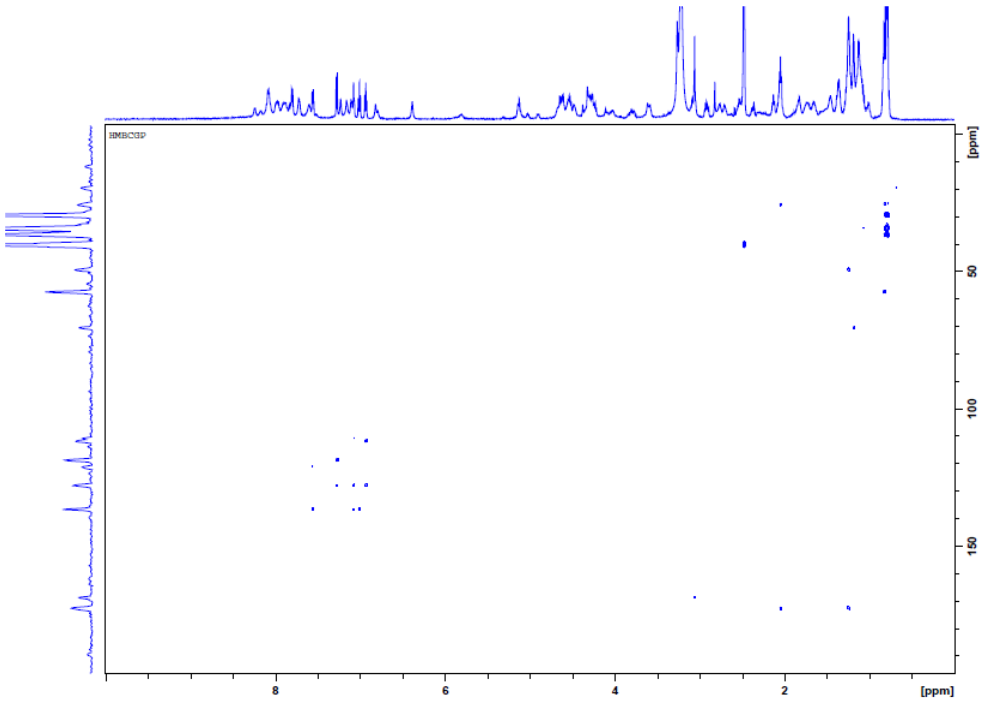

Figure A.15: ^{1}H-^{13}C HMBC spectrum A54145D-*t*HOAsn3-*t*MeOAsp9 (600 MHz, d_6-DMSO).

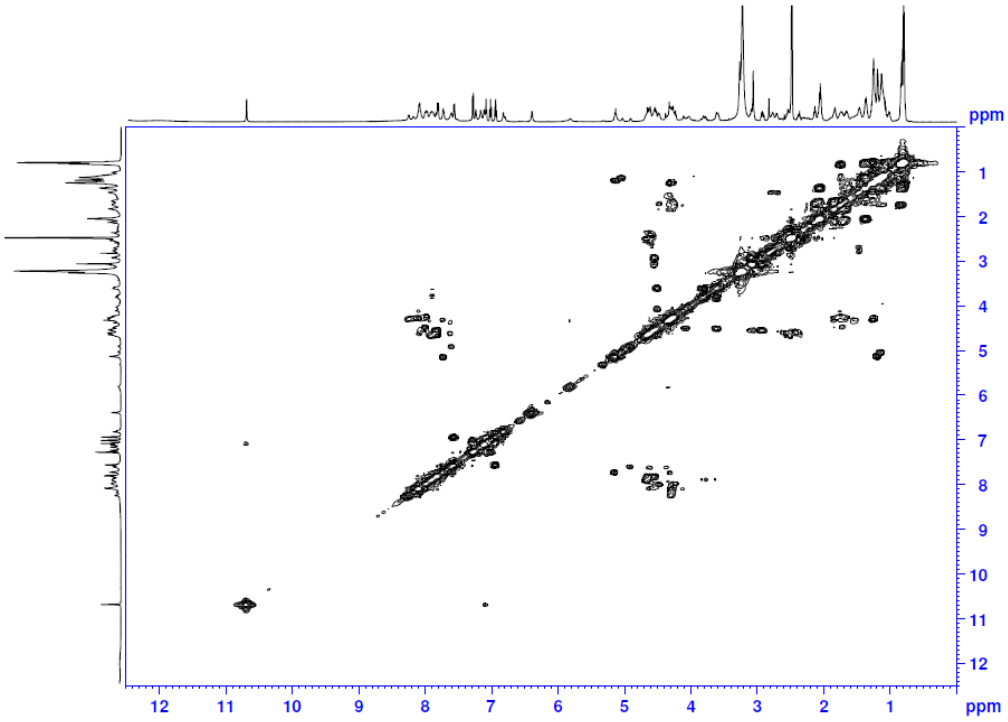

Figure A.16: ^{1}H-COSY spectrum of A54145D-*t*HOAsn3-*t*MeOAsp9 (600 MHz, d_6-DMSO).

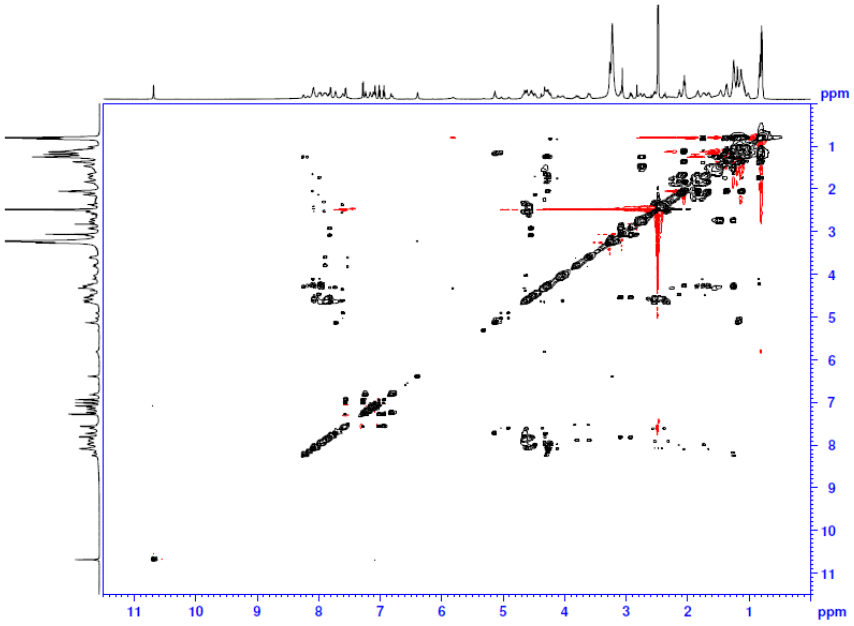

Figure A.17: ^{1}H-TOCSY spectrum of A54145D-*t*HOAsn3-*t*MeOAsp9 (600 MHz, d_6-DMSO).

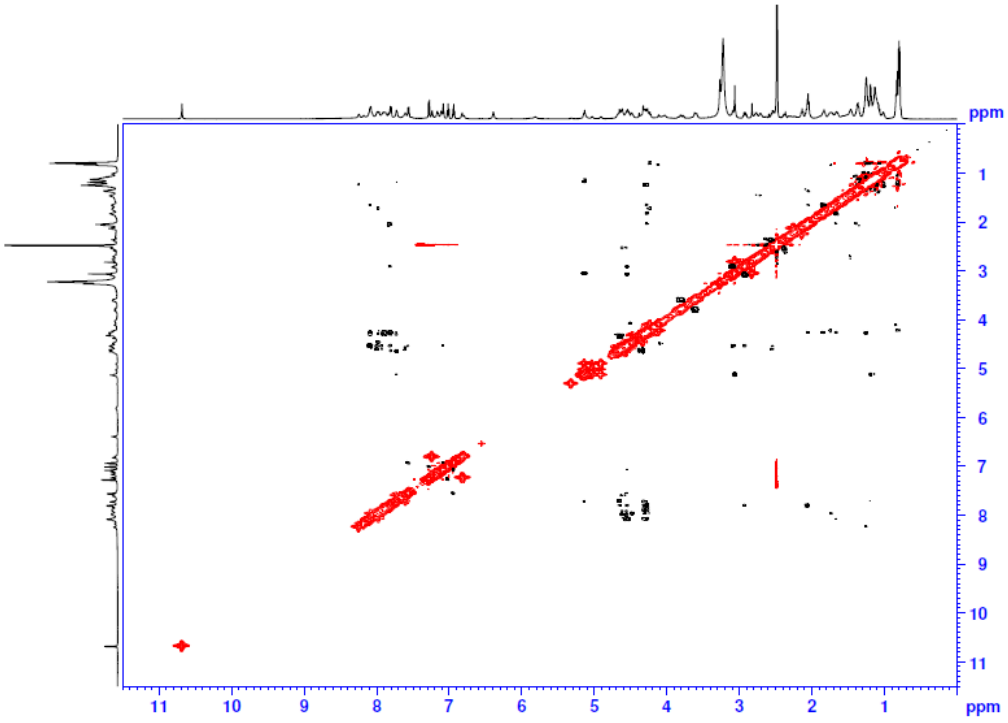

Figure A.18: ^{1}H-ROESY spectrum of A54145D-*t*HOAsn3-*t*MeOAsp9 (600 MHz, d_6-DMSO).

Table A.2: HSQC/HMBC Peak Coordinates for A54145D-*t*HOAsn3-*t*MeOAsp9 and A54145D-*t*HOAsn3-*e*MeOAsp9

	A54145D-*t*HOAsn3-*t*MeOAsp9 (600 MHz, DMSO)			A54145D-*t*HOAsn3-*e*MeOAsp9 (600 MHz, DMSO)		
		^{1}H	^{13}C		^{1}H	^{13}C
Trp[1]	N^{α}-H	7.83	---	N^{α}-H	7.84	---
	$C^{\alpha}H$	4.54	54.27	$C^{\alpha}H$	4.56	54.25
	$C^{\beta}H_2$	3.09, 2.92	28.38	$C^{\beta}H_2$	3.07, 2.92	28.45
	$N^{1}H$	10.68	---	$N^{1}H$	10.69	---
	$C^{2}H$	7.08	124.16	$C^{2}H$	7.08	124.07
	C^{3}	---	110.70	C^{3}	---	110.76
	C^{3a}	---	127.93	C^{3a}	---	127.86
	$C^{4}H$	7.56	118.83	$C^{4}H$	7.56	118.81
	$C^{5}H$	6.94	118.49	$C^{5}H$	6.94	118.54
	$C^{6}H$	7.01	121.27	$C^{6}H$	7.02	121.30
	$C^{7}H$	7.28	111.73	$C^{7}H$	7.28	111.80
	C^{7a}	---	136.62	C^{7a}	---	136.67
D-Glu[2]	N^{α}-H	8.09	---	N^{α}-H	8.11	---
	$C^{\alpha}H$	4.28	52.95	$C^{\alpha}H$	4.27	52.82
	$C^{\beta}H_2$	1.67, 1.85	27.76	$C^{\beta}H_2$	1.66, 1.84	27.70
	$C^{\gamma}H_2$	2.08	30.29	$C^{\gamma}H_2$	2.05	30.29
	COOH	12.1		COOH	12.1	
HOAsn[3]	N^{α}-H	7.79	---	N^{α}-H	7.76	---
	$C^{\alpha}H$	4.66	56.12	$C^{\alpha}H$	4.67	54.88
	$C^{\beta}H$	**4.33**	**71.52**	$C^{\beta}H$	4.33	71.52
	OH	5.31	---	OH	5.33	---
	$CONH_2$	5.81 [5.87][a]	---	$CONH_2$	5.79 [5.90][a]	---
Thr[4]	N^{α}-H	7.73 [7.60][a]	---	N^{α}-H	7.79 [7.58][a]	---
	$C^{\alpha}H$	5.13 [4.91][a]	49.92	$C^{\alpha}H$	5.11 [4.92][a]	50.91
	$C^{\beta}H$	5.13 [5.03][a]	70.40	$C^{\beta}H$	5.14 [5.03][a]	70.51
	$C^{\gamma}H_3$	1.19 [1.14][a]	15.35	$C^{\gamma}H_3$	1.18 [1.13][a]	15.77
Sar[5]	N^{α}-CH_3	3.07 [2.83][a]	37.16 [35.49][a]	N^{α}-CH_3	3.07 [2.82][a]	36.93 [35.58][a]
	$C^{\alpha}H_2$	4.07 [4.5][a] 3.59 [3.91][a]	50.60	$C^{\alpha}H_2$	4.54 3.80 [4.02][a]	50.65
Ala[6]	N^{α}-H	8.06	---	N^{α}-H	8.10	---
	$C^{\alpha}H$	4.30	49.43	$C^{\alpha}H$	4.23	49.56
	$C^{\beta}H_3$	1.25	18.19	$C^{\beta}H_3$	1.26	18.90
Asp[7]	N^{α}-H	7.82	---	N^{α}-H	7.80	---
	$C^{\alpha}H$	4.61	49.91	$C^{\alpha}H$	4.58	50.28
	$C^{\beta}H_2$	2.37, 2.55[b]	38.39	$C^{\beta}H_2$	2.43[b], 2.55[b]	38.07
	COOH	12.1		COOH	12.1	
D-Lys[8]	N^{α}-H	7.72	---	N^{α}-H	7.85	---
	$C^{\alpha}H$	4.31	53.93	$C^{\alpha}H$	4.27	52.82
	$C^{\beta}H_2$	1.51, 1.67	31.00	$C^{\beta}H_2$	1.52, 1.66	31.25
	$C^{\gamma}H_2$	1.25	21.89	$C^{\gamma}H_2$	1.25	22.53
	$C^{\delta}H_2$	1.46	27.33	$C^{\delta}H_2$	1.47	27.18
	$C^{\varepsilon}H_2$	2.71, 2.76	38.95	$C^{\varepsilon}H_2$	2.74	39.23
	$N^{\varepsilon}H_2$	7.62	---	$N^{\varepsilon}H_2$	7.61	---

Table A.2 (continued): HSQC/HMBC Peak Coordinates for A54145D-*t*HOAsn3-*t*MeOAsp9 and A54145D-*t*HOAsn3-*e*MeOAsp9

		A54145D-*t*HOAsn3-*t*MeOAsp9 (600 MHz, DMSO)			A54145D-*t*HOAsn3-*e*MeOAsp9 (600 MHz, DMSO)	
*t*MeOAsp[9] or *e*MeOAsp[9]	N^{α}-H	7.83	---	N^{α}-H	7.78	---
	$C^{\alpha}H$	4.66	56.12	$C^{\alpha}H$	4.67	55.83
	$C^{\beta}H$	**4.33**	**71.52**	$C^{\beta}H$	4.33	71.33
	O-CH_3	3.26[c]	58.20	O-CH_3	3.29[c]	58.73
	COOH	12.1	---	COOH	12.1	---
Gly[10]	N^{α}-H	7.89 [7.52][a]	---	N^{α}-H	7.89 [7.70][a]	---
	$C^{\alpha}H_2$	3.79 [3.82][a] 3.60 [3.61][a]	42.85	$C^{\alpha}H_2$	3.70, 3.80	42.87
D-Asn[11]	N^{α}-H	7.81	---	N^{α}-H	7.80	---
	$C^{\alpha}H$	4.58	49.35	$C^{\alpha}H$	4.56	50.49
	$C^{\beta}H_2$	2.30, 2.50[b]	36.85	$C^{\beta}H_2$	2.50[b], 2.42	36.51
	$CONH_2$	6.81, 7.24	---	$CONH_2$	6.80, 7.24	---
Glu[12]	N^{α}-H	8.00	---	N^{α}-H	7.99	---
	$C^{\alpha}H$	4.47	51.84	$C^{\alpha}H$	4.35	52.25
	$C^{\beta}H_2$	1.84, 1.74	28.00	$C^{\beta}H_2$	1.89, 1.73	27.85
	$C^{\gamma}H_2$	2.14	30.33	$C^{\gamma}H_2$	2.19	30.51
	COOH	12.1	---	COOH	12.1	---
Ile[13]	N^{α}-H	8.07	---	N^{α}-H	7.89	---
	$C^{\alpha}H$	4.22 [4.11][a]	57.33	$C^{\alpha}H$	4.14	57.62
	$C^{\beta}H$	1.74	36.44	$C^{\beta}H$	1.75	36.36
	$C^{\gamma}H_2$	1.36, 1.06	29.33	$C^{\gamma}H_2$	1.37, 1.11	29.33
	$C^{\delta}H_3$	0.80	12.77	$C^{\delta}H_3$	0.80	12.89
	$C^{\gamma}H_3$	0.83	15.88	$C^{\gamma}H_3$	0.83	15.77
MeDec[0]	$C^{2}H_2$	2.06	35.65	$C^{2}H_2$	2.05	35.70
	$C^{3}H_2$	1.36	25.44	$C^{3}H_2$	1.37	25.40
	$C^{4}H_2$	1.10	25.39	$C^{4}H_2$	1.11	25.18
	$C^{5}H_2$	**1.14**	**27.01**	$C^{5}H_2$	**1.13**	**27.00**
	$C^{6}H_2$	**1.14**	**27.01**	$C^{6}H_2$	**1.13**	**27.00**
	$C^{7}H_2$	1.01, 1.19	36.37	$C^{7}H_2$	1.01, 1.17	36.40
	$C^{8}H$	1.26	34.18	$C^{8}H$	1.25	34.18
	$C^{8'}H_3$	0.80	19.64	$C^{8'}H_3$	0.80	19.67
	$C^{9}H_2$	1.08, 1.13	29.19	$C^{9}H_2$	1.13, 1.08	29.10
	$C^{10}H_3$	0.80	11.81	$C^{10}H_3$	0.80	11.78

Note: bolded peaks overlap with one or more other peaks.

[a] square brackets denote the minor conformer's chemical shift.

[b] Partial overlap with DMSO-d_6 solvent residual peak.

[c] Partial overlap with H_2O peak.

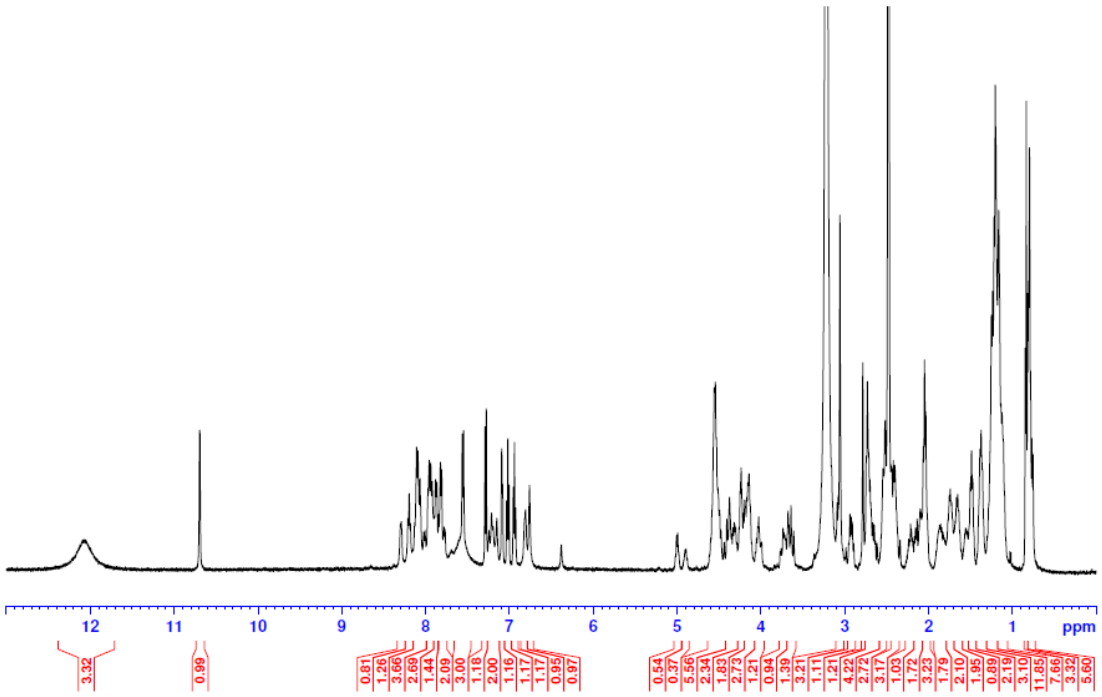

Figure A.19: ^{1}H-NMR spectrum of peptide **3.32** (500 MHz, DMSO-d_6).

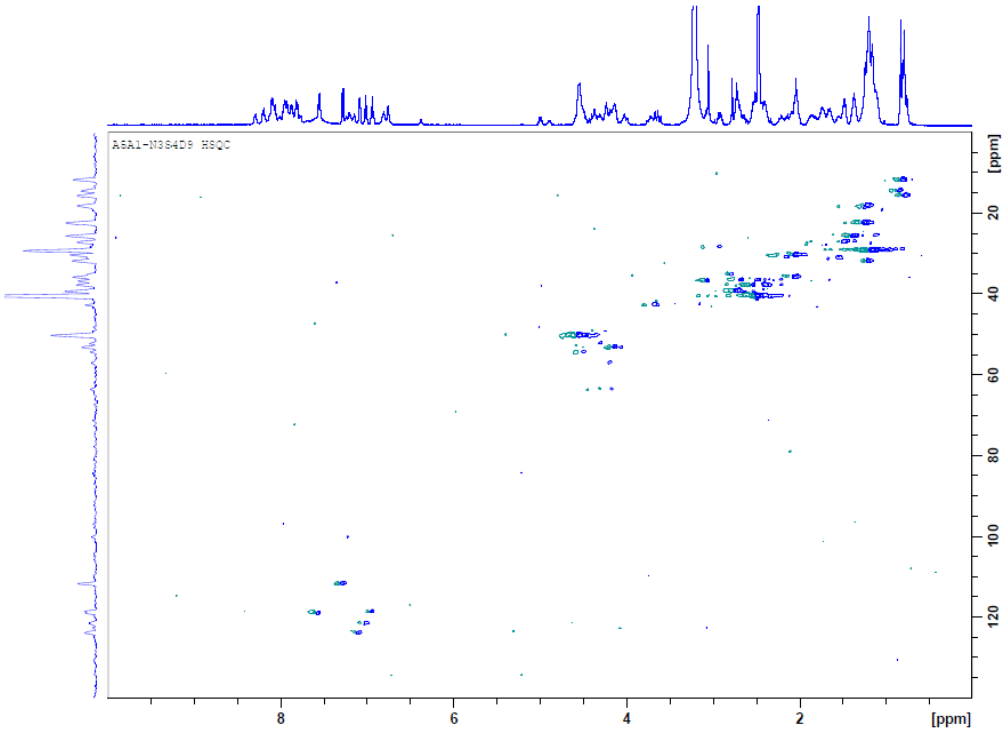

Figure A.20: ^{1}H-^{13}C HSQC spectrum of peptide **3.32** (500 MHz, DMSO-d_6).

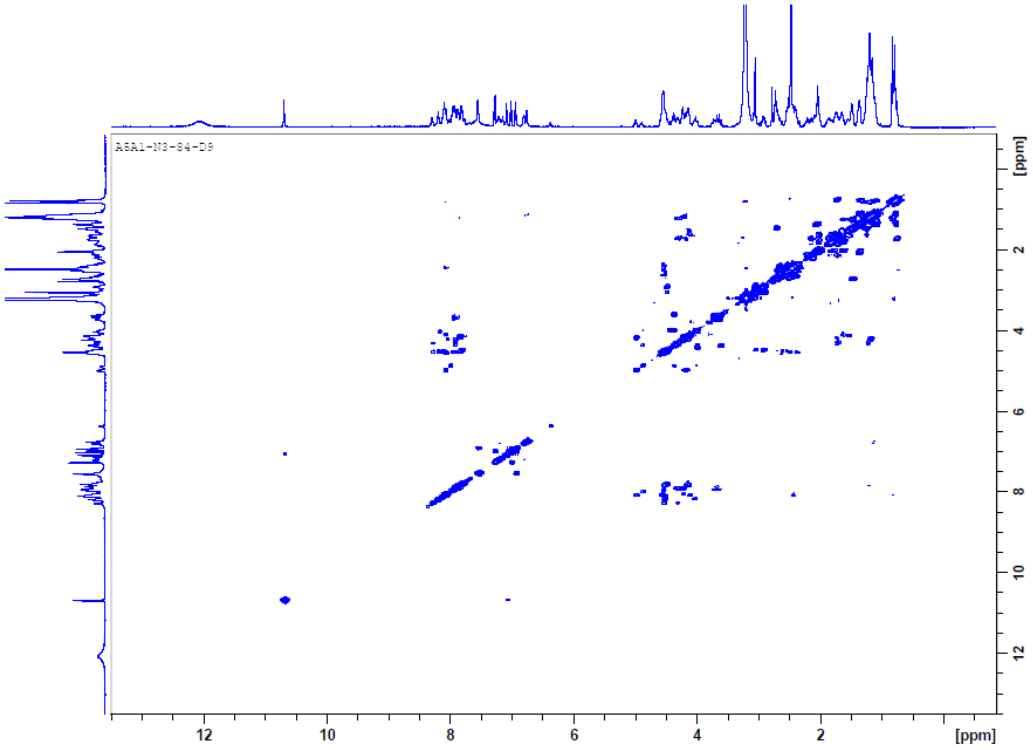

Figure A.21: ^{1}H-COSY spectrum of peptide **3.32** (500 MHz, DMSO-d_6).

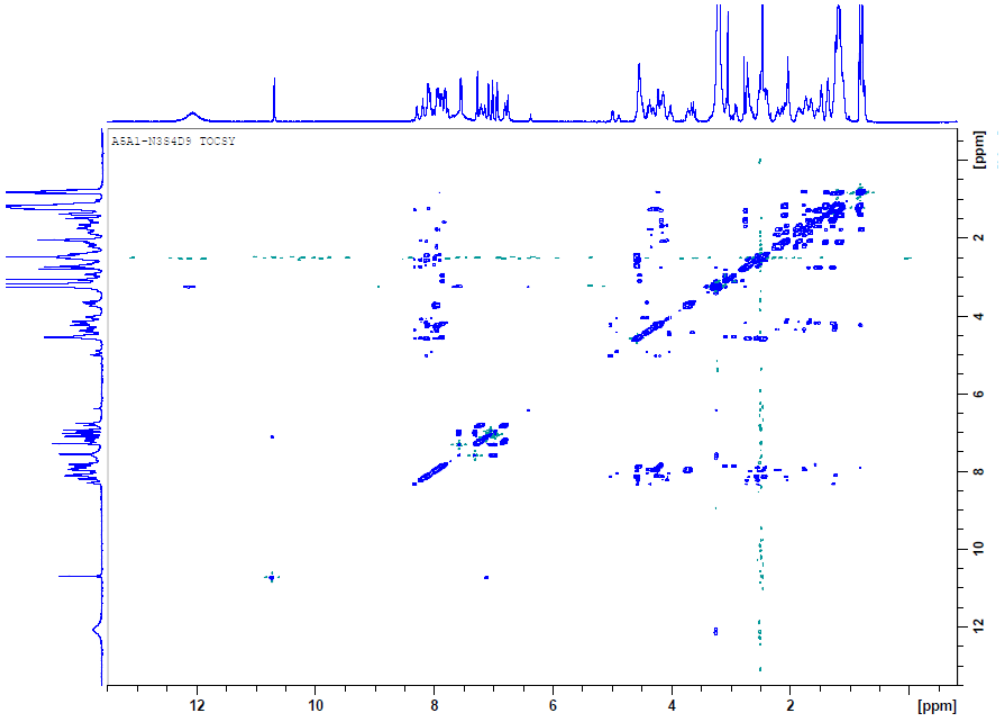

Figure A.22: ^{1}H-TOCSY spectrum of peptide **3.32** (500 MHz, DMSO-d_6).

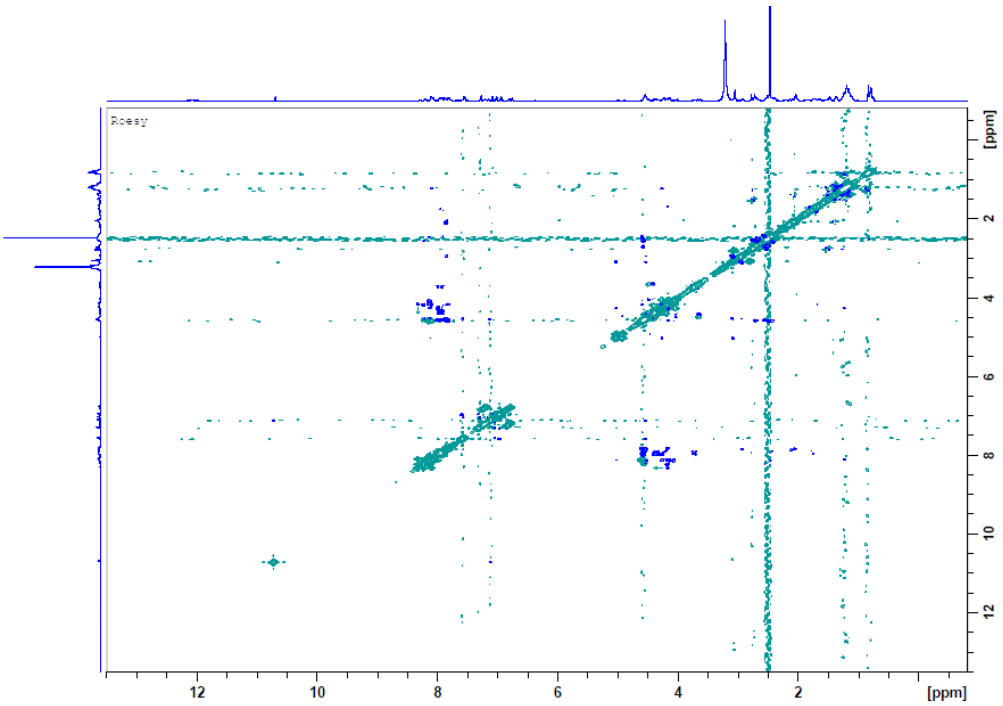

Figure A.23: ^{1}H-ROESY spectrum of peptide **3.32** (500 MHz, DMSO-d_6).

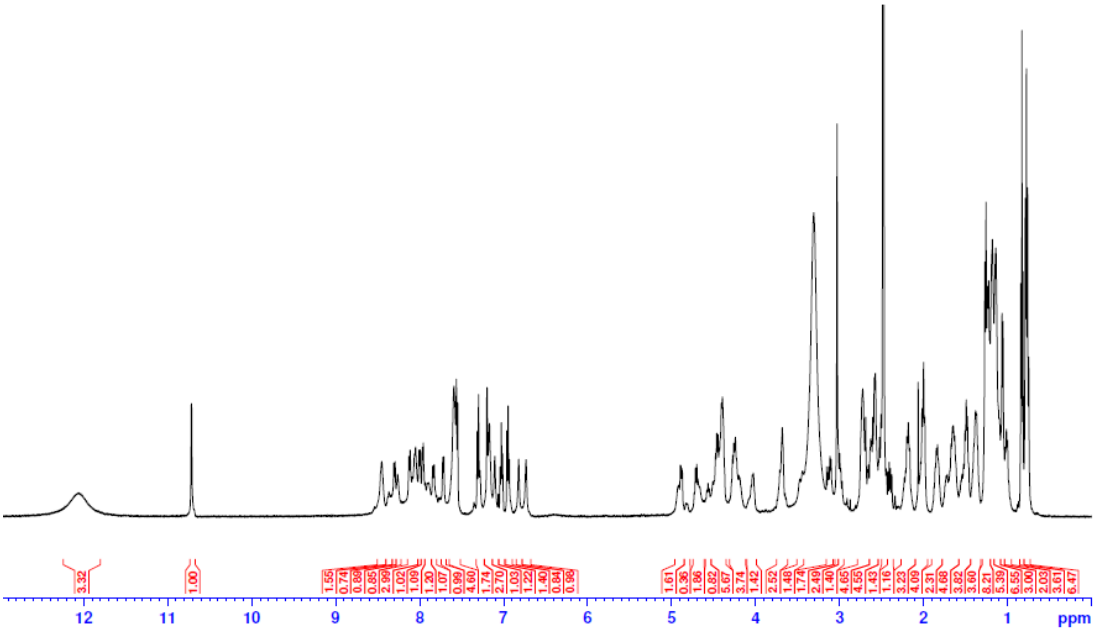

Figure A.24: ^{1}H-NMR spectrum of peptide **3.33** (500 MHz, DMSO-d_6).

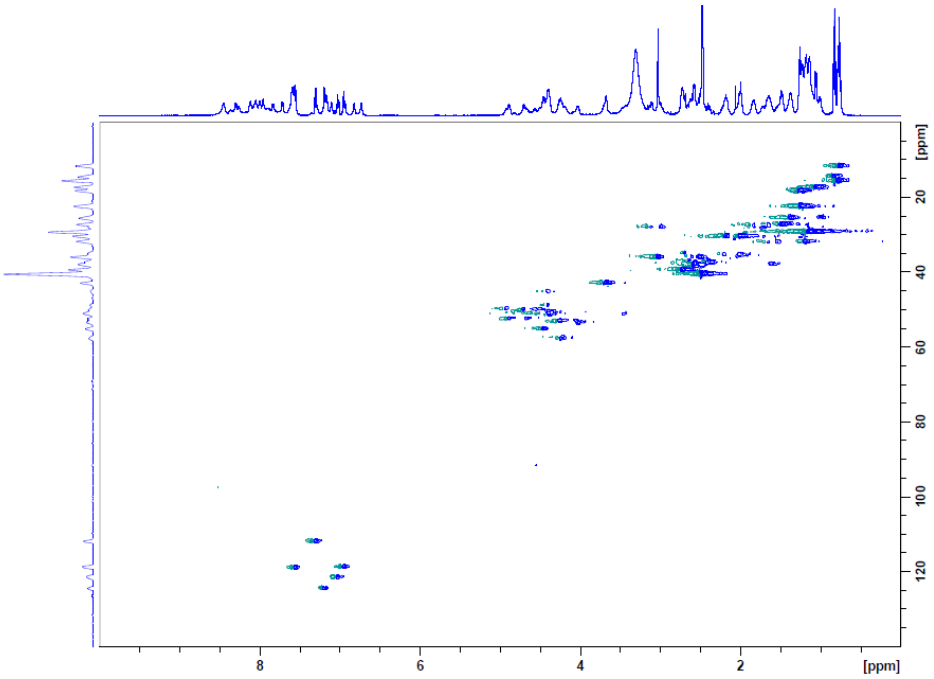

Figure A.25: ^{1}H-^{13}C HSQC spectrum of peptide **3.33** (500 MHz, DMSO-d_6).

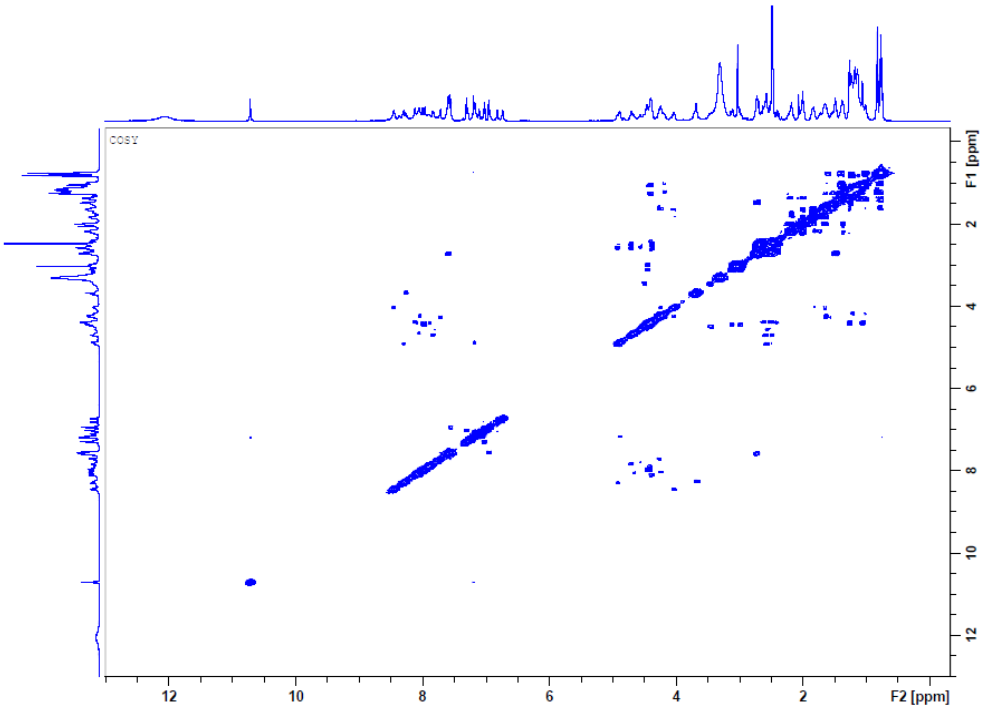

Figure A.26: ^{1}H-COSY spectrum of peptide **3.33** (500 MHz, DMSO-d_6).

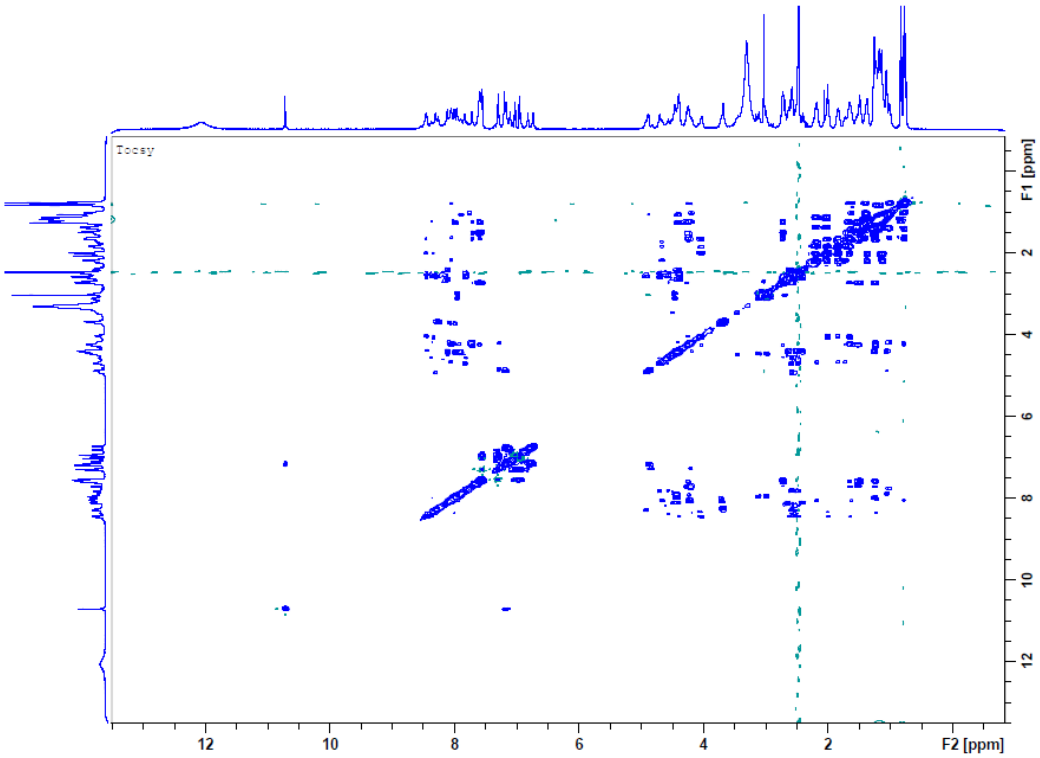

Figure A.27: ^{1}H-TOCSY spectrum of peptide **3.33** (500 MHz, DMSO-d_6).

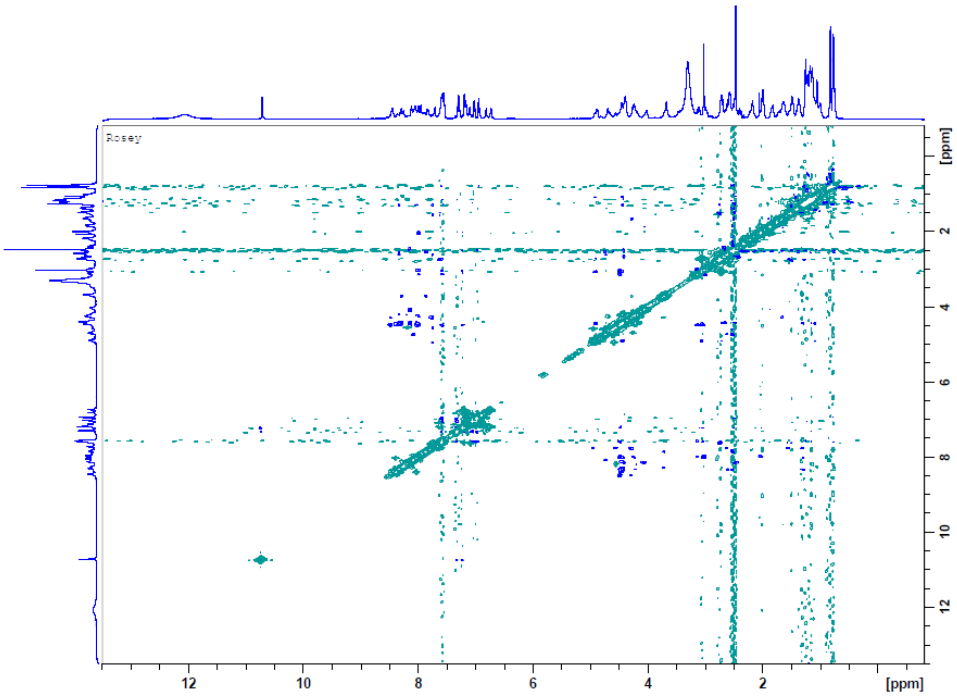

Figure A.28: ^{1}H-ROESY spectrum of peptide **3.33** (500 MHz, DMSO-d_6).

Table A.3: HSQC Peak Coordinates for peptides **3.32** and **3.33**.

	A54145A$_1$-Asn3-DABA4-Asp9 (peptide **3.33**) (500 MHz, DMSO)			A54145A$_1$-Asn3-Ser4-Asp9 (peptide **3.32**) (500 MHz, DMSO)		
		^{1}H	^{13}C		^{1}H	^{13}C
Trp^1	N^{α}-H	7.98	---	N^{α}-H	7.86	---
	$C^{\alpha}H$	4.45	55.0	$C^{\alpha}H$	**4.54**	**50.2**
	$C^{\beta}H_2$	2.99, 3.11	27.9	$C^{\beta}H_2$	3.11, 2.96	28.2
	N^1H	10.71	---	N^1H	10.70	---
	C^2H	7.20	124.5	C^2H	7.09	123.9
	C^4H	7.56	118.8	C^4H	7.55	119.0
	C^5H	6.95	118.7	C^5H	6.95	118.5
	C^6H	7.03	121.4	C^6H	7.02	121.5
	C^7H	7.31	111.8	C^7H	7.29	111.7
D-Glu^2	N^{α}-H	8.45	---	N^{α}-H	8.10	---
	$C^{\alpha}H$	4.03	53.3	$C^{\alpha}H$	4.12 [4.05]	53.2
	$C^{\beta}H_2$	1.84, 1.65	26.6	$C^{\beta}H_2$	1.83, 1.66	**27.9**
	$C^{\gamma}H_2$	2.00	30.4	$C^{\gamma}H_2$	2.04	30.3
	COOH	12.1	---	COOH	12.1	---
Asn^3	N^{α}-H	8.12	---	N^{α}-H	**8.10**	---
	$C^{\alpha}H$	4.42	50.8	$C^{\alpha}H$	**4.55**	**50.1**
	$C^{\beta}H$	2.66, 2.43 [a]	36.9	$C^{\beta}H_2$	**2.65-2.45**	**36.6/37.7**
	$CONH_2$	6.73, 7.18	---	$CONH_2$	7.17, 6.76	---
DABA^4 or Ser^4	N^{α}-H	7.19	---	N^{α}-H	8.10 [8.01]	---
	$C^{\alpha}H$	4.89	52.4	$C^{\alpha}H$	5.00 [4.90]	48.1
	$C^{\beta}H$	4.41	48.7	$C^{\beta}H_2$	4.24, 4.17 [4.39, 4.02]	63.5 [63.6]
	$C^{\gamma}H_3$	1.07	17.3			
	N^{γ}-H	7.21	---	---	---	---
Sar^5	N^{α}-CH_3	3.03	36.0	N^{α}-CH_3	3.06	36.7
	$C^{\alpha}H_2$	4.04, 4.26	53.0	$C^{\alpha}H_2$	3.63, 4.39	54.1
Ala^6	N^{α}-H	8.02	---	N^{α}-H	7.96 [7.93]	---
	$C^{\alpha}H$	4.41	48.7	$C^{\alpha}H$	4.24 [4.32]	49.2
	$C^{\beta}H_3$	1.26	18.3	$C^{\beta}H_3$	1.21 [1.24]	18.2
Asp^7	N^{α}-H	8.30	---	N^{α}-H	**8.10**	---
	$C^{\alpha}H$	4.56	49.9	$C^{\alpha}H$	**4.55**	**50.1**
	$C^{\beta}H_2$	**2.59, 2.54** [a]	**38.0**	$C^{\beta}H_2$	**2.65-2.45**	**36.6/37.7**
	COOH	12.1	---	COOH	12.1	---
D-Lys^8	N^{α}-H	8.05	---	N^{α}-H	7.87	---
	$C^{\alpha}H$	4.25	53.0	$C^{\alpha}H$	4.17	53.1
	$C^{\beta}H_2$	1.64, 1.56	32.0	$C^{\beta}H_2$	1.59, 1.52	31.1
	$C^{\gamma}H_2$	**1.25**	**22.4**	$C^{\gamma}H_2$	1.28	22.4
	$C^{\delta}H_2$	1.50	27.2	$C^{\delta}H_2$	1.50	27.1
	$C^{\varepsilon}H_2$	2.73	39.2	$C^{\varepsilon}H_2$	2.73	39.3
	$N^{\varepsilon}H_2$	7.60	---	$N^{\varepsilon}H_2$	7.60	---
Asp^9	N^{α}-H	7.83	---	N^{α}-H	**8.10**	---
	$C^{\alpha}H$	4.71	50.0	$C^{\alpha}H$	**4.55**	**50.1**
	$C^{\beta}H_2$	**2.59, 2.49** [a]	**38.0**	$C^{\beta}H_2$	**2.65-2.45**	**36.6/37.7**
	COOH	12.1	---	COOH	12.1	---

Table A.3 (continued): HSQC Peak Coordinates for peptides **3.32** and **3.33**.

	A5A$_1$-Asn3-DABA4-Asp9 (**5**) (500 MHz, DMSO)			A5A$_1$-Asn3-S4-Asp9 (**6**) (500 MHz, DMSO)		
		^{1}H	^{13}C		^{1}H	^{13}C
Gly^{10}	N$^{\alpha}$-H	8.26	---	N$^{\alpha}$-H	7.96	---
	C$^{\alpha}$H$_2$	3.69	42.9	C$^{\alpha}$H$_2$	3.65, 3.76	42.8
D-Asn^{11}	N$^{\alpha}$-H	8.44	---	N$^{\alpha}$-H	**8.10**	---
	C$^{\alpha}$H	4.40	48.7	C$^{\alpha}$H	**4.55**	**50.1**
	C$^{\beta}$H$_2$	2.61, 2.54[a]	36.0	C$^{\beta}$H$_2$	**2.65-2.45**	**36.6/37.7**
	CONH$_2$	6.83, 7.10	---	CONH$_2$	7.23, 6.81	---
Glu^{12}	N$^{\alpha}$-H	8.07	---	N$^{\alpha}$-H	8.29	---
	C$^{\alpha}$H	4.68	52.4	C$^{\alpha}$H	4.33	52.3
	C$^{\beta}$H$_2$	1.84, 1.74	28.1	C$^{\beta}$H$_2$	1.73, 1.89	**27.9**
	C$^{\gamma}$H$_2$	2.17	30.3	C$^{\gamma}$H$_2$	2.17	31.0
	COOH	12.1	---	COOH	12.1	---
Ile^{13}	N$^{\alpha}$-H	8.04	---	N$^{\alpha}$-H	7.96	---
	C$^{\alpha}$H	4.22	57.5	C$^{\alpha}$H	4.29	52.2
	C$^{\beta}$H	1.63	27.5	C$^{\beta}$H	1.77	27.9
	C$^{\gamma}$H$_2$	1.40, 1.01	25.3	C$^{\gamma}$H$_2$	1.38, 1.12	25.6
	C$^{\delta}$H$_3$	0.78	11.6	C$^{\delta}$H$_3$	0.80 [0.77]	11.7
	C$^{\gamma}$H$_3$	0.77	15.5	C$^{\gamma}$H$_3$	0.80	15.6
Dec^0	C^{2}H$_2$	2.21, 2.03	35.3	C^{2}H$_2$	2.04	35.8
	C^{3}H$_2$	1.37	25.5	C^{3}H$_2$	1.37	25.6
	C^{4}H$_2$	**1.2-1.1**	**31.7/29.2**	C^{4}H$_2$	**1.2-1.1**	**31.7/29.1**
	C^{5}H$_2$	**1.2-1.1**	**31.7/29.2**	C^{5}H$_2$	**1.2-1.1**	**31.7/29.1**
	C^{6}H$_2$	**1.2-1.1**	**31.7/29.2**	C^{6}H$_2$	**1.2-1.1**	**31.7/29.1**
	C^{7}H$_2$	**1.2-1.1**	**31.7/29.2**	C^{7}H$_2$	**1.2-1.1**	**31.7/29.1**
	C^{8}H$_2$	**1.2-1.1**	**31.7/29.2**	C^{8}H$_2$	**1.2-1.1**	**31.7/29.1**
	C^{9}H$_2$	**1.23**	**22.4**	C^{9}H$_2$	1.24	22.4
	C^{10}H$_3$	0.83	14.5	C^{10}H$_3$	0.83	14.4

Note: bolded peaks overlap with one or more other peaks.

[a] Partial overlap with DMSO-d$_6$ solvent residual peak.

Appendix B: Analytical HPLC Data of Purified Peptides

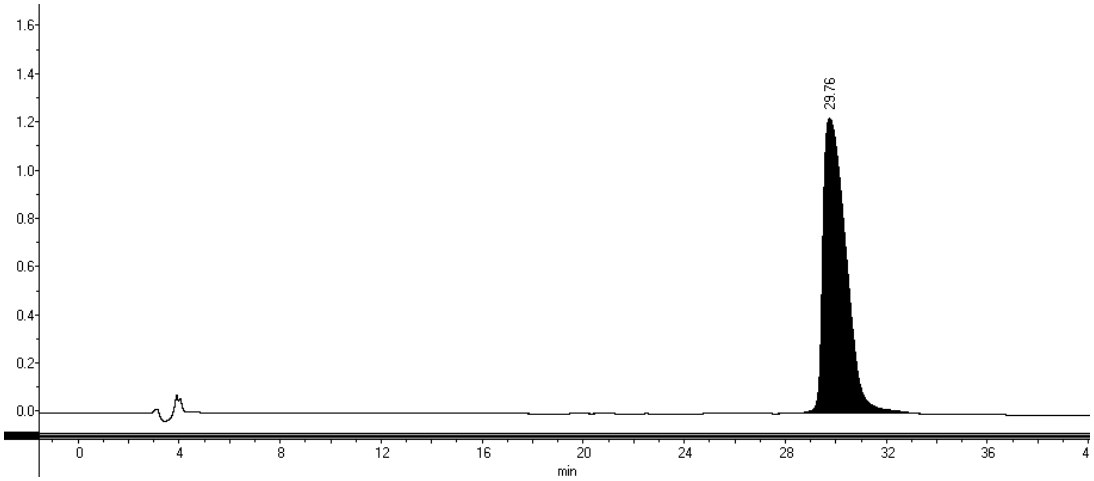

Figure B.1: HPLC chromatogram of pure A54145D-*t*HOAsn3-*t*MeOAsp9. Gradient: 30:70 MeCN:H_2O (+0.1% TFA) to 50:50 MeCN:H_2O (+ 0.1% TFA) in 40 min (λ = 220 nm).

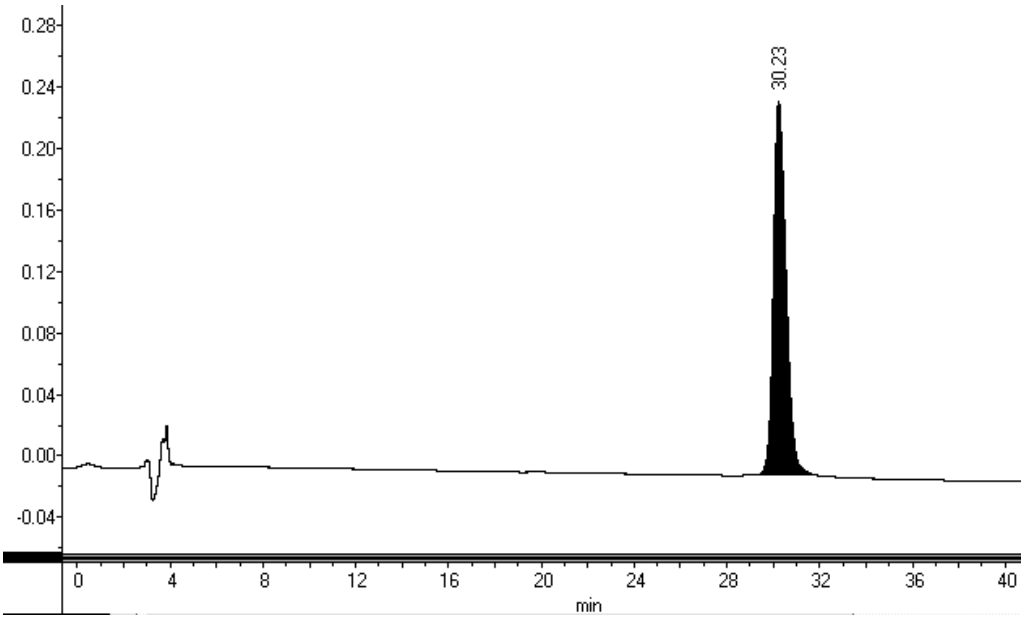

Figure B.2: HPLC chromatogram of pure synthetic A54145D (1.11). This peptide corresponds to A54145D-*t*HOAsn3-*e*MeOAsp9. Gradient: 30:70 MeCN:H_2O (+0.1% TFA) to 50:50 MeCN:H_2O (+ 0.1% TFA) in 40 min (λ = 220 nm).

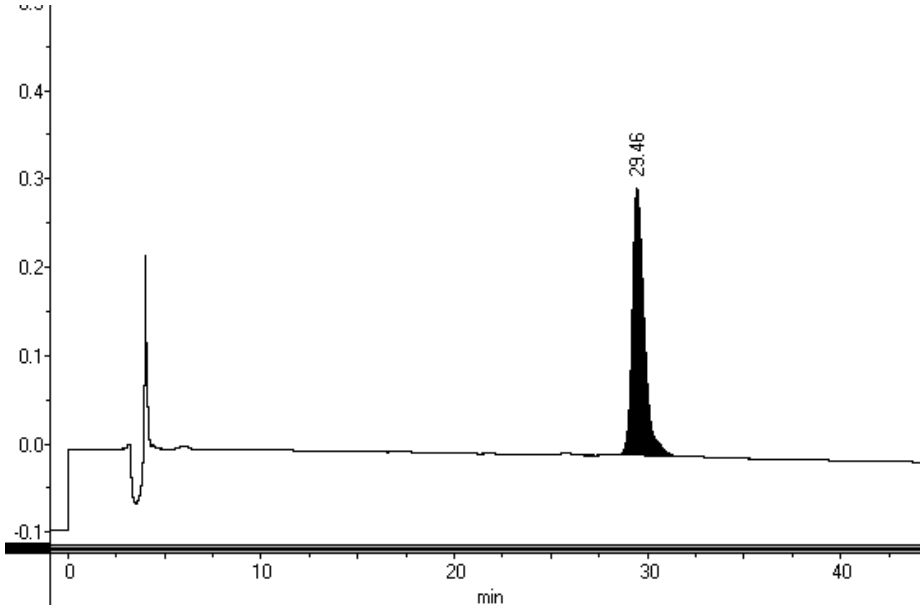

Figure B.3: HPLC chromatogram of pure A54145D-(8*S*)-*anteiso*. Gradient: 30:70 MeCN:H_2O (+0.1% TFA) to 50:50 MeCN:H_2O (+ 0.1% TFA) in 40 min (λ = 220 nm).

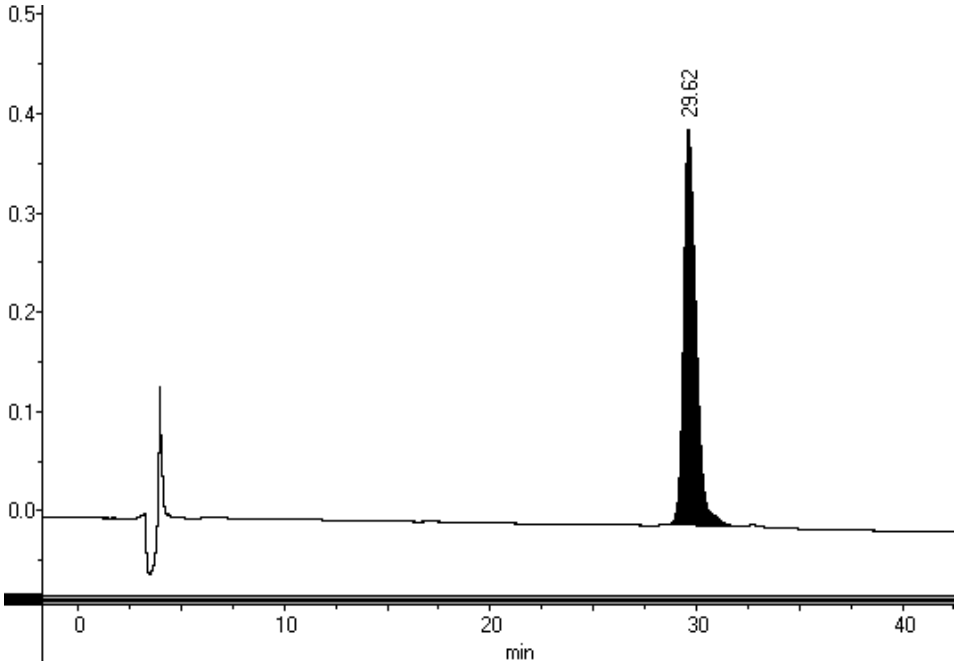

Figure B.4: HPLC chromatogram of pure A54145D-(8*R*)-*anteiso*. Gradient: 30:70 MeCN:H_2O (+0.1% TFA) to 50:50 MeCN:H_2O (+ 0.1% TFA) in 40 min (λ = 220 nm).

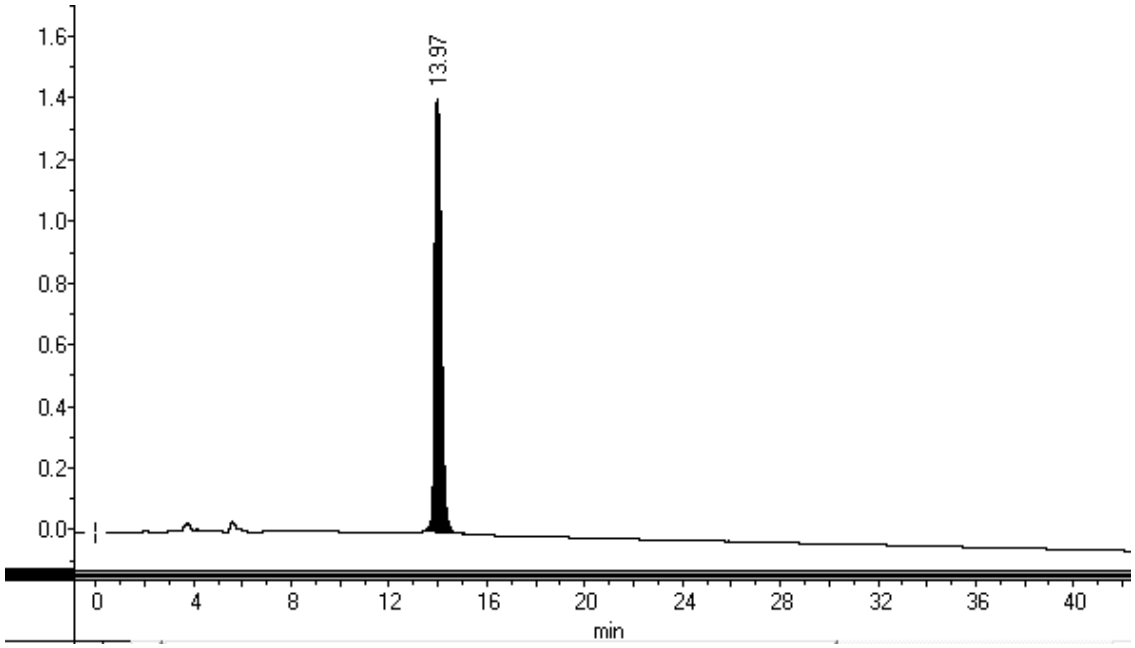

Figure B.5: HPLC chromatogram of pure A54145D-nucleus. Gradient: 10:90 MeCN:H_2O (+0.1% TFA) to 90:10 MeCN:H_2O (+ 0.1% TFA) in 40 min (λ = 220 nm).

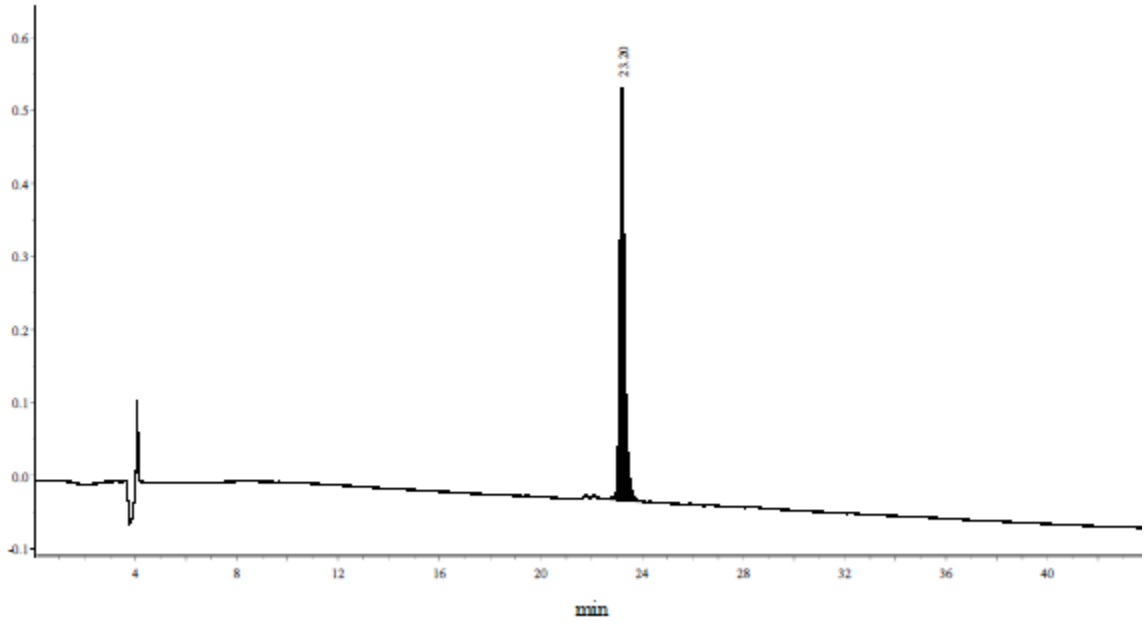

Figure B.6: HPLC chromatogram of pure A54145A_1-Asn3-DAPA4-Asp9 (**3.2**). Gradient: 10:90 MeCN:H_2O (+0.1% TFA) to 90:10 MeCN:H_2O (+ 0.1% TFA) in 40 min (λ = 220 nm).

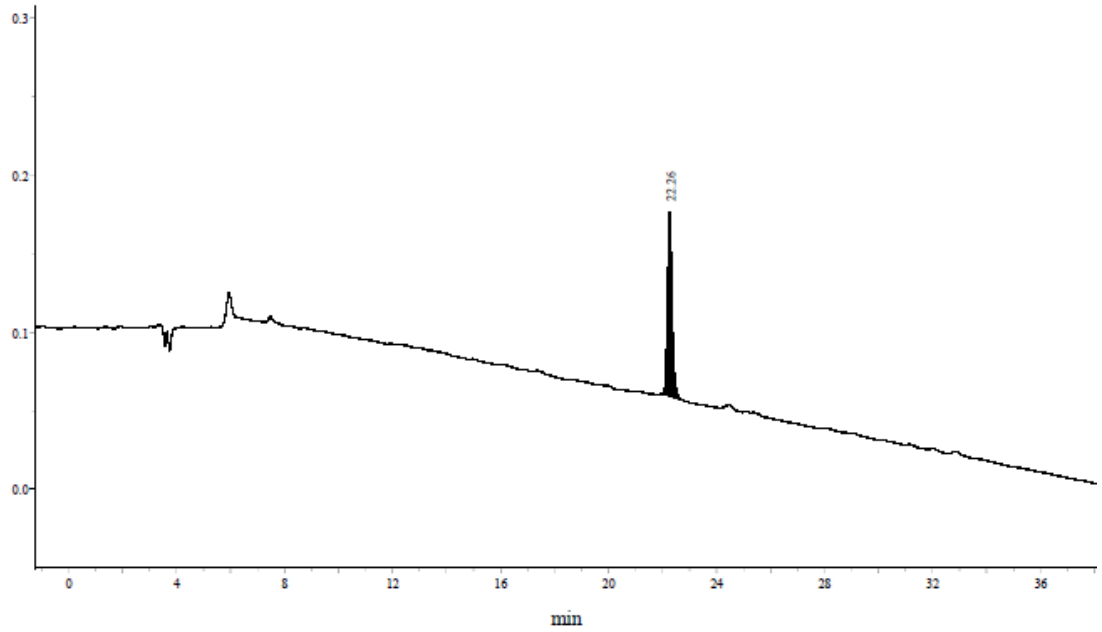

Figure B.7: HPLC chromatogram of pure A54145A$_1$-Asn3-Asp9 (**3.3**). Gradient: 10:90 MeCN:H_2O (+0.1% TFA) to 90:10 MeCN:H_2O (+ 0.1% TFA) in 40 min (λ = 220 nm).

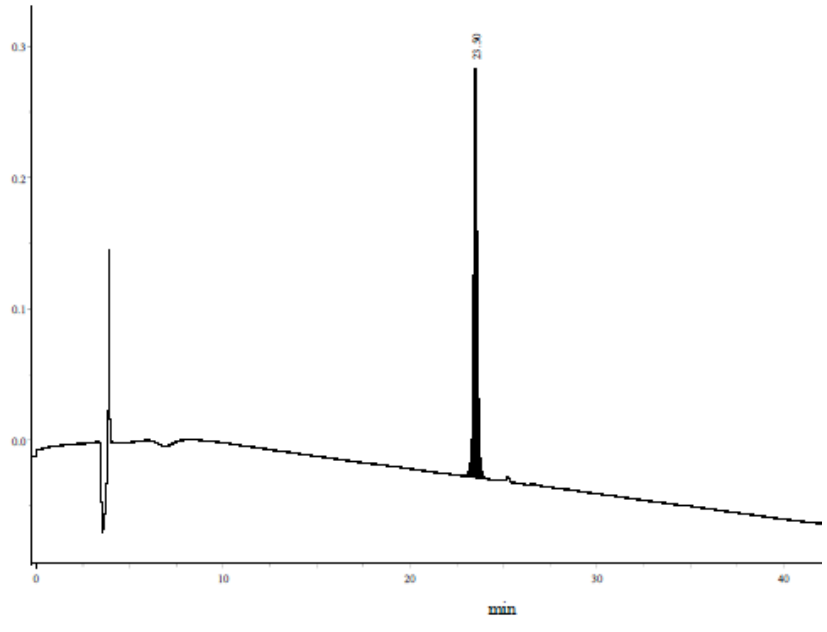

\

Figure B.8: HPLC chromatogram of pure A54145A$_1$-Asn3-Ser4-Asp9 (**3.32**). Gradient: 10:90 MeCN:H_2O (+0.1% TFA) to 90:10 MeCN:H_2O (+ 0.1% TFA) in 40 min (λ = 220 nm).

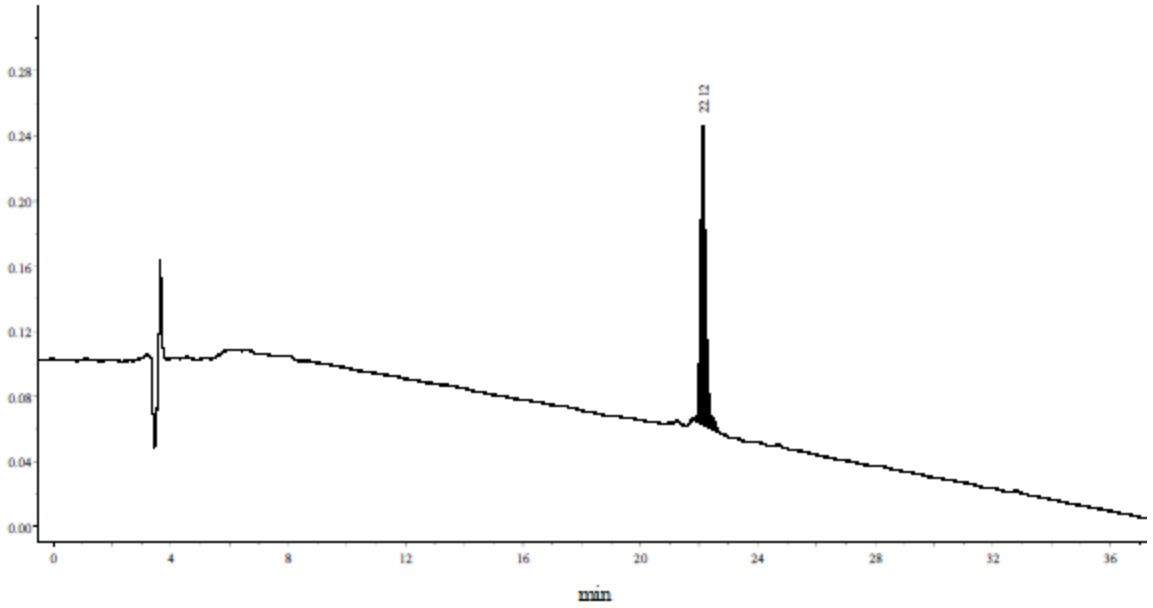

Figure B.9: HPLC chromatogram of pure A54145A$_1$-Asn3-DABA4-Asp9 (**3.33**). Gradient: 10:90 MeCN:H_2O (+0.1% TFA) to 90:10 MeCN:H_2O (+ 0.1% TFA) in 40 min (λ = 220 nm).

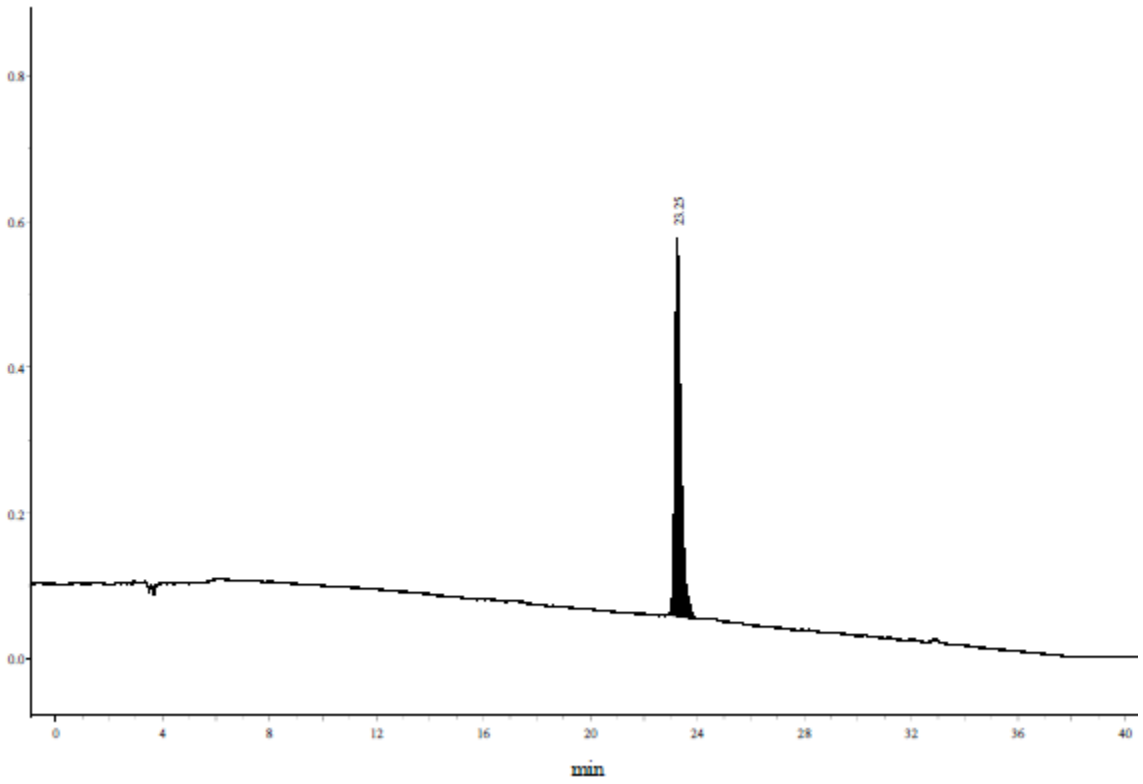

Figure B.10: HPLC chromatogram of pure A54145D-Asn3 (**3.44**). Gradient: 10:90 MeCN:H_2O (+0.1% TFA) to 90:10 MeCN:H_2O (+ 0.1% TFA) in 40 min (λ = 220 nm).

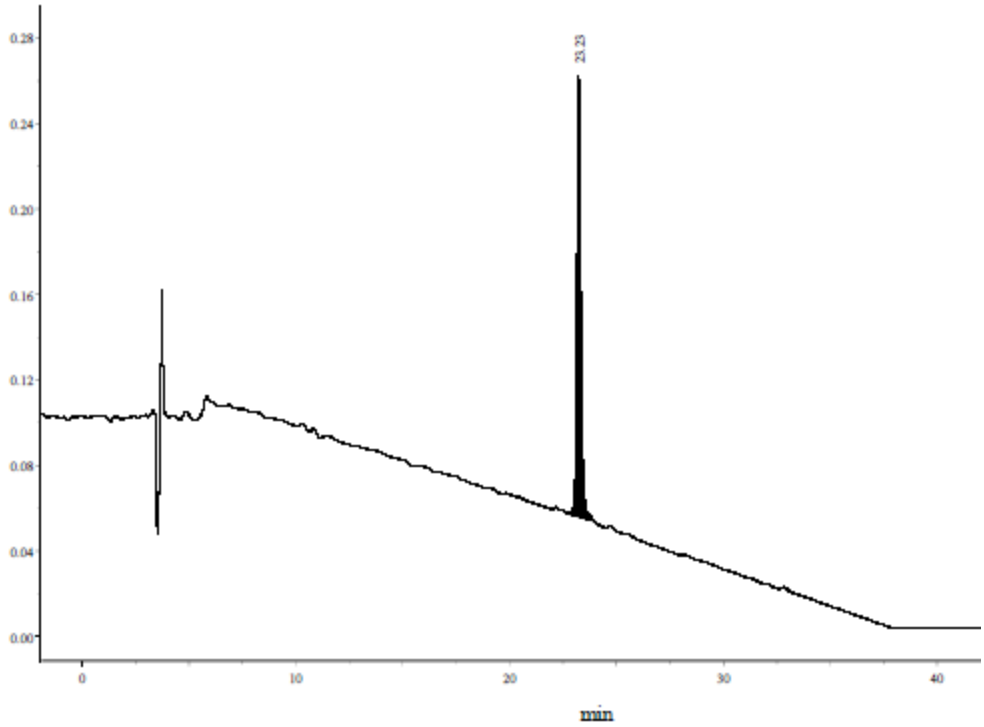

Figure B.11: HPLC chromatogram of pure A54145D-Asp9 (**3.45**). Gradient: 10:90 MeCN:H_2O (+0.1% TFA) to 90:10 MeCN:H_2O (+ 0.1% TFA) in 40 min (λ = 220 nm).

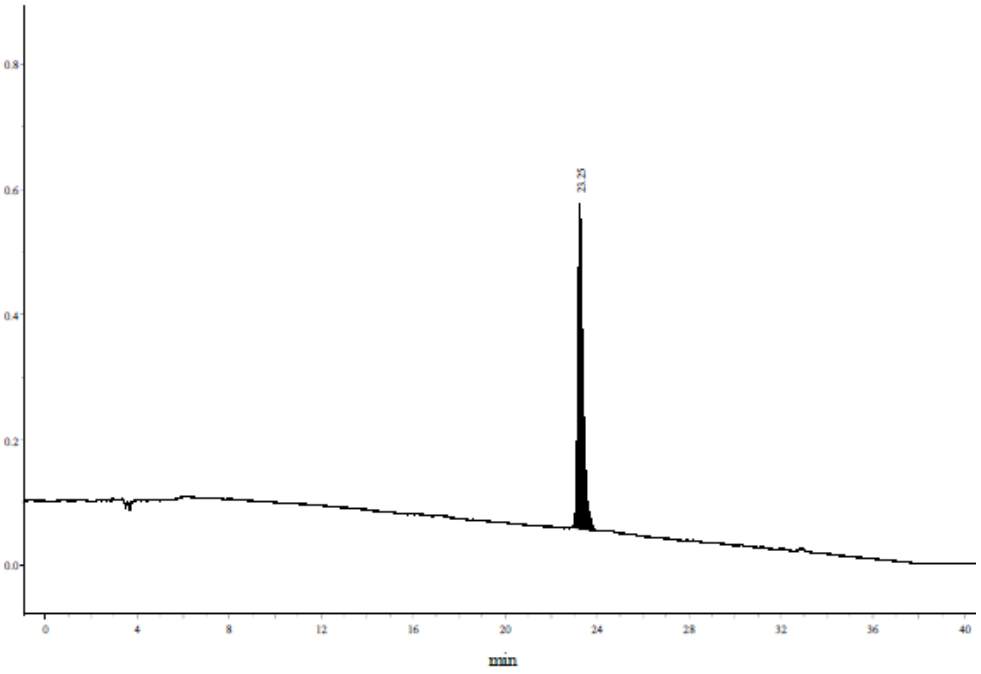

Figure B.12: HPLC chromatogram of pure synthetic A54145A_1 (**1.7**). Gradient: 10:90 MeCN:H_2O (+0.1% TFA) to 90:10 MeCN:H_2O (+ 0.1% TFA) in 40 min (λ = 220 nm).

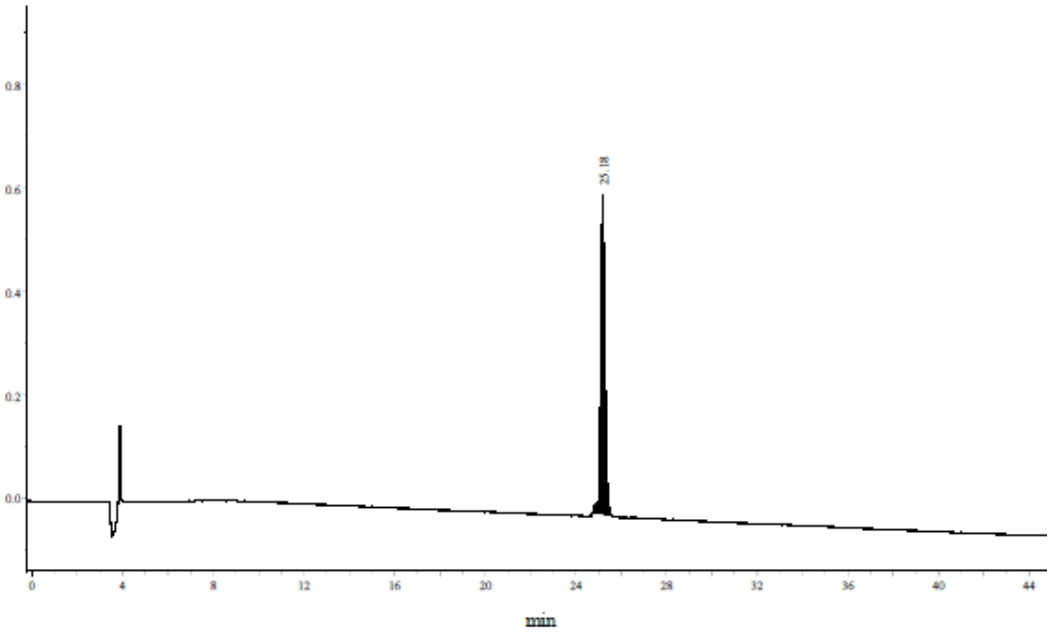

Figure B.13: HPLC chromatogram of pure 8-methyldecanoyl-daptomycin (**3.46**). Gradient: 10:90 MeCN:H_2O (+0.1% TFA) to 90:10 MeCN:H_2O (+ 0.1% TFA) in 40 min (λ = 220 nm).

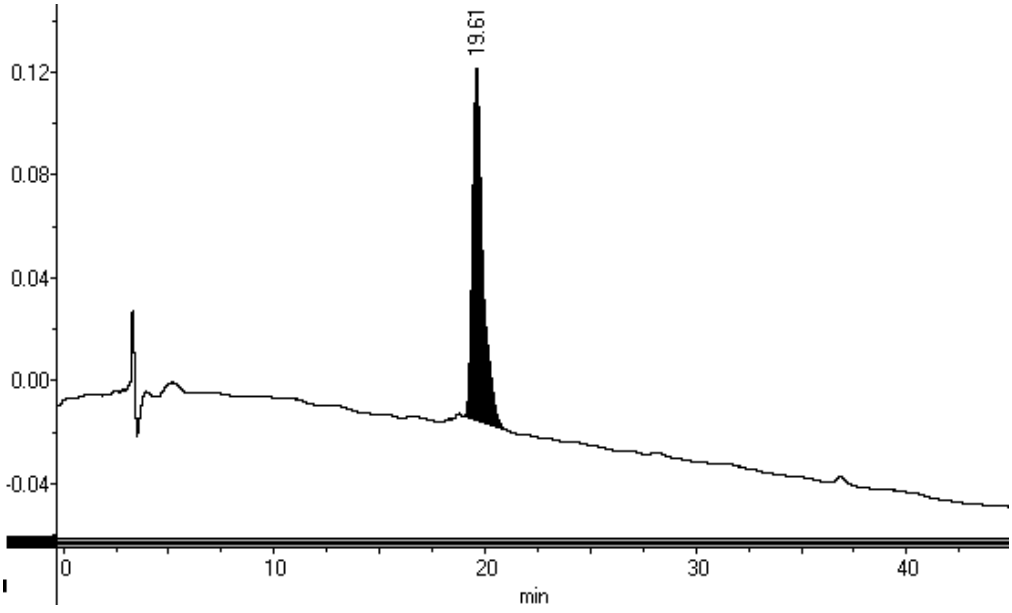

Figure B.14: HPLC chromatogram of pure 10-methyldodecanoyl-daptomycin (**3.47**). Gradient: 40:60 MeCN:H_2O (+0.1% TFA) to 70:30 MeCN:H_2O (+ 0.1% TFA) in 40 min (λ = 220 nm).

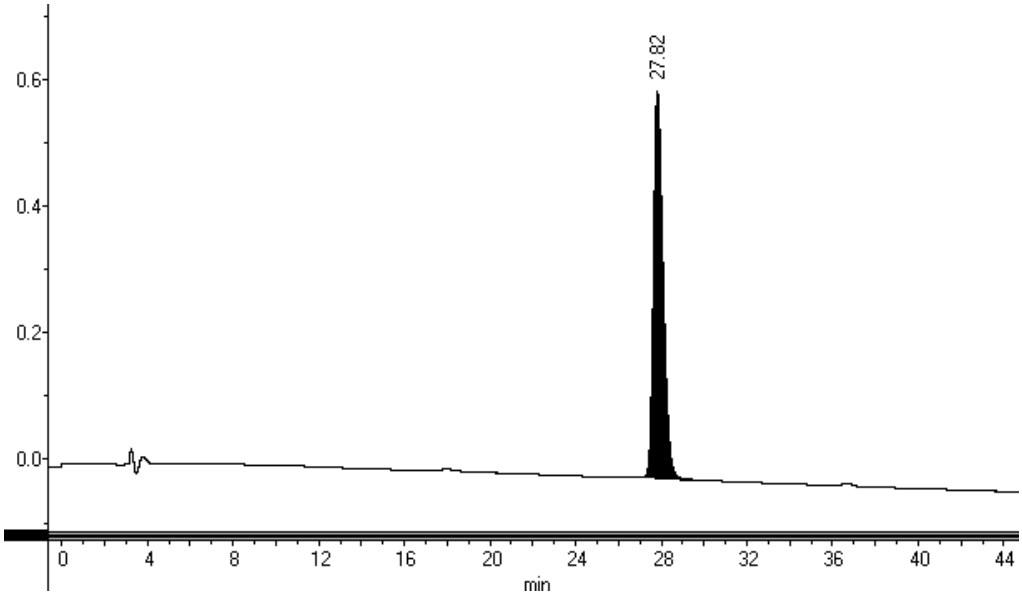

Figure B.15: HPLC chromatogram of pure pentadecanoyl-daptomycin (**3.48**). Gradient: 40:60 MeCN:H_2O (+0.1% TFA) to 70:30 MeCN:H_2O (+ 0.1% TFA) in 40 min (λ = 220 nm).

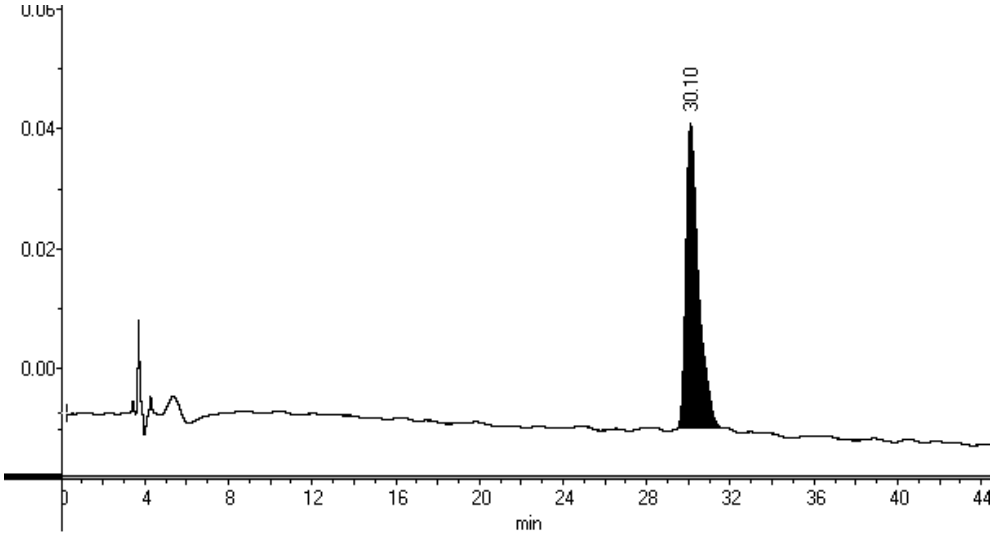

Figure B.16: HPLC chromatogram of pure 10,10,10-trifluorodecanoyl-daptomycin (**4.5**). Gradient: 30:70 MeCN:H_2O (+0.1% TFA) to 37:63 MeCN:H_2O (+ 0.1% TFA) in 40 min (λ = 220 nm).

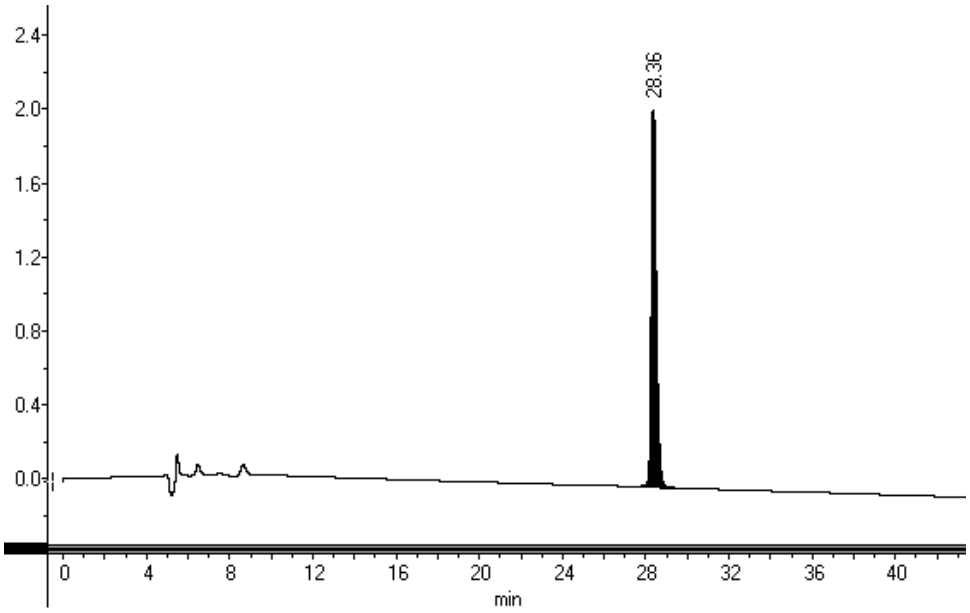

Figure B.17: HPLC chromatogram of pure Dap(^{TFM}benzyl)Orn6-daptomycin (**4.6**). Gradient: 10:90 MeCN:H_2O (+0.1% TFA) to 90:10 MeCN:H_2O (+ 0.1% TFA) in 40 min (λ = 220 nm).

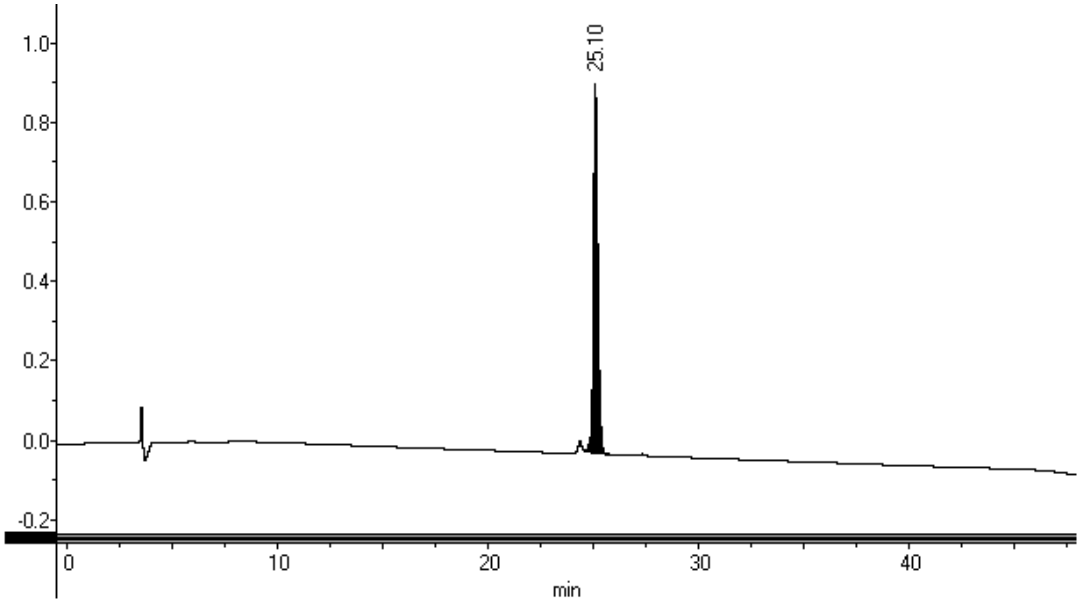

Figure B.18: HPLC chromatogram of pure Dap(^{TF}ethyl)Orn6-daptomycin (**4.7**). Gradient: 10:90 MeCN:H_2O (+0.1% TFA) to 90:10 MeCN:H_2O (+ 0.1% TFA) in 40 min (λ = 220 nm).

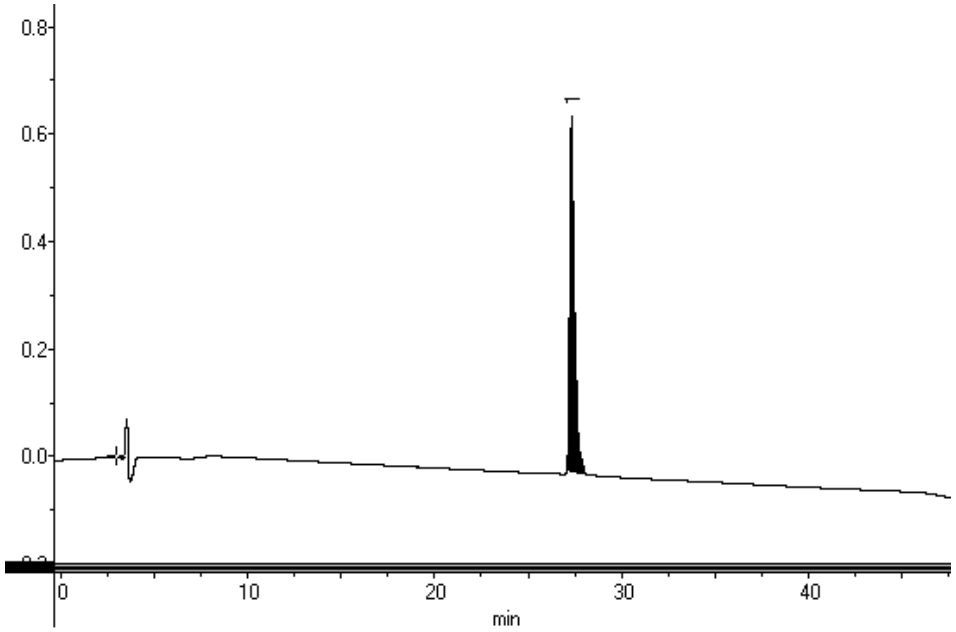

Figure B.19: HPLC chromatogram of pure Dap-(^{TFM}benzoyl)Orn6 (**4.8**). Gradient: 10:90 MeCN:H_2O (+0.1% TFA) to 90:10 MeCN:H_2O (+ 0.1% TFA) in 40 min (λ = 220 nm).

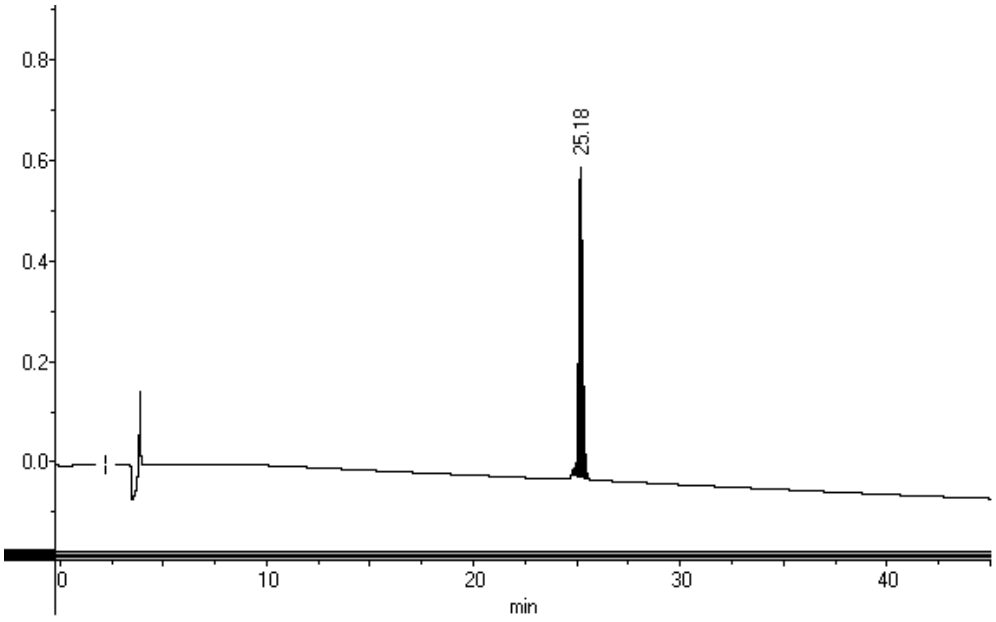

Figure B.20: HPLC chromatogram of pure Dap-(^{TF}acetyl)Orn6 (**4.9**). Gradient: 10:90 MeCN:H_2O (+0.1% TFA) to 90:10 MeCN:H_2O (+ 0.1% TFA) in 40 min (λ = 220 nm).

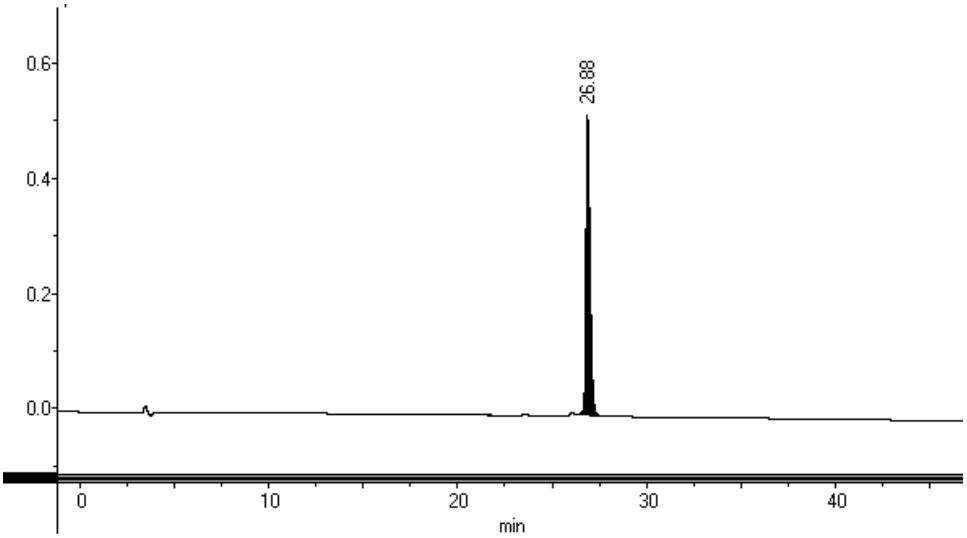

Figure B.21: HPLC chromatogram of pure Dap-^{TFM}Phe1-Lys6-Glu12-Trp13 (**4.15**). Gradient: 10:90 MeCN:H_2O (+0.1% TFA) to 90:10 MeCN:H_2O (+ 0.1% TFA) in 40 min (λ = 220 nm).

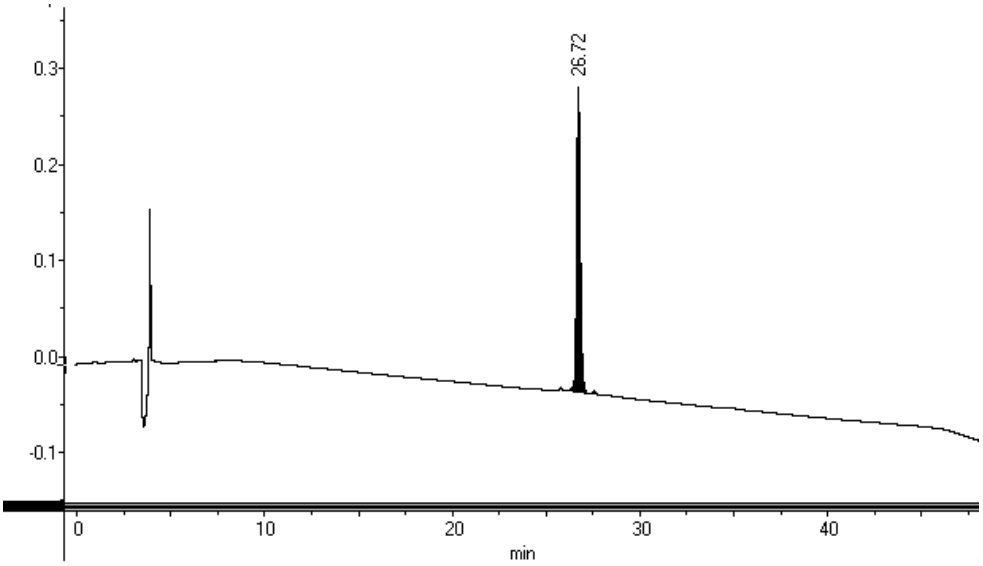

Figure B.22: HPLC chromatogram of pure Dap-Lys6-*D*-Ser(CF_3)11-Glu12-Trp13 (**4.38**). Gradient: 10:90 MeCN:H_2O (+0.1% TFA) to 90:10 MeCN:H_2O (+ 0.1% TFA) in 40 min (λ = 220 nm).

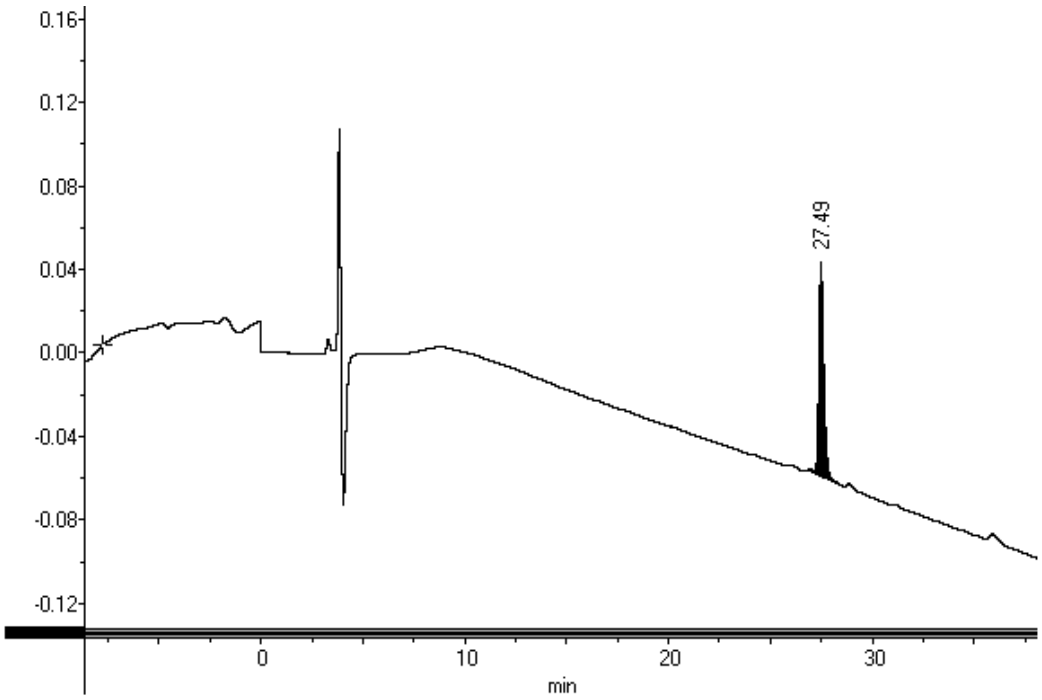

Figure B.23: HPLC chromatogram of pure Dap-Lys6-*D*-hCys(CF_3)8-Glu12-Trp13 (**4.55**). Gradient: 10:90 MeCN:H_2O (+0.1% TFA) to 90:10 MeCN:H_2O (+ 0.1% TFA) in 40 min (λ = 220 nm).

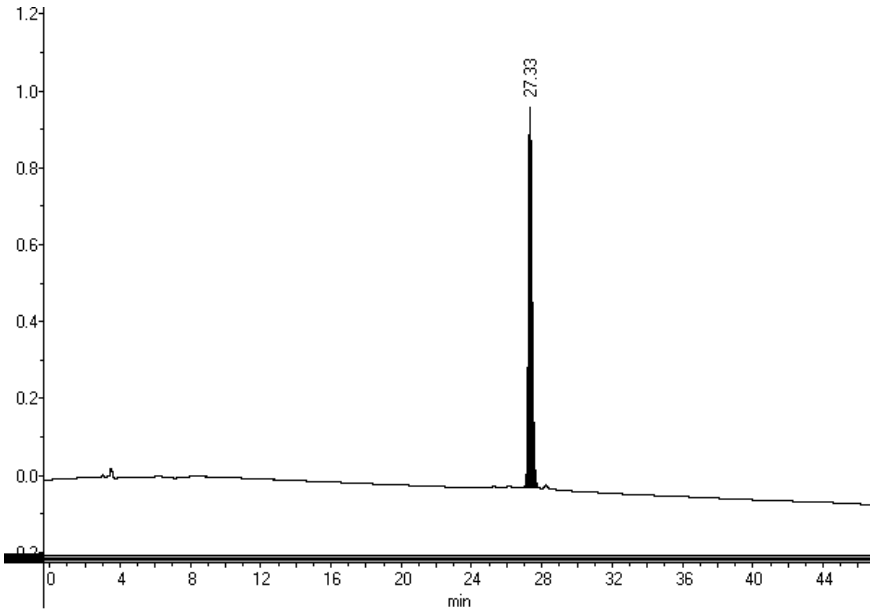

Figure B.24: HPLC chromatogram of pure Dap-Lys6-*D*-hCys(CF_3)11-Glu12-Trp13 (**4.56**). Gradient: 10:90 MeCN:H_2O (+0.1% TFA) to 90:10 MeCN:H_2O (+ 0.1% TFA) in 40 min (λ = 220 nm).

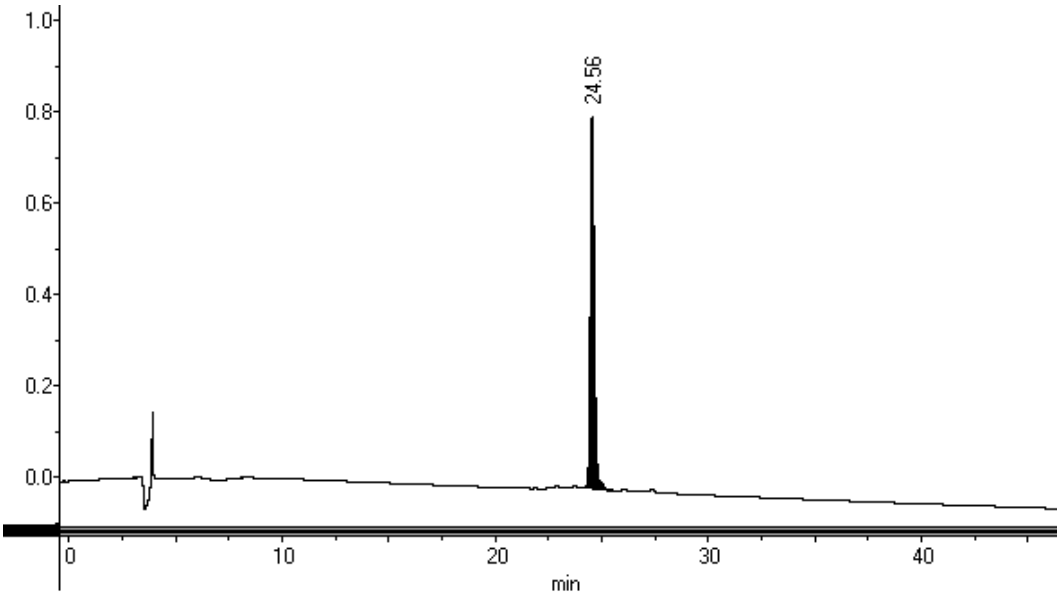

Figure B.25: HPLC chromatogram of pure Dap-^{TF}Dec0-Lys6-Glu12-Trp13 (**4.57**). Gradient: 10:90 MeCN:H_2O (+0.1% TFA) to 90:10 MeCN:H_2O (+ 0.1% TFA) in 40 min (λ = 220 nm).

Appendix C: HRMS Characterization Data of Purified Peptides

A

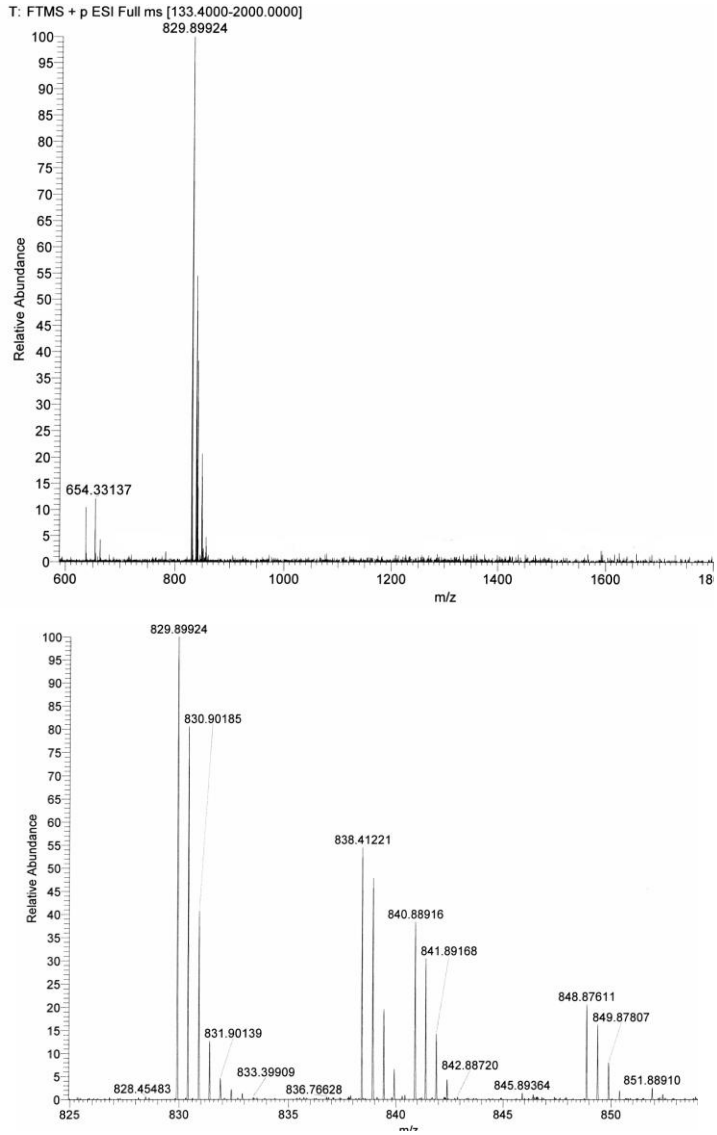

B

Elemental composition search on mass 829.89924

m/z= 824.89924-834.89924

m/z	Theo. Mass	Delta (ppm)	RDB equiv.	Composition
829.89924	829.89904	0.24	26.0	$C_{73}H_{113}O_{27}N_{17}$
	829.89993	-0.83	22.0	$C_{73}H_{118}O_{26}N_{15}K$
	829.89356	6.84	27.5	$C_{75}H_{112}O_{25}N_{16}Na$
	829.89343	7.01	26.0	$C_{74}H_{113}O_{28}N_{15}$
	829.90533	-7.34	25.5	$C_{74}H_{115}O_{27}N_{16}$

Figure C.1: HRMS data for A54145D-*t*HOAsn3-*t*MeOAsp9. (A) ESI^+ HRMS for A54145D-*t*HOAsn3-*t*MeOAsp9. The peak at *m/z* = 829.89924 corresponds to the $[M+2H]^+$ species. The peak at *m/z* = 838.41221 corresponds to the $[M+H+NH_4]^+$ species. The peak at *m/z* = 840.88916 corresponds to the $[M+H+Na]^+$ species. The peak at *m/z* = 848.87611 corresponds to the $[M+H+K]^+$ species. (B) HRMS data for the peak at *m/z* = 829.89924 is also shown.

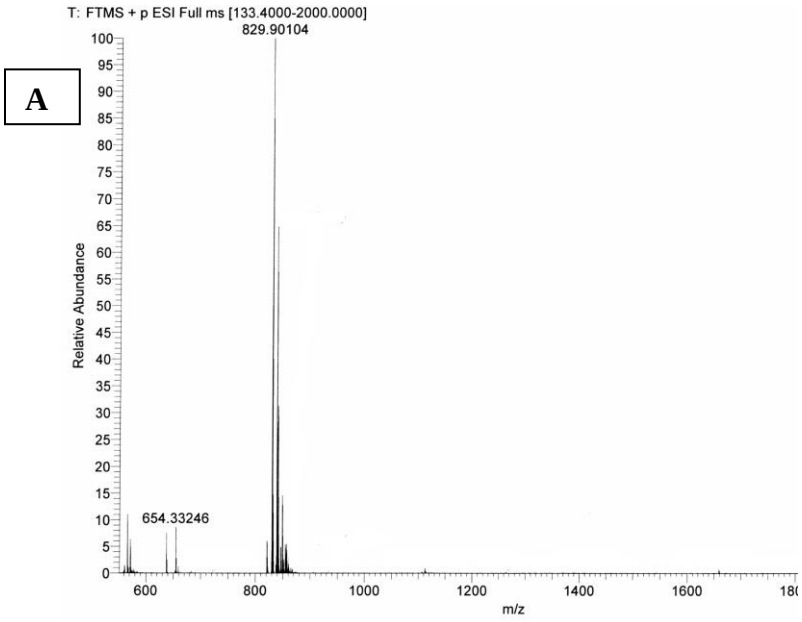

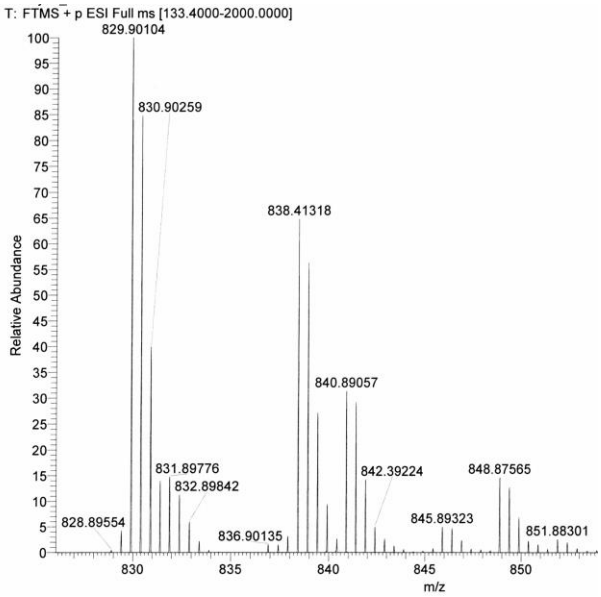

B

Elemental composition search on mass 829.90104

m/z= 824.90104-834.90104

m/z	Theo. Mass	Delta (ppm)	RDB equiv.	Composition
829.90104	829.89993	1.34	22.0	$C_{73}H_{118}O_{26}N_{15}K$
	829.89904	2.41	26.0	$C_{73}H_{113}O_{27}N_{17}$
	829.90533	-5.17	25.5	$C_{74}H_{115}O_{27}N_{16}$
	829.89356	9.01	27.5	$C_{75}H_{112}O_{25}N_{16}Na$
	829.89343	9.18	26.0	$C_{74}H_{113}O_{28}N_{15}$

Figure C.2: HRMS data for synthetic A54145D. This peptide corresponds to A54145D-*t*HOAsn3-*e*MeOAsp9. (A) ESI^+ HRMS for A54145D. The peak at *m/z* = 829.90104 corresponds to the $[M+2H]^+$ species. The peak at *m/z* = 838.41318 corresponds to the $[M+H+NH_4]^+$ species. The peak at *m/z* = 840.89057 corresponds to the $[M+H+Na]^+$ species. The peak at *m/z* = 848.87565 corresponds to the $[M+H+K]^+$ species. (B) HRMS data for the peak at *m/z* = 829.90104 is also shown.

A

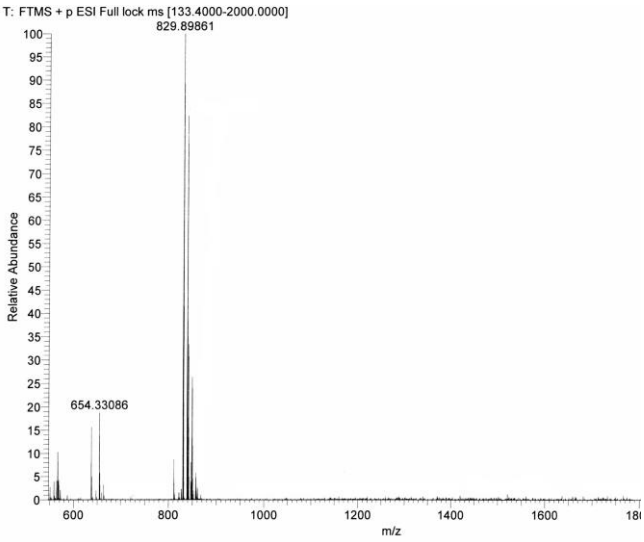

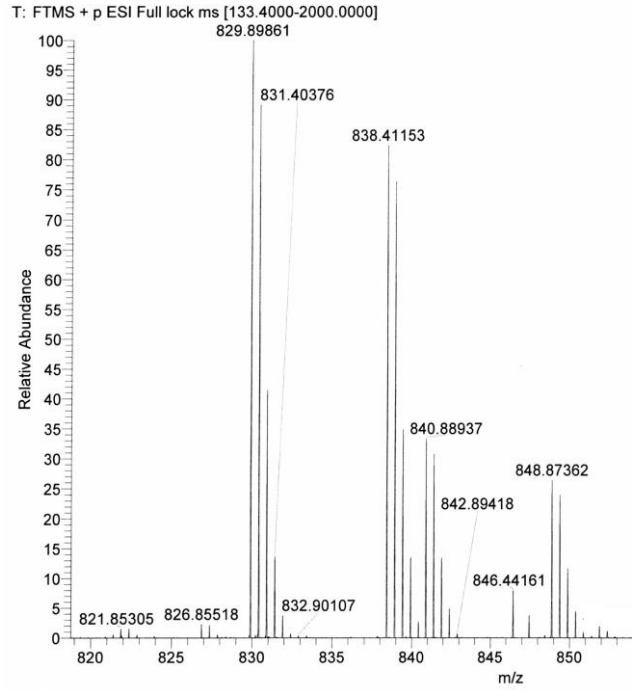

B

Elemental composition search on mass 829.89861

m/z= 824.89861-834.89861

m/z	Theo. Mass	Delta (ppm)	RDB equiv.	Composition
829.89861	829.89837	0.29	26.5	$C_{71}H_{111}O_{26}N_{20}$
	829.89904	-0.52	26.0	$C_{73}H_{113}O_{27}N_{17}$
	829.89770	1.09	21.5	$C_{70}H_{115}O_{30}N_{16}$
	829.89343	6.25	26.0	$C_{74}H_{113}O_{28}N_{15}$
	829.90399	-6.48	21.0	$C_{71}H_{117}O_{30}N_{15}$
	829.89275	7.06	26.5	$C_{72}H_{111}O_{27}N_{18}$
	829.90466	-7.29	26.0	$C_{72}H_{113}O_{26}N_{19}$
	829.90533	-8.10	25.5	$C_{74}H_{115}O_{27}N_{16}$

Figure C.3: HRMS data for A54145D-(8*S*)-*anteiso*. (A) ESI^+ HRMS for A54145D-(8*S*)-*anteiso*. The peak at *m/z* = 829.89861 corresponds to the $[M+2H]^{2+}$ species. The peak at *m/z* = 838.41153 corresponds to the $[M+H+NH_4]^{2+}$ species. The peak at *m/z* = 840.88937 corresponds to the $[M+H+Na]^{2+}$ species. The peak at *m/z* = 848.87362 corresponds to the $[M+H+K]^{2+}$ species. (B) HRMS data for the peak at *m/z* = 829.89861 is also shown.

A

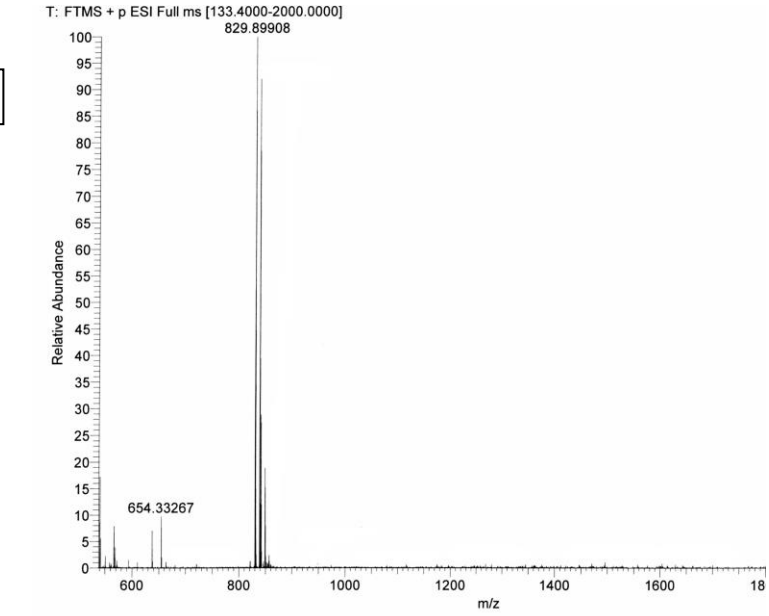

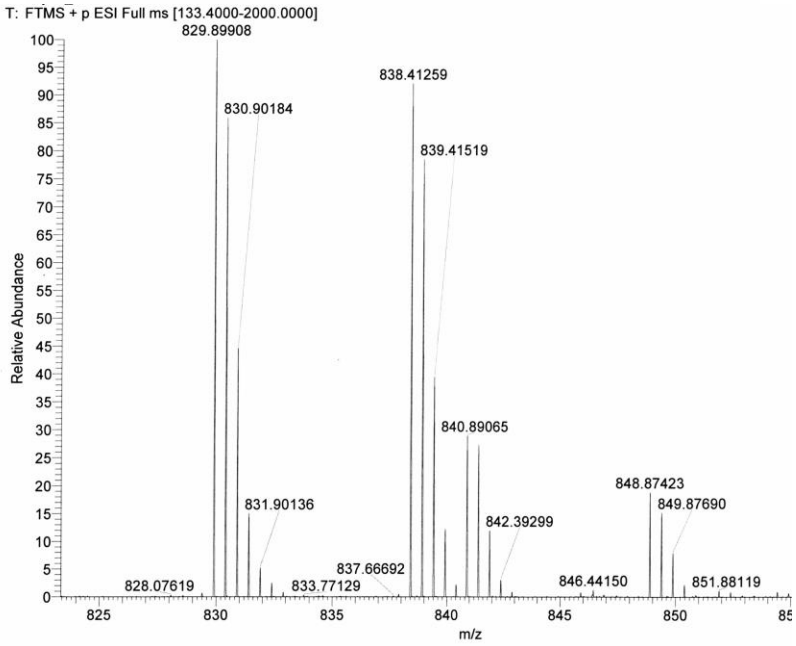

B

Elemental composition search on mass 829.89908

m/z= 824.89908-834.89908

m/z	Theo. Mass	Delta (ppm)	RDB equiv.	Composition
829.89908	829.89904	0.05	26.0	$C_{73}H_{113}O_{27}N_{17}$
	829.89993	-1.02	22.0	$C_{73}H_{118}O_{26}N_{15}K$
	829.89356	6.65	27.5	$C_{75}H_{112}O_{25}N_{16}Na$
	829.89343	6.81	26.0	$C_{74}H_{113}O_{28}N_{15}$
	829.90533	-7.53	25.5	$C_{74}H_{115}O_{27}N_{16}$

Figure C.4: HRMS data for A54145D-(8*R*)-*anteiso*. (A) ESI^+ HRMS for A54145D-(8*R*)-*anteiso*. The peak at *m/z* = 829.89908 corresponds to the $[M+2H]^{2+}$ species. The peak at *m/z* = 838.41259 corresponds to the $[M+H+NH_4]^{2+}$ species. The peak at *m/z* = 840.89065 corresponds to the $[M+H+Na]^{2+}$ species. The peak at *m/z* = 848.87423 corresponds to the $[M+H+K]^{2+}$ species. (B) HRMS data for the peak at *m/z* = 829.89908 is also shown.

A

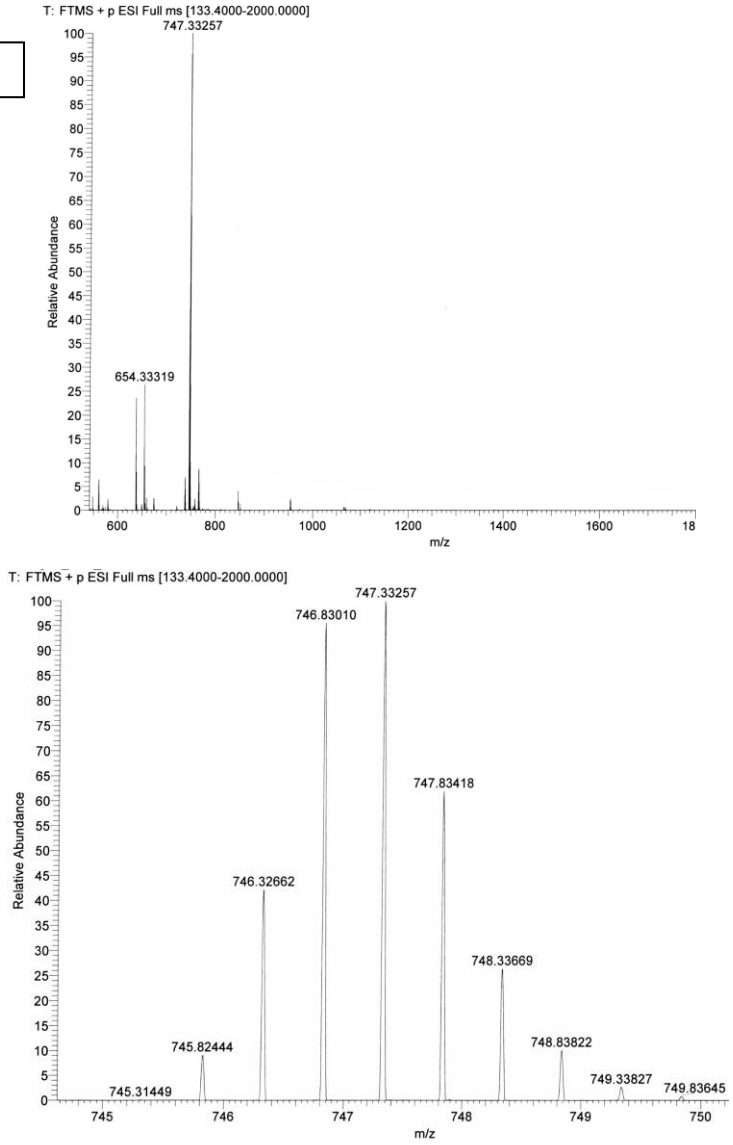

B

Elemental composition search on mass 745.82444

m/z= 740.82444-750.82444

m/z	Theo. Mass	Delta (ppm)	RDB equiv.	Composition
745.82444	745.82422	0.30	21.0	$C_{62}H_{98}O_{25}N_{15}K$
	745.82333	1.48	25.0	$C_{62}H_{93}O_{26}N_{17}$
	745.82842	-5.34	21.5	$C_{61}H_{96}O_{26}N_{16}Na$
	745.82895	-6.05	25.0	$C_{61}H_{93}O_{25}N_{19}$
	745.82962	-6.95	24.5	$C_{63}H_{95}O_{26}N_{16}$
	745.81793	8.73	21.5	$C_{61}H_{96}O_{25}N_{16}K$
	745.81772	9.01	25.0	$C_{63}H_{93}O_{27}N_{15}$
	745.81705	9.91	25.5	$C_{61}H_{91}O_{26}N_{18}$

Figure C.5: HRMS data for A54145D-nucleus. (A) ESI^+ HRMS for A54145D-nucleus. The peak at *m/z* = 745.82333 corresponds to the $[M+2H]^+$ species. (B) HRMS data for the peak at *m/z* = 745.82333 is also shown.

A

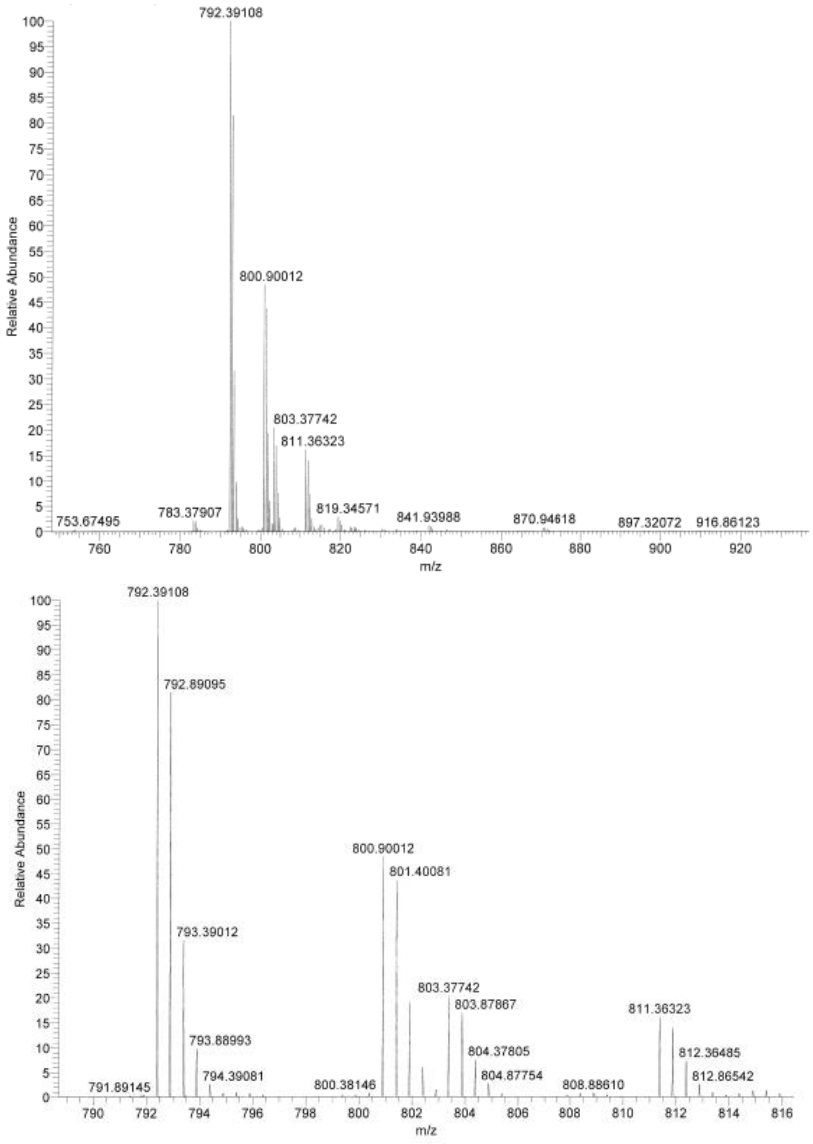

B

Elemental composition search on mass 792.39108

m/z= 787.39108-797.39108

m/z	Theo. Mass	Delta (ppm)	RDB equiv.	Composition
792.39108	792.38932	2.23	25.5	$C_{72}H_{110}O_{25}N_{15}$
	792.38864	3.07	26.0	$C_{70}H_{108}O_{24}N_{18}$
	792.39493	-4.86	25.5	$C_{71}H_{110}O_{24}N_{17}$

Figure C.6: HRMS data for A54145A$_1$-Asn3-DAPA4-Asp9 (**3.2**). (**A**) ESI+ HRMS of pure A54145A$_1$-Asn3-DAPA4-Asp9. The peak at *m/z* = 792.3911 corresponds to the $[M+2H]^{2+}$ species. The peak at *m/z* = 800.9001 corresponds to the $[M+H+NH_4]^{2+}$ species. The peak at *m/z* = 803.3774 corresponds to the $[M+H+Na]^{2+}$ species. The peak at *m/z* = 811.3632 corresponds to the $[M+H+K]^{2+}$ species. (**B**) HRMS data for the peak at 792.3911 is also shown.

A

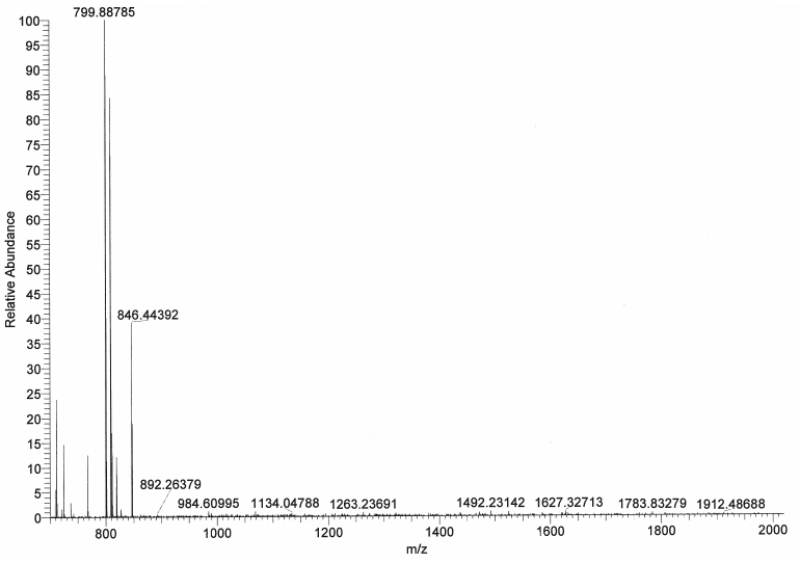

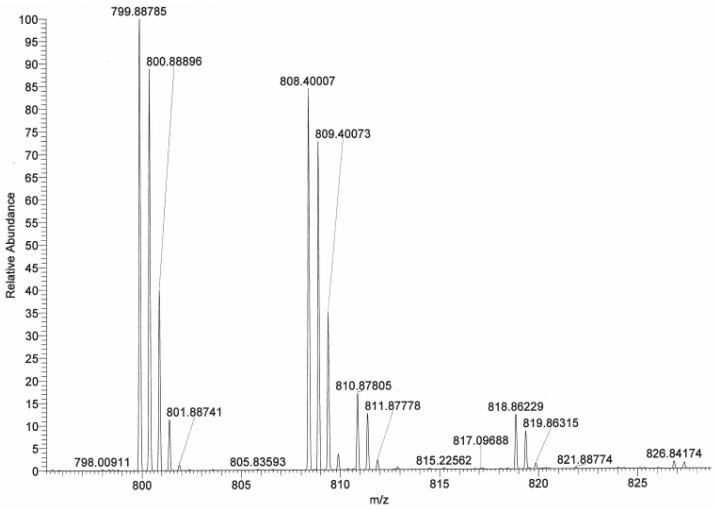

B

Elemental composition search on mass 799.88785

m/z= 794.88785-804.88785

m/z	Theo. Mass	Delta (ppm)	RDB equiv.	Composition
799.88785	799.88848	-0.78	26.0	$C_{71}H_{109}O_{25}N_{17}$
	799.88982	-2.46	30.5	$C_{74}H_{107}O_{22}N_{18}$
	799.88420	4.56	30.5	$C_{75}H_{107}O_{23}N_{16}$
	799.88353	5.40	31.0	$C_{73}H_{105}O_{22}N_{19}$
	799.88286	6.24	26.0	$C_{72}H_{109}O_{26}N_{15}$
	799.88219	7.08	26.5	$C_{70}H_{107}O_{25}N_{18}$
	799.89409	-7.81	26.0	$C_{70}H_{109}O_{24}N_{19}$
	799.89477	-8.65	25.5	$C_{72}H_{111}O_{25}N_{16}$
	799.89543	-9.48	30.5	$C_{73}H_{107}O_{21}N_{20}$

Figure C.7: HRMS data for A54145A$_1$-Asn3-Asp9 (**3.1**). (**A**) ESI+ HRMS of pure A54145A$_1$-Asn3-Asp9. The peak at *m/z* = 799.88785 corresponds to the $[M+2H]^{2+}$ species. The peak at *m/z* = 808.40007 corresponds to the $[M+H+NH_4]^{2+}$ species. The peak at *m/z* = 810.87805 corresponds to the $[M+H+Na]^{2+}$ species. The peak at *m/z* = 818.86229 corresponds to the $[M+H+K]^{2+}$ species. (**B**) HRMS data for the peak at *m/z* = 799.88785 is also shown.

A

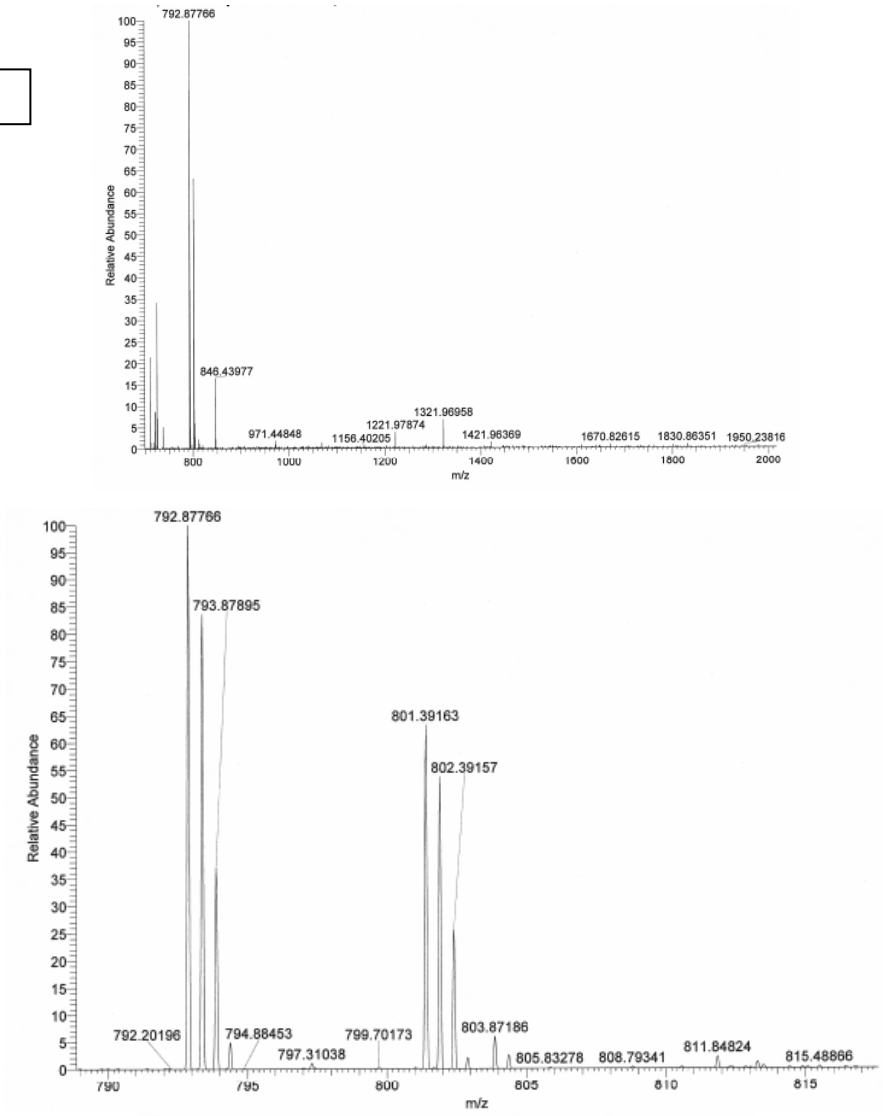

B

Elemental composition search on mass 792.87766

m/z- 787.87766-797.87766

m/z	Theo. Mass	Delta (ppm)	RDB equiv.	Composition
792.87766	792.87772	-0.07	35.0	$C_{77}H_{103}O_{20}N_{17}$
	792.87638	1.62	30.5	$C_{74}H_{105}O_{23}N_{16}$
	792.87570	2.47	31.0	$C_{72}H_{103}O_{22}N_{19}$
	792.87504	3.31	26.0	$C_{71}H_{107}O_{26}N_{15}$
	792.88065	-3.77	26.0	$C_{70}H_{107}O_{25}N_{17}$
	792.88199	-5.46	30.5	$C_{73}H_{105}O_{22}N_{18}$
	792.88266	-6.31	30.0	$C_{75}H_{107}O_{23}N_{15}$
	792.87210	7.01	35.0	$C_{78}H_{103}O_{21}N_{15}$
	792.87143	7.86	35.5	$C_{76}H_{101}O_{20}N_{18}$
	792.88400	-8.00	34.5	$C_{78}H_{105}O_{20}N_{16}$

Figure C.8: HRMS data for A54145A$_1$-Asn3-Ser4-Asp9 (**3.32**). (**A**) ESI+ HRMS of pure A54145A$_1$-Asn3-Ser4-Asp9. The peak at *m/z* = 792.87766 corresponds to the $[M+2H]^{2+}$ species. The peak at *m/z* = 801.39163 corresponds to the $[M+H+NH_4]^{2+}$ species. (**B**) HRMS data for the peak at *m/z* = 792.87766 is also shown.

A

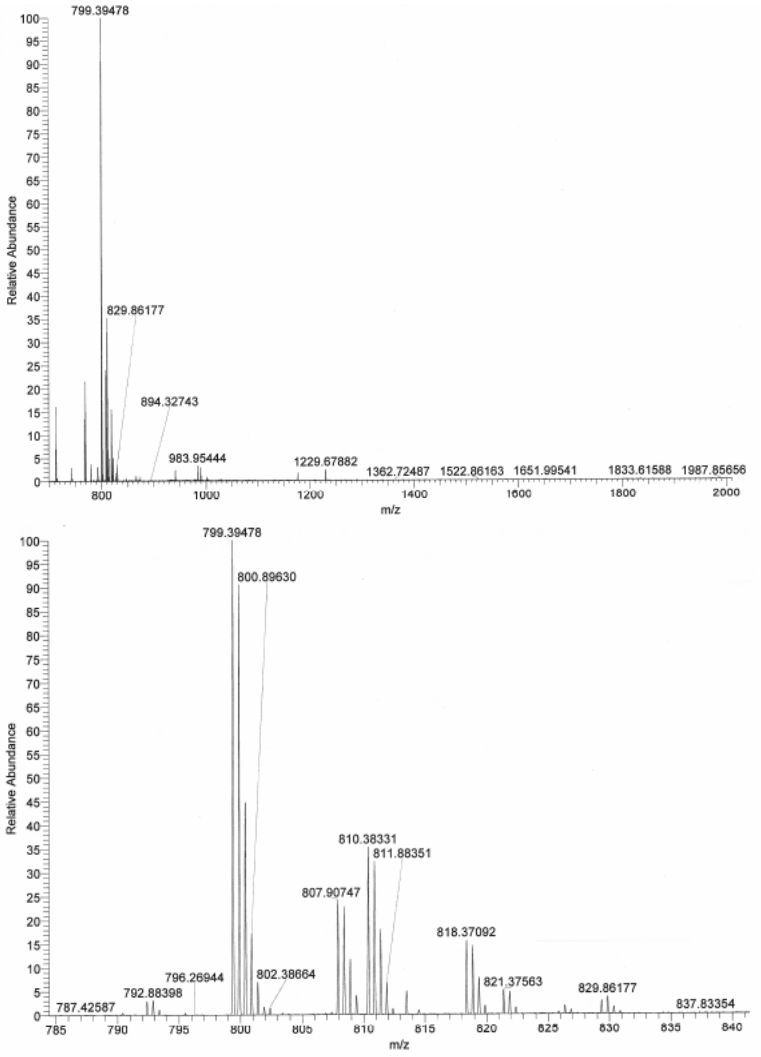

B

Elemental composition search on mass 799.39478

m/z= 794.39478-804.39478

m/z	Theo. Mass	Delta (ppm)	RDB equiv.	Composition
799.39478	799.39420	0.72	34.5	$C_{80}H_{108}O_{20}N_{15}$
	799.39647	-2.11	26.0	$C_{71}H_{110}O_{24}N_{18}$
	799.39219	3.24	30.5	$C_{75}H_{108}O_{22}N_{17}$
	799.39781	-3.79	30.5	$C_{74}H_{108}O_{21}N_{19}$
	799.39152	4.08	31.0	$C_{73}H_{106}O_{21}N_{20}$
	799.39848	-4.63	30.0	$C_{76}H_{110}O_{22}N_{16}$
	799.39085	4.91	26.0	$C_{72}H_{110}O_{25}N_{16}$
	799.39018	5.75	26.5	$C_{70}H_{108}O_{24}N_{19}$
	799.38792	8.59	35.0	$C_{79}H_{106}O_{20}N_{16}$
	799.40209	-9.14	26.0	$C_{70}H_{110}O_{23}N_{20}$

Figure C.9: HRMS data for A54145A$_1$-Asn3-DABA4-Asp9 (**3.33**). (**A**) ESI+ HRMS of pure A54145A$_1$-Asn3-DABA4-Asp9. The peak at *m/z* = 799.39478 corresponds to the $[M+2H]^{2+}$ species. The peak at *m/z* = 807.90747 corresponds to the $[M+H+NH_4]^{2+}$ species. The peak at *m/z* = 810.38331 corresponds to the $[M+H+Na]^{2+}$ species. The peak at *m/z* = 818.37092 corresponds to the $[M+H+K]^{2+}$ species. (**B**) HRMS data for the peak at *m/z* = 799.39478 is also shown.

A

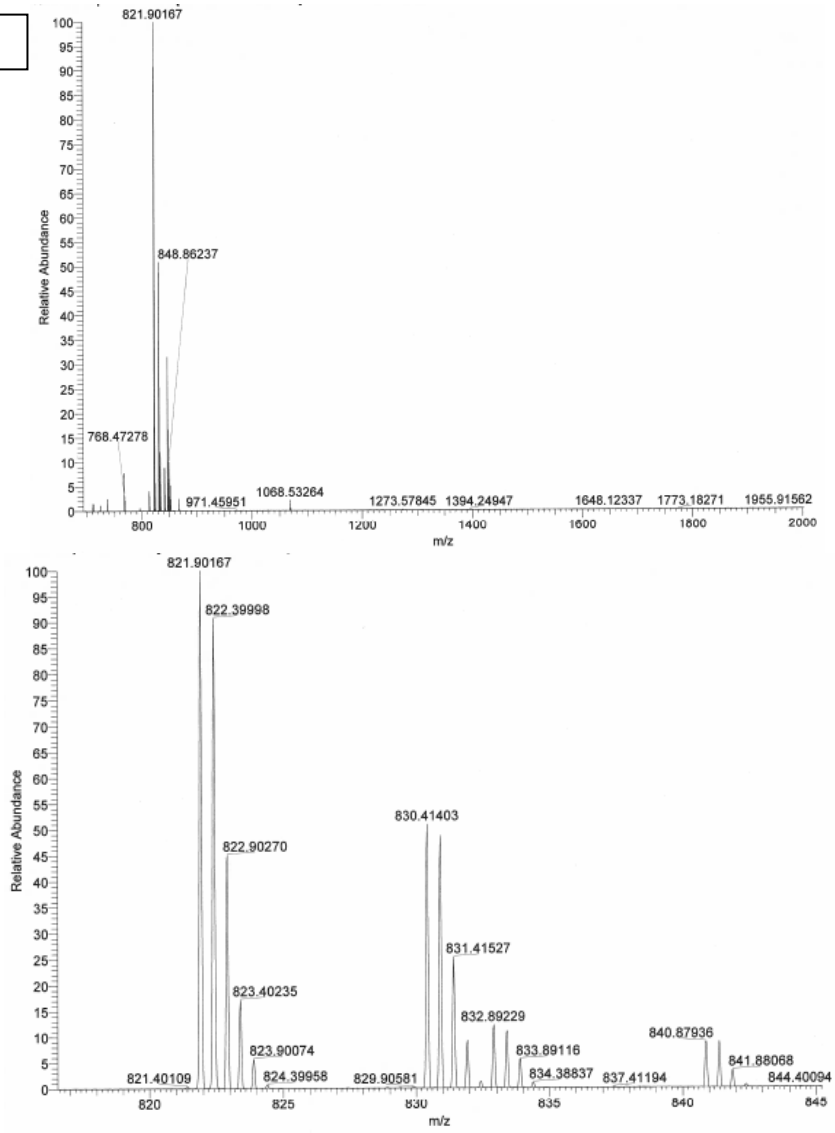

B

Elemental composition search on mass 821.90167

m/z= 816.90167-826.90167

m/z	Theo. Mass	Delta (ppm)	RDB equiv.	Composition
821.90167	821.90158	0.10	26.0	$C_{73}H_{113}O_{26}N_{17}$
	821.90091	0.92	26.5	$C_{71}H_{111}O_{25}N_{20}$
	821.90024	1.73	21.5	$C_{70}H_{115}O_{29}N_{16}$
	821.90653	-5.92	21.0	$C_{71}H_{117}O_{29}N_{15}$
	821.89664	6.12	31.0	$C_{75}H_{109}O_{23}N_{19}$
	821.90720	-6.73	26.0	$C_{72}H_{113}O_{25}N_{19}$
	821.89597	6.94	26.0	$C_{74}H_{113}O_{27}N_{15}$
	821.90787	-7.55	25.5	$C_{74}H_{115}O_{26}N_{16}$
	821.89530	7.75	26.5	$C_{72}H_{111}O_{26}N_{18}$
	821.90854	-8.36	30.5	$C_{75}H_{111}O_{22}N_{20}$

Figure C.10: HRMS data for A54145D-Asn3 (**3.44**). (**A**) ESI+ HRMS of pure A54145D-Asn3. The peak at *m/z* = 821.90167 corresponds to the $[M+2H]^{2+}$ species. The peak at *m/z* = 830.41403 corresponds to the $[M+H+NH_4]^{2+}$ species. The peak at *m/z* = 832.89229 corresponds to the $[M+H+Na]^{2+}$ species. The peak at *m/z* = 840.87936 corresponds to the $[M+H+K]^{2+}$ species. (**B**) HRMS data for the peak at *m/z* = 821.90167 is also shown.

A

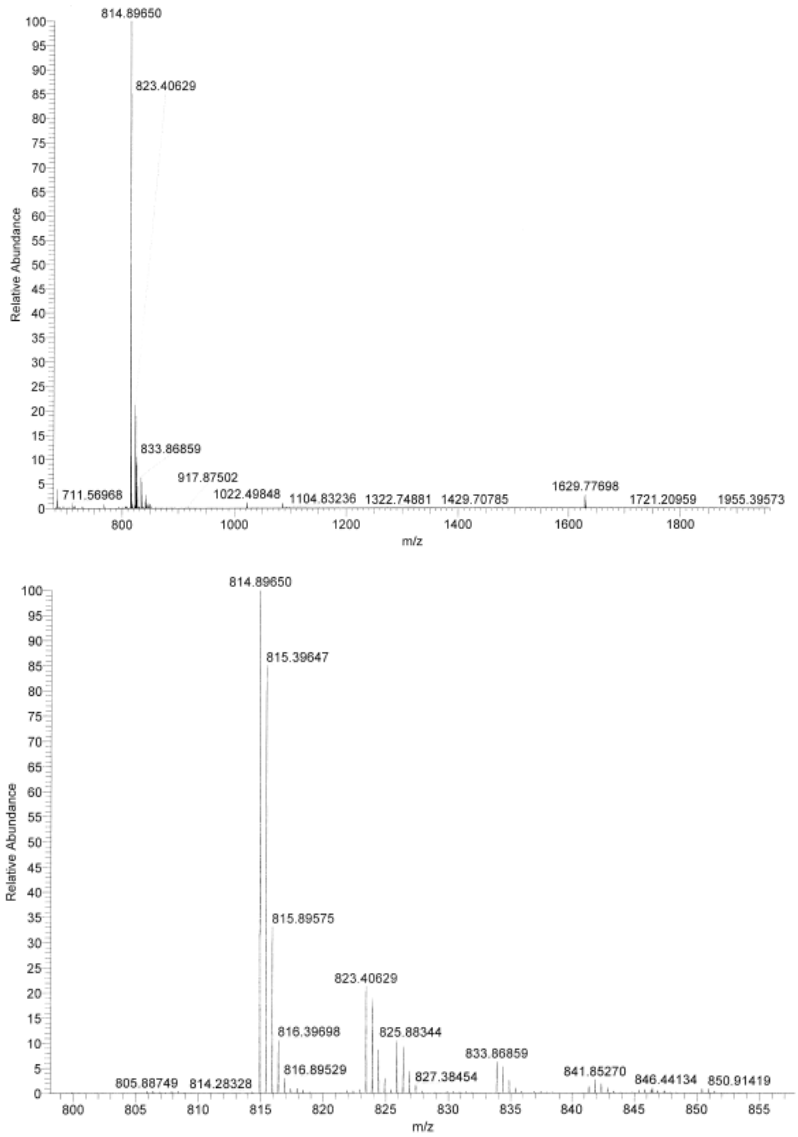

B

Elemental composition search on mass 814.89650

m/z= 809.89650-819.89650

m/z	Theo. Mass	Delta (ppm)	RDB equiv.	Composition
814.89650	814.89510	1.72	30.5	$C_{75}H_{109}O_{23}N_{18}$
	814.89376	3.36	26.0	$C_{72}H_{111}O_{26}N_{17}$
	814.89938	-3.53	26.0	$C_{71}H_{111}O_{25}N_{19}$
	814.89309	4.19	26.5	$C_{70}H_{109}O_{25}N_{20}$
	814.90005	-4.35	25.5	$C_{73}H_{113}O_{26}N_{16}$
	814.88881	9.43	31.0	$C_{74}H_{107}O_{23}N_{19}$

Figure C.11: HRMS data for A54145D-Asp9 (**3.45**). (**A**) ESI+ HRMS of pure A54145D-Asp9. The peak at *m/z* = 814.8965 corresponds to the $[M+2H]^{2+}$ species. The peak at *m/z* = 823.4063 corresponds to the $[M+H+NH_4]^{2+}$ species. The peak at *m/z* = 825.8834 corresponds to the $[M+H+Na]^{2+}$ species. The peak at *m/z* = 833.8686 corresponds to the $[M+H+K]^{2+}$ species. (**B**) HRMS data for the peak at *m/z* = 814.8965 is also shown.

A

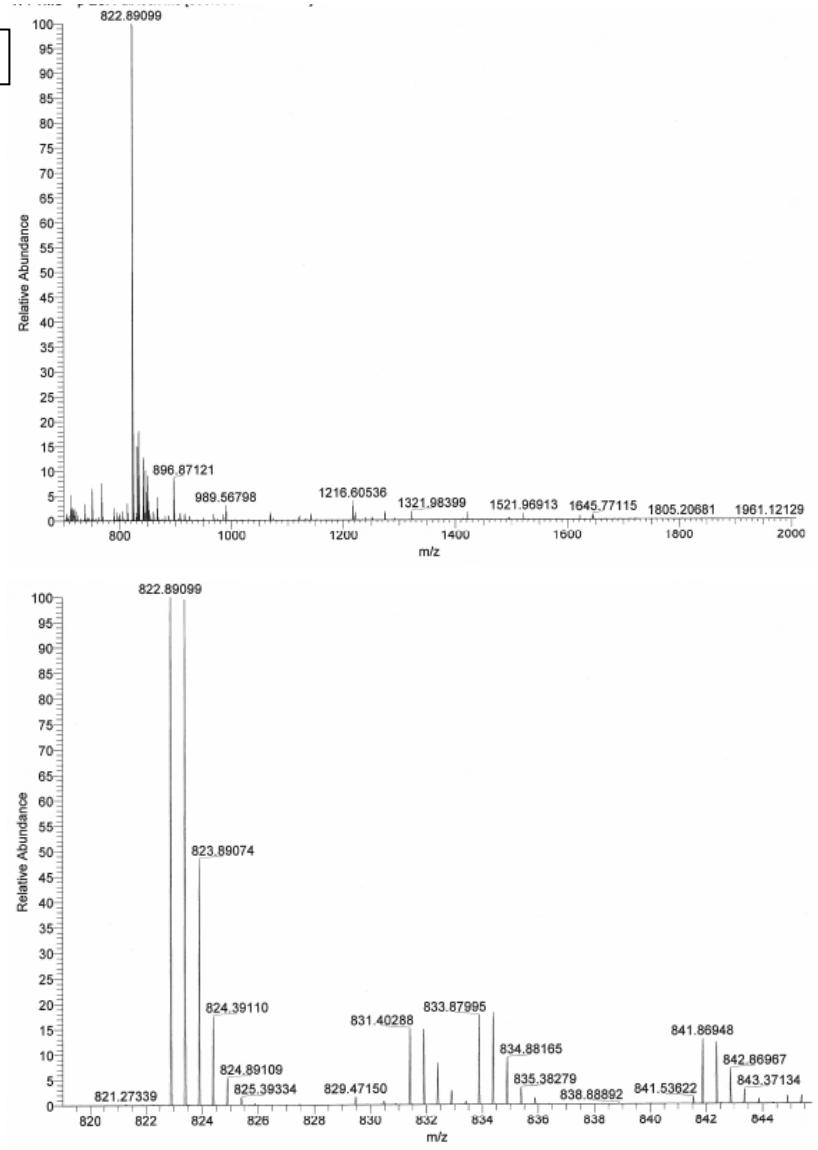

B

Elemental composition search on mass 822.89099

m/z= 817.89099-827.89099

m/z	Theo. Mass	Delta (ppm)	RDB equiv.	Composition
822.89099	822.89122	-0.28	26.0	$C_{72}H_{111}O_{27}N_{17}$
	822.89055	0.54	26.5	$C_{70}H_{109}O_{26}N_{20}$
	822.89323	-2.72	30.0	$C_{77}H_{111}O_{25}N_{15}$
	822.88694	4.92	30.5	$C_{76}H_{109}O_{25}N_{16}$
	822.89616	-6.29	21.0	$C_{70}H_{115}O_{30}N_{15}$
	822.88560	6.55	26.0	$C_{73}H_{111}O_{28}N_{15}$
	822.89683	-7.10	26.0	$C_{71}H_{111}O_{26}N_{19}$
	822.88493	7.37	26.5	$C_{71}H_{109}O_{27}N_{18}$
	822.89750	-7.92	25.5	$C_{73}H_{113}O_{27}N_{16}$

Figure C.12: HRMS data for synthetic A54145A$_1$ (**1.7**). (**A**) ESI+ HRMS of pure A54145A$_1$. The peak at *m/z* = 822.89099 corresponds to the $[M+2H]^{2+}$ species. The peak at *m/z* = 831.40258 corresponds to the $[M+H+NH_4]^{2+}$ species. The peak at *m/z* = 833.87995 corresponds to the $[M+H+Na]^{2+}$ species. The peak at *m/z* = 841.85948 corresponds to the $[M+H+K]^{2+}$ species. (**B**) HRMS data for the peak at *m/z* = 822.89099 is also shown.

A

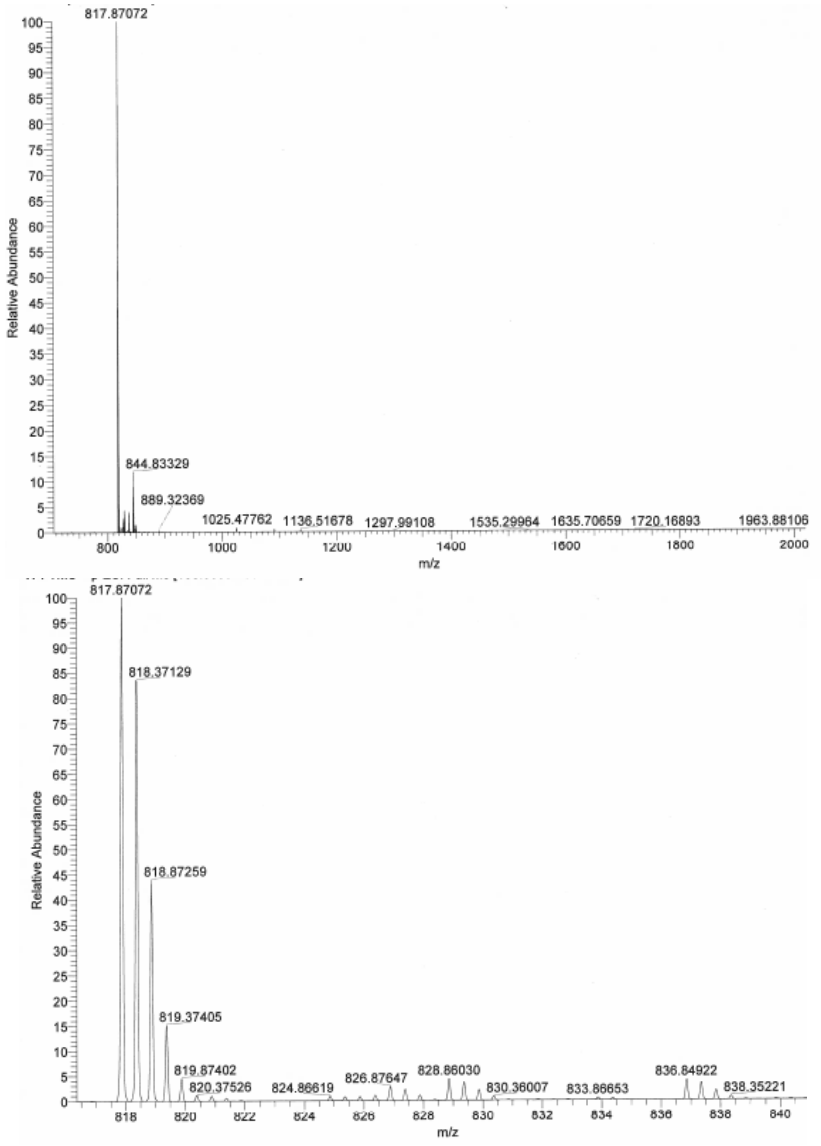

B

Elemental composition search on mass 817.87072

m/z= 812.87072-822.87072

m/z	Theo. Mass	Delta (ppm)	RDB equiv.	Composition
817.87072	817.87028	0.53	30.0	$C_{73}H_{105}O_{26}N_{17}$
	817.86961	1.35	30.5	$C_{71}H_{103}O_{25}N_{20}$
	817.86894	2.17	25.5	$C_{70}H_{107}O_{29}N_{16}$
	817.87523	-5.52	25.0	$C_{71}H_{109}O_{29}N_{15}$
	817.87590	-6.33	30.0	$C_{72}H_{105}O_{25}N_{19}$
	817.87657	-7.16	29.5	$C_{74}H_{107}O_{26}N_{16}$
	817.86467	7.40	30.0	$C_{74}H_{105}O_{27}N_{15}$
	817.86400	8.22	30.5	$C_{72}H_{103}O_{26}N_{18}$

Figure C.13: HRMS data for 8-methyldecanoyl-daptomycin (**3.46**). (**A**) ESI+ HRMS of pure 8-methyldecanoyl-daptomycin. The peak at *m/z* = 817.87072 corresponds to the $[M+2H]^{2+}$ species. The peak at *m/z* = 828.86030 corresponds to the $[M+H+Na]^{2+}$ species. The peak at *m/z* = 836.84922 corresponds to the $[M+H+K]^{2+}$ species. (**B**) HRMS data for the peak at *m/z* = 817.87072 is also shown.

A

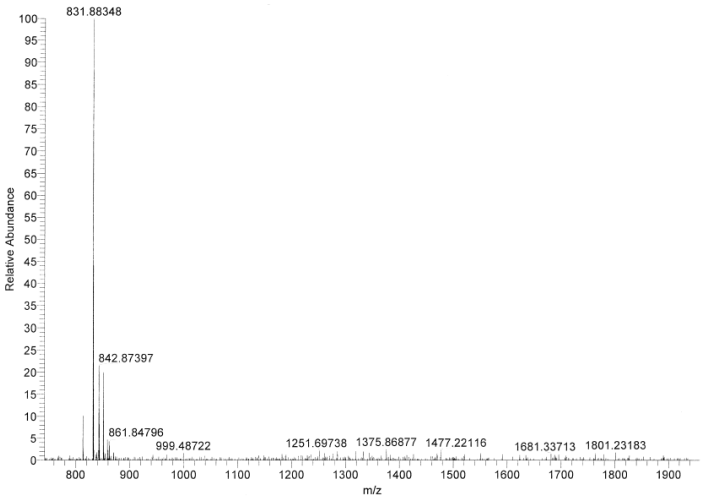

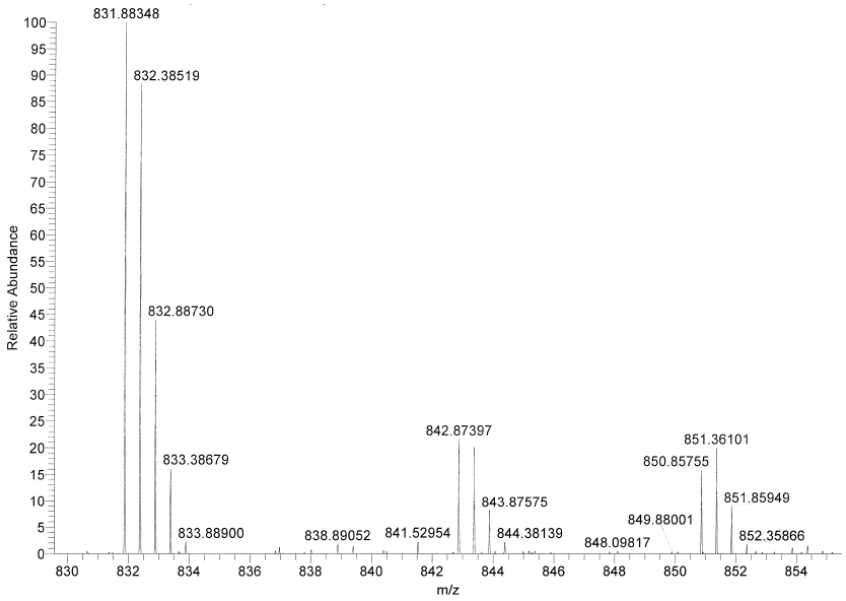

B

Elemental composition search on mass 831.88348

m/z= 826.88348-836.88348

m/z	Theo. Mass	Delta (ppm)	RDB equiv.	Composition
831.88348	831.88392	-0.53	26.0	$C_{70}H_{109}O_{28}N_{19}$
	831.88267	0.97	30.0	$C_{74}H_{109}O_{23}N_{19}S$
	831.88526	-2.14	30.5	$C_{73}H_{107}O_{25}N_{20}$
	831.88166	2.19	34.5	$C_{79}H_{107}O_{24}N_{16}$
	831.88593	-2.95	30.0	$C_{75}H_{109}O_{26}N_{17}$
	831.88099	3.00	35.0	$C_{77}H_{105}O_{23}N_{19}$
	831.88032	3.80	30.0	$C_{76}H_{109}O_{27}N_{15}$

Figure C.14: HRMS data for 10-methyldodecanoyl-daptomycin (**3.47**). (**A**) ESI+ HRMS of pure 10-methyldodecanoyl-daptomycin. The peak at *m/z* = 831.88348 corresponds to the $[M+2H]^{2+}$ species. The peak at *m/z* = 842.87397 corresponds to the $[M+H+Na]^{2+}$ species. The peak at *m/z* = 850.85755 corresponds to the $[M+H+K]^{2+}$ species. (**B**) HRMS data for the peak at *m/z* = 831.88348 is also shown.

A

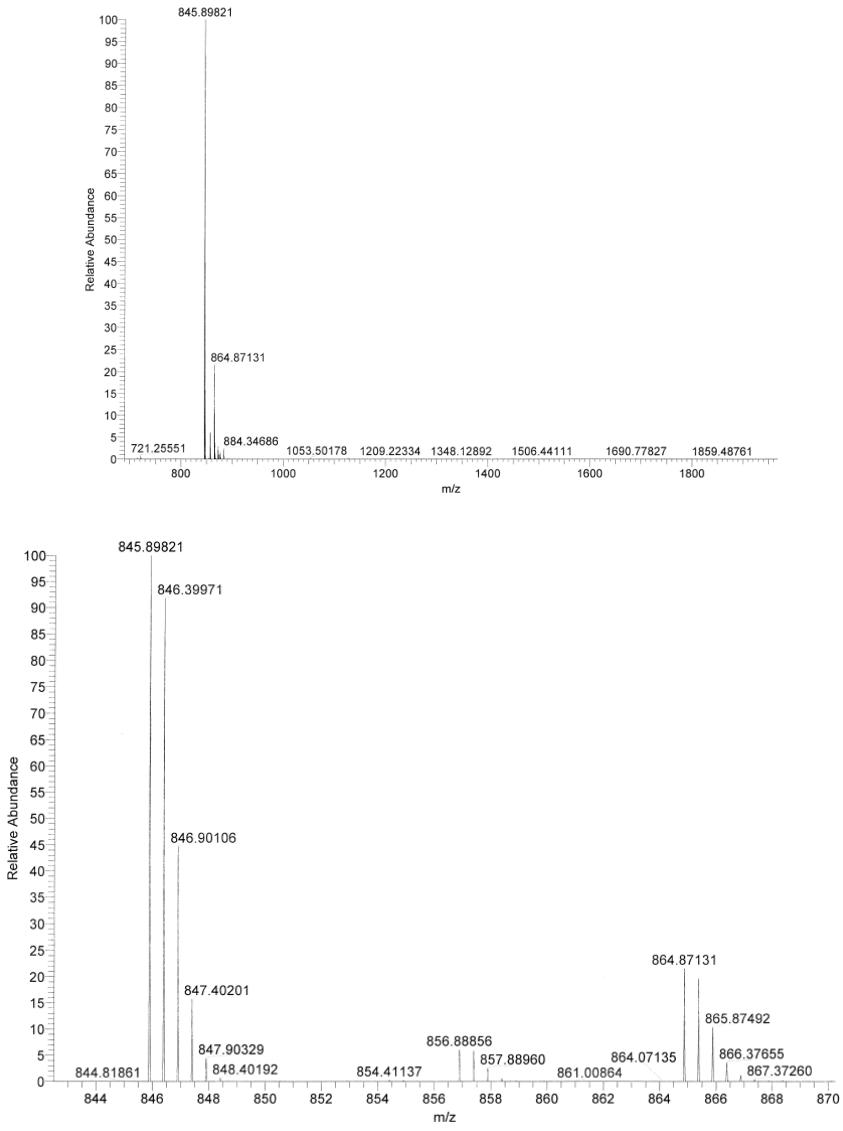

B

Elemental composition search on mass 845.89821

m/z= 840.89821-850.89821

m/z	Theo. Mass	Delta (ppm)	RDB equiv.	Composition
845.89821	845.89765	0.66	25.0	$C_{75}H_{117}O_{27}N_{15}S$
	845.89597	2.65	30.0	$C_{78}H_{113}O_{27}N_{15}$
	845.90091	-3.20	30.5	$C_{75}H_{111}O_{25}N_{20}$
	845.89530	3.44	30.5	$C_{76}H_{111}O_{26}N_{18}$
	845.90158	-3.99	30.0	$C_{77}H_{113}O_{26}N_{17}$

Figure C.15: HRMS data for pentadecanoyl-daptomycin (**3.48**). (**A**) ESI+ HRMS of pure pentadecanoyl-daptomycin. The peak at *m/z* = 845.89821 corresponds to the $[M+2H]^{2+}$ species. The peak at *m/z* = 856.88856 corresponds to the $[M+H+Na]^{2+}$ species. The peak at *m/z* = 864.871315 corresponds to the $[M+H+K]^{2+}$ species. (**B**) HRMS data for the peak at *m/z* = 845.89821 is also shown.

A

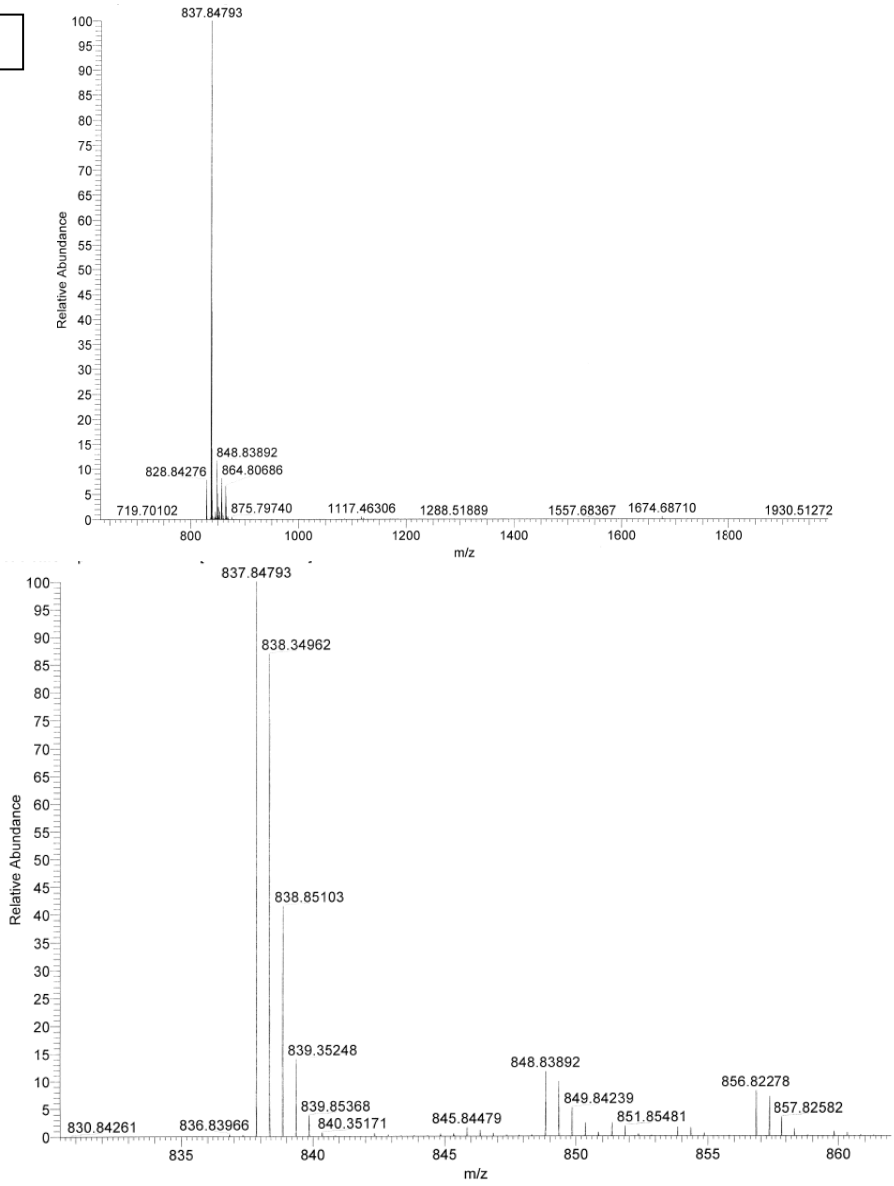

B

Elemental composition search on mass 837.84793

m/z= 832.84793-842.84793

m/z	Theo. Mass	Delta (ppm)	RDB equiv.	Composition
837.84793	837.84833	-0.47	30.0	$C_{72}H_{100}O_{26}N_{17}F_3$
	837.84574	2.62	29.5	$C_{73}H_{102}O_{24}N_{16}F_3S$
	837.85034	-2.87	34.0	$C_{77}H_{100}O_{24}N_{15}F_3$
	837.84506	3.42	30.0	$C_{71}H_{100}O_{23}N_{19}F_3S$

Figure C.16: HRMS data for 10,10,10-trifluorodecanoyl-daptomycin (**4.5**). (A) ESI+ HRMS Data for 10,10,10-trifluorodecanoyl-daptomycin. The peak at *m/z* = 837.84793 corresponds to the $[M+2H]^{2+}$ species. The peak at *m/z* = 848.83892 corresponds to the $[M+H+Na]^{2+}$ species. The peak at *m/z* = 856.82278 corresponds to the $[M+H+K]^{2+}$ species. (B) HRMS data for the peak at *m/z* = 837.84793 is also shown.

A

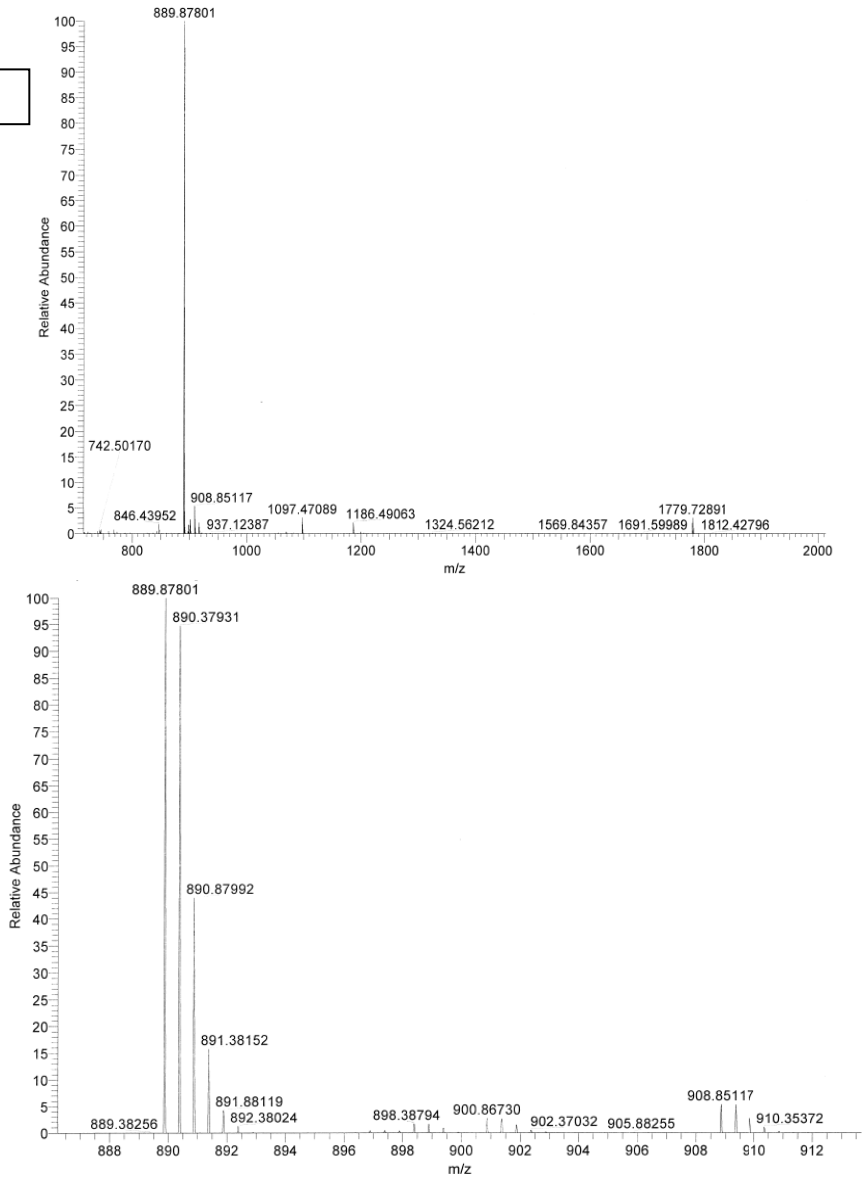

B

Elemental composition search on mass 889.87801

m/z= 884.87801-894.87801

m/z	Theo. Mass	Delta (ppm)	RDB equiv.	Composition
889.87801	889.87762	0.44	30.0	$C_{75}H_{108}O_{28}N_{19}F_3$
	889.87896	-1.06	34.5	$C_{78}H_{106}O_{25}N_{20}F_3$
	889.87704	1.09	33.5	$C_{81}H_{110}O_{24}N_{16}F_3S$
	889.87963	-1.82	34.0	$C_{80}H_{108}O_{26}N_{17}F_3$
	889.87636	1.85	34.0	$C_{79}H_{108}O_{23}N_{19}F_3S$
	889.88064	-2.96	29.5	$C_{75}H_{110}O_{25}N_{20}F_3S$
	889.87502	3.36	29.5	$C_{76}H_{110}O_{26}N_{18}F_3S$
	889.87468	3.74	39.0	$C_{82}H_{104}O_{23}N_{19}F_3$

Figure C.17: HRMS data for Dap-(^{TFM}Benzyl)Orn6 (**4.6**). (A) ESI+ HRMS Data for Dap-(^{TFM}Benzyl)Orn6. The peak at *m/z* = 889.87801 corresponds to the $[M+2H]^{2+}$ species. The peak at *m/z* = 908.85117 corresponds to the $[M+H+K]^{2+}$ species. (B) HRMS data for the peak at *m/z* = 889.87801 is also shown.

A

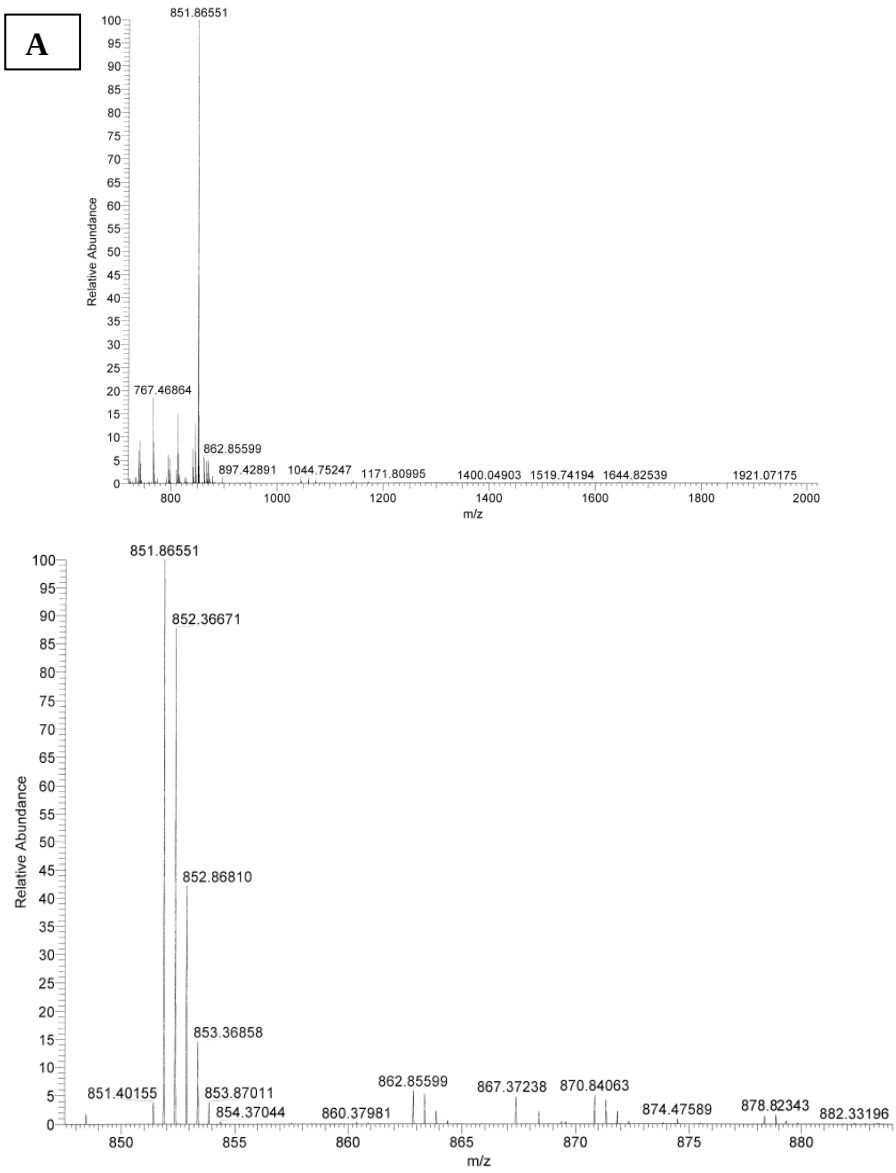

B

Elemental composition search on mass 851.86551

m/z= 846.86551-856.86551

m/z	Theo. Mass	Delta (ppm)	RDB equiv.	Composition
851.86551	851.86532	0.23	34.5	$C_{77}H_{102}O_{23}N_{18}F_3$
	851.86599	-0.56	34.0	$C_{79}H_{104}O_{24}N_{15}F_3$
	851.86700	-1.75	29.5	$C_{74}H_{106}O_{23}N_{18}F_3S$
	851.86398	1.80	30.0	$C_{74}H_{104}O_{26}N_{17}F_3$
	851.86331	2.59	30.5	$C_{72}H_{102}O_{25}N_{20}F_3$
	851.86825	-3.22	25.5	$C_{70}H_{106}O_{28}N_{18}F_3$

Figure C.18: HRMS data for Dap-(^{TF}ethyl)Orn6 (**4.7**). (A) ESI+ HRMS Data for Dap-(^{TF}ethyl)Orn6. The peak at *m/z* = 851.86551 corresponds to the $[M+2H]^{2+}$ species. The peak at *m/z* = 862.85599 corresponds to the $[M+H+Na]^{2+}$ species. The peak at *m/z* = 870.84063 corresponds to the $[M+H+K]^{2+}$ species. (B) HRMS data for the peak at *m/z* = 851.86551 is also shown.

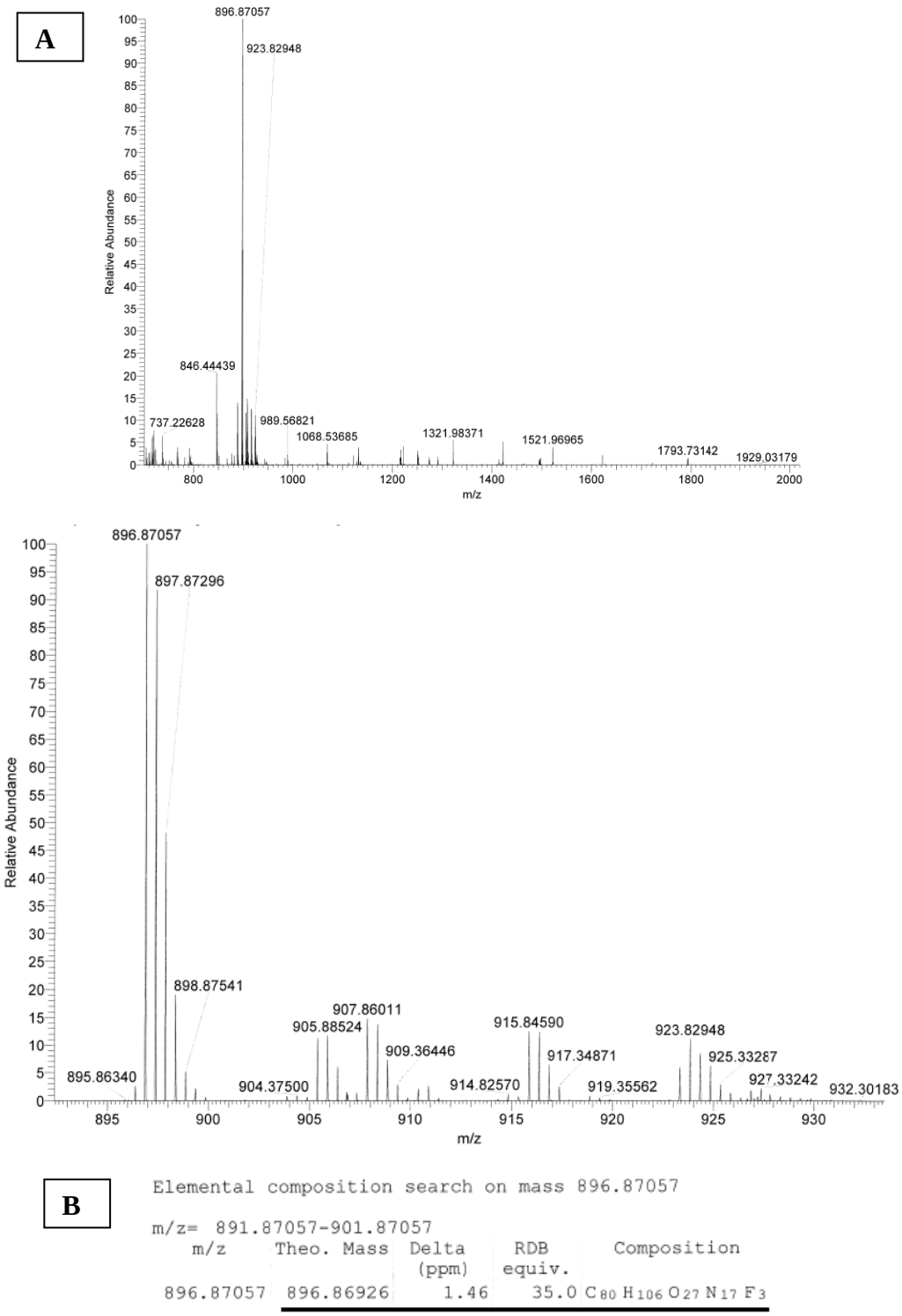

Figure C.19: HRMS data for Dap-(^{TFM}benzoyl)Orn6 (**4.8**). (A) ESI+ HRMS data for Dap-(^{TFM}benzoyl)Orn6. The peak at *m/z* = 896.87057 corresponds to the $[M+2H]^{2+}$ species. The peak at *m/z* = 907.86011 corresponds to the $[M+H+Na]^{2+}$ species. The peak at *m/z* = 915.84590 corresponds to the $[M+H+K]^{2+}$ species. (B) HRMS data for the peak at *m/z* = 896.87057 is also shown.

A

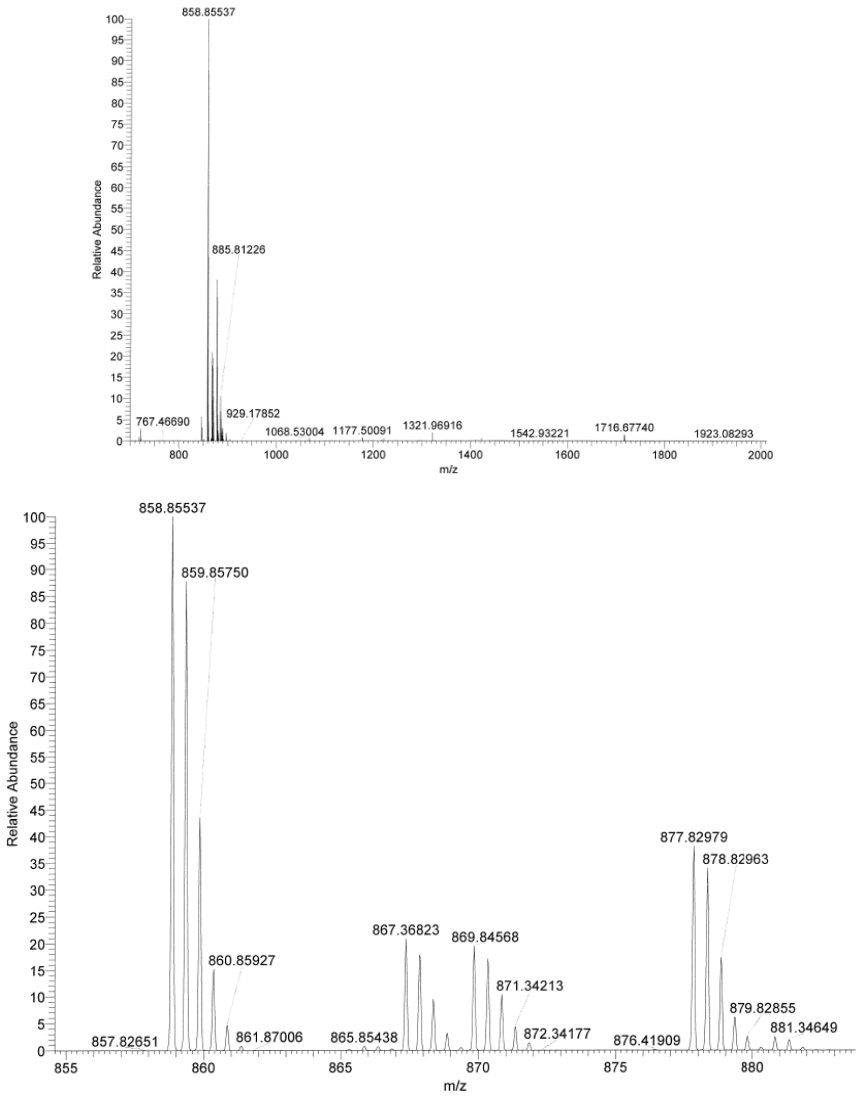

B

Elemental composition search on mass 858.85537

m/z= 853.85537-863.85537

m/z	Theo. Mass	Delta (ppm)	RDB equiv.	Composition
858.85537	858.85495	0.49	35.5	$C_{77}H_{100}O_{24}N_{18}F_3$
	858.85629	-1.07	40.0	$C_{80}H_{98}O_{21}N_{19}F_3$
	858.85361	2.05	31.0	$C_{74}H_{102}O_{27}N_{17}F_3$
	858.85294	2.83	31.5	$C_{72}H_{100}O_{26}N_{20}F_3$
	858.85789	-2.93	26.5	$C_{70}H_{104}O_{29}N_{18}F_3$
	858.85923	-4.49	31.0	$C_{73}H_{102}O_{26}N_{19}F_3$
	858.86057	-6.05	35.5	$C_{76}H_{100}O_{23}N_{20}F_3$
	858.85000	6.25	40.5	$C_{79}H_{96}O_{21}N_{20}F_3$
	858.86124	-6.83	35.0	$C_{78}H_{102}O_{24}N_{17}F_3$
	858.84866	7.81	36.0	$C_{76}H_{98}O_{24}N_{19}F_3$

Figure C.20: HRMS data for Dap-(^{TF}acetyl)Orn6 (**4.9**). (A) ESI+ HRMS data for Dap-(^{TF}acetyl)Orn6. The peak at *m/z* = 858.85537 corresponds to the $[M+2H]^{2+}$ species. The peak at *m/z* = 867.36823 corresponds to the $[M+H+NH_4]^{2+}$ species. The peak at *m/z* = 869.84568 corresponds to the $[M+H+Na]^{2+}$ species. The peak at *m/z* = 877.82979 corresponds to the $[M+H+K]^{2+}$ species. (B) HRMS data for the peak at *m/z* = 858.85537 is also shown.

A

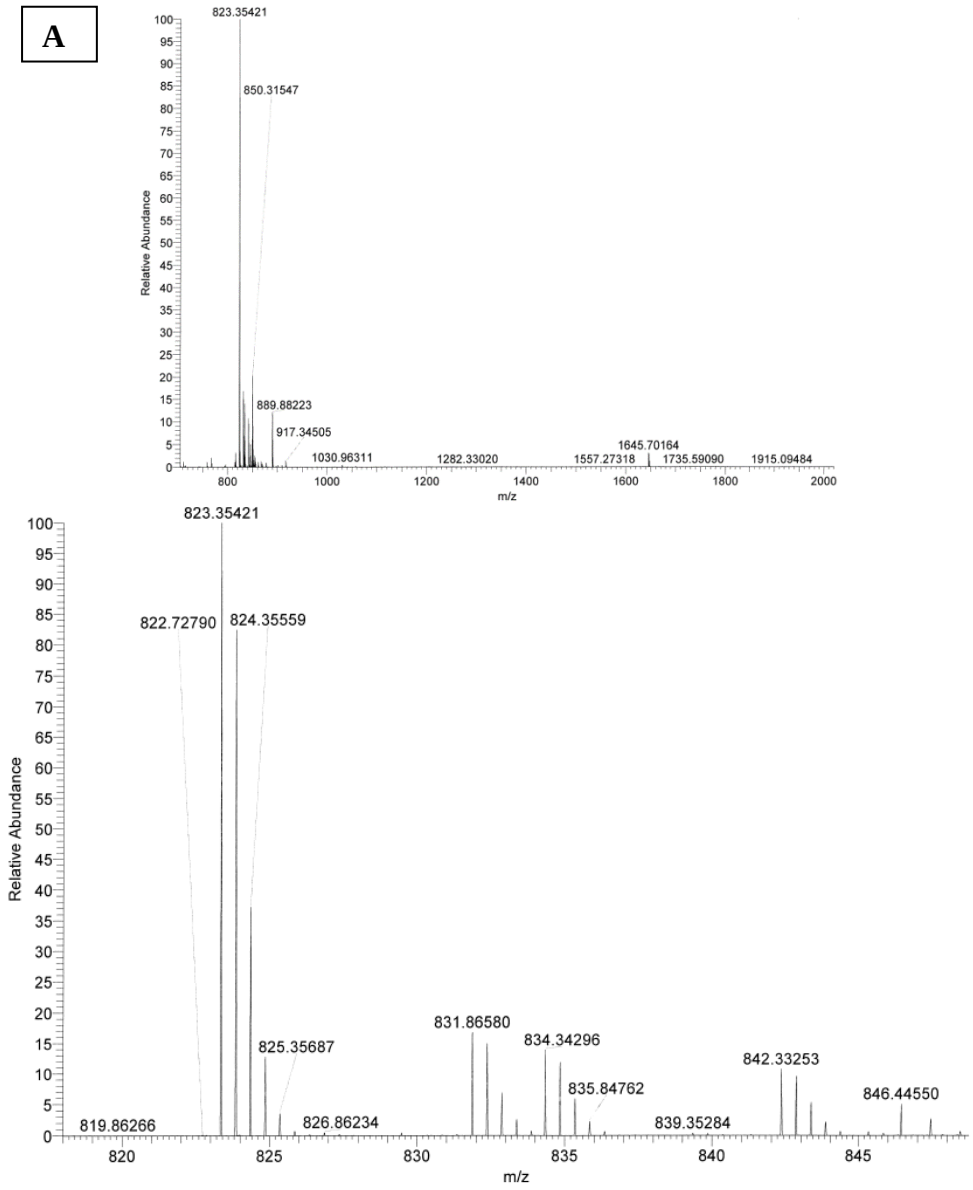

B

Elemental composition search on mass 823.35421

m/z= 818.35421-828.35421

m/z	Theo. Mass	Delta (ppm)	RDB equiv.	Composition
823.35421	823.35458	-0.46	33.5	$C_{75}H_{99}O_{22}N_{17}F_3$
	823.35324	1.17	29.0	$C_{72}H_{101}O_{25}N_{16}F_3$
	823.35257	1.99	29.5	$C_{70}H_{99}O_{24}N_{19}F_3$

Figure C.21: HRMS data for Dap-^{TFM}Phe1-Lys6-Glu12-Trp13 (**4.15**). (A) ESI+ HRMS data for Dap-^{TFM}Phe1-Lys6-Glu12-Trp13. The peak at *m/z* = 823.35421 corresponds to the $[M+2H]^{2+}$ species. The peak at *m/z* = 831.86580 corresponds to the $[M+H+NH_4]^{2+}$ species. The peak at *m/z* = 834.34296 corresponds to the $[M+H+Na]^{2+}$ species. The peak at *m/z* = 842.33253 corresponds to the $[M+H+K]^{2+}$ species. (B) HRMS data for the peak at *m/z* = 823.35421 is also shown.

A

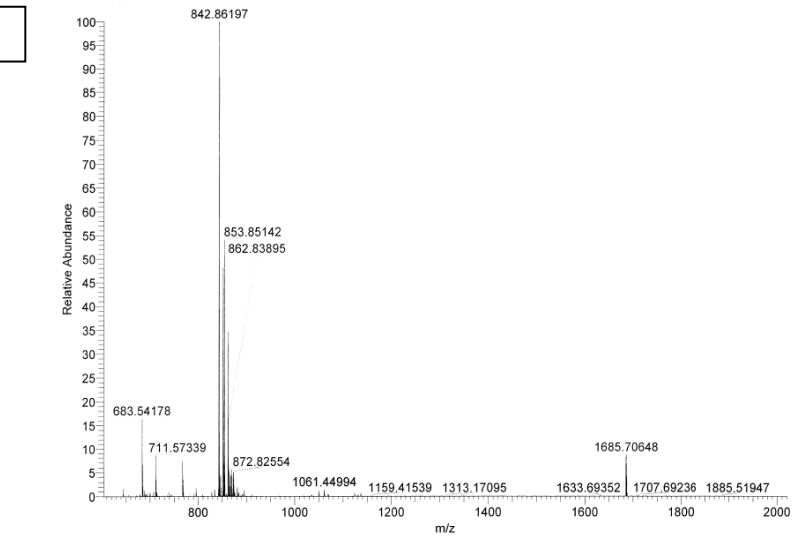

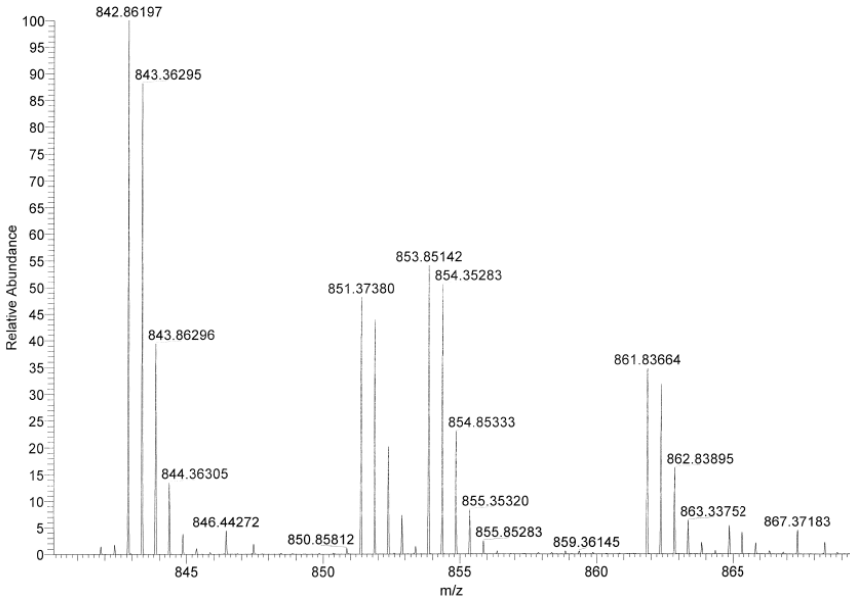

B

Elemental composition search on mass 842.86197

m/z= 837.86197-847.86197

m/z	Theo. Mass	Delta (ppm)	RDB equiv.	Composition
842.86197	842.86297	-1.19	26.5	$C_{70}H_{104}O_{27}N_{18}F_3$
	842.86071	1.50	35.0	$C_{79}H_{102}O_{23}N_{15}F_3$
	842.86364	-1.98	26.0	$C_{72}H_{106}O_{28}N_{15}F_3$
	842.86003	2.30	35.5	$C_{77}H_{100}O_{22}N_{18}F_3$
	842.86431	-2.78	31.0	$C_{73}H_{102}O_{24}N_{19}F_3$
	842.86498	-3.57	30.5	$C_{75}H_{104}O_{25}N_{16}F_3$
	842.85869	3.89	31.0	$C_{74}H_{102}O_{25}N_{17}F_3$

Figure C.22: HRMS data for Dap-Lys6-*D*-Ser(CF_3)11-Glu12-Trp13 (**4.38**). (A) ESI+ HRMS data for Dap-Lys6-*D*-Ser(CF_3)11-Glu12-Trp13. The peak at *m/z* = 842.86197 corresponds to the $[M+2H]^{2+}$ species. The peak at *m/z* = 866.37077 corresponds to the $[M+H+NH_4]^{2+}$ species. The peak at *m/z* = 868.84772 corresponds to the $[M+H+Na]^{2+}$ species. The peak at *m/z* = 876.83324 corresponds to the $[M+H+K]^{2+}$ species. (B) HRMS data for the peak at *m/z* = 857.85792 is also shown.

A

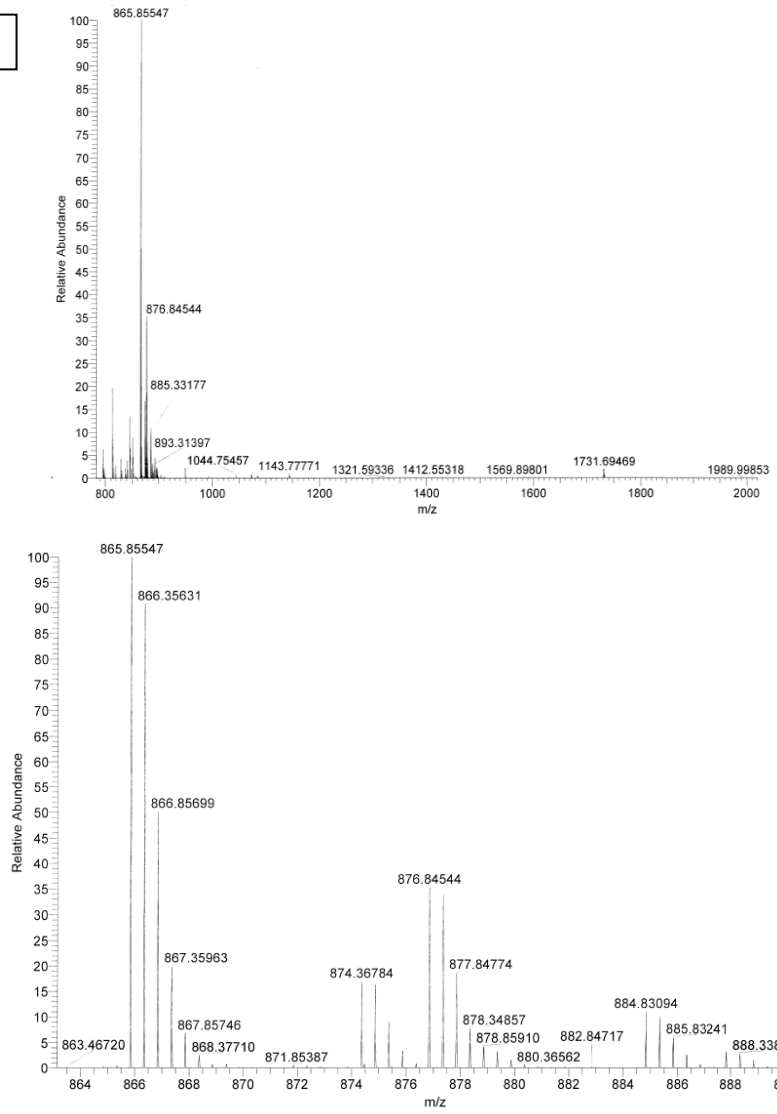

B

Elemental composition search on mass 865.85547

m/z= 860.85547-870.85547

m/z	Theo. Mass	Delta (ppm)	RDB equiv.	Composition
865.85547	865.85515	0.37	31.5	$C_{74}H_{102}O_{27}N_{18}F_3$
	865.85582	-0.40	31.0	$C_{76}H_{104}O_{28}N_{15}F_3$
	865.85649	-1.17	36.0	$C_{77}H_{100}O_{24}N_{19}F_3$
	865.85683	-1.57	26.5	$C_{71}H_{106}O_{27}N_{18}F_3S$
	865.85389	1.82	35.5	$C_{78}H_{102}O_{22}N_{18}F_3S$
	865.85716	-1.95	35.5	$C_{79}H_{102}O_{25}N_{16}F_3$
	865.85817	-3.12	31.0	$C_{74}H_{104}O_{24}N_{19}F_3S$
	865.85255	3.37	31.0	$C_{75}H_{104}O_{25}N_{17}F_3S$
	865.85884	-3.90	30.5	$C_{76}H_{106}O_{25}N_{16}F_3S$

Figure C.23: HRMS data for Dap-Lys6-*D*-hCys(CF_3)8-Glu12-Trp13 (**4.55**). (A) ESI+ HRMS data for Dap-Lys6-*D*-hCys(CF_3)8-Glu12-Trp13. The peak at *m/z* = 865.85547 corresponds to the $[M+2H]^{2+}$ species. The peak at *m/z* = 874.36784 corresponds to the $[M+H+NH_4]^{2+}$ species. The peak at *m/z* = 876.84544 corresponds to the $[M+H+Na]^{2+}$ species. The peak at *m/z* = 884.83094 corresponds to the $[M+H+K]^{2+}$ species. (B) HRMS data for the peak at *m/z* = 865.85547 is also shown.

A

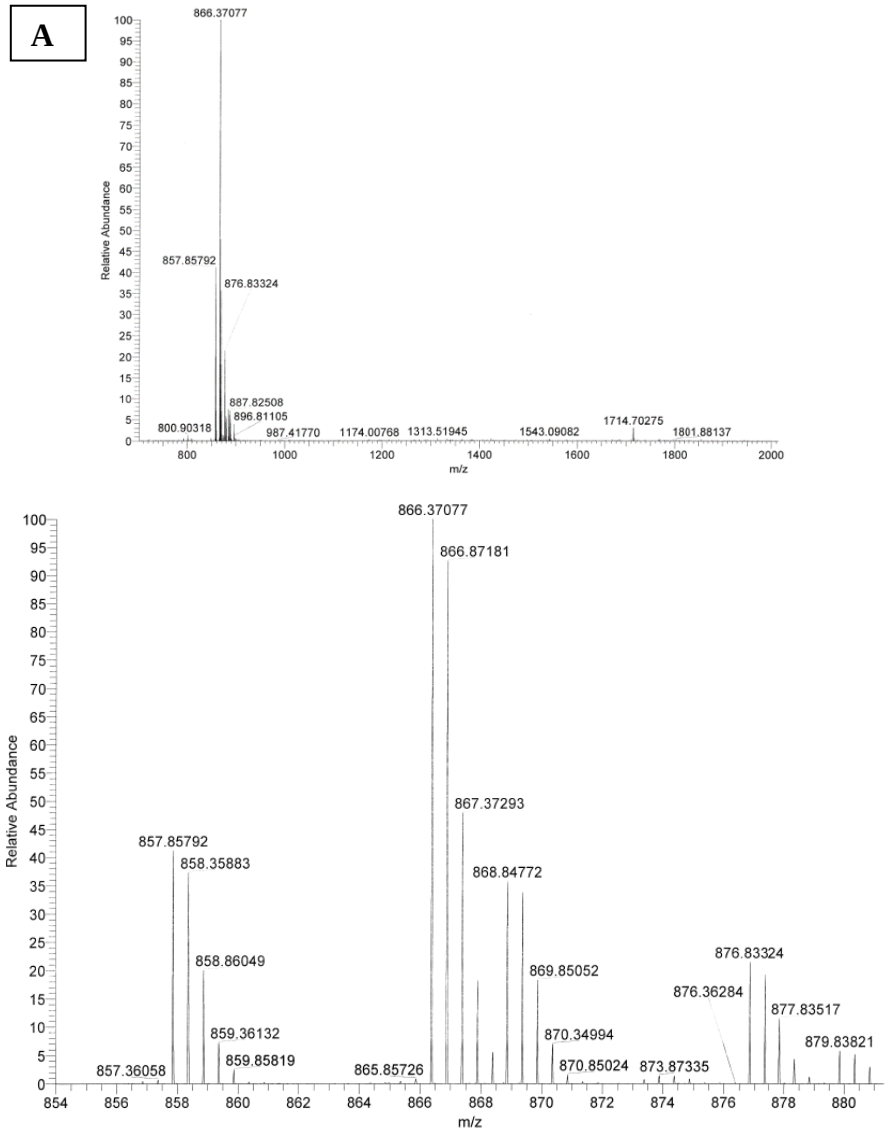

B

Elemental composition search on mass 857.85792

m/z= 852.85792-862.85792

m/z	Theo. Mass	Delta (ppm)	RDB equiv.	Composition
857.85792	857.85769	0.27	31.5	$C_{74}H_{102}O_{26}N_{18}F_3$
	857.85836	-0.51	31.0	$C_{76}H_{104}O_{27}N_{15}F_3$
	857.85903	-1.29	36.0	$C_{77}H_{100}O_{23}N_{19}F_3$
	857.85937	-1.70	26.5	$C_{71}H_{106}O_{26}N_{18}F_3S$
	857.85970	-2.08	35.5	$C_{79}H_{102}O_{24}N_{16}F_3$
	857.86071	-3.26	31.0	$C_{74}H_{104}O_{23}N_{19}F_3S$
	857.85510	3.29	31.0	$C_{75}H_{104}O_{24}N_{17}F_3S$

Figure C.24: HRMS data for Dap-Lys6-*D*-hCys(CF_3)11-Glu12-Trp13 (**4.56**). (A) ESI+ HRMS data for Dap-Lys6-*D*-hCys(CF_3)11-Glu12-Trp13. The peak at *m/z* = 857.85792 corresponds to the $[M+2H]^{2+}$ species. The peak at *m/z* = 866.37077 corresponds to the $[M+H+NH_4]^{2+}$ species. The peak at *m/z* = 868.84772 corresponds to the $[M+H+Na]^{2+}$ species. The peak at *m/z* = 876.83324 corresponds to the $[M+H+K]^{2+}$ species. (B) HRMS data for the peak at *m/z* = 857.85792 is also shown.

A

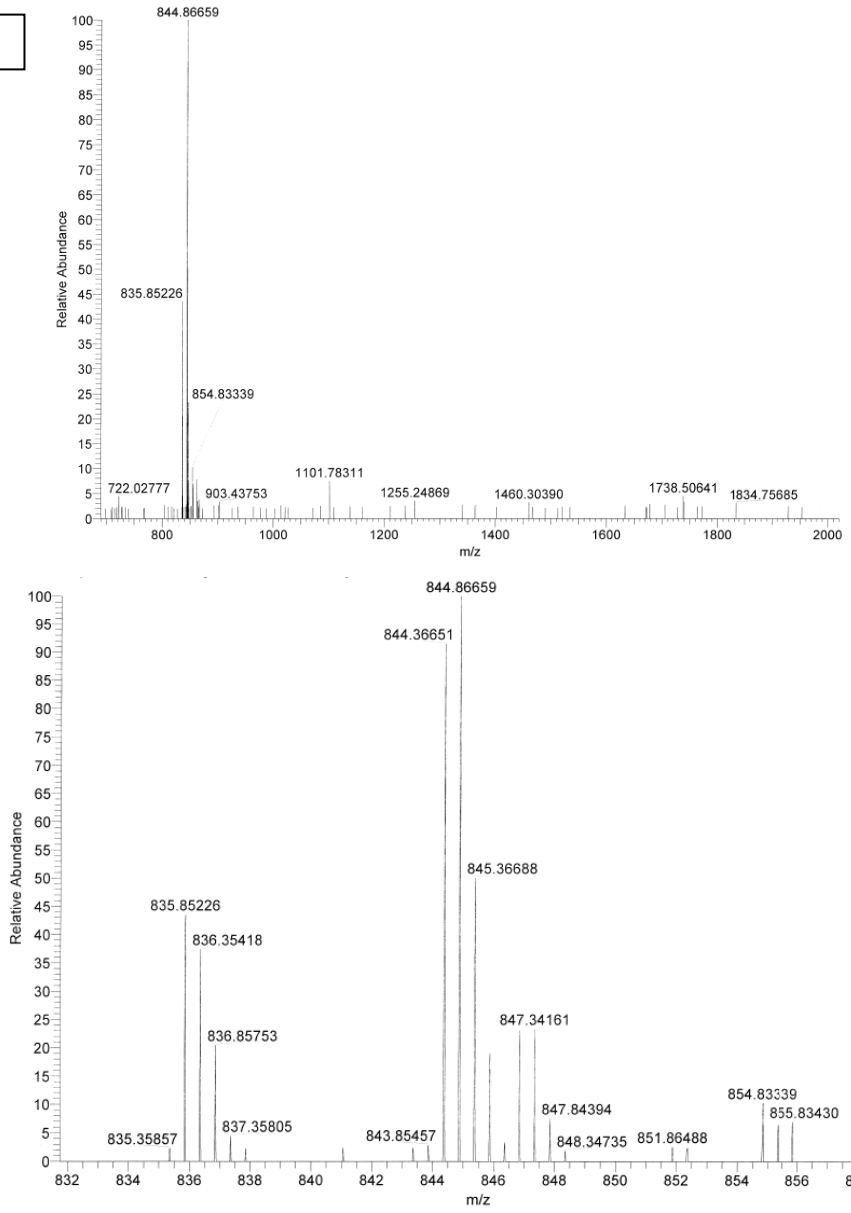

B

Elemental composition search on mass 835.85226

m/z= 830.85226-840.85226

m/z	Theo. Mass	Delta (ppm)	RDB equiv.	Composition
835.85226	835.85255	-0.35	26.0	$C_{70}H_{104}O_{25}N_{17}F_3S$
	835.85288	-0.74	35.0	$C_{78}H_{100}O_{23}N_{15}F_3$
	835.85087	1.66	31.0	$C_{73}H_{100}O_{25}N_{17}F_3$
	835.85389	-1.96	30.5	$C_{73}H_{102}O_{22}N_{18}F_3S$
	835.85457	-2.76	30.0	$C_{75}H_{104}O_{23}N_{15}F_3S$
	835.84953	3.27	26.5	$C_{70}H_{102}O_{28}N_{16}F_3$

Figure C.25: HRMS data for Dap-^{TF}Dec0-Lys6-Glu12-Trp13 (**4.57**). (A) ESI+ HRMS Data for Dap-^{TF}Dec0-Lys6-Glu12-Trp13. The peak at *m/z* = 835.85226 corresponds to the $[M+2H]^{2+}$ species. The peak at *m/z* = 844.36651 corresponds to the $[M+H+NH_4]^{2+}$ species. The peak at *m/z* = 854.83339 corresponds to the $[M+H+K]^{2+}$ species. (B) HRMS data for the peak at *m/z* = 835.85226 is also shown.

Appendix D: Peptide MS/MS Sequencing Data

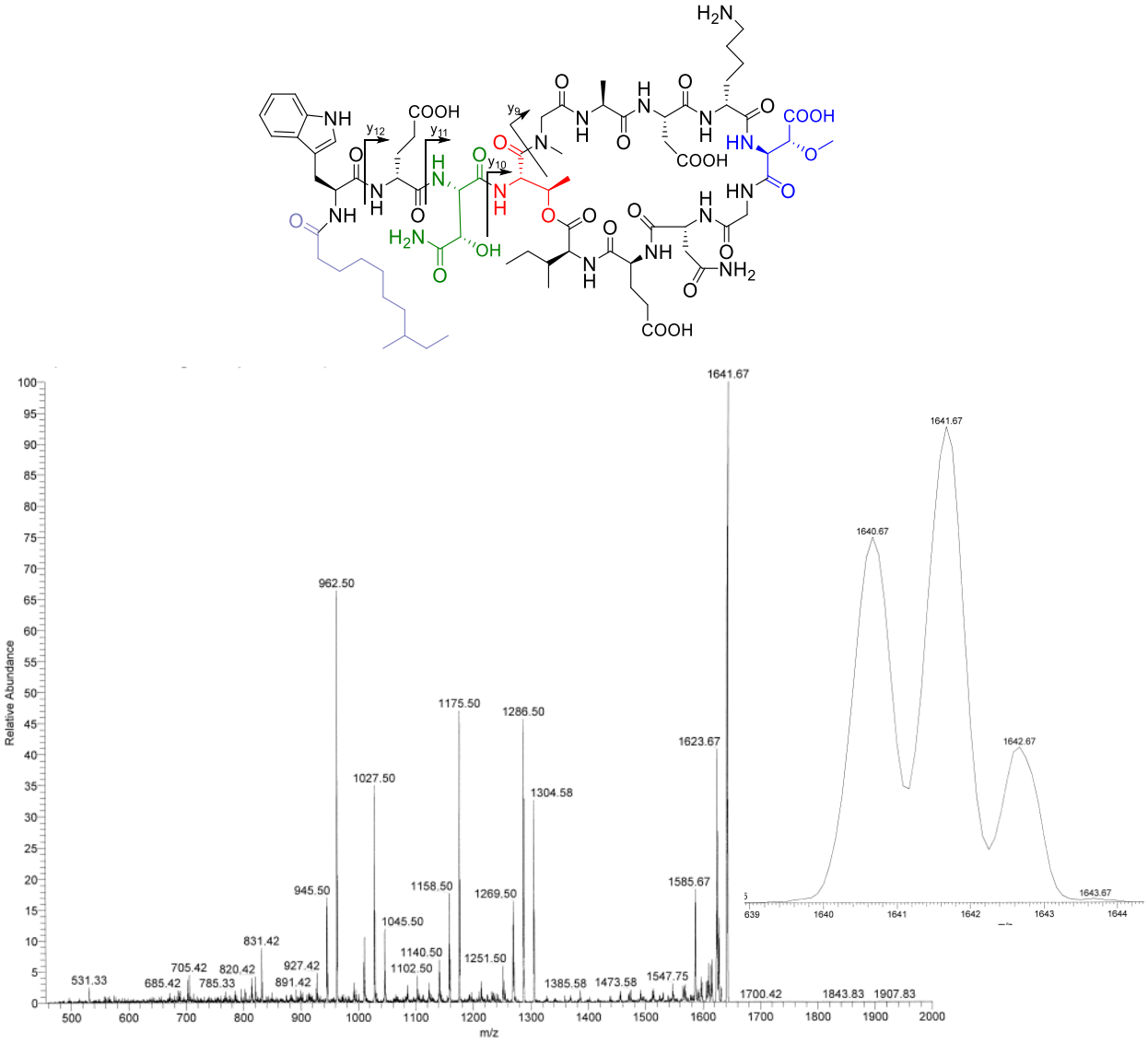

ion	molecular formula	Observed mass of fragment (Calculated mass) (Da)
$[M+H-H_2O]^+$	$C_{73}H_{110}N_{17}O_{26}^+$	1640.7 (1640.8)
$[M+H-NH_3]^+$	$C_{73}H_{109}N_{16}O_{27}^+$	1641.7 (1641.8)
y_9 + 18	$C_{38}H_{64}N_{11}O_{18}^+$	962.5 (962.4)
y_{10}	$C_{42}H_{69}N_{12}O_{19}^+$	1045.5 (1045.5)
y_{11}	$C_{45}H_{75}N_{14}O_{22}^+$	1175.5 (1175.5)
y_{12}	$C_{51}H_{82}N_{15}O_{25}^+$	1304.6 (1304.6)

Figure D.1: MS/MS sequencing of synthetic A54145D. This peptide is also referred to as A54145D-*t*HOAsn3-*e*MeOAsp9. Shown are single bond fragmentations corresponding to y_{10}, y_{11}, and y_{12}, as well as simultaneous cleavage of the ester bond with y_9.

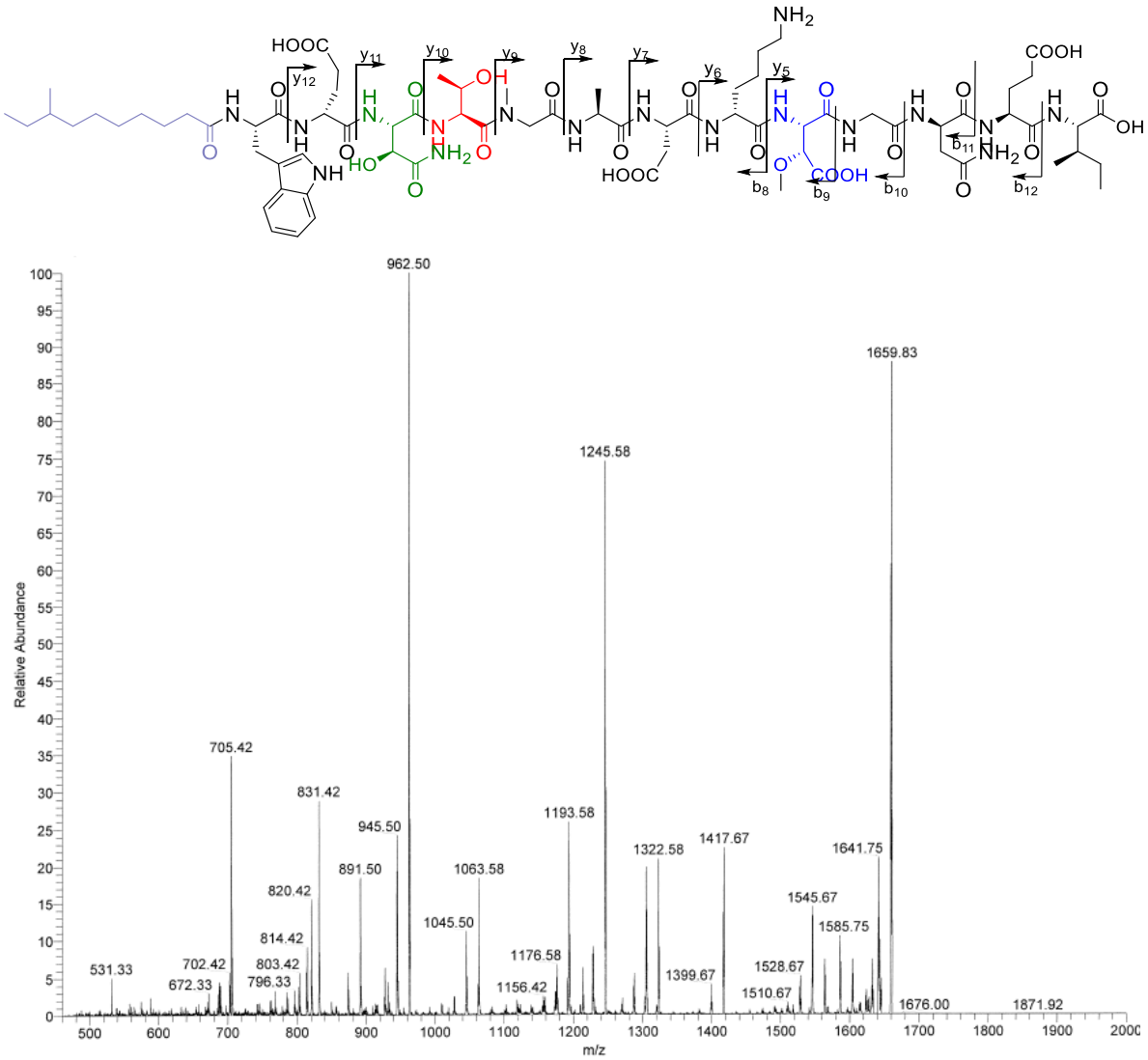

ion	molecular formula	Observed fragment (Calculated mass) (Da)	ion	molecular formula	Observed fragment (Calculated mass) (Da)
$[M+H-H_2O]^+$	$C_{73}H_{112}N_{17}O_{27}^+$	1658.8 (1658.8)	y_6	$C_{28}H_{49}N_8O_{13}^+$	705.4 (705.3)
$[M+H-NH_3]^+$	$C_{73}H_{111}N_{16}O_{28}^+$	1659.8 (1659.8)	y_7	$C_{32}H_{54}N_9O_{16}^+$	820.4 (820.4)
b_9	$C_{56}H_{85}N_{12}O_{20}^+$	1245.6 (1245.6)	y_8	$C_{35}H_{59}N_{10}O_{17}^+$	891.5 (891.4)
b_{10}	$C_{58}H_{88}N_{13}O_{21}^+$	1302.7 (1302.6)	y_9	$C_{38}H_{64}N_{11}O_{18}^+$	962.5 (962.4)
b_{11}	$C_{62}H_{94}N_{15}O_{23}^+$	1416.7 (1416.7)	y_{10}	$C_{42}H_{71}N_{12}O_{20}^+$	1063.6 (1063.5)
b_{12}	$C_{67}H_{101}N_{16}O_{26}^+$	1545.7 (1545.7)	y_{11}	$C_{46}H_{77}N_{14}O_{23}^+$	1193.6 (1193.5)
$y_5 - CO_2$	$C_{21}H_{35}N_6O_{10}^+$	531.3 (531.2)	y_{12}	$C_{51}H_{84}N_{15}O_{26}^+$	1322.6 (1322.6)

Figure D.2: MS/MS sequencing of hydrolyzed synthetic A54145D. The peptide was hydrolyzed with 0.1 M LiOH (aq). The fragment associated with y_5 was not observed, due to further fragmentation via decarboxylation.

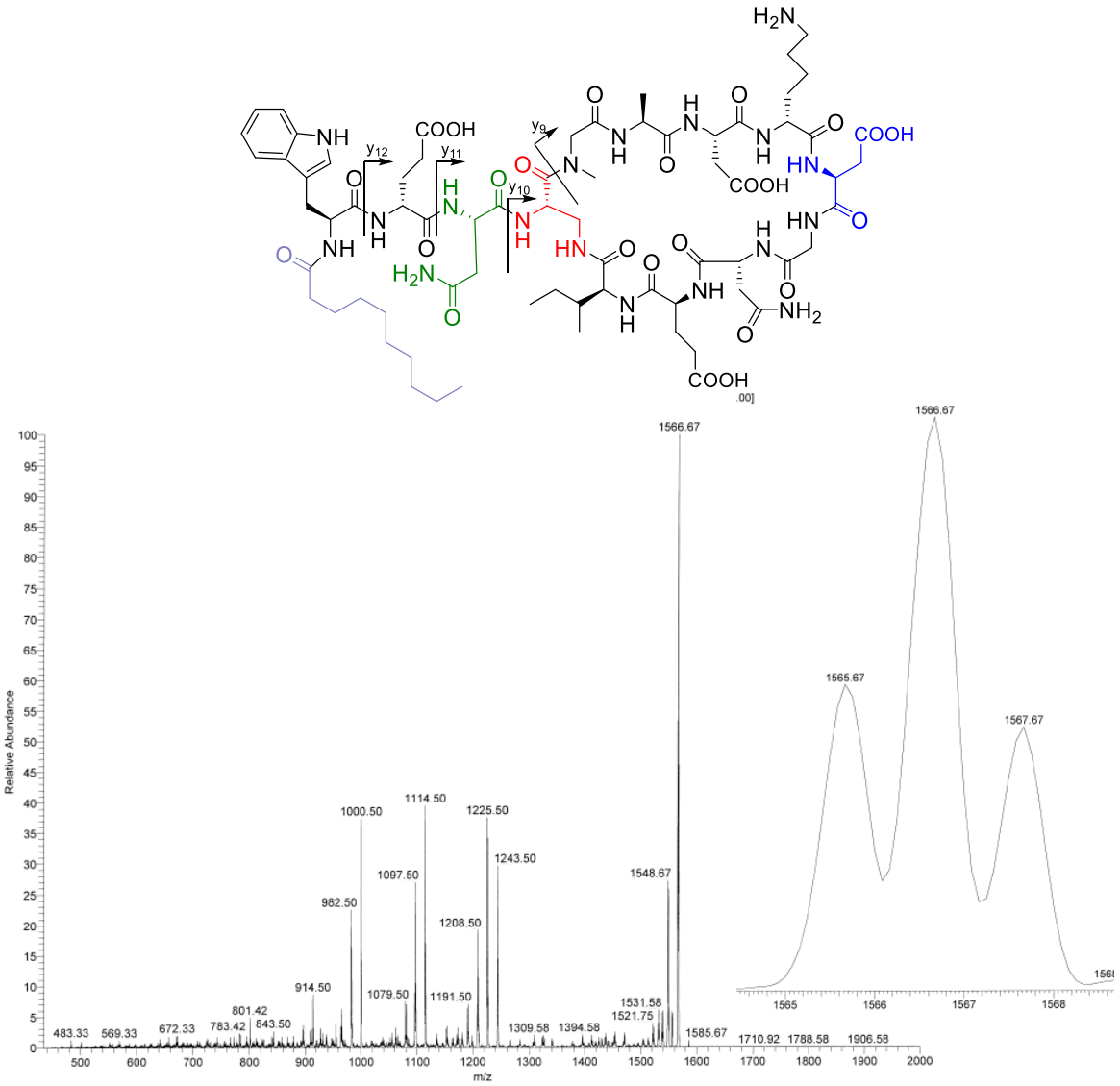

ion	molecular formula	Observed mass of fragment (Calculated mass) (Da)
$[M+H-H_2O]^+$	$C_{70}H_{105}N_{18}O_{23}^+$	1565.7 (1565.8)
$[M+H-NH_3]^+$	$C_{70}H_{104}N_{17}O_{24}^+$	1566.7 (1566.7)
$y_9 + 18$	$C_{37}H_{62}N_{11}O_{17}^+$	--- (932.4)
y_{10}	$C_{40}H_{66}N_{13}O_{17}^+$	1000.5 (1000.5)
y_{11}	$C_{44}H_{72}N_{15}O_{19}^+$	1114.5 (1114.5)
y_{12}	$C_{49}H_{79}N_{16}O_{22}^+$	1243.5 (1243.6)

Figure D.3: MS/MS sequencing of A54145A$_1$-Asn3-DAPA4-Asp9 (**3.2**). Shown are single bond fragmentations corresponding to y_{10}, y_{11}, and y_{12}. The lack of observation of a signal with *m/z* = 932.4 is indicative of an amide bond between DAPA4 and Ile13, as simultaneous cleavage of two amide bonds is less likely than simultaneous cleavage of an amide and ester bond. The spectrum above closely resembles the spectrum obtained by Kopp et al.[78]

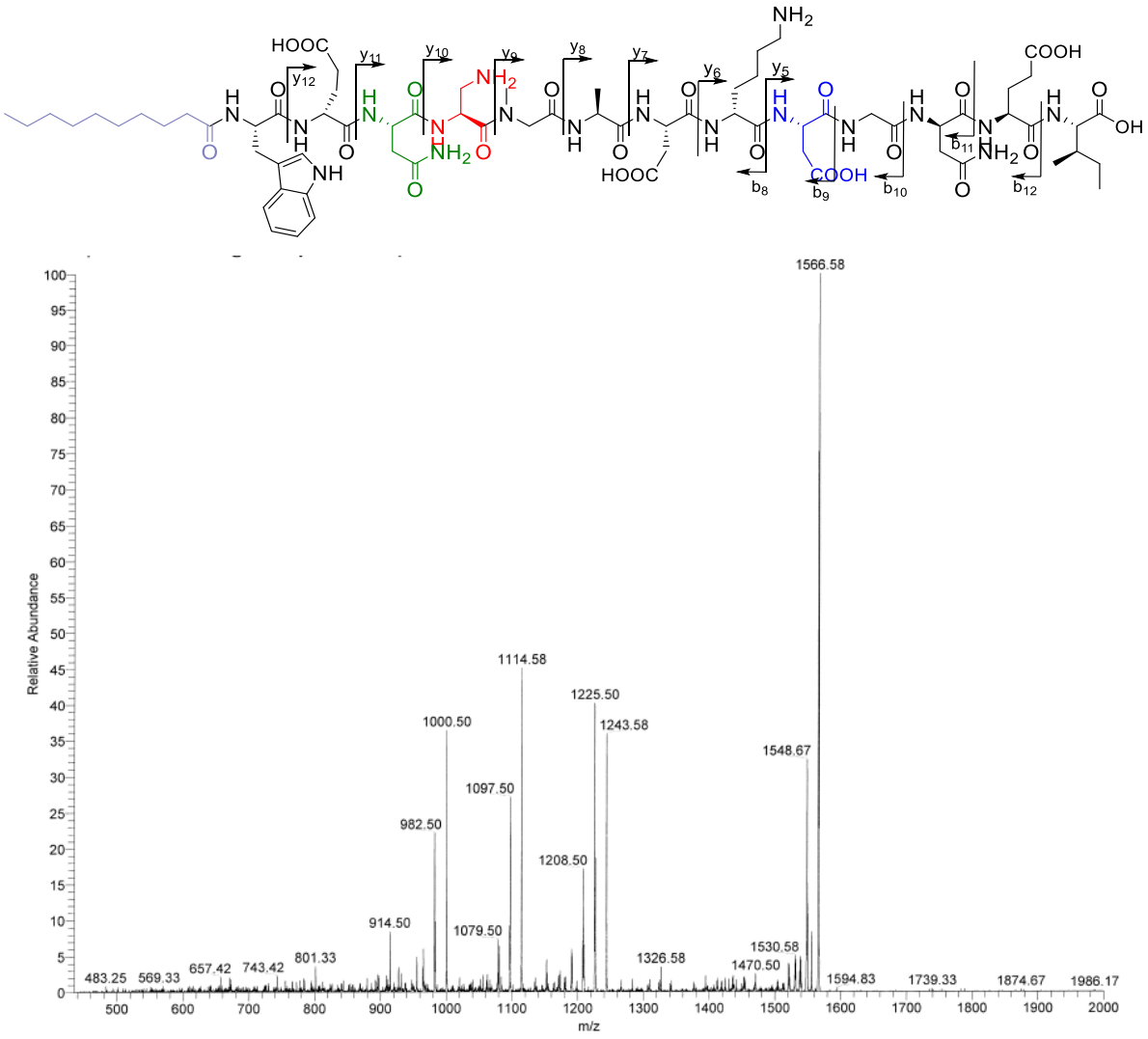

ion	molecular formula	Observed fragment (Calculated mass) (Da)	ion	molecular formula	Observed fragment (Calculated mass) (Da)
$[M+H-H_2O]^+$	$C_{70}H_{107}N_{18}O_{24}^+$	--- (1583.8)	y_6	$C_{27}H_{47}N_8O_{12}^+$	--- (675.3)
$[M+H-NH_3]^+$	$C_{70}H_{106}N_{17}O_{25}^+$	--- (1584.8)	y_7	$C_{31}H_{52}N_9O_{15}^+$	--- (790.4)
b_9	$C_{53}H_{80}N_{13}O_{17}^+$	--- (1170.6)	y_8	$C_{34}H_{57}N_{10}O_{16}^+$	--- (861.4)
b_{10}	$C_{55}H_{83}N_{14}O_{18}^+$	--- (1227.6)	y_9	$C_{37}H_{62}N_{11}O_{17}^+$	--- (932.4)
b_{11}	$C_{59}H_{89}N_{16}O_{20}^+$	--- (1341.6)	y_{10}	$C_{40}H_{68}N_{13}O_{18}^+$	--- (1018.5)
b_{12}	$C_{64}H_{96}N_{17}O_{23}^+$	--- (1470.7)	y_{11}	$C_{44}H_{74}N_{15}O_{20}^+$	--- (1132.5)
$y_5 - CO_2$	$C_{20}H_{33}N_6O_9^+$	--- (501.2)	y_{12}	$C_{49}H_{81}N_{16}O_{23}^+$	--- (1261.6)

Figure D.4: MS/MS after attempted hydrolysis of A54145A$_1$-Asn3-DAPA4-Asp9 (**3.2**). After subjecting A54145A$_1$-Asn3-DAPA4-Asp9 to 0.1 M LiOH (aq) for 24 h, no hydrolyzed product was observed, confirming that the side-chain of DAPA4 is attached to the α-carboxylic acid of Ile13 by an amide bond. Accordingly, the spectrum above is virtually identical to Figure D.3.

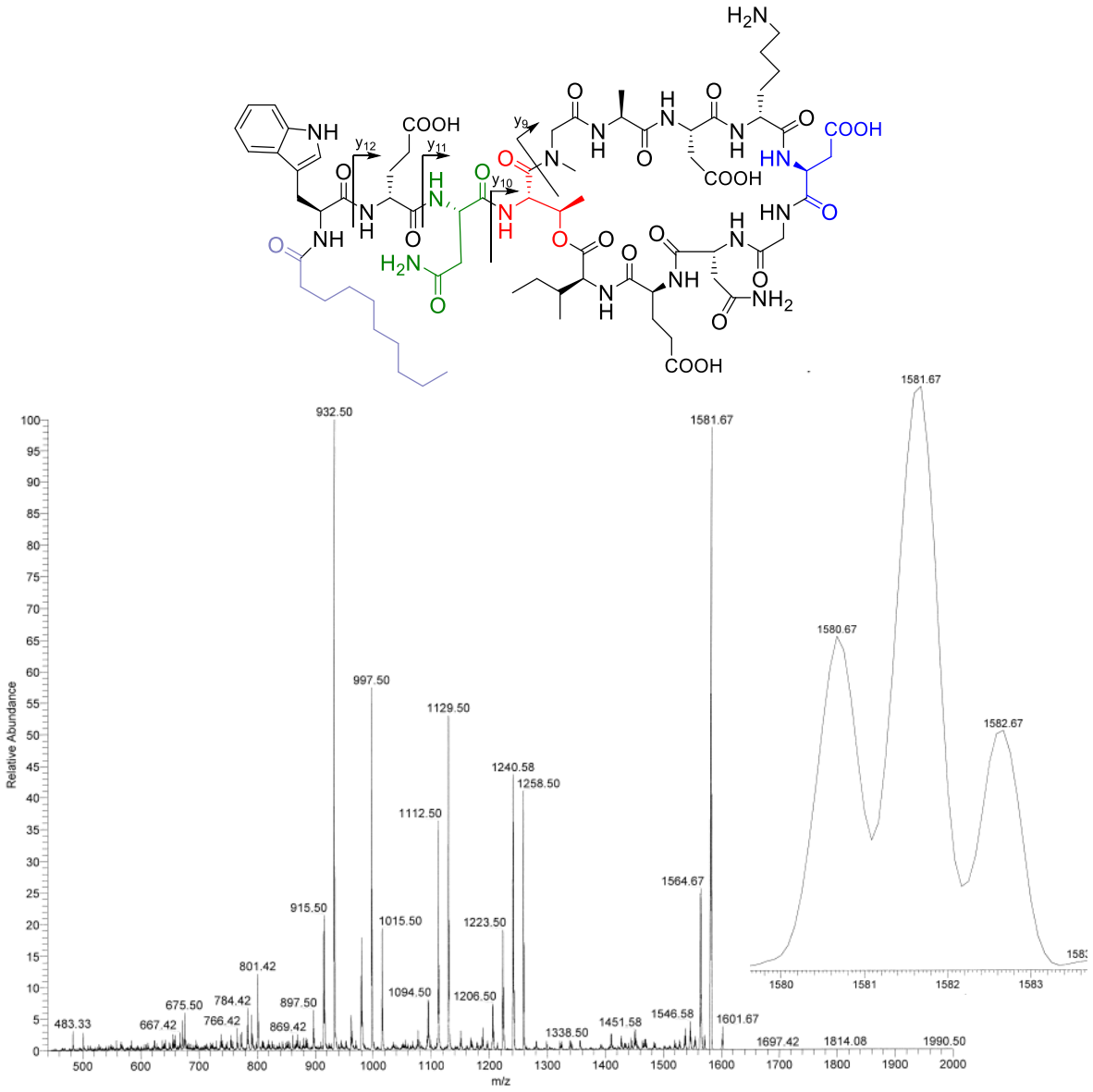

ion	molecular formula	Observed mass of fragment (Calculated mass) (Da)
$[M+H-H_2O]^+$	$C_{71}H_{106}N_{17}O_{24}^+$	1580.7 (1580.8)
$[M+H-NH_3]^+$	$C_{71}H_{105}N_{16}O_{25}^+$	1581.7 (1581.7)
y_9 + 18	$C_{37}H_{62}N_{11}O_{17}^+$	932.5 (932.4)
y_{10}	$C_{41}H_{67}N_{12}O_{19}^+$	1015.5 (1015.5)
y_{11}	$C_{45}H_{73}N_{14}O_{20}^+$	1129.5 (1129.5)
y_{12}	$C_{50}H_{80}N_{15}O_{23}^+$	1258.5 (1258.6)

Figure D.5: MS/MS sequencing of A54145A$_1$-Asn3-Asp9 (**3.1**). Shown are single bond fragmentations corresponding to y_{10}, y_{11}, and y_{12}, as well as simultaneous cleavage of the ester bond with y_9.

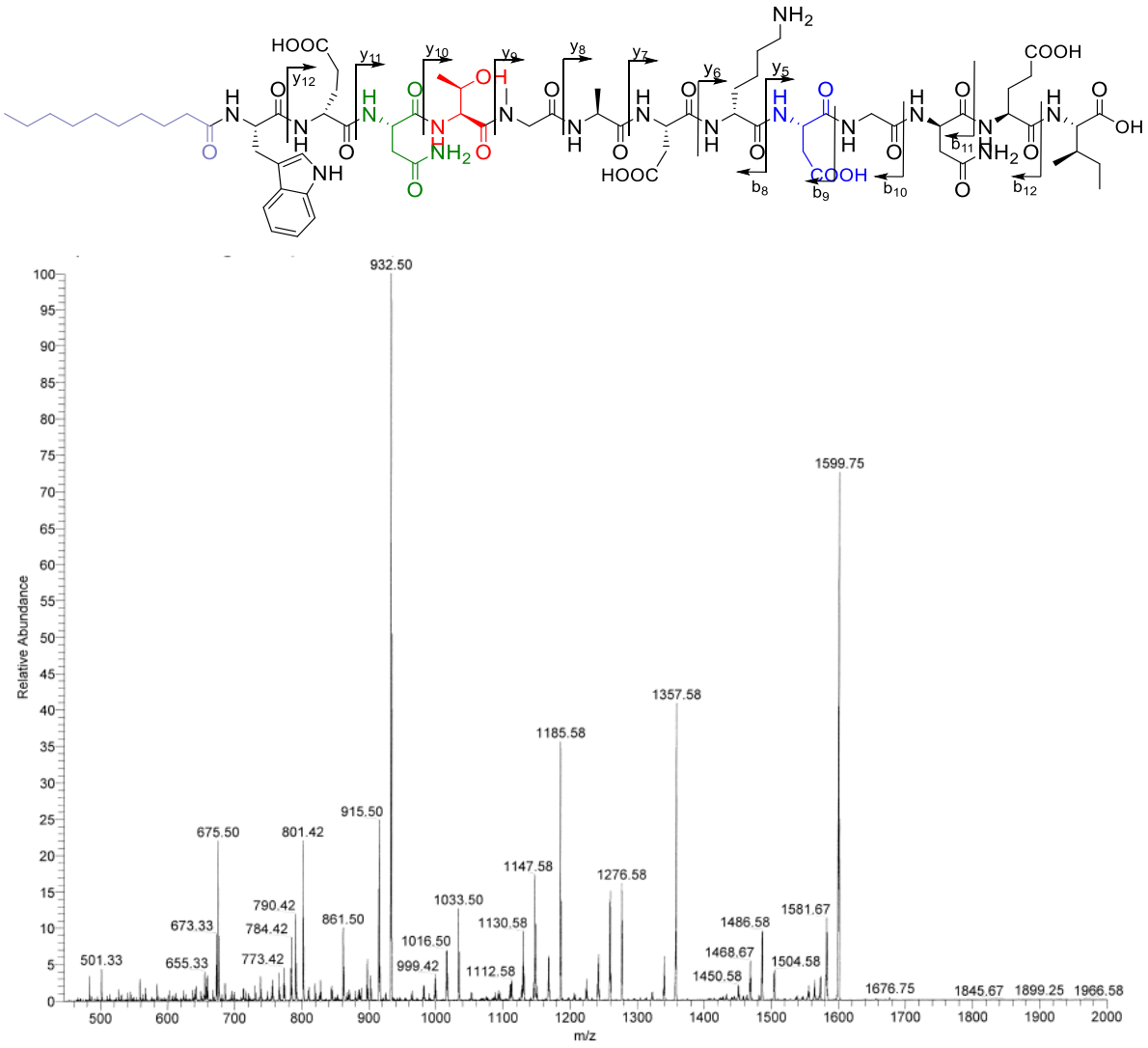

ion	molecular formula	Observed fragment (Calculated mass) (Da)	ion	molecular formula	Observed fragment (Calculated mass) (Da)
$[M+H-H_2O]^+$	$C_{71}H_{108}N_{17}O_{25}^+$	1598.8 (1598.8)	y_6	$C_{27}H_{47}N_8O_{12}^+$	675.5 (675.3)
$[M+H-NH_3]^+$	$C_{71}H_{107}N_{16}O_{26}^+$	1599.8 (1599.8)	y_7	$C_{31}H_{52}N_9O_{15}^+$	790.4 (790.4)
b_9	$C_{54}H_{81}N_{12}O_{18}^+$	1185.6 (1185.6)	y_8	$C_{34}H_{57}N_{10}O_{16}^+$	861.5 (861.4)
b_{10}	$C_{56}H_{84}N_{13}O_{19}^+$	1242.6 (1242.6)	y_9	$C_{37}H_{62}N_{11}O_{17}^+$	932.5 (932.4)
b_{11}	$C_{60}H_{90}N_{14}O_{21}^+$	1356.7 (1356.7)	y_{10}	$C_{41}H_{69}N_{12}O_{19}^+$	1033.5 (1033.5)
b_{12}	$C_{65}H_{97}N_{16}O_{24}^+$	1485.7 (1485.7)	y_{11}	$C_{45}H_{75}N_{14}O_{21}^+$	1147.6 (1147.5)
$y_5 - CO_2$	$C_{20}H_{33}N_6O_9^+$	501.3 (501.2)	y_{12}	$C_{50}H_{82}N_{15}O_{24}^+$	1276.6 (1276.6)

Figure D.6: MS/MS sequencing of hydrolyzed A54145A$_1$-Asn3-Asp9 (**3.1**). The peptide was hydrolyzed with 0.1 M LiOH (aq). The fragment associated with y_5 was not observed, due to further fragmentation via decarboxylation.

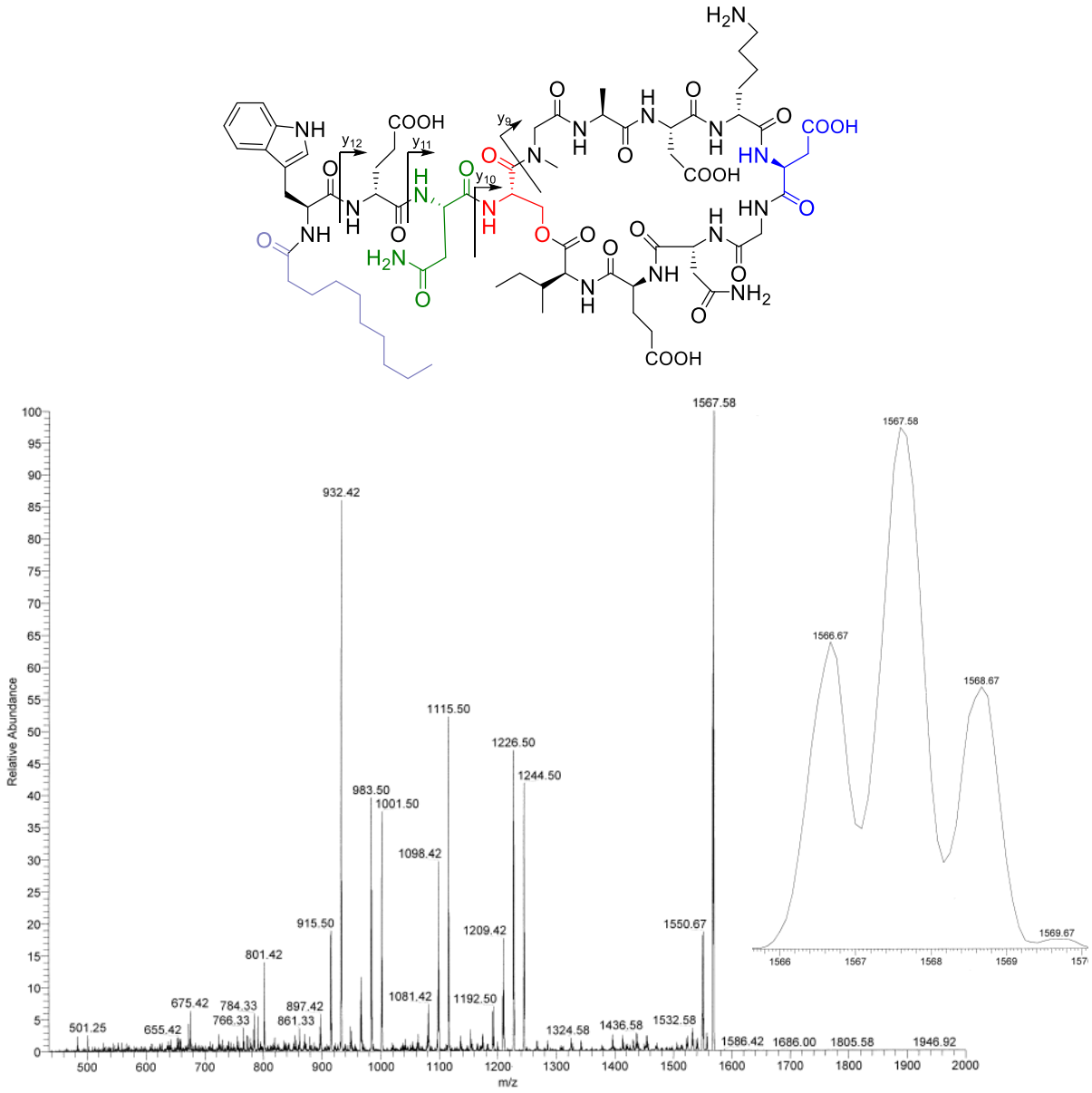

ion	molecular formula	Observed mass of fragment (Calculated mass) (Da)
$[M+H-H_2O]^+$	$C_{70}H_{104}N_{17}O_{24}^+$	1566.7 (1566.7)
$[M+H-NH_3]^+$	$C_{70}H_{103}N_{16}O_{25}^+$	1567.6 (1567.7)
$y_9 + 18$	$C_{37}H_{62}N_{11}O_{17}^+$	932.4 (932.4)
y_{10}	$C_{40}H_{65}N_{12}O_{19}^+$	1001.5 (1001.5)
y_{11}	$C_{44}H_{71}N_{14}O_{20}^+$	1115.5 (1115.5)
y_{12}	$C_{49}H_{78}N_{15}O_{23}^+$	1244.5 (1244.5)

Figure D.7: MS/MS sequencing of A54145A$_1$-Asn3-Ser4-Asp9 (**3.32**). Shown are single bond fragmentations corresponding to y_{10}, y_{11}, and y_{12}, as well as simultaneous cleavage of the ester bond with y_9.

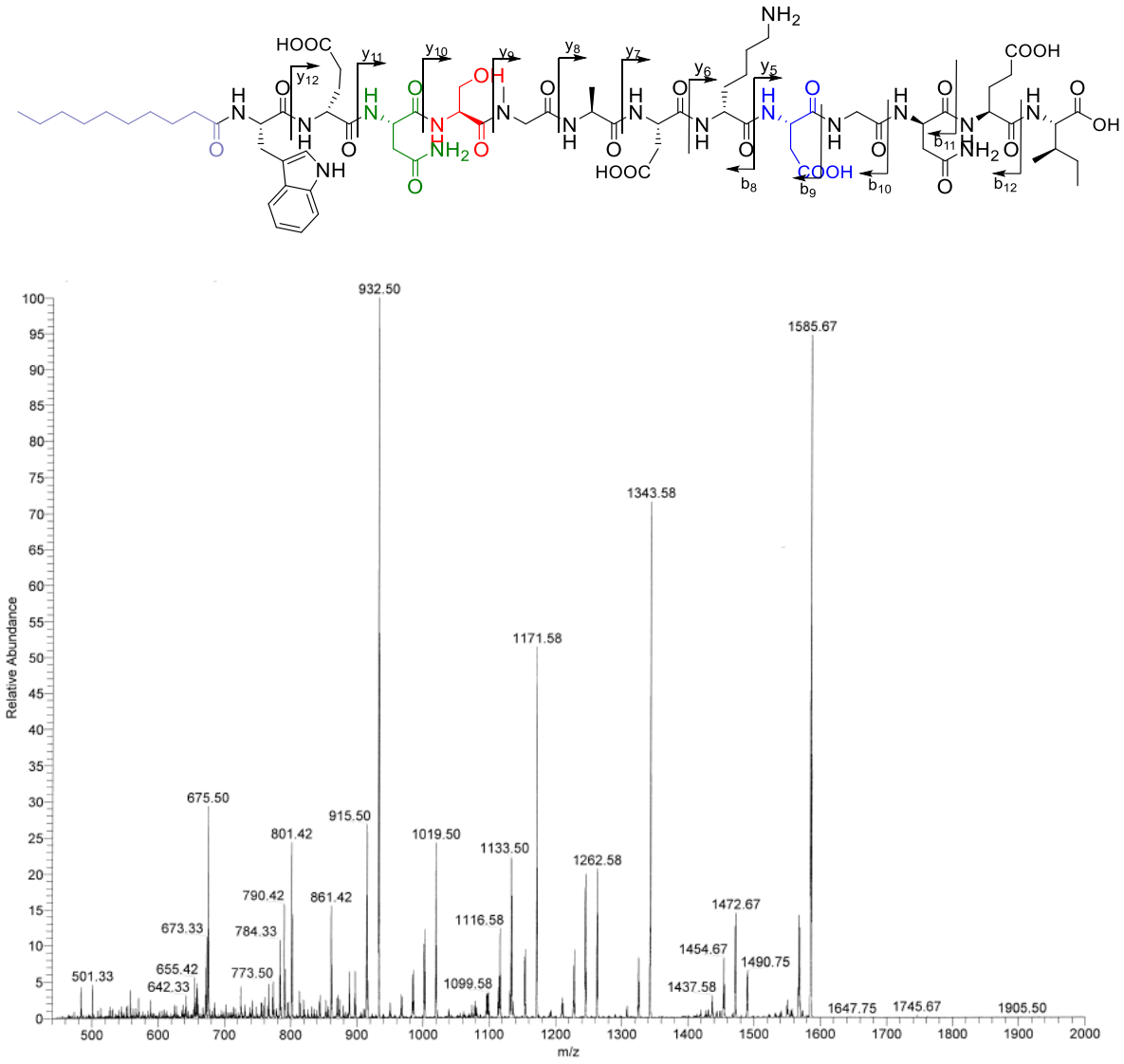

ion	molecular formula	Observed fragment (Calculated mass) (Da)	ion	molecular formula	Observed fragment (Calculated mass) (Da)
$[M+H-H_2O]^+$	$C_{70}H_{106}N_{17}O_{25}^+$	1584.8 (1584.8)	y_6	$C_{27}H_{47}N_8O_{12}^+$	675.5 (675.3)
$[M+H-NH_3]^+$	$C_{70}H_{105}N_{16}O_{26}^+$	1585.7 (1585.7)	y_7	$C_{31}H_{52}N_9O_{15}^+$	790.4 (790.4)
b_9	$C_{53}H_{79}N_{12}O_{18}^+$	1171.6 (1171.6)	y_8	$C_{34}H_{57}N_{10}O_{16}^+$	861.5 (861.4)
b_{10}	$C_{55}H_{82}N_{13}O_{19}^+$	1228.6 (1228.6)	y_9	$C_{37}H_{62}N_{11}O_{17}^+$	932.5 (932.4)
b_{11}	$C_{59}H_{88}N_{14}O_{21}^+$	1342.7 (1342.6)	y_{10}	$C_{40}H_{67}N_{12}O_{19}^+$	1019.5 (1019.5)
b_{12}	$C_{64}H_{95}N_{16}O_{24}^+$	1471.7 (1471.7)	y_{11}	$C_{44}H_{73}N_{14}O_{21}^+$	1133.5 (1133.5)
$y_5 - CO_2$	$C_{20}H_{33}N_6O_9^+$	501.3 (501.2)	y_{12}	$C_{49}H_{80}N_{15}O_{24}^+$	1262.6 (1262.6)

Figure D.8: MS/MS sequencing of hydrolyzed A54145A$_1$-Asn3-Ser4-Asp9 (**3.32**). The peptide was hydrolyzed with 0.1 M LiOH (aq). The fragment associated with y_5 was not observed, due to further fragmentation via decarboxylation.

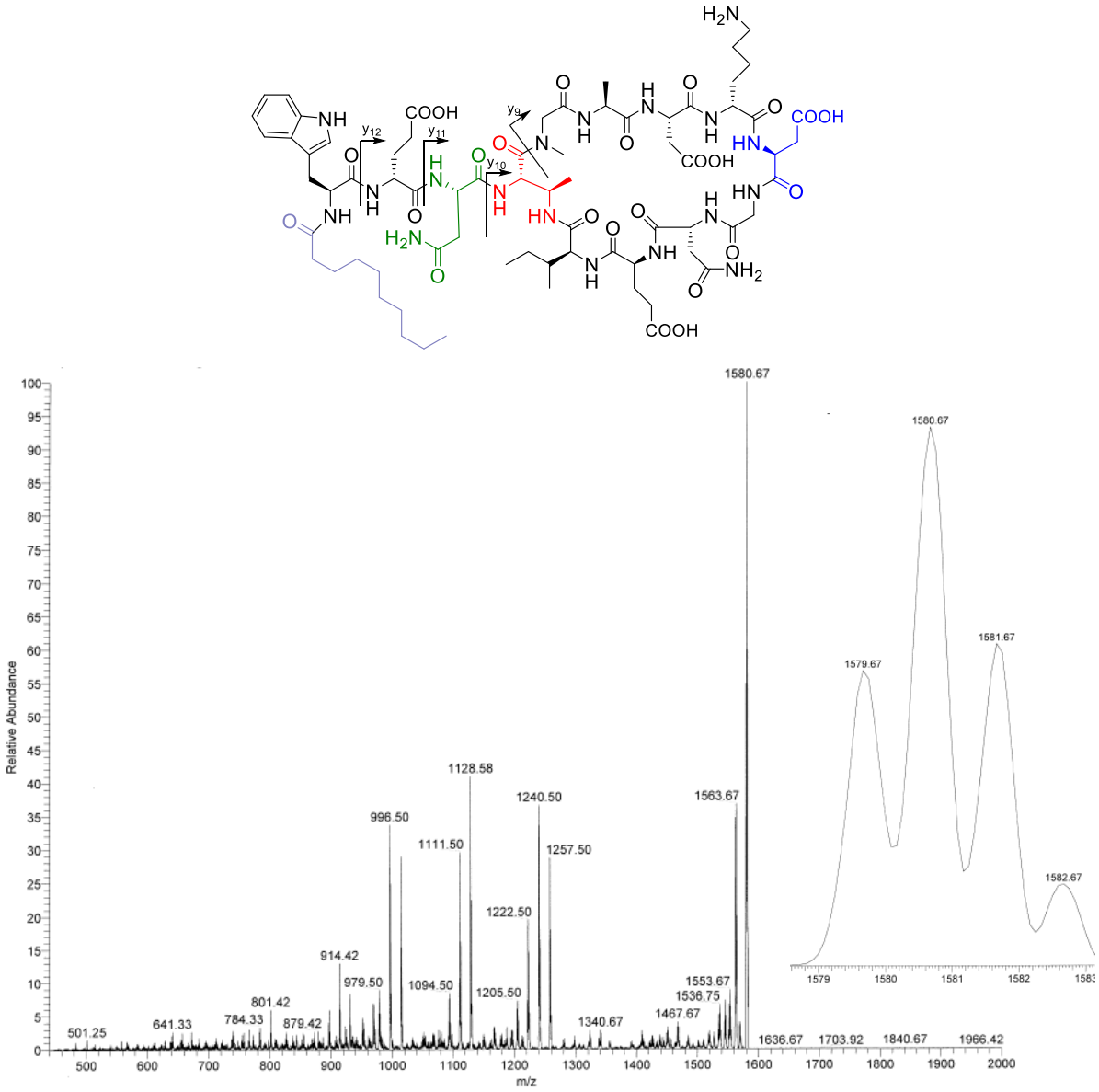

ion	molecular formula	Observed mass of fragment (Calculated mass) (Da)
$[M+H-H_2O]^+$	$C_{71}H_{107}N_{18}O_{23}^+$	1579.7 (1579.8)
$[M+H-NH_3]^+$	$C_{71}H_{104}N_{17}O_{24}^+$	1580.7 (1580.8)
$y_9 + 18$	$C_{37}H_{62}N_{11}O_{17}^+$	--- (932.4)
y_{10}	$C_{41}H_{68}N_{13}O_{17}^+$	1014.5 (1014.5)
y_{11}	$C_{45}H_{74}N_{15}O_{19}^+$	1128.6 (1128.5)
y_{12}	$C_{50}H_{81}N_{16}O_{22}^+$	1257.5 (1257.6)

Figure D.9: MS/MS sequencing of A54145A$_1$-Asn3-DABA4-Asp9 (**3.33**). Shown are single bond fragmentations corresponding to y_{10}, y_{11}, and y_{12}. The lack of observation of a signal with *m/z* = 932.5 is indicative of an amide bond between DABA4 and Ile13, as simultaneous cleavage of two amide bonds is less likely than simultaneous cleavage of an amide and ester bond.

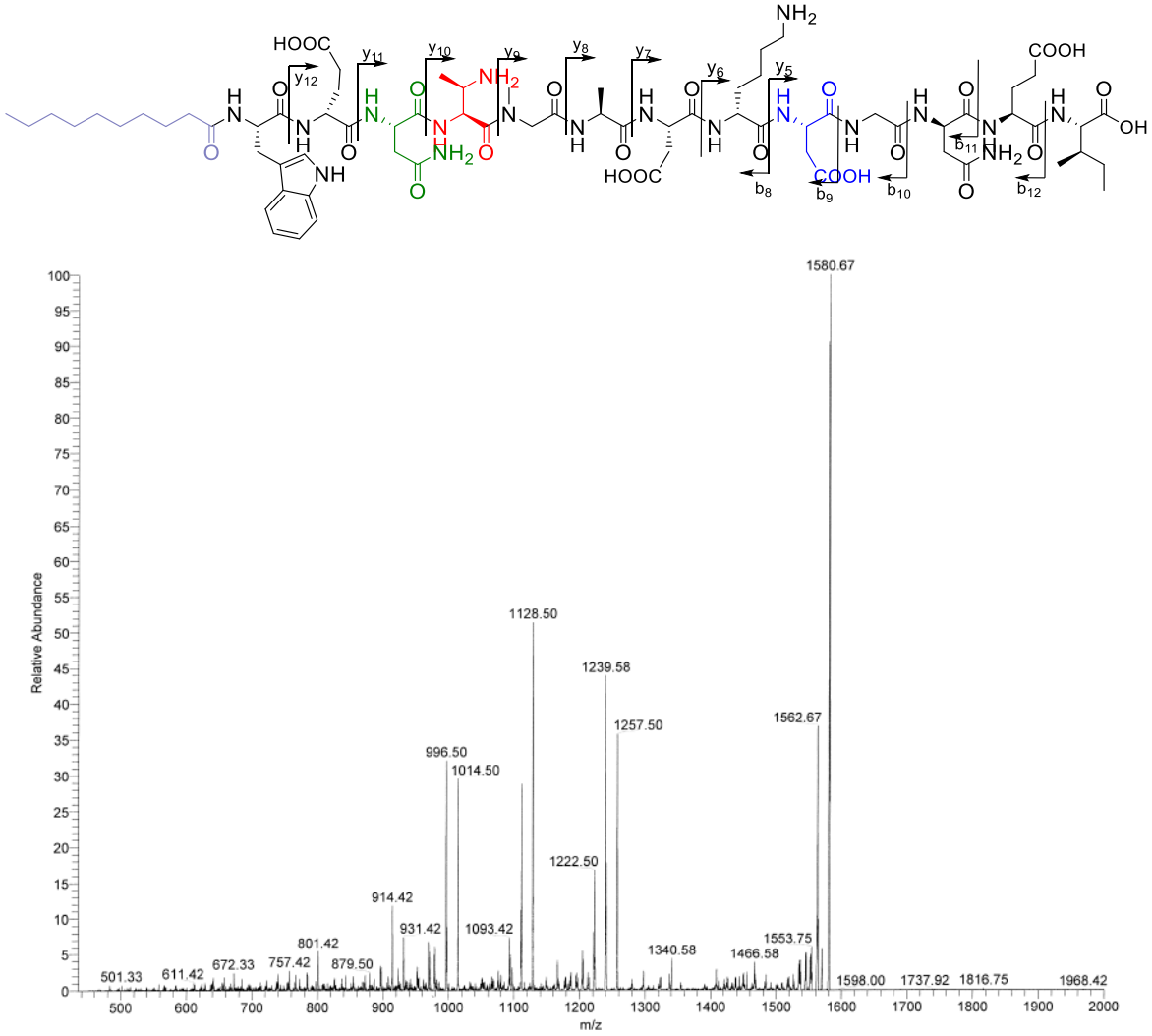

ion	molecular formula	Observed fragment (Calculated mass) (Da)	ion	molecular formula	Observed fragment (Calculated mass) (Da)
$[M+H-H_2O]^+$	$C_{71}H_{109}N_{18}O_{24}^+$	--- (1597.8)	y_6	$C_{27}H_{47}N_8O_{12}^+$	--- (675.3)
$[M+H-NH_3]^+$	$C_{71}H_{108}N_{17}O_{25}^+$	--- (1598.8)	y_7	$C_{31}H_{52}N_9O_{15}^+$	--- (790.4)
b_9	$C_{54}H_{82}N_{13}O_{17}^+$	--- (1184.6)	y_8	$C_{34}H_{57}N_{10}O_{16}^+$	--- (861.4)
b_{10}	$C_{56}H_{85}N_{14}O_{18}^+$	--- (1241.6)	y_9	$C_{37}H_{62}N_{11}O_{17}^+$	--- (932.4)
b_{11}	$C_{60}H_{91}N_{16}O_{20}^+$	--- (1355.7)	y_{10}	$C_{41}H_{70}N_{13}O_{18}^+$	--- (1032.5)
b_{12}	$C_{65}H_{98}N_{17}O_{23}^+$	--- (1484.7)	y_{11}	$C_{45}H_{76}N_{15}O_{20}^+$	--- (1146.5)
$y_5 - CO_2$	$C_{20}H_{33}N_6O_9^+$	--- (501.2)	y_{12}	$C_{50}H_{83}N_{16}O_{23}^+$	--- (1275.6)

Figure D.10: MS/MS after attempted hydrolysis of A54145A$_1$-Asn3-DABA4-Asp9 (**3.33**). After subjecting A54145A$_1$-Asn3-DABA4-Asp9 to 0.1 M LiOH (aq) for 24 h, no hydrolyzed product was observed, confirming that the side-chain of DABA4 is attached to the α-carboxylic acid of Ile13 by an amide bond. Accordingly, the spectrum above is virtually identical to Figure D.9.

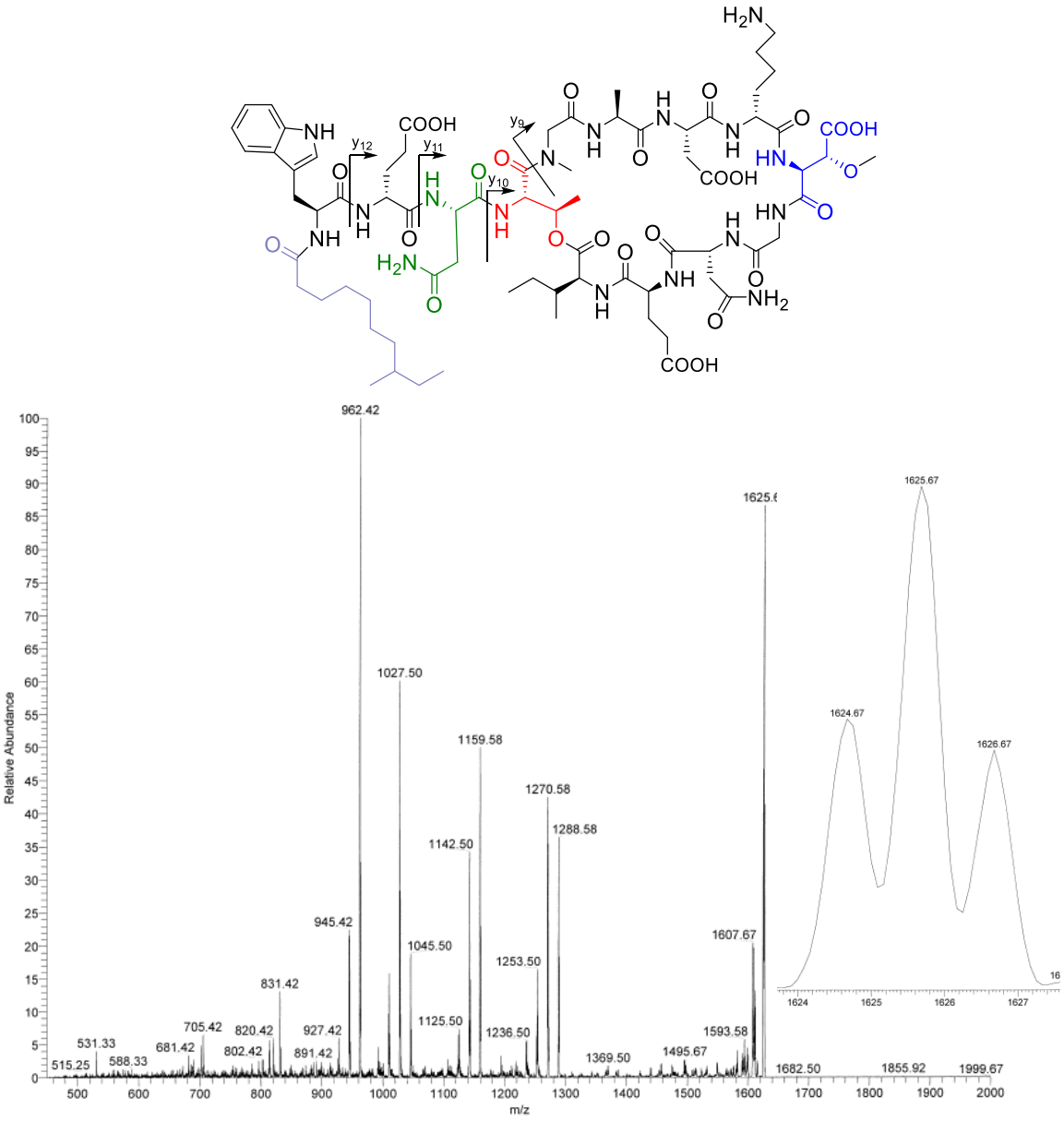

ion	molecular formula	Observed mass of fragment (Calculated mass) (Da)
$[M+H-H_2O]^+$	$C_{73}H_{110}N_{17}O_{25}^+$	1624.7 (1624.8)
$[M+H-NH_3]^+$	$C_{73}H_{109}N_{16}O_{26}^+$	1625.7 (1625.8)
$y_9 + 18$	$C_{38}H_{64}N_{11}O_{18}^+$	962.4 (962.4)
y_{10}	$C_{42}H_{69}N_{12}O_{19}^+$	1045.5 (1045.5)
y_{11}	$C_{46}H_{75}N_{14}O_{21}^+$	1159.6 (1159.5)
y_{12}	$C_{51}H_{82}N_{15}O_{24}^+$	1288.6 (1288.6)

Figure D.11: MS/MS sequencing of A54145D-Asn3 (**3.44**). Shown are single bond fragmentations corresponding to y_{10}, y_{11}, and y_{12}, as well as simultaneous cleavage of the ester bond with y_9.

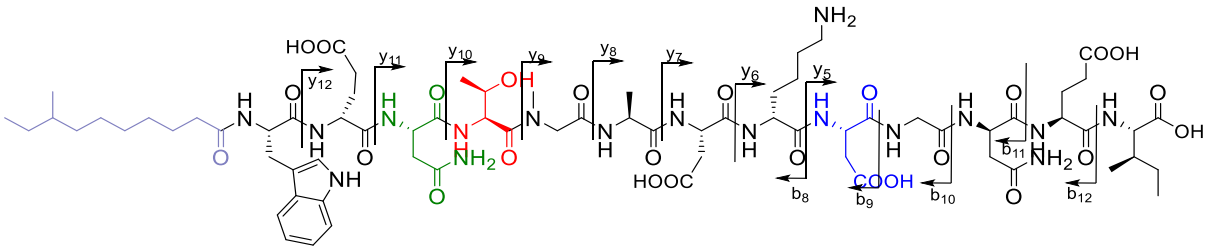

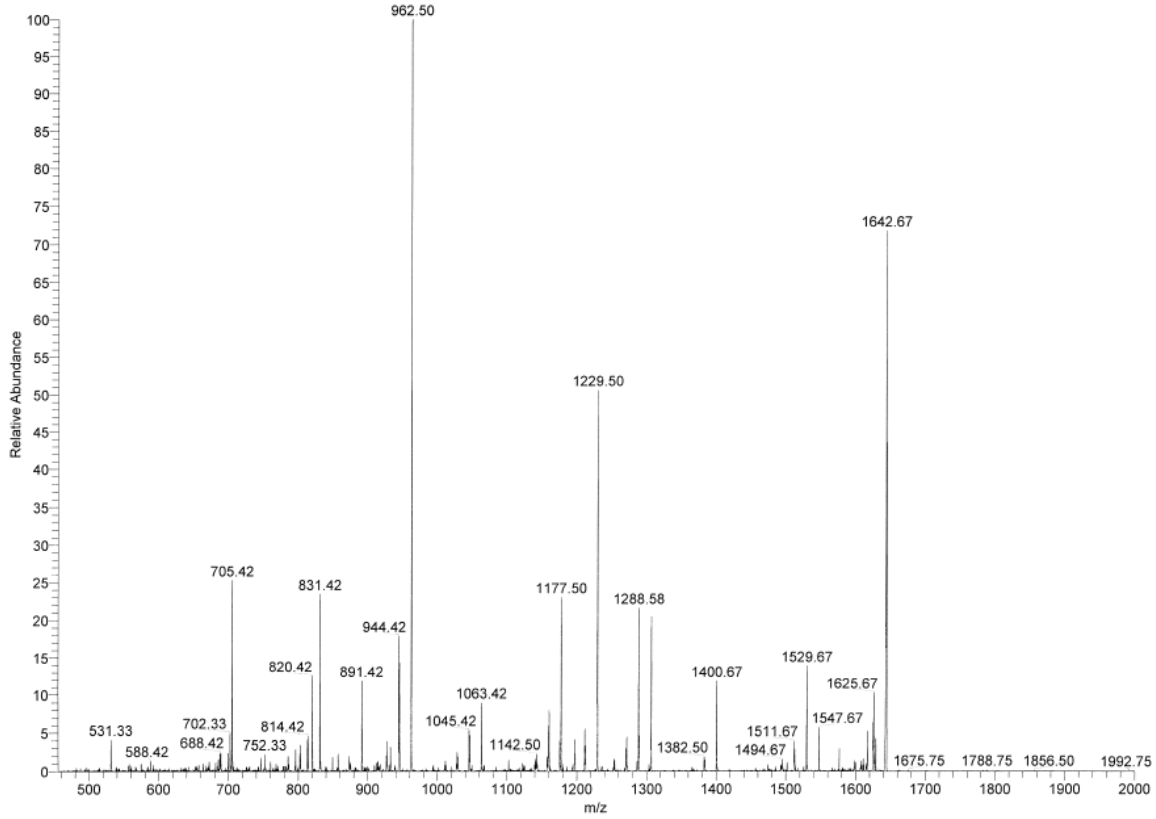

ion	molecular formula	Observed fragment (Calculated mass) (Da)	ion	molecular formula	Observed fragment (Calculated mass) (Da)
$[M+H-H_2O]^+$	$C_{73}H_{112}N_{17}O_{26}^+$	1642.7 (1642.8)	y_6	$C_{28}H_{49}N_8O_{13}^+$	705.4 (705.3)
$[M+H-NH_3]^+$	$C_{73}H_{111}N_{16}O_{27}^+$	1643.7 (1643.7)	y_7	$C_{32}H_{54}N_9O_{16}^+$	820.4 (820.4)
b_9	$C_{56}H_{85}N_{12}O_{19}^+$	1229.5 (1229.6)	y_8	$C_{35}H_{59}N_{10}O_{17}^+$	891.4 (891.4)
b_{10}	$C_{58}H_{88}N_{13}O_{20}^+$	1286.6 (1286.6)	y_9	$C_{38}H_{64}N_{11}O_{18}^+$	962.5 (962.4)
b_{11}	$C_{62}H_{94}N_{14}O_{22}^+$	1400.7 (1400.7)	y_{10}	$C_{42}H_{71}N_{12}O_{20}^+$	1063.4 (1063.5)
b_{12}	$C_{67}H_{101}N_{16}O_{25}^+$	1529.7 (1529.7)	y_{11}	$C_{46}H_{77}N_{14}O_{22}^+$	1177.5 (1177.5)
$y_5 - CO_2$	$C_{21}H_{35}N_6O_{10}^+$	531.3 (531.2)	y_{12}	$C_{51}H_{84}N_{15}O_{25}^+$	1306.5 (1306.6)

Figure D.12: MS/MS sequencing of hydrolyzed A54145D-Asn3 (**3.44**). The peptide was hydrolyzed with 0.1 M LiOH (aq). The fragment associated with y_5 was not observed, due to further fragmentation via decarboxylation.

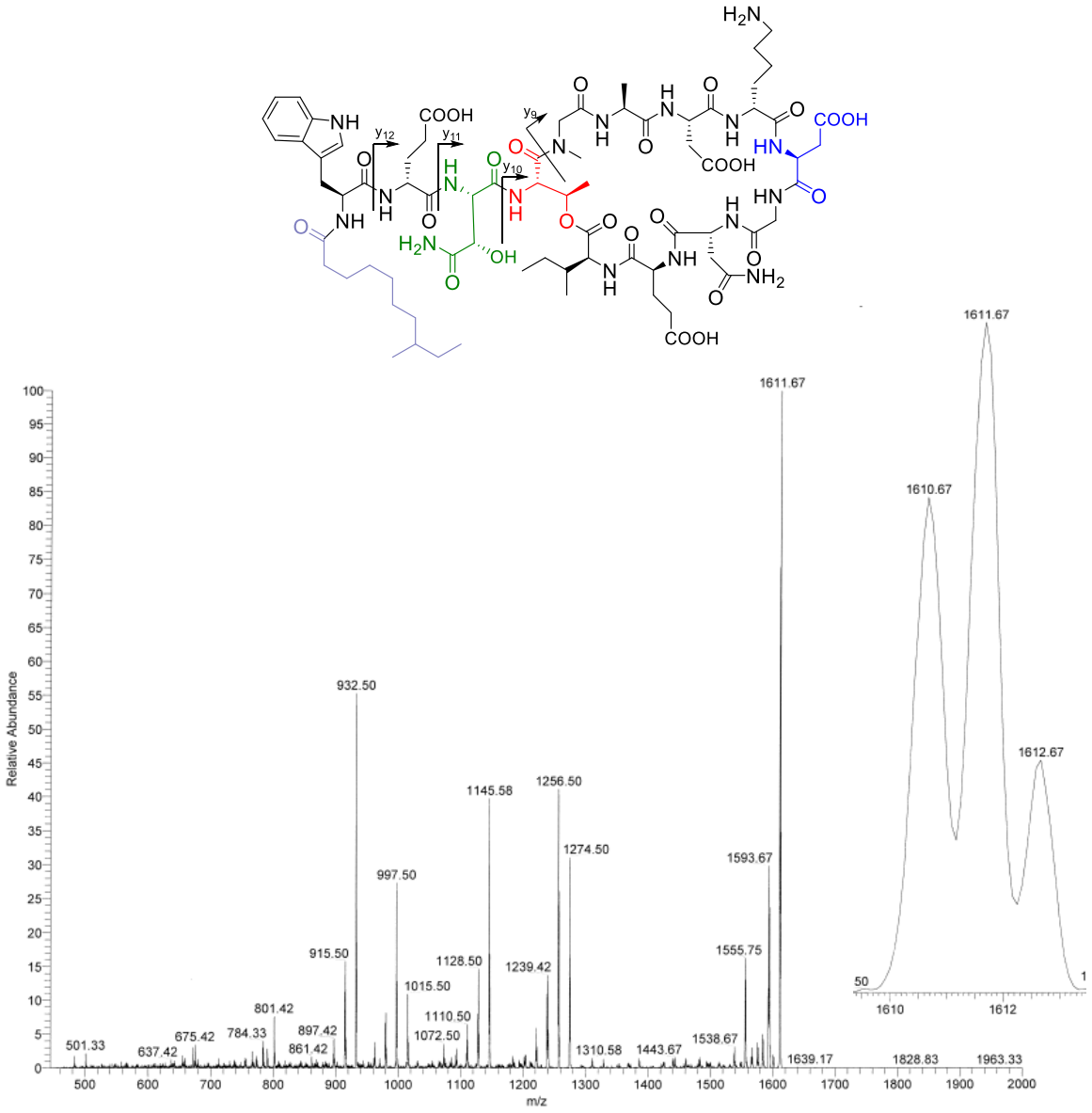

ion	molecular formula	Observed mass of fragment (Calculated mass) (Da)
$[M+H-H_2O]^+$	$C_{72}H_{108}N_{17}O_{25}^+$	1610.7 (1610.8)
$[M+H-NH_3]^+$	$C_{72}H_{107}N_{16}O_{26}^+$	1611.7 (1611.8)
y_9 + 18	$C_{37}H_{62}N_{11}O_{18}^+$	932.5 (932.4)
y_{10}	$C_{41}H_{67}N_{12}O_{19}^+$	1015.5 (1015.5)
y_{11}	$C_{45}H_{73}N_{14}O_{21}^+$	1145.6 (1145.5)
y_{12}	$C_{50}H_{80}N_{15}O_{24}^+$	1274.5 (1274.6)

Figure D.13: MS/MS sequencing of cyclic A54145D-Asp9 (**3.45**). Shown are single bond fragmentations corresponding to y_{10}, y_{11}, and y_{12}, as well as simultaneous cleavage of the ester bond with y_9.

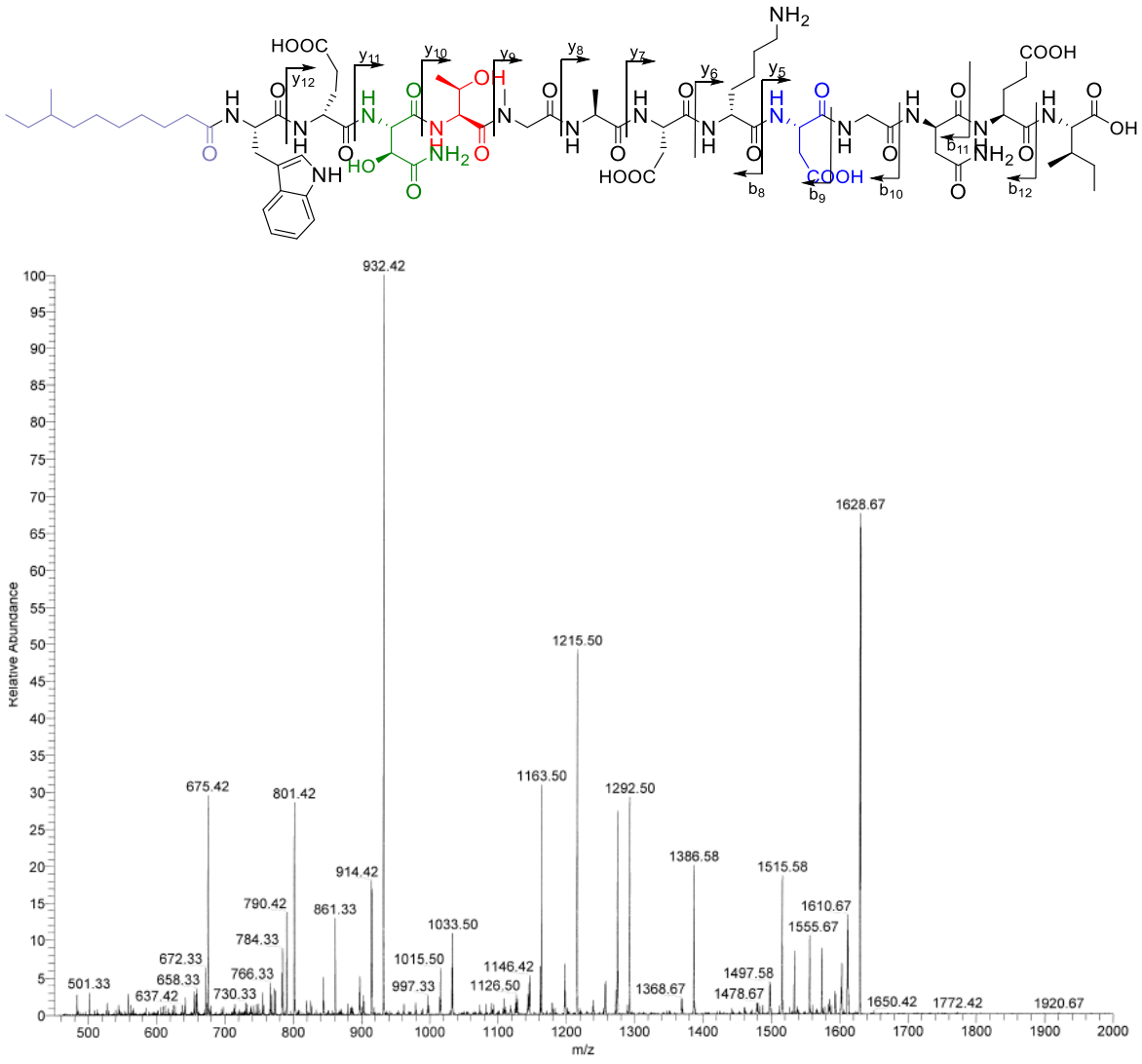

ion	molecular formula	Observed fragment (Calculated mass) (Da)	ion	molecular formula	Observed fragment (Calculated mass) (Da)
$[M+H-H_2O]^+$	$C_{72}H_{110}N_{17}O_{26}^+$	1628.7 (1628.8)	y_6	$C_{27}H_{47}N_8O_{12}^+$	675.4 (675.3)
$[M+H-NH_3]^+$	$C_{72}H_{109}N_{16}O_{27}^+$	1629.7 (1629.8)	y_7	$C_{31}H_{52}N_9O_{15}^+$	790.4 (790.4)
b_9	$C_{55}H_{83}N_{12}O_{19}^+$	1215.5 (1215.6)	y_8	$C_{34}H_{57}N_{10}O_{16}^+$	861.3 (861.4)
b_{10}	$C_{57}H_{86}N_{13}O_{20}^+$	1272.5 (1272.6)	y_9	$C_{37}H_{62}N_{11}O_{17}^+$	932.4 (932.4)
b_{11}	$C_{61}H_{92}N_{14}O_{22}^+$	1386.6 (1386.7)	y_{10}	$C_{41}H_{69}N_{12}O_{19}^+$	1033.5 (1033.5)
b_{12}	$C_{66}H_{99}N_{16}O_{25}^+$	1515.6 (1515.7)	y_{11}	$C_{45}H_{75}N_{14}O_{22}^+$	1163.5 (1163.5)
$y_5 - CO_2$	$C_{20}H_{33}N_6O_9^+$	501.3 (501.2)	y_{12}	$C_{50}H_{82}N_{15}O_{25}^+$	1292.5 (1292.6)

Figure D.14: MS/MS sequencing of hydrolyzed A54145D-Asp9 (**3.45**). The peptide was hydrolyzed with 0.1 M LiOH (aq). The fragment associated with y_5 was not observed, due to further fragmentation via decarboxylation.

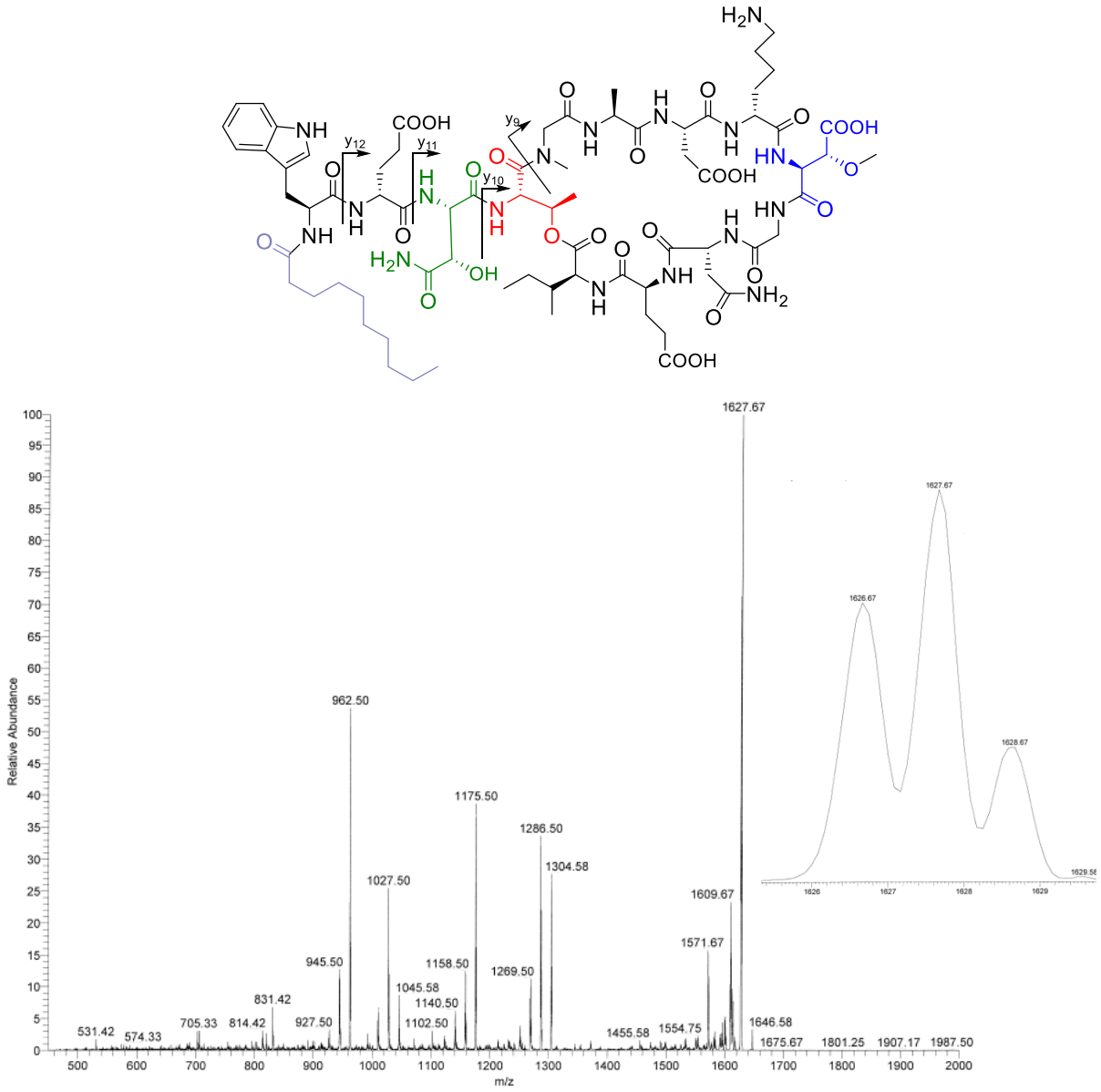

ion	molecular formula	Observed mass of fragment (Calculated mass) (Da)
$[M+H-H_2O]^+$	$C_{72}H_{108}N_{17}O_{26}^+$	1626.7 (1626.8)
$[M+H-NH_3]^+$	$C_{72}H_{107}N_{16}O_{27}^+$	1627.7 (1627.8)
y_9 + 18	$C_{38}H_{64}N_{11}O_{18}^+$	962.5 (962.4)
y_{10}	$C_{42}H_{69}N_{12}O_{19}^+$	1045.6 (1045.5)
y_{11}	$C_{45}H_{75}N_{14}O_{22}^+$	1175.5 (1175.5)
y_{12}	$C_{51}H_{82}N_{15}O_{25}^+$	1304.6 (1304.6)

Figure D.15: MS/MS sequencing of A54145A$_1$ (**1.7**). Shown are single bond fragmentations corresponding to y_{10}, y_{11}, and y_{12}, as well as simultaneous cleavage of the ester bond with y_9.

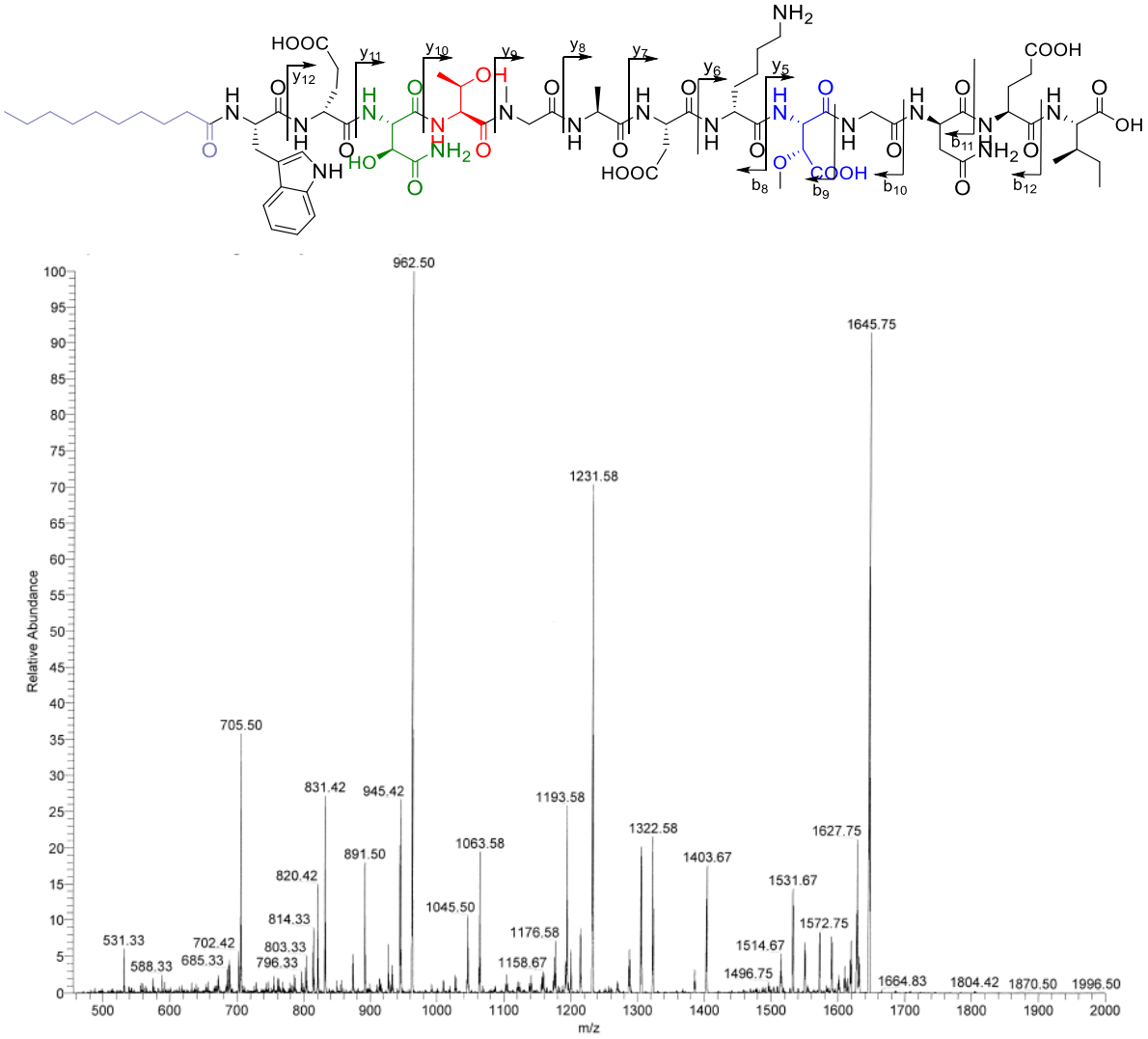

ion	molecular formula	Observed fragment (Calculated mass) (Da)	ion	molecular formula	Observed fragment (Calculated mass) (Da)
$[M+H-H_2O]^+$	$C_{72}H_{110}N_{17}O_{27}^+$	1644.8 (1644.8)	y_6	$C_{28}H_{49}N_8O_{13}^+$	705.5 (705.3)
$[M+H-NH_3]^+$	$C_{72}H_{109}N_{16}O_{28}^+$	1645.8 (1645.8)	y_7	$C_{32}H_{54}N_9O_{16}^+$	820.4 (820.4)
b_9	$C_{55}H_{83}N_{12}O_{20}^+$	1231.6 (1231.6)	y_8	$C_{35}H_{59}N_{10}O_{17}^+$	891.5 (891.4)
b_{10}	$C_{57}H_{86}N_{13}O_{21}^+$	1288.6 (1288.6)	y_9	$C_{38}H_{64}N_{11}O_{18}^+$	962.5 (962.4)
b_{11}	$C_{61}H_{92}N_{15}O_{23}^+$	1402.6 (1402.7)	y_{10}	$C_{42}H_{71}N_{12}O_{20}^+$	1063.6 (1063.5)
b_{12}	$C_{66}H_{99}N_{16}O_{26}^+$	1531.7 (1531.7)	y_{11}	$C_{46}H_{77}N_{14}O_{23}^+$	1193.6 (1193.5)
$y_5 - CO_2$	$C_{21}H_{35}N_6O_{10}^+$	531.3 (531.2)	y_{12}	$C_{51}H_{84}N_{15}O_{26}^+$	1322.6 (1322.6)

Figure D.16: MS/MS sequencing of hydrolyzed A54145A$_1$ (**1.7**). The peptide was hydrolyzed with 0.1 M LiOH (aq). The fragment associated with y_5 was not observed, due to further fragmentation via decarboxylation.

Appendix E: Letters of Copyright Permission

Permission for Figure 1.2:

Copyright Clearance Center Marketplace™

Nature Publishing Group (Permissions) - License Terms and Conditions

Order Date	11-Jan-2020
Order license ID	1005604-1
ISSN	1552-4450
Type of Use	Republish in a thesis/dissertation
Publisher	NATURE PUBLISHING GROUP
Portion	Image/photo/illustration

LICENSED CONTENT

Publication Title	Nature chemical biology	Rightsholder	Nature Publishing Group (Permissions)
Date	01/01/2005	Publication Type	Journal
Language	English	URL	http://www.nature.com/nchembio/index.html
Country	United Kingdom of Great Britain and Northern Ireland		

REQUEST DETAILS

Portion Type	Image/photo/illustration	Distribution	Worldwide
Number of images / photos / illustrations	1	Translation	Original language of publication
Format (select all that apply)	Print, Electronic	Copies for the disabled?	No
Who will republish the content?	Academic institution	Minor editing privileges?	No
Duration of Use	Life of current edition	Incidental promotional use?	No
Lifetime Unit Quantity	Up to 499	Currency	CAD
Rights Requested	Main product		

NEW WORK DETAILS

Title	Lipodepsipeptide Antibiotics: Total Synthesis and Mechanism of Action Studies Using 19F-NMR	Institution name	University of Waterloo
		Expected presentation date	2020-01-16
Instructor name	Braden Kralt		

ADDITIONAL DETAILS

Order reference number	N/A	The requesting person / organization to appear on the license	Braden Kralt

REUSE CONTENT DETAILS

Title, description or numeric reference of the portion(s)	Figure 1	Title of the article/chapter the portion is from	Targeting Virulence: A New Paradigm for Antimicrobial Therapy
Editor of portion(s)	N/A	Author of portion(s)	Clatworthy, A.E; Pierson, E.; Hung, D.T.
Volume of serial or monograph	3	Issue, if republishing an article from a serial	9
Page or page range of portion	541-548	Publication date of portion	2007-08-20

PUBLISHER TERMS AND CONDITIONS

Nature Publishing Group hereby grants you a non-exclusive license to reproduce this material for this purpose, and for no other use, subject to the conditions below: 1. NPG warrants that it has, to the best of its knowledge, the rights to license reuse of this material. However, you should ensure that the material you are requesting is original to Nature Publishing Group and does not carry the copyright of another entity (as credited in the published version). If the credit line on any part of the material you have requested indicates that it was reprinted or adapted by NPG with permission from another source, then you should also seek permission from that source to reuse the material. 2. Permission granted free of charge for material in print is also usually granted for any electronic version of that work, provided that the material is incidental to the work as a whole and that the electronic version is essentially equivalent to, or substitutes for, the print version. Where print permission has been granted for a fee, separate permission must be obtained for any additional, electronic re-use (unless, as in the case of a full paper, this has already been accounted for during your initial request in the calculation of a print

Permission for Figure 1.5:

Figure 1.5 was borrowed from Section 11.4.1 of Dr. Michael Palmer's online course notes for CHEM 731 - Biochemical Pharmacology. Dr. Michael Palmer gave written permission for this figure to be used in this thesis.

Permission for Figure 1.6:

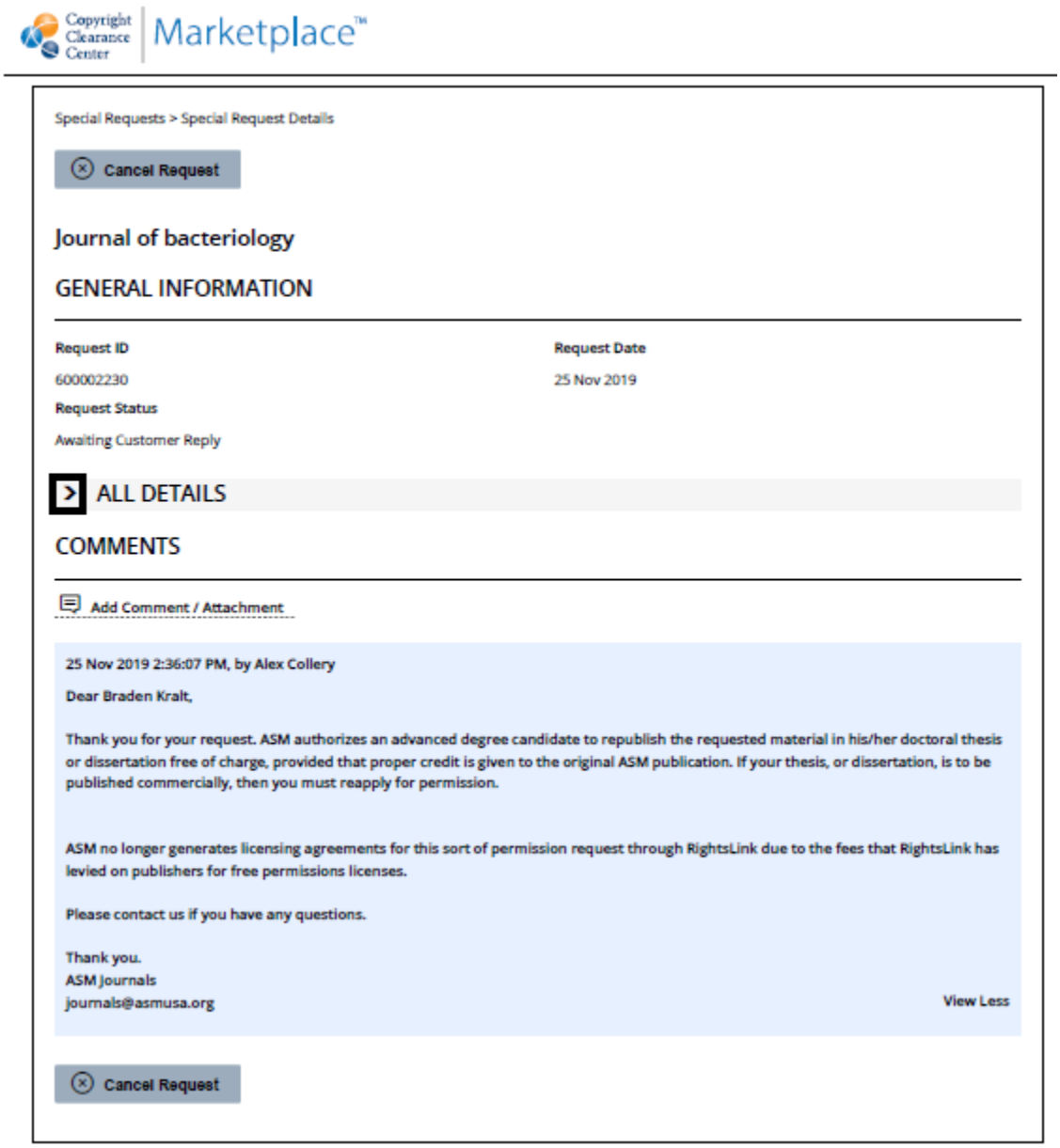

Copyright Clearance Center | Marketplace™

Special Requests > Special Request Details

Cancel Request

Journal of bacteriology

GENERAL INFORMATION

Request ID
600002230

Request Date
25 Nov 2019

Request Status
Awaiting Customer Reply

ALL DETAILS

COMMENTS

Add Comment / Attachment

25 Nov 2019 2:36:07 PM, by Alex Collery

Dear Braden Kralt,

Thank you for your request. ASM authorizes an advanced degree candidate to republish the requested material in his/her doctoral thesis or dissertation free of charge, provided that proper credit is given to the original ASM publication. If your thesis, or dissertation, is to be published commercially, then you must reapply for permission.

ASM no longer generates licensing agreements for this sort of permission request through RightsLink due to the fees that RightsLink has levied on publishers for free permissions licenses.

Please contact us if you have any questions.

Thank you.
ASM Journals
journals@asmusa.org

View Less

Cancel Request

Permission for Figure 1.7:

Dear Dr. Krait,

Your permission requested is granted and there is no fee for this reuse. In your planned reuse, you must cite the ACS article as the source, add this direct link https://pubs.acs.org/doi/10.1021/bi500779g , and include a notice to readers that further permissions related to the material excerpted should be directed to the ACS.

If you need further assistance, please let me know.

Sincerely,
Simran Mehra
ACS Publications Support
Customer Services & Information
Website: https://help.acs.org/

Incident Information:

Incident #:	3250124
Date Created:	2020-01-11T18:32:54
Priority:	3
Customer:	Braden Krait
Title:	Copyright Permissions Request
Description:	Dear Copyright Support Team: I'm writing to request the use of a Figure from an ACS Author Choice Journal article in my PhD thesis. Here is the link to the article: dx.doi.org/10.1021/bi500779g I wish to use one Figure (Figure 2A) in the introduction chapter of my thesis. Many thanks for your assistance in this matter. Braden Krait PhD Candidate, Organic Chemistry University of Waterloo, Ontario

Direct link to journal article:
https://pubs.acs.org/doi/10.1021/bi500779g

Notice to readers: further permissions related to the excerpted material should be directed to the ACS.

Permission for Figure 1.8:

PNAS Permissions 1:56 PM (41 minutes ago)

to me

Thank you for your message. Permission is granted for your use of the material as described in your request. Please include a full citation for the original PNAS article when reusing the material. Because this material published after 2008, a copyright note is not needed. There is no charge for this material, either. Let us know if you have any questions.

Sincerely,

Kay McLaughlin for
Diane Sullenberger
PNAS Executive Editor

...

From: Braden Kralt <bjkralt@gmail.com>
Sent: Saturday, January 11, 2020 8:21 AM
To: PNAS Permissions <PNASPermissions@nas.edu>
Subject: Requestion Permission

Dear PNAS Copyright permissions team:

I am writing to request the use of a Figure in my PhD Thesis.

My information / article information:

1. My name is Braden John Kralt, PhD Candidate at the University of Waterloo and would like to request the use of a Figure for my PhD Thesis.

2. email address: bjkralt@gmail.com

3. www.pnas.org/cgi/doi/10.1073/pnas.1611173113
Volume 113, Issue 45, 2016

4. Article title: Daptomycin inhibits cell envelope synthesis by interfering with fluid membrane microdomains

5. Author names:
Anna Müller, Michaela Wenzel, Henrik Strahl, Fabian Grein, Terrens N. V. Saaki, Bastian Kohl, Tjalling Siersma, Julia E. Bandow, Hans-Georg Sahl, Tanja Schneider,b,3, and Leendert W. Hamoen

6/7. Page number: Figure 7 on E7084

Intended use of material:

1 Thesis title, "Lipodepsipeptide Antibiotics: Total Synthesis and Mechanism of Action Studies Using 19F-NMR"

2. Author: Braden John Kralt

3. Publisher of work: University of Waterloo

4: Retail Price: $0.00

5. Number of copies to be produced, unknown

6. Intended audience: University of Waterloo

7. For Non-profit use.

Many thanks for your assistance on this matter!

Braden Kralt
PhD Candidate, Organic Chemistry
University of Waterloo, Ontario

Permission for Figure 1.9:

Copyright Clearance Center Marketplace™

Elsevier Science & Technology Journals - License Terms and Conditions

Order Date	11-Jan-2020
Order license ID	1005604-3
ISSN	0005-2736
Type of Use	Republish in a thesis/dissertation
Publisher	ELSEVIER BV
Portion	Chart/graph/table/figure

LICENSED CONTENT

Publication Title	Biochimica et biophysica acta. Biomembranes	Publication Type	Journal
Article Title	Daptomycin forms cation- and size-selective pores in model membranes	Start Page	2425
		End Page	2430
		Issue	10
Date	01/01/1967	Volume	1838
Language	Dutch		
Country	Netherlands		
Rightsholder	Elsevier Science & Technology Journals		

REQUEST DETAILS

Portion Type	Chart/graph/table/figure	Distribution	Worldwide
Number of charts / graphs / tables / figures requested	1	Translation	Original language of publication
		Copies for the disabled?	No
Format (select all that apply)	Print, Electronic	Minor editing privileges?	Yes
Who will republish the content?	Academic institution	Incidental promotional use?	No
Duration of Use	Life of current edition	Currency	CAD
Lifetime Unit Quantity	Up to 499		
Rights Requested	Main product		

NEW WORK DETAILS

Title	Lipodepsipeptide Antibiotics: Total Synthesis and Mechanism of Action Studies Using 19F-NMR	Institution name	University of Waterloo
		Expected presentation date	2020-01-16
Instructor name	Braden Kralt		

ADDITIONAL DETAILS

Order reference number	N/A	The requesting person / organization to appear on the license	Braden Kralt

REUSE CONTENT DETAILS

Title, description or numeric reference of the portion(s)	Figure 2	Title of the article/chapter the portion is from	Daptomycin forms cation- and size-selective pores in model membranes
Editor of portion(s)	Palmer, Michael; Silverman, Jared; MacCormick, Ben; Muraih, Jawad K.; Zhang, TianHua	Author of portion(s)	Palmer, Michael; Silverman, Jared; MacCormick, Ben; Muraih, Jawad K.; Zhang, TianHua
Volume of serial or monograph	1838		
Page or page range of portion	2425-2430	Issue, if republishing an article from a serial	10
		Publication date of portion	2014-05-21

PUBLISHER TERMS AND CONDITIONS

Elsevier publishes Open Access articles in both its Open Access journals and via its Open Access articles option in subscription journals, for which an author selects a user license permitting certain types of reuse without permission. Before proceeding please check if the article is Open Access on

http://www.sciencedirect.com and refer to the user license for the individual article. Any reuse not included in the user license terms will require permission. You must always fully and appropriately credit the author and source. If any part of the material to be used (for example, figures) has appeared in the Elsevier publication for which you are seeking permission, with credit or acknowledgement to another source it is the responsibility of the user to ensure their reuse complies with the terms and conditions determined by the rights holder. Please contact permissions@elsevier.com with any queries.

Permission for Figure 1.10 and Figure 1.11:

American Soc for Biochemistry & Molecular Biology - License Terms and Conditions

Order Date	11-Jan-2020
Order license ID	1005604-2
ISSN	1083-351X
Type of Use	Republish in a thesis/dissertation
Publisher	AMERICAN SOCIETY FOR BIOCHEMISTRY AND MOLECULAR BI
Portion	Chart/graph/table/figure

LICENSED CONTENT

Publication Title	Journal of biological chemistry	Publication Type	e-Journal
Article Title	Cardiolipin prevents membrane translocation and permeabilization by daptomycin.	Start Page	11591
		End Page	11591
Author/Editor	AMERICAN SOCIETY FOR BIOCHEMISTRY & MOLECULAR BIOL	Issue	17
		Volume	289
		URL	http://www.jbc.org/
Date	01/01/1905		
Language	English		
Country	United States of America		
Rightsholder	American Soc for Biochemistry & Molecular Biology		

REQUEST DETAILS

Portion Type	Chart/graph/table/figure	Distribution	Worldwide
Number of charts / graphs / tables / figures requested	2	Translation	Original language of publication
		Copies for the disabled?	No
Format (select all that apply)	Print, Electronic	Minor editing privileges?	No
Who will republish the content?	Academic institution	Incidental promotional use?	No
Duration of Use	Life of current and all future editions	Currency	CAD
Lifetime Unit Quantity	Up to 499		
Rights Requested	Main product		

NEW WORK DETAILS

Title	Lipodepsipeptide Antibiotics: Total Synthesis and Mechanism of Action Studies Using 19F-NMR	Institution name	University of Waterloo
		Expected presentation date	2020-01-16
Instructor name	Braden Kralt		

ADDITIONAL DETAILS

Order reference number	N/A	The requesting person / organization to appear on the license	Braden Kralt

REUSE CONTENT DETAILS

Title, description or numeric reference of the portion(s)	Figure 7, Figure 8	Title of the article/chapter the portion is from	Cardiolipin prevents membrane translocation and permeabilization by daptomycin.
Editor of portion(s)	Mintzer, Evan; Palmer, Michael; Taylor, Scott D; Uwumarenogie, Stephanie; Silverman, Jared; Victor, Rachel L; Herskowitz, Jennifer; Tishbi, Nasim; Muraih, Jawad K; Zhang, TianHua	Author of portion(s)	Mintzer, Evan; Palmer, Michael; Taylor, Scott D; Uwumarenogie, Stephanie; Silverman, Jared; Victor, Rachel L; Herskowitz, Jennifer; Tishbi, Nasim; Muraih, Jawad K; Zhang, TianHua
Volume of serial or monograph	289		
Page or page range of portion	11584-11591		

PUBLISHER TERMS AND CONDITIONS

Journal of Biological Chemistry permissions policies: • If you are an author of the content for which you are seeking permission, or if you are not an author but are requesting permission to copy, distribute, transmit and adapt the work for noncommercial purposes (e.g. reproduction of a figure for educational purposes such as schoolwork, or appending a reprinted article to a PhD dissertation), you do not need to seek permission using the options listed below, as long as any reuse includes the credit line in the reuse policies listed above. • Parties who are not authors on the article who wish to reuse content for commercial purposes such as reproducing a figure in a book, journal, or coursepack published by a commercial publisher, do need permission and should request permission by completing the form below. For more information please see Journal of Biological Chemistry: http://www.jbc.org/site/misc/edpolicy.xhtml#copyright

Permission for Figure 1.14 – Part 1:

Copyright Clearance Center Marketplace™

Royal Society of Chemistry - License Terms and Conditions

Order Date	11-Jan-2020
Order license ID	1005604-4
ISSN	0265-0568
Type of Use	Republish in a thesis/dissertation
Publisher	ROYAL SOCIETY OF CHEMISTRY,
Portion	Chart/graph/table/figure

LICENSED CONTENT

Publication Title	Natural product reports : a journal of current developments in bio-organic chemistry	Rightsholder	Royal Society of Chemistry
Article Title	Natural products to drugs: daptomycin and related lipopeptide antibiotics	Publication Type	Journal
Author/Editor	ROYAL SOCIETY OF CHEMISTRY (GREAT BRITAIN)	Start Page	717
Date	01/01/1984	Issue	6
Language	English	Volume	22
Country	United Kingdom of Great Britain and Northern Ireland		

REQUEST DETAILS

Portion Type	Chart/graph/table/figure	Distribution	Worldwide
Number of charts / graphs / tables / figures requested	1	Translation	Original language of publication
Format (select all that apply)	Print, Electronic	Copies for the disabled?	No
Who will republish the content?	Academic institution	Minor editing privileges?	Yes
Duration of Use	Life of current edition	Incidental promotional use?	No
Lifetime Unit Quantity	Up to 499	Currency	CAD
Rights Requested	Main product		

NEW WORK DETAILS

Title	Lipodepsipeptide Antibiotics: Total Synthesis and Mechanism of Action Studies Using 19F-NMR	Institution name	University of Waterloo
Instructor name	Braden Kralt	Expected presentation date	2020-01-16

ADDITIONAL DETAILS

Order reference number	N/A	The requesting person / organization to appear on the license	Braden Kralt

REUSE CONTENT DETAILS

Title, description or numeric reference of the portion(s)	Figure 3	Title of the article/chapter the portion is from	Natural products to drugs: daptomycin and related lipopeptide antibiotics
Editor of portion(s)	Baltz, Richard H.; Miao, Vivian; Wrigley, Stephen K.	Author of portion(s)	Baltz, Richard H.; Miao, Vivian; Wrigley, Stephen K.
Volume of serial or monograph	22	Issue, if republishing an article from a serial	6
Page or page range of portion	717	Publication date of portion	2005-11-25

Permission for Figure 1.14 – Part 2:

Copyright Clearance Center Marketplace™

Springer - License Terms and Conditions

Order Date	11-Jan-2020
Order license ID	1005604-5
ISSN	13675435
Type of Use	Republish in a thesis/dissertation
Publisher	SPRINGER-VERLAG
Portion	Chart/graph/table/figure

LICENSED CONTENT

Publication Title	Journal of industrial microbiology & biotechnology	Rightsholder	Springer
Article Title	The lipopeptide antibiotic A54145 biosynthetic gene cluster from Streptomyces fradiae	Publication Type	Journal
		Start Page	129
		End Page	140
Author/Editor	SOCIETY FOR INDUSTRIAL MICROBIOLOGY, Society for Industrial Microbiology (U.S.)	Issue	2
		Volume	33
Date	01/01/1986		
Language	English		
Country	Germany		

REQUEST DETAILS

Portion Type	Chart/graph/table/figure	Distribution	Worldwide
Number of charts / graphs / tables / figures requested	1	Translation	Original language of publication
		Copies for the disabled?	No
Format (select all that apply)	Print, Electronic	Minor editing privileges?	Yes
Who will republish the content?	Academic institution	Incidental promotional use?	No
Duration of Use	Life of current and all future editions	Currency	CAD
Lifetime Unit Quantity	Up to 499		
Rights Requested	Main product		

NEW WORK DETAILS

Title	Lipodepsipeptide Antibiotics: Total Synthesis and Mechanism of Action Studies Using 19F-NMR	Institution name	University of Waterloo
		Expected presentation date	2020-01-16
Instructor name	Braden Kralt		

ADDITIONAL DETAILS

Order reference number	N/A	The requesting person / organization to appear on the license	Braden Kralt

REUSE CONTENT DETAILS

Title, description or numeric reference of the portion(s)	Figure 2	Title of the article/chapter the portion is from	The lipopeptide antibiotic A54145 biosynthetic gene cluster from Streptomyces fradiae
Editor of portion(s)	Vivian, Miao; Renee, Brost; Joanne, Chapple; Kevin, She; Marie-FranÃ§ois, CoÃ«ffet-Le, Gal; Richard, H., Baltz	Author of portion(s)	Vivian, Miao; Renee, Brost; Joanne, Chapple; Kevin, She; Marie-FranÃ§ois, CoÃ«ffet-Le, Gal; Richard, H., Baltz
Volume of serial or monograph	33		
Page or page range of portion	129-140	Issue, if republishing an article from a serial	2
		Publication date of portion	2005-10-06

PUBLISHER TERMS AND CONDITIONS

A maximum of 10% of the content may be licensed for republication. The user is responsible for identifying and seeking separate licenses for any third party materials that are identified anywhere in the work. Without a separate license, such third party materials may not be reused.
If you are placing a request on behalf of/for a corporate organization, please use RightsLink.For further information visit
http://www.nature.com/reprints/permission-requests.html and
https://www.springer.com/gp/rights-permissions/obtaining-permissions/882

Permission for Figure 1.15:

Copyright Clearance Center Marketplace™

Elsevier Science & Technology Journals - License Terms and Conditions

Order Date	11-Jan-2020
Order license ID	1005604-6
ISSN	0968-0896
Type of Use	Republish in a thesis/dissertation
Publisher	PERGAMON
Portion	Chart/graph/table/figure

LICENSED CONTENT

Publication Title	Bioorganic & medicinal chemistry	Publication Type	Journal
Article Title	The action mechanism of daptomycin.	Start Page	6253
Date	01/01/1993	End Page	6268
Language	English	Issue	24
Country	United Kingdom of Great Britain and Northern Ireland	Volume	24
Rightsholder	Elsevier Science & Technology Journals		

REQUEST DETAILS

Portion Type	Chart/graph/table/figure	Distribution	Worldwide
Number of charts / graphs / tables / figures requested	1	Translation	Original language of publication
Format (select all that apply)	Print, Electronic	Copies for the disabled?	No
Who will republish the content?	Academic institution	Minor editing privileges?	Yes
Duration of Use	Life of current edition	Incidental promotional use?	No
Lifetime Unit Quantity	Up to 499	Currency	CAD
Rights Requested	Main product		

NEW WORK DETAILS

Title	Lipodepsipeptide Antibiotics: Total Synthesis and Mechanism of Action Studies Using 19F-NMR	Institution name	University of Waterloo
		Expected presentation date	2020-01-16
Instructor name	Braden Kralt		

ADDITIONAL DETAILS

Order reference number	N/A	The requesting person / organization to appear on the license	Braden Kralt

REUSE CONTENT DETAILS

Title, description or numeric reference of the portion(s)	Figure 2	Title of the article/chapter the portion is from	The action mechanism of daptomycin.
Editor of portion(s)	Taylor, Scott D.; Palmer, Michael	Author of portion(s)	Taylor, Scott D.; Palmer, Michael
Volume of serial or monograph	24	Issue, if republishing an article from a serial	24
Page or page range of portion	6253-6268	Publication date of portion	2016-05-28

PUBLISHER TERMS AND CONDITIONS

Elsevier publishes Open Access articles in both its Open Access journals and via its Open Access articles option in subscription journals, for which an author selects a user license permitting certain types of reuse without permission. Before proceeding please check if the article is Open Access on http://www.sciencedirect.com and refer to the user license for the individual article. Any reuse not included in the user license terms will require permission. You must always fully and appropriately credit the author and source. If any part of the material to be used (for example, figures) has appeared in the Elsevier publication for which you are seeking permission, with credit or acknowledgement to another source it is the responsibility of the user to ensure their reuse complies with the terms and conditions determined by the rights holder. Please contact permissions@elsevier.com with any queries.

Permission for Table 1.2:

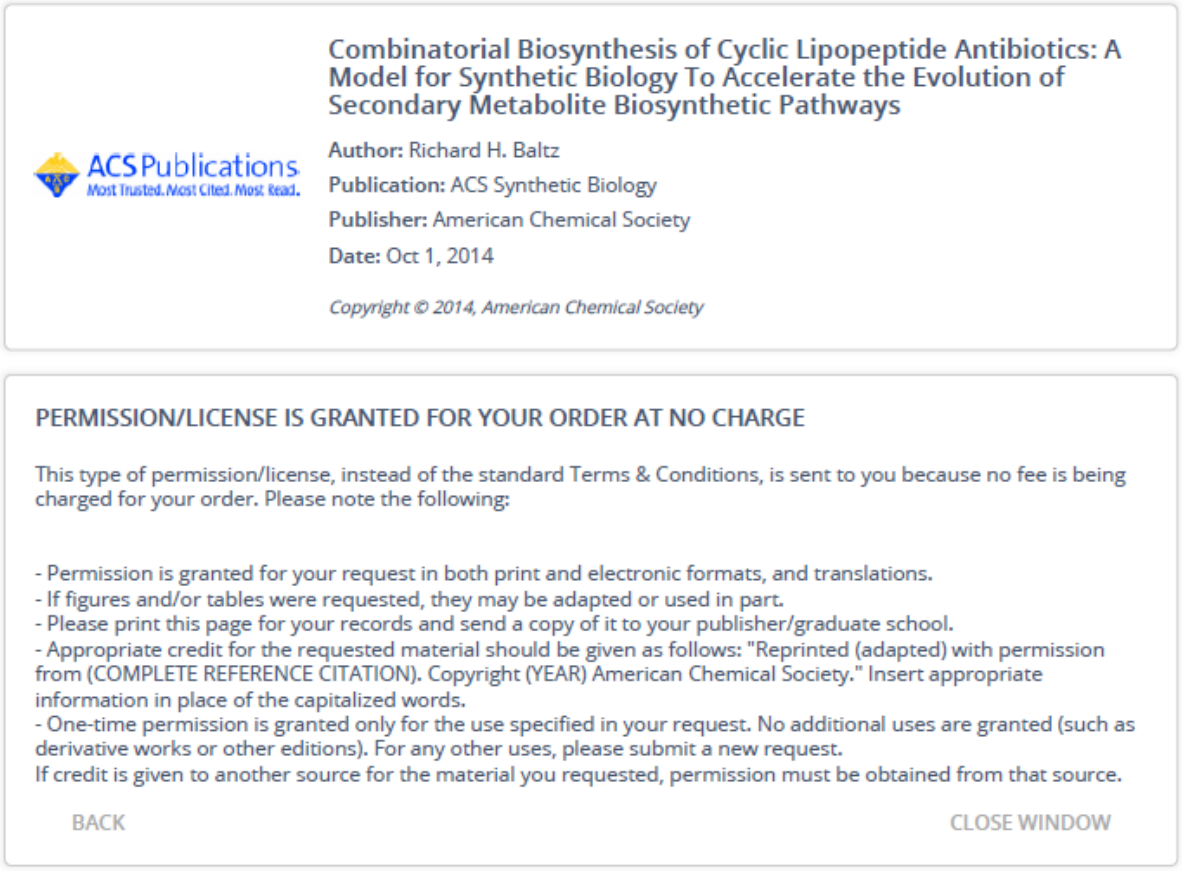

Combinatorial Biosynthesis of Cyclic Lipopeptide Antibiotics: A Model for Synthetic Biology To Accelerate the Evolution of Secondary Metabolite Biosynthetic Pathways

Author: Richard H. Baltz

Publication: ACS Synthetic Biology

Publisher: American Chemical Society

Date: Oct 1, 2014

Copyright © 2014, American Chemical Society

PERMISSION/LICENSE IS GRANTED FOR YOUR ORDER AT NO CHARGE

This type of permission/license, instead of the standard Terms & Conditions, is sent to you because no fee is being charged for your order. Please note the following:

- Permission is granted for your request in both print and electronic formats, and translations.
- If figures and/or tables were requested, they may be adapted or used in part.
- Please print this page for your records and send a copy of it to your publisher/graduate school.
- Appropriate credit for the requested material should be given as follows: "Reprinted (adapted) with permission from (COMPLETE REFERENCE CITATION). Copyright (YEAR) American Chemical Society." Insert appropriate information in place of the capitalized words.
- One-time permission is granted only for the use specified in your request. No additional uses are granted (such as derivative works or other editions). For any other uses, please submit a new request.

If credit is given to another source for the material you requested, permission must be obtained from that source.

BACK CLOSE WINDOW

References:

(1) Clatworthy, A. E.; Pierson, E.; Hung, D. T. Targeting Virulence: A New Paradigm for Antimicrobial Therapy. *Nat. Chem. Biol.* **2007**, *3* (9), 541–548.

(2) Palumbi, S. R. Humans as the World's Greatest Evolutionary Force. *Science* **2001**, *293*, 1786–1791.

(3) Yocum, R. R.; Rasmussen, J. R.; Strominger, J. L. The Mechanism of Action of Penicillin. *J. Biol. Chem.* **1980**, *255* (9), 3977–3986.

(4) Silver, L. L. Challenges of Antibacterial Discovery. *Clin. Microbiol. Revews* **2011**, *24* (1), 71–109.

(5) Venugopal, A. A.; Johnson, S. Fidaxomicin: A Novel Macrocyclic Antibiotic Approved for Treatment of Clostridium Difficile Infection. *Clin. Infect. Dis.* **2012**, *54*, 568–574.

(6) Fox, G. J.; Menzies, D. A Review of the Evidence for Using Bedaquiline (TMC207) to Treat Multi-Drug Resistant Tuberculosis. *Infect. Deseases Ther.* **2013**, *2*, 123–144.

(7) Fernandes, P.; Martens, E. Antibiotics in Late Clinical Development. *Biochem. Pharmacol.* **2017**, *133* (2017), 152–163.

(8) Swaney, S. M.; Aoki, H.; Ganoza, M. C.; Shinabarger, D. L. The Oxazolidinone Linezolid Inhibits Initiation of Protein Synthesis in Bacteria. *Antimicrob. Agents Chemother.* **1998**, *42* (12), 3251–3255.

(9) Jones, R. N.; Fritsche, T. R.; Sader, H. S.; Ross, J. E. Activity of Retapamulin (SB-275833), a Novel Pleuromutilin, against Selected Resistant Gram-Positive Cocci. *Antimicrob. Agents Chemother.* **2006**, *50* (7), 2583–2586.

(10) Srivastava, A.; Talaue, M.; Liu, S.; Degen, D.; Ebright, R. Y.; Sineva, E.; Chakraborty, A.; Druzhinin, S. Y.; Chatterjee, S.; Ebright, Y. W.; Zozula, A.; Shen, J.; Sengupta, S.; Rong, R.; Xin, C.; Kaneko, T.; Irschik, H.; Jansen, R.; Donadio, S.; Connell, N.; Ebright, R. H. New Target for Inhibition of Bacterial RNA Polymerase: "Switch Region." *Curr. Opin. Microbiol.* **2012**, *14* (5), 532–543.

(11) Yadav, S.; Rawal, G.; Baxi, M. Bedaquiline: A Novel Antitubercular Agent for the Treatment of Multidrug- Resistant Tuberculosis. *J. Clin. Diagnostic Res.* **2016**, *10* (8), FM01–FM02.

(12) Alanis, A. J. Resistance to Antibiotics: Are We in the Post-Antibiotic Era? *Arch. Med. Res.* **2005**, *36*, 697–705.

(13) Taylor, S. D.; Palmer, M. The Action Mechanism of Daptomycin. *Bioorganic Med. Chem.* **2016**, *24*, 6253–6268.

(14) Eisenstein, B. I.; Oleson, F. B.; Baltz, R. H. Daptomycin: From the Mountain to the Clinic, with Essential Help from Francis Tally, MD. *Clin. Infect. Dis.* **2010**, *50 Suppl 1* (Suppl 1), S10–S15.

(15) Counter, F. T.; Allen, N. E.; Fukuda, D. S.; Hobbs, J. N.; Ott, J.; Ensminger, P. W.; Mynderse, J. S.; Preston, D. A.; Wu, C. Y. E. A54145 a New Lipopeptide Antibiotic

Complex: Microbiological Evaluation. *J. Antibiot. (Tokyo).* **1990**, *43*, 616–622.

(16) Nguyen, K. T.; He, X.; Alexander, D. C.; Li, C.; Gu, J. Q.; Mascio, C.; Van Praagh, A.; Mortin, L.; Chu, M.; Silverman, J. a.; Brian, P.; Baltz, R. H. Genetically Engineered Lipopeptide Antibiotics Related to A54145 and Daptomycin with Improved Properties. *Antimicrob. Agents Chemother.* **2010**, *54* (4), 1404–1413.

(17) Alexander, D. C.; Rock, J.; Gu, J.; Mascio, C.; Chu, M.; Brian, P.; Baltz, R. H. Production of Novel Lipopeptide Antibiotics Related to A54145 by *Streptomyces fradiae* Mutants Blocked in Biosynthesis of Modified Amino Acids and Assignment of *LptJ*, *LptK* and *LptL* Gene Functions. *J. Antibiot. (Tokyo).* **2010**, *64* (1), 79–87.

(18) Liu, L.; Oza, S.; Hogan, D.; Perin, J.; Rudan, I.; Lawn, J. E.; Cousens, S.; Mathers, C.; Black, R. E. Global, Regional, and National Causes of Child Mortality in 2000–13 , with Projections to Inform Post-2015 Priorities: An Updated Systematic Analysis. *Lancet* **2015**, *385*, 430–440.

(19) Silverman, J. A.; Mortin, L. I.; Vanpraagh, A. D. G.; Li, T.; Alder, J. Inhibition of Daptomycin by Pulmonary Surfactant: In Vitro Modeling and Clinical Impact. *J. Infect. Dis.* **2005**, *191* (12), 2149–2152.

(20) Eliopoulos, G. M.; Thauvin, C.; Gerson, B.; Moellering, R. C. In Vitro Activity and Mechanism of Action of A21978C_1, a Novel Cyclic Lipopeptide Antibiotic. *Antimicrob. Agents Chemother.* **1985**, *27* (3), 357–362.

(21) Lakey, J. H.; Lea, E. J. A. The Role of Acyl Chain Character and Other Determinants on the Bilayer Activity of A21978C an Acidic Lipopeptide Antibiotic. *Biochim. Biophys. Acta* **1986**, *859*, 219–226.

(22) Jung, D.; Rozek, A.; Okon, M.; Hancock, R. E. W. Structural Transitions as Determinants of the Action of the Calcium-Dependent Antibiotic Daptomycin. *Chem. Biol.* **2004**, *11*, 949–957.

(23) Palmer, M. Biochemical Pharmacology. University of Waterloo: Waterloo 2012.

(24) Allen, N. E.; Hobbs, J. N.; Alborn, W. E. Inhibition of Peptidoglycan Biosynthesis in Gram-Positive Bacteria by LY146032. *Antimicrob. Agents Chemother.* **1987**, *31* (7), 1093–1099.

(25) Mengin-Lecreulx, D.; Allen, N. E.; Hobbs, J. N.; van Heijenoort, J. Inhibition of Peptidoglycan Biosynthesis in *Bacillus megaterium* by Daptomycin. *FEMS Microbiol. Lett.* **1990**, *69*, 245–248.

(26) Boaretti, M.; Canepari, P.; del Mar Lleo, M.; Satta, G. The Activity of Daptomycin on *Enterococcus faecium* Protoplasts: Indirect Evidence Supporting a Novel Mode of Action on Lipoteichoic Acid Synthesis. *J. Antimicrob. Chemother.* **1993**, *31*, 227–235.

(27) Canepari, P.; Boaretti, M.; del Mar Lleo, M.; Satta, G. Lipoteichoic Acid as a New Target for Activity of Antibiotics: Mode of Action of Daptomycin (LY146032). *Antimicrob. Agents Chemother.* **1990**, *34* (6), 1220–1226.

(28) Boaretti, M.; Canepari, P. Identification of Daptomycin-Binding Proteins in the Membrane of *Enterococcus hirae*. *Antimicrob. Agents Chemother.* **1995**, *39* (9), 2068–2072.

(29) Boaretti, M.; Canepari, P. Purification of Daptomycin Binding Proteins (DBPS) from the Membrane of *Enterococcus hirae*. *Microbiologica* **2000**, *23*, 305–317.

(30) Laganas, V.; Alder, J.; Silverman, J. A. In Vitro Bactericidal Activities of Daptomycin against *Staphylococcus aureus* and *Enterococcus faecalis* Are Not Mediated by Inhibition of Lipoteichoic Acid Biosynthesis. *Antimicrob. Agents Chemother.* **2003**, *47* (8), 2682–2684.

(31) Wehrli, W. Rifampin: Mechanisms of Action and Resistance. *Rev. Infect. Dis.* **1983**, *5*, S407–S411.

(32) Wale, L. J.; Shelton, A. P.; Greenwood, D. Scanning Electronmicroscopy of *Staphylococcus aureus* and *Enterococcus faecalis* Exposed to Daptomycin. *J. Med. Microbiol.* **1989**, *30*, 45–49.

(33) Cotroneo, N.; Harris, R.; Perlmutter, N.; Beveridge, T.; Silverman, J. A. Daptomycin Exerts Bactericidal Activity without Lysis of *Staphylococcus aureus*. *Antimicrob. Agents Chemother.* **2008**, *52* (6), 2223–2225.

(34) Jung, D.; Paul, J.; Straus, S. K.; Hancock, R. E. W. Lipid-Specific Binding of the Calcium-Dependent Antibiotic Daptomycin Leads to Changes in Lipid Polymorphism of Model Membranes. *Chem. Phys. Lipids* **2008**, *154*, 120–128.

(35) Pogliano, J.; Pogliano, N.; Silverman, J. a. Daptomycin-Mediated Reorganization of Membrane Architecture Causes Mislocalization of Essential Cell Division Proteins. *J. Bacteriol.* **2012**, *194* (17), 4494–4504.

(36) Chen, Y.; Sun, T.; Sun, Y.; Huang, H. W. Interaction of Daptomycin with Lipid Bilayers: A Lipid Extracting Effect. *Biochemistry* **2014**, *53*, 5384–5392.

(37) Müller, A.; Wenzel, M.; Strahl, H.; Grein, F.; Saaki, T. N. V; Kohl, B.; Siersma, T.; Bandow, J. E.; Sahl, H.-G.; Schneider, T.; Hamoen, L. W. Daptomycin Inhibits Cell Envelope Synthesis by Interfering with Fluid Membrane Microdomains. *Proc. Natl. Acad. Sci. U. S. A.* **2016**, *113* (45), E7077–E7086.

(38) Lee, M.-T.; Yang, P.-Y.; Charron, N. E.; Hseih, M.-H.; Chang, Y.-Y.; Huang, H. W. Comparison of the Effects of Daptomycin on Bacterial and Model Membranes. *Biochemistry* **2018**, *57* (38), 5629–5639.

(39) Lakey, J. H.; Ptak, M. Fluorescence Indicates a Calcium-Dependent Interaction between the Lipopeptide Antibiotic LY 146032 and Phospholipid Membranes. *Biochemistry* **1988**, *27*, 4639–4645.

(40) Alborn, W. E.; Allen, N. E.; Preston, D. A. Daptomycin Disrupts Membrane-Potential in Growing *Staphylococcus aureus*. *Antimicrob. Agents Chemother.* **1991**, *35* (11), 2282–2287.

(41) Allen, N. E.; Alborn, W. E.; Hobbs, J. N. Inhibition of Membrane Potential-Dependent Amino Acid Transport by Daptomycin. *Antimicrob. Agents Chemother.* **1991**, *35* (12), 2639–2642.

(42) Silverman, J. A.; Perlmutter, N. G.; Howard, M.; Shapiro, H. M. Correlation of Daptomycin Bactericidal Activity and Membrane Depolarization in *Staphylococcus aureus*. *Antimicrob. Agents Chemother.* **2003**, *47* (8), 2538–2544.

(43) Seydlová, G.; Sokol, A.; Liskova, P.; Konopasek, I.; Fiser, R. Daptomycin Pore Formation and Stoichiometry Depend on Membrane Potential of Target Membrane. *Antimicrob. Agents Chemother.* **2018**, *63* (1), e01589-18.

(44) Muraih, J. K.; Pearson, A.; Silverman, J.; Palmer, M. Oligomerization of Daptomycin on Membranes. *Biochim. Biophys. Acta* **2011**, *1808*, 1154–1160.

(45) Muraih, J. K.; Harris, J.; Taylor, S. D.; Palmer, M. Characterization of Daptomycin Oligomerization with Perylene Excimer Fluorescence: Stoichiometric Binding of Phosphatidylglycerol Triggers Oligomer Formation. *BBA - Biomembr.* **2012**, *1818*, 673–678.

(46) Muraih, J. K.; Palmer, M. Estimation of the Subunit Stoichiometry of the Membrane-Associated Daptomycin Oligomer by FRET. *Biochim. Biophys. Acta - Biomembr.* **2012**, *1818* (7), 1642–1647.

(47) Zhang, T.; Muraih, J. K.; MacCormick, B.; Silverman, J.; Palmer, M. Daptomycin Forms Cation- and Size-Selective Pores in Model Membranes. *Biochim. Biophys. Acta* **2014**, *1838*, 2425–2430.

(48) Zhang, T.; Muraih, J. K.; Herskowitz, J.; Victor, R. L.; Silverman, J.; Uwumarenogie, S.; Taylor, S. D.; Palmer, M.; Zhang, T.; Muraih, J. K.; Tishbi, N.; Herskowitz, J.; Victor, R. L.; Silverman, J.; Uwumarenogie, S.; Taylor, S. D.; Palmer, M.; Mintzer, E. Cardiolipin Prevents Membrane Translocation and Permeabilization by Daptomycin. *J. Biol. Chem.* **2014**, *289*, 11584–11591.

(49) Taylor, R.; Butt, K.; Scott, B.; Zhang, T.; Muraih, J. K.; Mintzer, E.; Taylor, S.; Palmer, M. Two Successive Calcium-Dependent Transitions Mediate Membrane Binding and Oligomerization of Daptomycin and the Related Antibiotic A54145. *BBA - Biomembr.* **2016**, *1858* (9), 1999–2005.

(50) Zhang, T.; Taylor, S. D.; Palmer, M.; Duhamel, J. Membrane Binding and Oligomerization of the Lipopeptide A54145 Studied by Pyrene Fluorescence. *Biophys. J.* **2016**, *111*, 1267–1277.

(51) Taylor, R.; Beriashvili, D.; Taylor, S.; Palmer, M. Daptomycin Pore Formation Is Restricted by Lipid Acyl Chain Composition. *ACS Infect. Dis.* **2017**, *3*, 797–801.

(52) Beriashvili, D.; Taylor, R.; Kralt, B.; Mazen, N. A.; Taylor, S. D.; Palmer, M. Mechanistic Studies on the Effect of Membrane Lipid Acyl Chain Composition on Daptomycin Pore Formation. *Chem. Phys. Lipids* **2018**, *216*, 73–79.

(53) Kreutzberger, M. A.; Pokorny, A.; Almeida, P. F. Daptomycin–Phosphatidylglycerol Domains in Lipid Membranes. *Langmuir* **2017**, *33* (47), 13669–13679.

(54) Friedman, L.; Alder, J. D.; Silverman, J. a. Genetic Changes That Correlate with Reduced Susceptibility to Daptomycin in *Staphylococcus aureus*. *Antimicrob. Agents Chemother.* **2006**, *50* (6), 2137–2145.

(55) Peleg, A. Y.; Miyakis, S.; Ward, D. V; Earl, A. M.; Rubio, A.; Cameron, D. R.; Pillai, S.; Moellering, R. C.; Eliopoulos, G. M. Whole Genome Characterization of the Mechanisms of Daptomycin Resistance in Clinical and Laboratory Derived Isolates of *Staphylococcus aureus*. *PLoS One* **2012**, *7*, e28316.

(56) Ernst, C. M.; Staubitz, P.; Mishra, N. N.; Yang, S.; Hornig, G.; Bayer, A. S.; Kraus, D.; Peschel, A. The Bacterial Defensin Resistance Protein MprF Consists of Separable Domains for Lipid Lysinylation and Antimicrobial Peptide Repulsion. *PLoS One* **2009**, *5* (11), e1000660.

(57) Ernst, C. M.; Peschel, A. Broad-Spectrum Antimicrobial Peptide Resistance by MprF-Mediated Aminoacylation and Flipping of Phospholipids. *Mol. Microbiol.* **2011**, *80* (2), 290–299.

(58) Yang, S.-J.; Mishra, N. N.; Rubio, A.; Bayer, A. S. Causal Role of Single Nucleotide Polymorphisms within the *MprF* Gene of *Staphylococcus aureus* in Daptomycin Resistance. *Antimicrob. Agents Chemother.* **2013**, *57* (11), 5658–5664.

(59) Yang, S.-J.; Xiong, Y. Q.; Dunman, P. M.; Schrenzel, J.; Francois, P.; Peschel, A.; Bayer, A. S. Regulation of MprF in Daptomycin-Nonsusceptible *Staphylococcus aureus* Strains. *Antimicrob. Agents Chemother.* **2016**, *53* (6), 2636–2637.

(60) Mishra, N. N.; Bayer, A. S. Correlation of Cell Membrane Lipid Profiles with Daptomycin Resistance in Methicillin-Resistant *Staphylococcus aureus*. *Antimicrob. Agents Chemother.* **2013**, *57* (2), 1082–1085.

(61) Pillai, S. K.; Gold, H. S.; Sakoulas, G.; Wennersten, C.; Moellering, R. C.; Eliopoulos, G. M. Daptomycin Nonsusceptibility in *Staphylococcus aureus* with Reduced Vancomycin Susceptibility Is Independent of Alterations in *MprF*. *Antimicrob. Agents Chemother.* **2007**, *51* (6), 2223–2225.

(62) Davlieva, M.; Zhang, W.; Arias, C. A.; Shamoo, Y. Biochemical Characterization of Cardiolipin Synthase Mutations Associated with Daptomycin Resistance in *Enterococci*. *Antimicrob. Agents Chemother.* **2013**, *57* (1), 289–296.

(63) Taylor, R. M.; Scott, B.; Taylor, S.; Palmer, M. An Acyl-Linked Dimer of Daptomycin Is Strongly Inhibited by the Bacterial Cell Wall. *ACS Infect. Dis.* **2017**, *3*, 462–466.

(64) Yang, S.; Nast, C. C.; Mishra, N. N.; Yeaman, M. R.; Fey, P. D.; Bayer, A. S. Cell Wall Thickening Is Not a Universal Accompaniment of the Daptomycin Nonsusceptibility Phenotype in *Staphylococcus aureus*: Evidence for Multiple Resistance Mechanisms. *Antimicrob. Agents Chemother.* **2016**, *54* (8), 3079–3085.

(65) D'Costa, V. M.; Mukhtar, T. a.; Patel, T.; Koteva, K.; Waglechner, N.; Hughes, D. W.; Wright, G. D.; De Pascale, G. Inactivation of the Lipopeptide Antibiotic Daptomycin by Hydrolytic Mechanisms. *Antimicrob. Agents Chemother.* **2012**, *56*, 757–764.

(66) Baltz, R. H.; Miao, V.; Wrigley, S. K. Natural Products to Drugs: Daptomycin and Related Lipopeptide Antibiotics. *Nat. Prod. Rep.* **2005**, *22*, 717–741.

(67) Miao, V.; Brost, R.; Chapple, J.; She, K.; Coëffet-Le Gal, M. F.; Baltz, R. H. The Lipopeptide Antibiotic A54145 Biosynthetic Gene Cluster from *Streptomyces fradiae*. *J. Ind. Microbiol. Biotechnol.* **2006**, *33*, 129–140.

(68) Robbel, L.; Marahiel, M. A. Daptomycin, a Bacterial Lipopeptide Synthesized by a Nonribosomal Machinery*. *J. Biol. Chem.* **2010**, *285* (36), 27501–27508.

(69) Debono, M.; Abbott, B. J.; Molloy, R. M.; Fukuda, D. S.; Hunt, A. H.; Daupert, V. M.; Counter, F. T.; Ott, J. L.; Carrell, C. B.; Howard, L. C.; Boeck, L. D.; Hamill, R. L. Enzymatic and Chemical Modifications of Lipopeptide Antibiotic A21978C: The Synthesis and Evaluation of Daptomycin (LY 146032). *J. Antibiot. (Tokyo).* **1988**, *41* (8), 1093–1105.

(70) Fukuda, D. S.; Bus, R. H. Du; Baker, P. J.; Mynderse, J. S.; Berry, D. M. A54145, a New Lipopeptide Antibiotic Complex: Isolation and Characterization. *J. Antibiot. (Tokyo).* **1990**, *43*, 594–600.

(71) Fukuda, D. S.; Debono, M.; Molloy, R. M.; Mynderse, J. S. A54145, a New Lipopeptide Antibiotic Complex: Microbial and Chemical Modification. *J. Antibiot. (Tokyo).* **1990**, *43*, 601–606.

(72) Hill, J.; Siedlecki, J.; Parr, I.; Morytko, M.; Yu, X.; Zhang, Y.; Silverman, J.; Controneo, N.; Laganas, V.; Li, T.; Lai, J.; Keith, D.; Shimer, G.; Finn, J. Synthesis and Biological Activity of *N*-Acylated Ornithine Analogues of Daptomycin. *Bioorganic Med. Chem. Lett.* **2003**, *13*, 4187–4191.

(73) Siedlecki, J.; Hill, J.; Parr, I.; Yu, X.; Morytko, M.; Zhang, Y.; Silverman, J.; Controneo, N.; Laganas, V.; Li, T.; Li, J.; Keith, D.; Shimer, G.; Finn, J. Array Synthesis of Novel Lipodepsipeptide. *Bioorganic Med. Chem. Lett.* **2003**, *13*, 4245–4249.

(74) He, Y.; Li, J.; Yin, N.; Herradura, P. S.; Martel, L.; Zhang, Y.; Pearson, A. L.; Kulkarni, V.; Mascio, C.; Howland, K.; Silverman, J. A.; Keith, D. D.; Metcalf, C. A. Reduced Pulmonary Surfactant Interaction of Daptomycin Analogs via Tryptophan Replacement with Alternative Amino Acids. *Bioorg. Med. Chem. Lett.* **2012**, *22* (19), 6248–6251.

(75) Leese, R. A.; Curran, W. V; Borders, D. B. Lipodepsipeptide Antiobiotics and Methods of Preparation. *US Pat.* **2003**, *US30224475*, 14.

(76) Grunewald, J.; Sieber, S. A.; Mahlert, C.; Linne, U.; Marahiel, M. A. Synthesis and Derivatization of Daptomycin : A Chemoenzymatic Route to Acidic Lipopeptide Antibiotics. *J. Am. Chem. Soc.* **2004**, *126*, 17025–17031.

(77) Miao, V.; Coeffet-LeGal, M. F.; Brian, P.; Brost, R.; Penn, J.; Whiting, A.; Martin, S.; Ford, R.; Parr, I.; Bouchard, M.; Silva, C. J.; Wrigley, S. K.; Baltz, R. H. Daptomycin Biosynthesis in *Streptomyces roseosporus*: Cloning and Analysis of the Gene Cluster and Revision of Peptide Stereochemistry. *Microbiology* **2005**, *151* (5), 1507–1523.

(78) Kopp, F.; Grunewald, J.; Mahlert, C.; Marahiel, M. A. Chemoenzymatic Design of Acidic Lipopeptide Hybrids: New Insights into the Structure-Activity Relationship of Daptomycin and A54145. *Biochemistry* **2006**, *45*, 10474–10481.

(79) Baltz, R. H. Combinatorial Biosynthesis of Cyclic Lipopeptide Antibiotics: A Model for Synthetic Biology To Accelerate the Evolution of Secondary Metabolite Biosynthetic Pathways. *ACS Synth. Biol.* **2014**, *3*, 748–758.

(80) Baltz, R. H. *Daptomycin and A54145: Structure-Activity Relationship (SAR) Studies Enabled by Combinatorial Biosynthesis*; Osbourne, A., Goss, R., Carter, G. T., Eds.; John Wiley and Sons, Inc.: Hoboken, NJ, 2014.

(81) Barnawi, G. Structure-Activity Relationship Studies on Daptomycin, 2018.

(82) Barnawi, G.; Noden, M.; Taylor, R.; Lohani, C.; Beriashvili, D.; Palmer, M.; Taylor, S. D. An Entirely Fmoc Solid Phase Approach to the Synthesis of Daptomycin Analogs. *Biopolymers* **2017**, *e23094*, doi.org/10.1002/bip.23094.

(83) Lam, H. Y.; Zhang, Y.; Liu, H.; Xu, J.; Wong, C. T. T.; Xu, C.; Li, X. Total Synthesis of Daptomycin by Cyclization via a Chemoselective Serine Ligation. *J. Am. Chem. Soc.* **2013**, *135*, 6272–6279.

(84) 't Hart, P.; Kleijn, L. H. J.; de Bruin, G.; Oppedijk, S. F.; Kemmink, J.; Martin, N. I. A Combined Solid- and Solution-Phase Approach Provides Convenient Access to Analogues of the Calcium-Dependent Lipopeptide Antibiotics. *Org. Biomol. Chem.* **2014**, *12* (6), 913–918.

(85) Lohani, C. R.; Taylor, R.; Palmer, M.; Taylor, S. D. Solid-Phase Total Synthesis of Daptomycin and Analogs. *Org. Lett.* **2015**, *17*, 748–751.

(86) Lohani, C. R.; Taylor, R.; Palmer, M.; Taylor, S. D. Solid-Phase Synthesis and *in vitro* Biological Activity of a Thr4 --> Ser4 Analog of Daptomycin. *Bioorganic Med. Chem. Lett.* **2015**, *25*, 5490–5494.

(87) Lohani, C. R.; Rasera, B.; Scott, B.; Palmer, M.; Taylor, S. D. α-Azido Acids in Solid-Phase Peptide Synthesis: Compatibility with Fmoc Chemistry and an Alternative Approach to the Solid Phase Synthesis of Daptomycin Analogs. *J. Org. Chem.* **2016**, *81*, 2624–2628.

(88) Strieker, M.; Kopp, F.; Mahlert, C.; Essen, L.-O.; Marahiel, M. A. Mechanistic and Structural Basis of Stereospecific Cβ-Hydroxylation in Calcium-Dependent Antibiotic, a Daptomycin-Type Lipopeptide. *ACS Chem. Biol.* **2007**, *2* (3), 187–196.

(89) von Eckardstein, L.; Petras, D.; Dang, T.; Cociancich, S.; Sabri, S.; Kerwat, D.; Seidel, M.; Pesic, A.; Dorrestein, P. C.; Royer, M.; Weston, J. B.; Sussmuth, R. D. Total Synthesis and Biological Assessment of Novel Albicidins Discovered by Mass Spectrometric Networking. *Chem. - A Eur. J.* **2017**, *2017* (23), 15316–15321.

(90) Imashiro, R.; Seki, M. A Catalytic Asymmetric Synthesis of Chiral Glycidic Acid Derivatives through Chiral Dioxirane-Mediated Catalytic Asymmetric Epoxidation of Cinnamic Acid Derivatives. *J. Org. Chem.* **2004**, *69*, 4216–4226.

(91) Moreira, R.; Taylor, S. D. Asymmetric Synthesis of Fmoc-Protected β-Hydroxy and β-Methoxy Amino Acids via a Sharpless Aminohydroxylation Reaction Using FmocNHCl. *Org. Lett.* **2018**, *20*, 7717–7720.

(92) Motoshima, K.; Ishikawa, M.; Hashimoto, Y.; Sugita, K. Peroxisome Proliferator-Activated Receptor Agonists with Phenethylphenylphthalimide Skeleton Derived from Thalidomide-Related Liver X Receptor Antagonists: Relationship between Absolute Configuration and Subtype Selectivity. *Bioorganic Med. Chem.* **2011**, *19* (10), 3156–3172.

(93) Siow, A.; Opiyo, G.; Kavianinia, I.; Li, F. F.; Furkert, D. P.; Harris, P. W. R.; Brimble, M. A. Total Synthesis of the Highly *N*-Methylated Acetylene-Containing Anticancer Peptide Jahanyne. *Org. Lett.* **2018**, *20*, 788–791.

(94) Pedroso, E.; Grandas, A.; de las Heras, X.; Eritja, R.; Giralt, E. Diketopiperazine Formation in Solid Phase Peptide Synthesis Using *p*-Alkoxybenzyl Ester Resins and Fmoc-Amino Acids. *Tetrahedron Lett.* **1986**, *27* (6), 743–746.

(95) Purdie, J. E.; Benoiton, N. L. Piperazinedione Formation from Esters of Dipeptides Containing Glycine, Alanine, and Sarcosine: The Kinetics in Aqueous Solution. *J. Chem. Soc. Perkin Trans. 1* **1973**, 1845–1853.

(96) Gude, M.; Ryf, J.; White, P. D. An Accurate Method for the Quantitation of Fmoc-Derivatized Solid Phase Supports. *Lett. Pept. Sci.* **2003**, *9*, 203–206.

(97) Thieriet, N.; Alsina, J.; Giralt, E.; Guibe, F.; Albericio, F. Use of Alloc-Amino Acids in Solid-Phase Peptide Synthesis. Tandem Deprotection-Coupling Reactions Using Neutral Conditions. *Tetrahedron Lett.* **1997**, *38* (41), 7275–7278.

(98) Zorn, C.; Gnad, F.; Salmen, S.; Herpin, T.; Reiser, O. Deprotection of *N*-Alloc Amines by Pd(0)/DABCO—an Efficient Method for *in situ* Peptide Coupling of Labile Amino Acids. *Tetrahedron* **2001**, *42*, 7049–7053.

(99) Malakoutikhah, M.; Teixidó, M.; Giralt, E. Toward an Optimal Blood-Brain Barrier Shuttle by Synthesis and Evaluation of Peptide Libraries. *J. Med. Chem.* **2008**, *51*, 4881–4889.

(100) Kim, H.; Cho, J. K.; Aimoto, S.; Lee, Y.-S. Solid-Phase Staudinger Ligation from a Novel Core-Shell-Type Resin: A Tool for Facile Condensation of Small Peptide Fragments. *Org. Lett.* **2006**, *8* (6), 1149–1151.

(101) Goddard-Borger, E. D.; Stick, R. V. An Efficient, Inexpensive, and Shelf-Stable Diazotransfer Reagent: Imidazole-1-Sulfonyl Azide Hydrochloride. *Org. Lett.* **2007**, *9* (19), 3797–3800.

(102) Ji, L.; Zhou, G.-Q.; Qian, C.; Chen, X.-Z. Synthesis of 1,2,3-Triazoles from Azide-Derivatised Aminocyclitols by Catalytic Diazo Transfer and CuAAC Click Chemistry. *European J. Org. Chem.* **2014**, *2014*, 3622–3636.

(103) Lohani, C. R.; Soley, J.; Kralt, B.; Palmer, M.; Taylor, S. D. α-Azido Esters in Depsipeptide Synthesis: C−O Bond Cleavage during Azido Group Reduction. *J. Org. Chem.* **2016**, *81*, 11831–11840.

(104) Wong, D.; Taylor, C. M. Asymmetric Synthesis of Erythro-β-Hydroxyasparagine. *Tetrahedron Lett.* **2009**, *50*, 1273–1275.

(105) Boeck, L. D.; Fukuda, D. S.; Mynderse, J. S.; Hoen, M. M.; Kastner, R. E.; Papiska, H. R. A54145 Antibiotics and Process for Their Production. *US Pat.* **1991**, *4994270*, 30.

(106) Fukuda, D. S.; Mynderse, J. S. A54145 Cyclic Peptides. *US Pat.* **1991**, *US5039789*, 23.

(107) Kaneda, T. *Iso*- and *Anteiso*-Fatty Acids in Bacteria: Biosynthesis, Function, and Taxonomic Significance. *Microbiol. Rev.* **1991**, *55* (2), 288–302.

(108) Boeck, L. D.; Wetzel, R. W. A54145, a New Lipopeptide Antibiotic Complex: Factor Control through Precursor Directed Biosynthesis. *J. Antibiot. (Tokyo).* **1990**, *43*, 607–

615.

(109) Wuster, T.; Kaczybura, N.; Bruckner, R.; Keller, M. Synthesis of Enantiomerically Pure Model Compounds of the Glucose-6-Phosphate-T1-Translocase Inhibitors Kodaistatins A-D. Inferences with Regard to the Stereostructure of the Natural Products. *Tetrahedron* **2013**, *69*, 7785–7809.

(110) Yang, Z.; Ma, M.; Yang, C.-H.; Gao, Y.; Zhang, Q.; Chen, Y. Determination of the Absolute Configurations of Microtermolides A and B. *J. Nat. Prod.* **2016**, *79*, 2408–2412.

(111) Chen, D.; Chow, H. Y.; Po, K. H. L.; Ma, W.; Leung, E. L. Y.; Sun, Z.; Liu, M.; Chen, S.; Li, X. Total Synthesis and Structural Establishment/Revision of Antibiotics A54145. *Org. Lett.* **2019**, *21*, 5639–5644.

(112) Wiegand, I.; Hilpert, K.; Hancock, R. E. W. Agar and Broth Dilution Methods to Determine the Minimal Inhibitory Concentration (MIC) of Antimicrobial Substances. *Nat. Protoc.* **2008**, *3* (2), 163–175.

(113) Hedenstrom, E.; Nguyen, B.-V.; Silks, L. A. I. Do Enzymes Recognise Remotely Located Stereocentres? Highly Enantioselective *Candida rugosa* Lipase-Catalysed Esterification of the 2- to 8-Methyldecanoic Acids. *Tetrahedron: Asymmetry* **2002**, *13*, 835–844.

(114) Paulsen, H.; Merz, G.; Brockhausen, I. Synthese von *L*-Prolin-Haltigen *O*-Glycopeptiden. *Liebigs Ann. der Chemie* **1990**, *1990* (8), 719–739.

(115) Groth, T.; Grøtli, M.; Meldal, M. Diffusion of Reagents in Macrobeads. *J. Comb. Chem.* **2001**, *3*, 461–468.

(116) Dartois, V.; Sanchez-Quesada, J.; Cabezas, E.; Chi, E.; Dubbelde, C.; Dunn, C.; Granja, J.; Gritzen, C.; Weinberger, D.; Ghadiri, M. R.; Parr, T. R. Systemic Antibacterial Activity of Novel Synthetic Cyclic Peptides. *Antimicrob. Agents Chemother.* **2005**, *49* (8), 3302–3310.

(117) Moreira, R.; Barnawi, G.; Beriashvili, D.; Palmer, M.; Taylor, S. D. The Effect of Replacing the Ester Bond with an Amide Bond and of Overall Stereochemistry on the Activity of Daptomycin. *Bioorganic Med. Chem.* **2019**, *27*, 240–246.

(118) Lau, Y. H.; Spring, D. R. Efficient Synthesis of Fmoc-Protected Azido Amino Acids. *Synlett* **2011**, 1917–1919.

(119) Pícha, J.; Budesinsky, M.; Machackova, K.; Collinsová, M.; Jiracek, J. Optimized Syntheses of Fmoc Azido Amino Acids for the Preparation of Azidopeptides. *J. Pept. Sci.* **2017**, *23*, 202–214.

(120) Thakkar, A.; Trinh, T. B.; Pei, D. Global Analysis of Peptide Cyclization Efficiency. *ACS Comb. Sci.* **2013**, *15*, 120–129.

(121) Knerr, P. J.; van der Donk, W. A. Chemical Synthesis and Biological Activity of Analogues of the Lantibiotic Epilancin 15X. *J. Am. Chem. Soc.* **2012**, *134*, 7648–7651.

(122) Alsina, J.; Barany, G.; Albericio, F.; Kates, S. A. Pyrrolidide Formation as a Side Reaction during Activation of Carboxylic Acids by Phosphonium Salt Coupling

Reagents. *Lett. Pept. Sci.* **1999**, *6*, 243–245.

(123) Eliopoulos, G. M.; Willey, S.; Reiszner, E.; Spitzer, P. G.; Caputo, G.; Moellering, R. C. *In vitro* and *in vivo* Activity of LY 146032, a New Cyclic Lipopeptide Antibiotic. *Antimicrob. Agents Chemother.* **1986**, *30* (4), 532–535.

(124) Luo, Y.; Evindar, G.; Fishlock, D.; Lajoie, G. A. Synthesis of *N*-Protected *N*-Methyl Serine and Threonine. *Tetrahedron Lett.* **2001**, *42*, 3807–3809.

(125) Aguda, A. H.; Lavallee, V.; Cheng, P.; Bott, T. M.; Meimetis, L. G.; Law, S.; Nguyen, N. T.; Williams, D. E.; Kaleta, J.; Villanueva, I.; Davies, J.; Andersen, R. J.; Brayer, G. D.; Bromme, D. Affinity Crystallography: A New Approach to Extracting High-Affinity Enzyme Inhibitors from Natural Extracts. *J. Nat. Prod.* **2016**, *79*, 1962–1970.

(126) Su, Y.; Degrado, W. F.; Hong, M. Orientation, Dynamics, and Lipid Interaction of an Antimicrobial Arylamide Investigated by ^{19}F and ^{31}P Solid-State NMR Spectroscopy. *J. Am. Chem. Soc.* **2010**, *132* (1), 9197–9205.

(127) Afonin, S.; Dürr, U. H. N.; Glaser, R. W.; Ulrich, A. S. 'Boomerang'-like Insertion of a Fusogenic Peptide in a Lipid Membrane Revealed by Solid-State ^{19}F NMR. *Magn. Reson. Chem.* **2004**, *42*, 195–203.

(128) Cobb, S. L.; Murphy, C. D. ^{19}F NMR Applications in Chemical Biology. *J. Fluor. Chem.* **2009**, *130*, 132–143.

(129) Prosser, R. S.; Evanics, F.; Kitevski, J. L.; Patel, S. The Measurement of Immersion Depth and Topology of Membrane Proteins by Solution State NMR. *Biochim. Biophys. Acta* **2007**, *1768*, 3044–3051.

(130) Marsh, E. N. G.; Suzuki, Y. Using ^{19}F NMR to Probe Biological Interactions of Proteins and Peptides. *ACS Chem. Biol.* **2014**, *9*, 1242–1250.

(131) Afonin, S.; Glaser, R. W.; Berditchevskaia, M.; Wadhwani, P.; Guhrs, K.-H.; Mollmann, U.; Perner, A.; Ulrich, A. S. 4-Fluorophenylglycine as a Label for ^{19}F NMR Structure Analysis of Membrane-Associated Peptides. *ChemBioChem* **2003**, *4*, 1151–1163.

(132) Anderluh, G.; Razpotnik, A.; Podlesek, Z.; Macek, P.; Separovic, F.; Norton, R. S. Interaction of the Eukaryotic Pore-Forming Cytolysin Equinatoxin II with Model Membranes: 19 F NMR Studies. *J. Mol. Biol.* **2005**, *347*, 27–39.

(133) Caaveiro, J. M. M.; Echabe, I.; Gutierrez-Aguirre, I.; Nieva, J. L.; Arrondo, J. L. R.; Gonzalez-Manas, J. M. Differential Interaction of Equinatoxin II with Model Membranes in Response to Lipid Composition. *Biophys. J.* **2001**, *80*, 1343–1353.

(134) Li, C.; Lutz, E. A.; Slade, K. M.; Ruf, R. A. S.; Wang, G.-F.; Pielak, G. J. ^{19}F NMR Studies of α-Synuclein Conformation and Fibrillation. *Biochemistry* **2009**, *48*, 8578–8584.

(135) Buer, B. C.; Chugh, J.; Al-hashimi, H. M.; Marsh, E. N. G. Using Fluorine Nuclear Magnetic Resonance To Probe the Interaction of Membrane-Active Peptides with the Lipid Bilayer. *Biochemistry* **2010**, *49*, 5760–5765.

(136) Suzuki, Y.; Buer, B. C.; Al-hashimi, H. M.; Marsh, E. N. G. Using Fluorine Nuclear

Magnetic Resonance to Probe Changes in the Structure and Dynamics of Membrane-Active Peptides Interacting with Lipid Bilayers. *Biochemistry* **2011**, *50*, 5979–5987.

(137) Buer, B. C.; Levin, B. J.; Marsh, E. N. G. Perfluoro-*tert*-Butyl-Homoserine as a Sensitive ^{19}F NMR Reporter for Peptide–Membrane Interactions in Solution. *J. Pept. Sci.* **2013**, *19*, 308–314.

(138) Wang, G.; Li, C.; Pielak, G. J. ^{19}F NMR Studies of α-Synuclein-Membrane Interactions. *Protein Sci.* **2010**, *19*, 1686–1691.

(139) Ball, L.-J.; Goult, C. M.; Donarski, J. A.; Micklefield, J.; Ramesh, V. NMR Structure Determination and Calcium Binding Effects of Lipopeptide Antibiotic Daptomycin. *Org. Biomol. Chem.* **2004**, *2*, 1872–1878.

(140) Rotondi, K. S.; Gierasch, L. M. A Well-Defined Amphipathic Conformation for the Calcium-Free Cyclic Lipopeptide Antibiotic, Daptomycin, in Aqueous Solution. *Biopolymers* **2005**, *80*, 374–385.

(141) Scott, W. R. P.; Baek, S.; Jung, D.; Hancock, R. E. W.; Straus, S. K. NMR Structural Studies of the Antibiotic Lipopeptide Daptomycin in DHPC Micelles. *Biochim. Biophys. Acta* **2007**, *1768*, 3116–3126.

(142) Graton, J.; Laurence, C.; Berthelot, M.; Questel, J.-Y. Le; Besseau, F.; Raczynska, E. D. Hydrogen-Bond Basicity pKH_B Scale of Aliphatic Primary Amines. *J. Chem. Soc. Perkin Trans. 2* **1999**, *2*, 997–1001.

(143) Konermann, L. Addressing a Common Misconception: Ammonium Acetate as Neutral pH "Buffer" For Native Electrospray Mass Spectrometry. *J. Am. Soc. Mass Spectrom.* **2017**, *28*, 1827–1835.

(144) Qiu, J.; Yu, L.; Kirsch, L. E. Estimated pK_A Values for Specific Amino Acid Residues in Daptomycin. *J. Pharm. Sci.* **2010**, *100* (10), 4225–4233.

(145) Haidle, A. M.; Burch, J.; Guay, D.; Gauthier, J. Y.; Robichaud, J.; Fournier, J. F.; Ellis, J. M.; Christopher, M.; Kattar, S. D.; Smith, G.; Northrup, A. B. Substituted Phenyl Spleen Tyrosine Kinase (Syk) Inhibitors. *WO Pat.* **2014**, *WO20140314*, 115.

(146) Bijan, P.; Shuo, Z.; Yixing, S.; van Oeveren, A.; Zhi, L. A1 Androgen Receptor Modulator Compounds and Methods. *US Pat.* **2009**, *US20093002*.

(147) Van Oeveren, A.; Motamedi, M.; Mani, N. S.; Marschke, K. B.; Lopez, F. J.; Schrader, W. T.; Negro-Vilar, A.; Zhi, L. 4-Trifluoromethylquinolin-2-(1H)-one as a Novel Selective Androgen Receptor Modulator. *J. Med. Chem.* **2006**, *49*, 6143–6146.

(148) van Oeveren, A.; Pio, B. A.; Tegley, C. M.; Higuchi, R. I.; Wu, M.; Zhi, L.; Jones, T. K.; Marschke, K. B.; Negro-Vilar, A.; Zhi, L. Discovery of an Androgen Receptor Modulator Pharmacophore Based on 2-Quinolinones. *Bioorganic Med. Chem. Lett.* **2007**, *17*, 1523–1526.

(149) Noden, M.; Marlyn, J.; Taylor, S. Unpublished Results.

(150) Kotoris, C. C. The Synthesis of Novel Organofluorines by Electrophilic Fluorination and Their Evaluation as Inhibitors of Protein Tyrosine Phosphatase 1B, University of Waterloo, 2000.

(151) Hill, B.; Ahmed, V.; Bates, D.; Taylor, S. D. Enantioselective Synthesis of Protected *L*-4-[Sulfonamido(Difluoromethyl)]Phenylalanine and *L*-4-[Sulfonamido(Methyl)]Phenylalanine and an Examination of Hexa-and Tripeptide Platforms for Evaluating PTyr Mimics for PTP1B Inhibition. *J. Org. Chem.* **2006**, *71*, 8190–8197.

(152) Chen, G.; Shigenari, T.; Jain, P.; Zhang, Z.; Jin, Z.; He, J.; Li, S.; Mapelli, C.; Miller, M. M.; Poss, M. A.; Scola, P. M.; Yeung, K.-S.; Yu, J.-Q. Ligand-Enabled β-C−H Arylation of α-Amino Acids Using a Simple and Practical Auxiliary. *J. Am. Chem. Soc.* **2015**, *137*, 3338–3351.

(153) Combret, Y.; Duflos, J.; Dupas, G.; Bourguignon, J.; Queguiner, G. Variations of the Nature of the Chiral Auxiliary with a Highly Enantioselective Chiral NADH Model. *Tetrahedron: Asymmetry* **1993**, *4* (7), 1635–1644.

(154) Lovelock, S. L.; Lloyd, R. C.; Turner, N. J. Phenylalanine Ammonia Lyase Catalyzed Synthesis of Amino Acids by an MIO-Cofactor Independent Pathway. *Angew. Chemie Int. Ed.* **2014**, *53*, 4652–4656.

(155) Parmeggiani, F.; Lovelock, S. L.; Weise, N. J.; Ahmed, S. T.; Turner, N. J. Synthesis of *D*- and *L*-Phenylalanine Derivatives by Phenylalanine Ammonia Lyases: A Multienzymatic Cascade Process. *Angew. Chemie Int. Ed.* **2015**, *54*, 4608–4611.

(156) Williams, R. M.; Im, M.-N. Assymetric Synthesis of Monosubstituted and α,α-Disubstituted α-Amino Acids via Diastereoselective Glycine Enolate Alkylations. *J. Am. Chem. Soc.* **1991**, *113*, 9276–9286.

(157) Van Den Nieuwendijk, A. M. C. H.; Kriek, N. M. A. J.; Brussee, J.; Van Boom, J. H.; van der Gen, A. Stereoselective Synthesis of (2*R*,5*R*)- and (2*S*,5*R*)-5-Hydroxylysine. *European J. Org. Chem.* **2000**, *2000*, 3683–3691.

(158) Allevi, P.; Anastasia, M. A Practical and Simple Synthesis of (2*S*,5*R*)- and (2*S*,5*S*)-5-Hydroxylysine and of a Related α-Amino Acid Required for the Synthesis of the Collagen Cross-Link Pyridinoline. *Tetrahedron: Asymmetry* **2004**, *15*, 2091–2096.

(159) Dastlik, K. A.; Sundermeier, U.; Johns, D. M.; Chen, Y.; Williams, R. M. An Improved Synthesis of Optically Pure 4-Boc-5,6-diphenylmorpholin-2-one and 4-Cbz-5,6-diphenylmorpholin-2-one. *Synlett* **2005**, *2005* (4), 693–696.

(160) Liu, J.; Xu, X.-H.; Qing, F.-L. Silver-Mediated Oxidative Trifluoromethylation of Alcohols to Alkyl Trifluoromethyl Ethers. *Org. Lett.* **2015**, *17*, 5048–5051.

(161) Brown, Z. Z.; Muller, M. M.; Jain, S. U.; Allis, C. D.; Lewis, P. W.; Muir, T. W. Strategy for "Detoxification" of a Cancer-Derived Histone Mutant Based on Mapping Its Interaction with the Methyltransferase PRC2. *J. Am. Chem. Soc.* **2014**, *136*, 13498–13501.

(162) Duewel, H.; Daub, E.; Robinson, V.; Honek, J. F. Incorporation of Trifluoromethionine into a Phage Lysozyme: Implications and a New Marker for Use in Protein ^{19}F NMR. *Biochemistry* **1997**, *36*, 3404–3416.

(163) Qiu, J.; Kirsch, L. E. Evaluation of Lipopeptide (Daptomycin) Aggregation Using Fluorescence, Light Scattering, and Nuclear Magnetic Resonance Spectroscopy. *J.*

Pharm. Sci. **2014**, *103*, 853–861.

(164) Ho, S. W.; Jung, D.; Calhoun, J. R.; Lear, J. D.; Okon, M.; Scott, W. R. P.; Hancock, R. E. W.; Straus, S. K. Effect of Divalent Cations on the Structure of the Antibiotic Daptomycin. *Eur. Biophys. J.* **2008**, *37*, 421–433.

(165) Wenisch, J. M.; Meyer, B.; Fuhrmann, V.; Saria, K.; Zuba, C.; Dittrich, P.; Thalhammer, F. Multiple-Dose Pharmacokinetics of Daptomycin during Continuous Venovenous Haemodiafiltration. *J. Antimicrob. Chemother.* **2012**, *67*, 977–983.

(166) Vilay, A. M.; Grio, M.; Depestel, D. D.; Sowinski, K. M.; Gao, L.; Heung, M.; Salama, N. N.; Mueller, B. A.; Nct, I.; Care, C. Daptomycin Pharmacokinetics in Critically Ill Patients Receiving Continuous Venovenous Hemodialysis. *Crit. Care Med.* **2011**, *39* (1), 19–25.

(167) Benvenuto, M.; Benziger, D. P.; Yankelev, S.; Vigliani, G. Pharmacokinetics and Tolerability of Daptomycin at Doses up to 12 Milligrams per Kilogram of Body Weight Once Daily in Healthy Volunteers. *Antimicrob. Agents Chemother.* **2006**, *50* (10), 3245–3249.

(168) Dvorchik, B. H.; Brazier, D.; Debruin, M. F.; Arbeit, R. D. Daptomycin Pharmacokinetics and Safety Following Administration of Escalating Doses Once Daily to Healthy Subjects Daptomycin Pharmacokinetics and Safety Following Administration of Escalating Doses Once Daily to Healthy Subjects. *Antimicrob. Agents Chemother.* **2003**, *47* (4), 1318–1323.

(169) Kleckner, I. R.; Foster, M. P. An Introduction to NMR-Based Approaches for Measuring Protein Dynamics. *Biochim. Biophys. Acta - Proteins Proteomics* **2011**, *1814*, 942–968.

(170) Kreutz, C.; Micura, R. Investigations on Fluorine-Labelled Ribonucleic Acids by ^{19}F NMR Spectroscopy. In *Modified Nucleosides*; 2008; pp 3–20.

(171) Rubin, H.; Cockrell, J.; Morgan, J. B. Scalable Synthesis of *N*-Acylaziridines from *N*-Tosylaziridines. *J. Org. Chem.* **2013**, *78*, 8865–8871.

(172) Busca, P.; Paradisi, F.; Moynihan, E.; Maguire, A. R.; Engel, P. C. Enantioselective Synthesis of Non-Natural Amino Acids Using Phenylalanine Dehydrogenases Modified by Site-Directed Mutagenesis. *Org. Biomol. Chem.* **2004**, *2*, 2684–2691.

(173) Takrouri, K.; Chen, T.; Papadopoulos, E.; Sahoo, R.; Kabha, E.; Chen, H.; Cantel, S.; Wagner, G.; Halperin, J. A.; Aktas, B. H.; Chorev, M. Structure-Activity Relationship Study of 4EGI-1, Small Molecule EIF4E/EIF4G Protein-Protein Interaction Inhibitors. *Eur. J. Med. Chem.* **2014**, *77*, 361–377.

(174) Lopez-Tapia, F.; Brotherton-Pleiss, C.; Yue, P.; Murakami, H.; Carolina Costa Araujo, A.; Reis dos Santos, B.; Ichinotsubo, E.; Rabkin, A.; Shah, R.; Lantz, M.; Chen, S.; Tius, M. A.; Turkson, J. Linker Variation and Structure–Activity Relationship Analyses of Carboxylic Acid-Based Small Molecule STAT3 Inhibitors. *ACS Med. Chem. Lett.* **2018**, *9*, 250–255.

(175) Yang, L.; Zhang, Z.; Cheng, B.; You, Y.; Wu, D.; Hong, C. Two Tandem Multicomponent Reactions for the Synthesis of Sequence-Defined Polymers. *Sci.*

China Chem. **2015**, *58*, 1734–1740.

(176) Langlois, B.; Montegre, D.; Roidot, N. Synthesis of *S*-Trifluoromethyl-Containing α-Amino Acids from Sodium Trifluoromethanesulfinate and Dithio-Amino Acids. *J. Fluor. Chem.* **1994**, *68*, 63–66.